DOE/MC/11089-3318
(DE93000254)

Pressurized Fluidized-Bed Hydroretorting of Eastern Oil Shales

Annual Report
June 1991 - May 1992

M.J. Roberts
M.C. Mensinger
D.M. Rue
F.S. Lau
C.W. Schultz (University of Alabama)
B.K. Parekh (University of Kentucky)
M. Misra (University of Nevada - Reno)
W.P. Bonner (Tennessee Technological University)

November 1992

Work Performed Under Contract No.: DE-AC21-87MC11089

For
U.S. Department of Energy
Office of Fossil Energy
Morgantown Energy Technology Center
Morgantown, West Virginia

By
Institute of Gas Technology
Chicago, Illinois

DISCLAIMER

DOE/MC/11089-3318
(DE93000254)

Pressurized Fluidized-Bed Hydroretorting of Eastern Oil Shales

Annual Report
June 1991 - May 1992

M.J. Roberts
M.C. Mensinger
D.M. Rue
F.S. Lau
C.W. Schultz (University of Alabama)
B.K. Parekh (University of Kentucky)
M. Misra (University of Nevada - Reno)
W.P. Bonner (Tennessee Technological University)

Work Performed Under Contract No.: DE-AC21-87MC11089

For
U.S. Department of Energy
Office of Fossil Energy
Morgantown Energy Technology Center
P.O. Box 880
Morgantown, West Virginia 26507-0880

By
Institute of Gas Technology
IIT Center
3424 S. State Street
Chicago, Illinois 60616

November 1992

EXECUTIVE SUMMARY

The Institute of Gas Technology (IGT) is developing the Pressurized Fluidized-Bed Hydroretorting (PFH) process for producing oil from the Devonian shales in the Eastern U.S. The original 3-year program was initiated in September 1987 under U.S. Department of Energy (DOE) Contract No. DE-AC21-87MC11089 for the project "Pressurized Fluidized-Bed Hydroretorting of Eastern Oil Shales." The Final Report (in four volumes) describing the results of that work has been published by IGT.[1] This report presents the work performed by IGT and its subcontractors during the program extension from June 1, 1991 through May 31, 1992. The objective of the program extension was to expand the data base for the PFH process to beneficiated shales. IGT is the prime contractor for the overall program to develop the PFH process. In addition, four universities are working with IGT as subcontractors; their responsibilities and achievements in the program are discussed below in the appropriate tasks.

Some of the tasks in the original 3-year program were completed and were not continued in the program extension; therefore, the task achievements discussed below represent the results of the active tasks.

The objective of Subtask 3.6 (Combustion of Hydroretorted Beneficiated Shales) was to evaluate the combustion of hydroretorted beneficiated shale for energy recovery prior to disposal. IGT conducted tests with hydroretorted shale in a thermogravimetric analyzer and in a 2-inch diameter fluidized-bed reactor at temperatures and pressures up to 1800°F and 1000 psig (982°C and 7.0 MPa). The results showed that hydroretorted shale could be readily combusted; carbon conversions ranging from 93 to 100 percent were achieved depending upon the operating conditions.

The objective of Subtask 3.7 (Innovative Reactor Concept Testing) was to determine the feasibility of generating hydrogen by cracking by-product hydrocarbon gases produced during shale hydroretorting to hydrogen and carbon. Hydrogen generated by the cracking reactions would be used to supply hydrogen for the PFH process. The carbon, subsequently deposited on spent shale, would be combusted to supply heat for the cracking reactions.

IGT conducted methane cracking tests in an experimental unit designed and built for this task. The cracking tests were conducted at temperatures up to 2260°F and pressures to 1000 psig. The results showed that methane could be cracked to near thermodynamic equilibrium. Also, as the temperature was increased, the nearer was the approach to equilibrium. In tests conducted with a mixture of methane, ethane, and butane, near equilibrium values were also achieved at temperatures in the range of 1900° to 2000°F. The stainless steel reactor wall was found to have a catalytic effect on the cracking reactions; therefore, most cracking tests were conducted after the reactor had been passivated with hydrogen sulfide at 1500°F.

The objective of Subtask 3.8 (Niche Market Studies) was to investigate the use of the asphalt fraction of shale oil produced by the PFH process as an additive for asphalt binder. IGT conducted tests in the laboratory-scale batch PFH reactor and determined the operating conditions that maximize the

yield of the asphalt fraction. Standardized tests were conducted to characterize blends of two shale oil additives (2 to 10 weight percent) and a commercially available binder. Characterization tests were also conducted on pavement briquettes made with the additive/binder blends. The results indicate that pavement briquettes made with the shale oil additive/binder blend have greater resistance to freeze-thaw cracking than those made with binder alone. These briquettes also retain more of their tensile strength when wet. A shale oil additive for asphalt that would have improved pavement characteristics could likely be produced from a higher-temperature boiling fraction of the shale oil.

The University of Alabama Mineral Resources Institute (MRI, Tuscaloosa) was responsible for the work conducted in Task 4 (Beneficiation Research). The objective of this task was to test new concepts for improving the shale beneficiation system.

MRI conducted three independent subtasks on Grinding-Flotation Circuit Design, Evaluation of Different Grinding Media, and Oil Agglomeration and Pelletizing.

The objective of Subtask 4.1.4 (Grinding-Flotation Circuit Design) was to evaluate various grinding and flotation circuit configurations to minimize the energy consumption and cost of producing kerogen concentrates. Prior research by MRI showed that the key to reducing energy consumption was in reducing the amount of material that was ground in the stirred ball mill by removing product material as soon as it is formed. MRI showed that a clean tailing could be produced from relatively coarse feedstock.

MRI performed tests to determine the amount of fines that would be produced at various levels of primary grinding. Batch tests indicated that grinding to 325 mesh produced only marginally more -12 micrometer (μm) material than grinding to 100 mesh. Therefore, a bulk sample was ground to -100 mesh to provide feedstock for subsequent studies.

Hydrocyclone tests performed on the -100-mesh sample showed that high inlet pressures and high solids concentrations were required to make an effective separation of finely sized shale. Reducing solids concentration tended to reduce the size of the overflow product but also significantly reduced the recovery of the -12 μm material in the overflow. A combination of cycloning followed by fine screening produced the most satisfactory sizing of the primary ball mill product.

Flotation tests indicated that satisfactory recovery could be achieved with either the cyclone overflow or the screen undersize. Two-stage column flotation tests were conducted on a sample of reground screen oversize (i.e., the oversize product from sizing the primary ball mill product). These tests showed that both a final concentrate and a final tailing could be produced from relatively coarse (d_{90} = 20 μm) shale.

Column flotation tests conducted with untreated recycled water showed that the quality of the kerogen/mineral matter separation diminished as the number of water recycles increased. Further work is recommended to isolate

the cause of the deterioration of the kerogen/mineral matter separation and to determine ways of alleviating it.

The objectives of Subtask 4.5 on Evaluation of Different Grinding Media were to evaluate the use of sand as a replacement for steel media in stirred ball mill grinding and to determine the preferred stirring mechanism and operating conditions for using sand. A comparison of the John and Molinex stirring mechanisms showed that the John option consumed less energy than did the Molinex option for most product sizes, including the size consist of interest (d_{90} = 15 μm).

A comparison of the effects of grinding using the same size sand and steel media showed that sand grinding was more energy efficient than steel at the fine product size (d_{50} <7 μm). Further, for the same grinding media particle size, sand media costs about 1 to 2 ¢/lb, while steel media costs 7 $/lb. Stirred ball milling operations typically consume 1 to 2 pounds of media per ton of material ground. Another advantage for using sand media is that is does not release alloy elements such as chromium, nickel, and manganese to the slurry as does steel media.

MRI also conducted oil agglomeration and pelletizing tests (Subtask 4.6.1) to develop a means of transforming flotation concentrates into agglomerates suitable for use in the PFH process, thereby excluding an energy intensive drying step. Additives or reagents were considered for evaluation if they were recoverable, contributed to the net product, and were not deleterious to the PFH process. Three systems were identified that met these criteria: oil agglomeration with asphalt emulsion, oil agglomeration with asphalt-pentane solution, and pelletizing. None of the tests conducted with these systems was successful in producing agglomerates that could be fed to the PFH reactor. Subsequent tests indicated that extrusion produced an agglomerate of uniform size without requiring a recycle loop (as does the briquetting system); however, the feed material was thermally dried before being extruded. Asphalt emulsion added to the extrusion mix was found to materially improve the resistance of the extrusions to attrition.

The University of Kentucky Center for Applied Energy Research (UK-CAER) conducted flotation tests in a flotation column and integrated grinding and column flotation tests in the "SYMUSEP" separator. The objective of the tests (Subtask 4.4) was to evaluate a one-step integrated grinding and flotation process using a BDR Mill column (SYMUSEP Separator) to obtain a high grade (>30 gallons per ton [GPT]) oil shale at more than 80 percent kerogen recovery. The SYMUSEP Separator uses a single stage grinding-cleaning column system to avoid over grinding the oil shale.

Baseline column flotation studies were conducted on Alabama shale with a Fischer Assay of about 14.5 GPT. The shale was ground to 90 percent passing 9 μm in an attritor mill. With the flotation column, a minimum retention time of 20 minutes was required to obtain both high carbon recovery (80 to 85 percent) and high concentrate grade (40 to 47 percent carbon). Optimum flotation conditions were 2 L/min air flow rate, 0.2 L/min wash water rate, 3 lb/ton M252 frother, and a retention time of greater than 20 minutes.

The objective of tests conducted with the SYMUSEP separator was to determine the effect of grinding charge, grind speed, air flow rate and feed point location on recovery and grade. The best results obtained with the SYMUSEP separator were obtained using a 900 rpm grind speed, 10 pounds of grinding media, and 5 L/min air flow rate, which provided a carbon recovery of 75 percent with a concentrate grade of 25 percent carbon.

In Subtask 4.6.2 (Bioflocculation of Kerogen), the University of Nevada, Reno (UNR) conducted tests to determine if a hydrophobic microorganism (Mycobacterium phlei) could be used to flocculate kerogen from enriched flotation concentrate to produce an ultra-high-grade product. UNR found that the presence of M. phlei improved the settling rate of kerogen across the range of pH values tested (3.0 to 10.6). Also, in vacuum and pressure dewatering tests, the presence of M. phlei reduced the moisture content of the dewatered kerogen cake from about 51 percent (no organism) to about 41 percent. The addition of surfactants to the solution with M. phlei was also shown to further reduce the moisture content of the dewatered kerogen to about 39 percent. UNR also found that using water recycled from the bio-thickener improved the grade and recovery of kerogen from a Denver flotation machine. These results suggest that the presence of some surfactant derived from M. phlei improved the flotation performance.

In Task 5 (Operation of PFH on Beneficiated Shale), IGT conducted tests in the laboratory-scale batch and continuous PFH reactors to expand the PFH data base to beneficiated Alabama shale. The laboratory-scale tests were conducted at temperatures, pressures, and residence times in the ranges of 850° to 1230°F, 400 to 1000 psig, and 5 to 75 minutes, respectively. Operating information obtained from these laboratory-scale tests was used to select conditions for the bench-scale test with beneficiated shale. Also, detailed results of tests to bracket conditions for producing asphalt additives from shale by the PFH process conducted as part of Subtask 3.8 are reported in this task.

IGT conducted a test in the 100-lb/h bench-scale unit (BSU) with beneficiated Alabama shale that had been pelletized and subsequently comminuted and screened to -20+80 mesh. The BSU test was conducted at 925°F, 1000 psig, and a residence time of 25 minutes. A total of 3-1/4 hours of steady-state operation was achieved, which included two separate sampling periods to determine the reproducibility of the data. The feed and hydroretorted shale samples as well as oil and water samples were analyzed for trace and minor elements. The environmental sampling train was used to collect product gas samples in acid and base scrubber solutions to determine the trace constituent composition. The oil yield from the test was 233 percent of Fischer Assay.

In Subtask 6.1 (Characteristics of Processed Shales), IGT determined the physical and chemical properties of raw and processed beneficiated shale samples that may affect the design and characteristics of embankments used for storing the material prior to ultimate disposal. The physical properties determined included particle size distribution, permeability, compressibility, compactability, consolidation, direct shear stress, cohesion, thermal conductivity, Atterberg liquid and plastic limits, and specific gravity. The results

from leaching tests were used to determine if spent shale must be treated as a hazardous material for disposal.

The results showed that the physical properties of the raw and thermally processed beneficiated shale samples varied significantly depending upon the processing steps that were employed. However, the stability of embankments designed with combusted or agglomerated shale can be ensured through proper design. Also, the results of TCLP tests showed that the raw and hydroretorted beneficiated shale are not leached to any significant amount and are, therefore, considered non-hazardous.

In Subtask 6.2.2 (Wastewater Treatability), Tennessee Technological University (TTU) conducted aerobic treatability studies on four compounds found in the wastewater from the PFH process. TTU was able to successfully acclimate microorganisms to phenol, methyl ethyl ketone, and aniline and demonstrate their biological treatability. Repeated attempts by TTU to acclimate microorganisms to 4-methyl pyridine, however, were not successful.

In Subtask 6.4.1 (PFH Process Analyses), IGT revised the correlations that describe the effects of hydroretorting process conditions on raw shales to include hydroretorting of beneficiated Alabama shale. These correlations can be used to predict the oil and gas yields for beneficiated shale hydroretorted in the PFH process.

In Subtask 6.4.3 (Plant Energy Optimization), TTU conducted a preliminary exergetic and thermoeconomic evaluation of the PFH process. Exergy is the part of energy in a process stream than can be transformed into useful energy. TTU focused on process plant areas, such as the hydrogen plant, that had high exergy destructions and suggested changes that would increase the overall exergetic efficiency of the process. In the thermoeconomic evaluation, the value of the exergy in each process stream was determined. Streams with high thermoeconomic value can be identified so that the exergy in that stream can be utilized in the most efficient manner.

TTU evaluated the performance of the PFH plant and of a steam power plant combined in a computer simulation. Overall, from a thermodynamic view, the PFH hydroretorting operation has an exergetic efficiency of about 86.7 percent. The exergetic efficiency of the steam power plant is 37.3 percent. When the PFH plant is combined with a conventional steam power plant that uses the spent shale as its primary fuel, the net oil cost is reduced from the base case by $4.37 per barrel. Other process modifications and improvements, such as recovering sulfuric acid from the power plant flue gas, reduce the net oil cost (from the base case) by $7.41 per barrel. The cost effectiveness of gas scrubbing, acid gas removal and hydrogen recovery can be increased mainly through savings in the investment costs. The cost effectiveness of the recycle gas compressors could be increased by increasing their efficiency. TTU also recommended changes in the heat exchanger network that aim at better matching the hot and cold streams and at avoiding cost ineffective exergy destruction, which result in a simpler and more cost effective overall design.

The design improvements discussed here and the reduction in the net oil cost demonstrate the capabilities of the advanced thermoeconomic evaluation techniques applied by TTU in this subtask.

In Subtask 6.4.4, on process economics, IGT prepared a preliminary economic evaluation of a commercial-scale PFH process based on beneficiated Kentucky New Albany shale. The PFH process plant incorporates electric power generation by combustion of hydroretorted shale. The sensitivity of product oil cost to changes in by-product and electric power credits, cost of capital, shale feed and beneficiation costs, plant size and operating conditions was determined. The base-case cost to produce 50,000 barrels per day of upgraded oil from beneficiated shale was estimated to be $33.13 per barrel (in 1990 dollars). The total capital cost for the base case was estimated to be $1,926 million. Improvements in the overall PFH process scheme suggested by TTU that could improve the economics of the process have not been included in the preliminary cost estimate.

In Task 7 (Sample Procurement, Preparation, and Characterization), MRI collected about 9 tons of shale from a site in Alabama for use by the program participants. This bulk sample was shipped to Michigan Technological University (MTU) and beneficiated in continuous equipment. Portions of the beneficiated shale were subsequently shipped to IGT, UK-CAER, and MRI for project-related studies.

TABLE OF CONTENTS

LIST OF FIGURES

LIST OF FIGURES (Continued)

LIST OF FIGURES (Continued)

LIST OF FIGURES (Continued)

LIST OF FIGURES (Continued)

LIST OF FIGURES (Continued)

LIST OF FIGURES (Continued)

LIST OF TABLES

LIST OF TABLES (Continued)

LIST OF TABLES (Continued)

LIST OF TABLES (Continued)

LIST OF TABLES (Continued)

LIST OF TABLES (Continued)

INTRODUCTION

The Devonian oil shales of the Eastern United States are a significant domestic energy resource. The overall objective of the multi-year program, initiated in October 1987 by the U.S. Department of Energy (Contract No. DE-AC21-87MC11089), is to perform the research necessary to develop the Pressurized Fluidized-Bed Hydroretorting (PFH) process for producing oil from Eastern oil shales. The program also incorporates research on technologies in areas such as raw shale preparation, beneficiation, product separation, and waste disposal that have the potential of improving the economics and/or environmental acceptability of recovering oil from oil shales using the PFH process.

The results of the original 3-year program, which was concluded in May 1991, have been summarized in a four-volume final report published by IGT. DOE subsequently approved a 1-year extension to the program to further develop the PFH process specifically for application to beneficiated shale as feedstock. Studies have shown that beneficiated shale is the preferred feedstock for pressurized hydroretorting. The program extension is divided into the following active* tasks:

- Task 3. Testing of Process Improvement Concepts
- Task 4. Beneficiation Research
- Task 5. Operation of PFH on Beneficiated Shale
- Task 6. Environmental Data and Mitigation Analyses
- Task 7. Sample Procurement, Preparation, and Characterization
- Task 8. Project Management and Reporting.

In order to accomplish all the program objectives, the Institute of Gas Technology (IGT), the prime contractor, worked with four other institutions: the University of Alabama/Mineral Resources Institute (MRI), the University of Kentucky Center for Applied Energy Research (UK-CAER), the University of Nevada (UN) at Reno, and Tennessee Technological University (TTU).

This report presents the work performed during the program extension from June 1, 1991 through May 31, 1992.

---

* Some of the tasks in the original program were not continued in the current program extension. The task achievements discussed below represent the active tasks of the program.

Task 3. Testing of Process Improvement Concepts

The objective of this task was to obtain data on novel process concepts that have the potential for improving the overall economics of PFH processing with Eastern oil shales. This task was divided into three subtasks corresponding to the concepts being tested: 3.6. Combustion of Hydroretorted Beneficiated Shales, 3.7. Innovative Reactor Concept Testing, and 3.8. Niche Market Studies.

Subtask 3.6. Combustion of Hydroretorted Beneficiated Shales

The overall objective of this subtask was to evaluate the combustion of hydroretorted shale for energy recovery prior to disposal. This subtask is comprised of two subtasks: 3.6.1. Combustion Characterization and 3.6.2. Combustion Tests.

Subtask 3.6.1. Combustion Characterization

The objective of this subtask was to determine the combustion characteristics of hydroretorted beneficiated shale.

Equipment and Test Procedure

The combustion characteristics of hydroretorted beneficiated Alabama shale were determined in a series of thermogravimetric analysis (TGA) tests. The tests were conducted in an existing high-pressure, high-temperature thermobalance unit. The unit, shown schematically in Figure 3-1, senses and records the instantaneous weight of a sample undergoing reaction at temperatures and pressures up to 2000°F (1095°C) and 1000 psig (7.0 MPa).

The thermobalance reactor is constructed from type 316 stainless steel pipe positioned inside a pressure shell. Furnace elements are placed inside the pressure shell (and outside the reactor tube). The pressure shell is filled with nitrogen and maintained at the same pressure as the reactor using a differential pressure controller. The feed gas flow is controlled with a mass flow controller. The exit gas system contains a back pressure controller, a dry test meter for measuring total gas flow, a liquids knockout trap, and a gas sampling loop.

In a typical thermobalance test, a weighed, representative 1 to 2 gram sample of hydroretorted shale is held in a stainless steel screen basket suspended from a force transducer by a stainless steel wire. The basket is pretreated at test conditions to prevent weight changes of the basket during the test. Thus, the transducer senses changes in the weight of the sample in the basket and not weight changes in the basket.

Tests were conducted in this subtask under isothermal and non-isothermal conditions. Before an isothermal test, the temperature, pressure, and feed gas flow rate are established in the thermobalance. The basket with the shale sample is kept in a higher, cool position above the reactor. When test

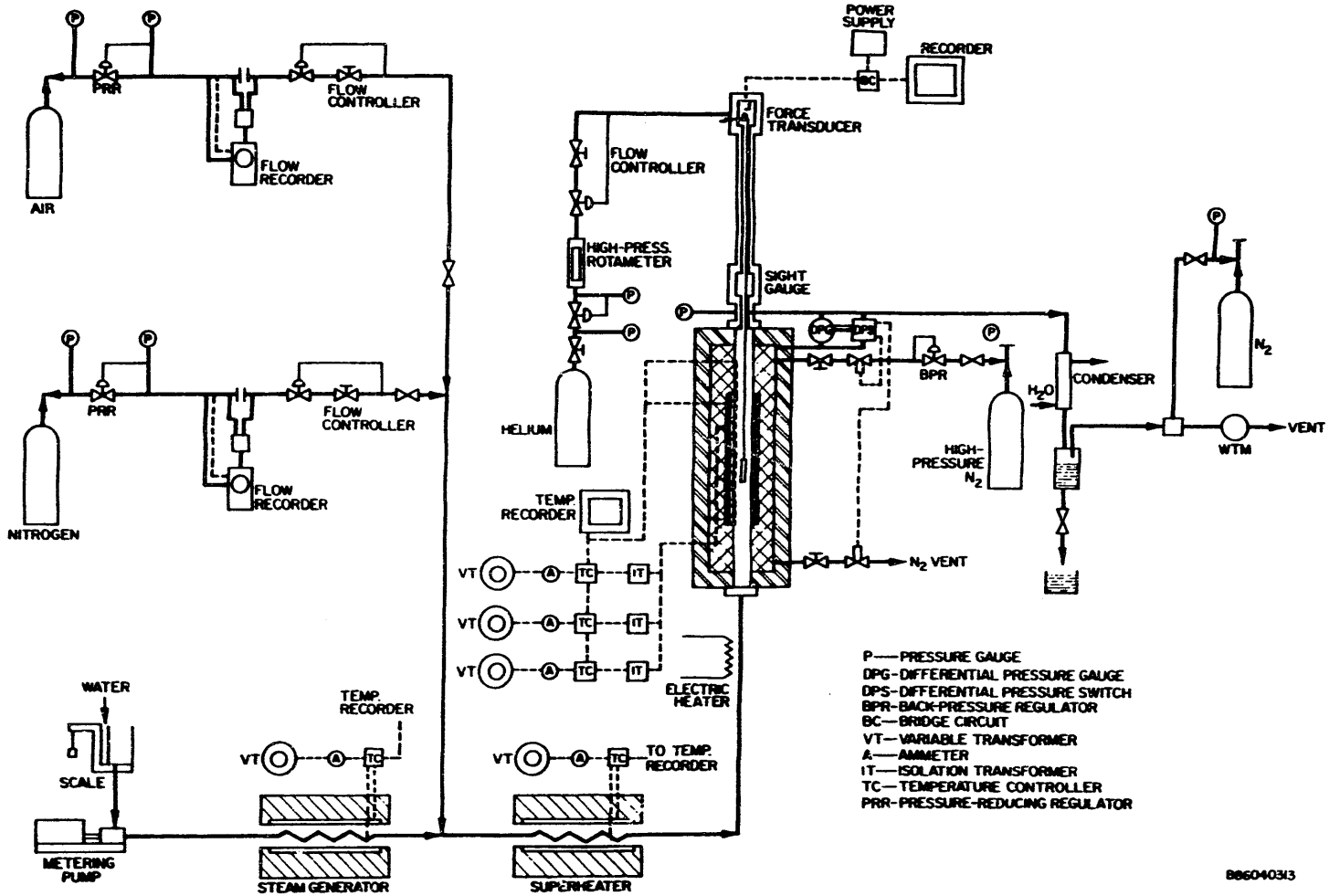

Figure 3-1. SCHEMATIC DIAGRAM OF THE THERMOBALANCE REACTOR

conditions are established, the sample is quickly lowered into the heated zone of the reactor. The basket hangs freely from the force transducer until the sample is raised into the cooler section above the reactor. The transducer signal is sent to a recorder so sample weight can be continuously recorded.

The procedure for a non-isothermal test requires lowering the sample basket into the reactor before starting the test. The pressure and gas flow rates are established, and the reactor is then heated at the desired rate. For these tests, the sample is heated at approximately 15°F/min (8°C/min). The sample weight is monitored throughout the heating period. When the maximum desired temperature is reached, the sample is raised into the cooler, upper part of the reactor. An isothermal holding period can be employed at the end of the heating period, but no isothermal period was used in the heat-up tests in this subtask.

Discussion

A total of seventeen thermobalance tests were conducted in this subtask to determine combustion characteristics of hydroretorted, beneficiated Alabama shale. The first three tests were non-isothermal and involved heating a shale sample to 1800°F (982°C) in air at 15, 200, and 1000 psig (0.2, 1.5, and 7.0 MPa). Eleven isothermal tests were conducted using a 20-minute residence time; three other isothermal tests were conducted using 1-, 2-, and 5-minute residence times. Isothermal test conditions ranged from 1500° to 2000°F (815° to 1095°C) at pressures of 15 to 1000 psig (0.2 to 7.0 MPa).

The hydroretorted shale used in the thermobalance tests was generated in a laboratory-scale continuous PFH test at 900°F (482°C) and 600 psig (4.2 MPa) in Subtask 5.2.1. The hydroretorted shale was screened to -20+40 mesh and riffled to produce the TGA feed shale. Analyses of the raw and hydroretorted Alabama shale are presented in Table 3-1. The sample weight totals more than 100 percent because metals in the shale mineral matter are oxidized during the analysis.

The carbon, sulfur, and nitrogen conversions achieved during the PFH test to generate the hydroretorted shale were 67, 44, and 55 percent, respectively. The hydrogen-to-carbon weight ratio was reduced from 0.099 to 0.053. The sample of hydroretorted shale residue contained a total of 24.2 weight percent carbon, hydrogen, sulfur, and nitrogen. The carbon, hydrogen and sulfur can be oxidized to produce energy during combustion. The shale gross calorific value was reduced from 6354 to 3060 Btu/lb during PFH processing, which represents 32 percent of the original shale heat content. Efficient recovery of this energy by combustion of the organic matter can improve the economics of the PFH process.

A summary of the operating conditions and elemental conversions for the combustion characterization tests is presented in Table 3-2. Conversions are not presented for Test 31-T-12 because at 2000°F (1093°C), the shale sample sintered and could not be separated from the basket after the test.

Table 3-1. ANALYSES OF RAW AND HYDRORETORTED BENEFICIATED ALABAMA SHALE*

Sample	Raw	Beneficiated
Feed	PFH	Combustion
Test Unit	Lab-Scale Continuous	Thermobalance
Moisture, wt %	1.53	0.00
Ultimate, wt % (dry)		
Ash	53.74	79.06
Carbon	31.90	15.37
Hydrogen	3.16	0.82
Sulfur	9.15	7.50
Nitrogen	0.77	0.51
Gross Calorific Value,		
Btu/lb	6354	3060
MJ/kg	14.8	7.1

* Ultimate analyses of shale samples may exceed 100% due to oxidation of mineral matter.

Table 3-2. COMBUSTION CHARACTERIZATION TEST CONDITIONS AND RESULTS†

Test No.	31-T-1	31-T-2	31-T-3	31-T-4	31-T-5	31-T-6
Operating Conditions						
Temperature, °F	--------- 1800 ---------			--------- 1700 ---------		
Pressure, psig	15	200	1000	15	200	1000
Res. Time,* min	---------- 20 ---------			---------- 20 ---------		
Heating Mode	---- Non-isothermal ----			------- Isothermal -----		
Results						
Residue Analysis, wt % (dry)						
Ash	98.87	98.77	98.58	99.75	99.17	96.48
Carbon	0.04	0.08	0.02	0.05	0.06	0.06
Hydrogen	0.08	0.06	0.05	0.03	0.03	0.03
Sulfur	0.22	0.15	0.37	0.14	0.49	1.59
Nitrogen	0.11	0.00	0.01	0.03	0.01	0.02
Component Loss, %						
Carbon	99.8	99.6	99.9	99.7	99.7	99.7
Hydrogen	92.3	94.3	95.2	97.1	97.1	97.1
Sulfur	97.7	98.4	96.1	98.5	94.8	82.9
Nitrogen	83.0	100.0	98.5	95.5	98.5	96.8
Total	21.3	21.6	20.9	20.9	20.9	19.4

* At maximum temperature

† Ultimate analyses of shale samples may exceed 100% due to oxidation of mineral matter.

Table 3-2 (continued). COMBUSTION CHARACTERIZATION TEST CONDITIONS AND RESULTS†

Test No.	31-T-7	31-T-8	31-T-9	31-T-10	31-T-11	31-T-12
Operating Conditions						
Temperature, °F	1500	1800	1700	1500	1800	2000
Pressure, psig	200	200	600	200	1000	200
Res. Time,* min	---------- 20 ---------			---------- 20 ---------		
Heating Mode	---------- Isothermal ----------					
Results						
Residue Analysis, wt % (dry)						
Ash	98.43	99.48	97.48	98.62	97.30	101.77
Carbon	0.00	0.00	0.00	0.00	0.03	0.17
Hydrogen	0.02	0.02	0.02	0.02	0.03	0.02
Sulfur	0.67	0.39	1.27	0.53	1.90	0.31
Nitrogen	0.00	0.00	0.00	0.01	0.02	0.00
Component Loss, %						
Carbon	100.0	100.0	100.0	100.0	99.8	--
Hydrogen	98.1	98.0	98.1	98.0	97.0	--
Sulfur	93.0	95.8	86.6	94.2	79.5	--
Nitrogen	100.0	100.0	100.0	98.4	96.8	--
Total	21.3	19.2	21.0	17.7	19.0	--

* At maximum temperature

† Ultimate analyses of shale samples may exceed 100% due to oxidation of mineral matter.

Table 3-2 (continued). COMBUSTION CHARACTERIZATION TEST CONDITIONS AND RESULTS†

Test No.	31-T-13	31-T-14	31-T-15	31-T-16	31-T-17
Operating Conditions					
Temperature, °F	----------	----------	1700	----------	----------
Pressure, psig	----------	----------	1000	----------	600
Res. Time,* min	2	20	5	1	20
Heating Mode	----------	----------	Isothermal	----------	----------
Results					
Residue Analysis, wt % (dry)					
Ash	87.96	98.67	97.36	87.29	98.82
Carbon	6.28	0.08	0.00	7.51	0.00
Hydrogen	0.10	0.05	0.03	0.08	0.01
Sulfur	5.53	0.62	1.24	5.30	0.49
Nitrogen	0.08	0.00	0.00	0.10	0.00
Component Loss, %					
Carbon	63.9	99.6	100.0	57.3	100.0
Hydrogen	89.2	95.2	97.1	91.5	99.0
Sulfur	34.9	93.5	86.8	38.3	94.8
Nitrogen	86.2	100.0	100.0	82.9	100.0
Total	11.7	21.0	20.1	12.7	21.0

* At maximum temperature.

† Ultimate analyses of shale samples may exceed 100% due to oxidation of mineral matter.

Non-isothermal TGA tests with hydroretorted shale were conducted in air at pressures of 15, 200, and 1000 psig (0.2, 1.5, and 7.0 MPa). The corresponding oxygen partial pressures were 0.2, 3.1, and 14.7 atm. Slow heating of the hydroretorted shale in air produced a large weight loss peak between 480° and 660°F (250° and 350°C). This was probably due to the onset of a self-sustained combustion reaction, which was not indicated by thermocouple readings. As the oxygen partial pressure increased, the combustion initiation temperature decreased. The results of the non-isothermal tests (Table 3-3) suggest that shale combustion can be initiated at temperatures as low as 478°F (248°C).

Table 3-3. EFFECT OF OXYGEN PARTIAL PRESSURE ON COMBUSTION INITIATION TEMPERATURES (Non-Isothermal Tests)

Test No.	O_2 Partial Pressure, atm	Combustion Initiation Temperature, °F
31-T-1	0.2	560-700
31-T-2	3.1	478-575
31-T-3	14.7	500-530

The thirteen isothermal thermobalance tests in which the shale did not sinter were conducted in air at temperatures of 1500° to 1800°F (815° to 982°C) and pressures of 15 to 1000 psig (0.2 to 7.0 MPa). Weight loss was high for all samples at this range of combustion conditions.

Carbon conversion increased from 57.3 percent at 1 minute to 63.9 percent at 2 minutes and to nearly 100 percent for tests at 5 minutes and 20 minutes. Detailed evaluations of carbon conversion rates at combustion temperatures above 1500°F (815°C) require thermogravimetric testing at residence times of less than 5 minutes. Shale residence times were too long to accurately measure the effects of temperature and pressure on carbon, but carbon conversions exceeded 99 percent after 20 minutes over the temperature and pressure ranges studied.

Sulfur conversion increased with increasing temperature but decreased with increasing pressure for similar residence times of 20 minutes. At 1700°F (925°C), sulfur conversion decreased from more than 98 percent at 15 psig to about 80 percent at a total pressure of 1000 psig. Results of residence time tests at 1700°F (927°C) showed that the rate of sulfur conversion was slower than the rate of carbon conversion during shale combustion.

The results of thermobalance tests conducted at 1500°, 1700°, and 1800°F (815°, 927°, and 980°C) and a pressure of 200 psig (1.5 MPa) are presented in Figure 3-2. Weight loss rate increases with increasing temperature. The time required to complete the combustion reactions decreases with increasing temperature. Combustion is complete in a relatively short time compared to the 20-minute residence time used. The time required to complete 95 percent of the total weight loss decreases from about 6 minutes at 1500°F to 4 minutes at

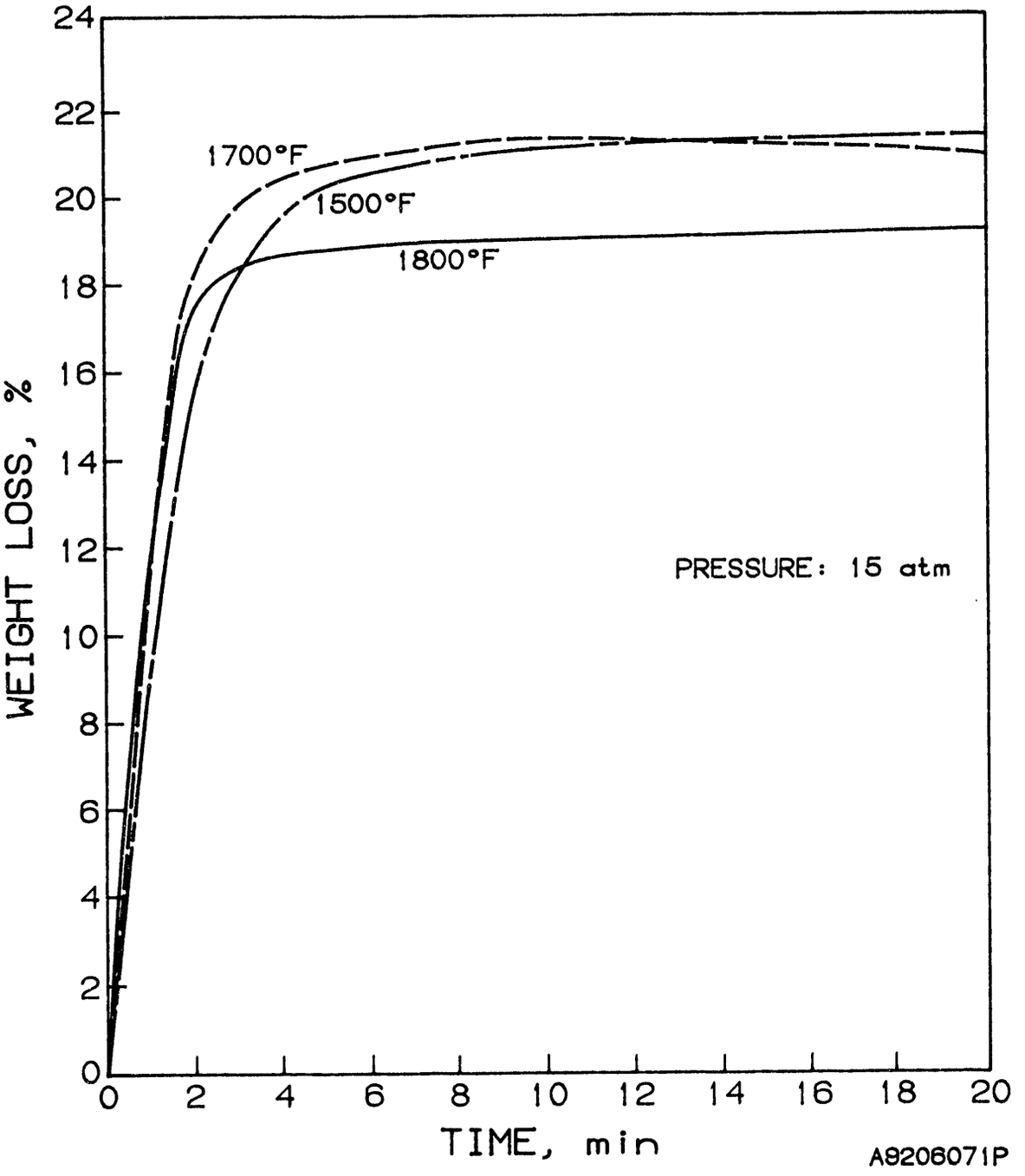

Figure 3-2. EFFECT OF TEMPERATURE ON SHALE WEIGHT LOSS IN THE THERMOBALANCE

1700°F and 3 minutes at 1800°F. Total weight loss appears to be a combination of organic matter conversion and mineral matter reactions. The decrease in total weight loss as temperature is increased from 1700° to 1800°F is comprised of an increase in organic matter conversion and a larger decrease in weight as a result of inorganic reactions.

Weight loss also increases with increasing oxygen pressure. The effect of pressure, however, is smaller than the effect of temperature. At 1700°F, the weight loss after 20 minutes was 21 percent at all pressures tested from 15 to 1000 psig (0.2 to 7.0 MPa). The weight loss after 2 minutes was 81 and 86 percent of the total weight loss at 15 and 1000 psig, respectively.

During combustion of hydroretorted shale, the mineral matter is not completely inert. The total weight changes in the thermobalance combustion tests were not consistent with the elemental conversions. At a pressure of 200 psig (1.5 MPa), conversions of the organic part of the shale (carbon, hydrogen, and sulfur) increased with increasing temperature. However, the total weight loss decreased with increasing temperature from 21.3 percent at 1500°F to 20.9 percent at 1700°F and to 19.2 percent at 1800°F. At a constant temperature of 1700°F, increasing the pressure increased the organic elemental conversions. Weight loss, however, decreased when pressure was increased from 600 to 1000 psig. These results indicate the mineral matter in the shale gains weight during combustion and that the mineral matter weight gain increases with increasing temperature and oxygen pressure.

Sintering was observed in the isothermal tests conducted at severe conditions. At 1700°F (925°C), part of the samples combusted at 600 and 1000 psig (4.2 and 7.0 MPa) was sintered. At higher temperatures of 1800° and 2000°F (980° and 1040°C) and a pressure of 200 psig (1.5 MPa), more of the sample sintered. The residue from Test 31-T-12 at 2000°F was entirely sintered and could not be separated from the sample basket after the test.

Ash fusion temperatures of combusted shale in reducing and oxidizing atmospheres are shown in Table 3-4. The initial deformation temperature (oxidizing atmosphere) of combusted shale was found to be 2350°F (1288°C). This temperature is well above the combustion temperature used in the thermobalance tests, but the combustion conditions used would lead to sintering in a packed bed. Combustion of hydroretorted beneficiated shale should be conducted in a more active reactor such as a fluidized bed to prevent sintering. The selection of a shale combustion temperature and a cracking temperature, if combusted shale is used as a substrate in the cracking unit, must be made with regard to the shale initial deformation temperatures.

Subtask 3.6.2. Combustion Tests

The objective of this subtask was to demonstrate the combustion of hydroretorted beneficiated shale in a fluidized-bed reactor. Laboratory-scale tests were conducted at various temperatures, pressures, and shale residence times to evaluate combustion characteristics and reactivity. Emissions from the tests were monitored for environmental purposes as well as for performing overall and elemental material balances.

Table 3-4. COMBUSTED HYDRORETORTED BENEFICIATED ALABAMA SHALE ASH FUSION TEMPERATURES

	Ash Fusion Temperature, °F	
	Reducing	Oxidizing
Initial Deformation	2025	2350
Softening	2145	2470
Hemispherical	2260	2550
Fluid	2375	2630

Equipment and Test Procedures

Laboratory-scale combustion tests were conducted in a 2-inch (5.08-cm) diameter fluidized-bed reactor. A schematic diagram of the unit configuration used for these tests is shown in Figure 3-3. All vessels and lines are constructed from 316 stainless steel and glass bombs are used to collect gas samples. A two-zone electric furnace is used to heat the reactor. Feed gas flow rates are controlled with mass flow controllers. A dry test meter is used to monitor the exit gas flow rate. All exit gas is scrubbed using a sodium hydroxide solution after metering the flow, but before venting.

Continuous operation is achieved by using a calibrated feed screw to transfer shale from the feed hopper to the reactor. Shale is fed to the bottom of the reactor and is discharged from the reactor through an overflow tube. Unsteady-state and steady-state receivers are used to collect the discharged residue shale. The feed gas is preheated with an electric furnace and fed through a sintered metal plate into the reactor. An internal sintered metal filter at the top of the reactor prevents the carryover of shale fines into the exit gas line.

A typical test is initiated by loading the feed hopper with a weighed amount of shale, sealing the pressure vessel, pressurizing the reactor and then preheating the reactor to 300°F (149°C) using a nitrogen purge. About 50 grams of shale is then charged to the unit and the bed is fluidized with nitrogen. Heating is continued and a small amount of air is added to the feed gas. When the bed reaches temperatures in the range of 500° to 800°F (260° to 427°C), the combustion reactions are initiated and become self-sustained. The feed screw is then restarted. The shale and air feed rates and the reactor heater temperatures are gradually increased until targeted conditions are achieved. This procedure prevents the combustion reactions from causing sudden changes in reactor temperature or pressure. Sudden changes in bed conditions can lead to defluidization and/or sintering.

Steady-state flow, temperature, and pressure conditions are readily established. However, steady-state operation is not declared until after a time period equivalent to three bed turnovers to ensure that the solids, which are sampled, have the proper time/temperature history. Samples of the product gas are taken during steady-state operation and analyzed for major components. Feed and residue solids are analyzed for ash, carbon, hydrogen, sulfur,

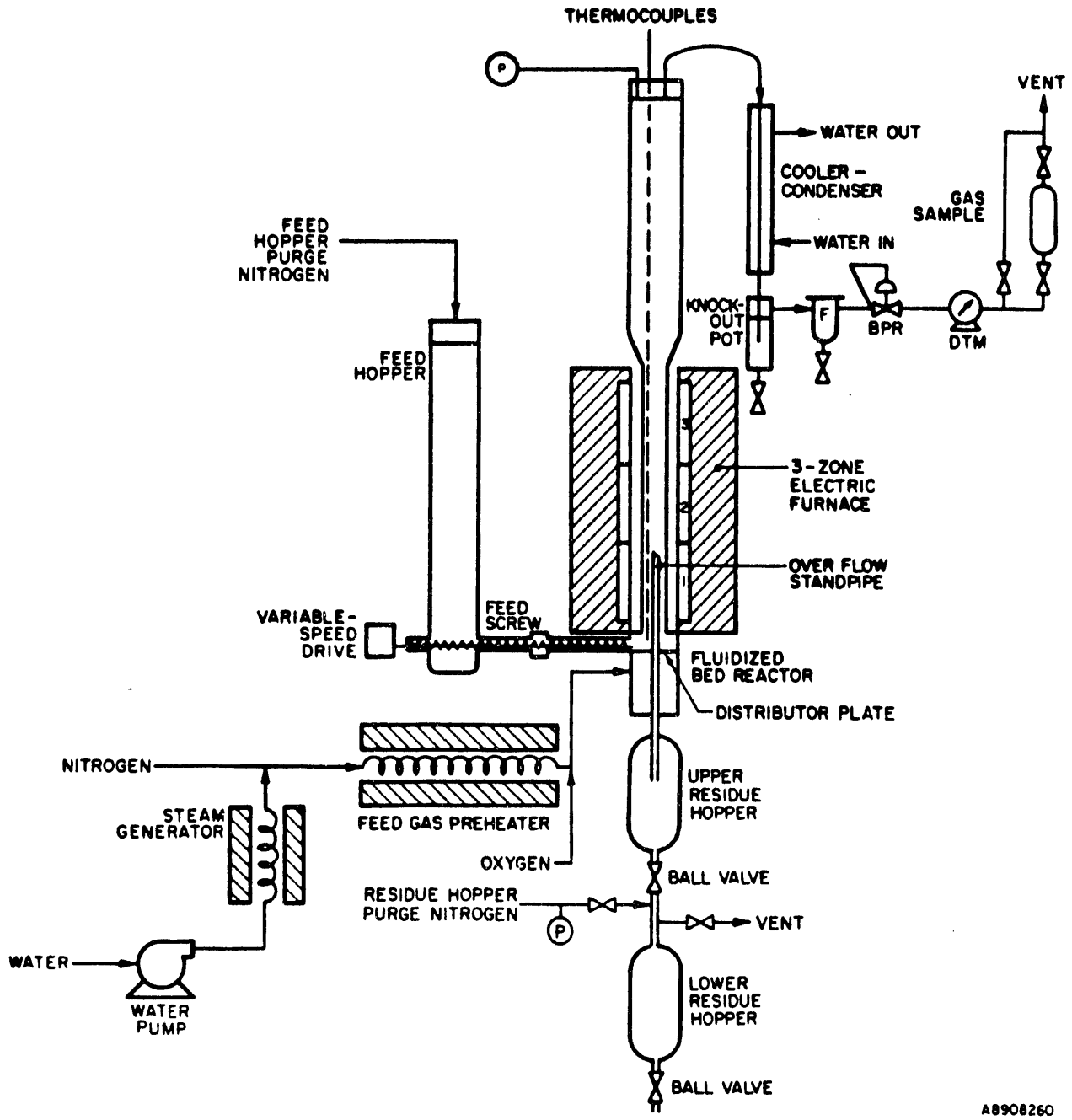

Figure 3-3. SCHEMATIC DIAGRAM OF THE 2-INCH DIAMETER FLUIDIZED-BED UNIT

nitrogen, high temperature water (HTW), and gross calorific value. Bulk density and screen analyses are also conducted on feed and residue solids samples.

Discussion

Six fluidized-bed combustion tests were conducted with hydroretorted beneficiated Alabama shale. The feed for the shale combustion tests was obtained from the receiver after a bench-scale test conducted in Subtask 5.2.2. The hydroretorted shale (steady-state residue) from the bench-scale test was screened to the desired size, riffled, and then charged to the combustion unit feed hopper. For the first combustion test, the shale was sized to -40+80 mesh; for the other five tests, the shale was sized to -30+80 mesh. The wider size consist was used in the latter tests so that a sufficient quantity of feed material would be available for tests. The -80 mesh fraction of the shale was removed to minimize problems associated with fines handling and also to facilitate a determination of the effects of fluidized-bed combustion on the extent of fines generation. The physical and chemical analyses of the feed and residue shale samples from the combustion tests are shown in Table 3-5.

Combustion tests were conducted at 1500° to 1700°F (816° to 927°C) with pressures of 50 to 200 psig (0.4 to 1.5 MPa). Shale residence times ranged from 14 to 50 minutes, and the bed height to diameter ratio was about 2. The feed gas superficial velocity was between 0.6 and 1.2 ft/s (0.18 to 0.37 m/s), which provided from 80 to 200 percent excess air to the reactor. Shale feed rates were 400 to 700 grams per hour. The operating conditions and results of the combustion tests are summarized in Table 3-6.

The superficial fluidization velocities for the tests were high (greater than complete fluidization for the largest particle size) to prevent sintering of the shale during combustion. At lower velocities (below complete fluidization velocity), the kinetic energy of the particles in the bed was insufficient to prevent sintering. The results showed that hydroretorted shale sinters easily during combustion at temperatures as low as 1200°F (649°C), but when the bed is well fluidized, sintering is avoided. Combustion tests were conducted without sintering at 1700°F (927°C) in the laboratory-scale, fluidized-bed reactor.

The fluidization velocities needed to avoid sintering did not result in any significant attrition of the shale particles. In Test 32-C-1, the feed shale contained 24.8 percent -60 mesh material; the combusted shale residue contained 22.4 percent -60 mesh material. The feed for the other five tests contained 9 percent -60 mesh material; the -60 mesh fraction of steady-state residue solids from these tests ranged from 8.1 to 17.9 weight percent. The increase in the -60 mesh fraction of the combusted shale observed in Tests 32-C-7 and 32-C-8 may have been due, in part, to higher gas flow, which caused more mixing and solid/solid contact in the bed. It was also observed that the residue shale particles were smoother and more spherical in shape than the feed. The scrubbing action of the fluidized bed apparently eroded small surface irregularities from the particles, but did not cause significant particle breakage.

Table 3-5. CHEMICAL AND PHYSICAL ANALYSES OF FEED AND RESIDUE SOLID SAMPLES FROM COMBUSTION TESTS†

Test No.	32-C-1	32-C-1	32-C-3 through 32-C-8	32-C-3	32-C-4	32-C-6	32-C-7	32-C-8
Sample	Feed	Residue	Feed	Residue	Residue	Residue	Residue	Residue
Ultimate, wt % dry								
Ash	81.08	96.85	81.08	98.63	97.37	98.83	96.33	99.01
Carbon	12.90	1.08	12.90	0.46	0.08	0.24	0.16	0.0
Hydrogen	0.78	0.03	0.78	0.02	0.0	0.0	0.0	0.0
Sulfur	7.32	1.23	7.32	0.33	1.03	0.35	1.43	0.29
Nitrogen	0.42	0.11	0.42	0.0	0.0	0.0	0.0	0.0
Oxygen (HTW)	2.39	0.44	2.39	0.67	0.44	0.50	0.62	0.34
Bulk Density, g/cm^3	0.57	0.59	0.57	0.59	0.52	0.59	0.53	0.60
Sieve Analysis (wt %), mesh								
+30	0.8	1.8	9.4	4.2	12.2	1.4	4.2	3.9
-30+40	5.2	1.3	49.8	61.5	56.8	49.5	50.9	35.4
-40+60	69.2	74.5	31.7	26.2	21.9	38.6	28.5	42.8
-60+70	13.6	10.6	5.1	5.1	6.3	5.0	9.3	8.3
-70+80	7.0	6.9	2.6	0.9	0.7	2.1	2.0	4.7
-80+Pan	4.2	4.9	1.4	2.1	2.1	3.4	5.1	4.9
Total	100.0	100.0	100.0	100.0	100.0	100.0	100.0	100.0
Gross Calorific Value, Btu/lb	2690	NA	2690	<10	<10	<10	<10	<10

† Ultimate analyses of shale samples may exceed 100% due to oxidation of mineral matter.

Table 3-6. OPERATING CONDITIONS AND RESULTS FROM SHALE COMBUSTION TESTS

Test No.	32-C-1	32-C-3	32-C-4	32-C-6	32-C-7	32-C-8
Temperature, °F	1525	1680	1510	1620	1490	1690
Pressure, psig	57	48	103	50	199	100
Shale Res. Time, min.	23	33	31	14	50	33
Bed Height/Diameter Ratio	----------	----------	----------	2.2	----------	----------
Steady-State Time, min.	60	60	60	55	38	55
Shale Feed Rate, g/h	569	404	391	718	382	476
Gas Feed Rate, SCFH	55.5	54.1	98.9	91.8	154.1	109.9
Gas Superficial Velocity, ft/s	0.63	0.76	0.75	1.21	0.58	0.84
Excess Air, %	80	156	162	144	299	306
Component Conversions, wt %						
Carbon	93.0	97.1	99.5	98.5	99.0	100.0
Sulfur	85.9	96.3	88.3	96.1	83.6	96.8
Nitrogen	78.1	100.0	100.0	100.0	100.0	100.0
Oxygen (HTW)	84.6	77.0	84.7	82.8	78.2	88.3
Calorific Value Reduction, %	NA	>99.5	>99.5	>99.5	>99.5	>99.5
Product Gas Composition, mol %						
O_2	9.9	10.1	4.6	9.7	6.9	11.7
N_2	79.2	81.2	91.1	80.7	90.6	82.9
CO_2	7.6	7.6	4.0	8.3	2.5	4.8
SO_2	3.3	1.1	0.3	1.3	0.0	0.6
Total	100.0	100.0	100.0	100.0	100.0	100.0
Recovered Carbon, % of Feed						
CO_2	73.1	98.8	101.1	99.9	98.4	105.0
Liquids	NA	0.02	0.03	0.03	0.04	0.02
Sulfur Recovered in Product Gas as SO_2, % of feed sulfur	148.8	66.3	40.2	73.6	2.0	58.8

The color of the solids was affected by combustion reactions. Hydroretorted beneficiated shale was black, which reflected the high level of carbon still present. After combustion, the shale had a light, reddish-brown color. The lighter the color, the lower was the carbon content of the combusted shale. The color of the combusted shale may reflect the presence of iron oxide. Elemental analyses of raw, beneficiated shale has shown iron concentrations in the range of 3 to 5 weight percent.

Combustion of hydroretorted beneficiated shale in a fluidized bed is a practical method for recovering the energy content in the residue from the PFH process. After hydroretorting at 950°F and 1000 psig (510°C and 7.0 MPa) in the bench-scale unit, the residue shale contained 12.9 percent carbon and 7.3 percent sulfur and had a gross calorific value of 2690 Btu/lb (6.3 MJ/kg).

Combustion reduced the calorific value of the solids by an average of more than 99.5 percent during the five tests. Because the calorific value reductions were so high, no specific effect of operating conditions on conversion was apparent.

High carbon and sulfur conversions were achieved in all combustion tests; measured gas-phase products were carbon dioxide and sulfur dioxide (SO_2) exclusively. Carbon conversions ranged from 93 to 100 percent. Sulfur conversions ranged from 84 to 97 percent. The elemental conversions from these tests were consistent with those from thermobalance combustion characterization tests in Subtask 3.6.1. Carbon conversion increased with increasing temperature, pressure, and residence time. The differences, however, were small. The carbon conversion achieved in Test 32-C-1 [conducted at 1500°F and 50 psig (816°C and 0.4 MPa)] was 93 percent; all other tests had carbon conversions of 97 to 100 percent. At 1600°F and 50 psig (871°C and 0.4 MPa), a 14-minute residence time yielded a carbon conversion of 98.5 percent. Tests conducted in a thermobalance (Subtask 3.6.1) indicated that 5 minutes should provide adequate solids residence time for high carbon conversions.

Sulfur conversions were lower than carbon conversions. Increases in sulfur conversion were achieved with increases in temperature and residence time, but increasing the pressure decreased sulfur conversion. This result was also observed in the thermobalance combustion tests (Subtask 3.6.1).

Essentially all of the converted sulfur was oxidized to form SO_2. Sulfur balances based on the SO_2 concentration in the spot gas samples were poor. Sulfur dioxide production was not steady during the combustion tests. Variations of more than 50 percent in the SO_2 concentration were obtained in the spot gas samples for each test. Non-uniform SO_2 production and/or interaction of SO_2 with steel vessels and tubing may account, in part, for the poor sulfur recovery in most tests.

The carbonyl sulfide (COS) content in the product gas from all tests was below the gas chromatography (GC) detection limit of 10 ppm. Therefore, less than 0.1 percent of the shale sulfur was converted to COS during combustion. The concentration of NO_x compounds in the product gas was not measured in these combustion tests. However, based on shale nitrogen conversions, the maximum possible NO_x concentration in the fluidized bed product gas would have been less than 15 ppm. Product gas compositions were determined in the combustion tests by averaging the compositions of several spot gas samples.

Subtask 3.7. Innovative Reactor Concept Testing

The objective of this subtask was to demonstrate the technical feasibility of generating hydrogen by cracking the by-product hydrocarbon gases on spent shale and combusting the carbon produced by the cracking reactions. Work was divided into two subtasks: 3.7.1. Cracking Tests and 3.7.2. Cracking-Combustion Tests.

Discussion

The industry standard method for generating hydrogen is by steam reforming of methane. The global chemistry of this process is the formation of hydrogen and carbon monoxide from methane and steam (Eq. 1).

$$CH_4 + H_2O \rightarrow CO + 3H_2 \quad (1)$$

The method of producing hydrogen that was investigated in this subtask is the cracking of by-product hydrocarbon gases to carbon and hydrogen as shown in Eq. 2. Spent shale, sand, or other suitable substrate provides a surface to collect the carbon in the cracker and, subsequently, carry it to a combustor. The combustion reaction (Eq. 3) generates the energy to heat the solids that are then returned to the cracking unit to supply heat needed for the cracking reaction.

$$CH_4 \rightarrow C + 2H_2 \quad (2)$$

$$C + O_2 \rightarrow CO_2 \quad (3)$$

Hydrocarbon cracking has several advantages over steam reforming of methane in the PFH process. First, the process requires less equipment and no steam generation. Second, less purchased natural gas is needed because much, but not all, of the process hydrogen could be generated from by-product hydrocarbon gases.

Finally, the cracking process (including combustion of carbon) is an exothermic process while steam reforming of methane is endothermic. A comparison of the two hydrogen generation schemes has been made by assuming reactants methane, oxygen, and water are at 298 K (77°F) and gaseous products are at 1400 K (2060°F). On this basis, cracking produces 47.2 kilocalories per gram mole of methane feed and reforming consumes 92.3 kilocalories per gram mole of methane.

Cracking the C_1 to C_5 hydrocarbon gases in the PFH product gas is limited by thermodynamic equilibrium, which is dependent on temperature and pressure. Methane, however, is the only light hydrocarbon gas that will not crack completely to carbon and hydrogen at 1150 K (1610°F). Therefore, only the cracking of methane was evaluated in this subtask. Figure 3-4 shows the equilibrium concentrations for methane in hydrogen as a function of temperature and pressure. Higher conversions of methane to carbon and hydrogen occur as temperature is increased, but the extent of methane cracking decreases as pressure is increased. Tests were conducted in Subtask 3.7.1 to determine the actual levels of methane cracking achieved in a batch reactor.

Subtask 3.7.1. Cracking Tests

The objective of this subtask was to demonstrate the generation of hydrogen by cracking by-product hydrocarbon gases.

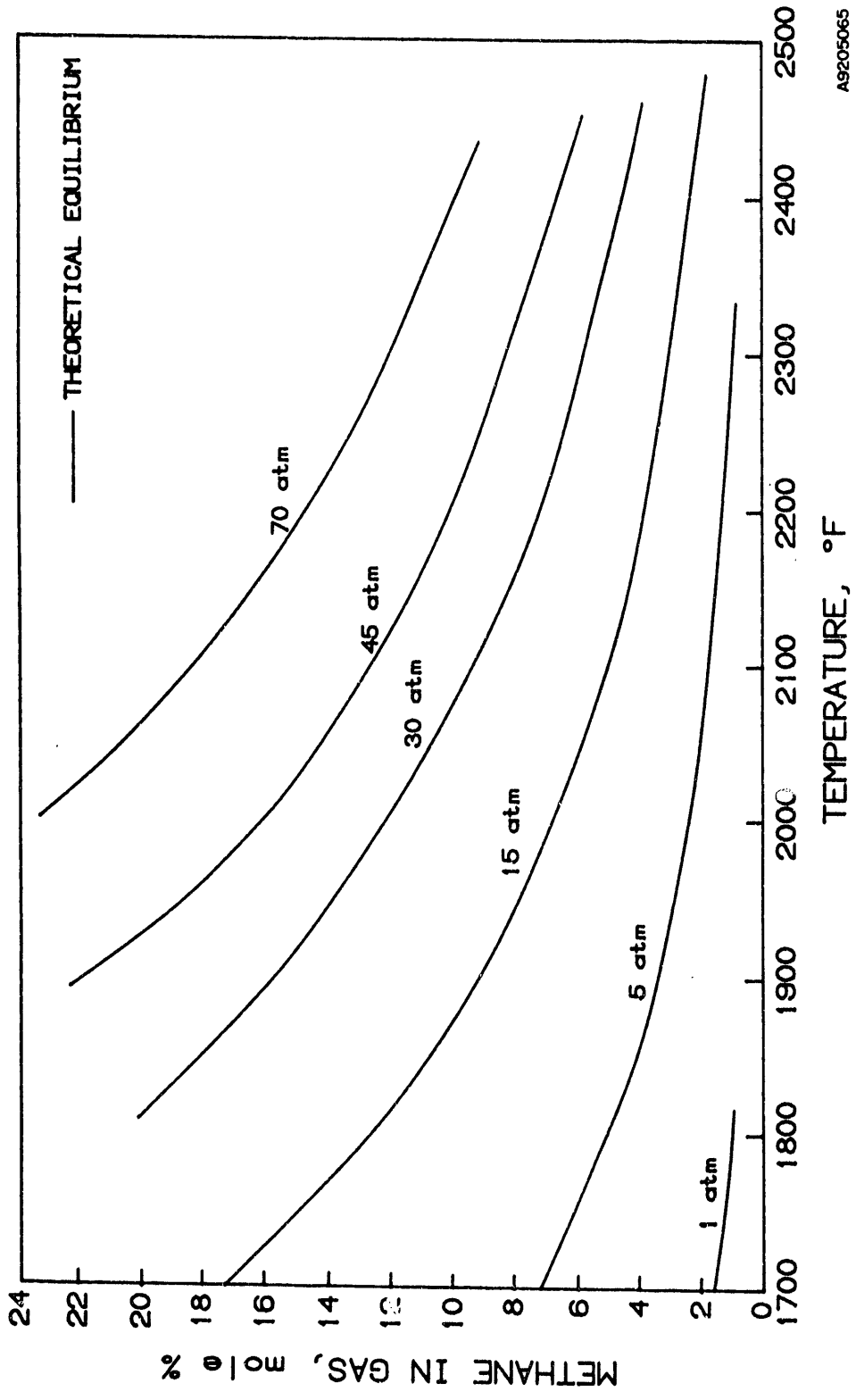

Figure 3-4. EFFECTS OF TEMPERATURE AND PRESSURE ON THE THERMODYNAMIC EQUILIBRIUM CONCENTRATION OF METHANE IN CRACKED GAS

Equipment and Test Procedures

A laboratory-scale cracking-combustion unit was designed and constructed to conduct the cracking and combustion tests in this subtask. A schematic diagram of the unit is presented in Figure 3-5. The unit includes the reactor tube, an outside pressure shell, a differential pressure controller, internal reactor thermocouples, thermocouples (tungsten-rhenium) outside the reactor for furnace control, a three-zone 2400°F (1316°C) furnace, and furnace controllers. Mass flow controllers are used to control the feed gas rate, and a dry test meter is used to measure the exit gas rate. A sampling manifold is used to obtain multiple gas samples. On-line infrared carbon monoxide, carbon dioxide, and methane detectors are downstream of the back-pressure regulator.

The unit design requires testing at conditions up to 2100°F and 1000 psig (1150°C and 7.0 MPa). To achieve these conditions, a balanced-pressure reactor design is utilized. A pressure shell containing the heaters and reactor is filled with nitrogen and held at the same pressure as the reactor. High temperature capabilities were enhanced by fabricating the reactor tube from type 309 stainless steel. All other components, including the pressure shell, are constructed of type 316 stainless steel.

The reactor tube is constructed of 1¼-inch schedule 40 pipe with an internal diameter (ID) of 1.38 inches (35.05 mm) and a length of 28.75 inches (73.03 cm). The reactor volume is 0.0230 ft^3 (0.65 L). An internal thermowell containing four thermocouples is used to measure the temperature of the reaction gas. A 1/8-inch diameter sampling tube is also positioned inside the reactor. Product gas is collected in small volume (10 mL) gas bombs connected to the sampling line. Gas bomb volume is low compared to reactor volume to minimize reactor pressure changes during sampling.

Cracking tests are initiated by charging solids (when solids are used as collection medium) and then pressure purging the reactor with nitrogen. Care must be taken to expel all oxygen and water vapor from the unit. The reactor is then pressurized with the hydrocarbon gas to be cracked. The furnaces are energized and the reactor is heated to the first temperature set point for gas sampling. One evacuated sample bomb is used to collect the unsteady-state gas present in the sampling line. Then the "representative" gas sample is taken. The reactor and sample are then heated to the next set point temperature, and the sampling procedure is repeated. This sampling procedure is continued until the highest desired set point temperature is achieved and sampling is complete.

After a test is concluded, the reactor is cooled and depressurized. If solids were used, the reactor is emptied, and the solids are collected and weighed. Gas samples and solids (if used) are submitted for analyses. The fraction of hydrocarbon gases in the gas mixture at each gas sampling temperatures are determined from the results.

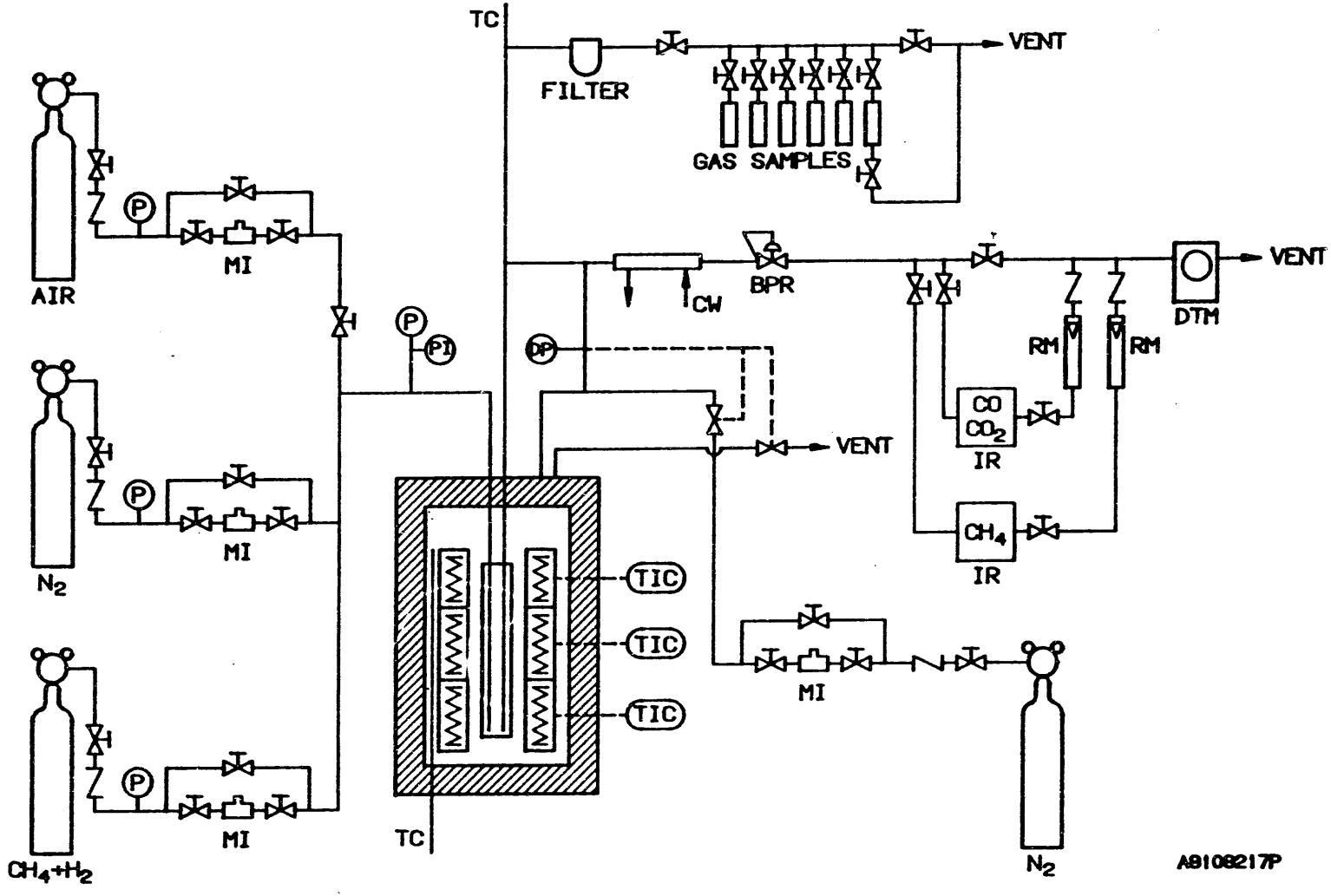

Figure 3-5. SCHEMATIC DIAGRAM OF CRACKING-COMBUSTION APPARATUS

Discussion

Twelve cracking tests were conducted in the batch unit. Eight tests were conducted with no solids in the reactor at pressures of 5 to 70 atm. These (empty reactor) tests were performed to determine the effect of temperature on the fraction of feed methane that will crack. Methane conversions were compared with those predicted from thermodynamic equilibrium for methane in the product methane:hydrogen mixture. Four tests were conducted with solids charged to the reactor. Solids were kept in a static, packed bed. The results of these tests were compared with those from other cracking tests at similar conditions with an empty reactor to determine the effects of shale solids. The operating conditions for all cracking tests are summarized in Table 3-7.

Table 3-7. OPERATING CONDITIONS FOR CRACKING TESTS

Test No.	Maximum Pressure atm	Maximum Temperature °F	Solids	Gas	Reactor Pretreated	Comment
32-CR-1	13.4	2260	No	CH_4	No	--
32-CR-2	4.4	2164	Shale[1]	CH_4	No	Sinter formed
32-CR-3	43.3	2115	No	CH_4	Yes	--
32-CR-4	4.4	2053	No	CH_4	Yes	--
32-CR-5	14.6	2087	No	Mix[2]	Yes	--
32-CR-6	67.3	2099	No	CH_4	Yes	--
32-CR-7	7.5	1820	Sand/ Shale[3]	CH_4	Yes	50:50 Sand-Shale No sinter
32-CR-8	5.3	2023	No	CH_4	Yes	--
32-CR-9	16.6	2020	No	CH_4	Yes	Sinter formed
32-CR-10	6.6	2018	No	CH_4	Yes	--
32-CR-11	45.4	1834	Sand/ Shale[3]	CH_4	Yes	50:50 Sand-Shale No sinter
32-CR-12	45.4	1830	Shale[3]	CH_4	Yes	Partial Sinter Formed

1. Combusted at 1400°F.
2. Combusted at 1700°F.
3. 55 mol % CH_4, 27 mol % C_2H_6, and 18 mol % C_4H_{10}.

The first cracking test was conducted with methane at a pressure of 15 atm and no solids in the reactor. Product gas in this test reached thermodynamic equilibrium, indicating that methane conversion was complete. Because the reactor wall may have acted as a catalyst for the cracking reaction, after the second test, the wall was passivated by heating a gas mixture of 15 percent hydrogen sulfide in hydrogen to 1500°F (816°C).

A test was performed at 15 atm using methane in the passivated reactor. A comparison of the methane content in the product gas for Tests 32-CR-1 and 32-CR-9 (Figure 3-6) shows that type 309 stainless steel wall does have a catalytic effect on methane cracking. The effect is neutralized with hydrogen sulfide pretreatment. At temperatures up to 1900°F (1038°C), a significantly

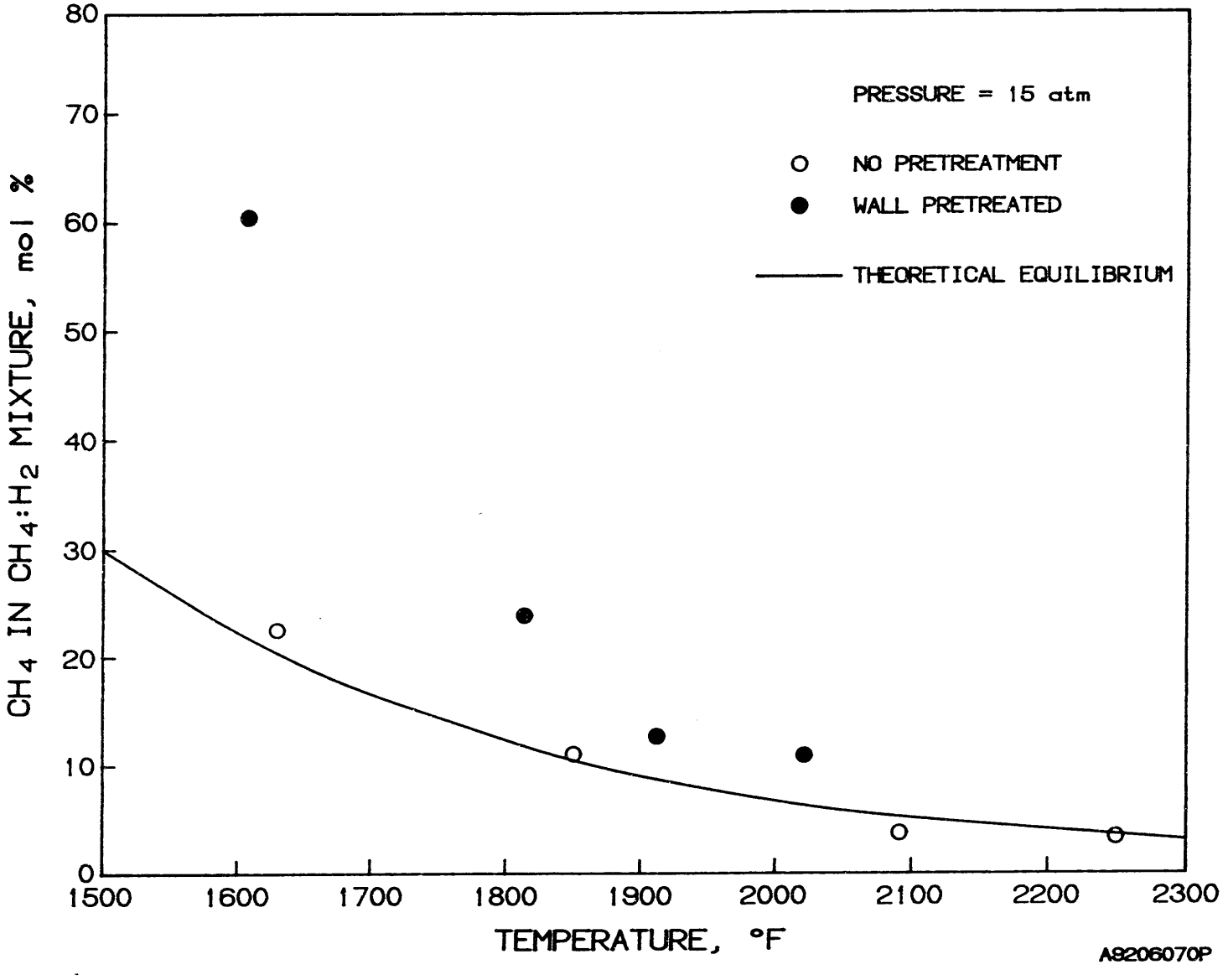

Figure 3-6. EFFECTS OF TEMPERATURE AND REACTOR PRETREATMENT ON METHANE CRACKING (Empty Reactor)

lower amount of methane conversion is achieved after the reactor has been treated. Methane conversion levels increase more rapidly with increasing temperature in the treated reactor. Above 2000°F (1093°C), the methane conversion to carbon and hydrogen is similar in the untreated and treated reactors.

Cracking tests were conducted at pressures of 5, 15, 45, and 70 atm with methane and no solids in the treated reactor. The results of these tests and the thermodynamic equilibrium values at these pressures are presented in Figure 3-7. The conversion of methane is lower than the equilibrium value at all pressures, but the difference decreases as the temperature increases. Cracking levels approximately equal to the equilibrium limit are achieved at temperatures above 2000°F (1093°C).

Methane cracking levels in Test 32-CR-6 at 67 atm are higher than those from Test 32-CR-3 at 43 atm. In both tests, the conversion levels were below the equilibrium values. However, the higher conversion levels obtained at higher pressure are unexpected. Additional high pressure testing should be conducted to evaluate this effect.

Product gas from the PFH process contains C_1 to C_6 hydrocarbon compounds. Equilibrium calculations show that at temperatures above 1600°F (871°C), all of the C_2 to C_6 hydrocarbon gases produced in the PFH process can be cracked to carbon and hydrogen. The cracking of higher molecular weight hydrocarbons was evaluated in Test 32-CR-5 using a simulated PFH product gas mixture containing 55 mole percent methane, 28 mole percent ethane, and 17 mole percent butane.

A comparison of the cracking conversion of methane and the simulated PFH product gas mixture is shown in Figure 3-8. Both tests were conducted at a pressure of 15 atm. The extent of cracking was similar for the methane and the mixture up to about 1900°F (1038°C). Above 1900°F, methane cracking is equal to the equilibrium limit and the mixture has a higher level of cracking. The higher hydrocarbon gases in the mixture cracked completely below the lowest sampling temperature of 1750°F (954°C). These results demonstrate that the hydrocarbon gases from the PFH process can be cracked to carbon and hydrogen.

The presence of water in the cracking unit was found to interfere with the cracking reactions. The product gas samples from Test 32-CR-8 contained more than 10 percent carbon monoxide but no carbon dioxide. At cracking temperatures, carbon monoxide and hydrogen can be generated by the reaction of steam with the carbon produced by cracking methane. The absence of carbon dioxide shows that the water-gas shift reaction did not occur. The production of carbon dioxide and hydrogen by the carbon-steam reaction can obscure the concentrations of methane and hydrogen based on methane cracking. Therefore, data from Test 32-CR-8 was disregarded, and care was taken in later tests to dry the reactor and to purge the unit with dry gases. Some carbon monoxide was formed in all tests with shale in the reactor. Steam for the carbon-steam reaction in these tests was supplied by residual high temperature water evolved from the combusted shale.

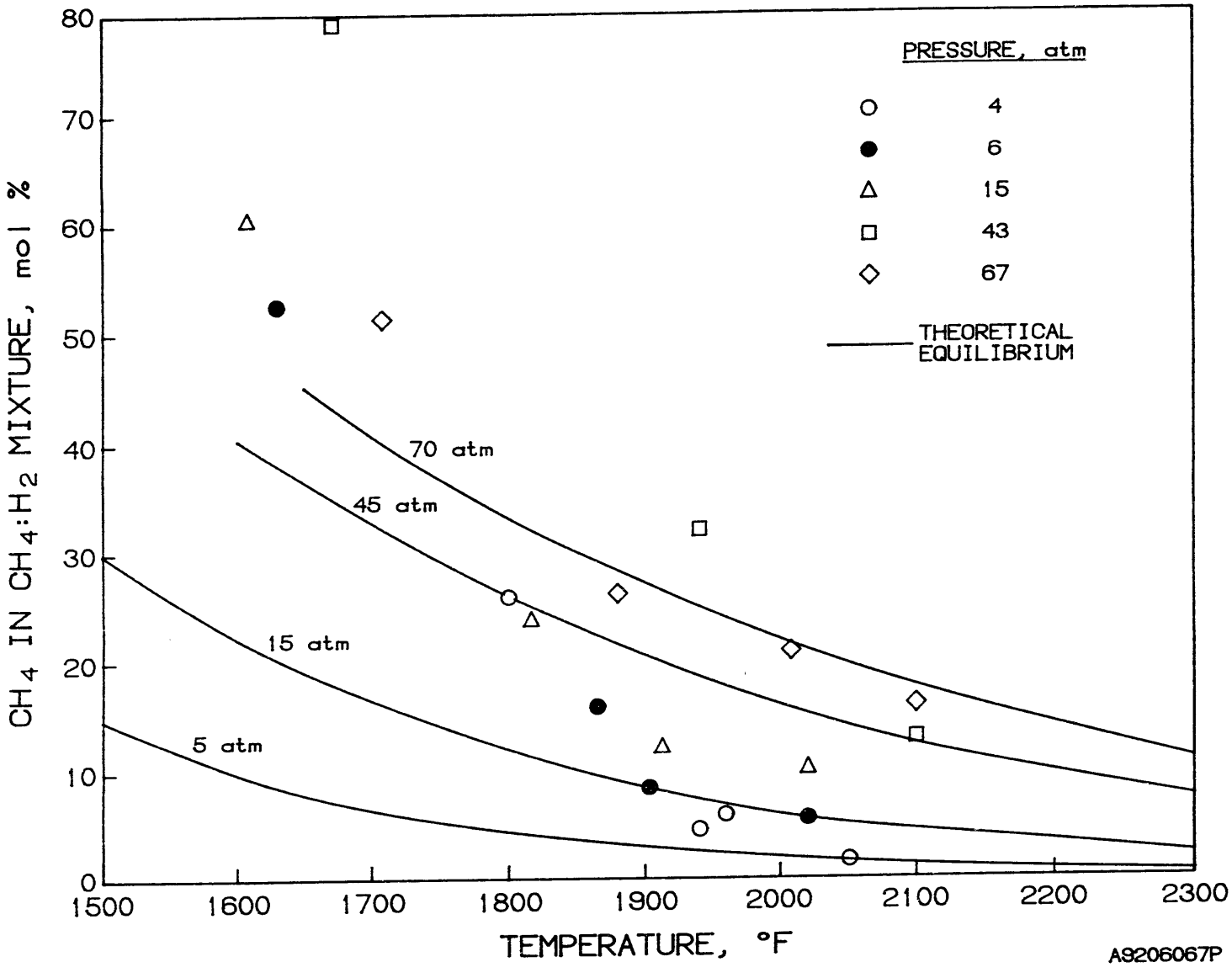

Figure 3-7. EFFECTS OF TEMPERATURE AND PRESSURE ON THE METHANE CRACKING REACTION (Empty Reactor)

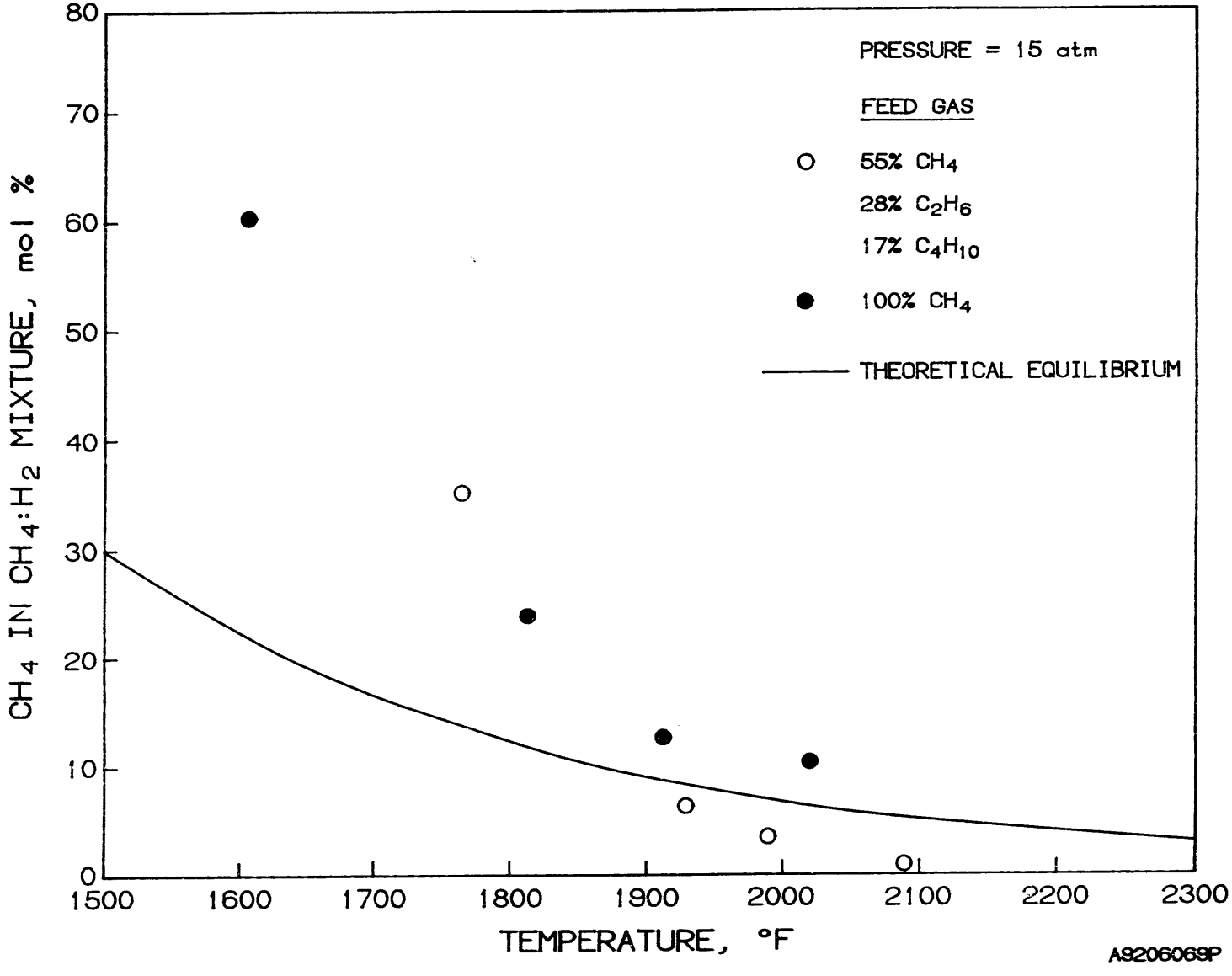

Figure 3-8. EFFECTS OF TEMPERATURE AND HYDROCARBON GAS COMPOSITION ON CRACKING REACTIONS

A total of four cracking tests, including three successful tests, were conducted with shale in the reactor. In the one unsuccessful test (32-CR-2), shale combusted at 1400°F (760°C) in a laboratory muffle furnace was put in the cracking reactor and heated to 2150°F (1177°C) at 4 atm. The shale residual carbon and sulfur produced high levels of carbon dioxide and hydrogen sulfide. Also, the packed bed of shale sintered at the high temperature used for cracking.

Several operational changes were made for the next three tests. The shale sample used previously in the reactor was changed to a representative combusted shale from a continuous fluidized-bed test conducted at 1700°F (927°C) in Subtask 3.6.2. The carbon and sulfur contents of this combusted shale sample were 0.09 and 1.07 weight percent, respectively. Temperatures used in the cracking reactor were reduced to a maximum of 1850°F (1010°C). Fluidized-bed combustion tests have shown that sintering can be avoided in some circumstances if an active bed is maintained. However, the batch cracking unit uses a packed bed that was known to sinter at temperatures above 2000°F (1093°C). Two tests were conducted with a packed bed of solids composed of 50 percent shale and 50 percent sand to reduce the possibility of sintering. The final test was conducted using a 100 percent shale charge to the reactor.

The results from the three cracking tests with solids are presented in Figure 3-9. Also shown in the figure are results of cracking tests at similar conditions with no shale in the reactor. The equilibrium values at the test pressures of 5 and 45 atm are included. The presence of shale in the cracking unit did not change the level of methane cracking at a pressure of 5 atm, but increased the level of methane cracking at 45 atm. At higher pressures, there is increased contact between gas and solid, which can explain the increase in methane cracking in the presence of solids at higher pressure. An increase in gas-solid contact by the use of a counter-current packed-bed or fluidized-bed reactor should improve methane cracking in the presence of solids.

Cracking tests conducted at 45 atm with combusted shale and with a mixture of 50 percent sand and 50 percent combusted shale showed that solids increased the level of methane conversion. The increase was the same for the shale and the mixture. The solids appear to increase the cracking of methane by providing additional surface area for carbon deposition. Combusted shale and sand do not show any catalytic effect on methane conversion to carbon and hydrogen.

Subtask 3.7.2. Cracking-Combustion Tests

The objective of this subtask was to demonstrate the combustion of carbon produced by the cracking of hydrocarbon gases.

Discussion

The same test unit constructed for the cracking tests in Subtask 3.7.1 was used for the cracking-combustion tests. Carbon was deposited on hydroretorted beneficiated shale at conditions determined in Subtask 3.7.1. A combustion cycle was then performed on each sample to determine the conditions

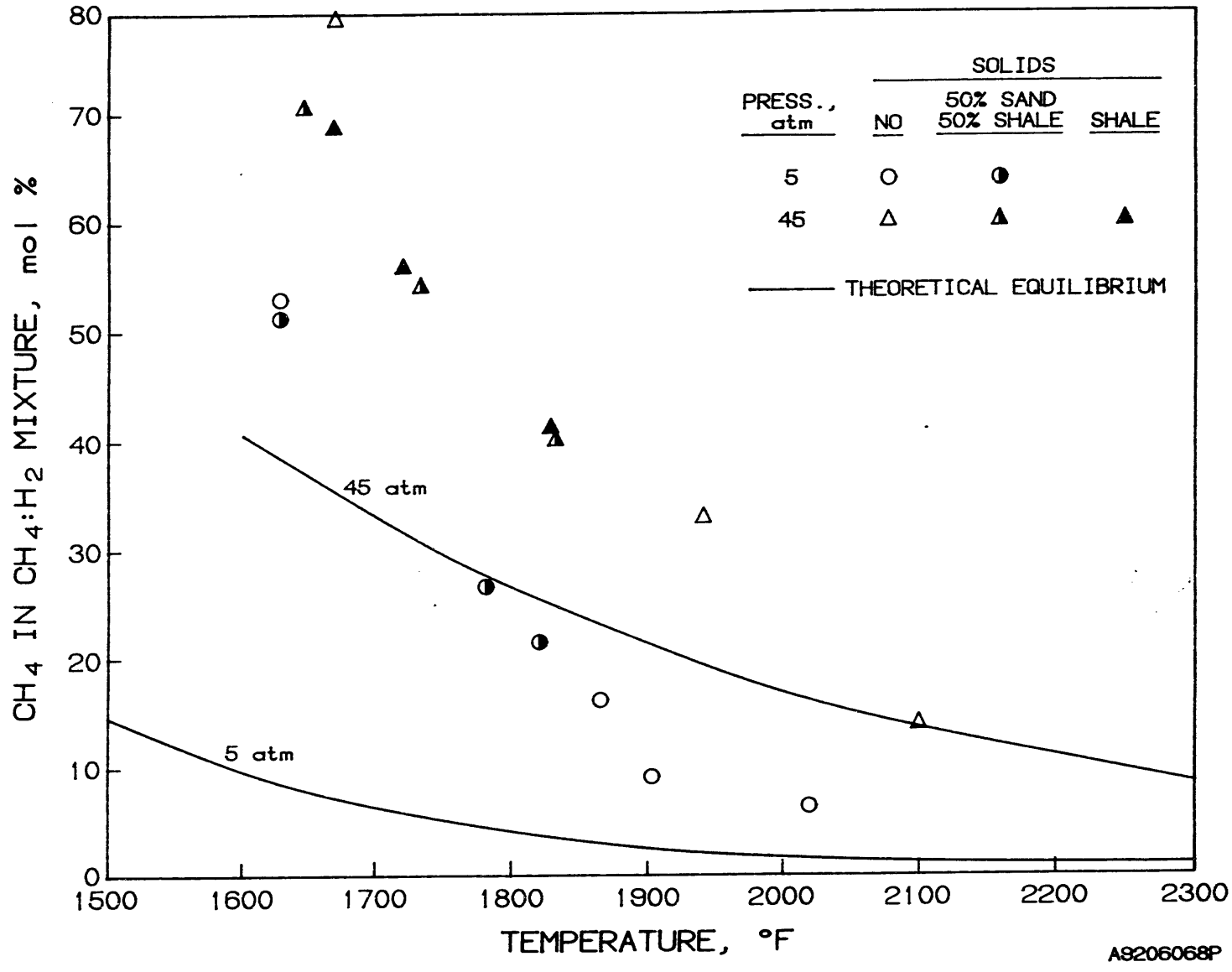

Figure 3-9. EFFECTS OF TEMPERATURE, PRESSURE, AND SOLIDS CHARACTERISTICS ON THE METHANE CRACKING REACTION

for removing the deposited carbon by combustion. One of the tests consisted of multiple cracking-combustion cycles and was conducted to determine the effects of recycling on the shale and its reactivity.

Equipment and Test Procedures

The unit used for these tests was described in detail in Subtask 3.7.1. A schematic diagram of the unit is presented in Figure 3-5.

Solids containing deposited carbon were collected from cracking tests in the cracking-combustion unit. About 150 grams of solids were charged to the reactor for each combustion test. A limited amount of solids was available from cracking tests. Therefore, cracking test solids were mixed with clean sand in a 1:1 ratio to obtain the needed amount of combustion test feed solids.

After charging solids to the reactor, the unit was pressurized with air. A steady flow of air was established and maintained throughout the combustion test. The reactor was heated from ambient temperature to 1800°F (982°C) at a heating rate of about 12°F/min (7°C/min). Throughout a test, gas flow rate and the exit gas carbon dioxide and carbon monoxide concentrations were monitored and recorded. The reactor was opened after each test, and the solids were collected. Product solids were weighed and then analyzed for total carbon content. Carbon conversions were determined by comparing the feed residue solids weights and carbon contents.

Discussion

Two combustion tests were conducted to demonstrate oxidative removal of carbon deposited on shale and sand solids during hydrocarbon gas cracking. Solids charged to the reactor in both tests consisted of 50 percent clean sand and 50 percent sand-shale mixture from methane cracking Tests 32-CR-7 and 32-CR-11. The solids used in the cracking tests were 50 percent sand and 50 percent combusted, densified, beneficiated Alabama shale from a fluidized-bed combustion test in Subtask 3.6.2.

Combustion Tests 32-CO-1 and 32-CO-2 were conducted at pressures of 5 and 45 atm. The carbon oxides infrared detectors indicated that combustion began at about 800°F (427°C). With a maximum temperature of 1850°F (1010°C), no solids sintering occurred.

Carbon conversions for the combustion tests are presented below. The feed solids contained 0.245 weight percent carbon, and the residue shale contained 0.24 and 0.18 weight percent carbon in Tests 32-CO-1 and 32-CO-2, respectively.

Test No.	Pressure, atm	Maximum Temp., °F	Carbon Conversion, %
32-CO-1	5	1850	1
32-CO-2	45	1850	26

The results of the combustion tests demonstrate that carbon deposited on sand and shale solids during cracking can be removed by combustion. Conversion of carbon to carbon oxides was low because the maximum temperature used was only 1850°F (1010°C). In a combustor combined with a cracking unit, the combustion temperature must be higher so solids can be used to recirculate heat to the cracking unit.

Using an oxygen-enriched air stream for combustion would provide complete oxidation of the deposited carbon. Laboratory analysis of residue solids carbon content by combustion in pure oxygen at 1750°F (954°C) removes 100 percent of the deposited carbon. Finally, combustion levels can be increased by changing the reactor configuration from a batch packed bed to a continuous flow reactor with greater gas-solids contact. Possible reactors include a fluidized bed and a riser column.

A test was conducted to determine the effects of multiple cracking and combustion cycles on methane cracking and carbon combustion. Five cycles were completed, which consisted of a cracking test at 45 atm and temperatures up to 2000°F (1093°C) followed by a combustion test at 45 atm and 1850°F (1010°C). The solids used for the cycle tests were the same as those used for Tests 32-CO-1 and 32-CO-2. Feed solids consisted of a mixture of 50 weight percent clean sand and 50 weight percent sand-shale mixture from methane cracking Tests 32-CR-7 and 32-CR-11.

A small sample (2 to 5 grams) of the reactor solids was collected after each cracking and combustion test and analyzed for carbon content. The remaining solids were returned to the reactor for the next test. No solids sintering occurred in the cracking tests. Spot gas samples were taken at a range of temperatures during the cracking tests. No gas samples were taken during the combustion tests, but the CO and CO_2 contents of the flowing air stream were monitored with infrared analyzers.

The results of the cracking tests are presented in Figure 3-10. No gas samples were taken in the fifth cracking test because a plug formed in the gas sample line. Data are also included for the equilibrium conversion of methane at 45 atm and for the average of three earlier tests conducted at 45 atm.

Methane cracking to carbon and hydrogen increases with increasing temperature at a constant pressure. At 45 atm, the methane in the gas decreased from 85 percent at 1650°F (899°C) to 42 percent at 1900°F (1038°C) and to 26 percent at 2040°F (1116°C). Methane conversions were lower than those from earlier tests at similar conditions and also lower than the equilibrium limit. As temperature increased, the methane conversions in the cycle tests and in the earlier cracking tests approached the equilibrium value. Conversions are close to equilibrium at 2000°F (1093°C) and should be almost equal to equilibrium at 2100°F (1149°C).

During the cycle test, each cracking test was followed by a combustion test. Combustion tests were conducted by heating the solids to about 1850°F (1010°C) in air. The product gas composition was monitored with infrared CO and CO_2 analyzers. A small amount of sintering, accounting for less than 10 weight percent of the solids, occurred during the combustion tests.

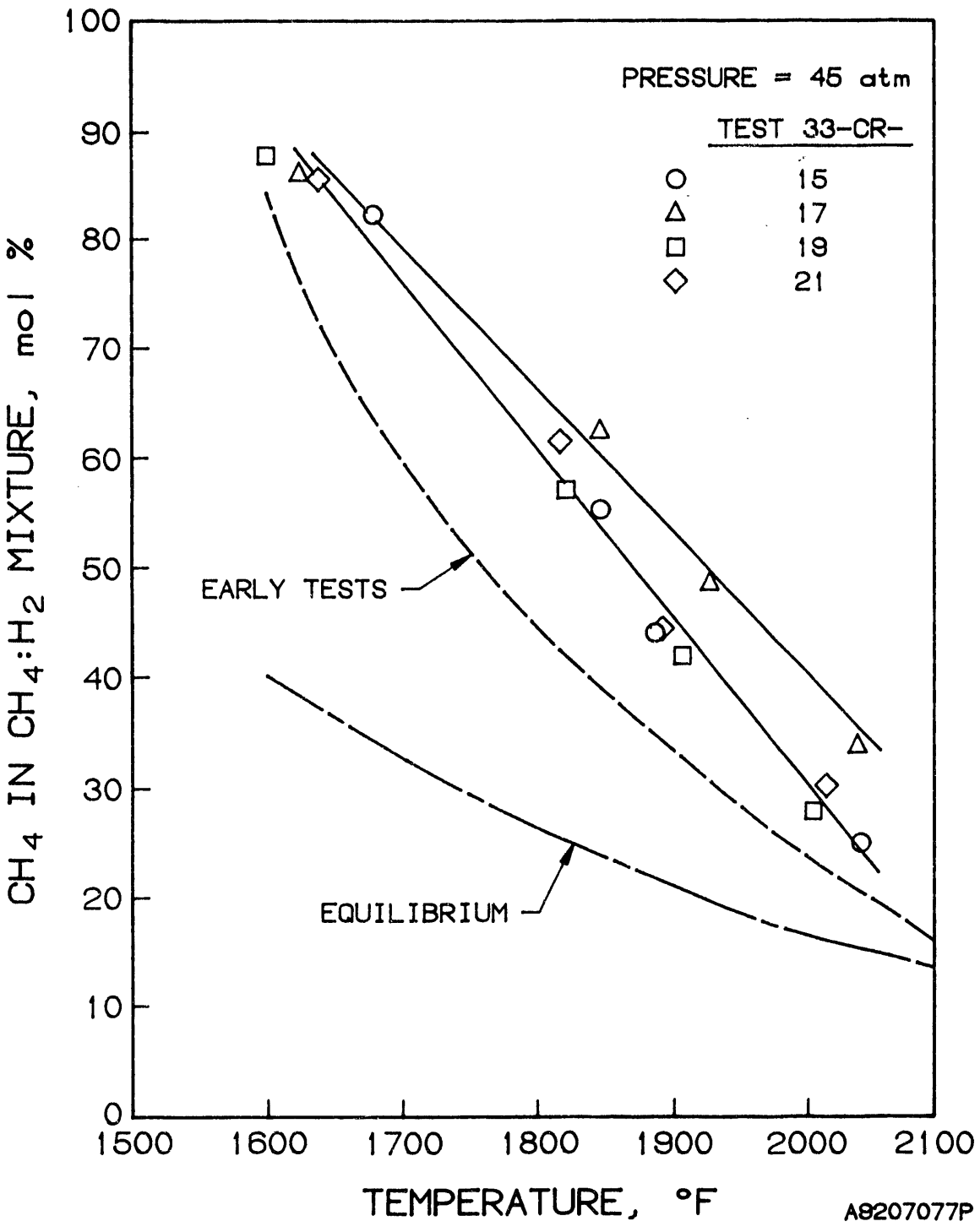

Figure 3-10. THE EFFECT OF MULTIPLE CYCLES ON METHANE CRACKING AT 45 ATMOSPHERES

Carbon conversions for the five combustion tests in the cycle test are presented in Table 3-8. Carbon cannot be accurately measured by ASTM methods below 0.5 percent. Therefore, the reported carbon conversions are estimates based on the ASTM procedures.

Table 3-8. CRACKING-COMBUSTION CYCLE TEST COMBUSTION RESULTS

Test No.	Solids Carbon Content, wt %		Carbon Conversion, wt %
	Feed	Residue	
32-CR-16	0.16	0.03	81
33-CR-18	0.16	0.10	38
33-CR-20	0.52	0.09	83
33-CR-22	0.37	0.05	86
33-CR-24	0.22	0.05	77

The average carbon conversion for combustion Tests 32-CR-16, 32-CR-20, 32-CR-22, and 32-CR-24 was 81 percent. Test 32-CR-18 had a lower carbon conversion, but this result may reflect inaccuracies in sampling or analytical procedures. Carbon conversions were high, but not all of the carbon was converted to oxides. Complete conversion of carbon to recover heat may require higher temperatures or the use of enriched air as oxidant. The combustion tests were conducted with the solids in a packed bed. Better gas-solid contact in a fluidized-bed reactor may also lead to higher carbon conversions.

The carbon conversions in the cycle combustion tests were significantly higher than those from the individual combustion Tests 32-CO-1 and 32-CO-2. This result may reflect more accurate carbon measurements in the cycle tests. Higher concentrations of deposited carbon in the cycle tests allows for more accurate carbon content measurements by the ASTM procedure used.

Subtask 3.8. Niche Market Studies

The objective of this subtask was to determine the potential for producing hydroretorted shale oil co-products, such as asphalt additives. A determination of the hydroretorting conditions needed to produce high yields of asphalt cement from an Eastern shale oil was also to be made. Characterization of the shale oil asphalt cements and pavement briquettes containing them will provide a detailed understanding of the shale asphalt cement properties and will allow evaluation of their performance in paving applications. The detailed objectives are:

- To conduct screening tests to find the hydroretorting conditions for obtaining the highest asphalt cement yields from an Eastern shale oil.
- To produce sufficient asphalt cement from an Eastern oil shale for characterization.

- To characterize the Eastern shale oil asphalt cements and pavement briquettes containing them.

- To compare the properties of shale oil and petroleum asphalts and determine the value of Eastern shale oil asphalts in paving applications.

Equipment and Test Procedures

A series of laboratory-scale batch PFH tests were conducted with densified beneficiated Alabama shale to determine the optimum conditions for producing shale oil asphalt. The equipment and test procedure used for these tests is described in Subtask 5.2.1. Shale oil from the batch PFH tests was separated into boiling point fractions by simulated distillation using a modified version of ASTM Method D3887. A sample of oil from the PFH tests in Subtask 5.2 was analyzed by high temperature simulated distillation with element-specific detectors to determine the carbon, hydrogen, sulfur, and nitrogen contents of the oil as a function of boiling point. A second PFH product oil sample from Subtask 5.2 was fractionated in a laboratory vacuum distillation column, and standard ASTM elemental analyses were performed on the four oil fractions.

Asphalt binder and asphalt pavement characterization tests were conducted with a standard AC-20 grade petroleum asphalt and mixtures of this binder and fractions of the PFH shale oil. The AC-20 asphalt for this study was donated by Seneca Petroleum. Mixtures were made containing two shale oil additives, SOA-1 and SOA-2. SOA-1 and SOA-2 were the fractions of the oil from the bench-scale PFH test that boil above 662° and 580°F (350° and 304°C), respectively. The shale oil additives were separated by vacuum distillation and then mixed with the AC-20 asphalt while heated to produce the desired mixtures. The asphalt binders were characterized by using ASTM methods for penetration at 39.2° and 77°F (4° and 25°C), kinematic viscosity at 275°F (135°C), absolute viscosity at 140°F (60°C), ductility at 77°F, specific gravity at 77°F, and thin film oven loss after 5 hours at 325°F (163°C). Aging characteristics were judged by measuring penetration, ductility, and viscosity after the thin film oven test and comparing the results with the unaged sample properties.

Pavement briquette samples were made from the AC-20 asphalt and mixtures containing the SOA-1 shale oil additive. The aggregate used was 3/8-inch limestone chips and fine sand. The aggregate and the Marshall test pavement formula were donated by Vulcan Materials specifically for this project. A Marshall test for resistance to plastic flow was performed on samples of each pavement briquette. The tensile strength and the effect of moisture on the pavements were determined by ASTM Method D4867. The final pavement characterization test was the Water Susceptibility Test (WST). In the WST, pavement briquettes are submerged in water and subjected to cycles including freezing at 15°F (-9°C) and heating at 140°F (60°C). A count is made of the number of freeze-thaw cycles needed to crack the briquettes. The WST is not an ASTM procedure but has been carefully described in the literature. Pavement samples containing both SOA-1 and SOA-2 were tested by the WST.

Discussion

Seven batch asphalt screening tests were conducted in this subtask in the laboratory-scale PFH unit. Tests were conducted at 900° to 1200°F (482° to 649°C) and pressures of 200 to 1000 psig (1.5 to 7.0 MPa). A 20-minute residence time was employed to ensure that the highest oil yield possible at that condition was achieved. Complete material balances were conducted for these tests and the detailed operating conditions and results are presented in Subtask 5.2.1 along with the results of other laboratory-scale batch tests.

The oil yield and oil fractionation data as a function of PFH conditions were of interest in this subtask. These results and the test operating conditions are presented in Table 3-9. Oil yield increases with increasing pressure between 200 and 1000 psig. Increasing the temperature from 900° to 1050°F (565°C) produces a decrease in oil yield, and increasing the temperature to 1200°F results in a much larger decrease in oil yield.

Changing the PFH conditions affects the carbon conversion to oil more than it does the oil split into boiling point fractions. Therefore, the highest PFH carbon conversion to oil was 71.2 percent at 900°F and 1000 psig. The highest conversion of carbon to higher boiling oil that can be used as an asphalt additive was also obtained at this condition. A large fraction of the PFH product oil boils in the temperature range of typical asphalts. For example, at PFH conditions of 940°F and 1000 psig (504°C and 7.0 MPa), 62 percent of the product oil boils above 650°F (343°C), 52 percent boils above 725°F (385°C), and 39 percent boils above 800°F (427°C).

The improvement of asphalt binders by the addition of shale oil fractions depends on the ability of the additives to improve asphalt pavement properties. Normal asphalt pavements are susceptible to weakening in the presence of moisture, and freezing and thawing of water on pavements tends to cause cracking by pulling the binder and aggregate apart. Studies have shown that nitrogen-containing compounds strengthen the binder-aggregate bond and reduce the susceptibility of asphalt pavements to moisture damage. Eastern shale oils have a high nitrogen content and may, therefore, improve asphalt properties when used as additives.

The shale oil fraction used as an asphalt additive may provide improved properties if the nitrogen content is high. Two groups of analyses were conducted on oil from PFH tests in Subtask 5.2 to determine the elemental content of shale oil as a function of boiling point. Before performing the first group of analyses, the unsteady-state oil produced from the bench-scale test in Subtask 5.2.2 was fractionated in a laboratory vacuum distillation column into four fractions boiling at less than 180°F (82°C), 180° to 360°F (182°C), 360° to 650°F (343°C), and above 650°F. Elemental analyses were conducted on all four fractions. The second group of analyses was conducted on oil from laboratory-scale continuous Test 51-C-3 in Subtask 5.2.1. The oil was subjected to a high temperature simulated distillation procedure in a GC using element-specific detectors.

TABLE 3-9. OPERATING CONDITIONS AND OIL SIMULATED BOILING POINT FRACTIONS FOR BATCH PFH TESTS

Test No.	Temp., °F	Press., psig	Carbon Conversion to Oil Boiling Below This Temperature, wt %								Total Carbon to Oil
			425°F	500°F	575°F	650°F	725°F	800°F	875°F	950°F	
35-B-1	937	227	6.4	9.5	13.1	16.9	21.1	26.7	31.0	36.4	49.5
35-B-2	1227	221	5.1	7.6	10.3	13.0	15.7	19.0	21.1	23.8	30.7
35-B-3	940	611	8.0	11.7	16.0	20.9	26.2	34.3	39.0	46.1	61.4
35-B-4	1072	613	7.5	9.6	14.4	19.4	22.1	27.8	34.1	40.6	56.1
35-B-5	1231	549	6.1	9.5	13.3	17.2	21.1	26.6	28.9	32.7	43.1
35-B-6	946	1055	9.9	15.0	20.7	27.0	34.0	43.4	48.4	55.3	71.2
35-B-7	1213	1017	3.7	7.1	10.5	14.3	18.1	23.6	26.0	29.9	39.3

Shale oil analyses as a function of boiling point are presented in Table 3-10. Results by the two analytical methods show the same trends of elemental content with varying boiling point even though the actual values are different. As boiling point increases, the carbon content increases and the hydrogen content decreases. The carbon to hydrogen weight ratio increases from 6.2 for the oil boiling below 180°F (82°C) to 9.3 for the oil boiling above 650°F (343°C). This corresponds with increasing shale oil aromaticity and aromatic ring number with increasing boiling point as determined by HPLC (high-pressure liquid chromatography) for the oil from the bench-scale test reported in Subtask 5.2.2. Sulfur content did not vary significantly with boiling point.

The nitrogen content in the oil increases with increasing boiling point. The fractionated oil boiling below 650°F had less than 0.32 weight percent nitrogen, and the oil boiling above 650°F had 1.63 weight percent nitrogen. The oil separated in the GC also showed a significant increase in nitrogen content with increasing boiling point, but the change was not as large. Oil boiling below 580°F (304°C) had less than 1 percent nitrogen, oil boiling between 580° and 800°F (°304 and 427°C) had 1.75 percent nitrogen, and oil boiling above 800°F had 2.3 percent nitrogen.

Asphalt Binder Characterization

Five asphalt binders were characterized. The first binder (SA-1) was a standard AC-20 grade asphalt binder donated by Seneca Petroleum. The other four asphalts were mixtures of the AC-20 asphalt and shale oil additives fractionated from the whole shale oil produced in the bench-scale test in Subtask 5.2.2. Two shale oil additives were used to make binder mixtures. SOA-1 was the shale oil fraction boiling above 662°F (350°C), and SOA-2 was the shale oil fraction boiling above 580°F (304°C). Three mixtures (SA-2, SA-3, and SA-4) were prepared with 2, 5, and 10 weight percent of SOA-1 mixed with the AC-20 asphalt. The final asphalt binder, SA-5, contained 5 weight percent SOA-2 combined with the AC-20 asphalt. A summary of the five asphalt binder mixture compositions is presented in Table 3-11.

The shale oil additives SOA-1 and SOA-2 boiling above 662° and 580°F, respectively, represent a large fraction of the whole shale oil. SOA-1 corresponds to 68 weight percent of the whole oil, and SOA-2 contains 78 percent of the whole oil. Production of shale oil asphalt additives could be the major product of a PFH plant.

Tests were conducted to determine the physical properties of the asphalt binders and the resistance of the asphalts to aging. Results of these characterization tests are presented in Table 3-12. The physical measurements included penetration at 39.2° and 77°F, kinematic viscosity at 275°F, absolute viscosity at 140°F, ductility at 77°F, specific gravity at 77°F, and vanadium content. All tests were ASTM procedures except that to determine vanadium content, which was determined by ion coupled plasma emission spectroscopy (ICP).

Table 3-10. OIL FRACTION ELEMENTAL ANALYSES

	Fraction of Whole Oil	Carbon	Hydrogen	Sulfur	Nitrogen
	----------	----------	wt % ----------	----------	----------
Fractionated Oil* Boiling Point					
Whole Oil	100.0	86.52	10.00	1.92	1.29
-180°F	1.4	83.45	13.39	1.61	0.18
180 - 360°F	7.6	84.49	12.72	1.56	0.20
360 - 650°F	16.1	85.95	11.59	1.57	0.32
+650°F	74.9	86.91	9.32	2.04	1.63
GC Separated Oil† Boiling Point					
Whole Oil	100.0	86.07	8.60	2.12	1.72
-360°F	8.1	--	--	1.67	0.44
360 - 580°F	21.5	--	--	2.10	0.93
580 - 662°F	10.1	--	--	2.72	1.40
662 - 800°F	17.9	--	--	2.79	1.98
+800°F	43.3	--	--	1.81	2.32

* Bench-scale test unsteady-state oil (Subtask 5.2.2).
† Lab-scale continuous Test 51-C-3 oil (Subtask 5.2.1).

Table 3-11. ASPHALT BINDERS AND PAVEMENT BRIQUETTES USED FOR CHARACTERIZATION TESTS

Binder Sample	SA-1	SA-2	SA-3	SA-4	SA-5
Binder Composition,* wt %					
AC-20	100.0	98.0	95.0	90.0	95.0
SOA-1	0.0	2.0	5.0	10.0	0.0
SOA-2	0.0	0.0	0.0	0.0	5.0
Total	100.0	100.0	100.0	100.0	100.0
Binder Characterization Tests	Yes	Yes	Yes	Yes	Yes
Pavement Briquette Composition, wt %					
Binder	----------		5.5	----------	
Limestone (3/8 inch)	----------		55.8	----------	
Sand	----------		38.7	----------	
Total					
Pavement Briquette Characterization Tests	Yes	Yes	Yes	Yes	No**

* AC-20 - Petroleum asphalt binder graded AC-20
SOA-1 - PFH shale oil boiling above 662°F
SOA-2 - PFH shale oil boiling above 580°F

** Water susceptibility test was performed.

Table 3-12. ASPHALT BINDER CHARACTERIZATION TEST RESULTS

Binder Sample	SA-1	SA-2	SA-3	SA-4	SA-5	ASTM Specification
Penetrations:						
At 77°F (100 g, 5 s)	55	60	65	66	69	>40
At 39.2°F (200 g, 1 min)	18	20	20	18	26	--
Viscosity,						
Kinematic at 275°F (cSt)	407	366	327	344	314	--
Absolute at 140°F (P)	2259	1938	1634	1607	1528	1600-2400
Ductility at 77°F, 5/60 (cm)	150+	150+	150+	150+	150+	--
Solubility in TCE*	99.9	99.9	99.9	99.9	99.9	>99.0
Vanadium Content, ppmw	260	250	280	250	230	--
Specific Gravity at 77°F	1.024	1.024	1.027	1.024	1.026	--
Thin Film Oven Loss						
5 h at 325°F, %	0.18	0.30	0.32	0.30	0.54	--
Tests on Residue from TFOL						
Penetration at 77°F, 100/5	34	35	36	36	35	--
% of Original	61.8	58.3	55.4	54.5	50.7	--
Ductility at 77°F, 5/60, cm	150+	150+	150+	150+	150+	>20
Viscosity, Absolute at 140°F (P)	5455	4974	4124	4312	4789	<10,000
Ratio After/Before	2.41	2.57	2.52	2.68	3.13	--

* Trichloroethylene.

Aging characteristics of the asphalts were evaluated by comparing the penetration at 77°F, ductility at 77°F, and absolute viscosity at 140°F before and after a thin film oven loss (TFOL) test. In the TFOL test, asphalt binder is heated to 325°F and held at this temperature for 5 hours. The weight loss from the TFOL gives an estimate of the asphalt volatility, and the characterization tests after the TFOL provide aging characteristics.

Many different grades of asphalt binders with various characteristics are used in pavements. A large number of binder analyses are performed to permit selection of an asphalt appropriate to the climate and use conditions expected for the pavement. The absolute viscosity at 140°F is most commonly used as the grading method for asphalt binders. AC-20 asphalt is used extensively in the midwestern U.S. and was, therefore, selected as the base-case asphalt for testing in this program. The absolute viscosity of AC-20 asphalt at 140°F must be between 1600 and 2400 poise (P) according to ASTM specifications.

The addition of shale oil additives SOA-1 and SOA-2 to the AC-20 reduced the absolute viscosity of the asphalt. The reduction was small when SOA-1 was added, and a mixture containing as much as 10 percent SOA-1 still had a viscosity within the range defined for AC-20 asphalt. Additive SOA-2, with a lower minimum boiling point, produced a mixture with a viscosity outside the range for AC-20. The kinematic viscosity at 275°F also showed some decrease with the addition of SOA-1 and a large decrease when SOA-2 was added. Penetration tests showed the asphalt mixtures containing SOA-1 were slightly softer than the AC-20 asphalt, and the SOA-2 mixture was significantly softer than the other asphalts. The AC-20 asphalt and all asphalt mixtures containing SOA-1 and SOA-2 had penetrations in excess of the AC-20 specification of 40.

The addition of shale oil additives to the AC-20 asphalt had no effect on the ductility, specific gravity, or vanadium content. The ductility and specific gravity of all samples were within the acceptable range for AC-20 asphalt. Vanadium is an undesirable contaminant of the asphalt. Analyses show that the vanadium contents of the shale oil additive mixtures are similar to those of standard AC-20 asphalts.

The TFOL test showed a volatile loss for AC-20 asphalt of 0.18 percent. The loss increased to about 0.3 percent for mixtures containing SOA-1. The loss was 0.54 percent for the asphalt containing the lower boiling SOA-2.

After aging in the TFOL test, the asphalts were again measured for ductility, penetration, and viscosity. The ductility of all five asphalts was still in excess of 150 cm, so no change was detected. This value is much higher than the minimum 20 cm specified by ASTM for this asphalt. The penetration of the AC-20 asphalt and the four mixtures were almost the same (34 to 36) after aging. Aging decreased the AC-20 penetration to 61.8 percent of the original value. Mixtures containing SOA-1 showed penetrations reduced to 55 to 58 percent of the original, and SOA-2 addition reduced the penetration to 50.7 percent of the original value.

The viscosity of an asphalt binder increases with age. All five asphalts showed an increase in viscosity after the aging test, but the

viscosities were well below the maximum 10,000 P specified by ASTM for AC-20 asphalt. The viscosity of the AC-20 asphalt was 5450 P after the TFOL aging test, and the ratio of viscosities before and after aging was 2.4. Mixtures containing SOA-1 show almost the same increase in viscosity. Viscosities after aging ranged from 4120 to 4970 P. The ratio of aged to "unaged" viscosity was 2.5 to 2.7. After aging, the SOA-2 asphalt mixture had a viscosity of 4790 P. However, aging produced a larger percentage increase in viscosity. The ratio of aged to unaged viscosity for SOA-2 asphalt was 3.1.

The results of asphalt binder property measurements and aging characteristics tests show that the binders containing SOA-1 have similar, but slightly lower viscosities and aging qualities than those of the AC-20 asphalt. Additive SOA-2 produces an asphalt with lower viscosity and aging characteristics. The characterization tests indicate the use of SOA-1 as an additive is not deleterious to the asphalt properties; the use of a higher boiling shale oil fraction as an additive could further improve the asphalt properties.

Asphalt Pavement Characterization

The AC-20 asphalt and the three asphalt mixtures containing AC-20 asphalt and the SOA-1 additive were tested for pavement tensile strength and resistance to plastic flow. The asphalt pavements were produced using the optimum mix formula for unmodified AC-20 asphalt cement and aggregate donated by Vulcan Materials. A Marshall test was conducted to measure resistance to plastic flow. Tensile strength under dry and wet conditions was measured by ASTM Method D4867.

The final pavement characterization test was measurement of the resistance of the pavement briquettes to cracking by alternate cycles of freezing and thawing. Resistance was measured by a water susceptibility test (WST). The objective of the WST is to determine the effects of different additives in the asphalt cement on resistance to freeze-thaw cracking. All five asphalt cements were used to make pavement samples for the WST. The asphalt cements included unmodified AC-20; AC-20 with 2, 5, and 10 weight percent SOA-1; and AC-20 with 5 weight percent SOA-2. Results of the pavement characterization tests are summarized in Table 3-13.

Addition of the SOA-1 additive improved the retention in tensile strength under wet conditions. The AC-20 asphalt retained only 63.3 percent of its strength (a loss of 37 percent). Addition of 2 to 10 percent SOA-1 improved the retention of strength to between 81.1 and 76.5 percent of the dry strength. Thus, loss in tensile strength was significantly reduced. The addition of the SOA-1 additive produced somewhat lower dry pavement tensile strengths but a higher wet pavement tensile strength compared to the unmodified AC-20 pavement. Pavement specific gravities, densities, air voids, stability, and resistance to flow were similar for the AC-20 asphalt and the mixtures containing the SOA-1 additive.

The WST was conducted on pavement briquettes containing 5.5 weight percent asphalt binder. The 50-gram briquettes were formed by pressing a hot pavement mix at 6200 psi for 20 minutes in a hydraulic press. Six briquettes of each of the four pavements were tested. The briquettes were cured for

Table 3-13. ASPHALT PAVEMENT BRIQUETTE CHARACTERIZATION TEST RESULTS

Binder Sample	SA-1	SA-2	SA-3	SA-4	SA-5
Asphalt Content, %	5.5	5.5	5.5	5.5	NA**
Maximum Specific Gravity, g/mL	2.522	2.523	2.522	2.522	NA
Marshall Density	2.338	2.330	2.336	2.342	NA
VMA,* %	19.9	20.2	20.0	19.8	NA
Air Voids, %	7.3	7.6	7.4	7.1	NA
Voids Filled,* %	63.3	62.4	63.0	64.1	NA
Stability at 140°F, lb	2460	2320	2410	2350	NA
Flow at 140°F, 0.01 in.	11.2	11.3	10.0	10.7	NA
Average Tensile Strength, Ratio, %	63.3	81.1	77.9	76.5	NA
Water Susceptibility Test, Average Cycles to Failure	1	1	2	2	1.5

* Voids in the mineral aggregate (VMA) and Voids Filled are calculated based on no asphalt absorption.
** Not analyzed.

three days at room temperature and then placed on stress pedestals in jars. Distilled water was added to the jars to a level about 1/2 (13 mm) inch above each briquette. A cycle was then performed consisting of freezing the jar at 12°F (-11°C) for 24 hours, warming the jar to room temperature, and then heating the sealed jar at 140°F (60°C) for 24 hours. At the end of each cycle, the briquettes were checked for cracks. If cracking did not occur, the briquette was subjected to another freeze-thaw cycle.

All six of the pavement briquettes containing unmodified AC-20 asphalt cement cracked severely during the first freeze-thaw cycle, as expected. As mentioned above, the WST is not intended to measure the properties of the unmodified asphalt cements; rather, its purpose is to evaluate the effects of additives or modifiers on the freeze-thaw resistance of the resulting asphalt cement mixtures. The six pavement samples containing AC-20 asphalt with 2 percent SOA-1 also failed during the first freeze-thaw cycle.

Increasing the fraction of SOA-1 in the asphalt cement mixture significantly improved the resistance of the pavement to freeze-thaw cracking. An average of 2 cycles were required to cause cracking when the asphalt cement contained 5 and 10 weight percent SOA-1. One of the six samples of both the 5 and 10 percent mixtures required 3 cycles to crack. The second additive, SOA-2, at a 5 percent concentration increased cracking resistance by a smaller amount to an average of 1.5 cycles before freeze-thaw cracking occurred.

A distinct improvement in freeze-thaw resistance to cracking was achieved with the addition of SOA-1 to the AC-20 asphalt cement. Five of six samples of pavement containing binder with 5 and 10 percent SOA-1 did not crack in the first cycle. Observation of the cracked pavement samples showed the unmodified AC-20 pavements had more severe cracking than the pavements containing the SOA-1 modifier. These results demonstrate the addition of the SOA-1 modifier improves the asphalt pavement resistance to freeze-thaw cracking.

Task 4. Beneficiation Research

The objective of this task was to test several novel and advanced grinding and beneficiation concepts, which have shown promising results with coal, for processing Eastern shales. This task is divided into four subtasks: 4.1. Grinding Studies (Subtask 4.1.4. Grinding Circuit Design), 4.4. Integrated Grinding and Flotation, 4.5. Evaluation of Different Grinding Media, and 4.6. Evaluation of Concentrate Preparation Techniques (Subtasks 4.6.1. Oil Agglomeration and Pelletizing and 4.6.2. Bioflocculation of Kerogen).

The overall responsibility for this task was assumed by the Mineral Resources Institute (MRI) of the University of Alabama. One of the subtasks (4.4) was conducted by the University of Kentucky Center for Applied Energy Research (UK-CAER), as a subcontractor to MRI. Subtask 4.6.2 was conducted by the University of Nevada (UN-Reno), also as a subcontractor to MRI. The achievements made during the program are described below.

Subtask 4.1. Grinding Studies

Subtask 4.1.4. Grinding-Flotation Circuit Design

Background and Objectives

The results of previous research by MRI[1] indicated that the most effective means of reducing grinding costs was to reduce the amount of material that is ground in the stirred ball mill. This in turn requires that material be removed from the circuit, as a final product, at the coarsest possible size compatible with effective flotation of the kerogen. Figure 4-1 presents a grinding and flotation flowsheet that was proposed at the conclusion of the prior research. The projected energy consumption for this flowsheet is presented in Table 4-1. These data represent the starting point of the current investigation.

The objective of this subtask was to evaluate various grinding/flotation circuit configurations that have the potential to reduce the energy consumption and cost of producing kerogen concentrates. Within that broad objective it is the further objective to test alternative means of accomplishing the unit operations, particularly sizing, within the various circuits.

Experimental Procedures and Results

Preliminary Sizing Tests. MRI conducted laboratory-scale rod mill grinding tests on -12 mesh Alabama oil shale. Samples were ground to pass 100, 200, and 325 mesh. Size analyses of these products showed that they contained, respectively, 31, 36, and 43 percent -12 micrometers (μm) - a size suitable for flotation. Hydraulic classifier tests were performed on a sample of the -100 mesh shale. The results, presented in Table 4-2, show that the hydraulic classifier captures essentially all of the -12 μm material, but the size split is relatively coarse (i.e. about 24 μm).

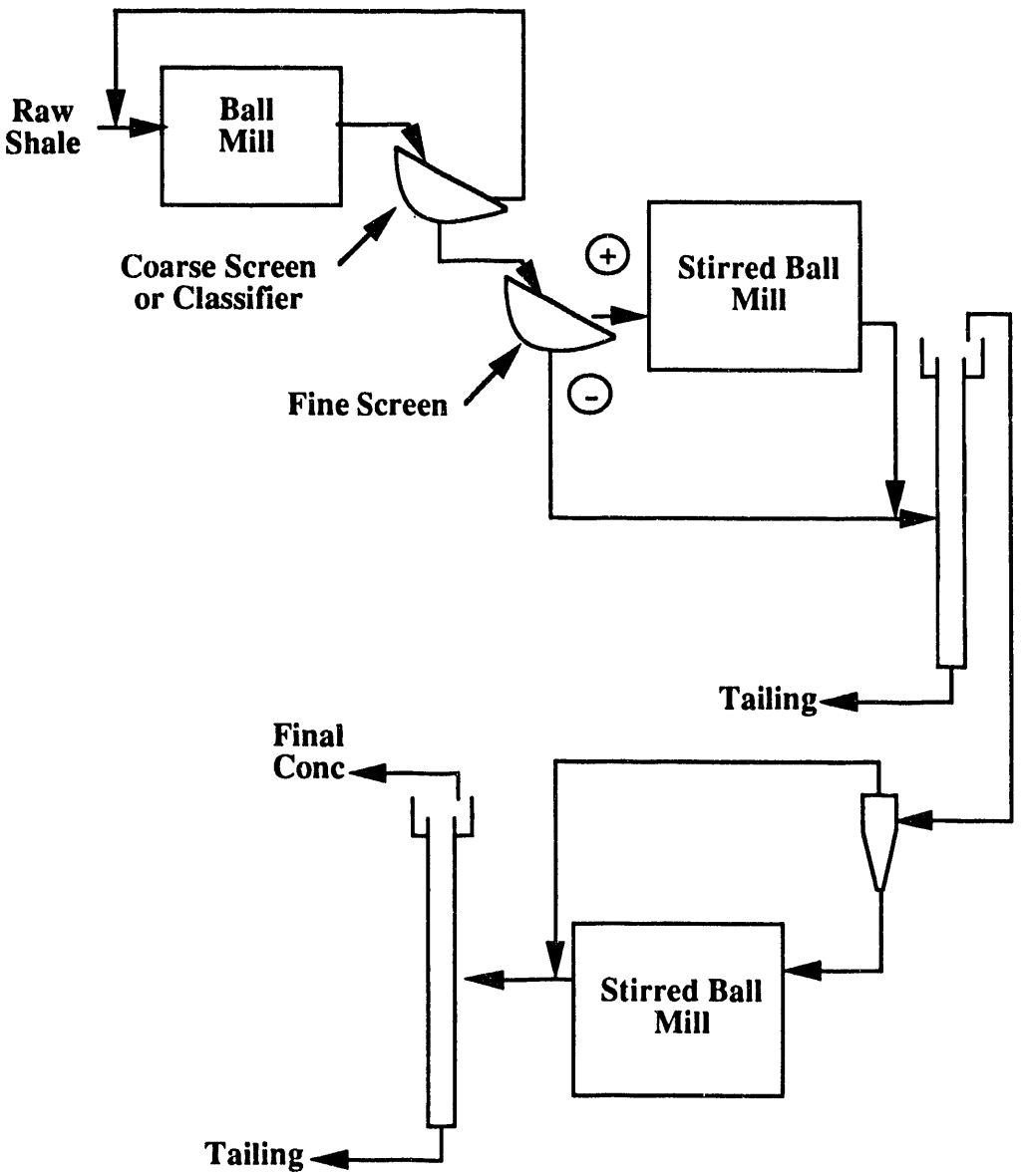

Figure 4-1. INITIALLY PROPOSED GRINDING-FLOTATION FLOWSHEET

The hydraulic classifier overflow (fines) was further classified by a hydrocyclone. The results of three stages of hydrocyclone are shown in Table 4-3. The hydrocyclone was not particularly efficient in capturing the -12 μm material. In the first pass, only 58.3 percent of the -12 μm fraction reported to the cyclone overflow. After three passes the total was only 77.5 percent. These data indicate the need to study the operating parameters affecting the size distribution in the cyclone products.

Table 4-1. BENEFICIATION FLOWSHEET PROJECTED ENERGY CONSUMPTION

Unit	Feed, %	kWh/t	Net kWh/t
Ball Mill	100	16.48	16.48
Primary Stirred Mill	50	40.00	20.00
Secondary Stirred Mill	25	49.52	12.38
Total Energy Consumption, Kwh/t			48.86

Table 4-2. HYDRAULIC CLASSIFICATION OF -100 MESH ALABAMA SHALE

Classifier Product	wt %	Size Distribution, %			Distr. of Size Fractions		
		+24 μm	24/12 μm	-12 μm	+24 μm	24/12 μm	-12 μm
Underflow	29	90.9	2.9	5.6	52.1	4.9	5.2
Overflow	71	34.2	23.2	41.8	47.9	95.1	94.8
Feed	100	50.6	17.3	31.3	100.0	100.0	100.0

Table 4-3. EFFECT OF HYDROCYCLONING THE HYDRAULIC CLASSIFIER OVERFLOW PRODUCT

Product	wt %	Size Distribution, %			Distr. of Size Fractions		
		+24 μm	24/12 μm	-12 μm	+24 μm	24/12 μm	-12 μm
Cyclone Overflow							
1st Pass	30.0	1.8	16.3	81.2	1.6	21.2	58.3
2nd Pass	7.0	2.3	12.7	84.4	0.5	3.8	14.1
3rd Pass	2.8	5.2	18.7	75.5	0.4	2.3	5.1
Cyclone Overflow							
1-3 Passes	39.8	2.1	15.8	1.4	2.5	27.2	77.5
Cyclone Underflow							
3rd Pass*	60.2	55.4	28.1	15.6	97.5	72.8	22.5
Cyclone Feed	100.0	34.2	23.2	41.8	100.0	100.0	100.0

* Cyclone underflow (3rd pass) calculated from known feed size.

Hydrocycloning Tests. About 800 pounds of Alabama shale was ground in a 19 x 36 inch Denver ball mill operating in closed circuit with a 100 mesh SWECO screen. The circuit was operated to maintain a relatively low

circulating load. The size distribution of the -100 mesh product is presented in Table 4-4.

Table 4-4. SIZE DISTRIBUTION OF -100 MESH ALABAMA SHALE

Size, μm	wt %	Cumulative wt % Retained
+128	2.2	2.2
-128+96	6.6	8.8
-96+64	12.2	21.0
-64+48	4.9	25.9
-48+32	11.2	37.1
-32+24	7.1	44.2
-24+16	10.1	54.7
-16+12	8.2	62.5
-12+8	8.4	70.9
-8+6	5.7	76.4
-6+4	6.5	83.1
-4+3	7.2	87.3
-3+2	4.4	91.7
-2+1	4.4	96.1
-1+pan	3.4	99.5

A representative sample of the -100 mesh product was split into three portions. One portion was retained, a second portion was screened to remove the +200 mesh material and the third fraction was screened to remove the +460 mesh material. The size distributions of the resulting three samples are compared in Table 4-5. These samples were the feedstocks used in a 3 x 3 factorial hydrocycloning experiment. The factors studied were feed size, feed density (percent solids), and the feed pressure (at the inlet to the cyclone). The objective of the experiment was to determine the operating conditions required for efficient size separation.

Table 4-5. SIZE CONSISTS OF COARSE GRINDING CIRCUIT DISCHARGE (Stirred Ball Mill Feed)

Size, mesh	wt %	Size Distribution, wt %			Distr. Parameters, μm	
		+24 μm	24/12 μm	-12 μm	d_{90}	d_{50}
-100	100.0	41.7	19.6	38.6	56.0	25.1
-200	80.0	33.2	22.4	44.4	46.3	18.7
-460	62.3	18.8	27.3	53.9	33.8	10.8

The results of the individual cyclone tests (Figures 4-2 through 4-4) show that at high feed solids, the finer feeds separate at a coarser size than do the coarser feed sizes. For example, in Figure 4-2 the -460 mesh sample yielded a cyclone overflow whose d_{90} was about 23 μm while the -100 mesh feed yielded an overflow product with a d_{90} of 13.5 μm. This tendency is diminished as the feed density is decreased.

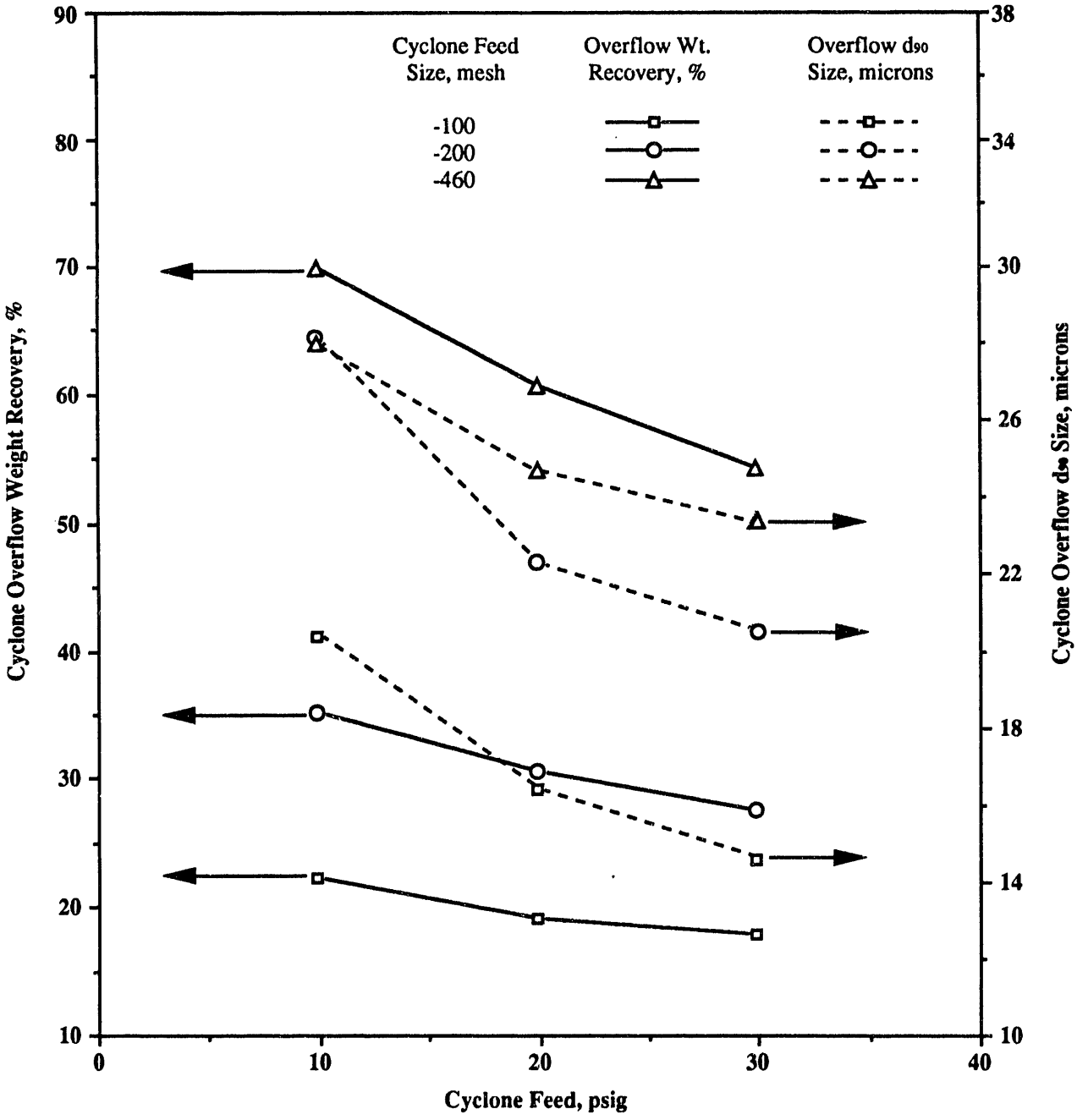

Figure 4-2. EFFECT OF CYCLONE PRESSURE AND CYCLONE FEED SIZE AT HIGH FEED (27 TO 31 wt %) SOLIDS

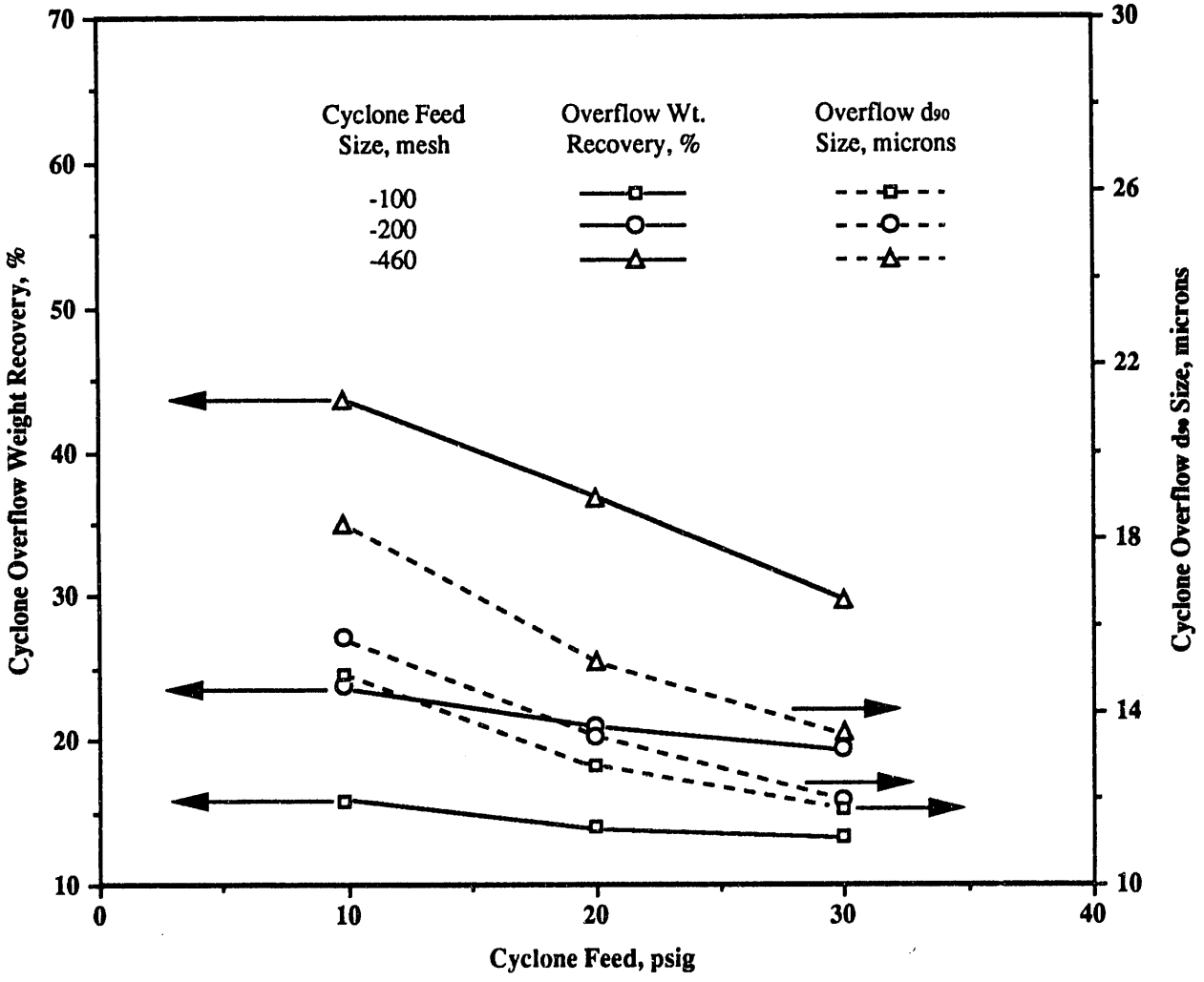

Figure 4-3. EFFECT OF CYCLONE PRESSURE AND CYCLONE FEED SIZE AT MEDIUM FEED (12.5 TO 15 wt %) SOLIDS

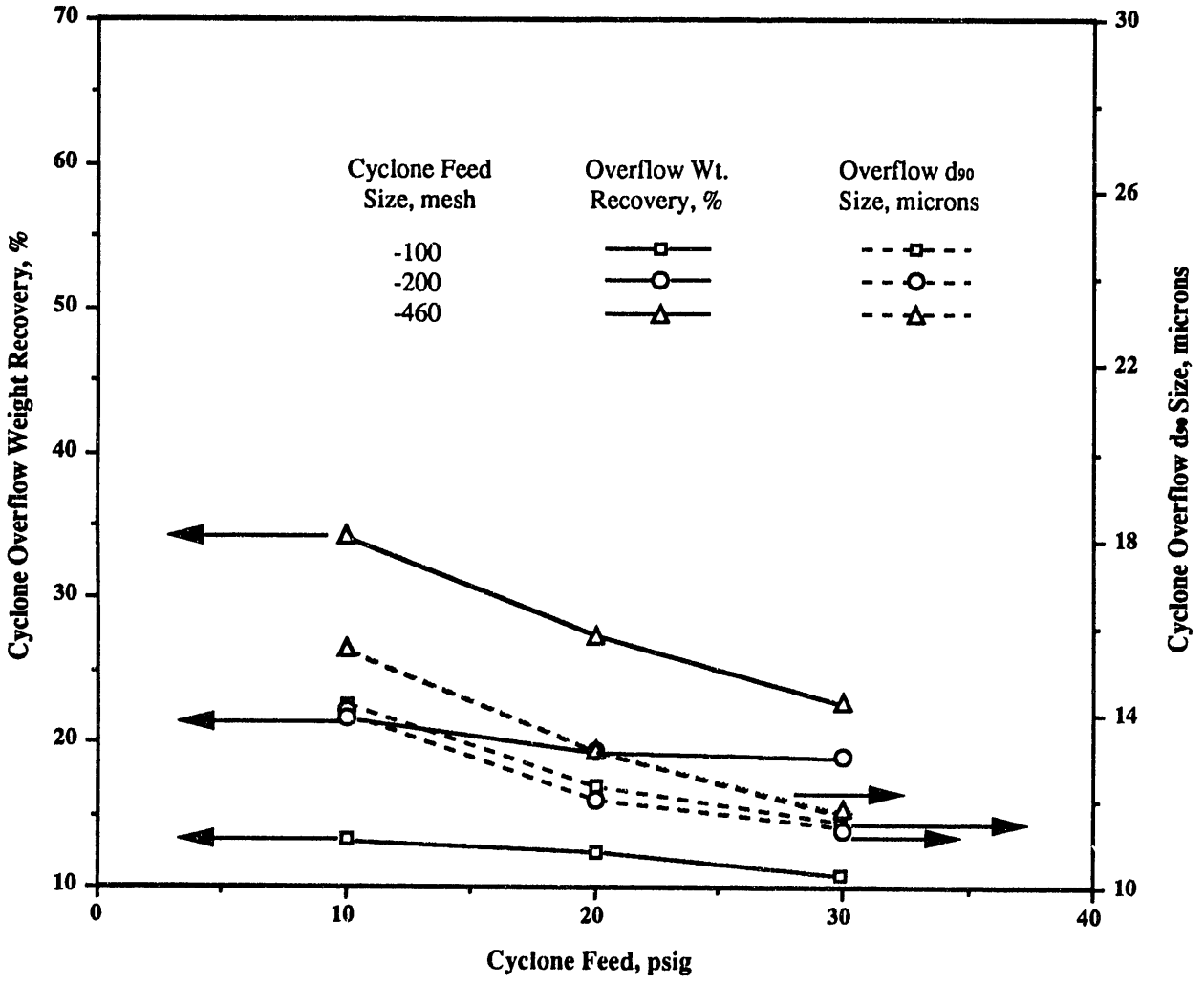

Figure 4-4. EFFECT OF CYCLONE PRESSURE AND CYCLONE FEED SIZE AT LOW FEED (4.8 TO 6.8 wt %) SOLIDS

In Figure 4-4, the overflow d_{90} of all three feeds is virtually the same at high pressures. It should also be noted that the weight recovery in the overflow diminishes as the feed solids concentration is decreased.

Bulk Sample Treatment. Data from these cycloning tests was used to establish operating conditions for sizing the remainder of the 800-pound bulk sample. The sample was first cycloned at high solids content. The cyclone underflow was then screened on a Derrick vibrating screen fitted with 460-mesh screen cloth. These sizing operations and the resulting weight splits are illustrated by Figure 4-5. Size distributions of the individual products are presented in Table 4-6.

Table 4-6. SIZE DISTRIBUTIONS OF BULK SAMPLE PRODUCTS

Size, μm	Screen Oversize		Screen Undersize		Cyclone Overflow	
	wt %	Cumulative % Retained	wt %	Cumulative % Retained	wt %	Cumulative % Retained
+96	15.7	15.7	--	--	--	--
-96+64	20.5	36.2	--	--	--	--
-64+48	7.9	44.1	3.5	3.5	--	--
-48+32	14.6	58.7	11.3	14.8	--	--
-32+24	7.4	66.1	11.2	26.0	1.0	1.0
-24+16	7.6	73.7	18.6	44.6	5.8	6.8
-16+12	6.4	80.1	12.5	57.1	7.9	14.7
-12+8	1.9	85.0	11.2	68.3	15.3	30.0
-8+6	14.4	99.4	6.7	75.0	12.0	42.0
-6+4	--	--	24.0	99.0	16.8	58.5
-4+3	--	--	--	--	10.4	69.2
-3+pan	--	--	--	--	30.7	99.9

Preliminary flotation tests were performed on the cyclone overflow (product A) and the screen undersize (product B) in a Denver laboratory mechanical flotation cell. The results (Table 4-7) show that in either case a clean tailing could be produced. The finer cyclone overflow produced a cleaner concentrate than did the screen undersize, however the screen undersize concentrate was not of a grade that could be considered a finished product. Column cell tests on the combined cyclone overflow and screen undersize are discussed later in this report.

Table 4-7. PRELIMINARY CELL FLOTATION TEST RESULTS (MECHANICAL)

Product A	Cleaner Concentrate Grade, GPT	26.8
	Oil Loss in Tailings, %	5.3
Product B	Concentrate Grade, GPT	15.7
	Oil Loss in Tailings, %	3.6
	Reduction, wt %	~30

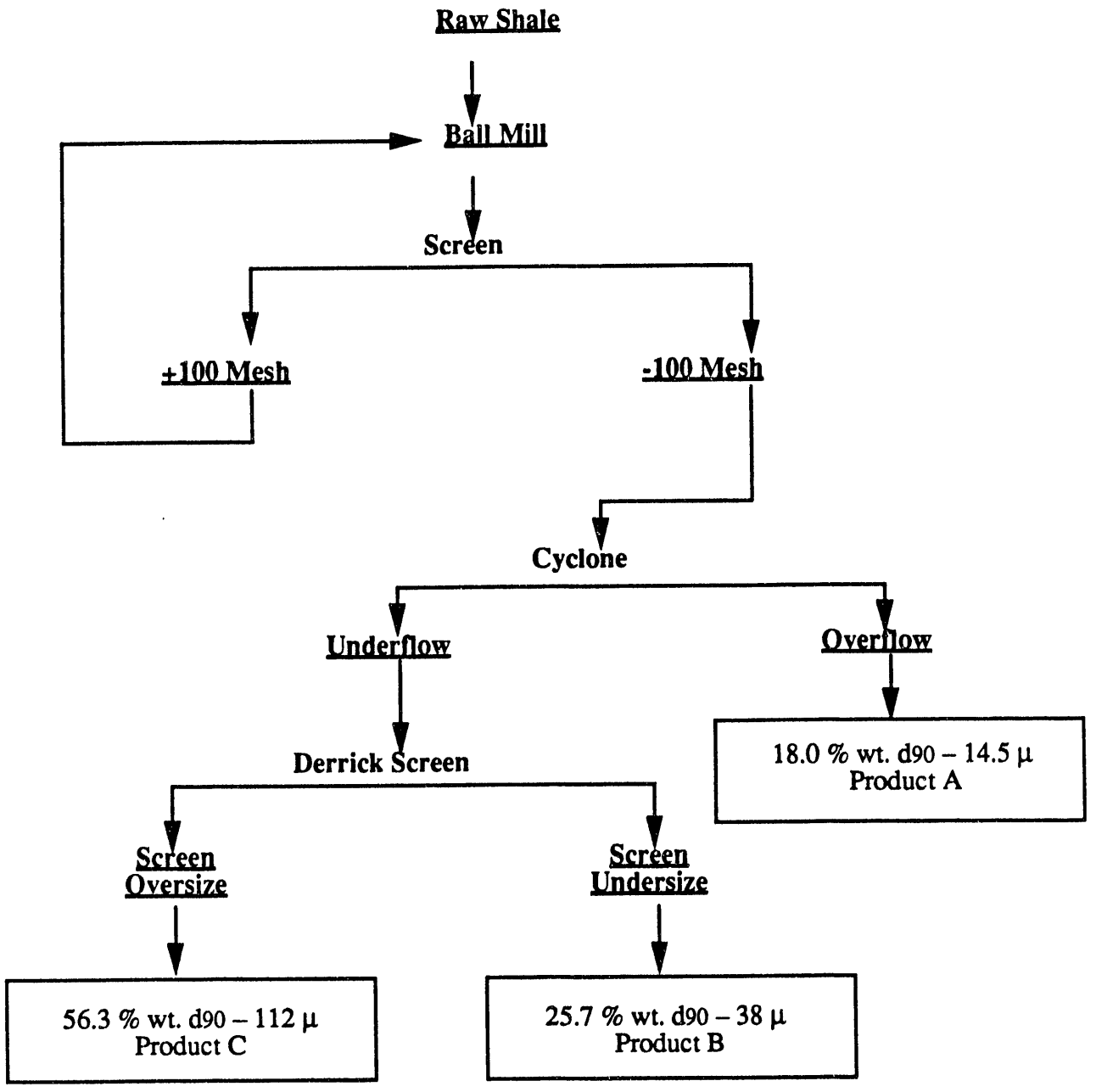

Figure 4-5. SIZING OF -100 MESH BULK SAMPLE

Grinding and Flotation of Screen Oversize. Stirred ball mill grinding tests on the Derrick screen oversize (Product C from Figure 4-5) were performed in the 4-L Netzsch stirred ball mill. The tests were performed at various feed rates and stirring speeds with 1.1 mm sand as the grinding media. The results of those tests are presented in Table 4-8. The significance of the test results are discussed in some detail in Task 4.5. The products from the grinding tests were composited for use in column flotation tests.

Table 4-8. STIRRED BALL MILL GRINDING TEST ON SCREEN OVERSIZE
(d_{90} = 112 μm, d_{50} = 39.5 μm)

rpm	Throughput, t/h	Specific Energy, kWh/t	Product Size, μm	
			d_{90}	d_{50}
1800	0.0343	69.2	20.4	8.1
2000	0.0343	103.3	19.7	6.7
2000	0.0257	145.7	16.9	6.3
2000	0.0428	84.6	19.9	7.1
2000	0.0556	64.7	22.8	7.9
2350	0.0556	116.8	17.4	6.6

Two-stage column flotation tests were performed in a composite of the reground screen oversize products. In this series of tests, concentrate (froth product) from the first stage of flotation was fed directly into the second column as shown in Figure 4-6.

Previous tests had shown that the cyclone overflow and screen undersize from the -100 mesh grind could each produce a clean tailing (Table 4-7). The purpose of these tests was to determine whether reground material of essentially the same size could also produce a clean tailing and further determine whether a final concentrate could be produced.

The results of the two-stage column test are presented in Table 4-9. The data show clearly that a clean tailing can be produced. Note that in five of the six tests the oil recovery in the rougher concentrate is greater than 90 percent. The data also indicate that it may be possible to produce a final concentrate containing more than 35 GPT oil. The cleaner concentrates from Test 4, 5, and 6 are trending in that direction with Test 6 yielding a 33.6 GPT concentrate grade.

Table 4-9. RESULTS OF TWO-STAGE COLUMN FLOTATION OF REGROUND SCREEN OVERSIZE

Test	Rougher Concentrate			Cleaner Concentrate			Cleaner Tailing (Middling)		
No.	wt %	Oil, GPT	Rec., %	wt %	Oil, GPT	Rec., %	wt %	Oil, GPT	Rec., %
1	40.2	24.0	78.2	25.7	29.1	65.0	12.7	12.8	13.2
2	46.2	25.6	94.2	39.8	27.9	90.6	5.3	8.3	3.6
3	54.3	20.3	91.4	41.9	24.6	84.6	12.4	6.7	6.8
4	47.0	25.4	96.4	34.2	31.3	86.1	12.8	9.8	10.0
5	60.3	20.1	97.4	30.8	32.7	81.0	29.5	6.9	16.4
6	58.3	20.7	97.4	31.5	33.6	85.3	26.8	5.6	12.1

Feed Size: d_{90} = 19.7 μm, d_{50} = 6.9 μm

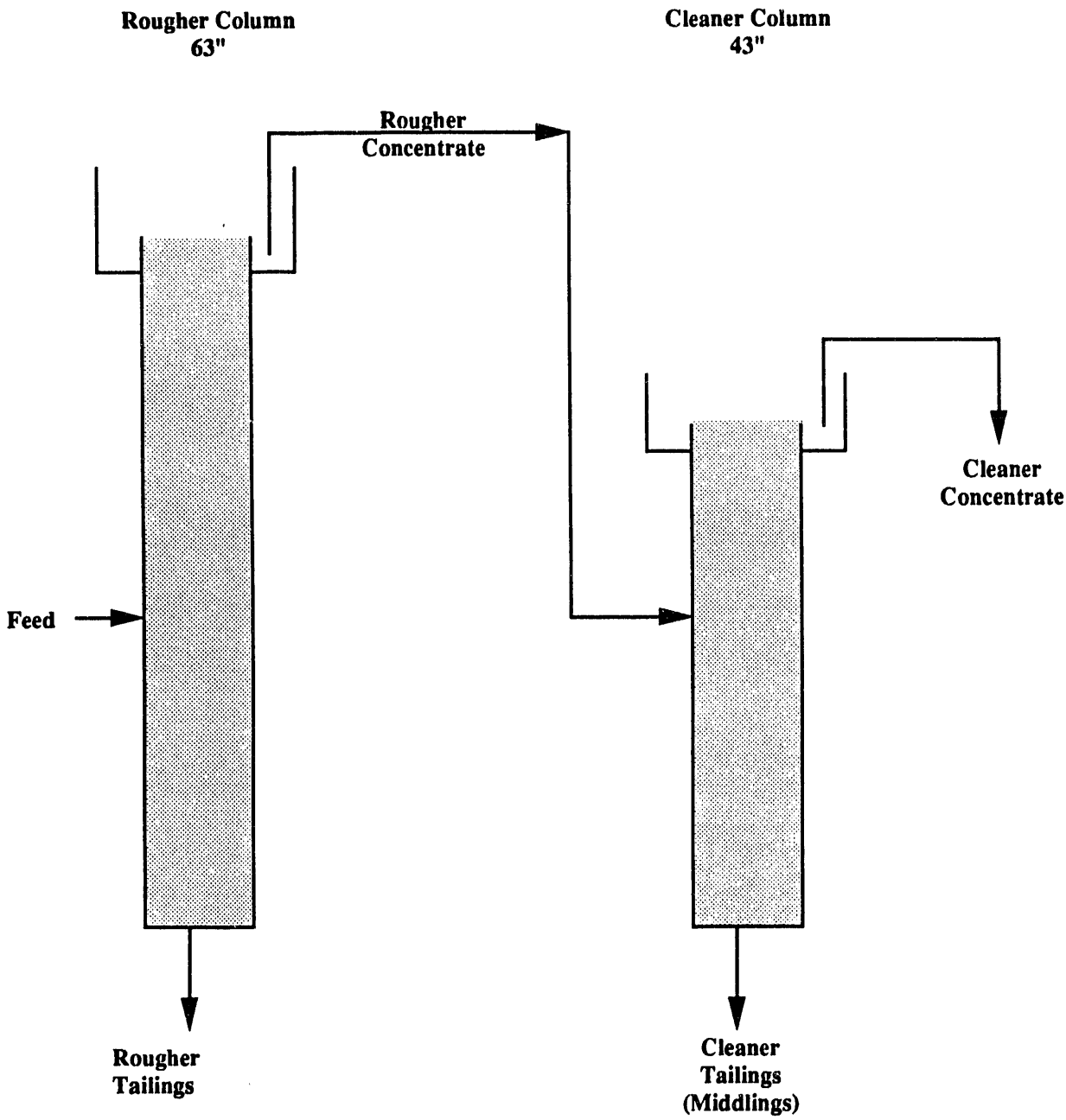

Figure 4-6. TWO-STAGE COLUMN FLOTATION CIRCUIT

Size analyses were performed on the products from Test 1. The cleaner concentrate was the coarsest product having a d_{90} of 21 μm. This suggests that no regrinding of the middling may be necessary and that it can be returned directly to the rougher column or to a scavenger cell. This conjecture must be experimentally confirmed.

Flotation Tests on -325 Mesh Shale. A sample of raw shale was ground to -325 mesh in a laboratory rod mill. The purpose was to determine whether grinding to a finer size in the primary mill would substantially decrease the weight of material that would require grinding in the stirred ball mill. The size distribution of the -325 mesh product is tabulated in Table 4-10 together with the size distribution of the -100 mesh shale discussed earlier. (Additional grinding tests performed on this sample are discussed in Task 4.5.)

Table 4-10. SIZE DISTRIBUTION OF SHALE SAMPLES GROUND TO -100 AND -325 MESH

	Cumulative % Retained	
Size, μm	100 mesh Grind	325 mesh Grind
+48	25.9	3.4
-48+32	37.1	15.5
-32+24	44.2	26.7
-24+16	54.7	43.1
-16+12	62.5	55.1
-12+8	70.9	66.6
-8+6	76.4	74.0
-6+4	83.1	81.7
-4+3	87.3	86.6
-3+2	91.7	91.5
-2+1	96.1	96.3
-1+pan	99.5	99.4

Column flotation tests were conducted on the -325 mesh sample to determine if oil shale flotation could be extended to coarser sizes. The results, however, were inconclusive and are not reported.

Column Flotation Tests With Recycled Water. In any commercial shale beneficiation plant, sizable quantities of water will be required. Flotation requires about 20 tons of water per ton of shale processed. To conserve water brought into the plant, and because the process water cannot be discharged to the environment without treatment, it will be necessary to recycle water from a closed tailings impoundment back to the primary plant. Because the flotation process is sensitive to the chemical environment, there is a question as to whether the use of recycled water also has a detrimental effect on the quality of separation achieved.

To answer this question, MRI set up a laboratory tailing pond system to permit repetitive batch column flotation tests with recycled water. A 55-gallon drum was filled with water used in grinding the 800-pound bulk sample discussed earlier. This water was used to grind batches of shale in the

laboratory rod and stirred ball mills. The same water was used to rinse the grinding media and to dilute the ground shale in flotation. Column flotation tests were performed at a series of air flow rates to establish a grade recovery curve. At the conclusion of daily operations, the accumulated tailings were returned to the "pond." Accumulated concentrates were filtered and the filtrate returned to the tailings pond. After two to three weeks, water was siphoned from the pond for a new cycle of grinding and flotation on a new shale sample.

This process was repeated through six cycles of regrinding and flotation. The results are summarized in Figure 4-7. Data from cycles 1 and 2 and from cycles 5 and 6 are compared with a grade-recovery curve established by several column flotation tests on the same sample. Clearly, the data from cycles 1 and 2 fall on the baseline curve, while those from cycles 5 and 6 show serious degradation in the quality of flotation. Data from cycles 3 and 4 have been omitted for clarity, but show intermediate effects.

Conclusions and Recommendations

The results indicate that a simplified flowsheet, such as shown in Figure 4-8, may be used to beneficiate oil shale. This scheme is simpler than that previously proposed (Figure 4-1) in that only one stage of stirred ball milling and one fine sizing operation are employed. In contrast, the previous flowsheet employed two stages of each. This conclusion is based primarily on the two-stage flotation test summarized in Table 4-9.

Questions remain in the implementation of such a system. First, what is the optimum size that the primary ball mill should produce? Table 4-10 shows that only moderately more fines are produced when grinding to -325 mesh compared to grinding to -100 mesh. However, grinding the oversize fraction to a d_{90} of 22.8 μm requires 64.7 kWh/t, while grinding the oversize fraction from a -325 mesh grind would require 53.9 kWh/ton. A detailed economic analysis that accounts not only for energy consumption, but also unit capacity (and hence capital cost) will be required to select the preferred alternative.

Sizing of the product from the primary ball mill remains a problem. If, as projected in Figure 4-8, the separation is made at about 20 μm, then it is important that all the -20 μm material be captured as screen undersize or cyclone overflow. Fine sizing operations are quite inefficient. For example in Table 4-6, the screen oversize (product C) still contains 20 percent -12 μm material after a combination of cycloning and screening. This represents an increase in the energy consumption on the stirred ball mill. MRI recommends that high efficiency sizing circuits be developed.

Flotation tests with recycled water show a degradation in the quality of separation achieved. It has not been determined whether the loss of flotation efficiency is due to the accumulation of excess frother in the water, the decrease in the pH of the water, or the build up of soluble ions in the water. MIT recommends that further work be performed with recycled water to isolate the cause of the degradation observed and to establish a water treatment method.

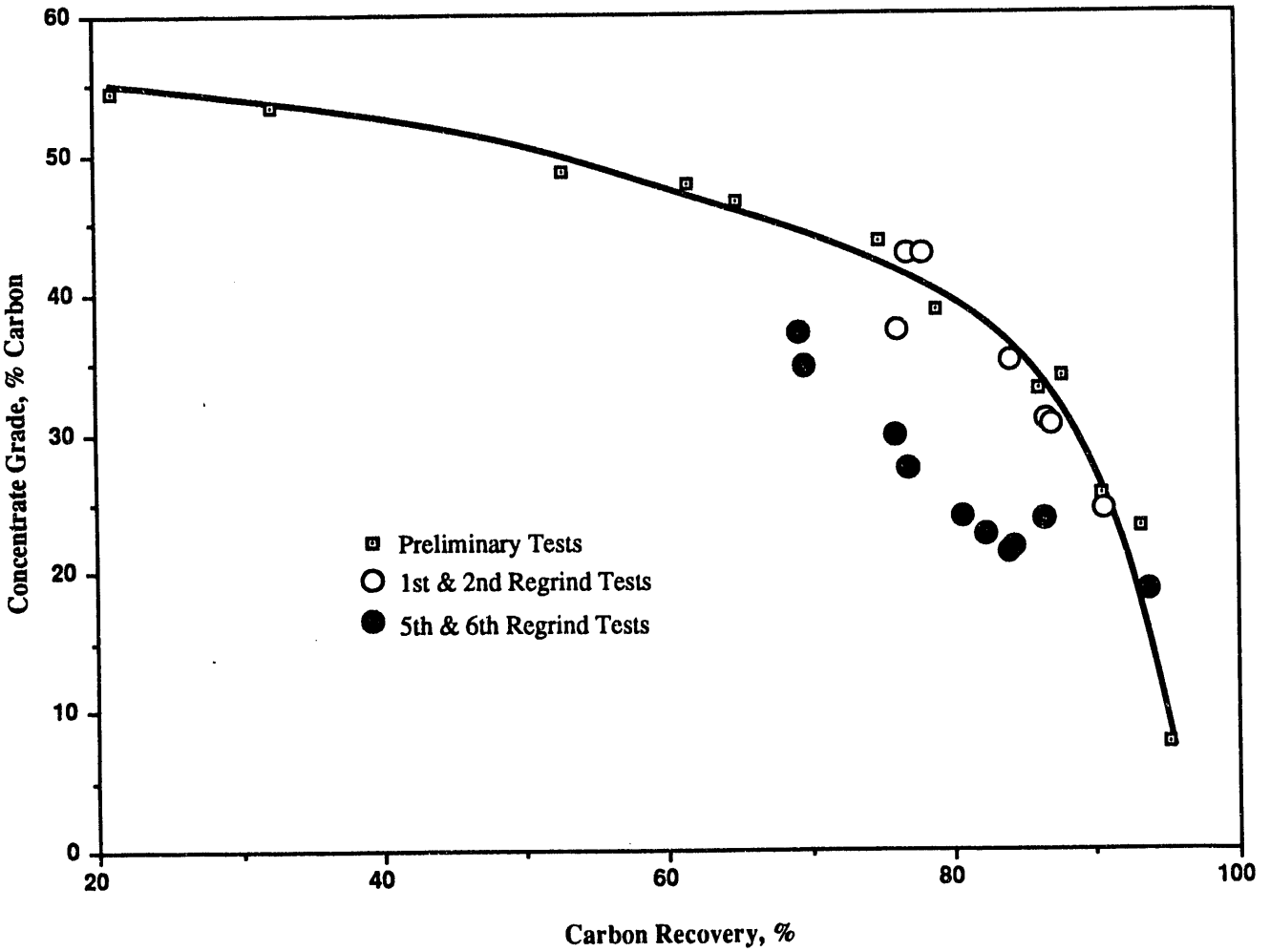

Figure 4-7. THE EFFECT OF WATER RECYCLING ON FLOTATION PERFORMANCE

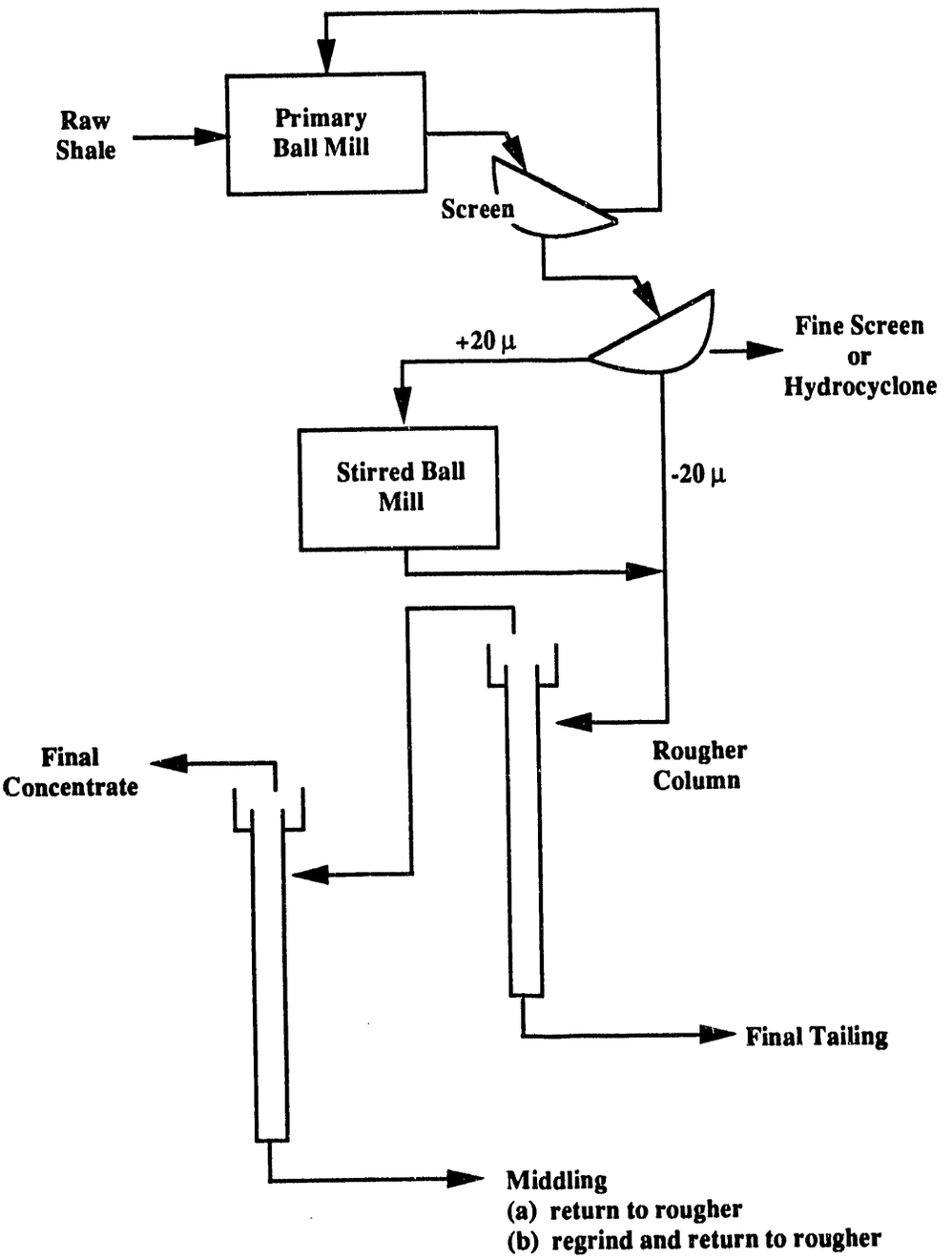

Figure 4-8. CURRENTLY PROPOSED GRINDING-FLOTATION FLOWSHEET

Subtask 4.4. Integrated Grinding and Flotation

The objectives of this subtask were to determine the column flotation characteristics of Eastern shale and to investigate the application of a novel integrated grinding and column flotation technique in a single-stage operation. The University of Kentucky Center for Applied Energy Research (UK-CAER) is evaluating the advanced Ken-Flote column flotation technique in conjunction with the BDR Mill column to obtain a high grade [>125.2 L/metric ton or >30 gallons per ton (GPT)] shale concentrate at more than 90 percent carbon recovery. The BDR Mill column utilizes a single-stage grinding/cleaning system that avoids overgrinding the shale. The goals of the project are to remove up to 90 percent of the inorganic minerals using minimum grinding energy.

Background

Oil shale beneficiation is typically considered as part of the above-ground processing technology for shale oil recovery. Reducing the cost and size of the retort for extracting shale oil via relatively low cost beneficiation is an area worthy of investigation. The physical beneficiation technique in mineral technology exploits differences in the physical-chemical properties between the mineral components of an ore. The major components in shale are organic matter (kerogen and bitumen), which is hydrophobic and inorganic matter, which is hydrophilic. Thus, separation of the organics from inorganics could be achieved using surface chemical-based processes such as froth flotation or oil agglomeration.

Various researchers have reported flotation and agglomeration results with Western and Eastern shales. Grinding of Eastern shale to 80 percent passing 7 μm size for flotation using pine oil provided upgrading of organics from 8 to 21 percent. Regrinding and refloating the concentrate improved the grade of the product; however, the overall recovery decreased.

Column flotation has been shown to be effective in beneficiation of ultrafine coal and mineral particles. MRI has conducted column flotation studies on Eastern shales and reported obtaining higher grade and recovery of kerogen when the feed was introduced into the froth phase. MRI also reported that addition of reagentized wash water improved concentrate grade, but diminished recovery, while increasing column height improved flotation performance.

At UK-CAER, the Ken-Flote column flotation process has achieved success in obtaining fine-size, low-ash clean coal at high recovery from ultrafine ground coal. The process has been in commercial use for the past two years. UK-CAER, in cooperation with B. Datta Research, has conducted fine coal cleaning research using the SYMUSEP separator that utilizes grinding and cleaning in a single stage column flotation unit. The SYMUSEP separator avoids overgrinding of material and, thus, saves energy during grinding. The current research program used the SYMUSEP Separator column system for beneficiation of Eastern shale. The Ken-Flote column flotation parameters were to be optimized for Eastern shale and then tests with the SYMUSEP Separator were to be conducted.

Equipment Descriptions

Initial fine grinding studies of the shale were conducted using a modified Attritor Mill (Figure 4-9), which can also monitor the amount of energy consumed during grinding. For most of the column flotation tests, shale grinding was done using the Drais-Werke Mill (Figure 4-10). Compared to the 60-minute grind time for the batch attritor mill, this mill produced 90 percent passing 12 μm particles in about 5 minutes retention time.

Column flotation experiments were conducted using the pilot-scale 2-inch ID, 20-foot high Ken-Flote column (Figure 4-11). A porous rubber tube was used for generating bubbles in the column. A few experiments were conducted using a foam jet sparger device (Figure 4-12). Samples of the froth and tailings were collected simultaneously for a known length of time and analyzed for organic carbon content. Column flotation tests conditions are given in Table 4-11.

Table 4-11. COLUMN FLOTATION TEST CONDITIONS

Column Dimensions	
Diameter, inches	2
Height, feet	20
Recovery Zone Height, feet	16-12
Froth Depth, feet	4-8
Froth Wash Zone, feet	2.5
Froth Drain Zone, feet	1.5
Feed Level, feet	14
Feed Rate (5 wt % solids), gal/min	0.13-0.39
Wash Water Rate, gal/min	0.05-0.16
Air Flow Rate, ft^3/min	0.05-0.10
Reagents, lb/ton	
Frother	1.5
Fuel Oil Collector	1.0

A schematic diagram of the SYMUSEP Separator that utilizes grinding and cleaning in a single stage is shown in Figure 4-13. A torque meter was attached to the separator to monitor grinding energy consumed. The flotation procedures used for tests conducted with the SYMUSEP separator were essentially the same as those utilized for the tests using the Ken-Flote column.

Results and Discussion

Chemical, maceral, and Fischer Assay (FA) analyses of a head sample of the Alabama shale are presented in Table 4-12. The FA oil yield was determined to be 14.6 GPT and the organic carbon content was 16.46 percent. The principle maceral present was lamalginite with smaller amounts of telaginite and vitrinite.

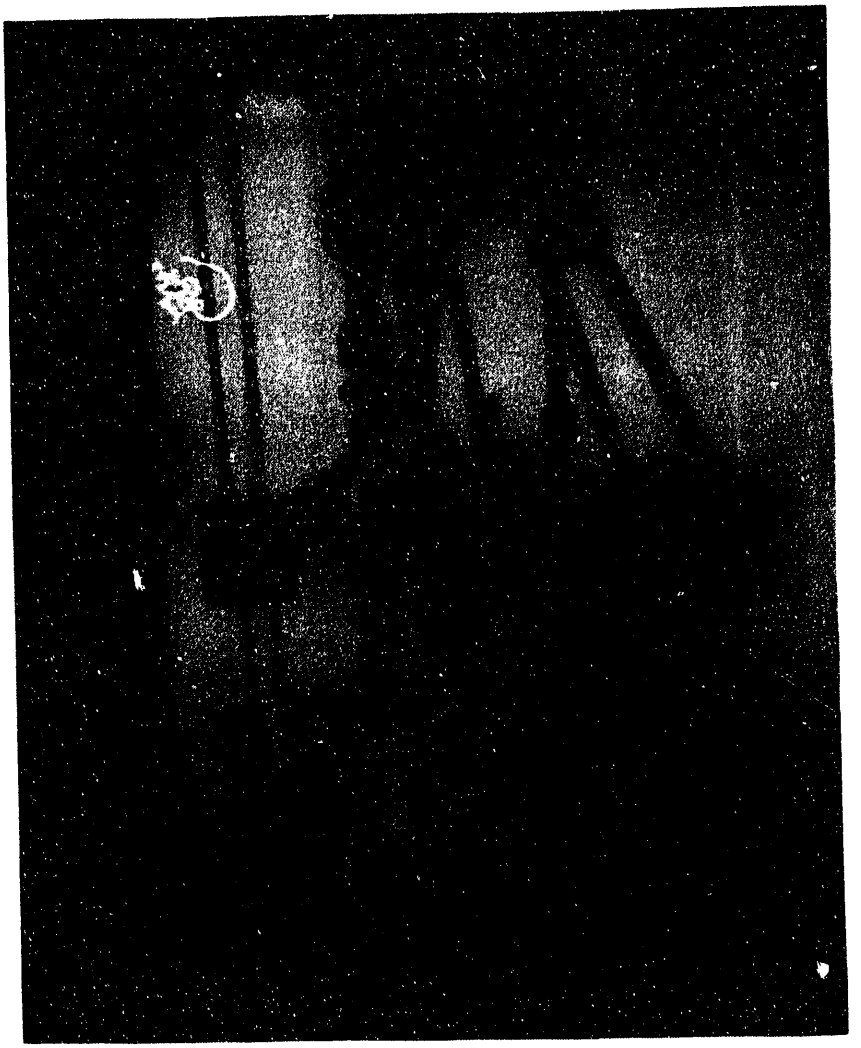

Figure 4-9. MODIFIED ATTRITOR MILL

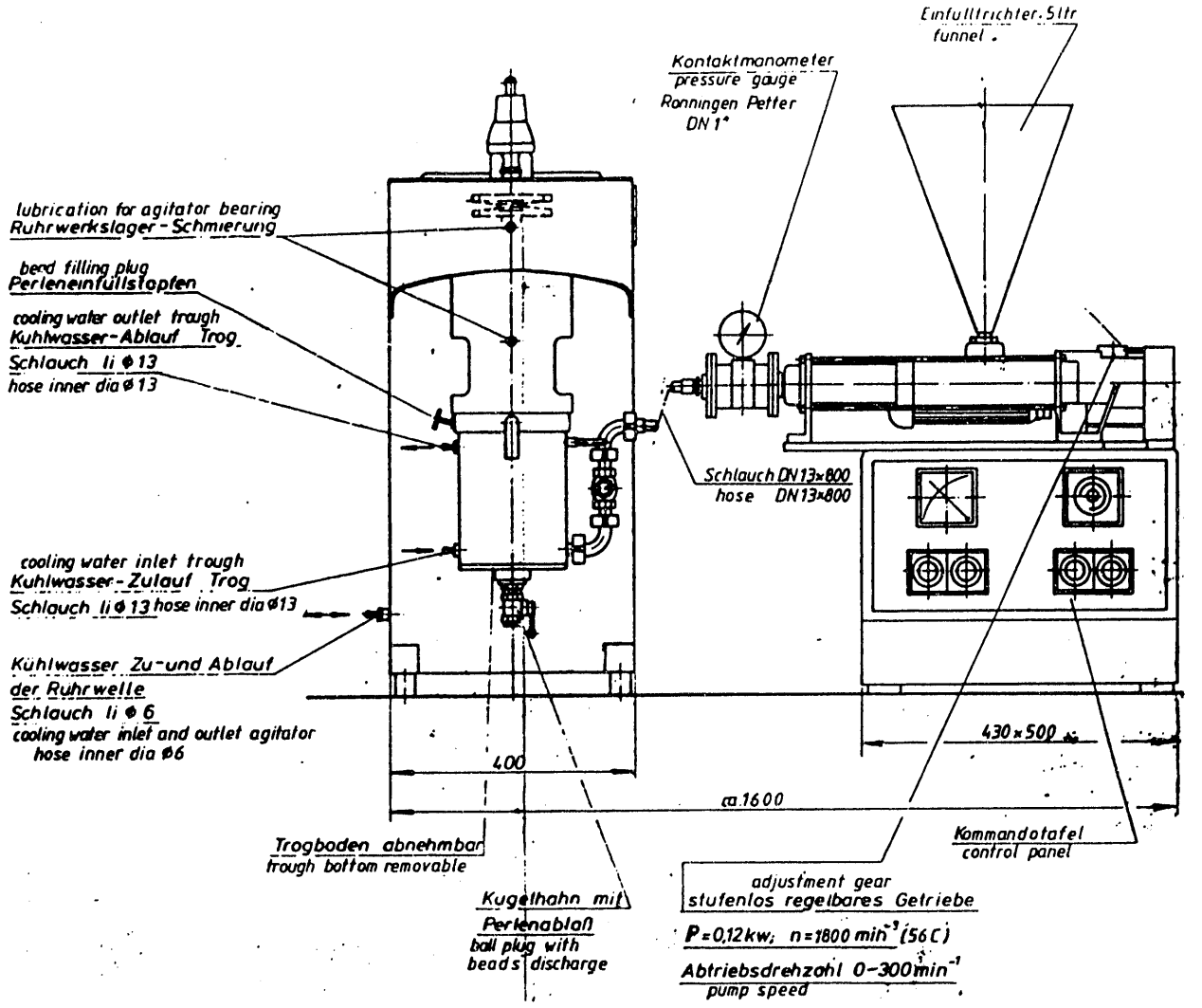

Figure 4-10. DRAIS-WERKE MILL

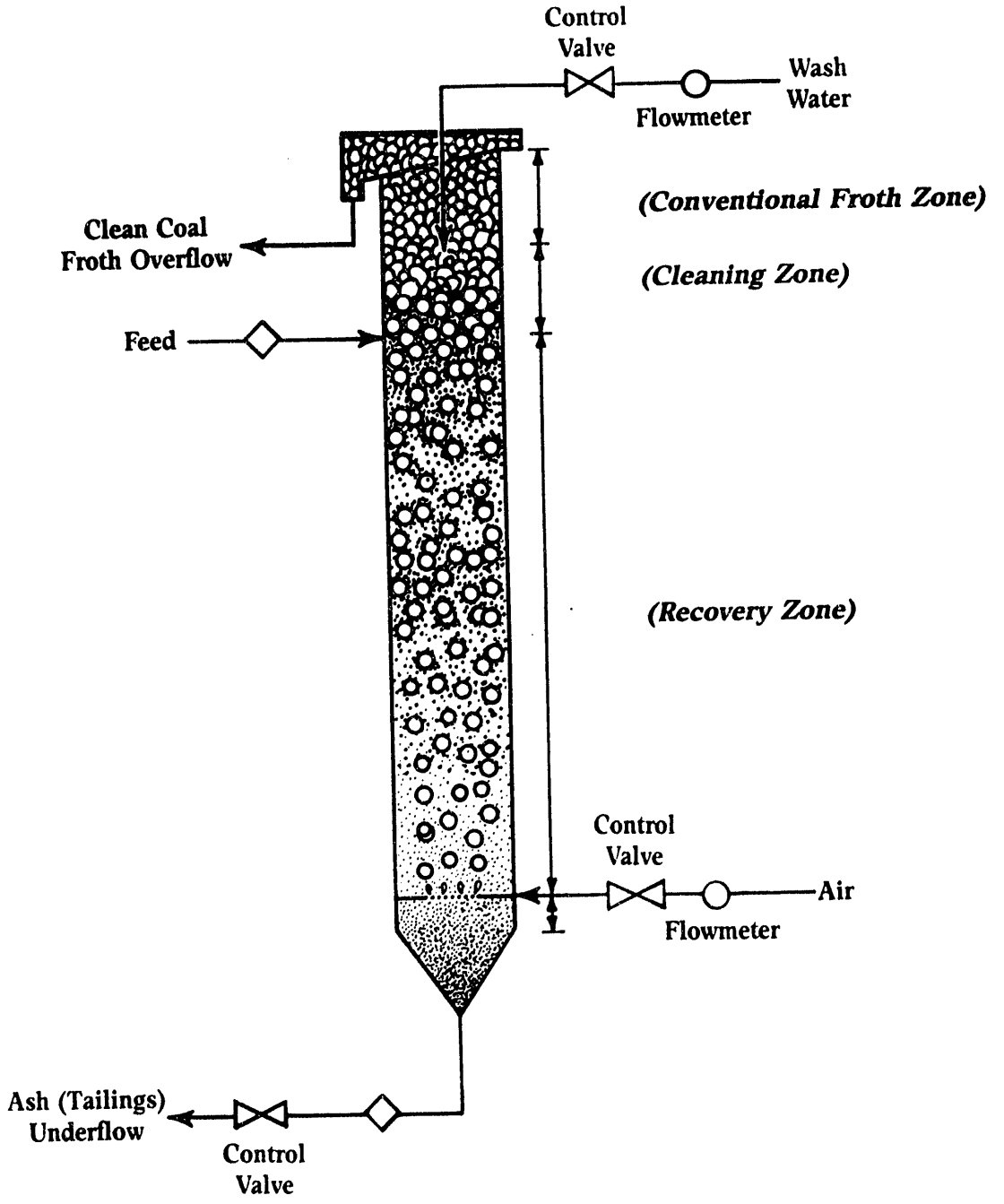

Figure 4-11. SCHEMATIC OF KEN-FLOTE COLUMN

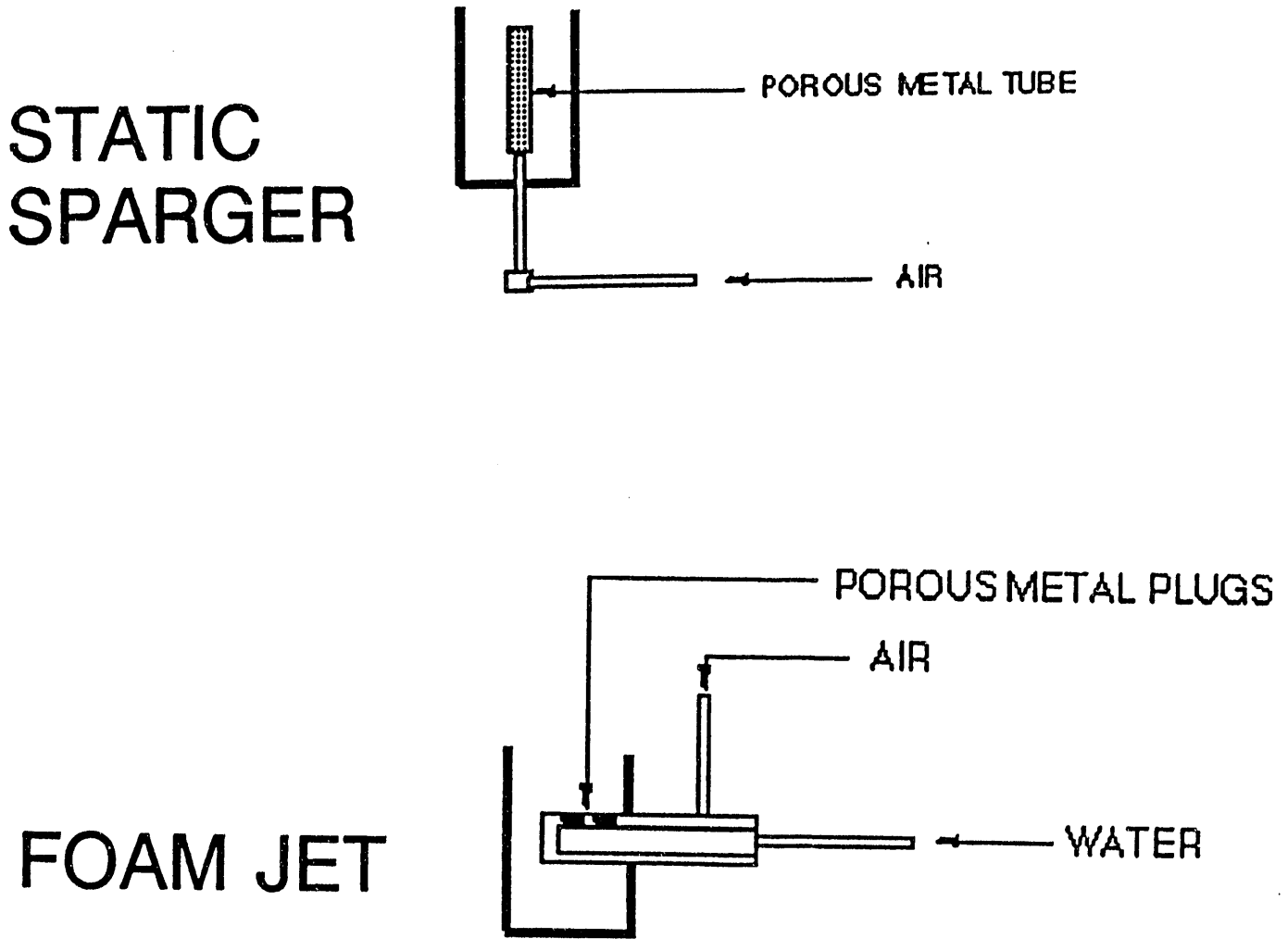

Figure 4-12. LINE DIAGRAMS OF STATIC AND FOAM JET SPARGERS

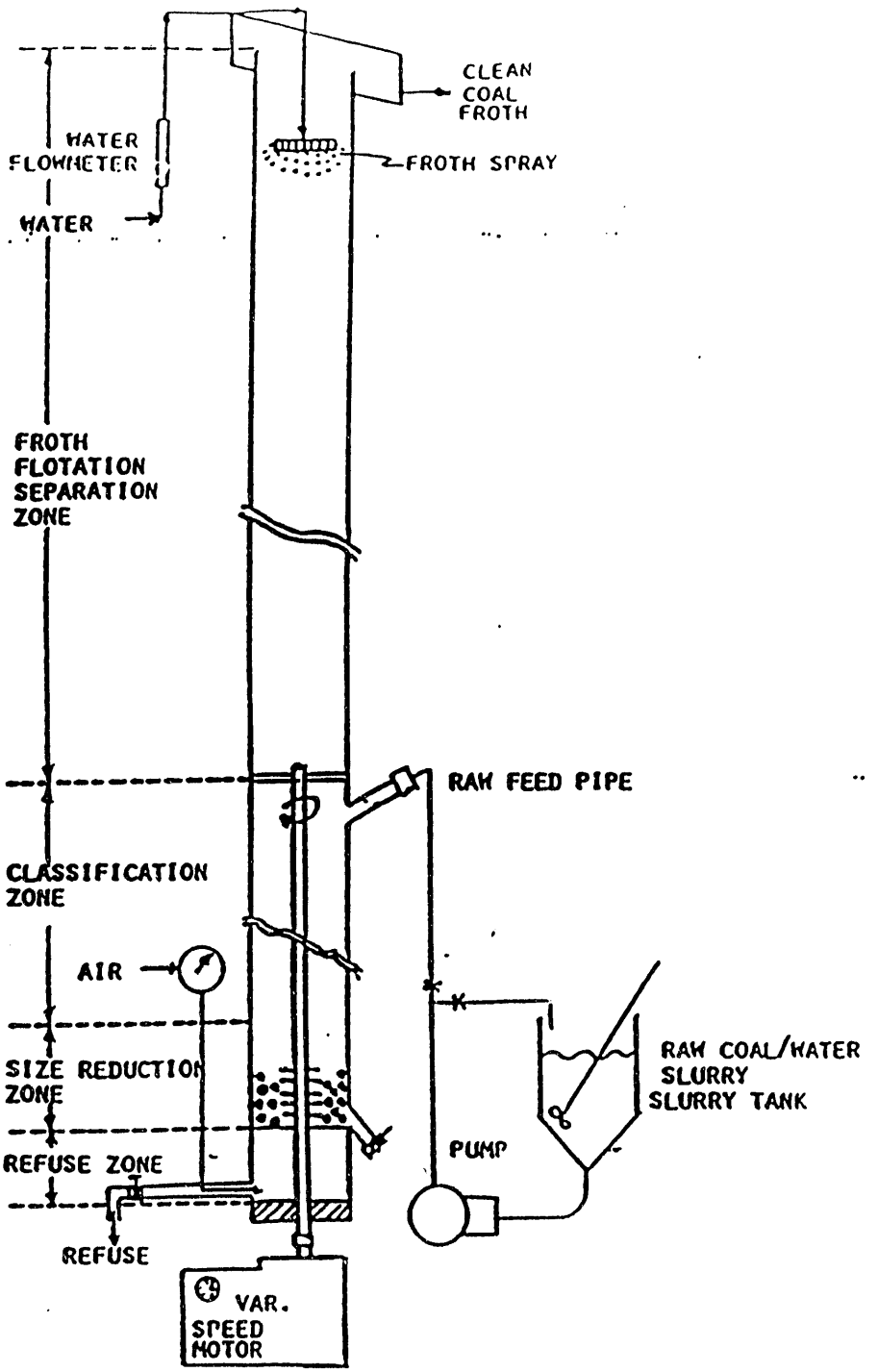

Figure 4-13. SCHEMATIC OF SYMUSEP SEPARATOR

TABLE 4-12. CHEMICAL AND MACERAL ANALYSES OF OIL SHALE

Component, wt %	
Moisture	1.18
Ash	72.80
Organic Carbon	16.46
Volatile Matter	15.80
Sulfur	8.20
Fischer Assay Oil Yield, GPT	14.6
Maceral Analysis, wt %	
Lamalginite	81.0
Telaginites (Tasmanite and Telaginite)	12.0
Vitrinite	5.6
Inertinite	1.4
Liptinite	Trace
Total	100.0

Figure 4-14 shows the cumulative energy consumption for grinding shale to 90 percent passing 10 μm using the Attritor Mill. To reduce the shale from 90 percent passing 15 μm to 90 percent passing 10 μm, the energy consumption increased from about 90 to 190 kWh/ton. The cumulative time to grind the sample from 90 percent passing 15 to 10 μm increased from about 30 to 60 minutes.

Baseline flotation tests were conducted using the Denver flotation machine to determine the optimum amount of frother and fuel oil for recovering 90 percent of the kerogen. Frother was tested in the range of 0.57 to 1.75 lb/ton. The effect of frother addition (Betz M252) on the yield of floatable material is shown in Figure 4-15. It is apparent that about 1.5 pound/ton of the frother is optimum. Fuel oil addition as high as 1.5 lb/ton had no significant effect on improving recovery of kerogen.

The Ken-Flote column flotation studies were conducted on shale ground to 90 percent passing 10 μm. The ground slurry was diluted to 5 percent solids and reagents were added before the slurry entered the column. Figure 4-16 shows the effect of air flow rate on organic carbon recovery and concentrate grade using the static porous tube sparger. Increasing the air flow from 1 to 3 L/min increased carbon recovery from 26 to 57 percent; however, the concentrate grade remained constant at about 62 percent carbon. Increasing the rate of wash water addition did not improve concentrate grade but did reduce recovery by diluting the froth phase and adversely effecting froth stability. Similarly, increasing froth height also lowered recovery by reducing retention time. Froth height had no significant effect on concentrate grade. The use of sodium metaphosphate as an ash dispersant adversely effected both recovery and concentrate grade.

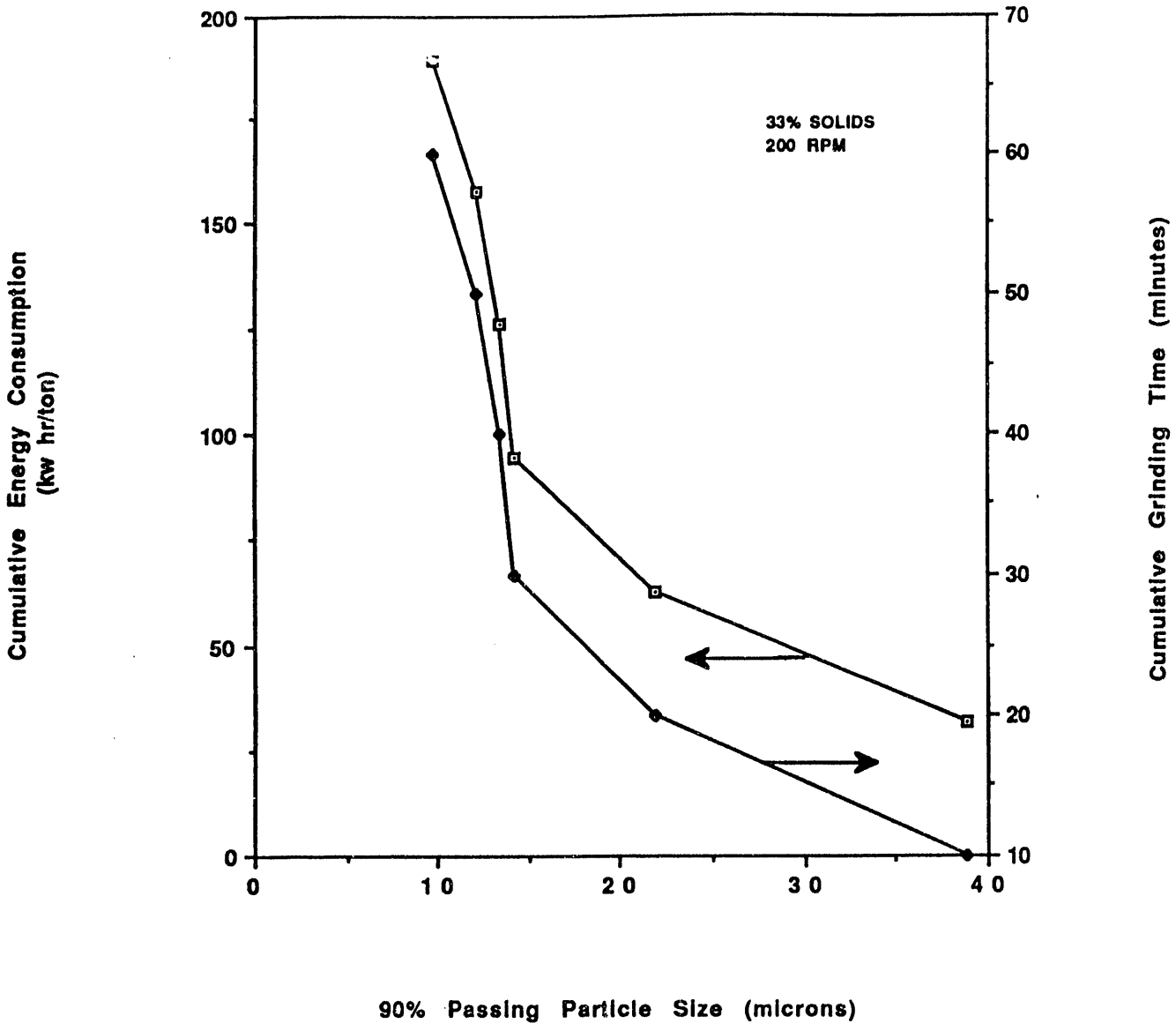

Figure 4-14. CUMULATIVE ENERGY CONSUMPTION FOR GRINDING OIL SHALE TO VARIOUS PARTICLE SIZES USING THE ATTRITOR MILL

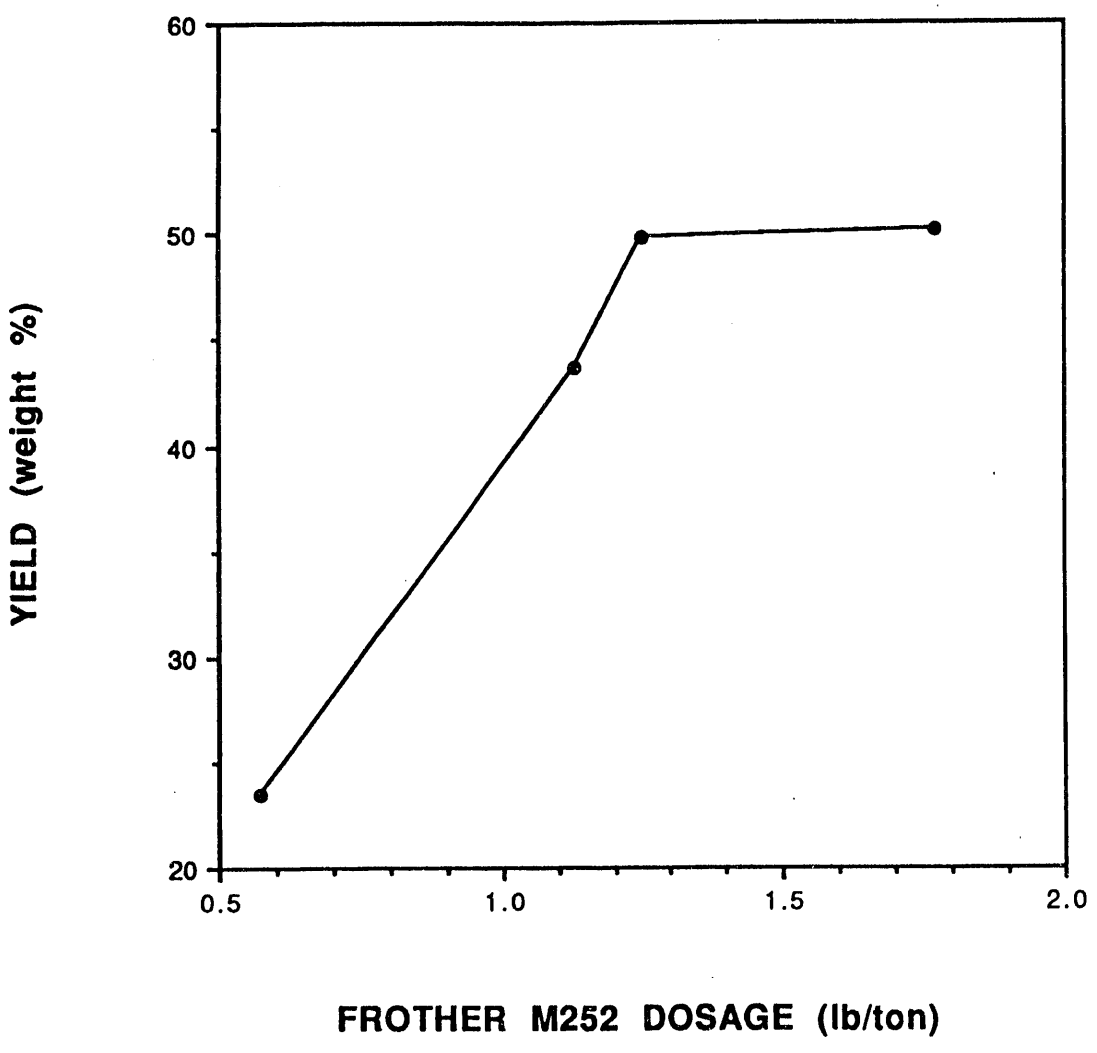

Figure 4-15. EFFECT OF FROTHER DOSAGE ON YIELD

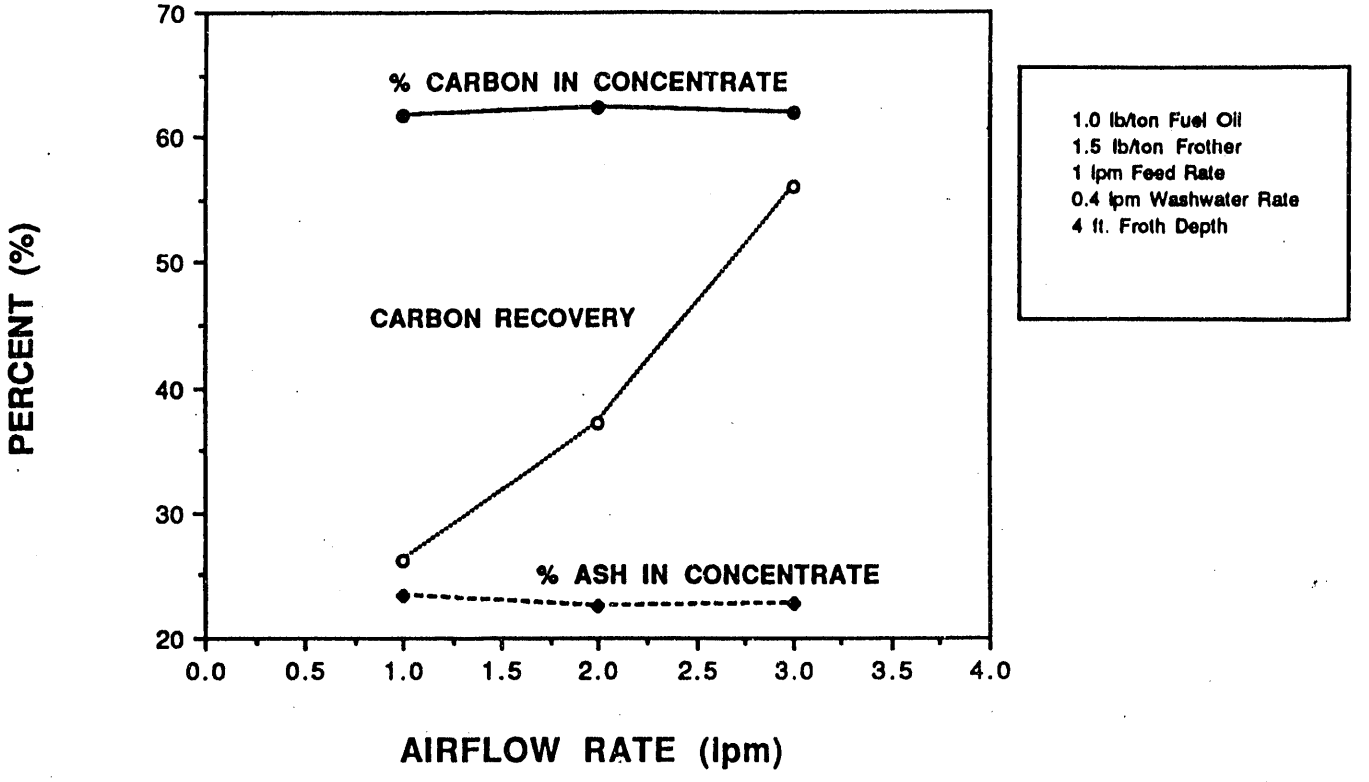

Figure 4-16. EFFECT OF AIR FLOW RATE ON RECOVERY AND GRADE FOR COLUMN FLOTATION TESTING

Figure 4-17 shows the effects of pine oil addition on the carbon recovery and concentrate grade for air flow rates of 2 and 3 L/min. At a pine oil dosage of 2 lb/ton and air flow rate of 3 L/min, a carbon recovery of 73 percent and concentrate grade of 43 percent carbon were achieved. Decreasing the air flow rate to 2 L/min, decreased the carbon recovery to 65 percent, but increased the concentrate grade to 52.4 percent carbon.

UK-CAER also conducted studies to evaluate two stages of column flotation in which the rougher concentrate obtained in the first stage was floated again in a cleaner stage to improve the grade of the column froth product. As shown in Figure 4-18, in the rougher stage, the recovery of carbon was 54.7 percent with a concentrate grade of 42.8 percent carbon. Cleaner flotation of this product provided 54.8 percent carbon recovery with a concentrate grade of 56.75 percent. The overall recovery of this two-stage process was 30.0 percent with a final grade of 56.75 percent carbon. These results show that cleaner flotation can increase the carbon content of the final product, however the overall recovery was poor. To improve the overall recovery, it would be necessary to significantly increase recovery in the rougher flotation stage.

Figure 4-19 shows that pH in the range of 5 to 10.5 did not have any significant effect on either the carbon recovery or concentrate grade. Further, neither increasing the fuel oil dosage, changing frothers or adding dispersants improved flotation performance. It was determined that the most effective method for increasing carbon recovery without reducing concentrate grade was to increase retention time. The results (Figure 4-20) indicate that a retention time of at least 10 minutes was required to obtain 80 percent carbon recovery; however, the grade of the concentrate obtained was only about 20 percent carbon. Increasing the retention time from 20 to 30 minutes provided 75 to 85 percent recovery of kerogen, while the concentrate grade improved to a range of 40 to 48 percent carbon.

Other column flotation tests were conducted with a foam jet sparger, which uses a pressurized mixture of water and air. The results of these tests showed that a low feed rate and high water flow through the sparger gave higher recovery (Figure 4-21). At feed and push water rates of 0.5 L/min each, carbon recovery was 68 percent at a concentrate grade of 37.5 percent carbon. Increasing the feed rate (decreasing retention time) resulted in decreased recovery with little effect on concentrate grade.

Beneficiation studies using the SYMUSEP Separator were conducted to determine the effects of grinding speed, air flow rate, feed point, and grinding media charge. The results in Figure 4-22 show that at a grinding speed of 800 rpm, the carbon recovery was 87 percent and the concentrate grade was 23 percent. Increasing the grinding speed to 900 rpm decreased the carbon recovery to about 75 percent and slightly increased the concentrate grade to 25 percent carbon. Decreasing the air flow rate from 6 to 5 L/min increased concentrate grade from 23 to 30 percent carbon (Figure 4-23), but significantly reduced carbon recovery from 87 to 46 percent.

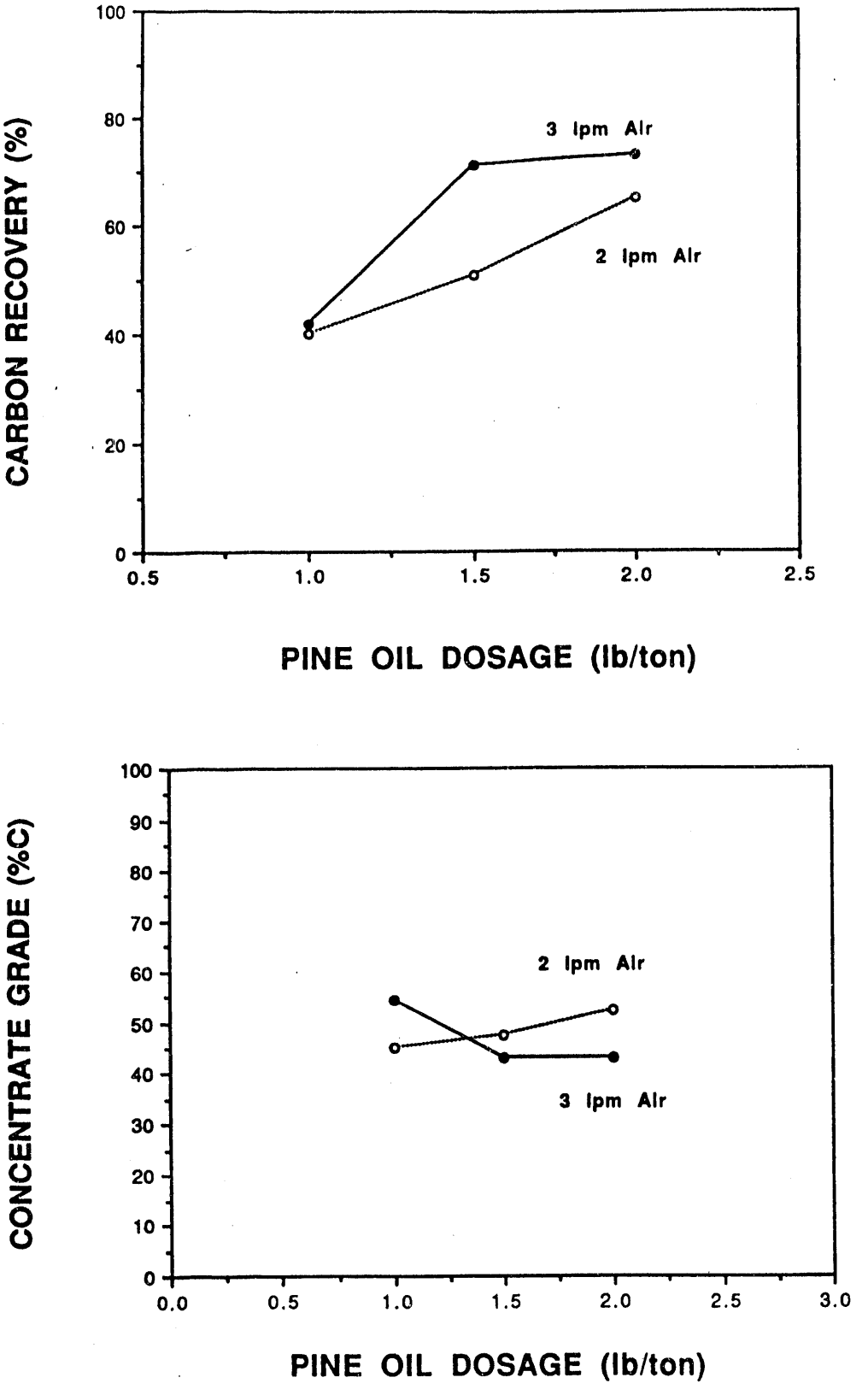

Figure 4-17. EFFECT OF PINE OIL ADDITION ON CARBON RECOVERY AND CONCENTRATE GRADE

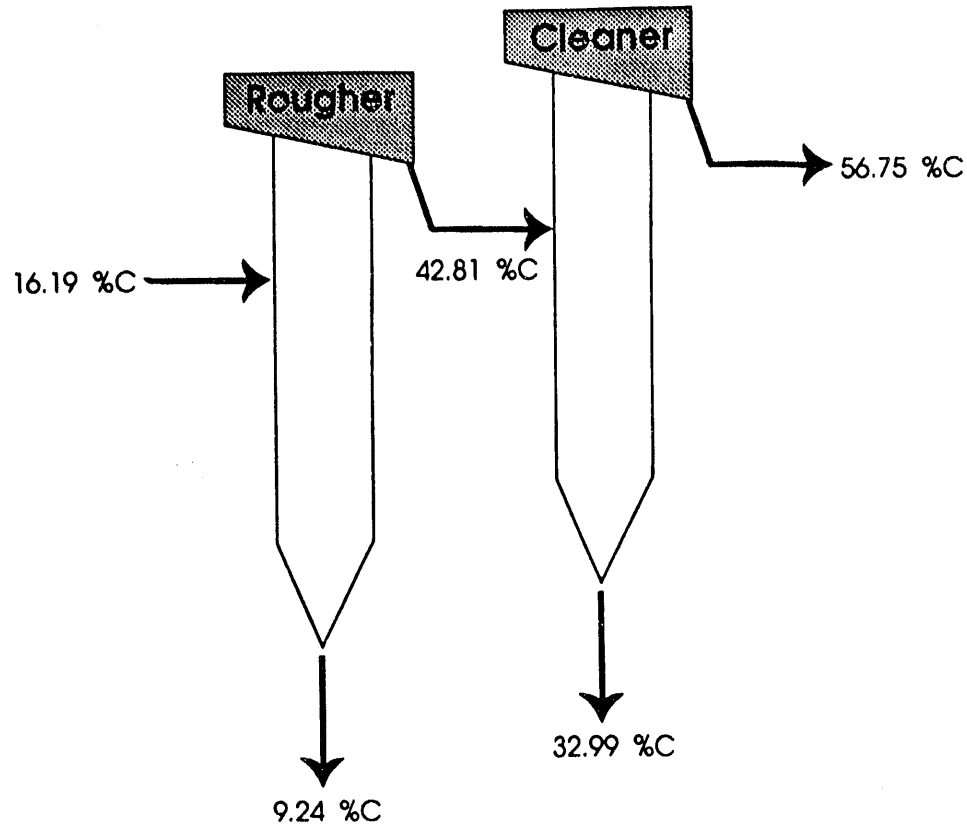

	Rougher Flotation	Cleaner Flotation
% Solids	5	2.6
Feed Rate (lpm)	1	6.5
Pine Oil Dosage (#/ton)	2	1
Washwater Rate (lpm)	0	0.4
Airflow Rate (lpm)	3	2
Carbon Recovery (%)	54.7	54.8
Yield (%)	20.7	41.3
Concentrate Grade (%)	42.81	56.75

Figure 4-18. TWO-STAGE COLUMN FLOTATION OF OIL SHALE

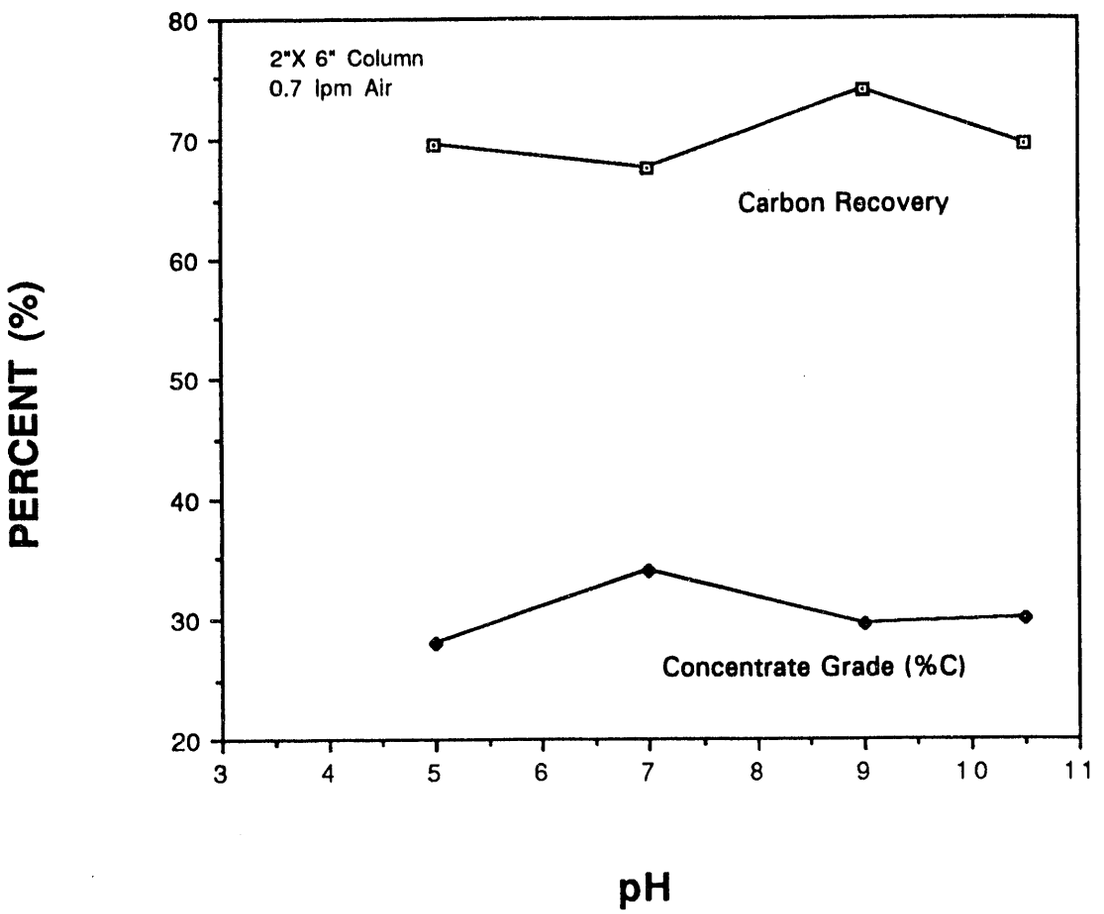

Figure 4-19. EFFECT OF pH ON CARBON RECOVERY AND CONCENTRATE GRADE

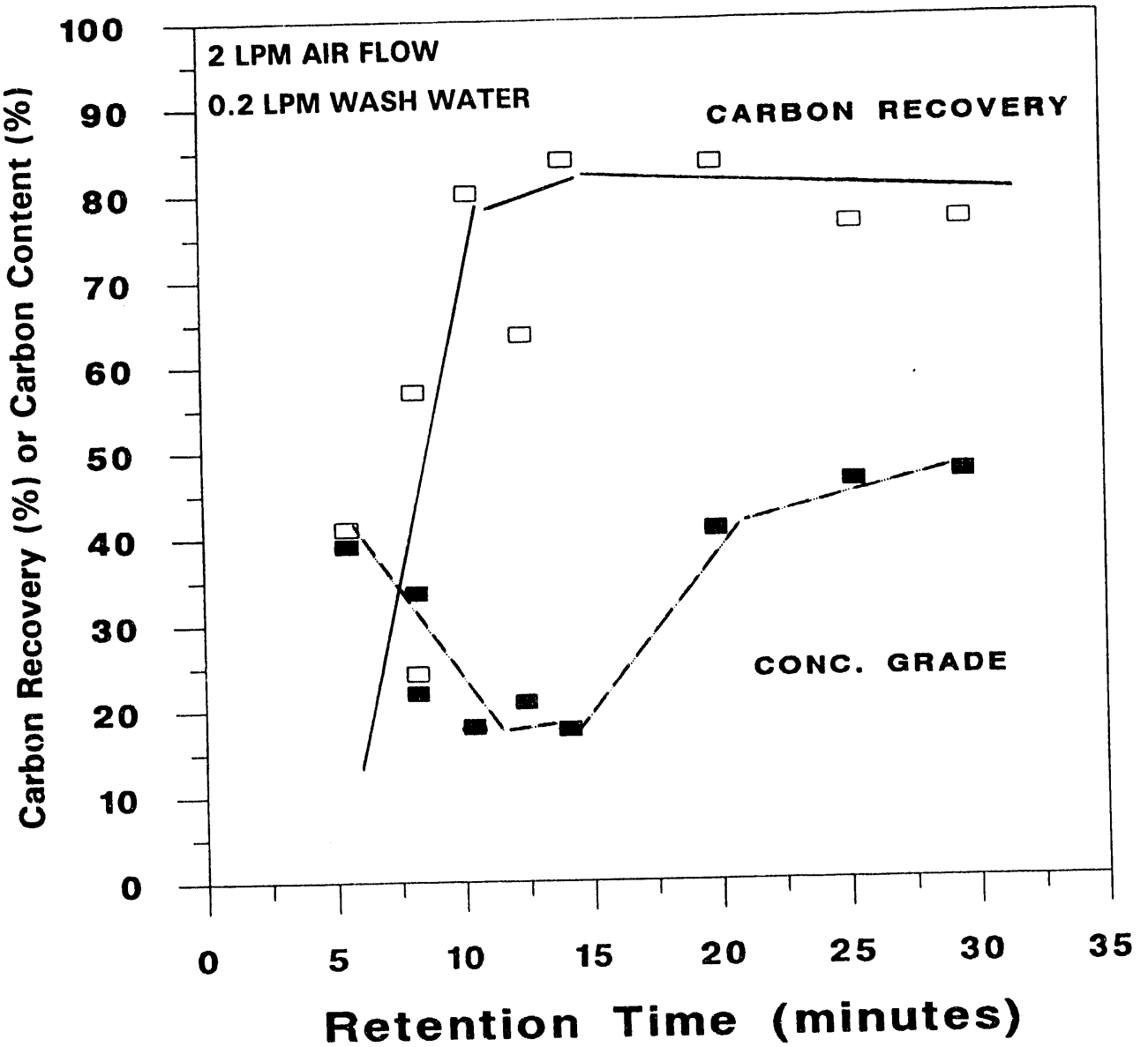

Figure 4-20. EFFECT OF RETENTION TIME ON CARBON RECOVERY AND CONCENTRATE GRADE

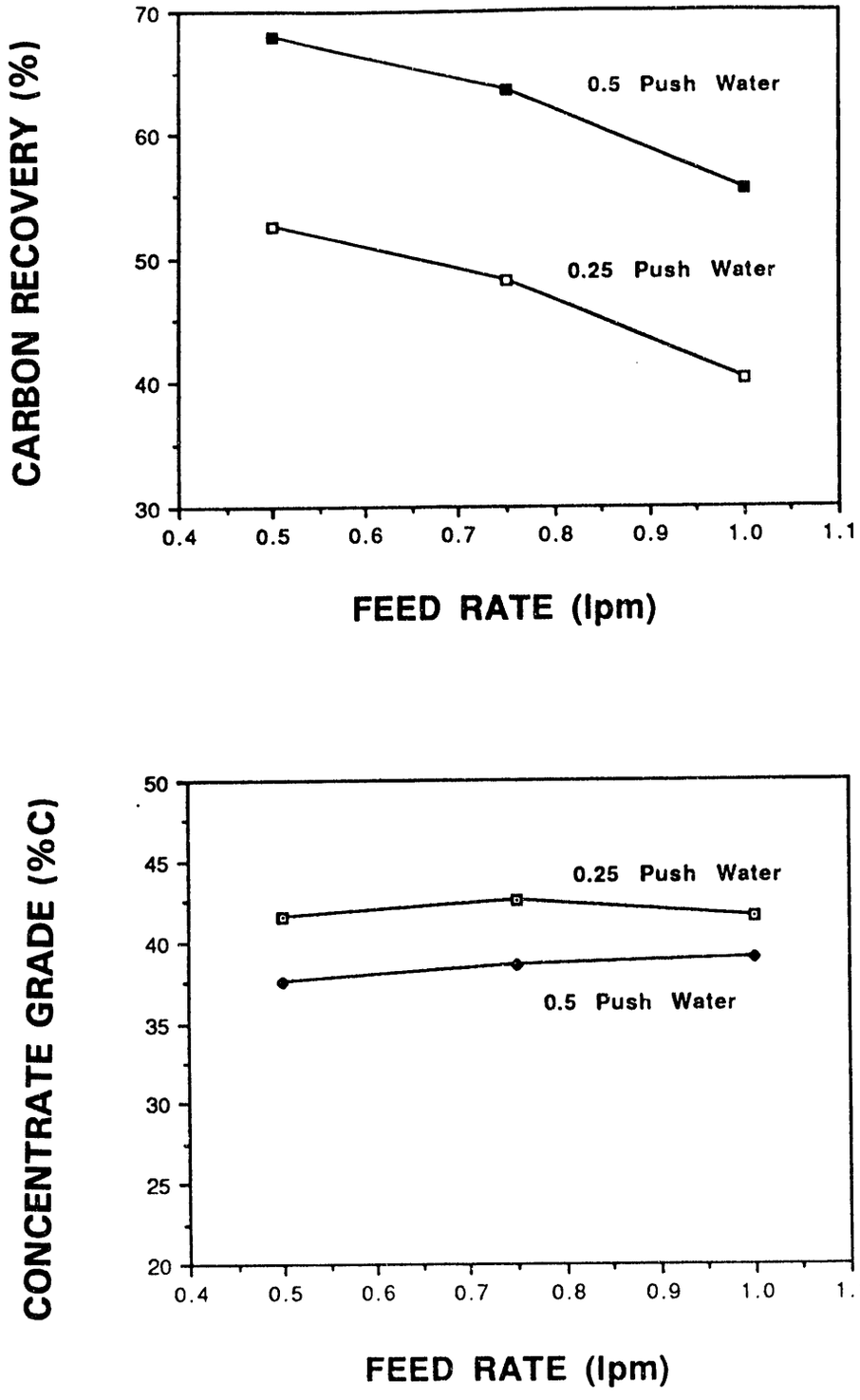

Figure 4-21. EFFECT OF FEED AND WASH WATER RATES THROUGH THE FOAM JET SPARGER ON CARBON RECOVERY AND CONCENTRATE GRADE

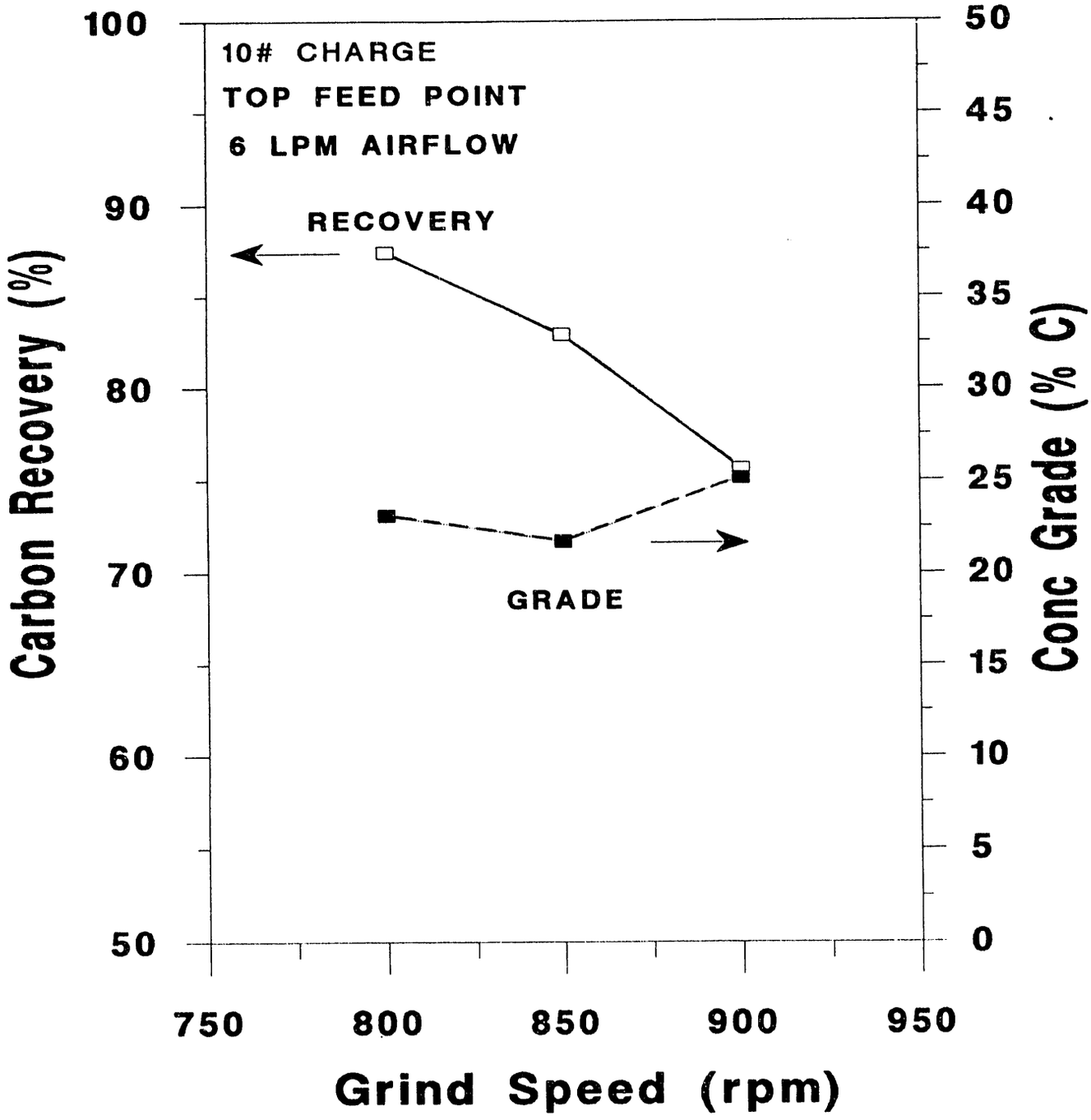

Figure 4-22. EFFECT OF GRIND SPEED ON CARBON RECOVERY AND CONCENTRATE GRADE IN THE SYMUSEP SEPARATOR

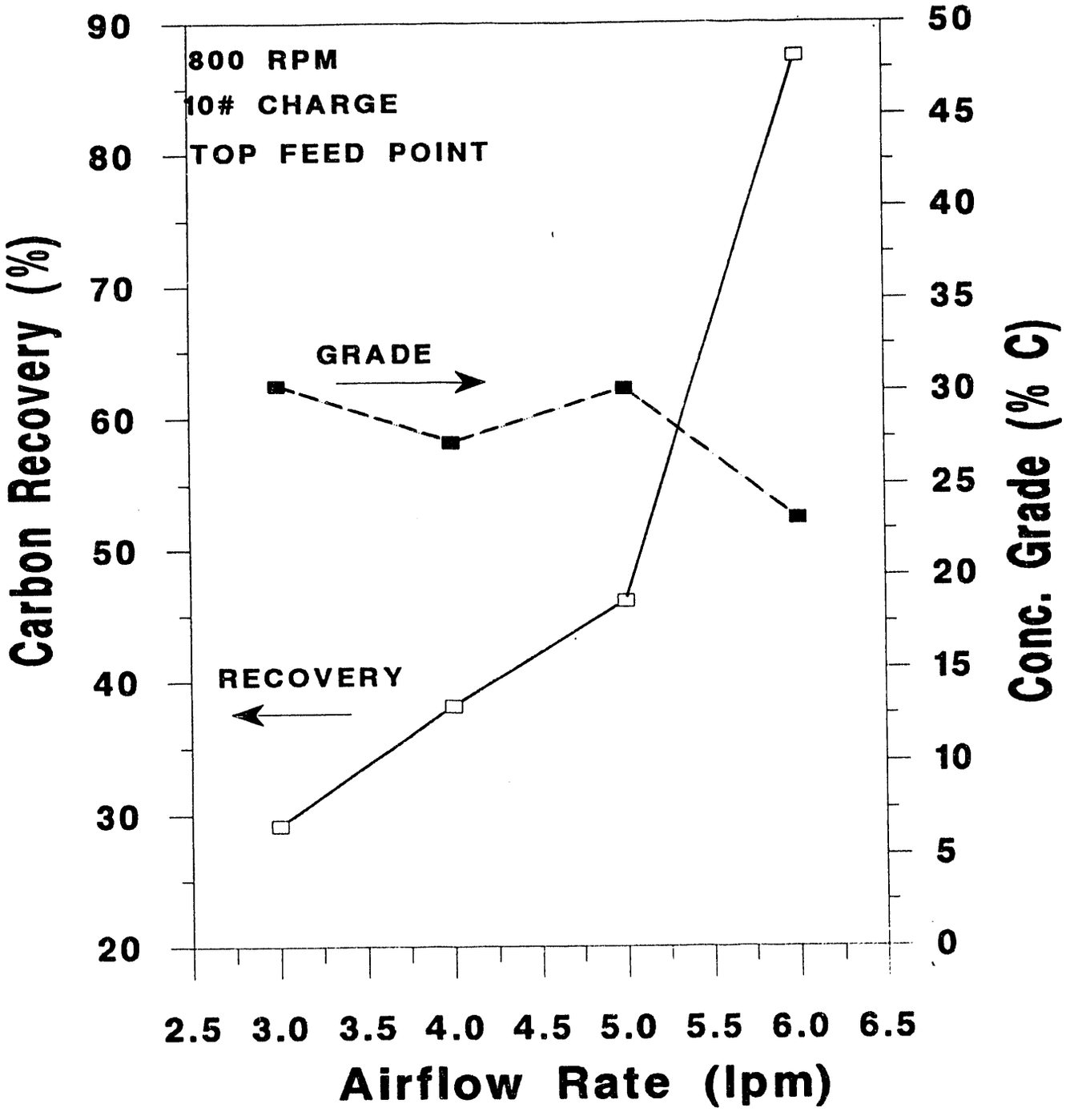

Figure 4-23. EFFECT OF AIR FLOW RATE ON CARBON RECOVERY AND CONCENTRATE GRADE IN THE SYMUSEP SEPARATOR

The effect of grinding media charge on concentrate grade and carbon recovery is shown in Figure 4-24. Increasing the grinding charge from 10 to 20 pounds at 900 rpm reduced the concentrate grade from 25 to 20 percent carbon, but did not significantly affect carbon recovery (76 to 77 percent). Grinding at 800 rpm showed large swings in carbon recovery and concentrate grade. The best combination of grade and recovery obtained with the limited number of tests conducted with the SYMUSEP separator was 25 percent carbon and 76 percent carbon recovery at 900 rpm.

Particle size analysis of the feed, concentrate and tailings (Figure 4-25) obtained from the SYMUSEP separator showed that the concentrate and tailings were essentially the same size (d_{90} = 16 μm), which was coarser than the grind size used in the Ken-Flote column (d_{90} = 10 μm). Low grade and recovery achieved with the SYMUSEP are attributed to incomplete kerogen liberation.

Conclusions

Based on these results, it can be concluded that -

- The kerogen liberation size was 90 percent passing 10 μm. The energy consumption required to achieve this size in the Attritor Mill was 190 kWh/ton.

- The Ken-Flote column with a static sparger for bubble generation achieved 57 percent carbon recovery with a concentrate grade of 60 percent carbon at an air flow rate of 3 L/min. Increasing air flow rate increased recovery, but significantly decreased concentrate grade.

- The Ken-Flote column with a foam jet bubble generator achieved 68 percent carbon recovery with a concentrate grade of 37.5 percent carbon at a feed rate of 0.5 L/min. Increasing the feed rate reduced retention time and decreased recovery.

- The minimum retention time required to obtain >80 percent recovery with high concentrate grade (>40 percent carbon) was 20 minutes. Decreasing retention time reduced concentrate grade.

- The best results obtained with the SYMUSEP separator were 75 percent carbon recovery with a concentrate grade of 25 percent carbon. The grind size to produce these results was 90 percent passing 16 μm, which was coarser than the grind used in the Ken-Flote column studies.

Recommendations

Based on the above, UK-CAER recommends that to obtain engineering and design data for larger-scale operation, pilot-plant studies in the beneficiation of the shale should be conducted using a 6-inch ID column.

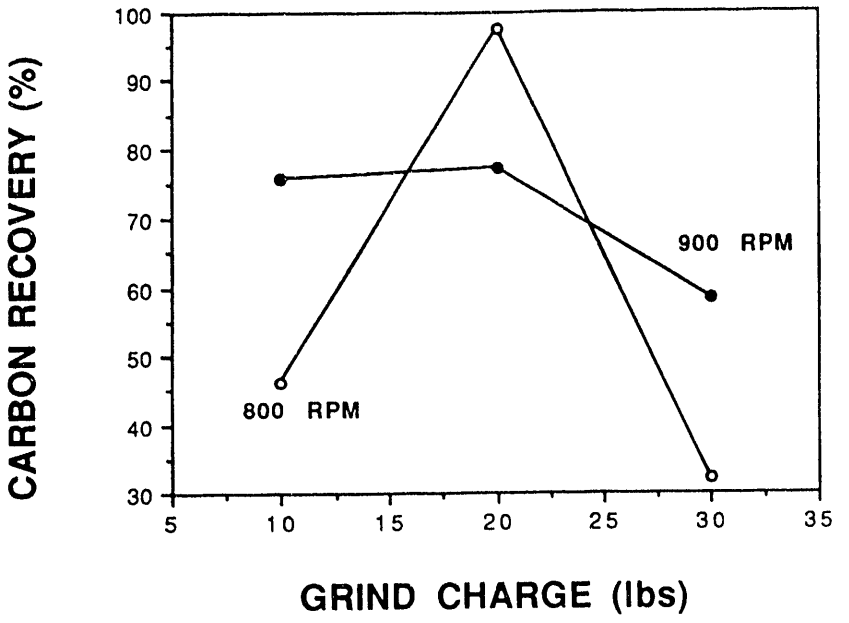

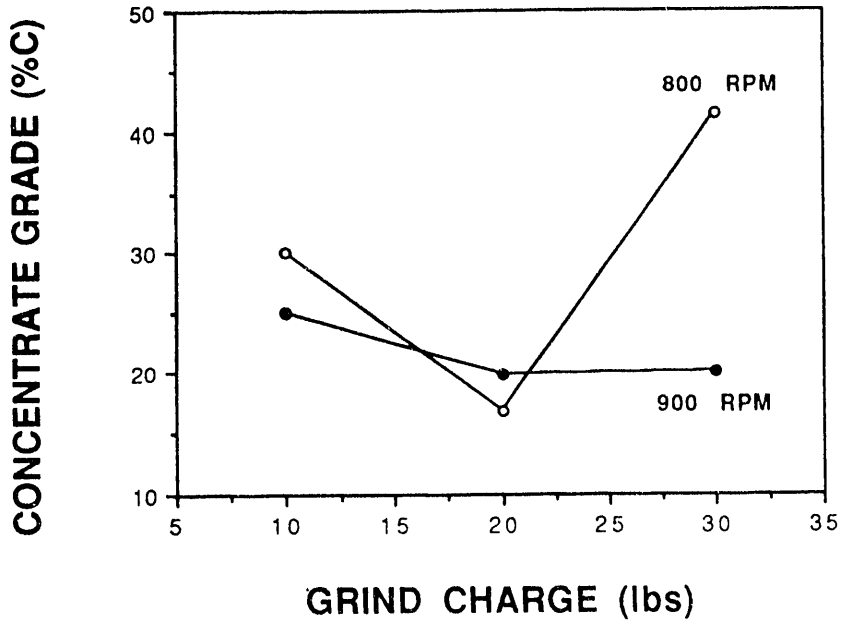

Figure 4-24. EFFECT OF GRIND CHARGE ON CARBON RECOVERY AND CONCENTRATE GRADE IN THE SYMUSEP SEPARATOR

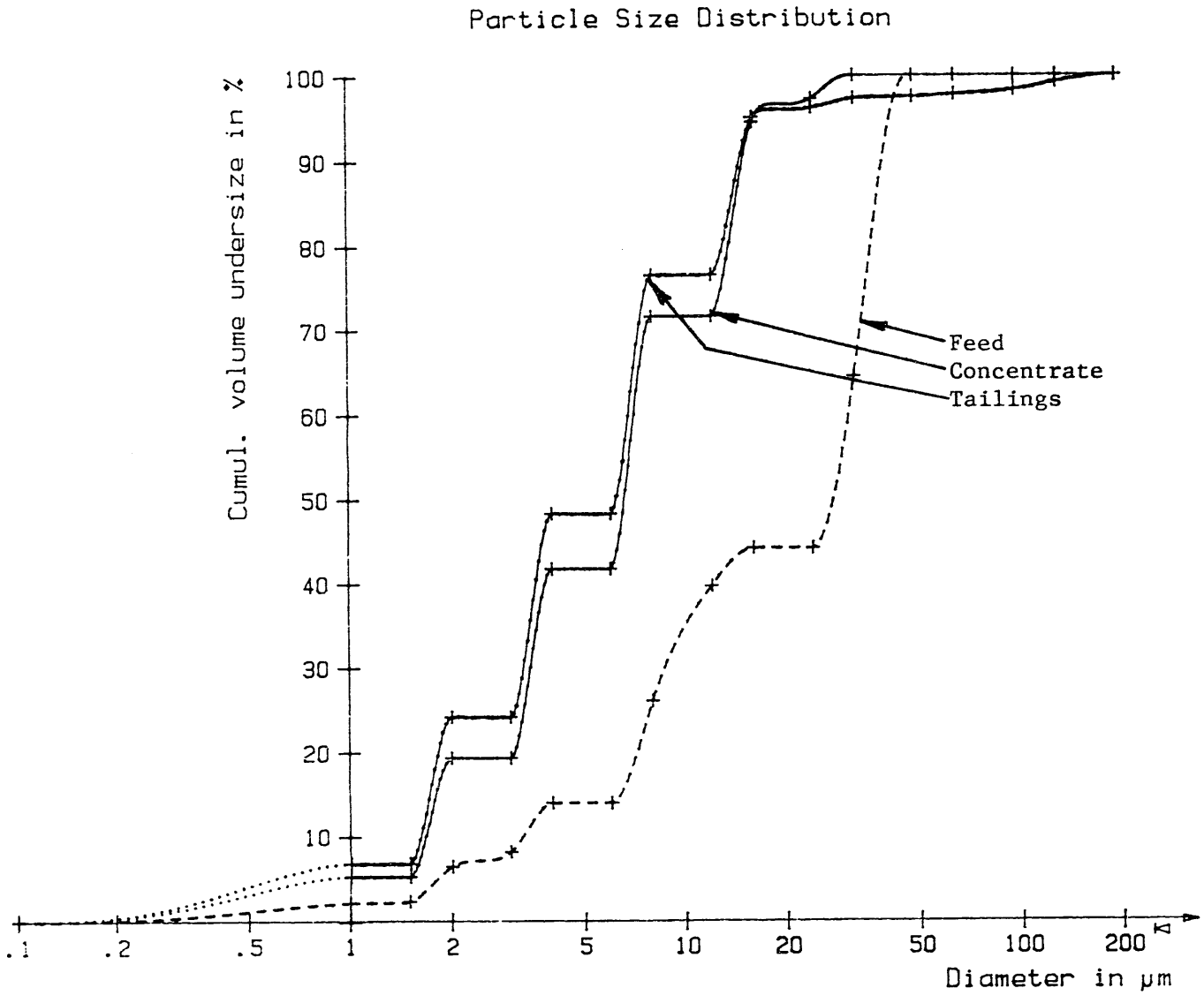

Figure 4-25. **PARTICLE SIZE ANALYSIS OF FEED, CONCENTRATE AND TAILINGS OBTAINED FROM THE SYMUSEP SEPARATOR**

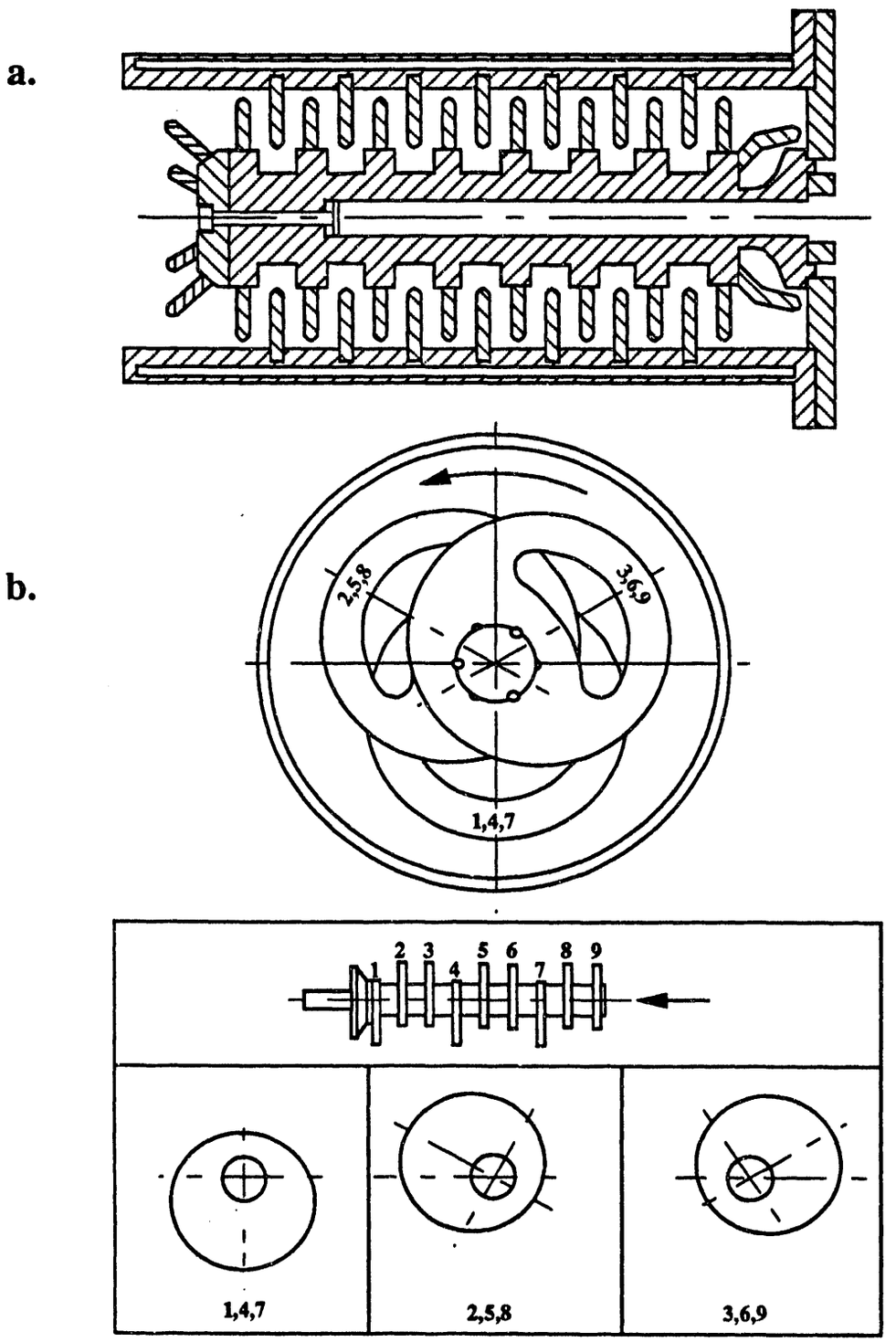

Figure 4-26. SCHEMATIC DIAGRAMS OF THE GRINDING MECHANISMS OF (a) THE JOHN AND (b) THE MOLINEX DEVICES

Dewatering of the kerogen concentrate is very difficult, hence, dewatering studies should be conducted to modify the kerogen surface so that it can be dewatered using conventional vacuum dewatering techniques.

Subtask 4.5. Evaluation of Different Grinding Media

The components of stirred ball milling costs are power, media consumption, and capital (installed equipment). Previous studies by MRI have focused on minimization of power consumption in a stirred ball mill using steel media (2-mm and 1.1-mm diameter balls) and the John Option stirring device. These studies have shown that smaller grinding media is more efficient in producing −10 μm product. However, the cost of 1.1-mm steel media is substantially higher than that of the 2-mm media. Thus, the power savings are offset by the higher media consumption costs.

Objective

Grinding is the highest unit cost operation in mineral processing. A major obstacle in the commercialization of oil shale beneficiation technology is the high cost of stirred ball mill grinding. The factors responsible for the high cost of stirred ball mill grinding are 1) the high level of energy expended in grinding, 2) the high wear rate of expensive grinding media, and 3) the high capital cost associated with complex mill design. The objective of this task was to demonstrate the feasibility of ultrafine grinding of shale using an inexpensive grinding media (sand) as a substitute for steel media in high-speed stirred ball mills. Sand is environmentally more acceptable because alloying elements such as chromium or nickel are not discharged to tailing impoundments. Within this general objective, specific objectives under this task were as follows:

- To determine the preferred stirring mechanism for use with sand media
- To determine the cost/energy effectiveness of replacing steel media in a stirred ball mill with sand media
- To establish the limiting conditions for the utilization of sand as grinding media
- To establish optimum operating conditions for the use of sand media

Equipment

Continuous Stirred Ball Mill. An LME-4 Horizontal Netzsch stirred ball mill was used in two configurations. These configurations are termed the John and Molinex options. The John option uses a large diameter agitator shaft with 8 annular rows of 4 stirrer pins each. The grinding tank for the John option has pins imbedded in the shell, forming a rotor-stator type of agitator. The Molinex option uses a relatively smaller diameter shaft with 9 eccentric disks. Figure 4-26 shows a schematic of these two options. The John option has a set volume of 2.5 liters and the Molinex option has a net volume of 4.0 liters. The larger net volume of the Molinex option is mainly due to the small diameter agitator shaft. The grinding chamber was typically

filled with media to 85 percent by volume. The grinding tests were performed using 2 mm and 1.1 mm chrome steel beads and -12+20 mesh (i.e., 1.2 mm) fracturing silica sand procured from the Unimin Corporation.

Batch Attrition Scrubber. Batch grinding tests were conducted using a modified Denver flotation machine equipped with a grinding chamber and rotor configuration shown in Figure 4-27. The chamber had a total net volume of 280 mL of which 250 mL was the net working volume. About 60 percent of the working volume was filled with both grinding media and slurry during each test to minimize spillage. The volumetric loading was kept constant for the two media types.

Particle Size Analyzer. The particle size analysis was carried out using a Marco Scientific Model No. 715 Granulometer.

Results and Discussion

Preliminary Testing of Molinex Option. Stirred ball milling tests were conducted with the Molinex agitator using 2-mm beads. The media weight was calculated to be 16 kg for the Molinex option, compared to 9.9 kg for the John option (Table 4-13). The tests were conducted using narrowly sized Alabama shale rougher concentrate as feed to the mill. This feed material was prepared using a hydraulic classifier followed by screening. The classifier was targeted to remove -20 μm material and the screening of underflow from the classifier was targeted to remove +100 mesh material. Thus, these operations removed the very fine and very coarse material. In the past, it was observed that oversize (+100 mesh) material gives rise to settling and clogging problems, whereas fine (-20 μm) material is overground in the stirred ball mill. The feed material prepared in this manner contained only 6.4 percent finer than 24 μm (the targeted d_{90} of the stirred mill product). It was observed that this feed material settled very fast in the sump, and therefore, the feed rate to the mill was kept relatively high at 1700 mL/min (i.e., residence time of 1.15 minutes). The experimental conditions and test results are listed in Table 4-14 and plotted in Figure 4-28. The results obtained at 1400 rpm showed that the grinding parameters, based on previous experience with the John option, were reasonable.

Table 4-13. CHARGE CALCULATION FOR THE MOLINEX AND JOHN OPTIONS

Option	Molinex	John
Net Volume, L	4.0	2.48
Fraction media filling	0.85	0.85
Fraction media void	0.40	0.40
Bulk media volume, L	3.4	2.1
True media volume, L	2.04	1.26
Media weight, kg	16	9.9
Mill void volume, L	1.96	1.22

A comparison of the efficiencies of the John and Molinex options could be made by grinding using either sand or steel media. Because the thrust of this research was to evaluate alternate grinding media, it was decided to make the comparison using -12+20 mesh sand as a grinding media.

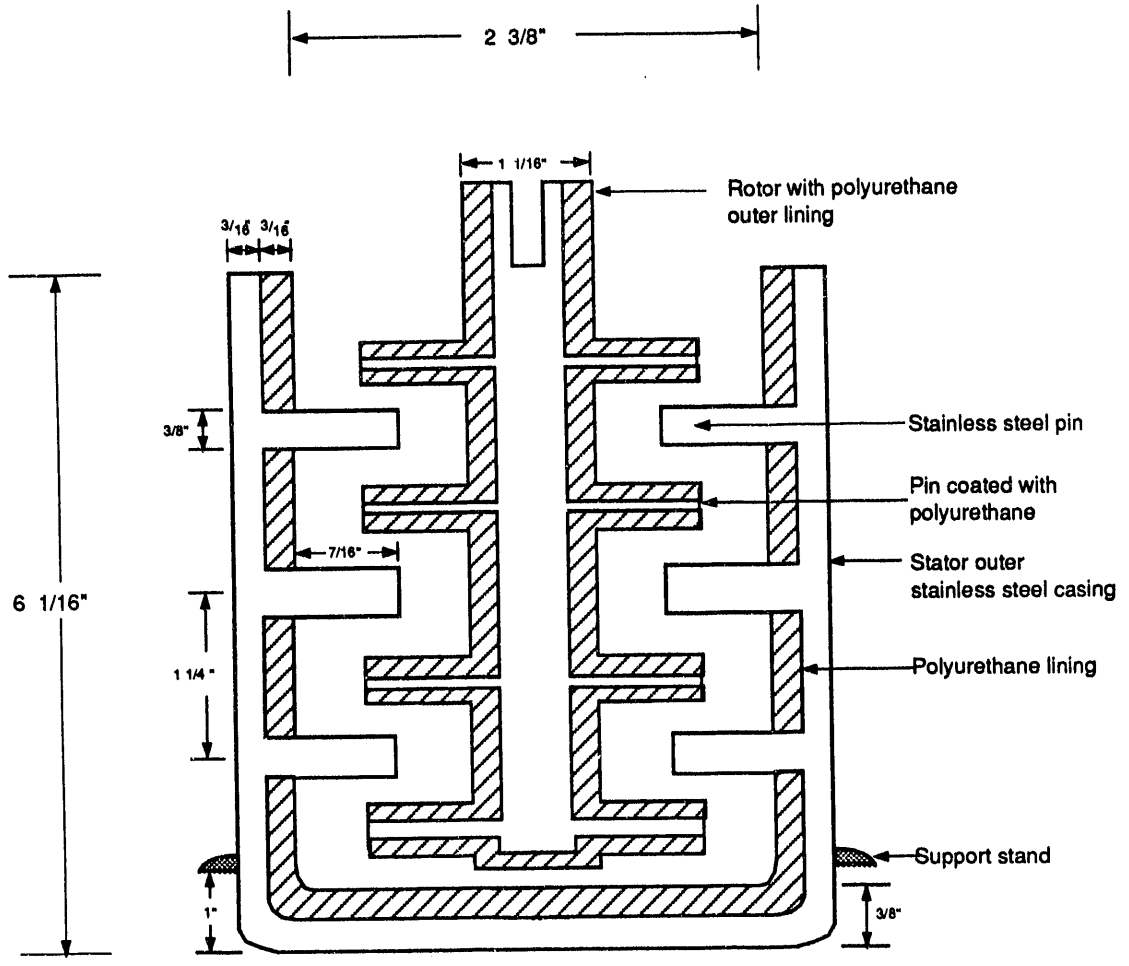

Figure 4-27. SCHEMATIC DIAGRAM OF THE MRI BATCH ATTRITION GRINDER WITH POLYURETHANE LINING

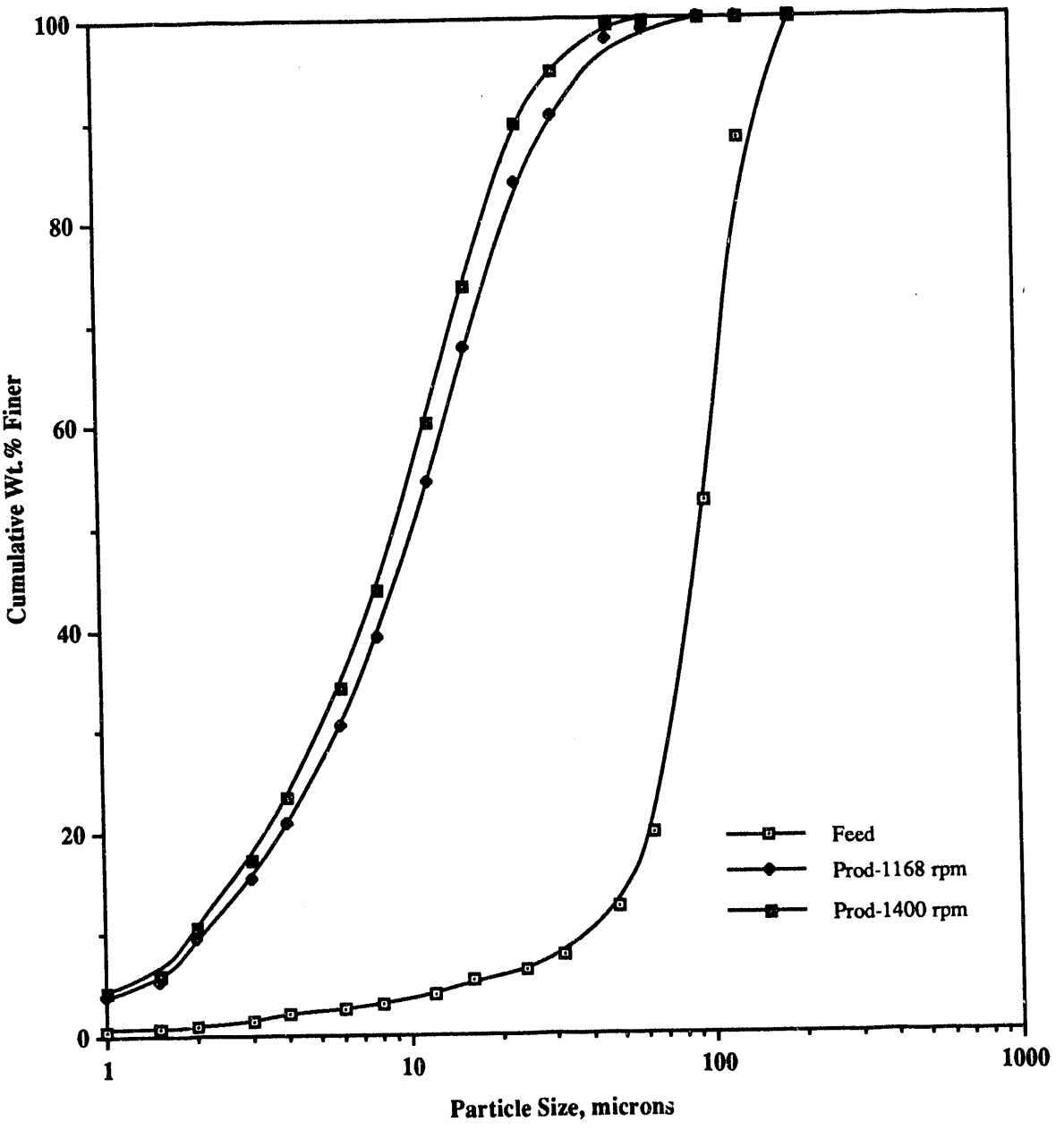

Figure 4-28. PARTICLE SIZE DISTRIBUTIONS OBTAINED USING MOLINEX OPTION FOR ALABAMA SHALE AT 41% SOLIDS

Comparison of the John and Molinex Options Using Sand. The comparison of the energy-size reduction efficiency of these two options was conducted in a regrinding mode. The stirred ball mill regrinding tests of Alabama shale rougher concentrate were conducted using -12+20 mesh (~1.1 mm) fracturing silica sand as a grinding media. The media loading was 85 percent by volume. The tests were conducted using higher rotor speed and lower feed rates to achieve relatively higher residence time and threshold energy due to lower density of sand (2.65 compared to 7.84 g/mL for steel beads). The experimental conditions and test results are shown in Table 4-15. It is rather difficult to say which option is more efficient. In other words, at an equal value of specific energy input, which option will yield a finer product? One observation from these data is that at comparable operating conditions, the power draft of the John option is twice that of the Molinex option (compare M-3 and J-3). Therefore, one would expect a greater size reduction in the John option than in the Molinex option at the same operating conditions.

Table 4-14. EXPERIMENTAL CONDITIONS AND RESULTS FOR THE LME-4 NETZSCH MILL OPEN CIRCUIT*

rpm	Throughput, t/h	Total Power, W	Net Power, W	Specific Energy, kWh/t	Particle Size, μm d_{90}	d_{50}
Feed	--	--	--	--	138.2	93.6
1168	0.0534	2260	1025	19.16	31.6	10.8
1400	0.0534	3330	2003	37.44	24.5	9.5

* Molinex Option, 41% Solids, Feed Rate 1700 mL/min, Closely Sized Alabama Shale Rougher Concentrate.

Table 4-15. A COMPARISON OF THE MOLINEX AND JOHN OPTIONS WITH SAND MEDIA*

Test	Option	rpm	Throughput, t/h	Net Power, W	Specific Energy, kWh/t	Particle Size, μm d_{90}	d_{50}
Feed	--	--	--	--	--	27.2	10.3
M-1	Molinex	1600	0.010	876	70.6	14.1	5.8
M-2	Molinex	1800	0.010	1440	116.1	11.9	5.0
M-3	Molinex	2000	0.014	1445	93.2	12.7	5.4
J-1	John	1600	0.014	1390	92.7	12.4	5.1
J-2	John	1800	0.014	2048	136.5	11.6	4.8
J-3	John	2000	0.014	2855	190.3	10.9	4.3
J-4	John	2000	0.016	2775	149.2	11.6	4.7
J-5	John	2000	0.020	2715	123.4	11.9	4.9

* Feed: Alabama Shale Rougher Concentrate, 41% Solids

Modified Charles energy size reduction relationships were developed from the data reported in Table 4-15. These relationships are as follows:

$E = 2.3157 \times 10^4 \ (d_{50,p})^{-3.2796}$ Molinex/Sand

$E = 1.07077 \times 10^5 \ (d_{50,p})^{-4.2853}$ John/Sand

E is specific energy and $d_{50,p}$ is product median size in micrometers. Simulated curves developed using these relationships for a product median size range of 3 to 10 μm are shown in Figure 4-29. It is interesting to note that for a product median size of 4 μm or greater, the John option is more energy efficient, but for a product median size smaller than 4 μm, the Molinex option becomes more energy efficient. This is indicative of the difference in a mode of grinding in these two devices. For the grinding regime of shale under consideration that rarely involves product median sizes of less than 4 μm, it can be concluded that the John option will result in energy savings. Therefore, it was decided to conduct future tests using the John option only.

After about 1 hour of grinding (Tests M-1 through M-3), the sand was removed from the John option and a representative sample was screened to determine if any size reduction occurred. The screen analysis of the sand and an indirect method of ash analysis of ground shale product both confirmed the hypothesis that comminution of sand media was not significant. These results are shown in Tables 4-16 and 4-17. The comminution of sand in the Molinex option was also found to be insignificant. The screen analysis of sand and ash analysis of ground shale product both confirm the presumed hypothesis.

Table 4-16. SIZE ANALYSIS OF SAND BEFORE AND AFTER GRINDING WITH JOHN OPTION

Size (mesh)	Before Grinding	After Grinding	
	grams	grams	% of feed
-12+20	836.1	829.5	99.21
-20+30	--	6.2	0.74
-30+40	--	0.3	0.04
-40+50	--	--	--
-50+70	--	--	--
-70+Pan	--	0.1	0.01

Table 4-17. ASH ANALYSES OF FEED AND PRODUCTS FROM SAND GRINDING TESTS

Sample	Ash Content, wt %
Feed	65.56
Product J-1	65.62
J-2	65.64
J-3	65.49
J-4	65.49
J-5	65.43

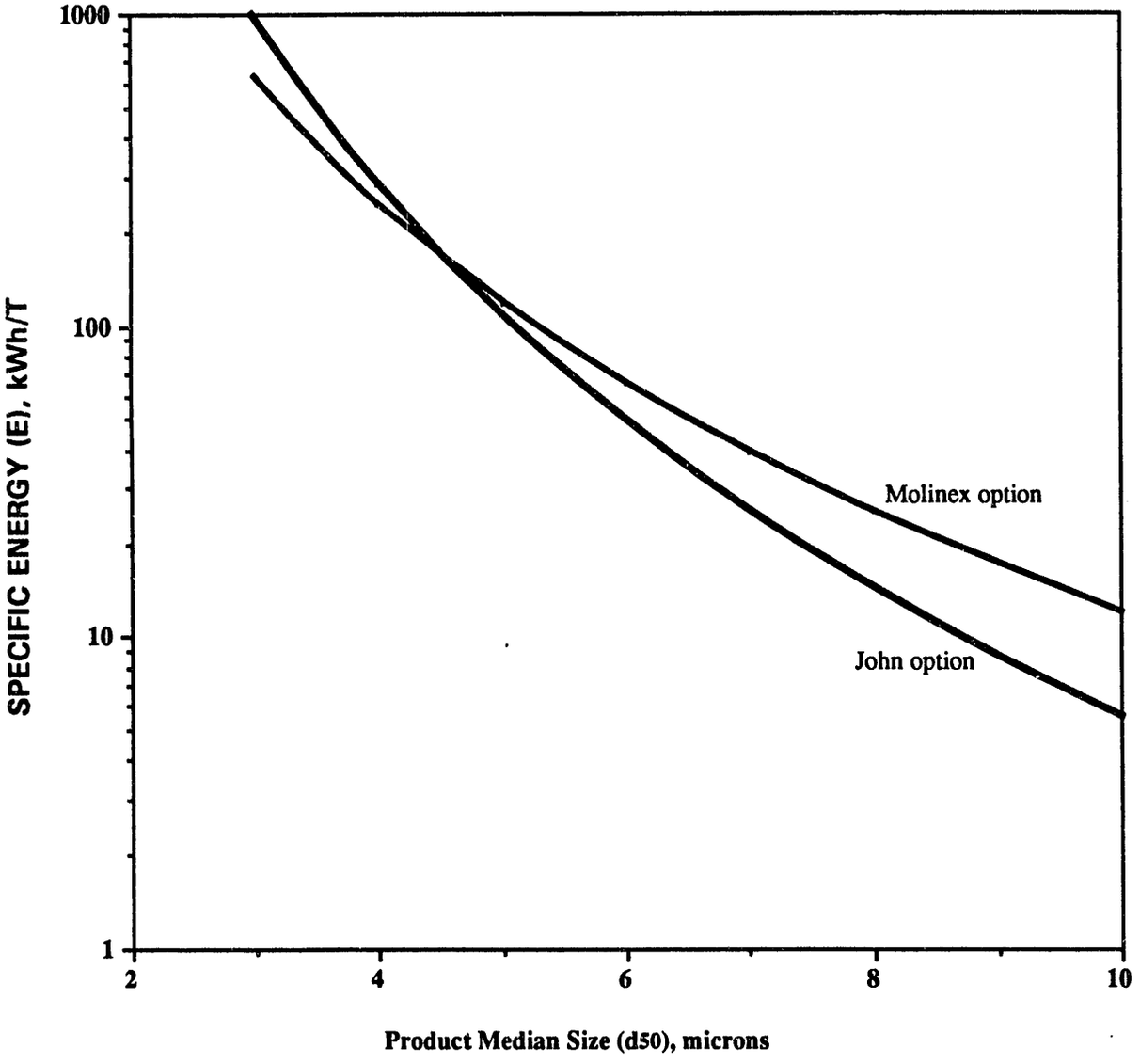

Figure 4-29. SIMULATED CHARLES CURVES COMPARING JOHN AND MOLINEX OPTIONS

The Fischer Assay (FA) of the shale concentrate fed to the Netzsch mill was 17.5 GPT. After grinding in the Molinex and John options using sand, the shale concentrate was assayed to determine whether any oil loss occurred during grinding. The FA of the ground products from the Molinex and John options were determined to be 16.3 and 16.5 GPT, respectively, indicating a loss of 1 GPT during sand grinding, whereas for steel media grinding a loss of 2 GPT was observed.

Comparison of Sand and Steel Grinding Media. To compare grinding efficiency of steel and sand media, a large feedstock of Alabama shale rougher concentrate having a d_{90} of 27.3 and d_{50} of 10.3 μm at 41 percent solids was used in all grinding experiments using the John option. These studies were conducted using equal size sand (12 x 20 mesh) and steel media (1.1 mm). Variables in this study were feed rate and rotor speed; these data are shown in Table 4-18. Subsequently, modified Charles size reduction energy relationships were developed as follows:

$$E = 1.07077 \times 10^3 \ (d_{50,p})^{-4.2853} \qquad \text{John/Sand}$$

$$E = 6.2950 \times 10^5 \ (d_{50,p})^{-5.2654} \qquad \text{John/Steel}$$

Table 4-18. A COMPARISON OF SAND AND STEEL MEDIA IN GRINDING ALABAMA SHALE ROUGHER CONCENTRATE*

Media Type	rpm	Throughput, t/h	Specific Energy, kWh/t	Particle Size, μm	
				d_{90}	d_{50}
Feed	--	--	--	27.2	10.3
1.1-mm Steel	1400	0.012	212.3	10.9	4.6
	1600	0.012	357.2	NR*	NR
	1800	0.012	595.8	NR	NR
	1400	0.024	117.8	11.8	5.0
	1600	0.024	182.6	11.2	4.7
	1800	0.024	297.5	9.7	4.2
	1600	0.033	119.5	NR	NR
	1800	0.033	119.5	11.3	4.8
1.1-mm Sand	1600	0.15	92.7	12.4	5.1
	1800	0.15	136.5	11.6	4.3
	2000	0.15	190.3	10.9	4.3
	2000	0.0186	149.2	11.6	4.7
	2000	0.022	123.4	11.9	4.9

* Test Conditions: Sand Size 12x20 mesh, 41% Solids, Media Loading 85 wt %.
NR - Not reported due to errors in particle size distribution.

An energy efficiency evaluation of these mill-media combination can be done by simulation in the same manner as shown in the previous section. The simulated values of (E versus d_{50}) are shown in Table 4-19. It is clear from the data that for ultrafine grinding to a d_{50} of less than 6 μm, sand media

will be much more energy efficient than steel media. For a smaller size reduction ratio, where a product d_{50} in the range of 6 to 9 μm is desired, steel media will be more energy efficient. It is also clear from the data of Table 4-18 that at comparable product size the sand uses less energy but at the cost of decreased mill capacity.

Table 4-19. CHARLES LAW PREDICTIONS FOR VARIOUS MILL-MEDIA COMBINATIONS USING ALABAMA SHALE ROUGHER CONCENTRATE

Product Median Size	1.1-mm Sand		1.1-mm Steel
$d_{50,p}$, μm	John	Molinex	John
	E (kWh/t)		
3	966.3	630.8	1935.4
4	281.8	245.6	425.5
5	108.2	118.1	131.4
6	49.6	65.0	50.3
7	25.6	39.2	22.3
8	14.4	25.3	11.1
9	8.7	17.2	6.0
10	5.6	12.2	3.4

Feed d_{90} = 10.3 μm

It was also of interest to determine if the characteristic shapes of the product shale distribution produced from steel and sand media were different. A reasonable way to compare this is of equal values to product d_{50}. Table 4-20 lists the product d_{50} obtained in sand and steel media runs. A meaningful comparison of the effect of media can be made by comparing sample 5 with sample 13, and sample 7 with sample 11. A strict comparison on the effect of mill type could not be made; however, a close approximation can be made by comparing sample 2 with samples 4 and 8. The effect of media and mill type on the shape of product size distribution is shown in Figures 4-30 and 4-31, respectively (figures showing similar effects are in Appendix A). It is clear that the shapes of the size distribution curves are similar for both media and mill comparisons.

Having established the suitability of sand media for secondary grinding (i.e., regrinding of rougher concentrate), it was decided to conduct the next series of tests to determine the feasibility of using sand media for primary grinding (i.e., raw shale grinding).

Testing of Sand Media for Primary Grinding. The Derrick screen oversize fraction (+460 mesh) having a d_{90} of 112 and d_{50} of 39.5 μm, respectively, was used to test sand grinding of raw shale. The as-received fracturing sand (-23+65 mesh) was used at 85 percent loading. The tests were conducted with the agitator speed at higher values (>1800 rpm), while the feed rate to the mill was varied. The energy-size reduction data collected are listed in Table 4-21. The data clearly show that it is feasible to grind the raw shale to the targeted d_{90} value ($\approx$20 μm) using sand media. The ground product samples collected were also analyzed for ash. These results (Table 4-22) are similar to those reported in the previous section for secondary grinding and show that sand media does not undergo any significant attrition in the mill.

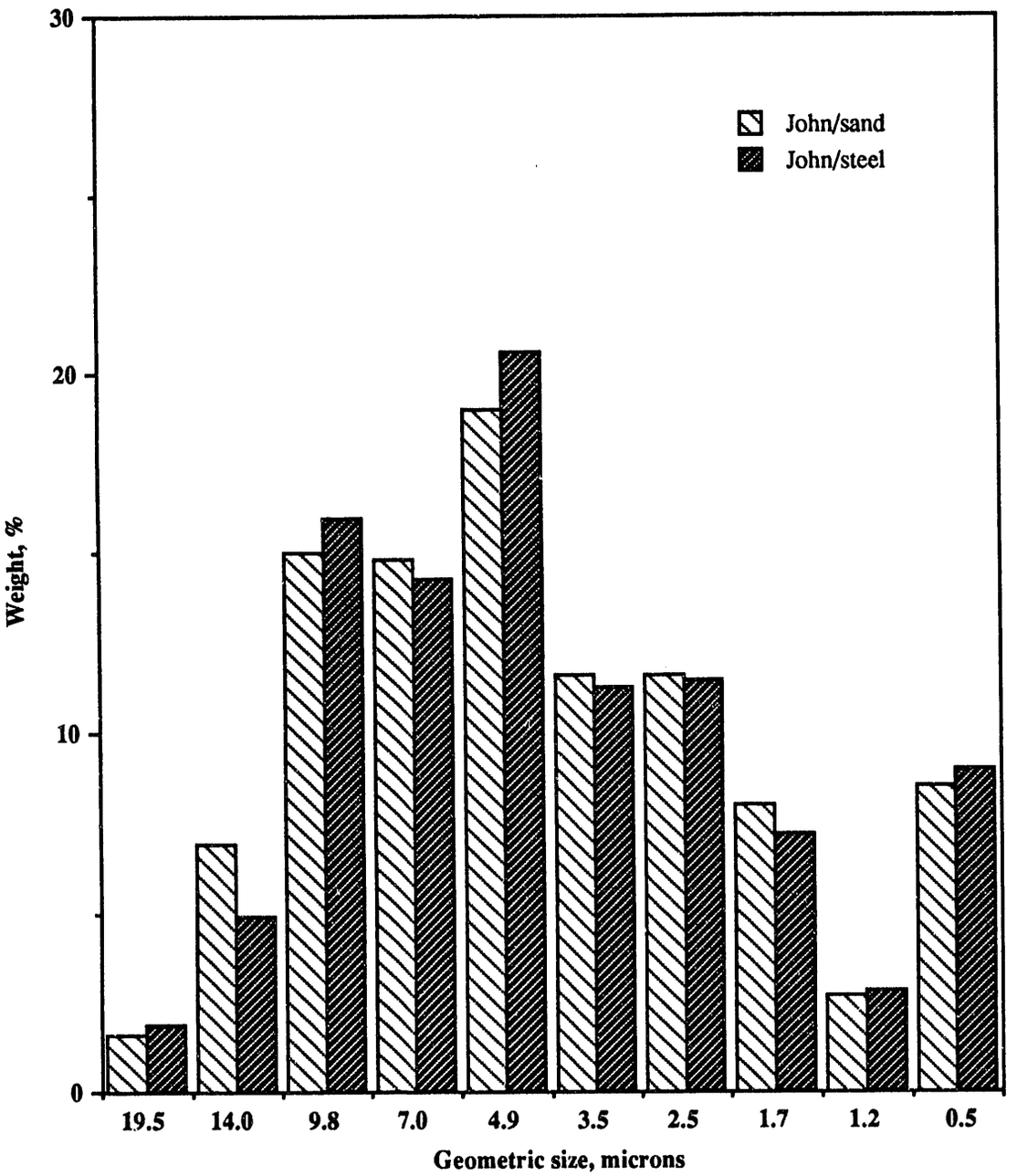

Figure 4-30. EFFECT OF MEDIA TYPE ON THE SHAPE OF PARTICLE SIZE DISTRIBUTION AT SIMILAR MEDIAN PRODUCT SIZE

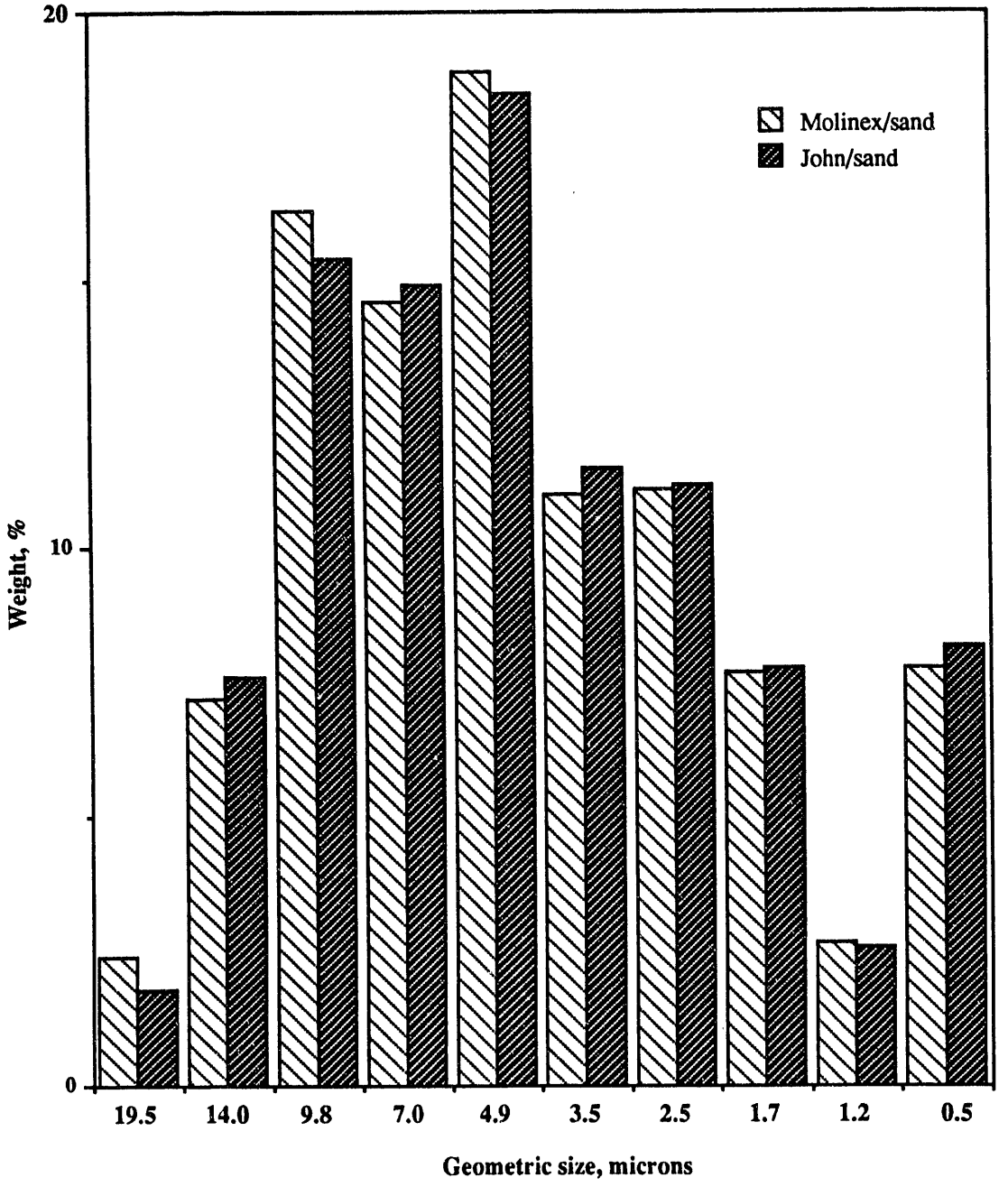

Figure 4-31. EFFECT OF MILL TYPE ON THE SHAPE OF PARTICLE SIZE DISTRIBUTION AT SIMILAR MEDIAN PRODUCT SIZE

Table 4-20. PRODUCT d_{50} VALUES FOR VARIOUS MILL-MEDIA COMBINATIONS

Sample	Mill-Media Combination	Product d_{50}, μm
1	Molinex-Sand	5.8
2	Molinex-Sand	5.0*
3	Molinex-Sand	5.4
4	John-Sand	5.1
5	John-Sand	4.8**
6	John-Sand	4.3
7	John-Sand	4.7***
8	John-Sand	4.9
9	John-Steel	4.6
10	John-Steel	5.0*
11	John-Steel	4.7***
12	John-Steel	4.2
13	John-Steel	4.8**

*, **, *** Represent equal product d_{50} values

Table 4-21. ENERGY CONSUMPTION IN GRINDING RAW SHALE WITH SAND MEDIA*

rpm	Throughput, t/h	Specific Energy, kWh/t	Particle Size, μm d_{90}	Particle Size, μm d_{50}
Feed	--	--	112	39.5
1800	0.0343	69.2	20.4	8.1
2000	0.0343	103.3	19.7	6.7
2000	0.0257	145.7	16.9	6.3
2000	0.0428	84.6	19.9	7.1
2000	0.0556	64.7	22.8	7.9
2350	0.0556	116.8	17.4	6.6

* Test Conditions: 51% Solids, Media Loading 85%, Shale density 2.39 g/mL.

Table 4-22. ASH ANALYSIS OF FEED AND PRODUCTS FROM GRINDING RAW SHALE WITH SAND MEDIA

Sample	Ash Content, wt %
Feed	74.42
Product 1	74.43
Product 2	74.24
Product 3	74.23
Product 4	74.29
Product 5	74.04
Average (Std. Dev.)	74.25 (0.14)
Overall Product	74.18

A series of batch grinding experiments were conducted on as-ground and classified shale feed in the polyurethane-lined attritor. The objective of these tests was to evaluate the effect of classification on the energy-size reduction efficiency of stirred ball mill grinding. Three feed samples were prepared. Sample 1 was prepared by grinding 1.5 kg of shale at 40 percent solids in a rod mill for 20 minutes followed by screening at 325 mesh. Samples 2 and 3 were prepared by grinding the shale under identical conditions but were screened to remove the -20 and -10 μm fractions. The size analysis of feed samples is listed in Table 4-23.

Table 4-23. SIZE ANALYSIS OF THE NARROWLY SIZED ALABAMA SHALE FEED AFTER SEDIMENTATION

Sample	wt %	Size Distribution, %					Size Distribution, μm	
		+96	96x48	48x24	24x12	12x0	d_{90}	d_{50}
1 (-45 μm)	100.0	--	9.8	24.6	25.9	39.1	47.9	15.9
2 (-45+10 μm)	63.7	0.9	17.4	44.0	30.9	5.9	65.7	29.5
3 (-45+20 μm)	30.7	4.4	37.7	48.2	7.7	1.4	88.0	44.4

The stirred ball milling conditions for these three samples were similar: 45 grams shale, 45 percent solids, sand loading of 150 grams, agitator speed of 2300 rpm. The samples were ground for 5, 7, 10 and 12 minutes. The energy-size reduction data obtained from these experiments is listed in Table 4-24. The results show that the viscosity of the feed slurry has a negligible contribution to the instantaneous power draft of the mill. The effect of removing the fine material is clearly shown by the net energy. The amount of fines generated during grinding (24x12 and -12 μm) for samples 2 and 3 are not significantly different. This means that the amount of fines (-24 μm) present in sample 2 actually adversely affected the grinding performance. If the grinding efficiency of samples 2 and 3 are compared on the basis of equal product size (eg., a d_{90} = 14 and d_{50} = 6 μm), then, at equal capacity (grind time of 10 min), sample 2 consumed almost twice the net specific energy as does sample 3. The data show that when a targeted product size (d_{90}) in the range of 20 μm is desired, it is advantageous to remove the -20 μm material from the feed.

The energy-size reduction data collected from the stirred ball mill grinding of raw shale and concentrate using sand was used to indirectly compare the relative breakage behavior of raw shale and concentrate. An indirect way of comparing the breakage behavior of raw shale and concentrate is by analyzing the energy size-reduction data in the context of modified Charles relationship. The relationships obtained from the data were as follows:

$$E = 1.07077 \times 10^5 \ (d_{50,p})^{-4.2853}$$ John/Sand/Concentrate

$$E = 3.7705 \times 10^4 \ (d_{50,p})^{-3.0565}$$ John/Steel/Raw Shale

Table 4-24. ENERGY SIZE REDUCTION DATA OBTAINED IN A BATCH STIRRED BALL MILL SHOWING THE EFFECT OF CLASSIFICATION

Sample No.	Feed Size, μm	Weight %	SBM Grinding Time, min	kWh/t		Size Distribution, wt %					Distribution Parameter, μm	
				Total	Net	+96	96x48	48x24	24x12	-12 μm	d_{90}	d_{50}
1	-45	100	--	--	--	--	9.8	24.6	25.9	39.1	47.9	15.9
1	-45	100	5	53.9	--	--	--	--	20.4	79.1	15.9	6.6
1	-45	100	7	75.4	--	--	--	--	14.6	84.6	14.0	5.8
1	-45	100	10	107.8	--	--	--	--	10.5	88.9	12.3	5.2
1	-45	100	12	129.4	--	--	--	--	8.1	91.1	11.6	4.9
2	-45+10	63.7	--	--	--	0.9	17.4	44.0	30.9	5.9	65.7	29.5
2	-45+10	63.7	5	53.9	34.3	--	--	1.0	29.2	69.2	18.7	8.4
2	-45+10	63.7	7	75.4	48.0	--	--	--	26.5	72.7	18.0	8.0
2	-45+10	63.7	10	107.8	68.7	--	--	--	14.9	84.4	14.1	6.0
2	-45+10	63.7	12	129.4	82.4	--	--	--	14.3	85.0	13.8	5.9
3	-45+20	30.7	--	--	--	4.4	37.7	48.2	7.7	1.4	88.0	44.0
3	-45+20	30.7	5	53.9	16.5	--	--	4.5	30.1	64.8	21.2	8.9
3	-45+20	30.7	7	75.4	23.1	--	--	--	25.1	74.4	17.7	7.4
3	-45+20	30.7	10	107.8	33.1	--	--	--	15.1	84.3	13.9	5.9
3	-45+20	30.7	12	129.4	39.7	--	--	--	11.6	87.6	12.9	5.5

These relationships are plotted in Figure 4-32. The data show that if raw shale and concentrate of the same feed size distribution are ground at equal energy inputs, then the concentrate will result in a finer d_{50}. In other words, the concentrate will require less specific energy than raw shale to achieve the same d_{50}. This finding indicates that concentrate is relatively easier to grind. On the contrary, the size distribution data of the column flotation concentrate and tails revealed the concentrate size distribution to be coarser than tailings. Hence, a direct comparison of their breakage behavior was needed.

Tests to determine the relative grindability of shale feed, concentrate and tailings are currently underway. In these tests, the feed material (-400 mesh) was prepared by grinding 5 pounds of Alabama shale for 20 minutes at 40 percent solids in a rod mill. Concentrate and tailing were prepared by conventional flotation. These products were in turn sized by microsieves into 4 fractions (37x30, 30x20, 20x10 and 10x0 μm). The tests will be conducted under identical conditions in the polyurethane-lined batch mill using 40 grams of material (a synthetic size distribution representing equal amount of particles from the 4 size fractions). The results from this series of tests will be reported in future research.

Conclusions

1. The John option consumes marginally less energy than the Molinex option in achieving a given product median size. At lower values of median size, the relationships converge. At values smaller than 4 μm, the reverse is true. For the range of fineness required by MRI's application, the John option is preferred.

2. Comparison of steel and sand media shows that at comparable product size, sand uses less energy, but at the cost of decreased mill capacity.

3. The shape of the product particle size distribution remains same at a given median size and is independent of the media and mill type.

4. It is feasible to grind raw shale using sand media to a nominal feed size for the stirred ball mill, thus completely eliminating the use of steel media. The biggest benefit of sand is reduced media cost.

5. The loss in mill capacity, when sand is used as the grinding media, is compensated by reduced energy and media cost. Therefore, in terms of overall cost, sand is a preferred media.

6. Size analysis of sand before and after grinding as well as the ash content of ground products, confirm that sand degradation during grinding is insignificant.

7. Important operating conditions for the use of sand are high agitation speed and high slurry density.

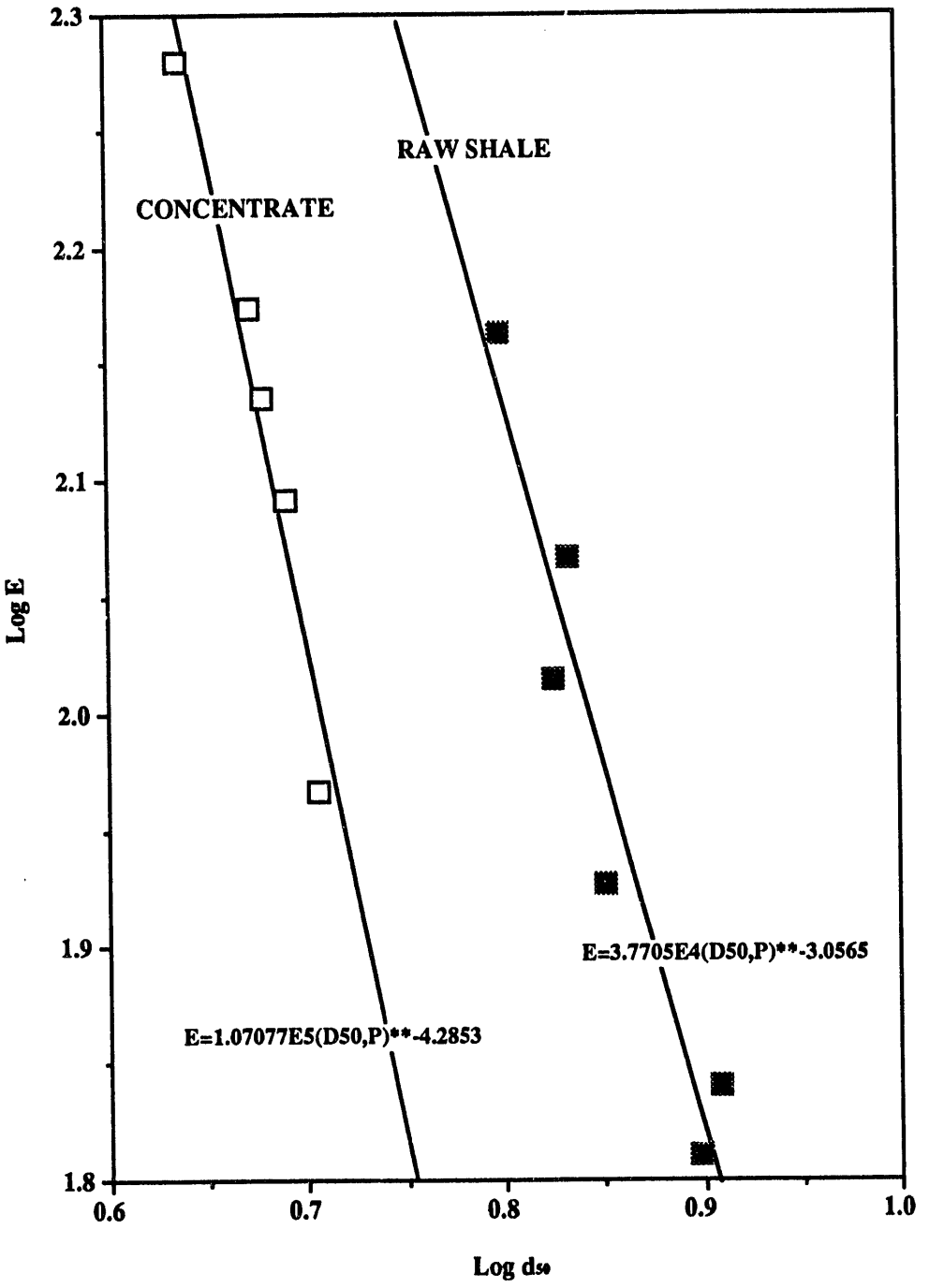

Figure 4-32. ENERGY-SIZE REDUCTION RELATIONSHIPS FOR JOHN OPTION AND STEEL MEDIA USING RAW ALABAMA SHALE AND CONCENTRATE

8. Stirred ball milling data using sand as the grinding media showed that the presence of fine material (-20 μm) in the feed does not go through primary breakage and adversely affects the grinding performance by decreasing the grinding rate of coarse particles.

Recommendations for Future Work

1. Fundamental studies on the breakage of different particle types should be considered.

2. The quantification of the optimum operating conditions for the sand media system should be examined to include an increase in the mill capacity by optimizing other variables.

Subtask 4.6 Evaluation of Concentrate Preparation Techniques

Subtask 4.6.1 Oil Agglomeration and Pelletizing

Background and Objectives

Beneficiation of Eastern shales by column flotation results in a product of superior chemical composition (ie., ~40 GPT), which requires further processing. The concentrate is obtained as a dilute (>95 percent water) slurry of fine kerogen (d_{90} >10 μm). One potential treatment scheme could consist of thickening, pressure filtration, briquetting, and thermal drying.

The objective of this task is to investigate other techniques that have the potential to reduce the cost of preparing concentrate for the PFH process, such as oil agglomeration. The potential advantages of oil agglomeration are that filtration is not required and, because the agglomerating oil tends to fill the interstices between kerogen grains, only surface moisture must be removed by thermal drying. MRI applied further constraints on what would be an acceptable solution. These constraints were that any additive must be recoverable, or non-deleterious to the process, and inexpensive.

In preparing batches of agglomerated concentrates for PFH tests, a system such as that shown in Flowsheet 1 of Figure 4-33 is adequate. In a commercial operation, however, such a scheme would be considered inefficient in that it requires crushing and screening subsequent to briquetting and also requires recycling of the fines produced in crushing.

Figure 4-33 presents four alternative agglomeration schemes. Flowsheet 1 is the process that has been used to prepare agglomerates for PFH tests. Flowsheets 2, 3, and 4 are schemes that, if workable, would meet the task objectives within the imposed constraints.

Oil Agglomeration with Asphalt Emulsion. This method of agglomeration is illustrated by Flowsheet 2. Oil agglomeration is most frequently performed with light oils such as diesel or fuel oils. However, because such oils would be converted to gases in the PFH process, asphalt emulsions were selected as an alternative. They are lower in cost and there is reason to believe that they would not be converted to light oils in the PFH process.

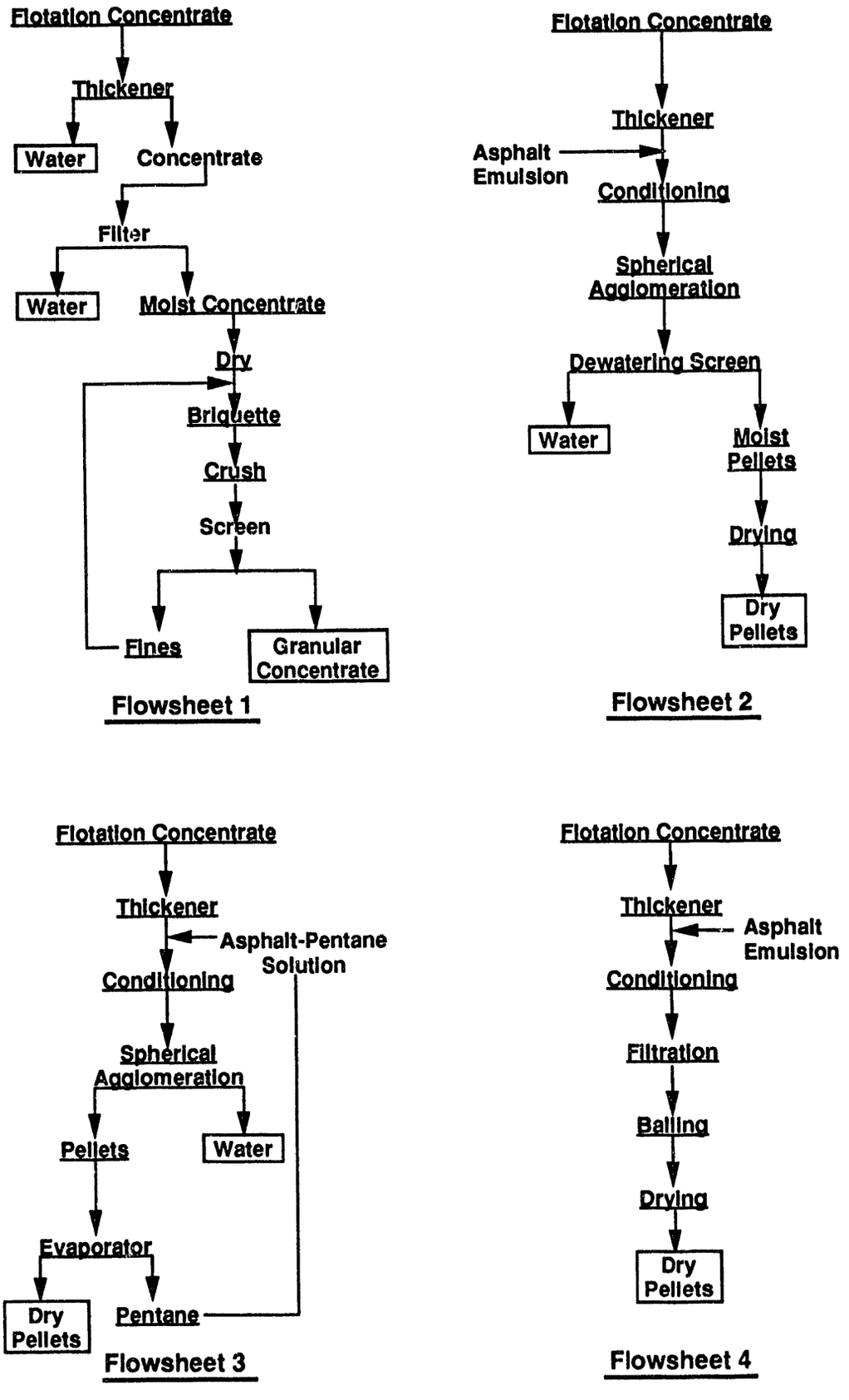

Figure 4-33. ALTERNATIVE AGGLOMERATION SCHEMES

Oil agglomeration is normally carried out in two stages. In the first stage, oil is added to a solid-water slurry and subjected to intense agitation. During this stage, the oil preferentially wets the hydrocarbon solids (in this instance, kerogen). In the second stage, the slurry is stirred at relatively low speeds to allow the wetted particles to collide and coalesce into small spheres.

In the present case, a slurry of about 100 grams of concentrate at 25 percent solids was conditioned in a Waring blender with variable additions of asphalt emulsion for a period of two minutes. The conditioned slurry was subsequently stirred at low speed for periods of time varying from 5 to 10 minutes. The range of asphalt emulsion addition was from one to five percent by weight. In no case was the formation of agglomerates noted. Examination of the slurry after conditioning indicated good dispersion of the asphalt and flocculation of the kerogen particles. These observations led MRI to believe that the conditioning was complete and satisfactory, and that increased conditioning time would not be required.

During the period of slow stirring, no growth of agglomerates was noted. In every case, however, there was a tendency toward phase separation. The concentrates tended to collect at the top of the vessel in a manner akin to a froth in a flotation cell. This effect was attributed to a high level of air entrainment in the conditioning stage. The failure to form spherical agglomerates was attributed to the non-fluid nature of the asphalt compared with the light oils that are normally used.

Oil Agglomeration with Asphalt-Pentane Solutions. This alternative, illustrated by Flowsheet 3 is a slight variation on Flowsheet 2. Pentane was selected as a solvent to increase the fluidity of the asphalt. Pentane has a high vapor pressure that enables it to be readily recovered and it has been shown to be effective in the oil agglomeration of coal. A series of tests, similar to those described previously, were performed with much the same result. Conditioning appeared to be complete, but the strong odor of pentane indicated that a significant evaporation loss occurred in this stage. Phase separation occurred strongly in the second stage, but no tendency to form agglomerates was noted.

In a parallel test on coal, a tendency to form agglomerates was noted when the slurry was heated. That possibility was considered to be too costly to apply to oil shale.

Pelletizing. Pelletizing is the most widely practiced method of agglomeration in the U.S. Each year some 60 million tons of iron ore concentrates are pelletized to prepare them for use in blast furnaces. The pelletizing process is simple. Moist granular solids are metered onto an inclined rotating disc. They tend to form into small balls. As the small balls roll over fresh unconsolidated solids, the new material tends to accrete onto the surface of the balls. The process has been likened to the formation of a snow ball as it grows in size while rolling down a hill.

The pelletizing process is illustrated by Flowsheet 4. In laboratory tests, thickened flotation concentrates were conditioned with various levels of asphalt emulsion as described earlier. The slurry was then filtered on a laboratory pressure filter. The filter cake was broken up then stirred with a hand mixer to get it into an unconsolidated state. The moist-unconsolidated concentrates were then hand fed onto a laboratory pelletizing disk. The moist concentrates formed rapidly into "seed" pellets of about 1/8 inch diameter. As this occurred, the seeds became denser (more tightly packed) and the internal moisture was squeezed to the surface. When that happened, the seeds rapidly coalesced into "raspberry like" agglomerates that in turn grew uncontrollably. The net result then is that while the material agglomerated well, there was no control of the agglomerate size. The agglomerates could not be used in the fluidized bed systems that requires relatively small agglomerates that are closely sized.

Extrusion. Extrusion was not originally considered for inclusion in this program. However, given the failure of the other three systems that were tested, extrusion was included as an alternative. The extrusion process most closely resembles Flowsheet 4. After filtration, the moist concentrate was packed into the cylinder of a clay extrusion press. The press was fitted with an extrusion die having seven 3/16-inch diameter holes. The concentrate was extruded through the die as a cylindrical ribbon. The extrude was then oven dried overnight at 50°C. After drying, the extruded ribbon was broken into short sections or pellets ranging from 1/4 to 1/2 inch in length. In industrial practice, this would be done by cutting the ribbon as it exits the die.

Four batches of extruded pellets having additions of 0, 1, 3, and 5 percent asphalt were made by this process. To test the effect of the asphalt additions on the durability of the extruded pellets, the pellets were tumbled in a rotating drum. The drum was 18 inches in diameter and was filled with three 3-inch wide lifters attached to the inner periphery. The pellets were tumbled for a period of 1 minute at 20 rpm. The charge of pellets was then screened on a 10 mesh screen to determine the amount of size degradation or abrasion loss. After screening, the entire charge was returned to the drum and tumbled for an additional five minutes. The charge was again screened to determine additional abrasion losses.

This process was devised to simulate the effect of loading, handling, and flow in bins to which pellets or other agglomerates would normally be subjected. The results of the tumbling tests, presented in Figure 4-34, show that the asphalt emulsion significantly reduces the breakdown or abrasion loss. Additions of asphalt on the order of 5 percent virtually eliminated particle breakdown.

Conclusions and Recommendations

A method of agglomerating oil shale concentrates in a single pass without recycling has been demonstrated. The method (extrusion) however, does not have the desirable attributes of an oil agglomeration process in that it does not reject water from the concentrates. The cost of drying the product remains a part of the overall cost of the production of oil from Eastern shales.

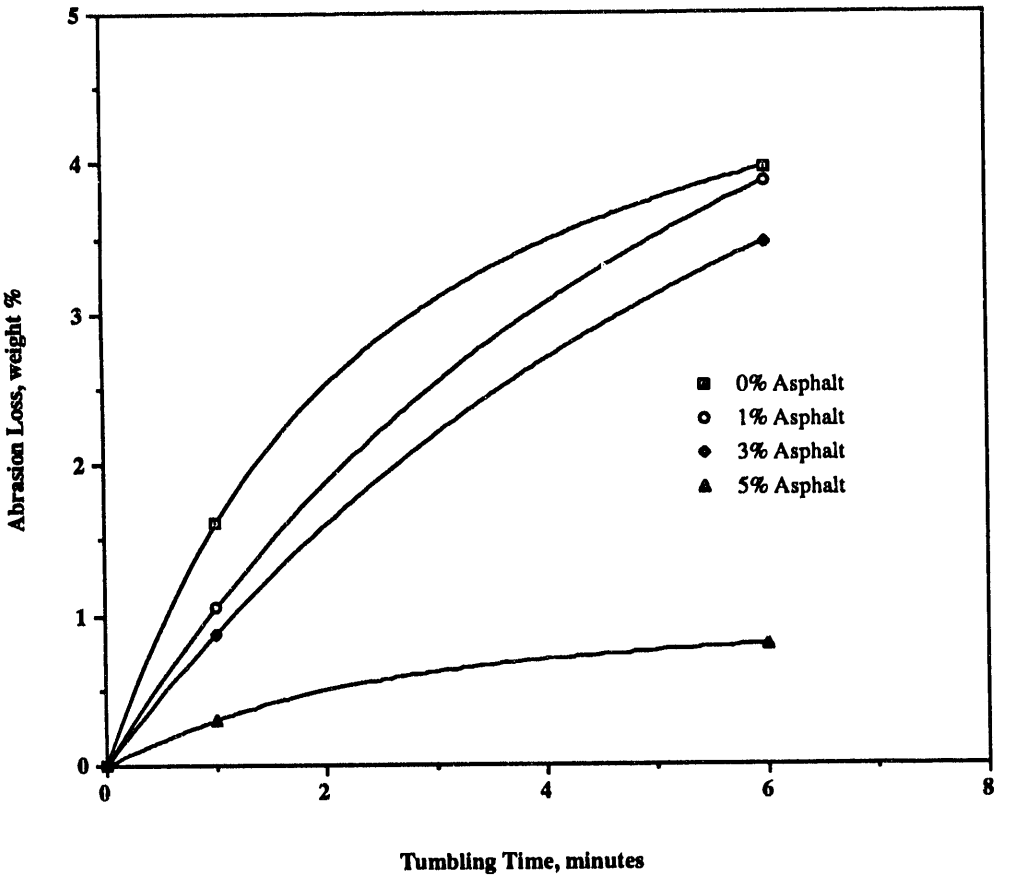

Figure 4-34. EFFECT OF ASPHALT CONCENTRATION ON AGGLOMERATE STRENGTH

The extrusion process does offer the potential for close control of product size and readily accommodates the addition of binders. Further work may be required to determine whether drying is more easily accomplished with agglomerates than with non-agglomerated concentrates. A more fruitful area of future research may be in filtration. Recent advances in filtration technology offer the potential for cost reduction in drying by reducing the moisture content of the filter cake. Moisture reduction may also yield a high quality (i.e. more abrasion resistant) product because it would result in higher extrusion pressures.

Subtask 4.6.2. Bioflocculation of Kerogen

The objective of this subtask is to use a hydrophobic microorganism to selectively flocculate kerogen from enriched flotation concentrate to produce an ultrahigh-grade product and simultaneously enhance subsequent dewatering of the concentrate. Another objective is to use the hydrophobic microorganism as precursor for oil-assisted spherical agglomeration to produce oil enriched-water-repellent kerogen agglomerates. This subtask was conducted by the University of Nevada, Reno (UN).

Background

The microorganism Mycobacterium phlei is a powerful flocculant. It has both a hydrophobic character and a negatively charged surface. Its hydrophobic character is due to the presence of fatty groups at the surface; the negative charge is due to surface carboxylate groups. Because of the combination of these two surface properties, it is unique for selective flocculation of kerogen particulates from beneficiated flotation concentrates. The nature of aggregation and flocculation with M. phlei is completely different from that of polymeric synthetic flocculants. The entwining effects generally observed with synthetic flocculant are absent in the case of M. phlei. The aggregation and flocculation of kerogen from dilute flotation concentrate can be accomplished very rapidly at moderately acidic pH and with the addition of appropriate amounts of organism. In a short time, a significant amount of process water can be recycled without having any deleterious effect on process performance. M. phlei not only acts as a flocculating agent, but also increases the rate of filtration. The residual moisture content in the filter cake can be reduced significantly by organism-surfactant combination.

Introduction

In recent years, physical separation processes, particularly the beneficiation process, have been utilized to separate the kerogen from oil shale. Successful separation requires grinding to a size of about 10 μm followed by froth flotation in a column cell. The concentrate produced by column flotation is dilute and difficult to dewater. Because of the fine size and intrinsic laminated shape of kerogen, it is difficult to settle even after an extended time. Further, the presence of soluble dissolved ions and slime coating on the kerogen particles keeps the particles in suspension. Typical column flotation concentrate contains 25 to 30 percent organic carbon and 9 to 11 percent sulfur with the remainder being clay and quartz. The presence of water in the beneficiated kerogen concentrate is a recognized problem in

storage, transportation, and retorting. It has been established that the removal of water from kerogen can significantly reduce the heat load during combustion due to the evaporation of surface and intrinsic moisture and eliminate, to some extent, the problems associated with corrosion and erosion.

Description of M. phlei

M. phlei is a Gram positive procaryotic cell. In general, it has a rod-like shape 1 to 1.5 μm in diameter and 5 μm in length. The shape can be altered depending on the culture method and rate of growth.[15] A conceptual surface chemical structure of the microorganism as envisioned by UN is depicted in Figure 4-35.[17] The plasma membrane (on the surface of M. phlei) is a semipermeable barrier that regulates the passage of molecules into the cell structure, which consists of free lipids, phospholipids and glycolipids. On the surface of M. phlei, two main functional groups i.e polar groups (carboxyl, hydroxyl, amino and phosphate groups) and nonpolar (alkyl groups) are present. The presence of large amounts of polar groups impart a high negative surface charge. It has been shown that M. phlei is both highly hydrophobic and negatively charged with an isoelectic point (iep) at a pH of about 1.8.[5-11] It readily adheres to hydrophobic particulates mainly due to hydrophobic interactions. Since the bacterium has a rod/ellipsoid/coccal shape, the flocculation characteristics are completely different from that of synthetic polymeric flocculants that have long chain structures. Schematic diagrams of bioflocculation and conventional flocculation processes are given in Figure 4-36. While both the bacterium and long chain polymers, in part, flocculate mineral particles by bridging, the entwining characteristics of the long chain molecules are absent in the case of M. phlei. Thus, the hydrophobic interaction between adhering microorganisms on adjacent solid particles is of greater importance in the formation of mineral aggregations. As a result, the aggregates are selective and tightly held.

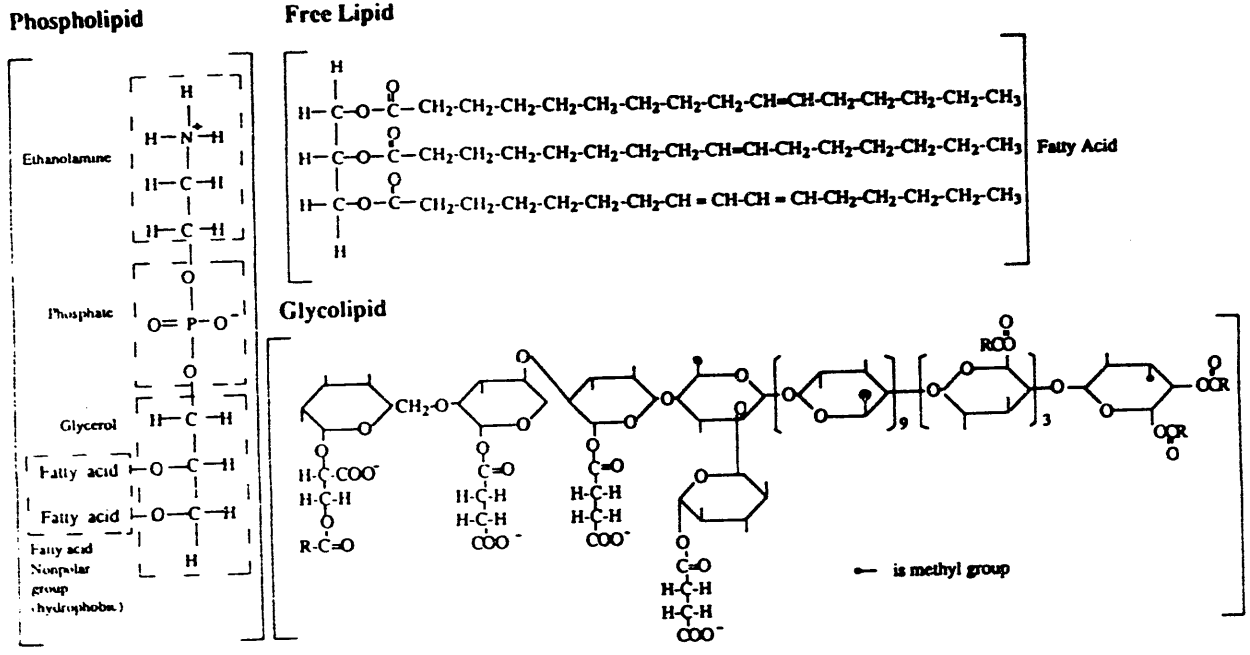

Figure 4-35. APPROXIMATE CELL COMPOSITION OF Mycobacterium phlei

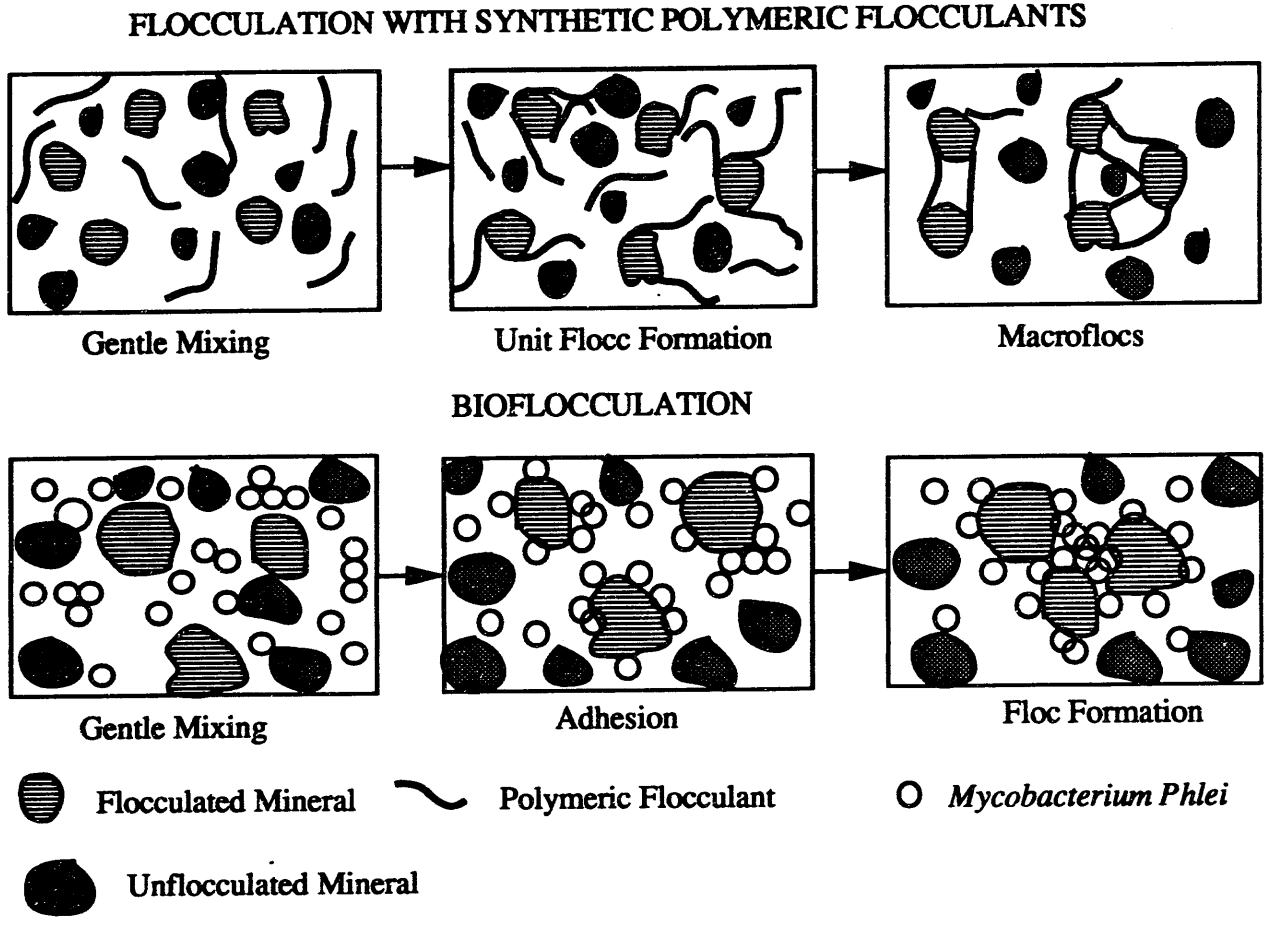

Figure 4-36. STEPS IN CONVENTIONAL FLOCCULATION AND BIOFLOCCULATION PROCESSES

Experimental Approach

Oil Shale, M. phlei and Surfactants

The sample of shale used for tests in this subtask was obtained from Madison County, Alabama. The sample was first ground to -10 mesh. The -10 mesh material was further ground to the desired size (90 percent passing 10 μm) in a ball mill. Kerogen-enriched concentrate was collected by flotation with the addition of Dow frother. The rougher flotation concentrate was cleaned three times. The organic carbon content in the cleaner flotation concentrate was about 30 percent. The solid content in the flotation concentrate slurry was in the range of 0.5 to 1 percent by weight. The M. phlei used in the experiments was grown from culture obtained from Carolina Biological Supply Company. The bacterium is ubiquitous and found in soils and on the leaves of plants, particularly grasses and sometimes referred to as hay or timothy bacillus.[12,13] It is non-pathogenic to all animals so far tested. The medium and growth procedure are given by Pratt and Guirard et al.[14,15] The culture medium contains the following (per liter of distilled water): 10 g glucose, 2 g casein, 1 g beef extract and 1 g yeast, which was sterilized at 120°C for 30 minutes. The incubation temperature was 35°C. After 48 hours of incubation, M. phlei was harvested by centrifugation and washed twice and suspended in distilled water. The approximate number of microorganisms per milliliter of solution were in the range of 10^{12} to 10^{13}. The concentration of M. phlei is reported as mg of dry M. phlei per liter of suspension (ppm).

Surfactants from Rhone-Poulene Company were chosen for this investigation. The trade name of the surfactants is IGEPAL series compounds (IGEPAL CO-430, -510, -610, and -630). The empirical formula is $(C_2H_4O)_nC_{15}H_{24}O$, where n = 4, 6, 7.5, 9. Their Hydrophobic-Lipophile Balance (HLB) numbers were calculated following the procedure given in reference 18. The HLB number of IGEPAL series compounds are given in Table 4-25. The cationic surfactant used in the investigation was dodecyl ammonium chloride, manufactured by ICN Pharmaceuticals, Inc.

Table 4-25. HYDROPHOBIC-LIPOPHILE BALANCE NUMBER

IGEPAL Compound	HLB Number
CO-430	2.50
CO-530	3.16
CO-610	3.92
CO-630	4.14

Experimental Methods

Flocculation Experiments

A schematic diagram of the flocculation and filtration experimental arrangement is shown in Figure 4-37. Flocculation tests were performed by first mixing 1000 mL of freshly prepared kerogen concentrate in a controlled stirring vessel. In order to have good mixing, cultured bacteria were added to the slurry suspension at a moderate speed of 250 rpm. After 2 to 3 minutes of stirring, the stirrer speed was reduced to 30 rpm for 5 to 7 minutes for initial growth of the flocs. The suspension was transferred to a 1000-mL graduated cylinder. Samples were removed at a specified distance from the top of the cylinder at different time intervals. The solid concentration was determined gravimetrically. From the data obtained, it was then possible to calculate the relative stabilities of the suspension as a function of time by dividing the weight percent solids in the sample taken at time (t) by weight percent solids in the sample at the beginning of the experiment (W_t/W_o). For convenience, the values were converted to percentages by multiplying them by 100.

Filtration Experiments

The flocculated part of the material was filtered by addition of different surfactants. Most of the filtration experiments were conducted using vacuum filtration. The residual moisture content in the filter cake was determined by drying in an oven at 60°C. The equilibrium moisture content of the filter cake was calculated using Eq. 1.

$$\text{Equilibrium Moisture} = (W_o - W_d)/W_o \times 100 \qquad (1)$$

where W_o is weight of wet filter cake and W_d is weight of dried filter cake of the sample.

Zeta Potential Experiments

Electrophoretic mobilities were determined using a ZR-11 ZetaReader. Mobilities are precise to 0.1 mV. Dispersion pH was measured using an accurate Fisher 925 pH meter combination Fisher glass electrode.

Suspensions of oil shale and M. phlei were prepared by dispersing oil shale (0.1 to 0.2 gram) in dilute electrolyte (100 mL of 10^{-3} M NaCl) and adjusting the pH with HCl or NaOH. The suspension was then conditioned for 15 minutes by magnetic stirring. The suspension was pumped to the cell of the Zeta Reader.

Surface Tension Experiments

To measure surface tension of M. phlei solutions and surfactants, the Fisher Model 215 Autotensiomat Surface Tension Analyzer was used. In this method the force required to detach a ring from a solution surface is measured by suspending the ring from the arm of a balance. The detachment force is related to the surface tension by the expression -

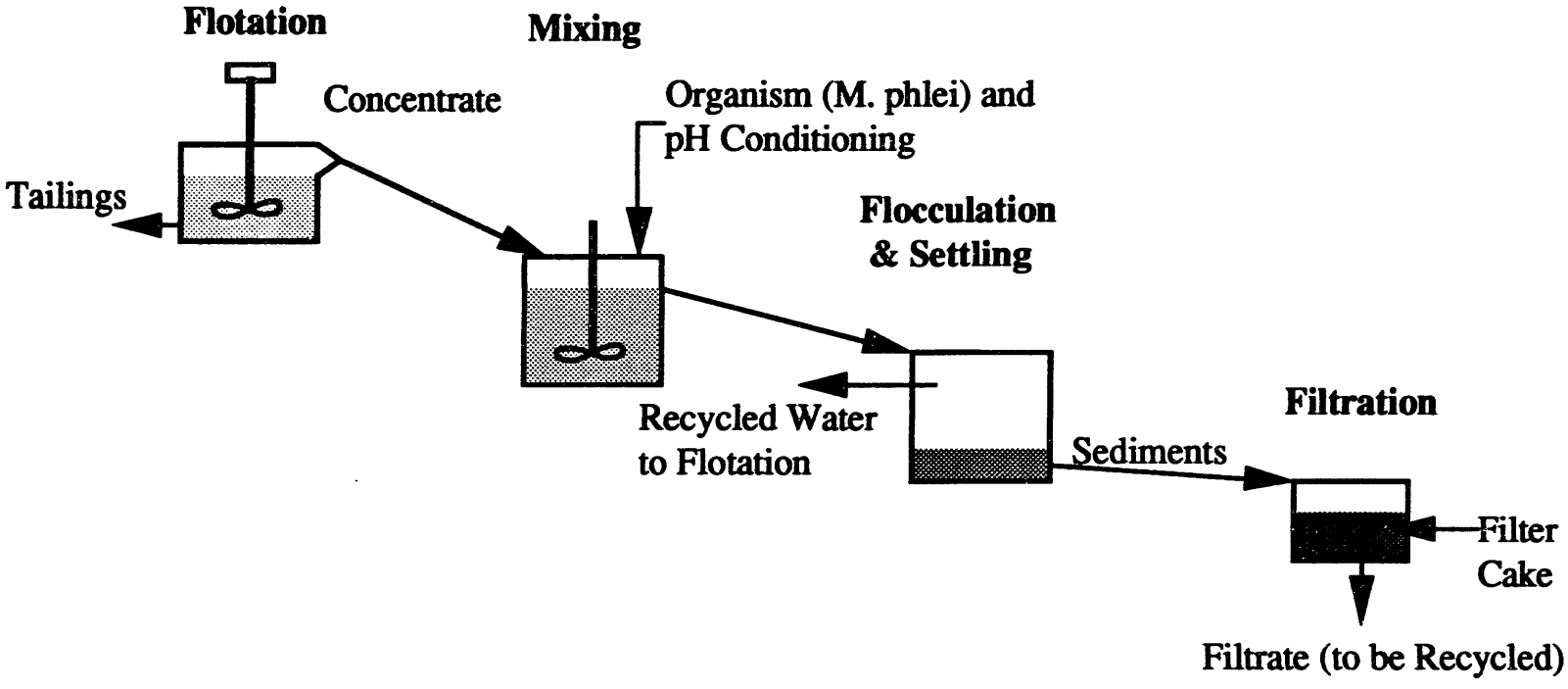

Figure 4-37. FLOCCULATION AND FILTRATION EXPERIMENTAL APPROACH

$$\tau = \beta F/(4\pi R) \qquad (2)$$

where F is the pull on the ring, R is the mean radius of the ring, and ß is a correction factor. To obtain valid results, the ring and sample vessel were cleaned thoroughly with suitable solvents. For sample vessels, a cleaning with fresh chromic-sulfuric acid mixture, followed by a thorough rinsing in distilled water, was used. The ring was rinsed in benzene, squirted with acetone and allowed to dry, then brought to the oxidizing portion of a gas flame. The solution pH was adjusted by NaOH or HCl. The solution of M. phlei was agitated for 3 minutes and then kept 5 more minutes without any agitation.

Results and Discussion

Flocculation. The effects of pH and the presence or absence of microorganisms on the settling rate of kerogen are shown in Figures 4-38 through 4-40. Flocculation and settling of kerogen is rapid around pH 3 and improved flocculation can be observed with addition of organism at that pH. Most of the kerogen (excluding shale and pyrite) settled in 5 minutes. At pH 3, more than 87 percent of the materials settled in 5 minutes, whereas only 40 percent of it settled without the addition of M. phlei.

Flocculation and settling of freshly prepared flotation kerogen concentrate as a function of pH is given in Figure 4-41. For comparison, flocculation tests of column flotation concentrate obtained from IGT were conducted as a function of pH. For these tests, the predried solid concentrate (containing 26 percent organic carbon) was suspended in water for 30 minutes and the slurry was mixed at 900 rpm for 10 minutes. After 10 minutes mixing, the slurry was diluted and dispersed again with ultrasonic treatment. The results (Figure 4-42) show that the flocculation characteristics of the sample received from IGT were slightly different from those of the freshly prepared sample.

The flocculation and settling of kerogen concentrate as a function of M. phlei concentration is given in Figure 4-43. It can be seen that rapid settling can be obtained with the addition of 60 ppm M. phlei and no significant improvement is noticed by increasing the M. phlei concentrate beyond 160 ppm. The flocculation of kerogen as a function of solid concentration in the pulp is given in Figure 4-44. The solid concentrate for good flocculation is about 0.5 percent. Scanning electron microphotographs of flocculated kerogen with M. phlei show a significant attachment of M. phlei to the kerogen particles. It is likely that flocculation of kerogen particles is due to the adhesion of organisms and subsequent bridging of particles.

Filtration. Dewatering of flocculated and unflocculated beneficiated kerogen concentrate was conducted by vacuum filtration. Initial experiments show that the residual moisture content in the filter cake without microorganism addition was in the range of 49 to 52 percent. The residual moisture content is strongly dependent upon the particle size, carbon and ash content, and concentration of dissolved metals.

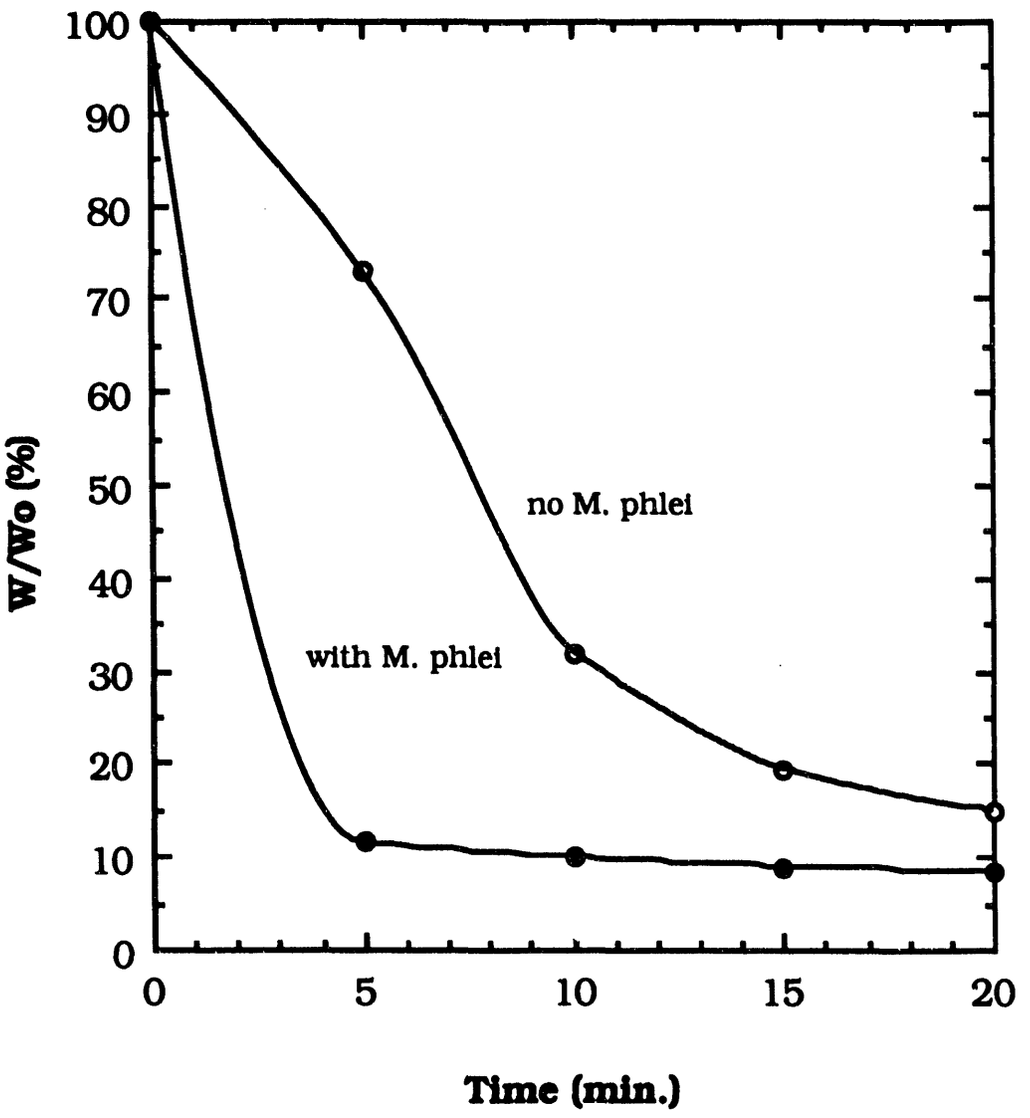

Figure 4-38. SETTLING RATE OF KEROGEN CONCENTRATE WITH AND WITHOUT M. phlei AT pH 3.03

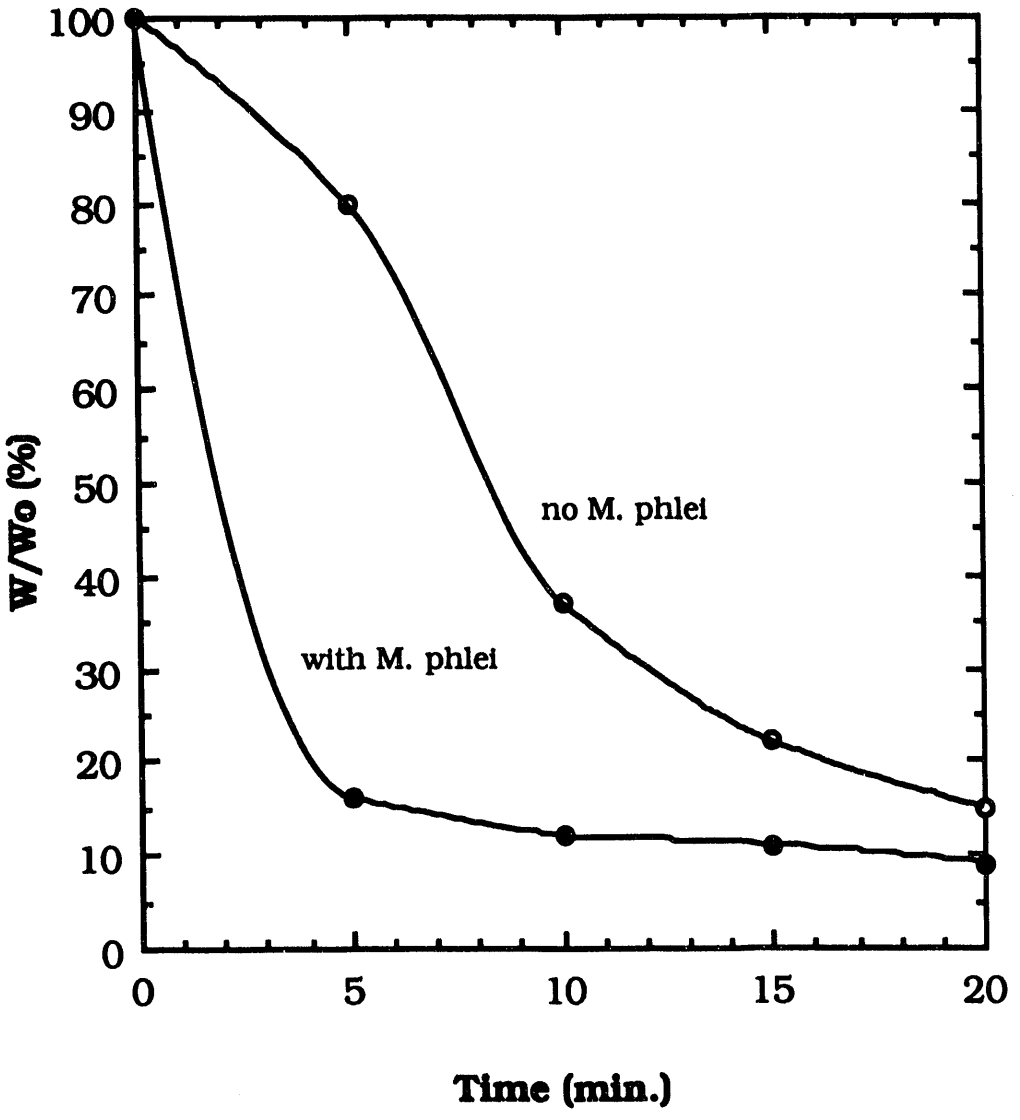

Figure 4-39. SETTLING RATE OF KEROGEN CONCENTRATE WITH AND WITHOUT M. phlei AT pH 7.32

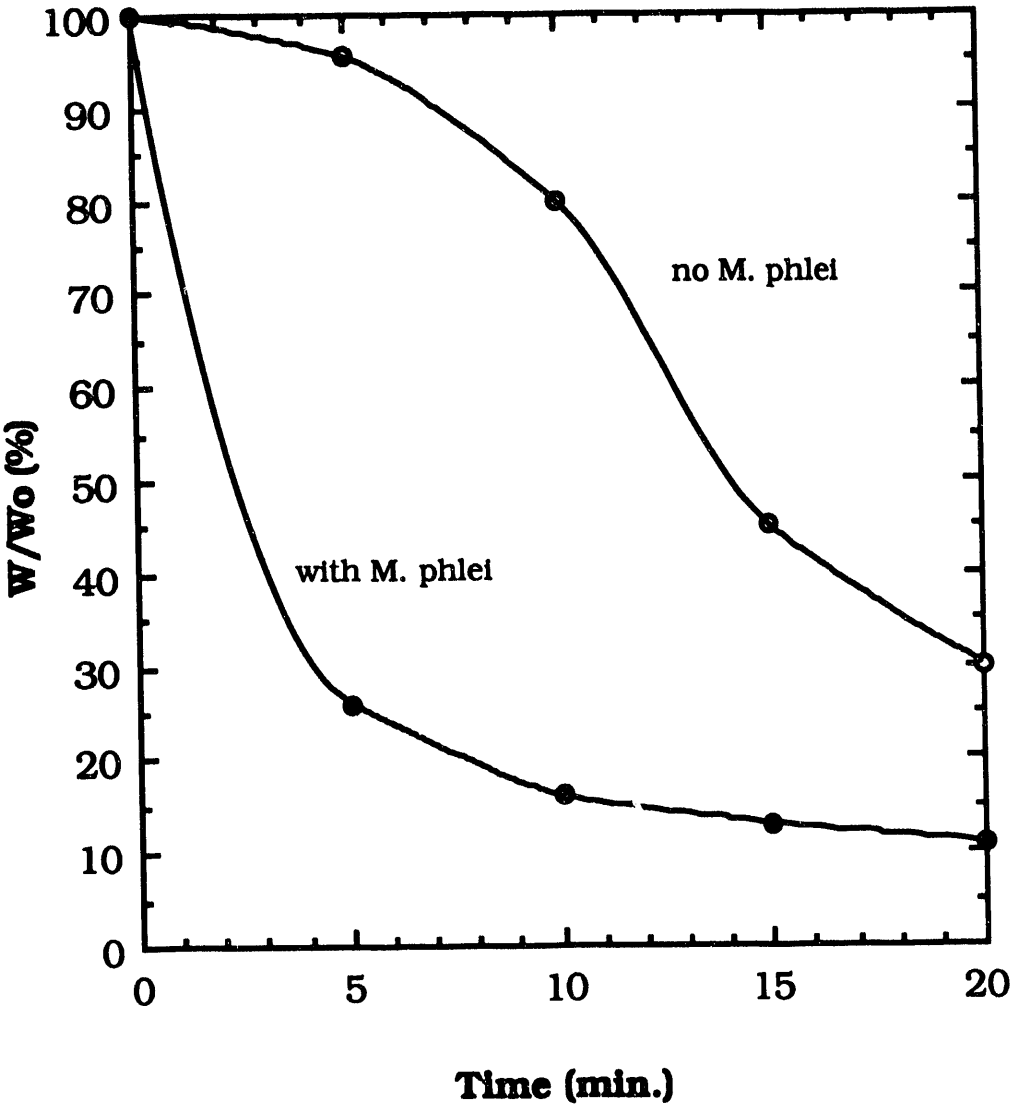

Figure 4-40. SETTING RATE OF KEROGEN CONCENTRATION WITH AND WITHOUT M. phlei AT pH 10.63

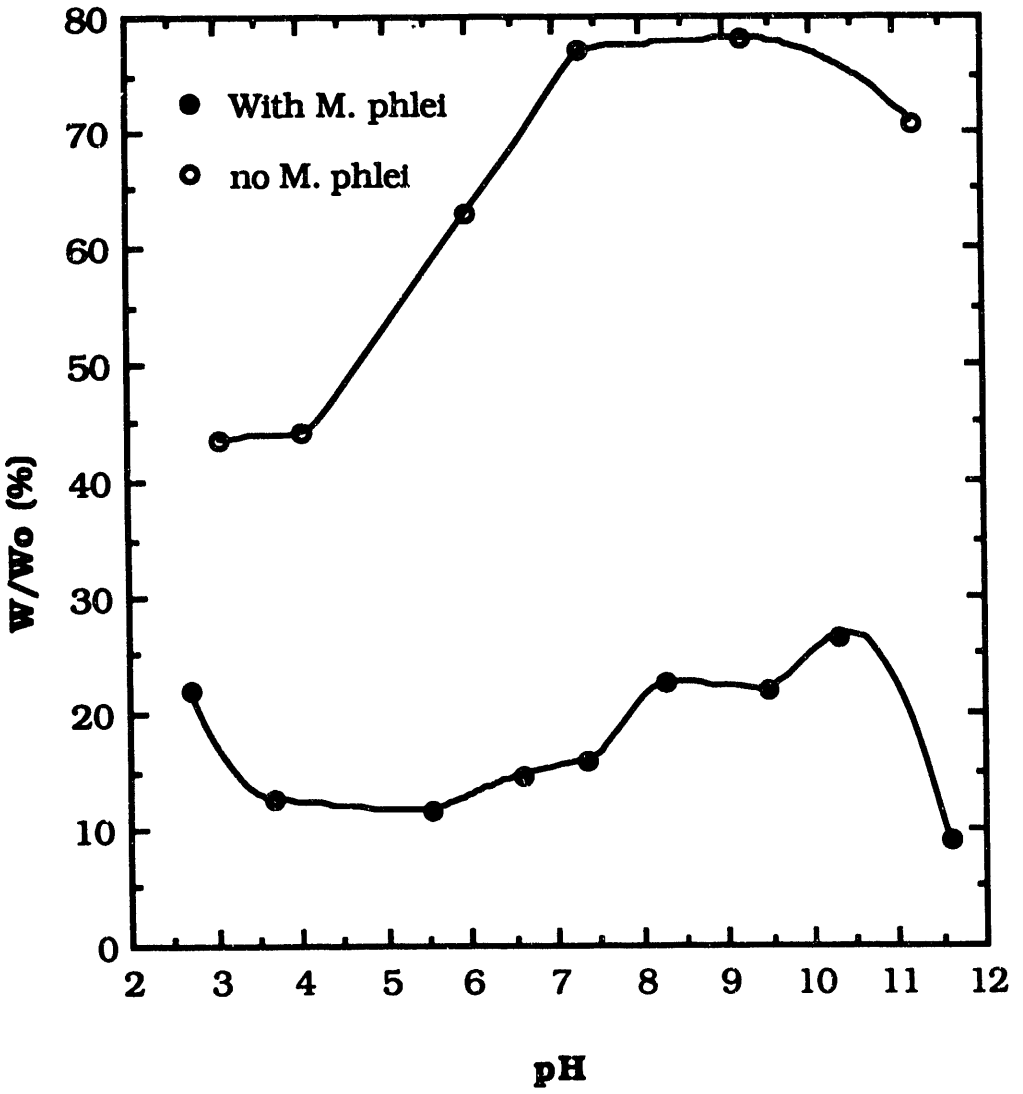

Figure 4-41. EFFECT OF pH AND THE PRESENCE OR ABSENCE OF M. phlei ON THE SEDIMENTATION (After 5 Minutes) OF FRESHLY PREPARED BENEFICIATED FLOTATION CONCENTRATE

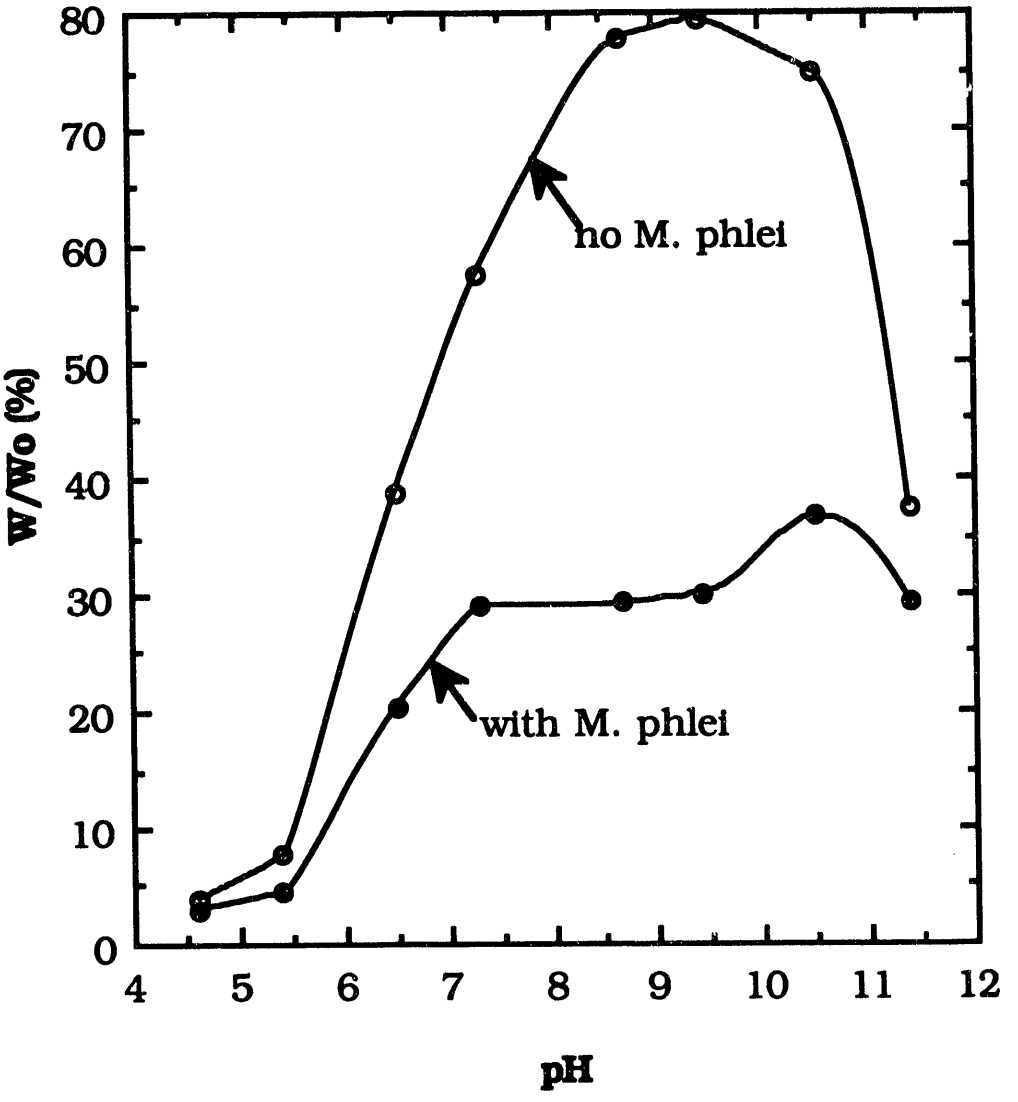

Figure 4-42. EFFECT OF pH AND THE PRESENCE OR ABSENCE OF M. phlei ON THE SEDIMENTATION (After 5 Minutes) OF DRIED KEROGEN CONCENTRATE

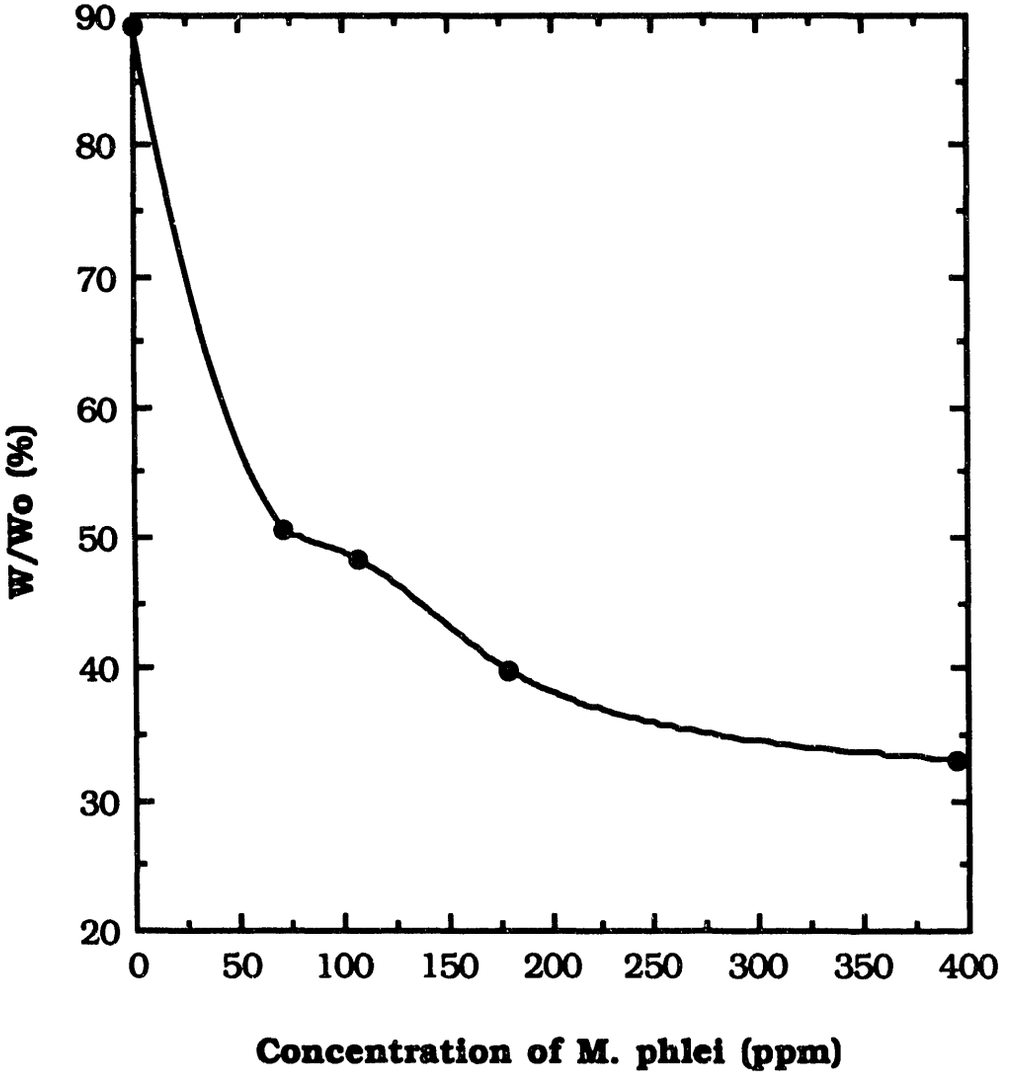

Figure 4-43. EFFECT OF M. phlei CONCENTRATION ON SEDIMENTATION (After 5 Minutes) OF KEROGEN CONCENTRATE AT pH 11.0

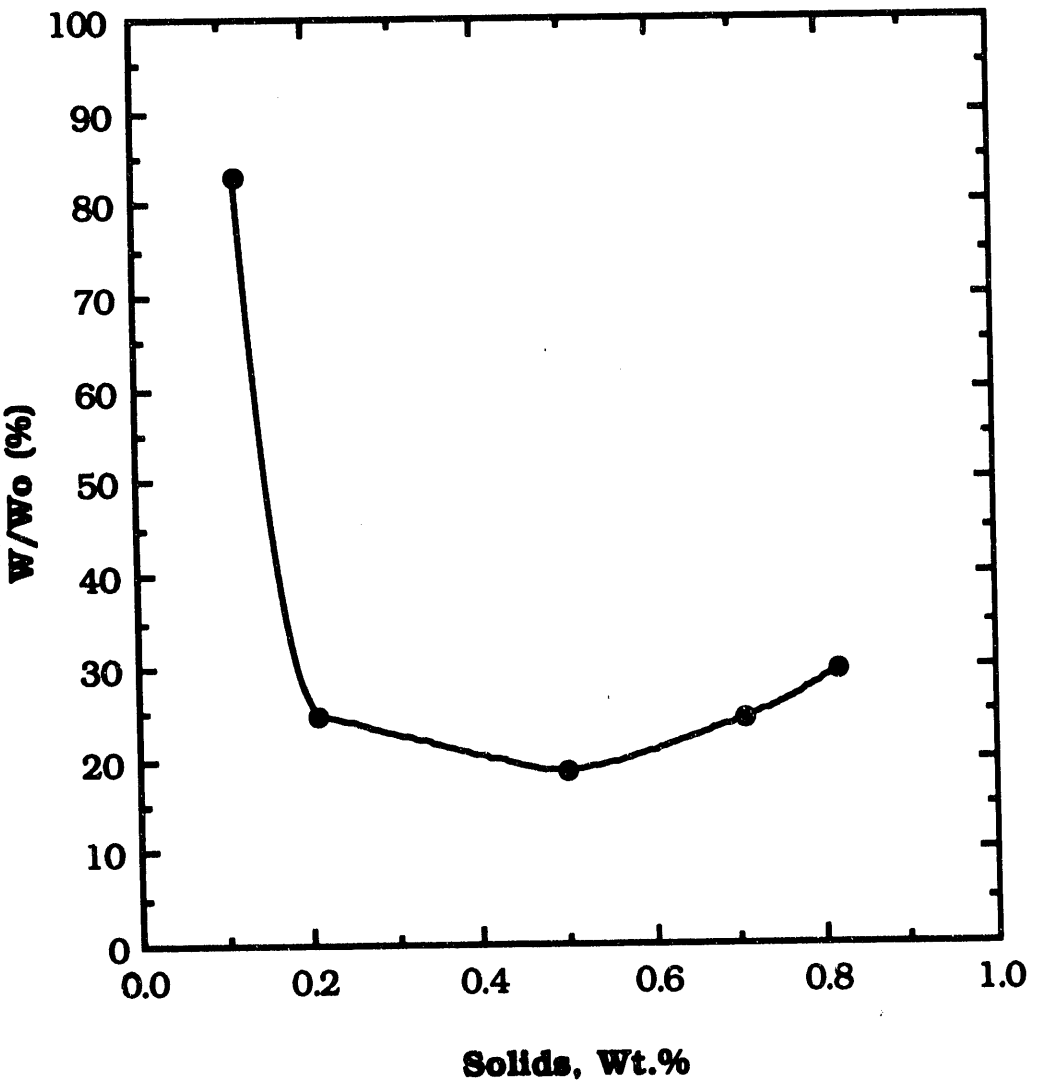

Figure 4-44. EFFECT OF KEROGEN CONCENTRATION WITH M. phlei ON SEDIMENTATION (After 5 Minutes)

The residual moisture content in the filter cake with different nonionic IGEPAL series surfactants are given in Figures 4-45 through 4-48. With increasing surfactant concentration, the equilibrium moisture of the filter cake decreased. For example, when the concentration of CO-630 was 80 ppm, the equilibrium moisture was about 40.5 percent. By increasing the surfactant concentration, the residue moisture increased again. Residual moisture content in the filter cake was evaluated as a function of HLB of the surfactants used (Figure 4-49). It was noticed that the increase in HLB number showed a concomitant decrease in the residual moisture in the filter cake.

Following the experiments with nonionic surfactants, a few experiments were conducted with a cationic surfactant, dodecyl ammonium chloride. Filtration of residual moisture as a function of concentration of dodecyl ammonium chloride is given in Figure 4-50. It can be seen that the residual moisture content can be decreased from 42 to 39.2 percent with the addition of dodecyl ammonium chloride. Further, it appears that dodecyl ammonium chloride is a good dewatering aid compared to nonionic surfactants.

UN also conducted tests to determine the dewatering rate of kerogen (without organism, with organisms, and with organism-surfactant combinations). The rate of filtration as a function of time was measured. The results were rearranged to give the filter cake resistance (see Appendix B). As can been seen from Figure 4-51, filter cake resistance decreased with the addition of organism and the effect is significant for organism-surfactant combinations.

Zeta Potential. The effect of pH on the zeta potentials of M. phlei and raw shale and the flotation concentrate (containing 30 percent organic carbon) is shown in Figure 4-52. It should be noted that the isoelectric points of shale and kerogen concentrate are at pH values of about 3 to 4, whereas the isoelectric point of M. phlei is at a pH of about 1.8 to 2. Further, the zeta potential of M. phlei is more negative than that of shale up to a pH of 7.

Surface Tension. Generally, most dewatering aids are nonionic, cationic or anionic surfactants. Surfactants decrease interfacial tension and enhance dewatering. In order to test the validity of this concept, the interfacial tension of the air/M. phlei solution was measured as a function of pH and organism concentration. In addition, the interfacial tension of two selected nonionic surfactants (IGEPAL series compounds) and cationic surfactant (dodecyl ammonium chloride) was also measured and compared. As Figure 4-53 shows, the interfacial tension of water decreased from 70 to 53 dyne/cm with increase in M. phlei concentration and stayed constant beyond 2500 ppm. Interfacial tension as a function of pH at constant concentration of M. phlei is given in Figure 4-54. The interfacial tension increased with increase in pH up to 8 and then decreased. The interfacial tension of IGEPAL series compounds for different concentrations is given in Figures 4-55 through 4-57. The interfacial tension decreases dramatically with IGEPAL compound addition.

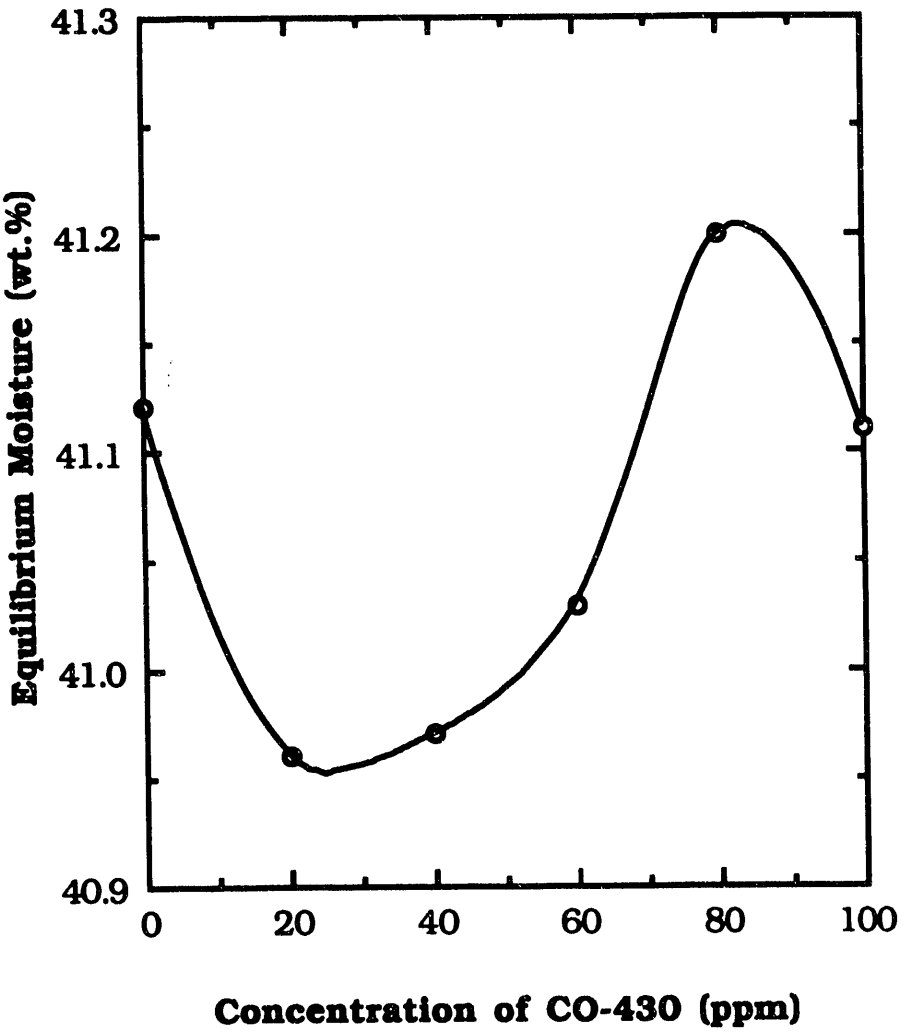

Figure 4-45. EQUILIBRIUM MOISTURE OF FILTER CAKE AS A FUNCTION OF CONCENTRATION OF CO-430

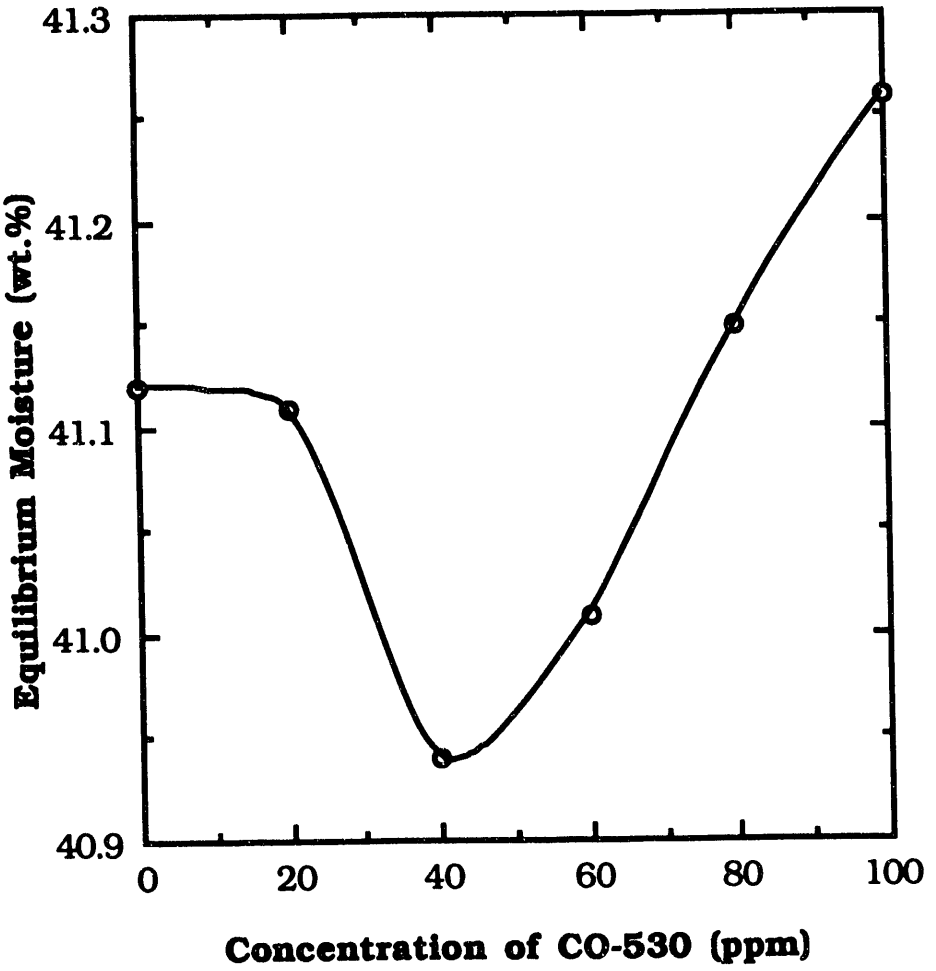

Figure 4-46. EQUILIBRIUM MOISTURE OF FILTER CAKE AS A FUNCTION OF CONCENTRATION OF CO-530

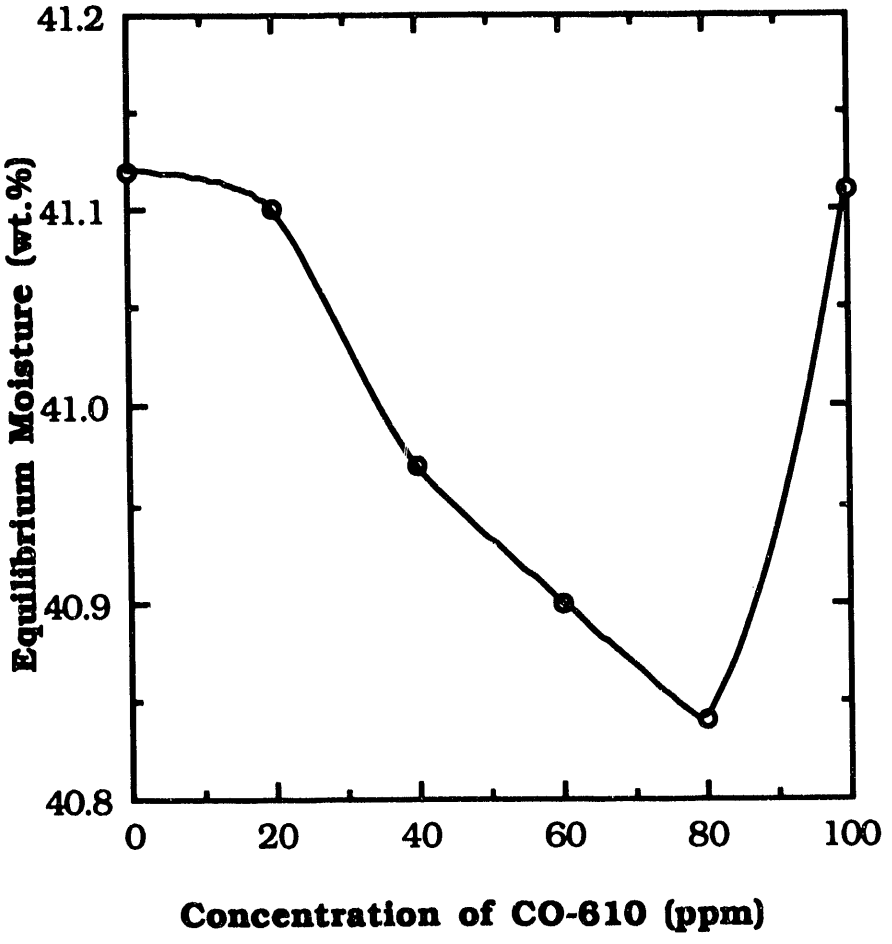

Figure 4-47. EQUILIBRIUM MOISTURE OF FILTER CAKE AS A FUNCTION OF CONCENTRATION OF CO-610

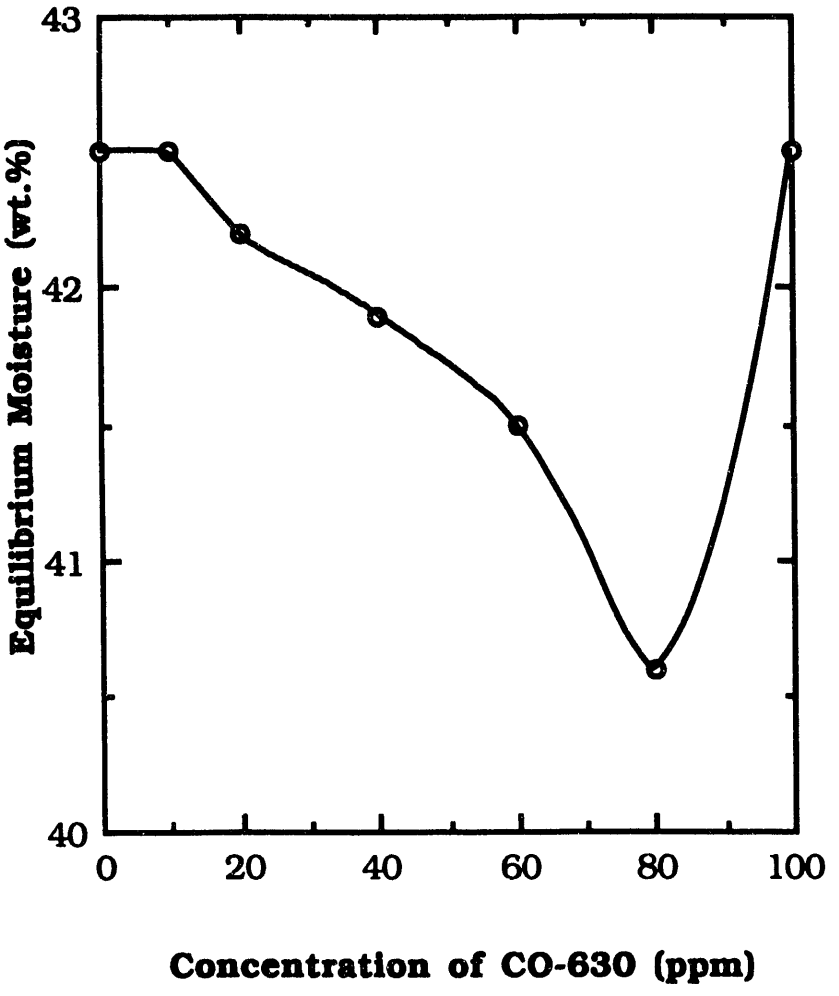

Figure 4-48. EQUILIBRIUM MOISTURE OF FILTER CAKE AS A FUNCTION OF CONCENTRATION OF CO-630

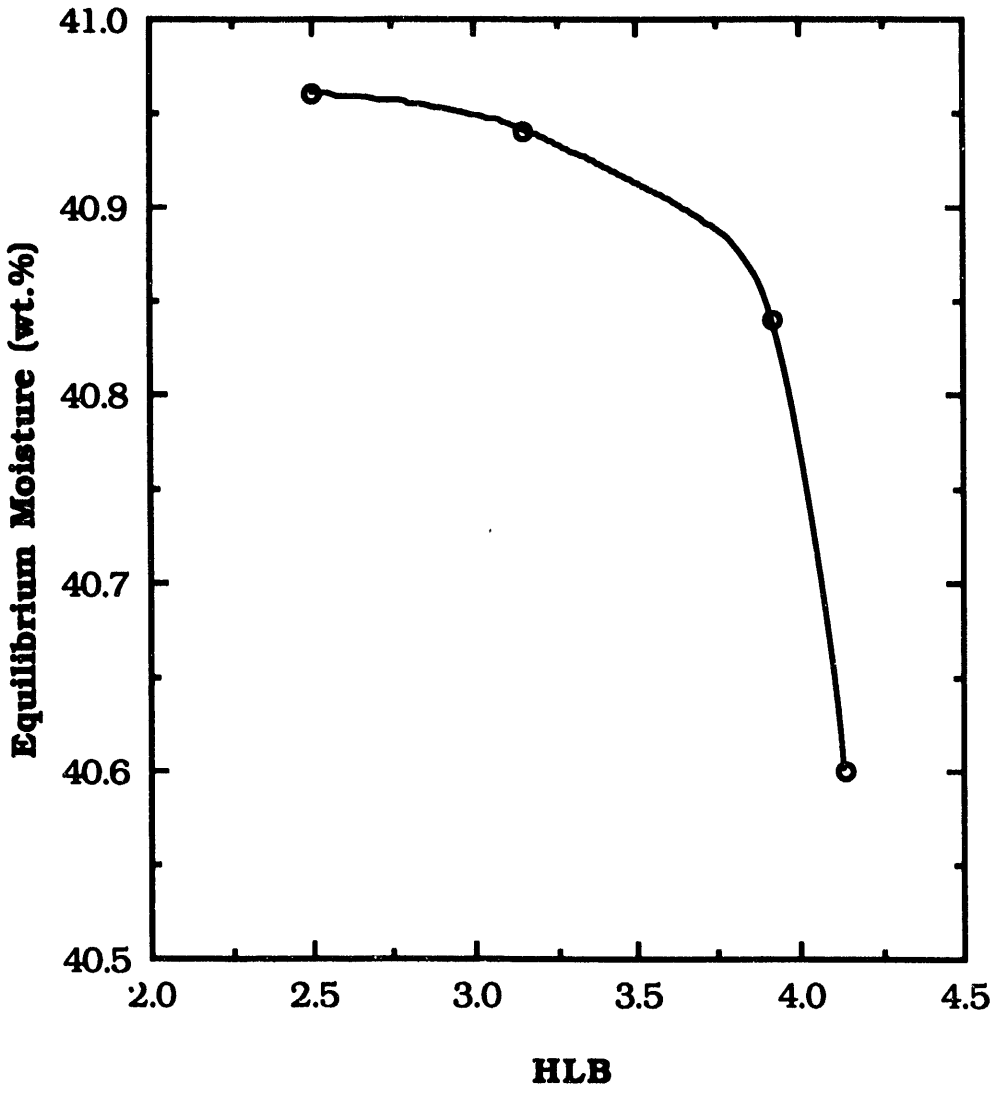

Figure 4-49. EQUILIBRIUM MOISTURE OF CAKE AS A FUNCTION OF HLB NUMBER OF SURFACTANTS

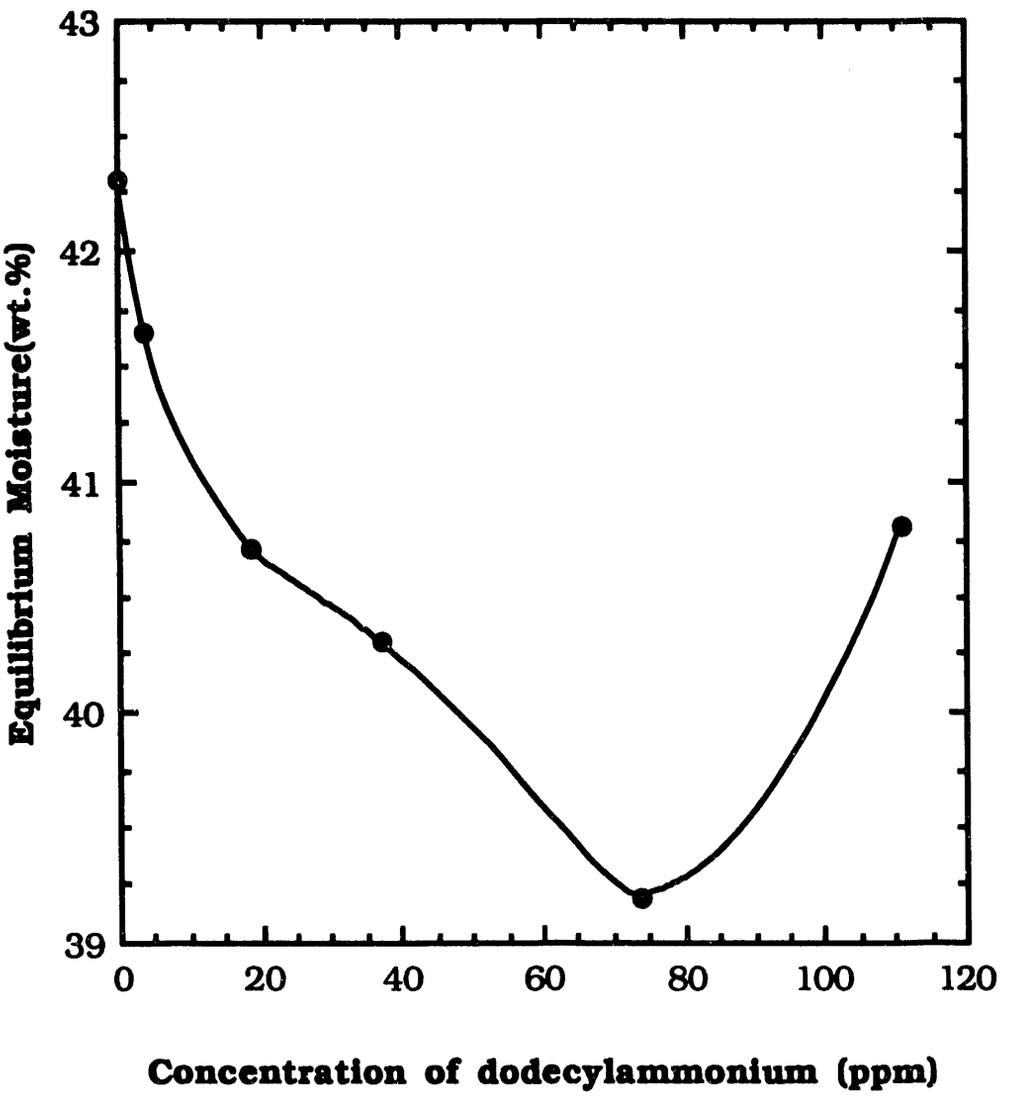

Figure 4-50. EQUILIBRIUM MOISTURE OF FILTER CAKE AS A FUNCTION OF CONCENTRATION OF DODECYL AMMONIUM CHLORIDE

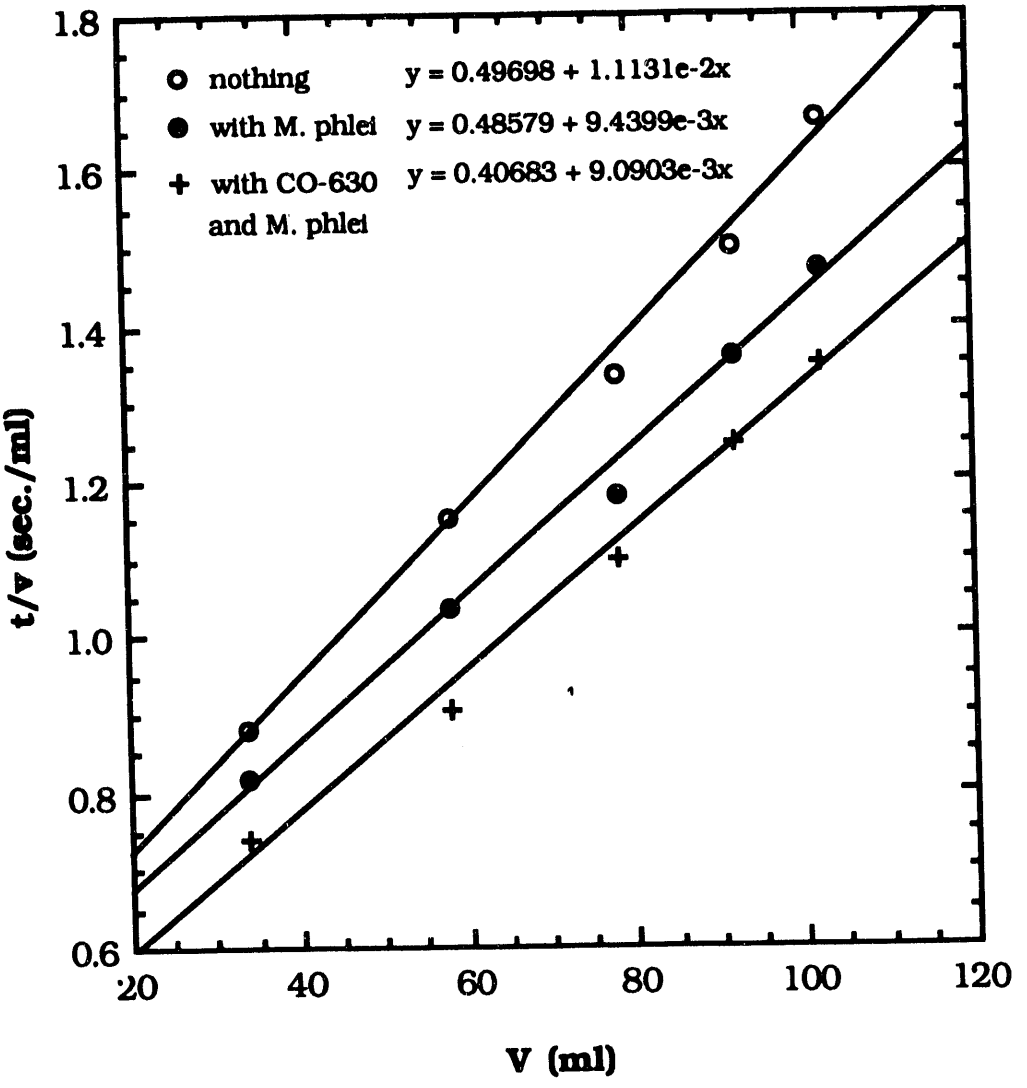

Figure 4-51. TIME/FILTRATE VOLUME (t/v) AS A FUNCTION OF FILTRATE VOLUME RECOVERED (v)

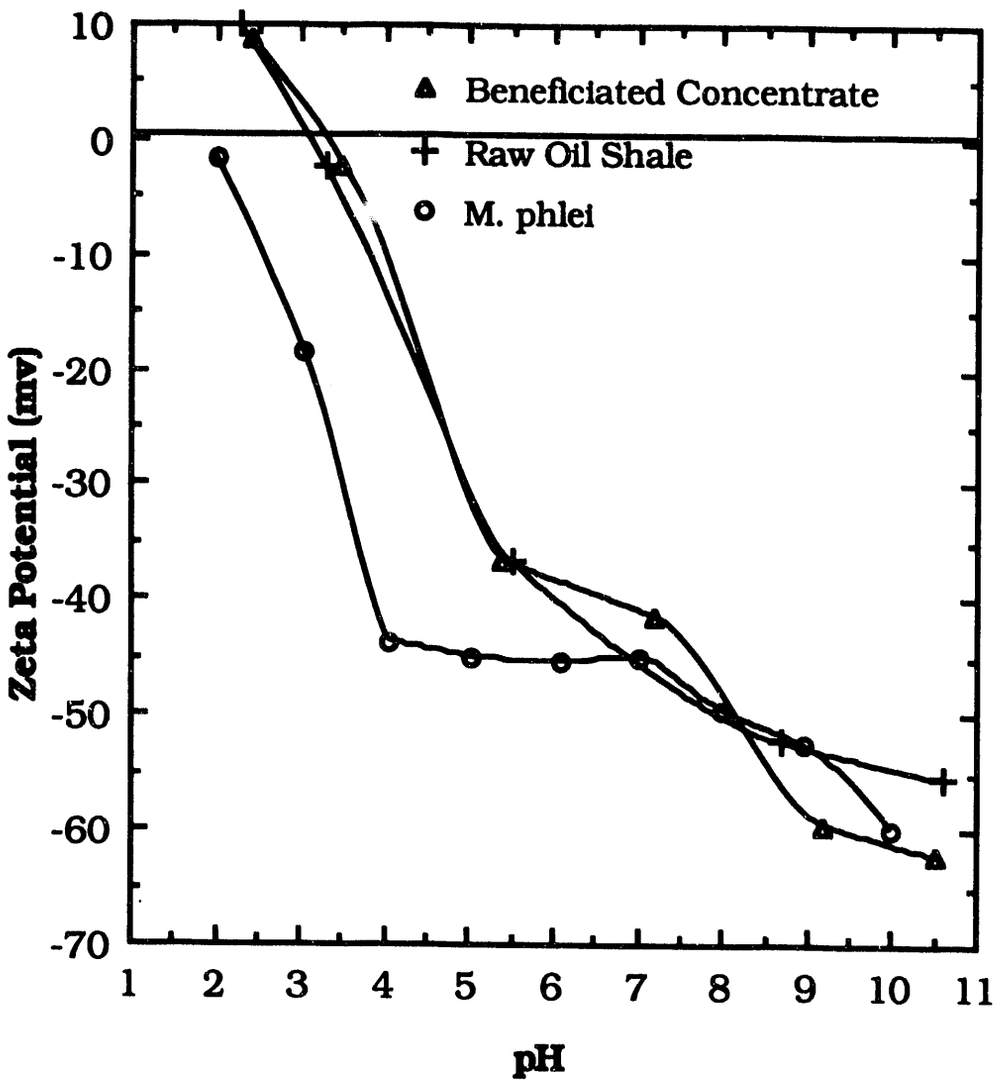

Figure 4-52. EFFECT OF pH ON THE ZETA POTENTIAL OF M. phlei, RAW SHALE AND BENEFICIATED CONCENTRATE

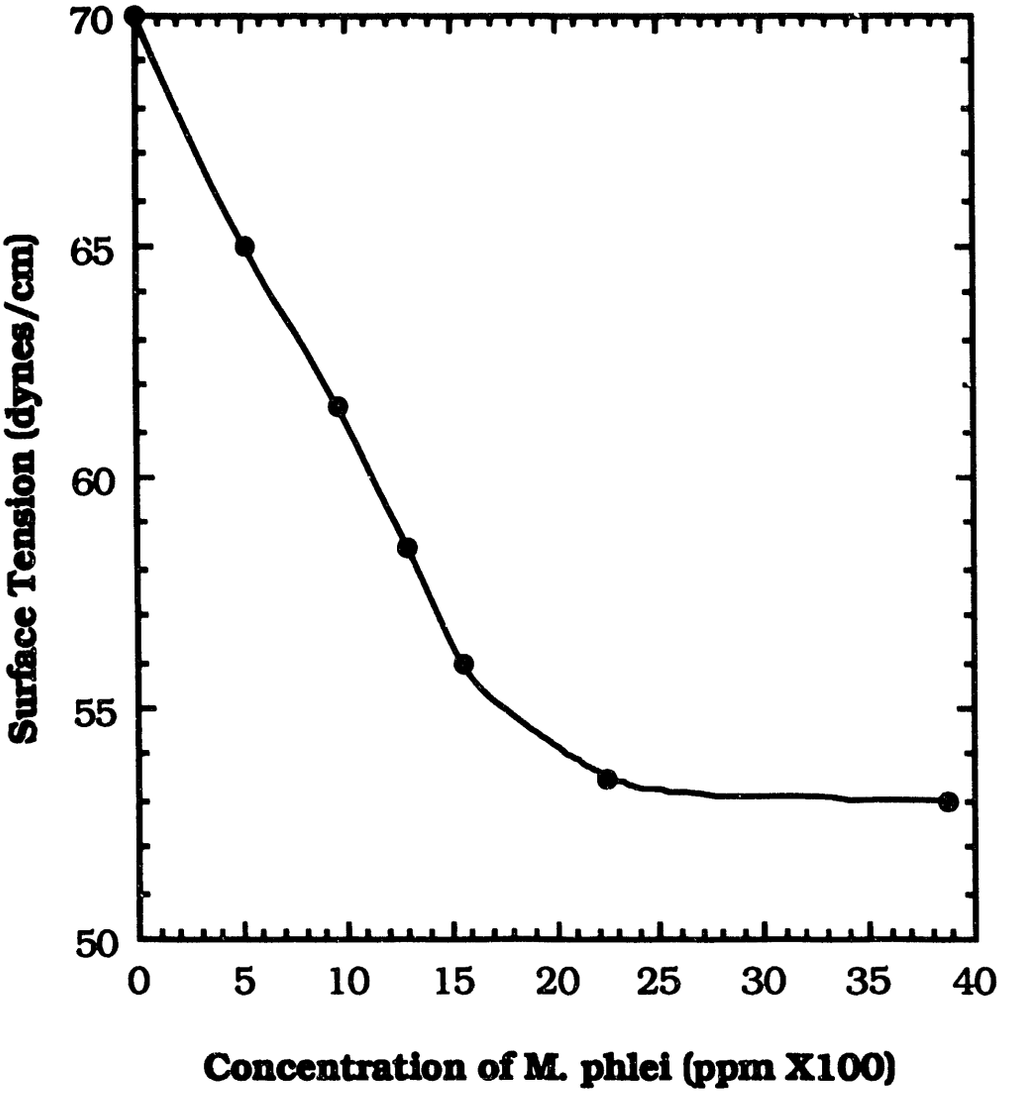

Figure 4-53. SURFACE TENSION OF M. phlei SOLUTION AS A FUNCTION OF ITS CONCENTRATION AT pH 9.30

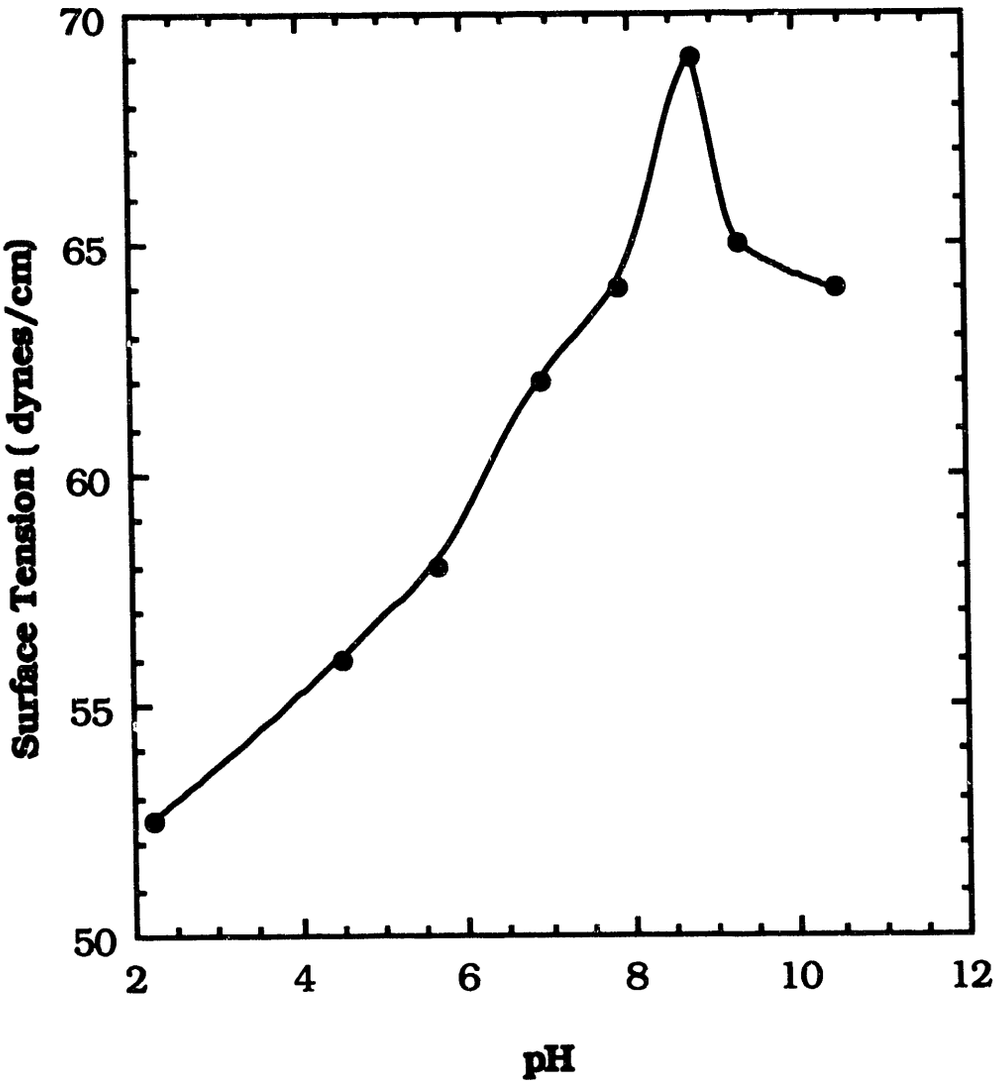

Figure 4-54. SURFACE TENSION OF M. phlei SOLUTION AS A FUNCTION OF pH WITH 560 ppm M. phlei

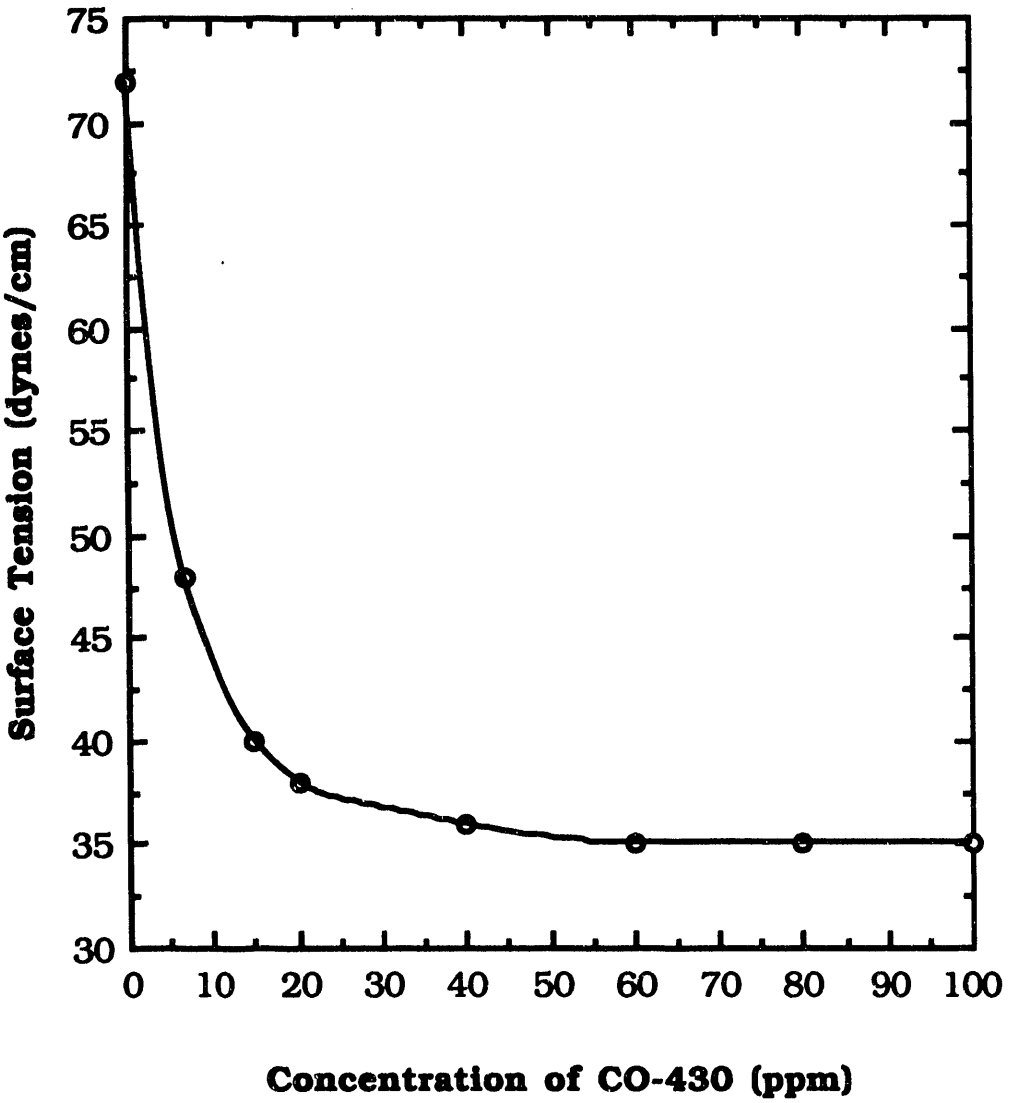

Figure 4-55. SURFACE TENSION AS A FUNCTION OF CONCENTRATION OF CO-430

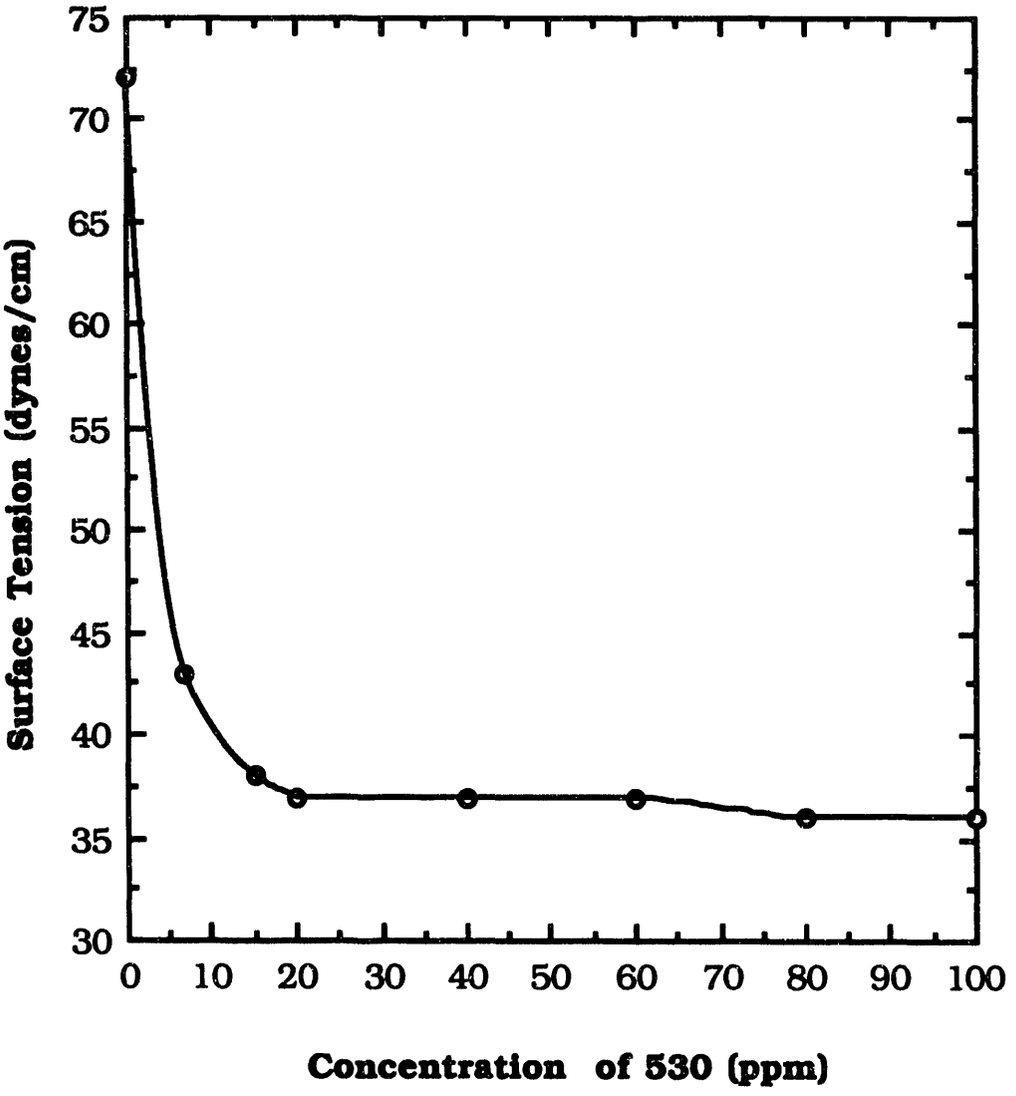

Figure 4-56. SURFACE TENSION AS A FUNCTION OF CONCENTRATION OF CO-530

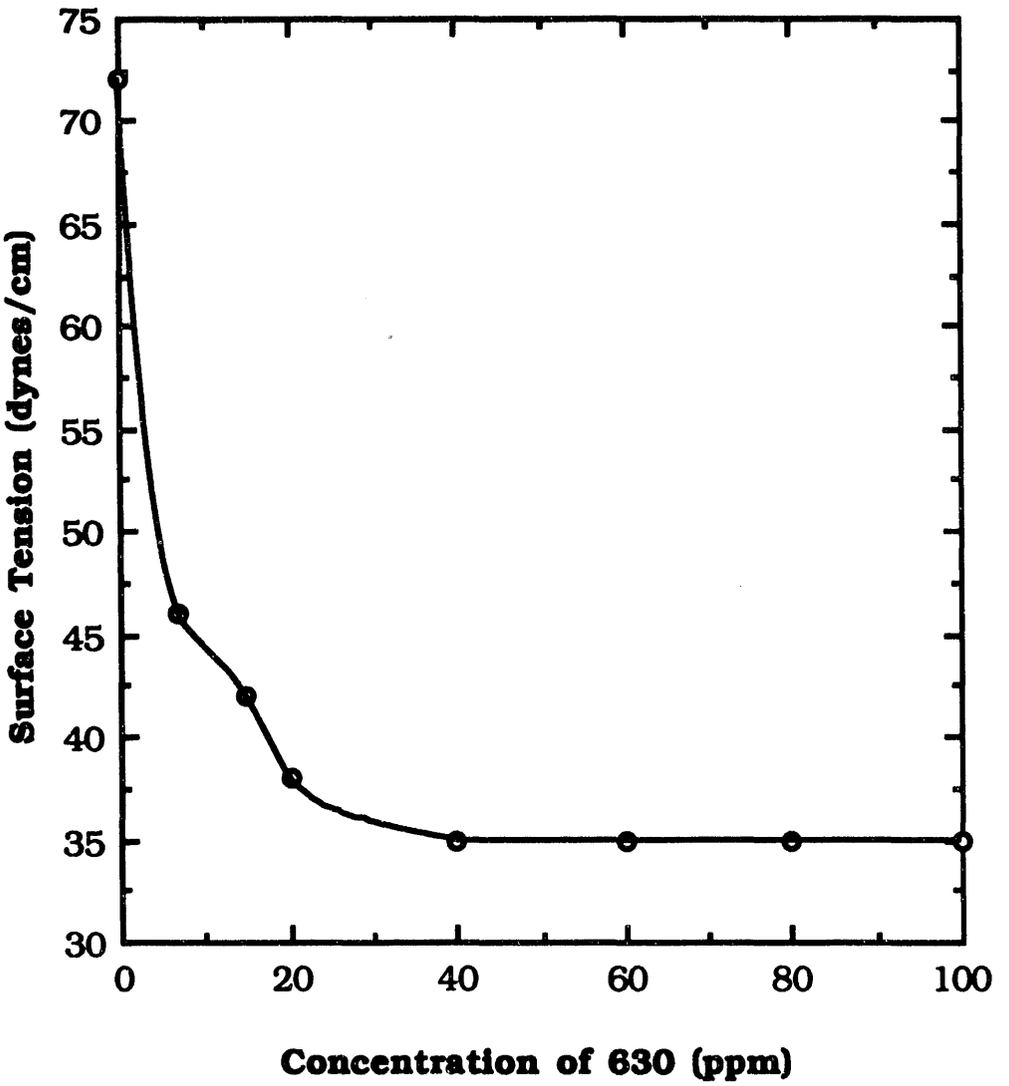

Figure 4-57. SURFACE TENSION AS A FUNCTION OF CONCENTRATION OF CO-630

The interfacial tension was not much affected with dodecyl ammonium chloride (Figure 4-58). However, the surface tension measurement obtained with dodecyl ammonium chloride is comparable to that of solutions containing M. phlei. These results suggest that M. phlei is capable of acting as a surfactant.

Effect of Recycled Water. A few experiments were conducted to determine the effect of recycled process water on the flotation process. It is well known that the recycled process water generated by conventional thickening using polymeric flocculants, invariably has an adverse effect on flotation. As can be seen from Figure 4-59, the kerogen concentrate produced by the recycled water (recycled from the bio-thickener) improved the grade and recovery compared to a clean tap water. Results presented in the figure are from a single-stage Denver flotation experiment. These results suggest that the presence of some surfactant derived from the M. phlei is improving both the concentrate grade and recovery.

Summary

The finely dispersed kerogen particles present in beneficiated flotation concentrate can be aggregated with the addition of a novel microorganism M. phlei. M. phlei possesses both a hydrophobic surface and a highly negative electrostatic charge. It adheres to the kerogen surface selectively. The rate and extent of kerogen aggregation and flocculation is dependent upon the system pH, organism concentration and solids concentration. It was demonstrated that most of the process water can be recycled using bioflocculation technology. With the addition of microorganism, more than 80 percent of the process water can be recycled. The recycled process water apparently does not have any deleterious effect on flotation performance.

Not only is the bacterium a strong flocculant, it also acts as a dewatering aid. M. phlei had a positive effect on the vacuum filtration of flocculated kerogen. The residual moisture content in the filter cake can be decreased from about 50 to 51 percent (without any organism) to about 41 to 42 percent with M. phlei. Further, the addition of surfactant decreased residual moisture in the filter cake to as low as 39 percent.

It is recommended that flocculation and dewatering process technology be investigated on a continuous and larger scale. The data obtained from a continuous unit can be used for scale-up and design of a biothickener and vacuum filtration unit for dewatering of kerogen containing beneficiated flotation concentrates.

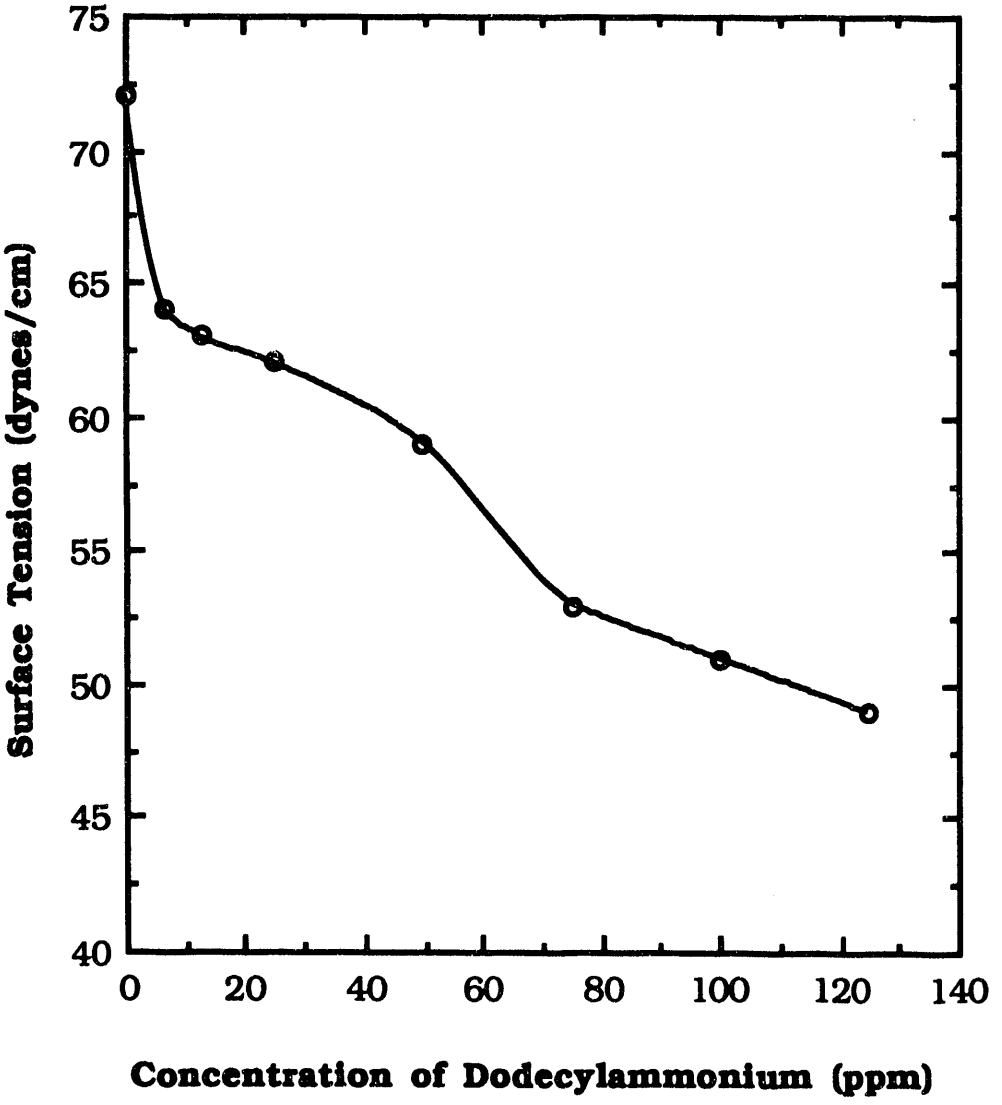

Figure 4-58. SURFACE TENSION AS A FUNCTION OF CONCENTRATION OF DODECYL AMMONIUM CHLORIDE

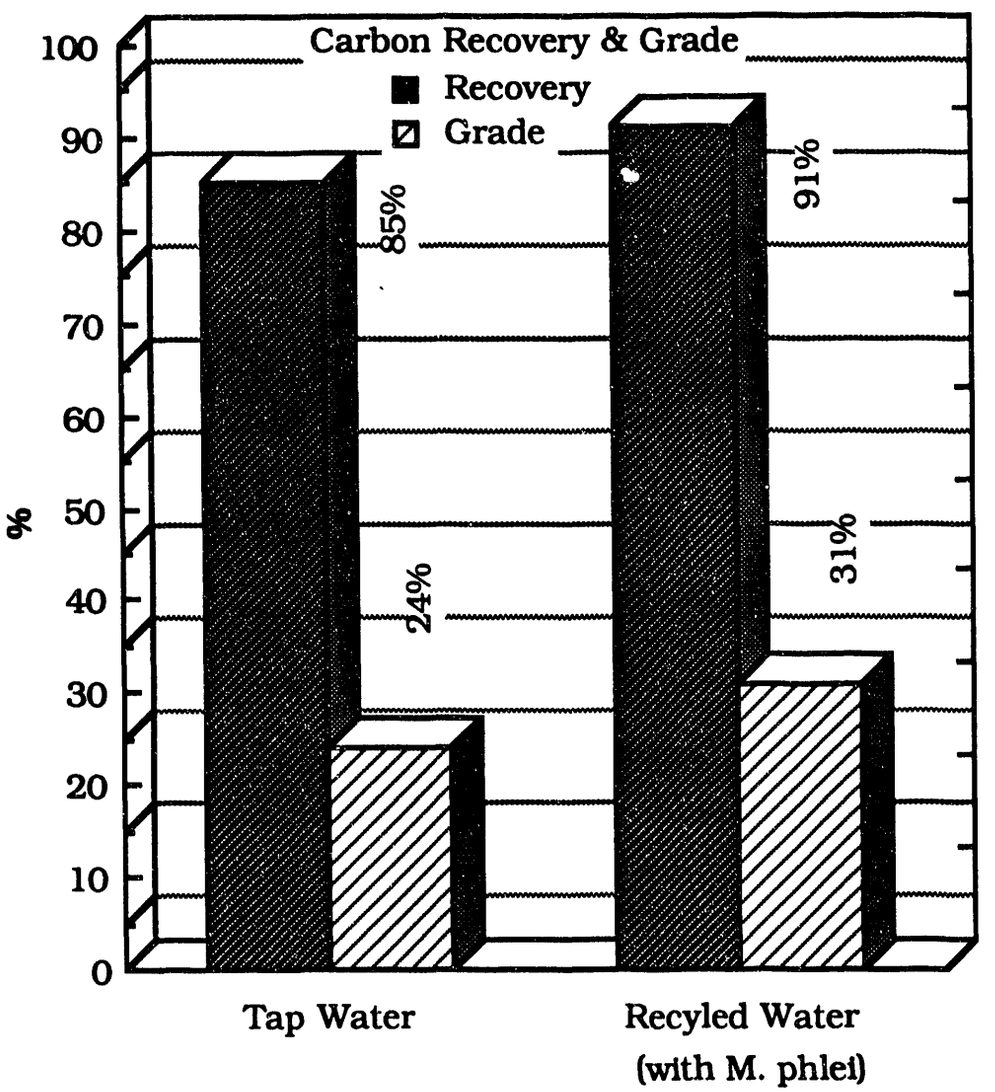

Figure 4-59. THE EFFECT OF RECYCLED WATER ON FLOTATION RECOVERY AND GRADE

Task 5. Operation of PFH on Beneficiated Shale

The objectives of this task were to expand the PFH data base by conducting laboratory- and bench-scale tests with beneficiated Alabama shale, and to characterize the effluent streams from these tests. This task is divided into two subtasks: 5.2.1. (Laboratory-Scale Tests) and 5.2.2. (Bench-Scale Continuous Tests), which were performed by IGT.

Subtask 5.2. Reactive Testing

Subtask 5.2.1. Laboratory-Scale Tests

The objective of this subtask was to conduct laboratory-scale batch and continuous tests with beneficiated shale to determine the operating conditions for bench-scale testing in Subtask 5.2.2.

IGT conducted twenty batch tests and seven continuous tests in the 2-inch (5.1-cm) diameter laboratory-scale PFH reactors. Seven of the batch tests were conducted in the performance of Subtask 3.8. Thirteen of the batch tests and all of the continuous tests were conducted in this subtask. Batch test conditions were selected to determine the effects of temperature, hydrogen pressure, residence time, and particle size on carbon conversions and oil yield. Lab-scale continuous tests were then used to confirm the batch test conversions in a continuous PFH reactor. The bench-scale PFH test in Subtask 5.2.2 was conducted at the optimum temperature, pressure, and residence time for oil yield determined in the batch PFH tests. The continuous tests confirmed the batch test results and provided information on the feeding and discharging of beneficiated shale from a continuous fluidized-bed reactor.

The lab-scale batch tests were conducted with samples riffled from a large batch of pelletized, beneficiated Alabama shale. The pelletized shale was sized to -16+70 mesh with the great majority between 20 and 50 mesh. The analysis of the feed shale is shown below. The operating conditions of the batch PFH tests include temperatures of 850° to 1070°F (455° to 575°C), pressures of 200 to 1000 psig (1.4 to 7.0 MPa), particle sizes of -20+30 mesh to -50+80 mesh, and residence times of 5 to 30 minutes. The operating conditions, carbon conversions, and oil yields for the batch PFH tests are summarized in Table 5-1. The operating conditions and results of the successful tests conducted in the continuous PFH unit are presented in Table 5-2.

Moisture, wt %	1.87
Ultimate Analysis, wt % dry	
Ash	54.30
Carbon	32.15
Hydrogen	3.11
Sulfur	9.15
Nitrogen	0.85
Oxygen (HTW)	4.72
FA Oil Yield, GPT	22.5
L/metric ton	94.0
Bulk Density, g/cm^3	0.741

Table 5-1, Part 1. SUMMARY OF TEST CONDITIONS AND RESULTS OF BATCH PFH TESTS WITH BENEFICIATED ALABAMA SHALE

Test No.	35-B-1	35-B-2	35-B-3	35-B-4	35-B-5
Average Feed Hopper Temperature, °F	141	163	110	165	160
Feed Hopper Residence Time, min	10	15	10	10	5
Average Reactor Temperature, °F	937	1227	940	1072	1231
Reactor Residence Time, min	20	20	19	19	19
Pressure, psig	227	221	611	613	549
Shale Particle Size, mesh	----------	----------	-20+50	----------	----------
Superficial Gas Velocity, ft/s	0.093	0.106	0.081	0.088	0.108
Minimum Fluidization Velocity, ft/s	----------	----------	0.047	----------	----------
Product Distribution, % of feed carbon					
Residue Shale	40.1	41.6	27.5	27.5	26.6
Product Gas	10.4	27.7	11.1	16.5	30.3
Oil	49.5	30.7	61.4	56.0	43.1
Total	100.0	100.0	100.0	100.0	100.0
Oil Specific Gravity	0.983	1.057	0.995	1.012	1.067
°API	12.4	2.4	10.7	8.3	1.1
Oil Yield, GPT	45.5	27.5	55.6	49.9	36.9
Product Gas,* mol %					
H_2	96.55	73.76	98.43	97.14	94.72
CO	0.04	0.19	0.00	0.00	0.00
CO_2	0.00	0.12	0.00	0.00	0.00
CH_4	1.74	17.09	0.85	1.66	3.47
C_2H_6	0.76	7.62	0.38	0.69	1.60
C_2H_4	0.06	0.02	0.00	0.00	0.00
C_3H_8	0.46	0.65	0.19	0.31	0.14
C_3H_6	0.10	0.12	0.03	0.03	0.02
C_4H_{10}	0.12	0.13	0.07	0.10	0.03
C_4H_8	0.05	0.08	0.00	0.01	0.00
C_5H_{12}	0.04	0.00	0.01	0.02	0.00
C_6^+	0.08	0.22	0.04	0.04	0.02
Total	100.00	100.00	100.00	100.00	100.00

* H_2S-free basis.

Table 5-1, Part 2. SUMMARY OF TEST CONDITIONS AND RESULTS OF BATCH PFH TESTS WITH BENEFICIATED ALABAMA SHALE

Test No.	35-B-6	35-B-7	51-B-1	52-B-2	51-B-3
Average Feed Hopper Temperature, °F	145	132	225	200	220
Feed Hopper Residence Time, min	10	10	15	25	15
Average Reactor Temperature, °F	946	1213	969	956	926
Reactor Residence Time, min	20	20	30	10	5
Pressure, psig	1055	1017	977	977	988
Shale Particle Size, mesh	----------	----------	-20+50	----------	----------
Superficial Gas Velocity, ft/s	0.062	0.090	0.078	0.087	0.078
Minimum Fluidization Velocity, ft/s	----------	----------	0.047	----------	----------
Product Distribution, % of feed carbon					
Residue Shale	15.6	23.0	19.0	23.6	30.8
Product Gas	13.2	37.6	14.5	11.8	10.7
Oil	71.2	39.4	66.5	64.6	58.5
Total	100.0	100.0	100.0	100.0	100.0
Oil Specific Gravity	0.980	1.113	1.009	1.012	1.009
°API	12.9	-4.4	8.7	8.3	8.7
Oil Yield, GPT	65.7	32.0	59.3	57.3	51.9
Product Gas,* mol %					
H_2	98.95	98.12	98.48	98.88	98.88
CO	0.00	0.00	0.00	0.00	0.00
CO_2	0.00	0.00	0.06	0.00	0.09
CH_4	0.53	1.15	0.78	0.56	0.52
C_2H_6	0.28	0.62	0.40	0.26	0.26
C_2H_4	0.00	0.00	0.00	0.00	0.00
C_3H_8	0.14	0.08	0.20	0.16	0.13
C_3H_6	0.01	0.01	0.01	0.02	0.02
C_4H_{10}	0.06	0.02	0.05	0.06	0.06
C_4H_8	0.00	0.00	0.00	0.00	0.00
C_5H_{12}	0.01	0.00	0.00	0.02	0.01
C_6+	0.02	0.00	0.02	0.04	0.03
Total	100.00	100.00	100.00	100.00	100.00

* H_2S-free basis.

Table 5-1, Part 3. SUMMARY OF TEST CONDITIONS AND RESULTS OF BATCH PFH TESTS WITH BENEFICIATED ALABAMA SHALE

Test No.	51-B-4	51-B-5	51-B-6	51-B-7	51-B-8
Average Feed Hopper Temperature, °F	210	195	90	265	102
Feed Hopper Residence Time, min	10	30	5	20	10
Average Reactor Temperature, °F	848	1040	951	984	969
Reactor Residence Time, min	21	18	10	10	9
Pressure, psig	988	981	977	620	604
Shale Particle Size, mesh	---	-20+50	----	-50+80	-20+50	-50+80
Superficial Gas Velocity, ft/s	0.064	0.083	0.038	0.088	0.032
Minimum Fluidization Velocity, ft/s	----	0.047	----	0.024	0.047	0.024
Product Distribution, % of feed carbon					
Residue Shale	39.6	20.0	22.2	26.6	31.0
Product Gas	8.5	15.9	11.8	14.4	12.6
Oil	51.9	64.1	66.0	59.0	56.4
Total	100.0	100.0	100.0	100.0	100.0
Oil Specific Gravity	0.998	1.013	1.013	1.010	0.997
°API	10.3	8.2	8.2	8.6	10.4
Oil Yield, GPT	46.7	57.0	58.8	52.7	51.4
Product Gas,* mol %					
H_2	99.36	98.36	98.95	97.90	98.30
CO	0.00	0.00	0.00	0.00	0.00
CO_2	0.03	0.00	0.00	0.02	0.00
CH_4	0.28	0.88	0.55	1.11	0.92
C_2H_6	0.17	0.39	0.24	0.47	0.36
C_2H_4	0.00	0.00	0.00	0.00	0.02
C_3H_8	0.10	0.23	0.13	0.24	0.17
C_3H_6	0.01	0.02	0.03	0.05	0.05
C_4H_{10}	0.03	0.07	0.05	0.10	0.08
C_4H_8	0.00	0.00	0.00	0.02	0.04
C_5H_{12}	0.00	0.02	0.02	0.03	0.02
C_6+	0.02	0.03	0.03	0.06	0.04
Total	100.00	100.00	100.00	100.00	100.00

* H_2S-free basis.

Table 5-1, Part 4. SUMMARY OF TEST CONDITIONS AND RESULTS OF BATCH PFH TESTS WITH BENEFICIATED ALABAMA SHALE

Test No.	51-B-9	51-B-10	51-B-11	51-B-12	51-B-13
Average Feed Hopper Temperature, °F	125	175	90	145	210
Feed Hopper Residence Time, min	5	20	10	10	10
Average Reactor Temperature, °F	941	885	980	1030	950
Reactor Residence Time, min	10	13	9	9	10
Pressure, psig	603	409	429	402	1000
Shale Particle Size, mesh	-20+30	----------	-20+50	----------	
Superficial Gas Velocity, ft/s	0.120	0.093	0.095	0.109	0.078
Minimum Fluidization Velocity, ft/s	0.250	----------	0.047	----------	
Product Distribution, % of feed carbon					
Residue Shale	29.1	35.0	31.9	30.1	22.5
Product Gas	10.3	9.2	11.3	12.2	13.1
Oil	60.6	55.8	56.8	57.7	64.4
Total	100.0	100.0	100.0	100.0	100.0
Oil Specific Gravity	0.997	0.999	0.994	1.000	1.019
°API	10.4	10.1	10.8	10.0	7.4
Oil Yield, GPT	54.9	50.5	51.4	51.9	56.7
Product Gas,* mol %					
H_2	98.46	98.38	97.68	92.50	98.72
CO	0.00	0.00	0.00	0.00	0.00
CO_2	0.00	0.00	0.00	0.06	0.00
CH_4	0.78	0.78	1.25	4.34	0.63
C_2H_6	0.35	0.39	0.50	2.29	0.33
C_2H_4	0.00	0.00	0.05	0.00	0.00
C_3H_8	0.18	0.23	0.23	0.55	0.20
C_3H_6	0.04	0.04	0.06	0.06	0.02
C_4H_{10}	0.08	0.09	0.09	0.08	0.06
C_4H_8	0.02	0.02	0.04	0.00	0.00
C_5H_{12}	0.02	0.02	0.03	0.00	0.01
C_6+	0.07	0.05	0.07	0.12	0.03
Total	100.00	100.00	100.00	100.00	100.00

* H_2S-free basis.

Table 5-2. SUMMARY OF OPERATING CONDITIONS AND RESULTS OF CONTINUOUS PFH TESTS WITH BENEFICIATED ALABAMA SHALE

Test No.	51-C-2	51-C-3	51-C-4
Operating Conditions			
Average Temperature, °F			
Feed Hopper	--	--	--
Reactor	946	998	940
Reactor Residence Time, min	78	36	25
Pressure, psig	612	626	636
Shale Particle Size, mesh	----------	-40+80	---------
Gas Velocities, ft/s			
Superficial	0.155	0.161	0.155
Complete Fluidization	----------	0.122	---------
Operating Results			
Product Distribution, % of feed carbon			
Spent Shale	27.8	29.7	31.5
Product Gas	55.7	53.3	55.3
Oil	16.5	17.0	13.2
Total	100.0	100.0	100.0
Oil Yield, GPT	48.5	45.7	48.3
Oil Yield, % of FA	217	204	216
Oil Gravity, °API	6.0	5.0	7.0
Oil Density, g/mL	1.029	1.037	1.022
Product Gas Composition,* mol %			
H_2	95.17	94.08	94.69
CO	0.00	0.00	0.00
CO_2	0.00	0.00	0.00
CH_4	2.11	2.74	2.14
C_2H_6	1.16	1.53	1.30
C_2H_4	0.04	0.05	0.05
C_3H_8	0.24	0.02	0.19
C_3H_6	0.03	0.04	0.03
C_4H_{10}	0.04	0.04	0.02
C_4H_8	0.00	0.00	0.00
C_5H_{12}	0.00	0.00	0.00
C_6+	0.01	0.02	0.01
H_2S	1.20	1.28	1.57
Total	100.00	100.00	100.00

* At the end of the steady-state period.

Table 5-2 (Cont.). SUMMARY OF OPERATING CONDITIONS AND RESULTS OF CONTINUOUS PFH TESTS WITH BENEFICIATED ALABAMA SHALE

Test No.	51-C-5	51-C-6	51-C-7
Operating Conditions			
Average Temperature, °F			
Feed Hopper	--	--	--
Reactor	931	931	929
Reactor Residence Time, min	20	40	20
Pressure, psig	400	396	1014
Shale Particle Size, mesh	----------	-40+80	----------
Gas Velocities, ft/s			
Superficial	0.168	0.183	0.121
Complete Fluidization	----------	0.122	----------
Operating Results			
Product Distribution, % of feed carbon			
Spent Shale	38.4	42.4	27.0
Product Gas	48.2	47.1	61.0
Oil	13.4	10.5	12.0
Total	100.0	100.0	100.0
Oil Yield, GPT	42.3	41.8	54.1
Oil Yield, % of FA	190	187	243
Oil Gravity, °API	7.8	8.7	9.2
Oil Density, g/mL	1.016	1.009	1.006
Product Gas Composition,* mol %			
H_2	94.99	94.92	95.25
CO	0.00	0.00	0.00
CO_2	0.03	0.04	0.00
CH_4	1.98	2.24	1.87
C_2H_6	1.19	1.22	1.12
C_2H_4	0.06	0.06	0.04
C_3H_8	0.09	0.03	0.23
C_3H_6	0.03	0.02	0.02
C_4H_{10}	0.02	0.01	0.04
C_4H_8	0.00	0.01	0.00
C_5H_{12}	0.00	0.00	0.00
C_6+	0.03	0.03	0.02
H_2S	1.58	1.42	1.41
Total	100.00	100.00	100.00

* At the end of the steady-state period.

The effects of temperature, pressure, and residence time on carbon conversion to gas and oil and total carbon conversion are presented in Figures 5-1 through 5-4. There was no apparent effect of particle size on gas or oil yield over the range tested. The feed shale was sized to -20+50 mesh for all tests except Tests 51-B-6 and 51-B-8 with a -50+80 mesh consist and Test 51-B-9 with a -20+30 mesh consist. Carbon conversions to oil and gas in these three tests are comparable to those in tests with -20+50 mesh shale at similar conditions.

As shown in Figure 5-1, carbon conversion to gas in the batch PFH tests increased with increasing temperature but was unaffected by changes in hydrogen pressure between 200 and 1000 psig (1.4 and 7.0 MPa). Gas production appears to be complete within 5 minutes at typical PFH conditions, because residence times of 5 to 30 minutes produced the same gas yield. The increase in carbon conversion to gas is linear between 850°F (455°C) and 1060°F (570°C). Above 1060°F, the carbon conversion to gas increases more rapidly with increasing temperature.

Figure 5-2 shows the effects of temperature and hydrogen partial pressure on carbon conversion to oil. Oil yield increases with increasing hydrogen pressure and has a maximum value at about 940°F (505°C). At 940°F, the carbon conversion to oil increases from 49 percent at 200 psig (1.4 MPa), to 60 percent at 600 psig (4.2 MPa), to 66 percent at 1000 psig (7.0 MPa). Increasing the temperature from 850° to 940°F (455° to 505°C) produces a large increase in carbon conversion to oil. Further temperature increase, up to 1060°F (570°C), produces a slight decrease in oil yield. Finally, increasing the temperature above 1060°F (570°C) causes a large decrease in the carbon conversion to oil.

The data indicate that the oil production rate is slower than the gas production rate. Test 51-B-3, conducted at 1000 psig (7.0 MPa), had a solids residence time of 5 minutes; the other tests had residence times in the range of 10 to 30 minutes. The carbon conversion to oil in this test was lower than that of the other tests and apparently not complete after only 5 minutes in the batch reactor. Tests with solids residence times between 10 and 30 minutes show no effects of residence time on oil yield. The carbon conversion to gas was the same for the 5-minute test and the 10- to 30-minute tests. These results suggest that carbon conversion to gas is completed more quickly than carbon conversion to oil.

Oil yields of up to 265 percent of Fischer Assay were achieved in the batch reactor. Batch test oil yields on a normalized basis - GPT (gallon per ton) per weight percent organic carbon - are presented in Figure 5-3. The Fischer Assay oil yield for the beneficiated Alabama shale was 22.5 GPT or 0.70 GPT per weight percent organic carbon. The oil yield increased with increasing hydrogen pressure and was at a maximum at about 940°F (505°C). The maximum oil yield as a function of pressure increased from 1.42 to 1.68 to 1.85 GPT per weight percent organic carbon at 200, 600, and 1000 psig (1.4, 4.2, and 7.0 MPa), respectively. These normalized yields are equivalent to actual yields of 46, 54, and 59 GPT, which are 205, 240, and 265 percent of the Fischer Assay oil yield at the same pressures.

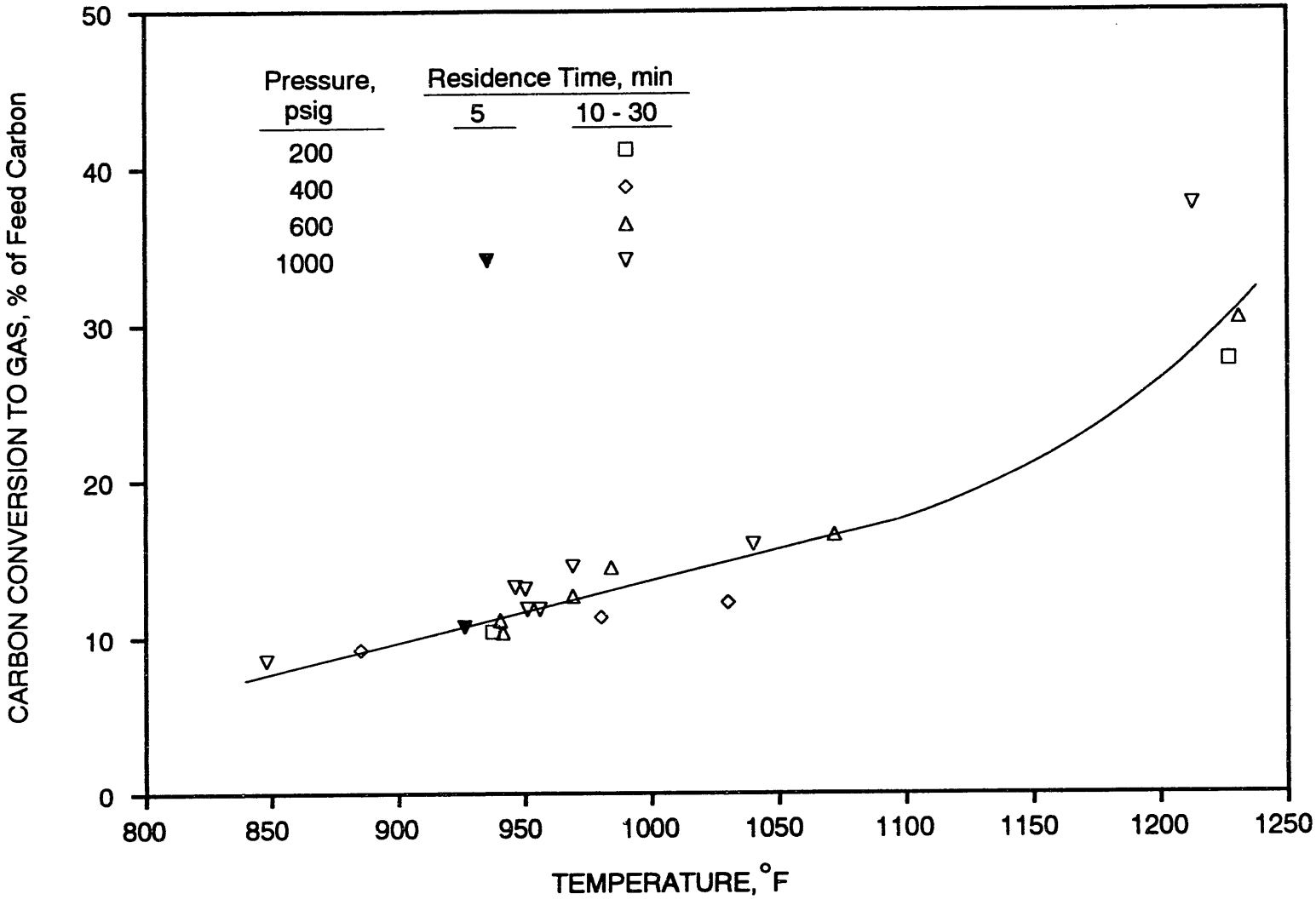

Figure 5-1. THE EFFECTS OF TEMPERATURE AND PRESSURE ON THE CARBON CONVERSION TO GAS FROM HYDRORETORTING BENEFICIATED ALABAMA SHALE

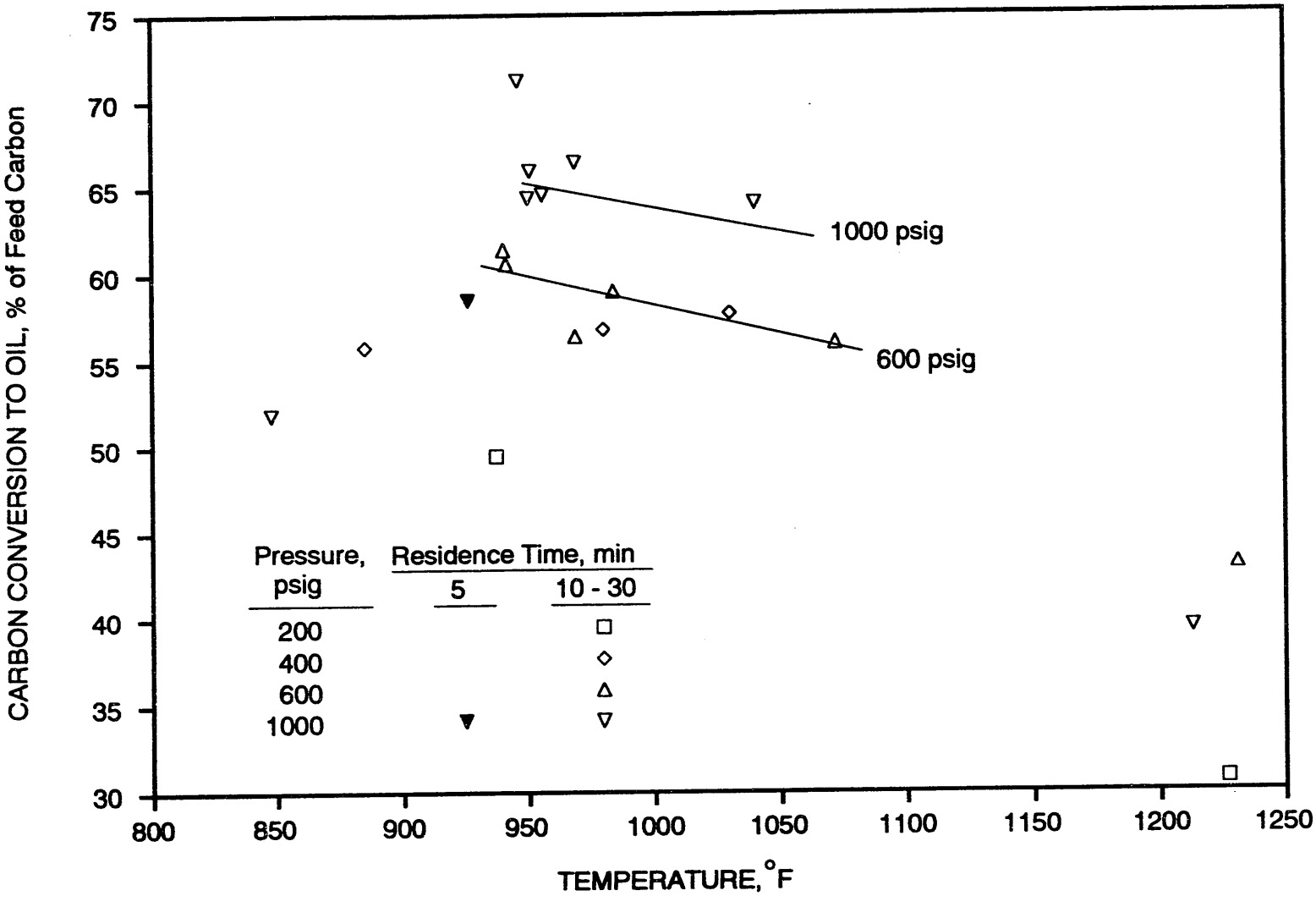

Figure 5-2. THE EFFECTS OF TEMPERATURE AND PRESSURE ON THE CARBON CONVERSION TO OIL FROM HYDRORETORTING BENEFICIATED ALABAMA SHALE

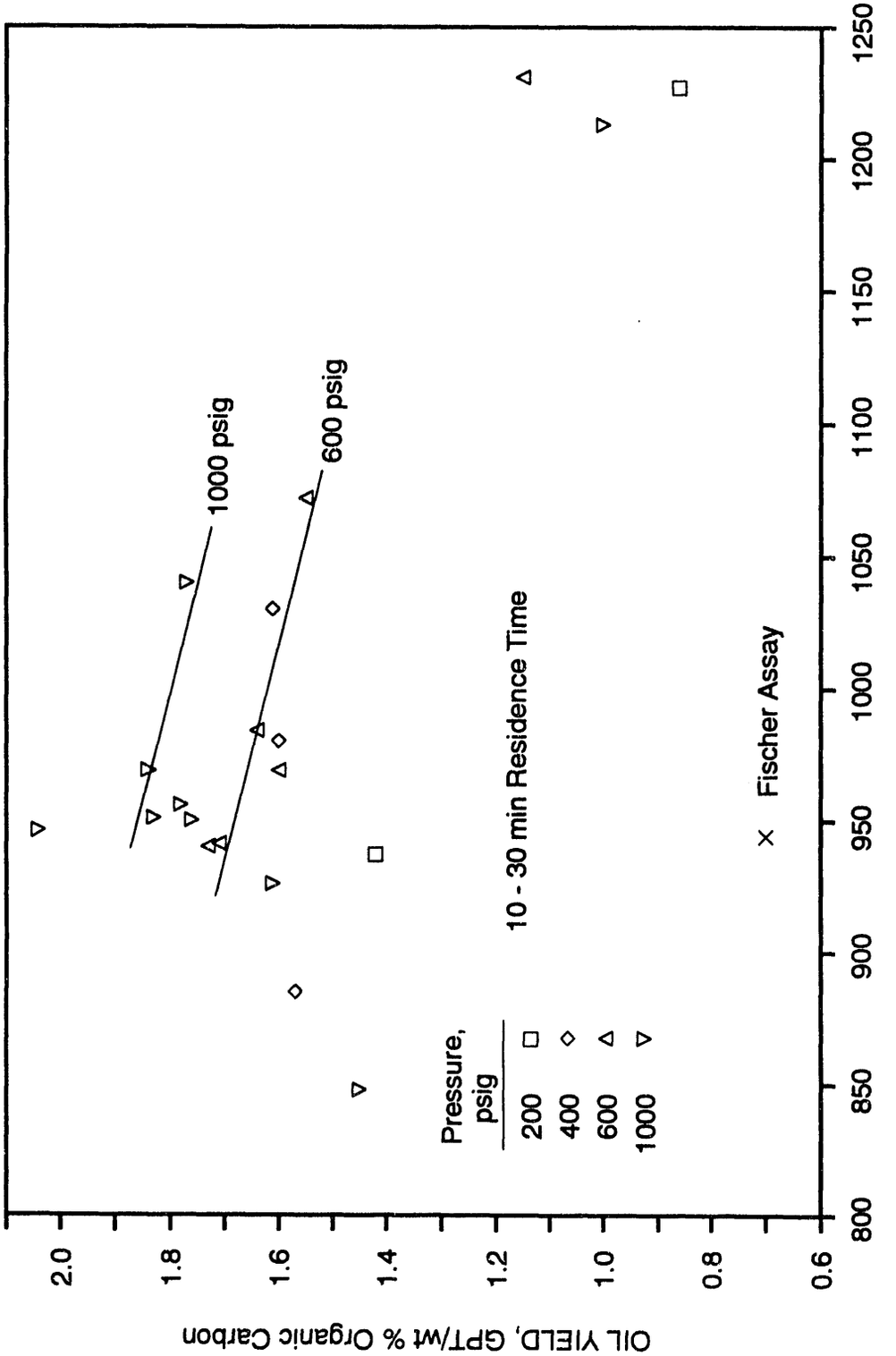

Figure 5-3. THE EFFECTS OF TEMPERATURE AND PRESSURE ON THE NORMALIZED OIL YIELD FROM HYDRORETORTING BENEFICIATED ALABAMA SHALE

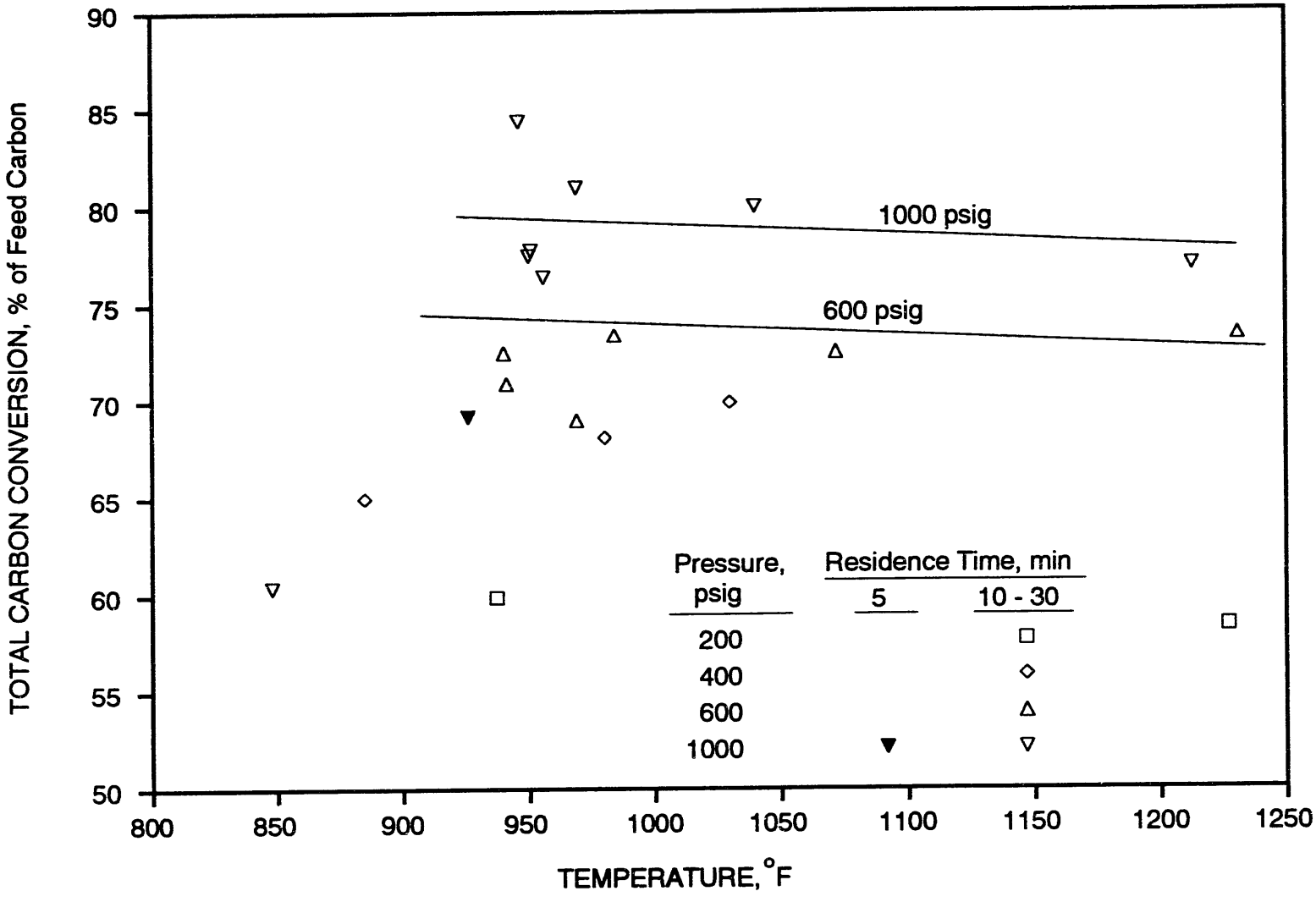

Figure 5-4. THE EFFECTS OF TEMPERATURE AND PRESSURE ON THE TOTAL CARBON CONVERSION FROM HYDRORETORTING BENEFICIATED ALABAMA SHALE

The total carbon conversion to gas and oil is presented in Figure 5-4. Carbon conversion increases with increasing pressure. Increasing the temperature to about 930°F (500°C) produces an increase in total carbon conversion, but between 930° and 1230°F (500° and 665°C) there is very little change in total carbon conversion with changes in temperature. Over this temperature range, the increase in carbon conversion to gas is almost equal to the decrease in carbon conversion to oil with increasing temperature. Therefore, the highest oil yield and highest selectivity of carbon to oil both occur at the same temperature of 940°F (510°C).

The effects of operating conditions on oil quality are shown in Figures 5-5 and 5-6. Oil quality is measured by both specific gravity and carbon-to-hydrogen weight ratio (C/H). Typically oils that have lower specific gravities and C/H ratios are of a higher quality than those with higher gravities and C/H ratios. The results show that increasing temperature and pressure reduces the quality of the oil. Increasing the PFH hydrogen pressure generates significantly more oil, but the oil quality decreases slightly as the yield increases. Increasing hydrogen pressure to 1000 psig (7.0 MPa) produces a larger percentage increase in oil yield than decrease in oil quality. However, a trade-off must be made between oil yield and oil quality. The relationship between both oil specific gravity and C/H and the PFH temperature is linear between 850° and 1060°F (455° and 570°C). Above 1060°F (570°C), the oil quality decreases much more rapidly with increasing temperature.

IGT conducted seven tests, including six successful tests, in the laboratory-scale continuous PFH unit. Two tests were conducted at 400 psig (2.8 MPa), three tests at 600 psig (4.2 MPa), and one test at 1000 psig (7.0 MPa). Temperatures and residence times ranged from 929° and 998°F (498° and 537°C) and 20 and 78 minutes, respectively. The beneficiated Alabama shale was sized to -40+80 mesh for all tests. The shale was riffled from the same large batch of beneficiated Alabama shale used for the batch PFH tests. The objective of the continuous tests was to confirm the results obtained in the laboratory-scale batch unit tests.

A summary of the continuous test operating conditions and results is presented in Table 5-2. The feed hopper was not preheated, so ambient-temperature shale was fed directly to the top of the reactor. Steady-state periods ranged from 75 and 120 minutes for the tests and the operating conditions given are averages of the steady-state values. The superficial gas velocity for all tests was above the complete fluidization velocity, defined as the velocity at which the largest particle in the bed is fluidized. The results include the carbon distribution to products, oil yield, product oil specific gravity, and the exit gas composition at the end of steady-state operation.

The effects of temperature, hydrogen pressure, and residence time on carbon conversion to gas and oil and normalized oil yield are presented in Figures 5-7 through 5-9. Lines are included on the figures showing the best fit of results from the batch PFH tests conducted at similar conditions. No variation was made in shale particle size for the continuous tests because batch test results indicate no effect of particle size on carbon conversion over the range of particle sizes used.

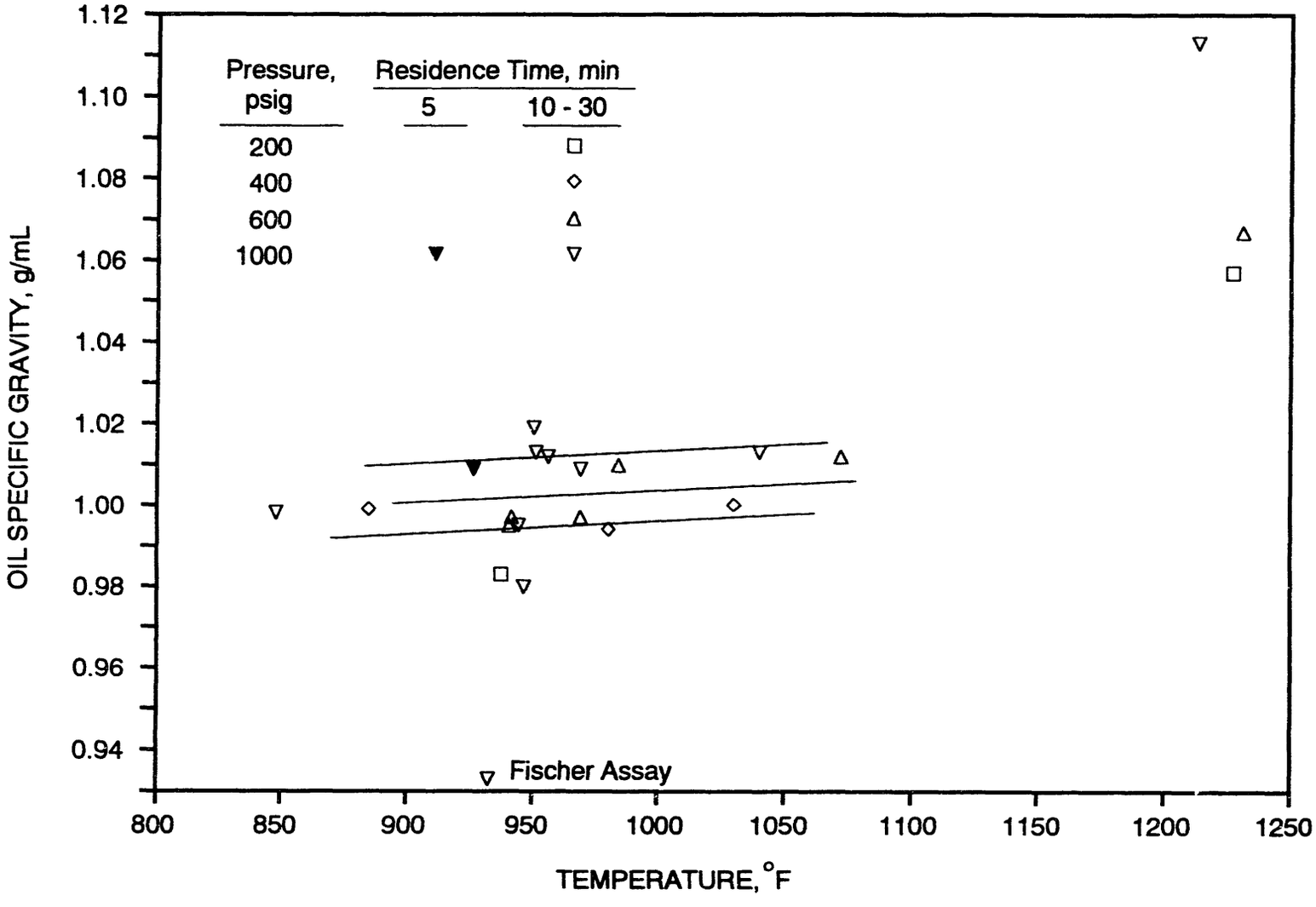

Figure 5-5. THE EFFECTS OF TEMPERATURE AND PRESSURE ON THE SPECIFIC GRAVITY OF THE OIL PRODUCED FROM HYDRORETORTING BENEFICIATED ALABAMA SHALE

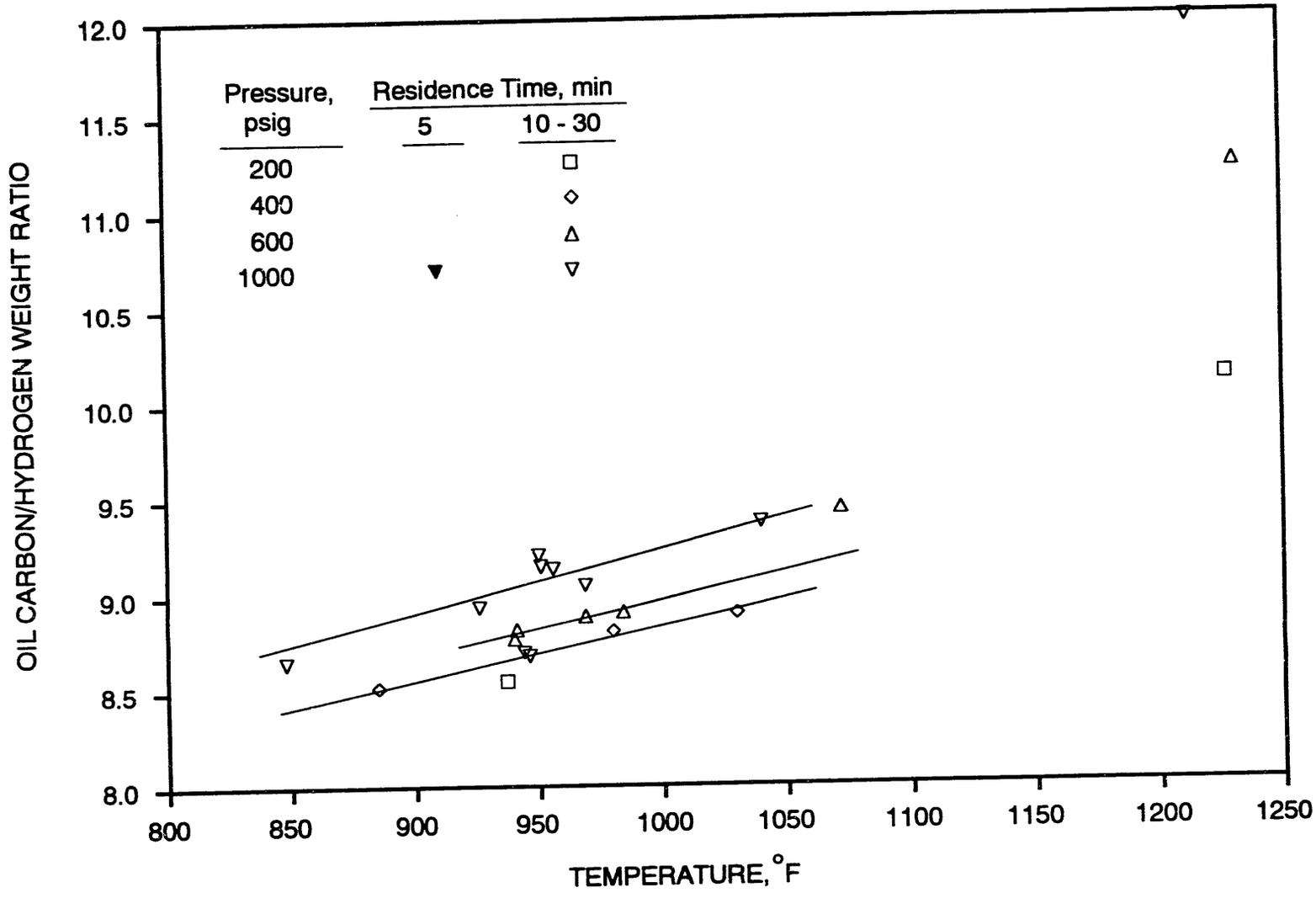

Figure 5-6. THE EFFECTS OF TEMPERATURE AND PRESSURE ON THE C/H RATIO OF THE OIL PRODUCED FROM HYDRORETORTING BENEFICIATED ALABAMA SHALE

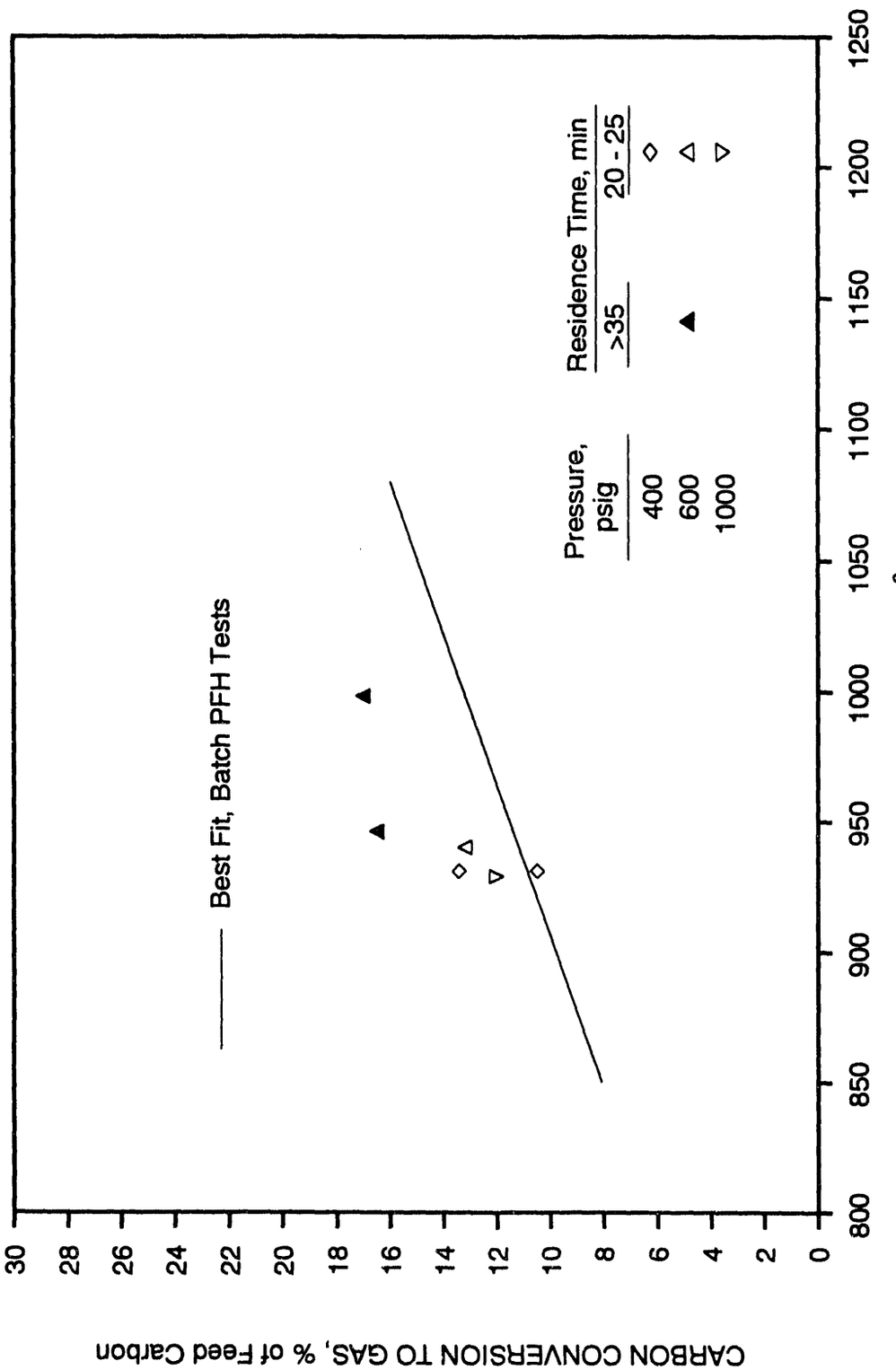

Figure 5-7. COMPARISON OF THE CARBON CONVERSIONS TO GAS IN THE CONTINUOUS PFH UNIT WITH THOSE IN THE BATCH PFH UNIT

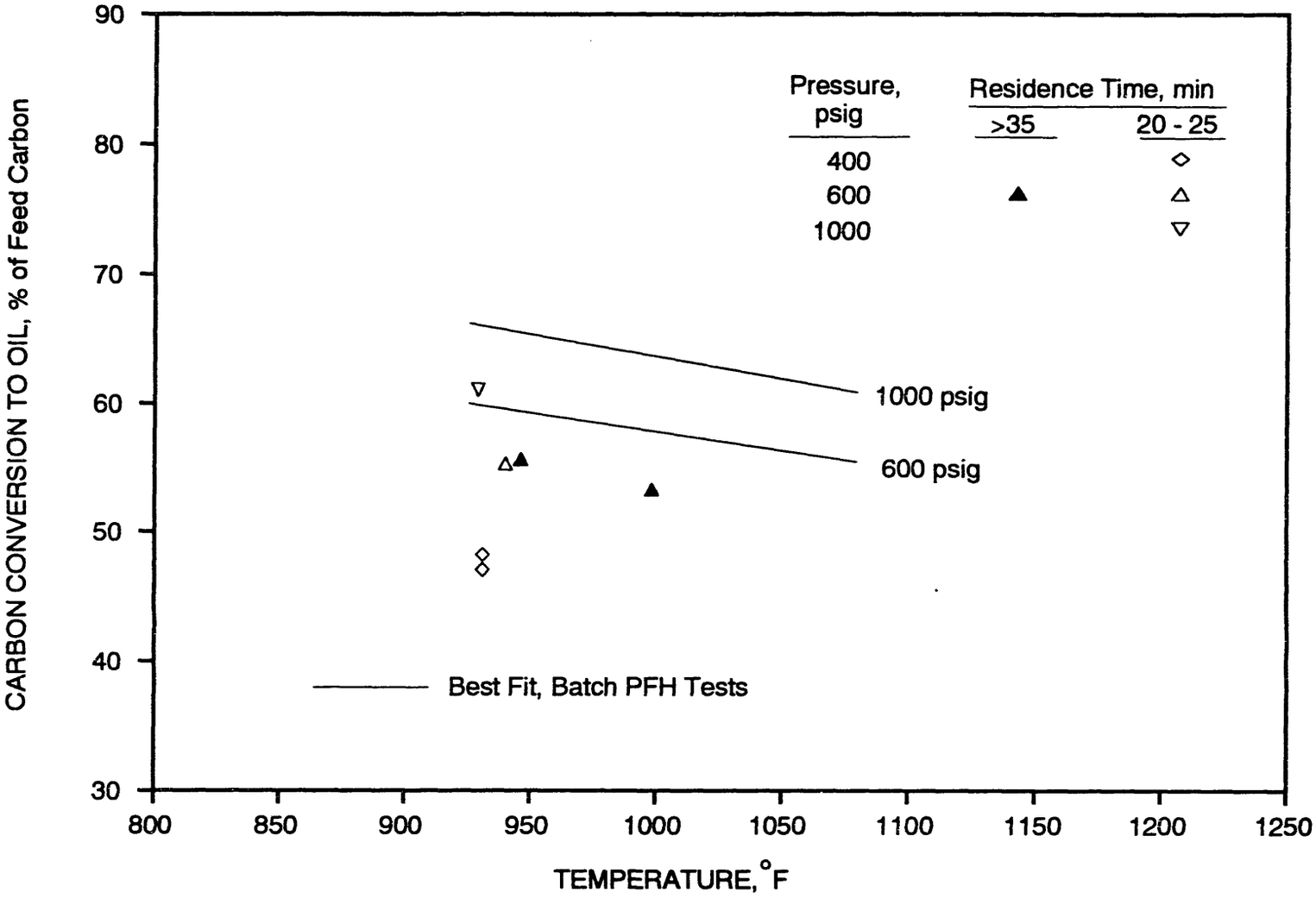

Figure 5-8. COMPARISON OF THE CARBON CONVERSIONS TO OIL IN THE CONTINUOUS PFH UNIT WITH THOSE IN THE BATCH PFH UNIT

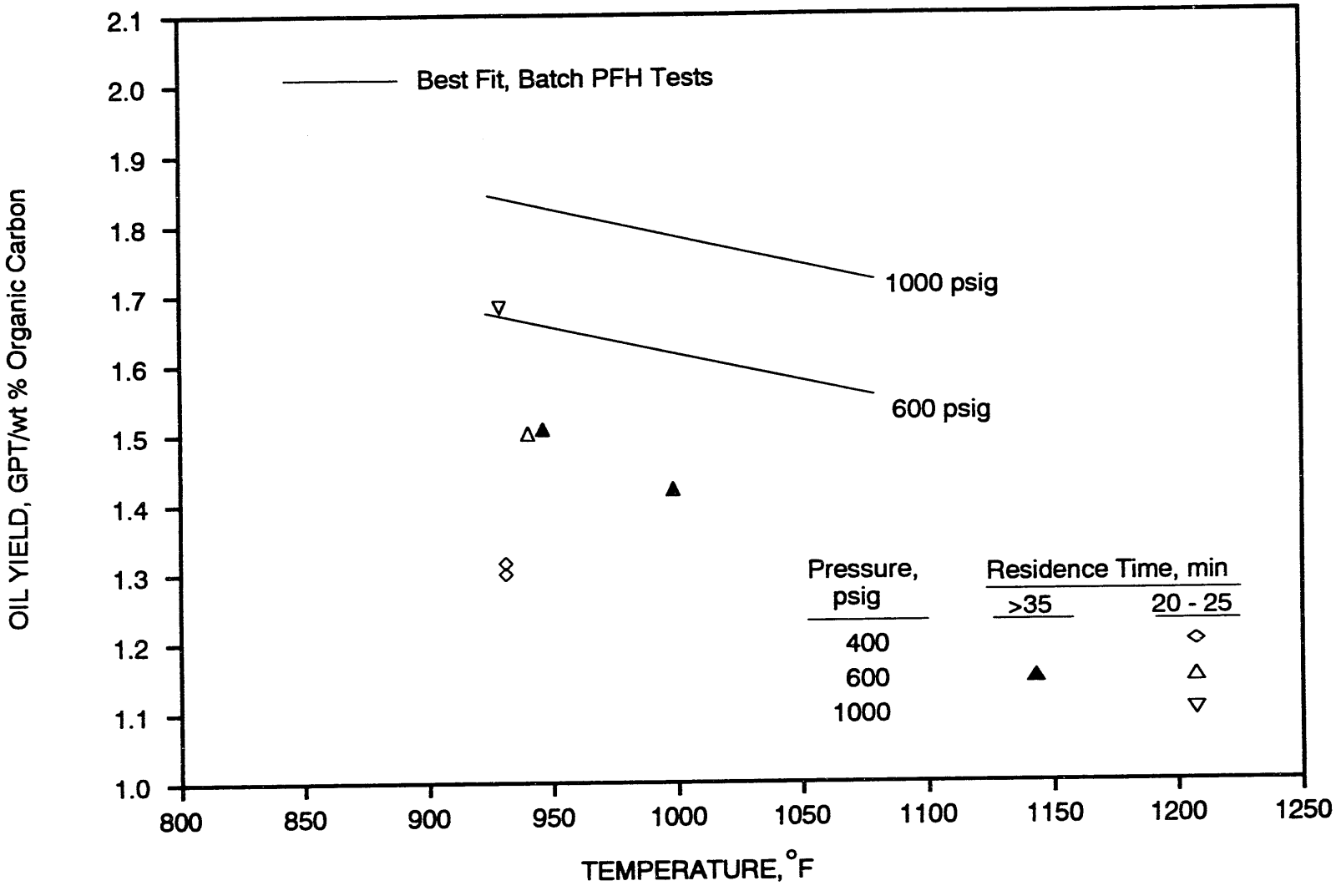

Figure 5-9. COMPARISON OF THE NORMALIZED OIL YIELDS OBTAINED IN THE CONTINUOUS PFH UNIT WITH THOSE IN THE BATCH PFH UNIT

The amount of carbon converted to gas was similar in the batch and continuous PFH reactors (Figure 5-7). Batch tests demonstrated that gas yield increases with increasing temperature but is not affected by changes in pressure. The results of continuous tests also showed no effect of hydrogen pressure on carbon conversion to gas. For residence times of less than 25 minutes, the carbon conversion to gas was 10 to 13 percent. Longer residence times (greater than 35 minutes) produced a higher carbon conversion to gas of 17 percent.

A comparison of continuous and best fit batch PFH carbon conversion to oil is shown in Figure 5-8. In both test units the carbon conversion to oil increased with increasing hydrogen pressure and decreased with increasing temperature. The maximum carbon conversion to oil is obtained at about 930°F (500°C) over the 400 to 1000 psig (2.8 to 7.0 MPa) range of pressures tested. The maximum oil yield is obtained at the same temperature for all hydrogen pressures.

In the continuous tests, the carbon conversion to oil was high but somewhat lower than for comparable batch PFH tests. Oil yields well above 200 percent of FA were achieved. Carbon conversion to oil increased from 48 percent at 400 psig (2.8 MPa) to 55 percent at 600 psig (4.2 MPa) and to 61 percent at 1000 psig (7.0 MPa). These carbon conversions correspond to oil yields of 190, 210, and 240 percent of FA. In the batch PFH unit, carbon conversion to oil was about 4 percent (20 percent of FA) higher with the maximum oil yield of 265 percent of FA achieved at 1000 psig (7.0 MPa) and 930°F (500°C). The reasons for the slightly lower oil yield in the continuous unit are unclear, but may relate to the faster heating rate, the shale particle distribution in the bed, or physical characteristics of the reactors.

The normalized oil yields achieved in the continuous tests are shown in Figure 5-9 along with the best-fit lines for the batch tests. Oil yield results are similar to the carbon conversion to oil results. The continuous unit produced high yields, but the oil yields in the batch unit under similar conditions were slightly higher. Tests at 600 and 1000 psig (4.2 and 7.0 MPa) generated oil yields of more than 200 percent of FA with the highest oil yield of 243 percent of FA obtained at 1000 psig (7.0 MPa). Oil produced in the continuous and batch units appeared to have similar compositions and qualities. The specific gravity of the oil from both units was similar.

Batch and continuous PFH tests have confirmed the ability of the PFH process to produce high oil yields and high selectivities of carbon to oil. Oil yields of greater than 200 percent of FA have been achieved in both units with slightly higher oil yields obtained in the batch unit. These encouraging results with beneficiated Alabama shale can be directly scaled to larger continuous PFH reactors.

Subtask 5.2.2. Bench-Scale Continuous Tests

The objective of this subtask was to expand the PFH data base by processing densified, beneficiated Alabama shale, to characterize the effluent streams for environmental mitigation analyses, to provide process scale-up from laboratory-scale to bench-scale, and to provide shale and shale oil for use in Subtasks 3.6 and 3.8 and Task 6.1.

Equipment and Test Procedure

The bench-scale experimental work was conducted at a nominal feed rate of 100 lb/h (45 kg/h) in an existing fluidized-bed bench-scale unit (BSU), which was modified during the previous PFH program to allow for liquid quench and collection. The BSU is an experimental fluidization unit capable of operating simultaneously at high temperatures [up to 1800°F (982°C)] and high pressures [up to 1000 psig (7.0 MPa)]. The temperature of the pressure shell is kept near ambient by the addition of 7½ inches of bulk Fiberfrax insulation between the shell and the internal electrical heaters. A schematic diagram of the reactor is shown in Figure 5-10 with a 6-inch (15.2-cm) diameter internal column. The BSU process flow schematic is shown in Figure 5-11. The BSU is extremely flexible and can be used to feed multiple, preheated gas streams to the fluidized bed in the test vessel.

During a test, it is necessary to continuously bleed off product gases containing hydrocarbons and supply hydrogen as a makeup gas to maintain a high hydrogen partial pressure in the reactor. Makeup hydrogen is supplied by high-pressure "jumbo" trailers with a storage capacity of about 100,000 SCF. The hydrogen is supplied to the unit at a pressure of about 2600 psig (18.0 MPa) and then regulated down to the desired supply pressure.

Gases can be preheated in either of two large gas-fired heaters capable of supplying gases at about 1000°F and 1100 psig (540°C and 7.7 MPa). After passing through the coils of the fired heater, the primary fluidizing gas can be further heated to bed temperatures, or a maximum of about 1600°F (870°C), inside the pressure shell prior to entering the fluidized bed. This is accomplished by passing the preheater gas through an annular space between the inner and outer walls of the reactor insert. About 130 pounds (60 kg) of coiled stainless steel wire are in this annular volume to enhance heat transfer from the outer wall of the insert to the gas passing through the annulus. Additional heat is supplied by six, 25-kW electrical resistance heaters stacked inside the pressure shell surrounding the reactor insert. Thermal expansion of the reactor insert relative to the pressure shell is allowed to occur in a sleeve at the top of the reactor. The pressure shell annulus is continuously purged to prevent product gases from entering the insulated shell and cooling, causing condensation of some of the liquids.

The product gas is recycled around the system to 1) increase the concentrations of products of reaction in the exit gas stream to levels high enough to obtain accurate on-line gas analyses, and 2) reduce net hydrogen requirements by about 95 percent compared with a once-through gas flow system. Gas enters the top of the reactor, passes through an annular space where it is heated and enters the bed through a multi-holed bubble cap distributor. Gas

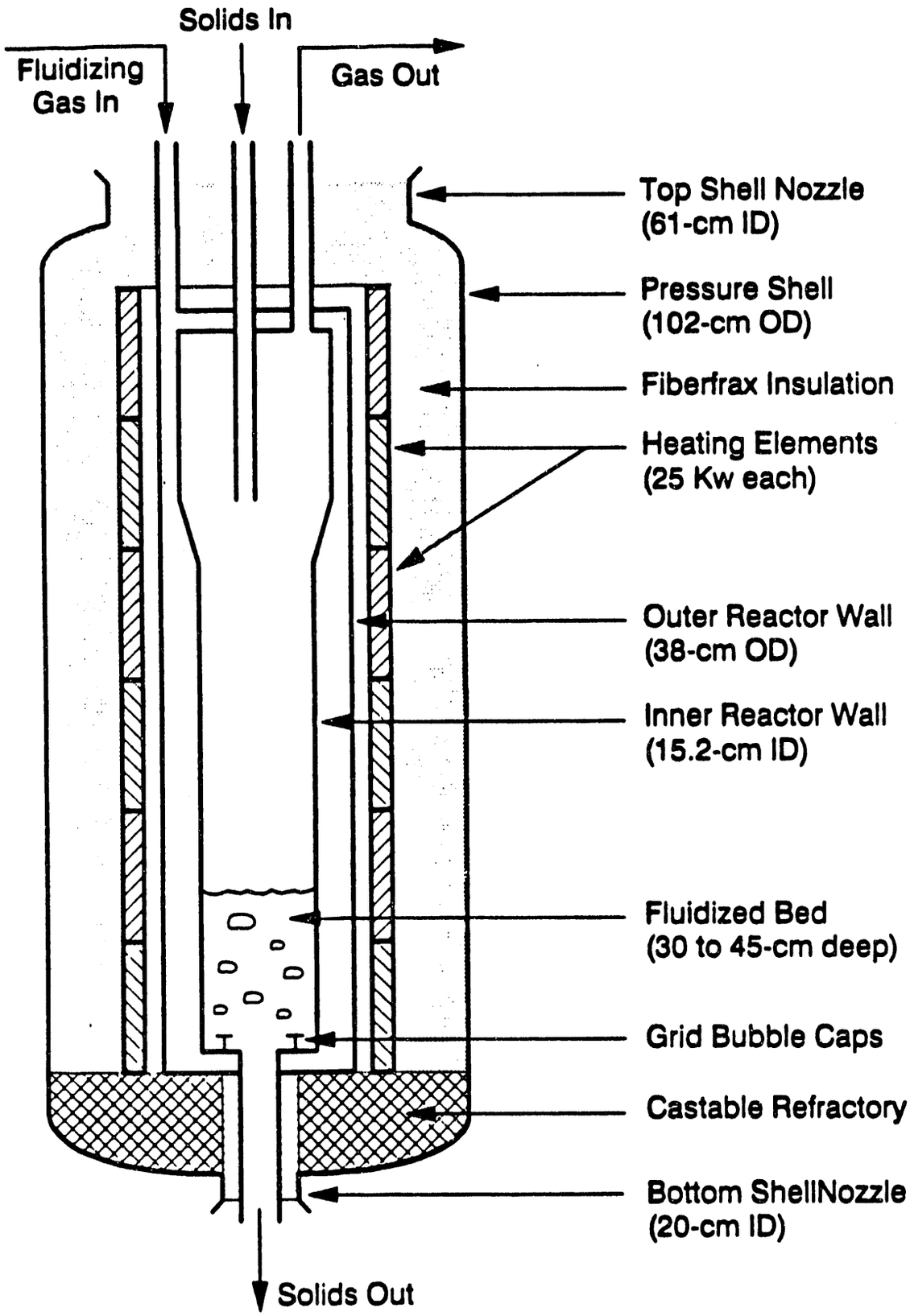

Figure 5-10. BENCH-SCALE UNIT REACTOR AND PRESSURE SHELL CONSTRUCTION

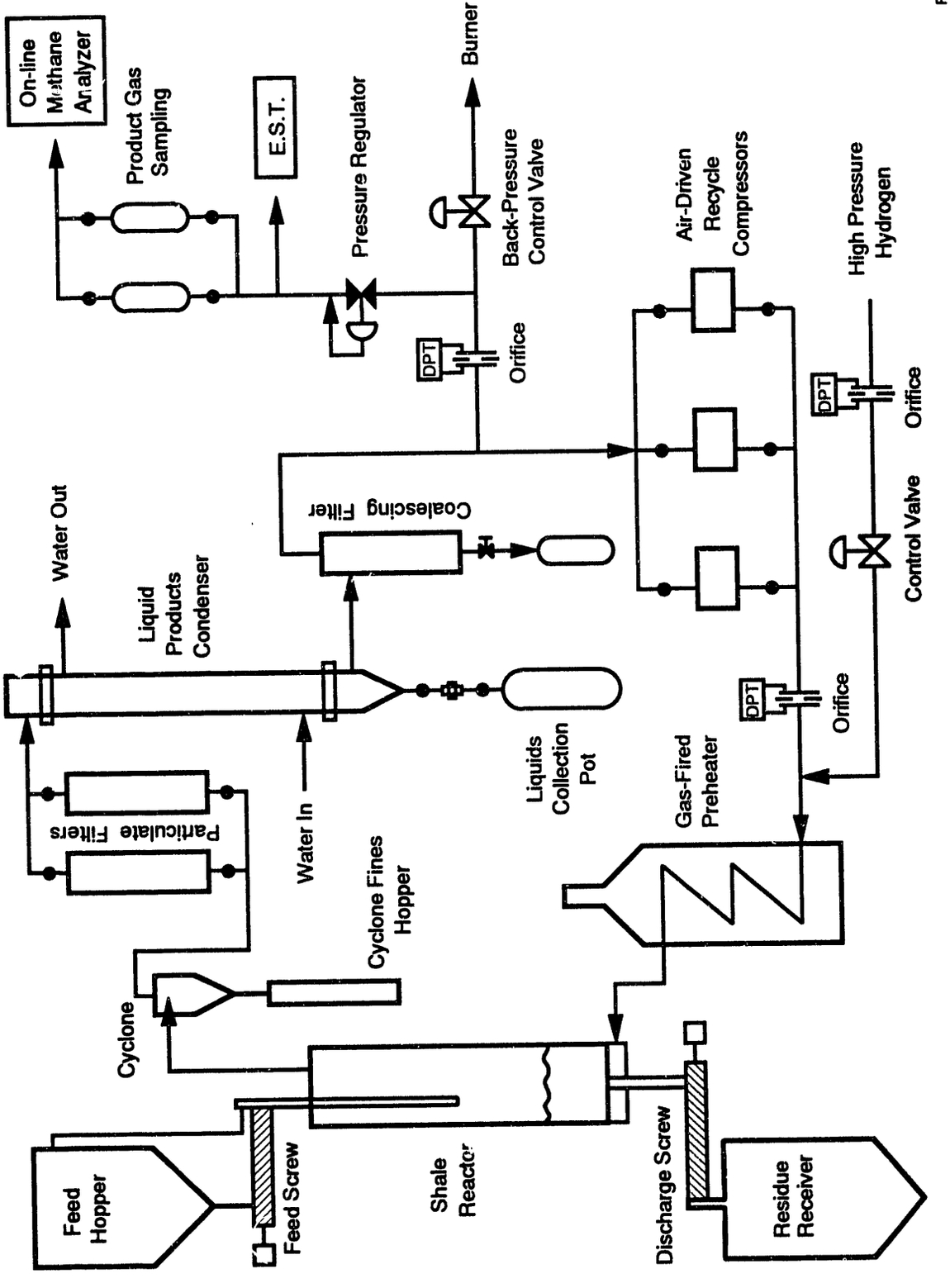

Figure 5-11. SCHEMATIC DIAGRAM OF THE BENCH-SCALE PFH TEST UNIT

leaving the reactor passes through a cyclone before flowing through particulate filters to remove any remaining entrained fines prior to condensing the liquids.

Two single-pass, shell-and-tube heat exchangers cool the recycled gas and condense the liquid products. A shell-and-tube design was utilized for optimum liquid drainage and ease of maintenance. An integral gas-liquids disengaging section forms the bottom of the unit, which drains into an in-line collection pot. The gas then enters a coalescing filter. At this point, the gas is at a much lower temperature and, therefore, a lower volumetric flow rate and contains only a fraction of the total condensable liquids. These factors allowed a smaller, more efficient coiled concentric-tube design to be used to complete the cooling of the product gas. Two sets of three dual heat-transfer coils are connected in series. Each coil has 1.9 ft^2 (0.18 m^2) of heat transfer surface.

A high-pressure mist coalescing filter is immediately downstream of the heat exchanger to recover any entrained oil or water droplets as liquid product. It also ensures clean gas flow to the recycle compressors and for sampling and analysis. An orifice meter is used to measure the product gas flow rate leaving the recycle loop. An on-line infrared analyzer monitors the concentration of hydrocarbon gases in the exit gas and provides an indication of steady-state operation.

An environmental sampling train (EST) collects samples that are subsequently analyzed for environmental mitigation purposes. This equipment consists of separate acid and base scrubbers for the removal of oils and other organic and inorganic compounds from the BSU exit gas stream. The acid scrub used 3-M hydrogen chloride (HCl) in three 1-liter chilled bubblers in series. After the test, the resulting solutions were analyzed for oil, grease, NO_x, total ammonia, total nitrogen, phenols organic carbon, and chemical oxygen demand (COD). The base scrub used 6-N sodium hydroxide (NaOH) in three 1-L bubblers. The resulting solutions were analyzed for sulfides, sulfates, total sulfur, total cyanides, and total thiocyanates.

Prior to a test, the feed material is loaded into the solids feed hopper, which is 30 inches (76.2 cm) in diameter and 12½ feet (3.81 m) tall. A 70° angled, stainless-steel mass flow cone at the bottom of the vessel ensures even, nonsegregated flow of solids from the hopper. The feed hopper is loaded with sufficient shale for the planned test and sealed and the entire reactor system is pressure tested. With a capacity of about 42 ft^3 (1.19 m^3), solids can be fed continuously at a rate of 5 ft^3/h (0.14 m^3/h) for up to 8 hours. A 3-inch (7.6-cm) diameter, variable speed screw conveyor is used to feed solids to the freeboard of the fluidized-bed reactor. A non-mechanical L-valve has also been used in place of a screw conveyer in previous work for continuous solids feeding when the particle attrition common in screw conveyers is unacceptable.

Solids were transferred from the reactor to the residue receiver via a 3-inch (7.6-cm) diameter, variable speed, solids discharge screw. The residue receiver is 36 inches (91.4 cm) in diameter and 8½ feet (2.6 m) tall. A cone at the bottom of the receiver allows easy removal of all solids after a test.

Spent shale exits the bed through a 3-inch-diameter (7.6 cm) underflow standpipe. Solids are recovered weighed and analyzed after the test.

Bed pressure taps and thermocouples enter the fluidized bed from below through the solids underflow standpipe. For this reason the pressure taps must be continuously purged to prevent solids from plugging the small diameter (1/4-inch) 0.635 cm tubes. The tap lines were designed to minimize the effect of purge gas velocity on the measured differential-pressure between individually purged taps.

BSU Operation with Beneficiated Shale

There had been some difficulty in feeding solids to the reactor and especially discharging spent solids to the receiver in previous testing. In fact, several BSU tests had been conducted in which an L-valve was used to discharge spent shale solids to the residue receiver. Therefore, prior to testing the densified beneficiated Alabama shale in the BSU, a solids flow test was conducted with a shale with a similar particle size distribution as the proposed feed material. Solids were loaded to the feed hopper and were successfully transferred to the reactor and then to the receiver via the feed and discharge screw conveyors, respectively. The solids flow test was conducted at atmospheric pressure and ambient temperature.

Since the BSU had also undergone several modifications and been equipped with some new instrumentation, a hot-flow test was conducted prior to operation with beneficiated shale. The unit was pressurized and the gas-fired heater was activated and the liquids condenser and collection systems were successfully tested as well as the instrumentation used for controlling the flows and recording data. In this test, sand was fed from the feed hopper to the reactor to establish a bed in the BSU. After the hot-flow test, the sand was discharged from the reactor to the receiver and the unit was depressurized. The feed hopper was then loaded with shale solids in preparation for the planned BSU test.

After the feed hopper was loaded with sufficient shale for the test, the BSU was successfully pressure tested with nitrogen and subsequently purged and pressurized with hydrogen to 1000 psig (7.0 MPa). Gas flow to the unit was adjusted to the targeted conditions and the fired heater was energized. Test 52-A-1 was initiated when the feed screw was activated to establish a bed in the reactor. While feeding solids to the reactor, the feed screw control electronics malfunctioned. While idling the fired heater and maintaining gas pressure and flow, the feed screw control unit was repaired and put back into service. Solids were subsequently fed to the reactor at a rate of about 68 lb/h (31 kg/h) for 5 hours including 3-1/4 hours of steady-state operation. During the test, the amount of solids elutriated and collected in the external cyclone was continuously monitored. The run was terminated when the level of solids in the cyclone dipleg indicated that the cyclone collection container was nearly full. The run was separated into two steady-state periods to determine reproducibility of the data over an extended run time. Separate gas, liquid, and EST samples were obtained and analyzed for each of the steady-state periods.

Discussion

The results of batch and continuous laboratory-scale PFH tests from Subtask 5.2.1 were used to select the operating conditions for the BSU test in this task. Lab-scale batch and continuous tests were conducted over a wide range of temperatures, pressures, and residence times. Optimum batch test oil yields were as high as 290 percent of Fischer Assay (FA) at 900°F and 1000 psig (482°C and 7.0 MPa). Oil yield increases with increasing temperature up to 900°F, decreases as temperature is raised to 1050°F, and finally decreases significantly as temperature is increased above 1050°F. Increasing pressure from 200 to 1000 psig produces an increase in oil yield. Longer residence times produce an increase in oil yield, but the increase is small for residence times greater than 10 minutes. Lab-scale continuous test oil yields are slightly lower than those from the batch PFH tests. Residence times of 20 to 75 minutes produced similar oil yields in the continuous unit.

The nominal operating conditions selected for the BSU test were 925°F and 1000 psig with a shale residence time of 20 minutes. These conditions were chosen to obtain a high oil yield. Based on batch PFH test results, a temperature of 900°F would give a slightly higher oil yield, but conditions were selected to allow for possible temperature excursions of ±25°F and yet not have the oil yield drop significantly.

During the bench-scale PFH test, steady-state operation was divided into two separate periods. The steady-state operating periods for Tests 52-A-1 and 52-A-2 were 2.0 and 1.25 hours long, respectively. Complete sets of gas samples and EST samples were taken during each steady-state period.

A summary of the operating conditions and overall results of the BSU test with densified, beneficiated Alabama shale is presented in Table 5-3. Test conditions and results were similar for the two steady-state periods. The Alabama shale was beneficiated, densified, and sized to -20+80 mesh (0.2 to 1.0 mm) before shipment to IGT. Details of the procedures used to prepare the beneficiated shale are included in Task 7 of this report. Shale was charged to the feed hopper and fed at a rate of 68 pounds per hour. Average steady-state temperatures and pressures were 943°F and 1000 psig. The average shale residence time was 26 minutes. The bed height was about 30 inches for a height-to-diameter ratio of 5. The superficial gas velocity of 0.85 feet per second was four times the minimum fluidization velocity. Results of lab-scale continuous tests demonstrated the need to keep the bed of beneficiated shale active in the BSU to avoid packing of the solids.

A carbon recovery of 92 percent was obtained in the BSU test. The carbon balance was reconciled by assuming the residue analyses were correct and adjusting the carbon to oil and gas by the same factor. This is the same procedure used reconciling balances in the batch-scale tests. Carbon conversions to oil and gas are 58 and 14 percent, respectively, for both steady-state periods. Gas yield is similar to lab-scale batch and continuous test results. Oil yield in both cases is 52 GPT or 233 percent of the FA yield. The oil yields in the BSU tests are similar to those from laboratory-scale continuous tests.

Table 5-3. OPERATING CONDITIONS AND RESULTS OF THE BSU TEST WITH BENEFICIATED ALABAMA SHALE

Test No.	52-A-1	52-A-2
Shale	Alabama Beneficiated	Alabama Beneficiated
Operating Conditions		
Average Temperature, °F		
Feed Hopper	--	--
Reactor	943	944
Reactor Residence Time, min	26	26
Pressure, psig	1000	1000
Shale Particle Size, mesh	-20+80	-20+80
Shale Feed Rate, lb/h	67.4	69.4
Gas Rate, SCFH	15,290	15,390
Gas Velocities, ft/s		
Superficial	0.85	0.85
Complete Fluidization	0.58	0.58
Shale Feeding Time, h	5.0	--
Steady-State Period, h	2.0	1.25
Product Carbon, % feed carbon		
Residue Shale	26.8	26.8
Product Gas	14.9	14.8
Oil	58.1	58.2
Water (as soluble hydrocarbons)	0.2	0.2
Total	100.0	100.0
Oil Yield, GPT	52.6	52.5
Oil Yield, % of FA	234	233
Oil Density, °API	10.6	10.8
Oil Density, g/mL	0.996	0.994
Product Sulfur, % feed sulfur		
Residue Shale	54.0	54.0
Product Gas	36.8	37.2
Oil	6.6	6.2
Water	2.6	2.6
Total	100.0	100.0

The evaluation of results from batch tests in Subtasks 3.8 and 5.2.1 indicate a carbon conversion to oil of 65 percent or 260 percent of FA yield at these conditions. The difference in batch and continuous PFH oil yields has been observed in earlier projects with raw (non-beneficiated) Eastern oil shales. No decrease in oil yield was detected in scaling up by a factor of 50 from the lab-scale continuous unit to the bench-scale continuous unit. Carbon

conversions to oil and gas for densified beneficiated Alabama shale tested in the BSU are the same as those for raw Alabama shale tested at the same conditions.

In the BSU test, the conversion of feed sulfur was 46 percent. Conversions to hydrogen sulfide, oil (in heterocyclic compounds), and water (in sulfides and sulfates) were 37, 6.4, and 2.6 percent, respectively. Beneficiation has been found in earlier IGT tests[1] to reduce the conversion of carbon to gas. In a BSU test with raw Alabama shale at similar conditions, the sulfur conversion to gas was 51 percent. The sulfur in the beneficiated shale is comprised of 9 percent sulfate, trace sulfide, 67 percent pyrite, and 24 percent organic in form. The sulfur in the residue from the PFH process is 3 percent sulfate, 73 percent sulfide, 5 percent pyrite, and 18 percent organic in form. The large increase in the sulfide form of sulfur is typical for the PFH processing of Eastern shales and results from the conversion of pyrite to FeS. The individual conversions of sulfate and organic sulfur were higher than that of total sulfur. The conversion of sulfide plus pyritic sulfur to other forms (38 percent), is lower than the total sulfur conversion of 46 percent.

Chemical and screen analyses of the feed and residue shale samples are presented in Table 5-4. The shale was riffled but not screened before charging to the feed hopper. Sieve analyses show that 95 weight percent of the feed shale was between 18 and 60 mesh.

The beneficiated Alabama shale has about twice the organic carbon content (32.06 compared with 16.46 weight percent) and produces twice the product oil yield of raw shale. The densified, beneficiated shale particle and true densities (1.16 and 1.87 g/cm^3, respectively) are different indicating a high particle porosity after pelletization. The difference in particle (0.92 g/cm^3) and true densities (2.48 g/cm^3) is even greater after PFH processing. The conversion of kerogen to liquid and gaseous products during hydroretorting greatly increases particle void fraction and porosity. Processing of the beneficiated Alabama shale in the BSU reduced the shale bulk density by about 16 percent from 0.73 to 0.61 g/cm^3, or roughly twice that observed for raw shale.

Attrition of the densified shale due to retorting was low during the BSU test. The feed shale was sized to 38 percent below 30 mesh and 5 percent below 60 mesh. After the BSU test, 76 percent of the residue was below 30 mesh and 16 percent was under 60 mesh. These size distributions show a decrease in particle size in the fluidized bed that resulted from particle breakage with only a small decrease caused by attrition. The low cyclone fines production (primarily feed shale) of 11 percent of the feed shale also indicates that particle attrition is low for the densified, beneficiated Alabama shale in the BSU.

Beneficiation of the Alabama shale increased the carbon content to 32 percent and increased the calorific value to 6310 Btu per pound. After the BSU test in which 73 percent of the carbon and 46 percent of the sulfur were converted to products, the residue shale contained 13 percent carbon and had a calorific value of 2710 Btu per pound. The carbon content and calorific value

Table 5-4. ANALYSES OF THE FEED AND RESIDUE SAMPLES FROM THE BSU TEST WITH BENEFICIATED ALABAMA SHALE

Test No.	--	52-A-1 and 52-A-2
Sample	Feed Beneficiated Alabama Shale	Residue Shale
Moisture, wt %	1.51	0.0
Ultimate Analysis, wt % dry		
Ash	53.85	81.07
Carbon	32.08	12.95
Organic Carbon	32.06	12.94
CO_2	0.07	0.02
Hydrogen	3.02	0.82
Sulfur	9.12	7.43
Nitrogen	0.84	0.47
High Temperature Water	6.08	2.56
Oxygen (from HTW)	5.40	2.27
Gross Calorific Value, Btu/lb	6310	2710
Density, g/cm^3		
Bulk	0.73	0.61
Particle (Hg)	1.16	0.92
True (He)	1.87	2.48
Sieve Analysis (wt%), mesh		
+30	61.7	24.1
-30+40	19.6	27.8
-40+60	13.8	32.5
-60+70	4.0	13.2
-70+80	0.3	0.9
-80+Pan	0.6	1.5
Total	100.0	100.0
Fischer Assay, GPT (L/m ton)	22.5 (94.0)	--

in the residue shale are similar to those of raw shale. After hydroretorting, the residue shale contains 28 percent of the original shale energy content and has high enough carbon content and heating values to be used as a fuel.

Analyses of the feed and residue shale samples for 30 trace and minor element are shown in Table 5-5. The most abundant elements (excluding carbon, hydrogen, sulfur, nitrogen, and oxygen) are aluminum, calcium, iron, potassium, magnesium, and silicon with concentrations between 0.7 and 7.6 percent in the feed and between 1.8 and 16 percent in the residue. Aluminum and silicon concentrations are lower in the residue, and calcium, potassium, and magnesium concentrations are higher in the residue. The other 24 trace elements are present in the feed and residue shales in concentrations at or below 0.1 percent and range from 0.1 percent for titanium to 0.25 ppm for mercury.

Table 5-5. TRACE AND MINOR ELEMENT ANALYSES OF THE FEED AND RESIDUE SHALE SAMPLES FROM THE BSU TEST

Test No.	--	51-A-1 and 52-A-2
Sample	Alabama Ben. Shale	Residue Shale
Element, ppmw		
Ag	2.1	2.2
Al	29,600	17,900
As	120	150
B	<5.0	<5.0
Ba	120	51
Be	<0.5	<0.5
Ca	76,400	161,000
Cd	1.6	4.0
Cl	200	91
Cr	94	120
Cu	160	200
F	430	240
Fe	37,400	37,000
Hg	0.034	<0.070
K	6,700	20,400
Li	<6.0	<6.0
Mg	44,600	96,900
Mn	210	230
Mo	350	480
Na	470	140
Ni	340	250
P	550	790
Pb	<20	<20
Sb	35	44
Se	21	25
Si	51,400	39,100
Sr	120	75
Ti	1,700	960
V	320	220
Zn	270	260

Toxicity Characteristic Leaching Procedure (TCLP) tests were conducted on the feed and residue shales. The results presented in Table 5-6 show that silver, lead, and mercury are not leached at levels above the analytical detection limit. Selenium levels were about 10 percent of the TCLP limit and all other elements were leached at less than 2 percent of the TCLP limit. All eight elements were leached from the feed and residue shales at levels below the TCLP leachability limits.

The average product gas compositions for the two steady-state periods are presented in Table 5-7. Gas compositions did not change significantly during either steady-state period of the test. The high hydrogen concentrations and low concentrations of hydrocarbons and hydrogen sulfide compared to

the lab-scale continuous tests in Subtask 5.2.1 are a result of the high hydrogen-to-shale ratio used in these tests.

Table 5-6. TCLP RESULTS WITH FEED AND RESIDUE SHALE SAMPLES FROM THE BSU TEST

Sample	TCLP Leachability Limit	Feed Alabama Ben. Shale	Residue 52-A-1 and 52-A-2
Element	----------	mg/L ----------	
Arsenic	5	0.0023	0.081
Barium	100	0.073	0.082
Cadmium	1	0.038	<0.020
Chromium	5	0.13	<0.050
Lead	5	<0.20	<0.20
Mercury	0.2	<0.005	<0.005
Selenium	1	0.13	0.096
Silver	5	<0.050	<0.050

Table 5-7. ANALYSIS OF THE PRODUCT GAS FROM THE BSU TEST

Test No.	52-A-1	52-A-2
Component,* mol %		
Hydrogen	96.90	96.97
Carbon Dioxide	0.00	0.00
Carbon Monoxide	0.00	0.00
Methane	1.23	1.12
Ethane	0.75	0.66
Propane	0.15	0.20
Propene	0.01	0.01
i-Butane	0.01	0.02
n-Butane	0.02	0.03
C_6+	0.01	0.01
Hydrogen Sulfide	0.92	0.98
Total	100.00	100.00

* Representative steady-state gas.

Chemical analyses of the product oils, including specific gravities, heating values, and distillation data are presented in Table 5-8. Distillation was by ASTM method D86. Componential analyses of the oils are summarized in Table 5-9, including 13 compounds with molecular weights less than C_{32} identified as present in the oils by GC-FID analysis. Acetone is probably present in the oils, but the reported concentrations may be high because acetone is used to flush the BSU lines and vessels during cleaning. The identified oil components comprise only a small fraction of the product oils since more than 98 percent of the oils consists of unidentified compounds.

Table 5-8. ELEMENTAL ANALYSIS AND DISTILLATION DATA FOR PRODUCT OIL FROM THE BSU TEST

Test No.	52-A-1	52-A-2
Ultimate Analysis, wt %		
Ash	0.0	0.0
Carbon	85.40	85.95
Hydrogen	9.86	9.83
Sulfur	2.75	2.59
Nitrogen	1.44	1.48
Specific Gravity (60°/60°F)	0.996	0.994
Gross Calorific Value, Btu/lb	17,750	17,710
Distillation wt % (D86), °F		
Initial Boiling Point	248	254
5	308	316
10	367	367
20	460	473
30	568	581
40	634	652
50	680	701
60	708	733
70	722	755
Oil Recovery by 760°F, wt %	74.5	75.0

Table 5-9. COMPONENT ANALYSES OF THE COMPOSITE OIL FROM THE BSU TEST

Test No.	52-A-1	52-A-2
Component, wt %		
Acetone	0.02	0.02
Benzene	0.21	0.19
Toluene	0.32	0.34
Ethylbenzene	0.15	0.16
m, p-Xylenes	0.29	0.30
Styrene	BDL*	BDL
o-Xylene	0.16	0.17
Phenol	0.09	0.09
Naphthalene	0.09	0.08
2-methylnaphthalene	0.15	0.14
1-methylnaphthalene	0.14	0.13
Phenanthrene	BDL	BDL
Anthracene	BDL	BDL
Total Unidentified	98.38	98.38

* Below detection limit.

Analyses of the product oil group types are presented in Table 5-10. The oils from the two tests are similar, and the great majority of both oils (91 percent) is soluble in hexane. The oils are composed mostly of aromatic and polar group types. One and two-ring group types comprise the largest fraction of the oil (38 percent). Aliphatic groups account for 21 percent and 4-ring and polar compounds account for 26 percent of the oil.

Table 5-10. HYDROCARBON GROUP TYPES OF THE OIL PRODUCED DURING THE BSU TEST

Test No.	52-A-1	52-A-2
Hexane Soluble Groups,* wt %	92.0	91.5
Aliphatic	19.0	20.0
1-Ring	21.5	22.0
2-Ring	13.5	13.0
3-Ring	6.0	6.0
4-Ring + Polar Groups	32.0	30.5
Hexane Insoluble Groups, wt %	8.0	7.5

* Oil:Hexane dilution of 1:100.

The oil product from Test 52-A-1 was vacuum distilled into five boiling point fractions: -180°F, 180°-360°F, 360°-650°F, 650°-850°F, and +850°F. The +850°F fraction of oil was fractionated at a total pressure of 1 mm Hg (133.3 Pa) to prevent coking. The five fractions were analyzed for elemental composition, specific gravity, cetane index, group type analysis, and trace metals. Simulated boiling point curves were determined for the three lowest boiling fractions and for a combined +650°F fraction. Test results are presented in Tables 5-11 and 5-12.

Simulated boiling point curves for the four fractions are shown in Figure 5-12. These curves were obtained for the oil fractions by a modified version of the ASTM gas chromatography method D2887. The results show that the vacuum distillation achieved clean separations between the cuts. Only the lightest fraction (-180°F) showed significant overlap with the next fraction.

The majority of the shale oil boils above 650°F and more than 40 percent boils above 850°F. The carbon content of the oil increases and the hydrogen content decreases with increasing boiling point. The carbon-to-hydrogen weight ratio increases from 6.2 for the -180°F fraction to 10.1 for the +850°F fraction. The specific gravity also increases with increasing boiling point. The -180°F fraction gravity is 0.750 g/mL (57.2 °API) and the +850°F fraction gravity is 1.089 g/mL (-1.6 °API). Cetane index values were calculated for two of the oil fractions. The lightest and two heaviest oil fractions are outside the range defined for diesel fuels. The calculated cetane index was 26.6 for the 180°-360°F fraction and 27.5 for the 360°-650°F fraction.

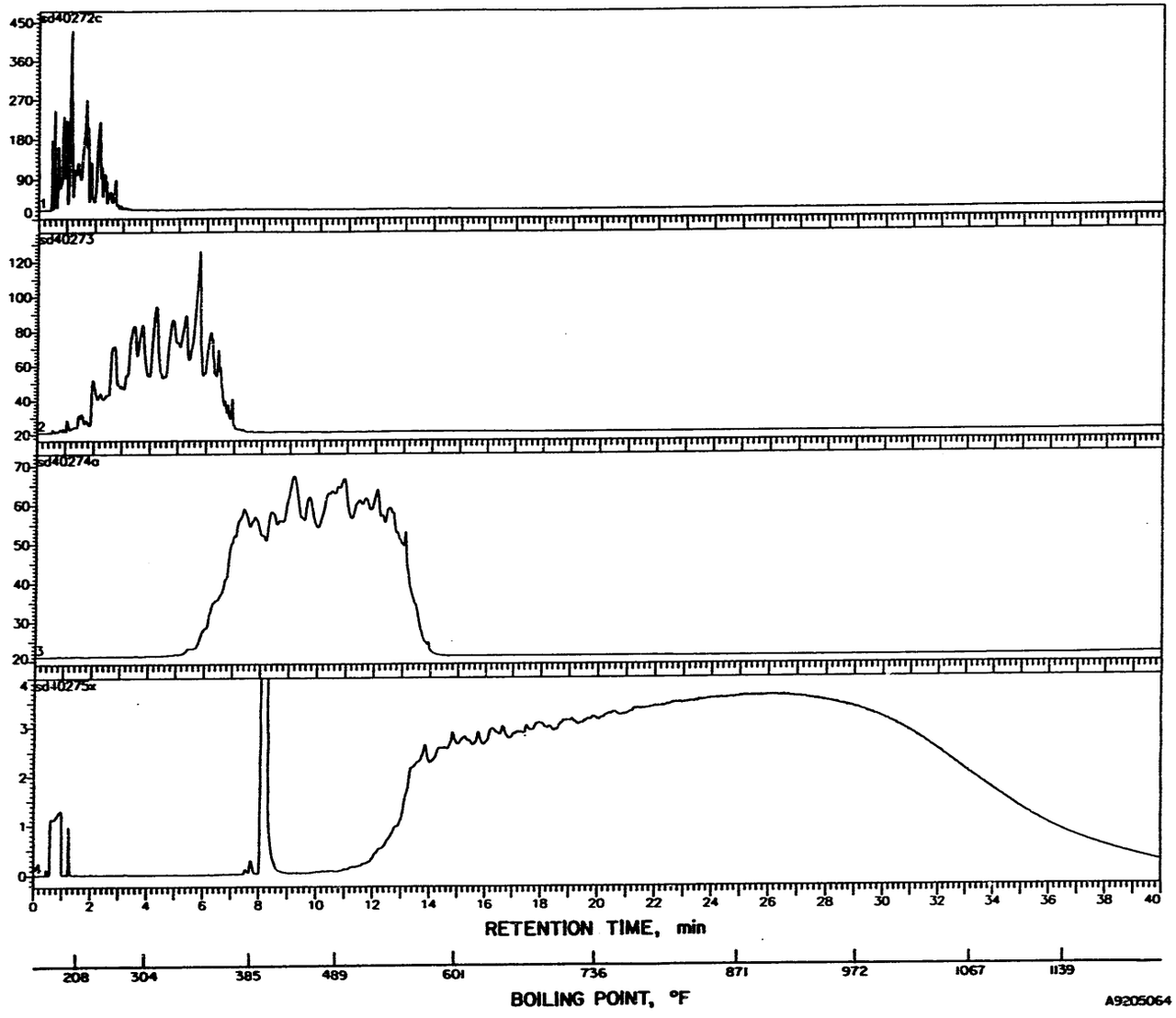

Figure 5-12. SIMULATED BOILING POINT CURVES FOR THE FOUR FRACTIONS OF OIL OBTAINED FROM THE BENCH-SCALE TEST WITH BENEFICIATED ALABAMA SHALE

Table 5-11. ANALYSES OF THE OIL FRACTIONS FROM THE BSU TEST WITH BENEFICIATED ALABAMA SHALE

Distillation Fraction, °F	-180	180-360	360-650	650-850	850+
Fraction of Whole Oil, wt %	1.4	7.6	16.1	30.4	44.5
Ultimate Analysis, wt %					
Ash	0.00	0.00	0.00	0.00	0.00
Carbon	83.45	84.49	85.95	86.56	86.89
Hydrogen	13.39	12.72	11.59	10.03	8.61
Sulfur	1.61	1.56	1.57	2.00	1.77
Nitrogen	0.18	0.20	0.32	1.13	1.98
Specific Gravity (60°/60°F)	0.750	0.809	0.888	0.984	1.089
Calculated Cetane Index*	OR†	26.6	27.5	OR	OR
Oil Gravity, °API	57.2	43.5	27.9	12.3	-1.6
Group Types,** wt %					
Aliphatic	62.5	58.5	42.0	19.0	9.0
1-Ring	37.5	41.0	47.0	30.0	12.0
2-Ring	<0.5	<0.5	9.5	26.0	12.0
3-Ring	<0.5	<0.5	<0.5	10.0	6.0
4-Ring + Polar Groups	<0.5	0.5	1.5	12.0	45.0
Hexane Insoluble	0.0	0.0	0.0	3.0	16.0
Total	100.0	100.0	100.0	100.0	100.0
Trace Elements, ppmw					
Arsenic	0.8	2.4	4.6	7.3	11.6
Chlorine	300	89	42	540	550
Iron	29	27	46	<4.3	250
Nickel	3.9	3.4	10	<4.3	25
Vanadium	<0.2	<0.2	<0.2	<2.6	9.1

* ASTM D976
** Oil:Hexane dilution of 1:100
† Outside diesel fuel range

Table 5-12. SIMULATED DISTILLATION OF THE PRODUCT OIL FRACTIONS FROM THE BSU TESTS

Distillation Fraction, °F	-180	180-360	360-650	+650
Simulated Distillation Temperature, °F*	wt %			
208	52.7	1.3	0.0	
259	96.6	10.6	0.1	
304	100.0	36.3	0.1	
345		69.8	0.4	
385		98.4	6.3	
421		99.4	23.9	
489		99.5	61.1	0.0
549		99.6	93.9	0.8
601		99.8	99.7	6.2
651		99.9	99.9	13.0
736		100.0	100.0	26.2
808				38.6
871				50.1
925				60.9
972				70.5
1013				78.7
1067				87.7
1139				95.1

* By modified ASTM Method D3887.

The sulfur content does not vary significantly with boiling point. The highest sulfur concentration was found in the 650°-850°F oil fraction. The nitrogen content, however, increases with boiling point and is concentrated in the higher boiling point fractions. The nitrogen concentration increases from 0.18 to 0.32 percent for the lowest three boiling fractions to 1.13 and 1.98 percent in the 650°-850°F and +850°F fractions. The samples were also analyzed for arsenic, chlorine, iron, nickel, and vanadium. The concentrations of these elements increase with increasing boiling point.

The analyses of the five boiling point fractions show that the aliphatic content decreases with increasing boiling point. More than half of the oil that boils below 360°F is aliphatic; however, the aliphatic contents of the 650°-850°F and +850°F boiling fractions are 19.0 and 9.0 percent, respectively. The aromatic content of the oil increases and aromatic groups become larger as the boiling point increases. Almost all of the 3-ring and larger aromatic groups are concentrated in the fractions boiling above 650°F. Four-ring and larger compounds comprise almost half of the 850°F fraction, and a large fraction of asphaltenes is present in the highest temperature fraction.

The product water from the densified, beneficiated Alabama shale was analyzed by GC-FID for major organic components (Table 5-13). Compared to raw shale, processing beneficiated shale generates less product water per gallon of oil but has higher concentrations of organic compounds.[1] Product water

from processing of beneficiated shale contains more than 11,500 mg/L of organic compounds. Two-thirds of the organic compounds contain oxygen and nitrogen; the remaining one-third of the organic compounds are unidentified species. The compounds present in the highest concentration are acetic acid, acetonitrile, acetone, pyrrole, methyl pyrroles, and methanol. The acetone concentrations may be artificially high because the unit vessels and lines are cleaned with acetone between tests.

Table 5-13. ANALYSES OF THE PRODUCT WATER FROM THE BSU TEST

Test No.	52-A-1	52-A-2
Oxygenated Compounds, ppmw		
Methanol	600	450
Ethanol	60	80
1-Propanol	150	120
Acetone	840	650
Methyl Ethyl Ketone	470	380
2-Pentanone	160	110
Acetic Acid	2100	1600
Propanoic Acid	BDL*	BDL
Butanoic Acid	BDL	BDL
Phenol	420	360
Methyl Phenols	110	100
Nitrogen Compounds		
Acetonitrile	880	700
Propionitrile	280	110
Aniline	460	390
Methyl Aniline	360	300
Pyrrole	660	570
Methyl Pyrroles	700	490
C_2-Pyrroles	340	290
Oxygen and Nitrogen Compounds		
Acetamide	95	60
Propamide	25	30
Pyrrolidinone	BDL	BDL
Unidentified	4400	4700
Total	13,110	11,490

* Below detection limit.

Trace element analyses of the product oils and waters from the two BSU test sample periods are presented in Table 5-14. The product oils contain almost 400 ppm of chlorine and from 10 to 25 ppm of arsenic, cadmium, nickel, selenium, and vanadium. Twenty-four other elements are present in lower concentrations. Product waters contain almost 200 ppm of fluorine, between 5 and

10 ppm of chlorine, iron, and sodium, and 3 ppm of calcium and zinc. Twenty-four other elements are present in concentrations of less than 3 ppm.

Table 5-14. TRACE ELEMENT ANALYSES OF THE PRODUCT OIL AND WATER FROM THE BSU TEST

Test No.	52-A-1		52-A-2	
Sample	Oil	Water	Oil	Water
Element, ppmw				
Ag	<5.0	<0.20	<5.0	<0.20
Al	<2.5	2.2	<2.5	0.90
As	9.8	1.8	16	2.3
Ba	<3.0	0.11	<3.0	<0.10
Ca	11	3.2	11	2.2
Cd	<3.0	<0.10	<3.0	<0.10
Cl	360	6.8	380	4.0
Cr	2.5	1.4	1.7	1.2
Cu	<0.50	0.36	<0.50	0.96
F	20	190	<20	180
Fe	9.6	6.9	3.6	4.3
Hg	1.1	0.86	1.5	0.81
K	<15	1.4	<15	<0.70
Li	<15	<0.70	<15	<0.70
Mg	1.1	0.70	1.3	0.43
Mn	<0.50	3.0	<0.50	2.2
Na	<3.0	6.6	<3.0	1.4
Ni	24	1.2	24	1.0
Pb	<50	<2.0	<50	<2.0
Sb	<50	<2.0	<50	<2.0
Se	21	<0.30	23	<0.30
V	9.3	<0.20	11	<0.20
Zn	2.7	3.3	1.5	3.5

The EST was used in steady-state periods 52-A-1 and 52-A-2. A portion of the product gas was passed through 3N HCl and 6N NaOH solutions to collect nitrogen compounds, sulfur compounds, oil, phenols, cyanide, and thiocyanate. In both periods, the acid scrub was used for 60 minutes and the base scrub was used for 30 minutes. The second steady-state period lasted only 75 minutes, but the full 90-minute EST sampling period was achieved by including 15 minutes of the unsteady-state period with the steady-state period.

Acid and base scrub EST results are presented in Table 5-15. Acid scrub results show very little oil is carried past the condenser and coalescing filters. Nitrogen and phenol levels were below analytical limits and, therefore, can not be used to determine recoveries. Base scrub results show the majority of the sulfur collected is in sulfide form with very little sulfate sulfur collected.

Table 5-15. ANALYSES OF THE ACID AND BASE SCRUB SOLUTIONS FROM THE ENVIRONMENTAL SAMPLING TRAIN

Test No.	52-A-1	52-A-2
Acid Scrub Concentration	---------- mg/L ----------	
COD	11400	9900
Oil and Grease	13	3
Total Nitrogen	<20	<20
NO_2	<5	<5
NO_3	<5	<5
Ammonia Nitrogen	<20	<20
Phosphorous	0.22	0.15
Phenols	<5	<5
Organic Carbon	40	33
Base Scrub Concentration		
Cyanide	2.51	3.21
Thiocyanates	5.7	21
Total Sulfur	8100	9000
Sulfate Sulfur	190	220
Sulfide Sulfur	7700	8800

Task 6. Environmental Data and Mitigation Analyses

The overall objectives of this task were to obtain environmental data relating to PFH and shale beneficiation, to analyze the potential environmental impact of the integrated PFH process, and to conduct a preliminary economic evaluation. This task was divided into five subtasks: 6.1. Characterization of Processed Shales, 6.2.2 Wastewater Treatability, 6.4.1. PFH Process Analyses, 6.4.3. Plant Energy Optimization, and 6.4.4. Economics.

Subtask 6.1. Characterization of Processed Shales

The objective of this subtask was to determine the effects of PFH processing and thermal posttreatment on the physical and chemical characteristics of raw and hydroretorted beneficiated Alabama shale. The specific posttreatment processes considered are combustion and thermal agglomeration.

Discussion

The physical properties of raw and hydroretorted beneficiated shale dictate the geometry and size of an embankment in which the spent shale will be stored. Post-retorting processing, such as combustion and agglomeration, will also affect the embankment characteristics. The angle of internal friction provides the maximum slope for the sides of the embankment to prevent sliding failure. The compactability and compressibility of the spent shale relate to the volume occupied by the shale at its optimum moisture content. The relative flow of water through the pile, which may affect leaching of environmentally sensitive (priority) metals, is related to the permeability or hydraulic conductivity. The Atterberg liquid and plastic limit tests determine the moisture content of the solid sample (shale, soil, or other) at the boundary between the a) liquid and plastic and the b) plastic and semisolid states, respectively. Thermal conductivity affects the rate at which hot shale from the retort or combustion process will cool to temperatures appropriate for moisturization and disposal.

The chemical properties of shale determined during this project relate specifically to the leaching of raw and spent beneficiated shale by precipitation in storage piles. Raw beneficiated shale will be exposed to weather during storage in stockpiles prior to hydroretorting. After hydroretorting and combustion, spent shale will also be exposed to weather in stockpiles prior to ultimate disposal. It is during these exposures that the most significant environmental impacts could be realized by the leaching of trace metals (in addition to other components) into water in the shale. The test used to evaluate the leaching characteristics of shale samples is the Toxicity Characteristic Leaching Procedure (TCLP), promulgated by the U.S. Environmental Protection Agency (EPA).[1]

If the concentration of any trace element in the leachate from the TCLP test with shale exceeds the Federal limits shown in Table 6-1, the material is classified as hazardous and must be disposed of in suitably constructed and monitored landfills. If the leachate is not effectively contained or collected, it could percolate down to the water table or combine with surface runoff to contaminate fresh water supplies. The sulfur content of the shale

affects its leachability. A shale high in sulfur will yield leachate that is more acidic.

Table 6-1. EPA TCLP LIMITS FOR METALS[1]

Element	Leachate Limit, mg/L
Arsenic	5
Barium	100
Cadmium	1
Chromium	5
Lead	5
Mercury	0.2
Selenium	1
Silver	5

Thermal processing reduces the concentration of acid-forming components in shale and yields leachate that is less acidic. Other elements of importance have been considered for inclusion on the list of priority metals. Regulations promulgated by the EPA in the future may include these elements as well as others determined to pose significant environmental threats.

During the initial 3-year program, IGT conducted physical and chemical properties tests on shales from six states in the Eastern U.S. The results of these tests are presented in the final report on the program.[2]

Shale Samples and Preparation

Four samples of raw and processed beneficiated Alabama shale were prepared for the physical and chemical properties tests. The samples of raw and hydroretorted beneficiated shale were obtained from a BSU test conducted at a temperature of 925°F (496°C) in hydrogen and a pressure of 1000 psig (7.0 MPa) with a residence time of 26 minutes. Descriptions of the BSU equipment and test procedures are presented in Task 5. The particle size consist of the raw beneficiated feed shale was -20+80 mesh. The combusted and hydroretorted beneficiated shale sample was obtained from tests conducted in Subtask 3.6.1. The agglomerated and hydroretorted beneficiated shale sample was prepared with solids from the BSU test, which were subsequently agglomerated in a 2-inch diameter, laboratory-scale batch unit shown in Figure 6-1.

In the process of agglomeration, particles in a fluidized bed are heated to near their softening temperature. Under specific hydrodynamic conditions, the particles stick together and grow in size by accretion. When the particles become large enough, the fluidizing gas can no longer support them and they can be removed from the bed by gravity. In uncontrolled agglomeration, the particles combine into a single agglomerate or sinter.

Prior to the agglomeration test, a weighed amount (about 220 grams) of hydroretorted shale was charged to the reactor. During heat up, nitrogen was fed to the reactor grid and central jet at 5 SCF/h (2.35 L/min) each to

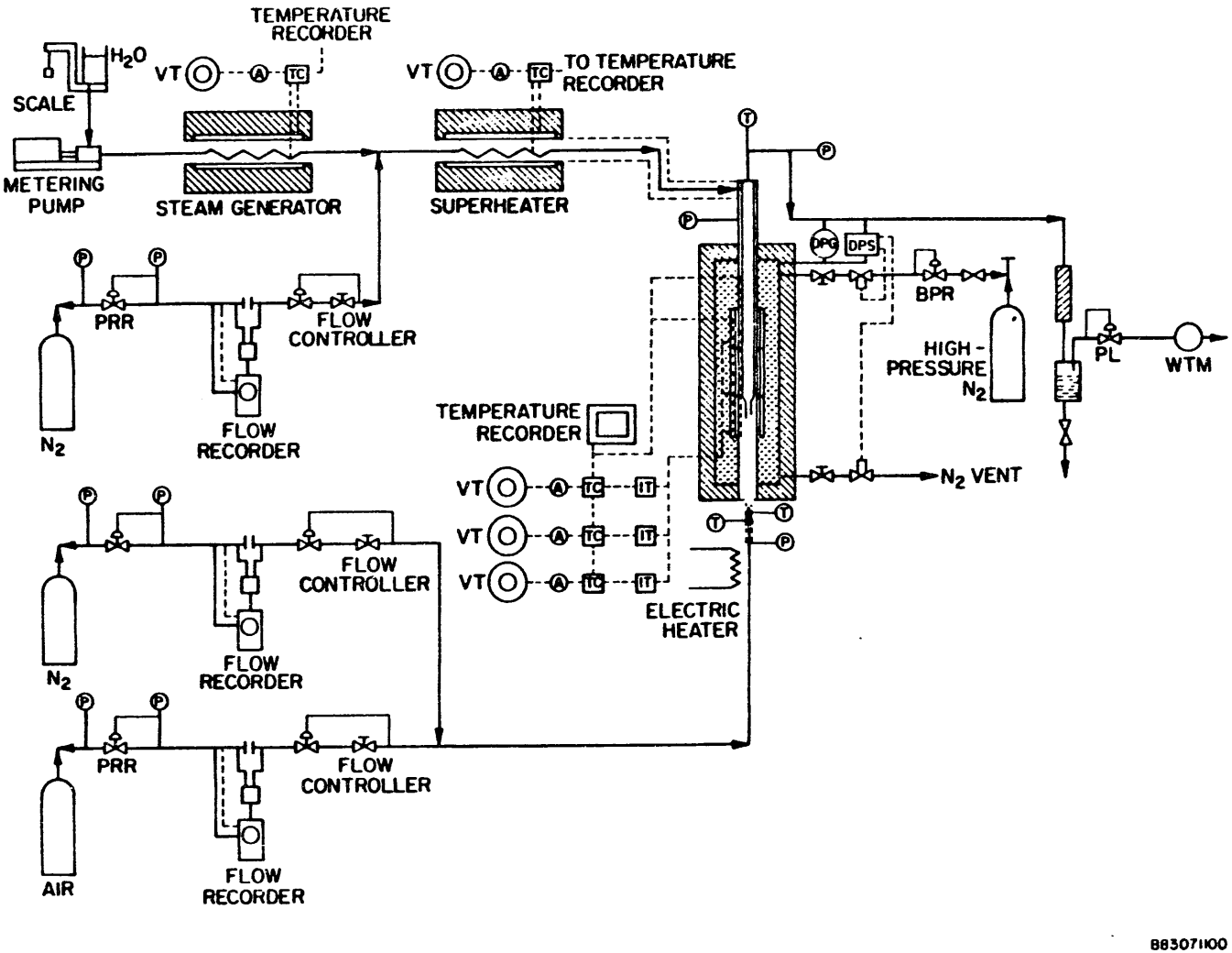

Figure 6-1. SCHEMATIC DIAGRAM OF THE 2-INCH DIAMETER FLUIDIZED-BED SHALE AGGLOMERATION UNIT

maintain a fluidized bed. When a temperature of about 1800°F (982°C) was achieved, the nitrogen flow to the central jet was replaced by air at 5 SCFH (2.35 L/min). The oxygen content of the total gas to the reactor was then about 10 mole percent. Heat liberated by the combustion reactions further increased the temperature to the target of about 2000°F (1093°C). The sample was held at these conditions for 90 minutes to ensure complete combustion. Previous tests with hydroretorted raw shale had demonstrated that these conditions were adequate to agglomerate the shale. The product from the agglomeration test consisted of a sinter and a small quantity of unincorporated fine particles.

Physical Properties

The physical properties tests were conducted by the Illinois Institute of Technology (IIT) Department of Civil Engineering. When IIT completed the tests, the samples were returned to IGT and subjected to the TCLP test.

The physical properties of the samples of raw and processed PFH shales were determined using ASTM (American Society for Testing and Materials) standards or laboratory procedures developed by the IIT Civil Engineering Department. The tests and procedures, listed in Table 6-2, were conducted in the indicated order to minimize the impact on subsequent tests.

Table 6-2. PHYSICAL PROPERTY TESTS AND SEQUENCE USED FOR RAW AND PROCESSED BENEFICIATED SHALE SAMPLES

Sequence	Physical Property	Test/ASTM Standard
1	Particle Size	D 421-85
2	Permeability	D 2434-74 (Falling Head)
3	Thermal Conductivity	IIT Laboratory Test
4	Consolidation/ Compressibility	D 2435-80
5	Direct Shear Strength	D 3080-72
6	Compactability	D 698-78 (Harvard miniature)
7	Atterberg Liquid and Plastic Limit	D 4318-84
8	Specific Gravity	D 854-83

Chemical Properties

The toxic or non-toxic character of the shale samples was determined by TCLP test (EPA Method 1311). In the TCLP test, the shale sample is mixed with 20 times its weight of an appropriate aqueous extraction fluid (depending upon alkalinity) for 18 hours. After mixing, the solids are separated from the extraction fluid and the extract is analyzed for metals and specific volatile and nonvolatile organic compounds. If the concentration of any metal (or organic compound) in the leachate exceeds the regulatory limit, the material is said to exhibit a toxic character and is classified as a hazardous waste. The solid must then be disposed of in suitably constructed and monitored land-

fills. Because this task focused on the heavy metals in shale, the leachate was not analyzed for organic compounds.

TCLP tests were conducted on the following four samples of beneficiated Alabama shale: 1) raw, 2) hydroretorted, 3) hydroretorted and combusted, and 4) hydroretorted and agglomerated. If the results of TCLP tests on "as received" and agglomerated spent shales were similar, the spent shale could be disposed of without further processing.

Discussion of Results

Physical Properties. Overall, the physical properties of four samples showed considerable variability. The results of particle size, thermal conductivity, permeability, consolidation (compressibility), shear strength, compactability, and Atterberg liquid and plastic limit tests are presented in Tables 6-3 through 6-7.

Table 6-3 shows that the particle size distributions for the raw and hydroretorted beneficiated shale samples were quite similar before compaction. About 85 percent of these samples were between 10 and 50 mesh. The hydroretorted and combusted (H&C) sample has about 69 percent in the -10+50 mesh particle size range. The hydroretorted and agglomerated (H&A) sample was crushed with a mortor and pestle at IIT to -10 mesh for the physical properties tests, which explains the relatively high fraction of fine (-100 mesh) particles.

Table 6-3. PARTICLES SIZE DISTRIBUTION OF SAMPLES OF RAW AND PROCESSED BENEFICIATED ALABAMA SHALE (Before Compaction)

Sample	Raw	Hydroretorted	Hydroretorted & Combusted	Hydroretorted & Agglomerated
Particle Size Distribution, wt %				
Mesh, U.S.S.				
+10	0.0	0.0	0.0	0.0
-10+20	21.4	12.0	0.2	25.0
-20+40	44.8	55.3	36.7	28.7
-40+50	17.8	18.0	31.9	10.9
-50+80	9.8	9.5	24.2	9.2
-80+100	2.6	1.9	3.1	3.0
-100+200	2.0	2.3	3.3	11.8
-200+pan	1.6	1.0	0.6	11.4
Total	100.0	100.0	100.0	100.0

The thermal conductivity (TC) of the raw beneficiated shale sample was 0.67 W/m-K (refer to Table 6-4). Hydroretorting the beneficiated shale sample reduced the TC to 0.08 W/m-K. Combustion of the hydroretorted shale sample resulted in a slight increase in TC (compared to that of the hydroretorted sample) to 0.11 W/m-K. Agglomeration of the hydroretorted shale sample reduced the TC slightly to 0.06 W/m-K. For comparison, in previous work, IGT

determined the thermal conductivity of a sample of hydroretorted Alabama shale to be 0.21 W/m-K.[2]

The permeability (k_{20}) of the raw beneficiated shale sample was 3.2×10^{-3} cm/s. Hydroretorting the beneficiated sample reduced the permeability somewhat to 2.74×10^{-3} cm/s. Combustion of the hydroretorted sample reduced the permeability by an order of magnitude to 4.8×10^{-4} cm/s. The permeability of the H&A sample (2.94×10^{-3} cm/s) was essentially the same as that of the hydroretorted sample. The permeability of a sample of hydroretorted Alabama shale was determined previously to be 1.34×10^{-2} cm/s.[2]

Table 6-4. RESULTS OF THERMAL CONDUCTIVITY AND PERMEABILITY TESTS CONDUCTED ON SAMPLES OF RAW AND PROCESSED BENEFICIATED ALABAMA SHALE

Sample	Raw	Hydroretorted	Hydroretorted & Combusted	Hydroretorted & Agglomerated
Thermal Conductivity, W/m-K	0.67	0.08	0.11	0.06
(Btu/h-ft-°F)	(0.39)	(0.05)	(0.06)	(0.04)
At Density, g/cm^3	0.75	0.67	0.58	0.72
Permeability, cm/s, k_{20}	3.2E-3	2.74E-3	4.8E-4	2.94E-3
At Density, g/cm^3	0.99	0.88	0.77	0.96

The results of consolidation tests (Table 6-5) showed that the initial void ratio (volume of voids per volume of solids) of the raw sample was 1.17, which decreased with hydroretorting to 0.88 and with combustion to 0.76. The void ratio of the agglomerated sample (1.24) was higher than that of the raw beneficiated shale sample. After consolidation, the H&C shale sample had the lowest void ratio (0.36). The compacted bulk density of the samples ranged from about 1.26 g/cm^3 (78.6 lb/ft^3) for the hydroretorted shale to 1.83 g/cm^3 (114.1 lb/ft^3) for the H&A shale, which was similar to that of the raw beneficiated shale sample (1.80 g/cm^3 or 112.3 lb/ft^3). The final void ratio and compacted bulk density of a sample of hydroretorted Alabama shale were determined to be 0.68 and 1.55 g/cm^3 (96.7 lb/ft^3), respectively.[2]

The factors, C_c' and C_c, are obtained from the consolidation tests. C_c' is an indication of the rebound (springiness) of the sample during unloading - a higher value for C_c' indicates a higher rebound. C_c is a measure of the extent to which the sample will consolidate. A sample with a high C_c will consolidate to a larger extent than one with a low value of C_c.

The angle of internal friction was determined to be 37.2° for raw beneficiated shale and 26.0° and 27.0° for the hydroretorted and H&C shale samples. The angle of internal friction for the H&A sample was 32.8°. The cohesion (c) was 0.0 kPa (0.0 psi) for the raw beneficiated shale and 17.2 and 27.0 kPa (2.5 and 0.8 psi) for the hydroretorted and H&C shale samples. The

cohesion for the H&A sample was the same as that of the raw sample. The angle of internal friction and cohesive strength for a sample of hydroretorted Alabama shale were previously determined to be 40.9° and 0.0 kPa, respectively.[2]

Table 6-5. RESULTS OF CONSOLIDATION AND SHEAR STRENGTH TESTS CONDUCTED ON SAMPLES OF RAW AND PROCESSED BENEFICIATED ALABAMA SHALE

Sample	Raw	Hydroretorted	Hydroretorted & Combusted	Hydroretorted & Agglomerated
Consolidation; Void Ratio, Vol. Void/Vol. Solid				
Initial	1.17	0.88	0.76	1.24
Final	0.65	0.44	0.36	0.69
Density, g/cm^3				
Initial	1.36	0.96	1.19	1.38
Final	1.80	1.26	1.53	1.83
Consolidation factors				
C_c'	0.046	0.047	0.021	0.091
C_c	0.25	0.17	0.17	0.22
Shear Strength				
Angle of Internal Friction, degrees	37.2	26.0	27.0	32.8
Cohesion (c), kPa	0.0	17.2	5.5	0.0
(psi)	(0.0)	(2.5)	(0.8)	(0.0)
At Density, g/cm^3	0.99	0.85	0.79	1.23

The results of the compaction tests are presented in Table 6-6. The compaction tests were conducted using a Harvard miniature mold, which has a 3.3-cm ID, a height of 7.15 cm, and a capacity of 61.15 cm^3. The standard mold for this procedure has an ID of 10.16 cm, a height of 11.64 cm, and a capacity of 944 cm^3. The optimum moisture contents (OMC) for the raw, hydroretorted, and H&C samples of beneficiated shale were about 25 percent. The OMC of the H&A sample was 10 percent. The maximum dry density (at the OMC) decreased from 1.23 g/cm^3 (76.7 lb/ft^3) for the raw sample, to 1.11 g/cm^3 (69.2 lb/ft^3) for the hydroretorted sample to 0.96 g/cm^3 (59.9 lb/ft^3) for the H&C sample. The MDD was determined to be 1.19 g/cm^3 (74.2 lb/ft^3) for the H&A sample. The OMC and MDD a sample of hydroretorted Alabama shale were previously determined to be 22.0 percent and 1.36 g/cm^3 (84.8 lb/ft^3).[2]

The results show that the hydroretorted samples (including combustion and agglomeration) experienced particle size reduction during the compaction procedure. The fines (-100 mesh) content in the hydroretorted sample increased from 3.3 before to 33.0 percent after compaction. In the H&C sample, the fines content increased from 3.9 to 30.0 percent. The fines content of the H&A sample increased by the least amount, from 23.2 to 33.5 percent.

Table 6-6. RESULTS OF COMPACTION TESTS AND GRAIN SIZE ANALYSES OF SAMPLES OF RAW AND PROCESSED BENEFICIATED ALABAMA SHALE

Sample	Raw	Hydroretorted	Hydroretorted & Combusted	Hydroretorted & Agglomerated
Compaction Test Results (Harvard Miniature)				
Optimum Moisture Content, wt %	26.0	25.0	25.0	10.0
Maximum Dry Density, g/cm^3	1.23	1.11	0.96	1.19
Particle Size Distribution, wt % (after compaction)				
Mesh, U.S.S.				
+10	0.0	0.0	0.0	0.0
-10+20	23.0	16.0	15.0	12.1
-20+40	24.0	21.0	20.0	25.5
-40+50	14.0	11.0	14.0	12.2
-50+80	16.0	12.0	15.0	12.2
-80+100	14.0	7.0	6.0	4.5
-100+200	5.0	12.0	9.0	15.2
-200+pan	4.0	21.0	21.0	18.3
Total	100.0	100.0	100.0	100.0

The results of the Atterberg Liquid and Plastic Limits tests are presented in Table 6-7. Per the ASTM definition, the Liquid Limit is defined as the water content of a sample, expressed as a percentage of the dry sample weight, at the boundary between the liquid and plastic states. It is defined arbitrarily as the water content at which two halves of a soil cake will flow together for a distance of 1/2 inch along the bottom of a groove separating the two halves, when the sample cup is dropped 25 times for a distance of 1 cm at a rate of two drops per second. The sample cup is a rounded brass bowl, 3.68 inches in diameter and 1.063 inches deep. Typically, tests at three different water contents are needed to determine the Liquid Limit.

Table 6-7. RESULTS OF ATTERBERG LIQUID AND PLASTIC LIMIT TESTS CONDUCTED ON SAMPLES OF RAW AND PROCESSED BENEFICIATED ALABAMA SHALE

Sample	Raw	Hydroretorted	Hydroretorted & Combusted	Hydroretorted & Agglomerated
Liquid Limit, %	31.8	32.4	48.0	25.3
Plastic Limit, %	16.5	18.5	23.2	14.6
Plasticity Index, %	15.3	13.9	24.8	10.7
Flow Index	-10.9	-6.5	-18.3	-14.5
Specific Gravity (G_s), g/mL	1.84	1.64	2.40	2.22

The results of the three Liquid Limit tests are plotted on semilog paper with the water content on the ordinate and the number of drops required on the abscissa (log scale). The water content at which the line intercepts the 25 drop value is the Liquid Limit. The slope of the line is defined as the Flow Index. For materials that exhibit the same Liquid Limit value, a low Flow Index (shallow slope) means that the sample will be in the liquid state with less liquid addition than a sample with high Flow Index (steep slope).

The Plastic Limit is defined as the water content of the sample, also expressed as a percentage of the dry sample weight, at the boundary between the plastic and semisolid states. It is also arbitrarily defined as the lowest moisture content at which the soil sample can be rolled (by hand) into threads 1/8 inch in diameter without the threads breaking into pieces. The Plasticity Index (I_p) is defined as the difference between the Liquid and Plastic Limits.

The results show that the Liquid Limits for the raw and hydroretorted beneficiated shale samples are quite similar at about 32 percent. The H&C sample exhibits the highest Liquid Limit value (48.0 percent); the H&A sample the lowest (25.3 percent). The H&C sample also has the highest Plastic Limit (23.2 percent) and Plasticity Index (24.8 percent) of the other samples and the highest value (absolute) of Flow Index (-18.3).

For considerations of slope stability and strength in embankments, the lower the value for the Plasticity Index (PI), the higher is the relative sample strength. Therefore, based on the PI value, the H&A sample exhibits characteristic that are more desirable than those of the other samples. However, because the PI values fall within a fairly narrow range of about 10 to 25, the other sample characteristics are not detrimental to slope stability.

Chemical Properties. The results of the TCLP tests conducted on the shale samples are presented in Table 6-8. The results show that for the raw, hydroretorted, H&C, and H&A beneficiated shale samples, neither silver, lead, nor mercury are leached at levels above the analytical detection limit. Selenium levels were about 10 percent of the TCLP limit and all other elements were leached at less than 2 percent of the TCLP limit. All eight elements were leached from the feed and residue shales at levels below the TCLP leachability limits. Therefore, these samples do not exhibit the toxicity characteristic.

Embankment Design. The following general guidelines could be used for designing an embankment for storing raw, hydroretorted, or H&C or H&A shale. To ensure stability, the slope of the embankment should not exceed a rise/run ratio of 0.5 (~26.5°). A cohesion of 0 psi should be assumed. The shale could be compacted to about 1.3 to 1.55 g/cm^3 (80 to 95 lb/ft^3) at a moisture content of 20 to 24 percent. Reclamation could be initiated with a surfacial coverage of top soil (or overburden) of about 1 to 3 feet in thickness. Because hydroretorted beneficiated shale does not exhibit the toxicity characteristic, it can be stored in ordinary surface or landfills.

Table 6-8. RESULTS OF TCLP TESTS CONDUCTED ON SAMPLES OF RAW AND PROCESSED BENEFICIATED ALABAMA SHALE

Sample		Raw	Hydroretorted	Hydroretorted & Combusted	Hydroretorted & Agglomerated
Analysis of TCLP Extract					
Element	Max. Allowable Conc.	mg/L			
Arsenic	5	0.0028	0.084	0.078	0.0069
Barium	100	0.025	0.059	0.034	0.085
Cadmium	1	0.029	<0.02	<0.02	0.12
Chromium	5	0.28	<0.05	<0.05	<0.05
Lead	5	<0.2*	<0.2	<0.2	<0.2
Mercury	0.2	<0.001	<0.001	<0.001	<0.001
Selenium	1	0.038	0.0091	0.026	<0.013
Silver	5	<0.05	<0.05	<0.05	<0.05

* "<" indicates detection limit of the analytical technique used.

Conclusions

The physical properties of raw, hydroretorted, hydroretorted and combusted (H&C), and hydroretorted and agglomerated (H&A) beneficiated Alabama shale samples were determined. Based on the results of the tests conducted during this program, the following conclusions can be drawn:

- Thermal conductivity ranged from 0.06 to 0.11 W/m-K for thermally processed shales, and was 0.67 W/m-K for raw beneficiated Alabama shale.
- Permeabilities of the shale samples were in the range of 10^{-3} cm/s; that of the H&C shale sample was lowest at about 10^{-4} cm/sec.
- The angle of internal friction was 37.2° for the raw sample, 26.0° for the hydroretorted sample, 27.0° for the H&C sample, and 32.8° for the H&A sample. Cohesive strengths were similar for the raw and H&A shale samples (0 psi).
- Beneficiated shale can be compacted to a density of 1.23 g/cm^3 (76.7 lb/ft^3) at an optimum moisture content of 26 percent. The H&A sample can be compacted to 1.19 g/cm^3 (74.2 lb/ft^3) at an optimum moisture content of 10 percent.
- Embankments with processed beneficiated shale can be constructed safely with a slope of 26.5° (1:2 rise/run).
- The results of leaching tests conducted with raw and hydroretorted beneficiated shale samples indicate that none exhibit the toxicity characteristic according to the TCLP.

- Spent shale from the PFH process can be disposed in ordinary surface or landfills.

Recommendations

Larger-scale and long-term testing should be conducted on evaluating the embankment design and slope stability of hydroretorted and thermally processed beneficiated shale. Large-scale lysimeter tests should be conducted on bulk samples of hydroretorted and thermally processed beneficiated shale to determine long-term leaching characteristics. Trace elements, in addition to those specified by the TCLP, such as Ni and Mo, should be analyzed in the leachate from TCLP tests to determine the extent of leaching.

Subtask 6.2. Water Availability and Treatment Studies

Subtask 6.2.2. Wastewater Treatability

The objective of this subtask was to determine suitable techniques for treating the wastewater generated during shale processing. Tennessee Technological University (TTU) conducted the work on this subtask.

The liquid waste produced during the production of oil from oil shales by the PFH process is expected to vary in its composition and to depend on the operating conditions and the type of shale being processed. Component analyses of water produced as a result of laboratory- and bench-scale hydroretorting tests have demonstrated the presence of numerous components (Table 6-9).[1] Hydrogen sulfide (H_2S) and ammonia (NH_3) would normally be removed prior to any wastewater treatment in a commercial-scale facility.

Some of the compounds listed in Table 6-9 are considered to be harmful to health and the environment by the EPA. Among those listed, acetone, methyl ethyl ketone (MEK), phenol, acetonitrile, aniline, methyl pyridine, and pyridine are classified under the Resource Conservation and Recovery Act (RCRA) as hazardous wastes.[2]

During the previous program, TTU evaluated the biological treatability of four of the compounds that were detected in the PFH sour water. These compounds were acetone, thiocyanate, propionitrile, and pyrrole. TTU determined that all of these compounds could be degraded biologically at various concentrations in a modified continuous flow extended aeration activated sludge process. The waste used in that study was synthetic, since sufficient quantities of the actual sour water from the PFH process experimental program were not available.[3]

In the current work, four other compounds expected to occur in the PFH sour water were selected for treatability evaluation. These compounds are aniline, phenol, MEK, and 4-methyl pyridine. Synthetic wastes were prepared including each of these compounds individually and in mixtures. A biological seed was acclimated to each compound and treatability was evaluated in batch reactors.

Table 6-9. COMPOSITION OF WATER GENERATED BY HYDRORETORTING TENNESSEE CHATTANOOGA SHALE

Compound	Concentration, ppm
Thiocyanate	7350
Sulfides	58,500
Sulfates	7150
Acetone	200
Methyl ethyl ketone	50
Pentanone	15
Phenol	40
Methyl phenol	30
Ammonia	42,700
Acetonitrile	360
Propionitrile	40
Aniline	500
Methyl anilines	180
Pyrrole	130
Methyl pyrrole	70
C_2-pyrrole	15
C_2-pyridines	5
Cyanide	45
Methyl pyridines	30

Literature Review

Phenol. Phenol (C_6H_6O) exists as a solid or liquid at 15°C and 1 atm. The crystals are white and the liquid is pink. The melting point is 43°C and the boiling point is 181.8°C at 1 atm. The specific gravity of phenol is 1.058 g/mL at 41°C and its molecular weight is 94.11.[4] Phenol is soluble in water to a concentration of 66.7 g/L at 20°C. It is very soluble in alcohol, chloroform, ether, glycerol, and carbon disulfide.[5] The LD_{50} (lethal dose for 50 percent of a population) for rats is 530 mg/kg.[4]

The biodegradability of phenol has been reported by researchers for many years. Zobell[6] reported in 1950 that numerous phenolic compounds and hydrocarbons were oxidizable by bacteria. The work of Ludzack and Ettinger[7] indicated that mono- or dihydric phenols or cresols showed relatively little resistance to acclimated organisms.

Tabak, Chambers, and Kabler[8] showed a 99 percent reduction in the phenol concentration using an initial concentration of up to 100 mg/L. They also reported that microorganisms previously acclimated to phenol were able to reduce an initial concentration of 300 mg/L by 95 percent within 1 to 2 days. The microorganisms that were acclimated to phenol as a sole carbon source exhibited a marked lag time when a secondary carbon source was introduced after the phenol was depleted. The microorganisms used in this study were obtained from sediments in a lagoon receiving petroleum refining wastes.

Bayly and Wigmore[9] reported that aerobic microorganisms were able to metabolize phenol by converting it to catechol and methylcatechols, which then

underwent meta fission of the benzene nucleus to eventually become pyruvate and other compounds that can go through the energy productive Krebs (or tricarboxylic acid) cycle.

Lallai and Mura[10] reported that phenol was biodegradable at initial concentrations up to 1000 mg/L by previously acclimated biomass. It was also reported in this work that the pH in a batch reactor decreased along with the biodegradation of phenol, due to the production of organic acids as metabolic by-products. Once phenol was depleted, the acids were then degraded and the pH increased, but not to its original level.

Aniline. Aniline, or benzenamine (C_6H_7N), is an oily liquid that is colorless when first distilled but darkens when exposed to air and light. The specific gravity of aniline is 1.022 g/mL at 20°C, its boiling point is 184.2°C, and its molecular weight is 93.1.[4]

Since aniline is a substituted benzene, beyond the initial step, its metabolic breakdown is similar to that of phenol. Lyons, Katz and Bartha[11] studied the fate of aniline in polluted and unpolluted pond water and reported that removal by microbial processes, resulting ultimately in carbon dioxide and biomass, was by far the most efficient removal mechanism. They indicated that no acclimation period was required, or was not detected, prior to degradation of aniline. The principal biodegradation pathway apparently involves attack by dioxygenase resulting in oxidative deamination to catechol. Catechol was not detected, but the intermediates leading through the tricarboxylic acid cycle to the release of CO_2 were detected.

Wyndham[12] reported that aniline in a batch reactor was removed at a rate of 0.34 μM/liter/h from river water after a lag period of 24 hours. The aniline was removed to below the detection level of 2 μM/L in the reactor. It was also noted that the aniline was used as a source of both carbon and nitrogen in the reactor.

Paris and Wolfe[13] studied the effect of compound structure on the biological degradation of a series of anilines. It was determined that catechol was an intermediate of the metabolism.

4-Methyl Pyridine. The common name for 4-methyl pyridine (C_6H_7N) is 4-picoline. The compound is a colorless liquid and has a disagreeable odor. The boiling point of 4-methyl pyridine is 145°C at 1 atm., its specific gravity is 0.9571 g/mL, and its molecular weight 93.14.[14,15]

The Henry's Law constant of 7.07×10^{-7} atm-m^3/mol at 25°C indicates that volatilization of 4-methyl pyridine from environmental waters should be extremely slow.[15] The available literature on the biological degradability of this compound is limited.

Ettinger, Lishka and Kroner[16] reported in 1954 that 4-methyl pyridine was biodegradable but only if the biological seed had been given long periods of acclimation to the compound. The seed that was found to be effective was taken from the Ohio River downstream from industrial discharges that included 4-methyl pyridine. It was also noted in the study that it was unlikely that

organisms would split the pyridine ring just to obtain the nitrogen. In the current study there was an ample amount of more readily available nitrogen.

Stafford and Callely[17] reported that a seed taken from an activated sludge plant treating pyridine compounds would biodegrade 4-methyl pyridine. Interestingly, this same seed would not biodegrade 2-and 3-methyl pyridine.

Watson and Cain[18] isolated two bacteria, a Bacillus sp. and a Nocardia sp. by enrichment with 0.1 percent (v/v) of pyridine. These microorganisms grew rapidly on pyridine but would not grow on 2- or 4-methyl pyridine. The pyridine supplied both carbon and nitrogen to the microorganisms.

Kuhn and Suflita[19] evaluated the potential for using anaerobic biodegradation on twelve heterocyclic compounds including pyridine and its methyl substitutes. They reported that 4-methyl pyridine was biodegradable in a methanogenic environment.

No references were available that proposed a metabolic pathway for 4-methyl pyridine.

Methyl Ethyl Ketone (MEK). The International Union of Pure and Applied Chemistry (IUPAC) name for MEK (C_4H_8O) is 2-butanone. It is a colorless liquid with a boiling point of 79.6°C. The specific gravity of MEK is 0.805 g/mL at 20°C and its molecular weight is 72.11.[20]

No literature information was found on biological treatability of MEK.

Discussion

The microorganisms were acclimated to the individual compounds prior to the treatability tests. The acclimation solution consisted of distilled water and the compounds, either individually or combined, at the concentrations to be used in the treatability studies. Also added to the solution were the nutrients required for biological growth and sufficient phosphates to buffer the pH at about 7. The concentrations of nutrients and buffer are listed in Table 6-10.

Table 6-10. NUTRIENTS ADDED TO THE SYNTHETIC WASTEWATER

Nutrient or Buffer	Concentration, mg/L
$(NH_4)_2SO_4$	500
$MnSO_4$ (Hydrated)	10
$CaCl_2$	7.5
$MgSO_4$	1
$FeCl_3$	0.5
KH_2PO_4	526
K_2HPO_4	1070

The acclimation vessels were 250 mL Erlenmeyer flasks placed in a shaker apparatus. The individual compounds were placed in the shaker flasks at the desired concentrations. Each compound was prepared in a series of concentrations as follows: phenol at 100, 250, and 450 mg/L; aniline at 150, 300, and

600 mg/L; MEK at 50, 100, and 250 mg/L; and 4-methyl pyridine at 50, 100 and 250 mg/L. These flasks were seeded from the supernatant of a continuous flow reactor being used to treat a combination synthetic waste containing 150 mg/L each of acetone, pyrrole, propionitrile, and thiocyanate. Once a visible biological growth was obtained in the first series of flasks for a given compound, a second series was prepared and seeded from the supernatant of the first. This serial process was repeated three times.

After the serial acclimation experiments were completed, a 1.5-liter cylindrical acclimation vessel was prepared with the same concentrations of substrate and the essential nutrients. The reactor was aerated with air supplied through a diffuser stone. A seed was taken out of the appropriate shaker flask supernatant and placed in the acclimation vessel. The biological culture was maintained in this reactor by operating the system in batch mode. Every 3 to 4 days the solids in the reactor were allowed to settle and then about two-thirds of the volume was removed from the supernatant. The reactor was then brought back to its original volume with distilled water, substrate, and nutrients so that the substrate and nutrients were recharged to their required concentrations. A shaker flask was maintained at the highest concentration of each acclimated compound throughout the project.

The treatability studies were initiated once a dense biomass was achieved in the acclimation vessels containing a specific compound. Phenol, MEK, and aniline treatability studies were performed in that order. A separate set of 1.5-L cylindrical reactors was prepared, one for each concentration. Prior to seeding the reactors from the acclimation vessels, a time-zero sample was taken. Then 25 mL of seed was taken out of each of the associated acclimation vessels and placed in the treatability reactors. At appropriate intervals, samples were taken to determine the biological uptake of the substrate. The samples were filtered immediately through a 0.45 μm nylon membrane filter. Vials for chemical oxygen demand (COD) were prepared and the remainder of the sample was refrigerated.

During the MEK treatability tests, it was found that a significant quantity of MEK was being stripped from the reactor vessels by the air bubbling through them. Therefore, the observed reduction in MEK concentration from these reactors reflected both biological degradation as well as removal by air stripping. To account for that portion of substrate removed by air stripping, a series of sterilized reactors identical to the treatability reactors was prepared. These reactors, without biological seed, were operated to determine the removal of MEK by air stripping alone. These data were then used to correct the results of the biological treatability tests with MEK.

After the biological treatability tests with the individual compounds were completed, TTU conducted tests to determine the treatability of combination of each compound. Seed taken from each of the acclimation reactors was acclimated to a mixture of the phenol (250 mg/L), MEK (250 mg/L), 4-methyl pyridine (250 mg/L), and aniline (300 mg/L). Once the microbial seed showed evidence that acclimation had been achieved, treatability studies were performed with the same procedures used for the individual studies. Three combination reactors were prepared: 1) included all of the compounds, 2) in-

cluded phenol and aniline, and 3) included phenol and MEK. The effect of MEK air stripping was also taken into consideration in the experiments.

The experiments were duplicated to ensure reproducibility and complete microbial acclimation. Samples were analyzed for COD to determine the change in the concentration of total organics. The method used was the closed reflux, ampule variation of colorimetric analysis, as specified by Standard Methods.[21] The concentration of specific substrate were determined by GC. A Hewlett-Packard 5890A was used for GC analyses.

Results and Discussion

TTU successfully acclimated microorganisms to phenol, aniline, and MEK. They conducted numerous tests to acclimate microorganisms to 4-methyl pyridine. The tests are described in Table 6-11. Each test consisted of a series of flasks with concentrations of 4-methyl pyridine of 50, 100, and 250 mg/L. The overall results of these tests were negative; no microbial growth was detected on 4-methyl pyridine in any attempt.

Table 6-11. RESULTS OF 4-METHYL PYRIDINE ACCLIMATION TESTS

Test	Description
1A	Seed taken from continuous flow activated sludge reactor treating a synthetic waste with 150 mg/L each of acetone, pyrrole, propionitrile, and thiocyanate.
1B	Seed from 1A flasks, the continuous flow reactor, and sewage treatment plant (STP) activated sludge.
1C	Test prepared with seed from 1B, STP activated sludge, and microorganisms acclimated to phenol.
1D	Test with seed from 1B, 1C, STP activated sludge, and microorganisms acclimated to MEK.
1E	Test with phenol seeded from STP activated sludge and from microorganisms acclimated to phenol.
2E	Repeated 1E with seed from 1E.
1D	Seeded 1D from 1E
3E	Repeated 2E with seed from 2E.
1D	Seeded 1D from 2E.
1F	Prepared new flasks seeded from soil sample.
1D	Seeded flask 1D with seed from 3E.
1G	Test with 250 mg/L sucrose seeded from industrial activated sludge treatment plant.
1H	Repeated 1G with seed from creek containing sediments polluted with petroleum wastes.
1I	Test with barbituric acid seeded with industrial activated sludge.

Six replicate treatability tests were performed with phenol prior to achieving complete acclimation. These experiments were performed over a period of 60 days. A comparison of these experiments is given in Table 6-12. Experiment 6 maintained the initiation and completion times reported in

Experiments 4 and 5. The differences observed are considered to be within reasonable limits for heterogeneous biological populations.

Table 6-12. COMPARISON OF PHENOL BATCH EXPERIMENTS 2 THROUGH 6

Initial Phenol Conc., mg/L	100		250		450	
	Start	Complete	Start	Complete	Start	Complete
Test	hours					
2	30	75	30	90	30	120
3	20	80	20	80	20	130
4	15	40	15	55	15	40
5	10	41	10	41	10	41
6	10	35	10	35	10	58

The results from the final phenol batch experiment are shown in Figures 6-2 through 6-5. Figure 6-2 gives the change in COD with time for each reactor at different initial concentrations. The reactor with an initial phenol concentration of about 450 mg/L had a total COD of 975 mg/L initially. This COD was reduced to 21 mg/L after 75 hours. A total reduction of 97.9 percent was achieved.

The reactor with an initial phenol concentration of about 250 mg/L had an initial COD of 526 mg/L. This COD was decreased to 10 mg/L within 38 hours for a 98 percent decrease. In the reactor with an initial phenol concentration of about 100 mg/L, the initial COD was determined to be 222 mg/L. After 35 hours this COD was decreased by 94.6 percent to 12 mg/L.

Figures 6-3, 6-4, and 6-5 show the change in COD and phenol concentration with time for the final phenol experiment. The reduction in COD for each concentration was associated with a drop in phenol concentration.

As mentioned above, MEK was air stripped under the conditions of these experiments. Figure 6-6 shows the results of the air stripping tests. A constant MEK concentration of about 250 mg/L was exposed to air flow rates of 133, 257, and 474 mL/min/L, under sterile conditions to prevent biological interference. The overall decreases in COD after 29 hours for the different air flow rates were 27, 58, and 85 percent, respectively.

To obtain data that would allow correcting for the air stripping of MEK, six reactors were required. For each treatability reactor used, a reactor was prepared that was identical, except it did not receive a biological seed and was operated under sterile conditions. The reactor operated under sterile conditions was used to determine the amount of MEK being removed as a result of air stripping. The flow rate of air to the diffusers in all reactors was maintained at 180 mL/min/L. The data generated by the treatability reactors gave the total amount of MEK removed as a result of biodegradation and air stripping and the data from the sterile reactors gave the amount removed as a result of air stripping. Therefore, by subtracting the amount removed by air stripping from the amount removed by both biodegradation and air stripping, the amount removed by biodegradation only was determined.

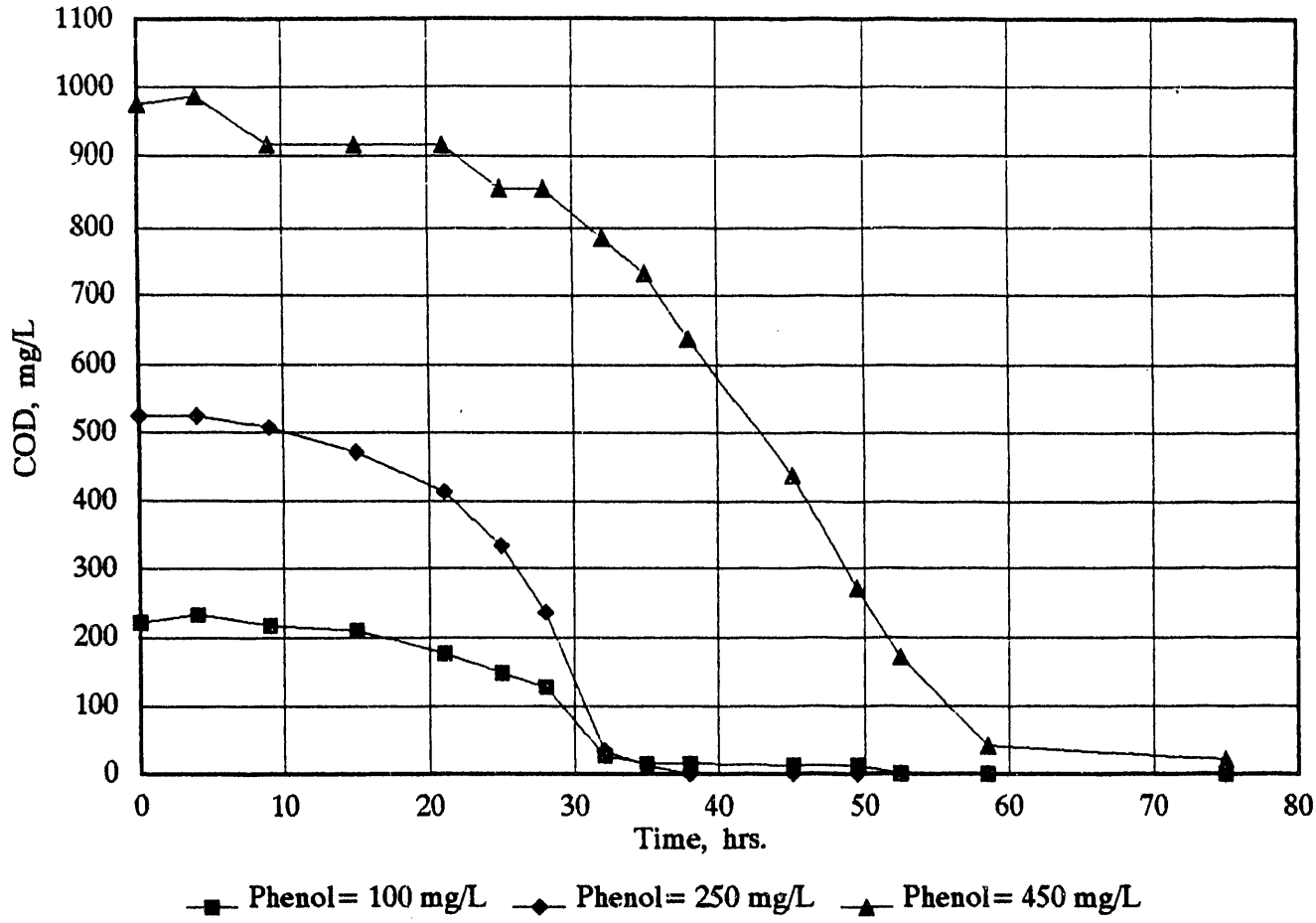

Figure 6-2. COD VERSUS TIME FOR PHENOL BATCH EXPERIMENTS
(Initial Phenol Concentrations of 100, 250, and 450 mg/L)

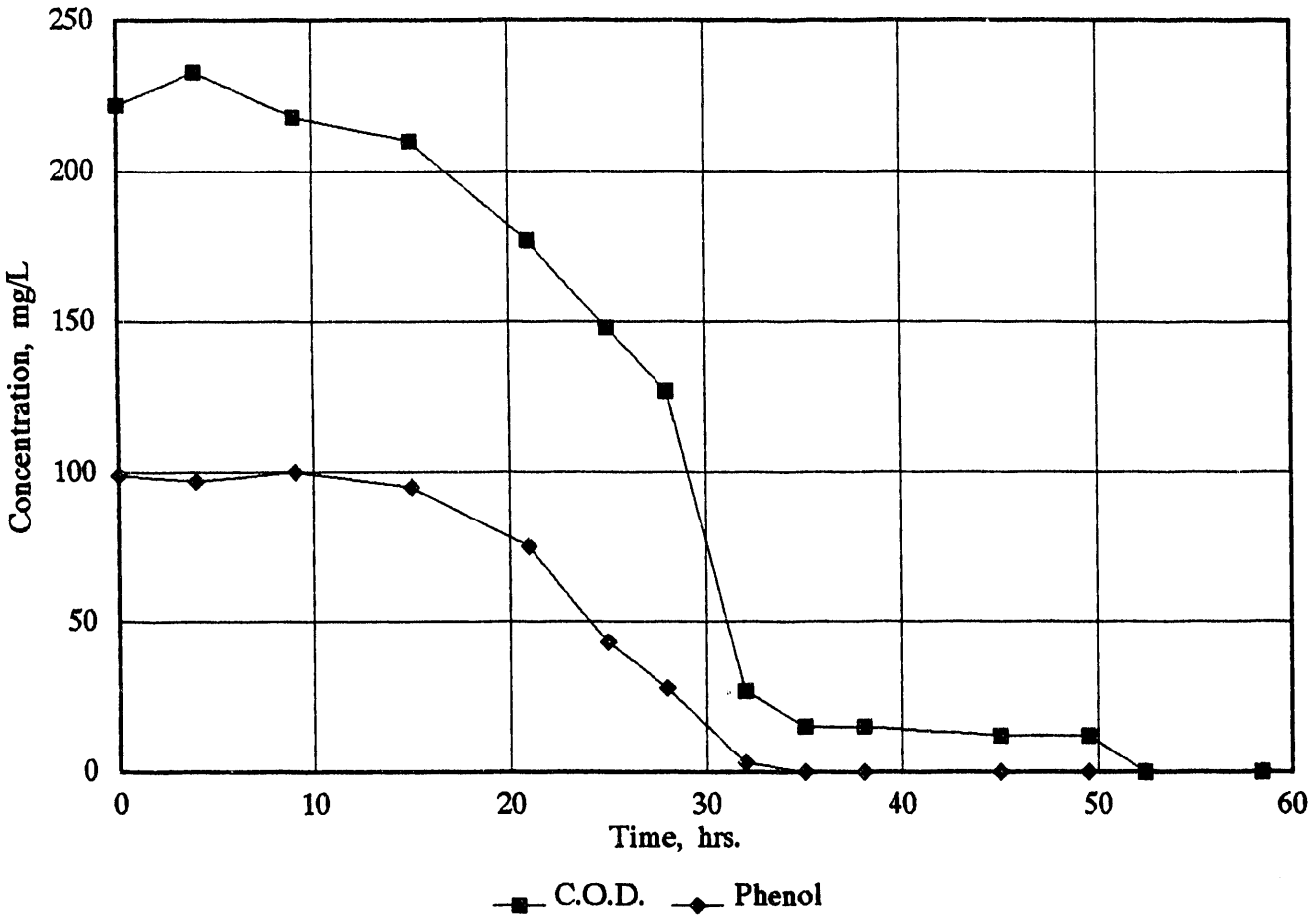

Figure 6-3. COD AND PHENOL VERSUS TIME FOR BATCH EXPERIMENT
(Initial Phenol Concentration of 100 mg/L)

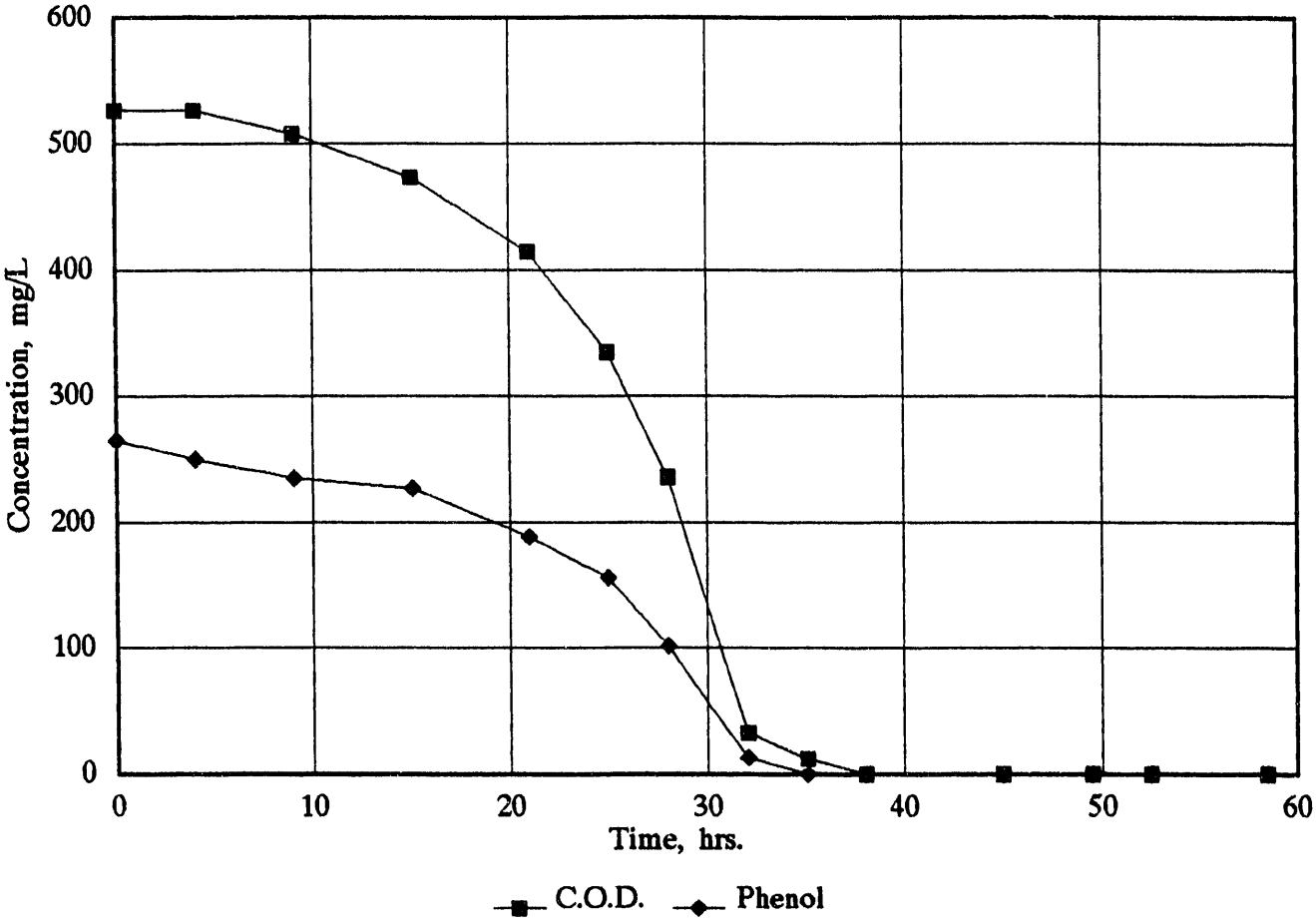

Figure 6-4. COD AND PHENOL VERSUS TIME FOR BATCH EXPERIMENT
(Initial Phenol Concentration of 250 mg/L)

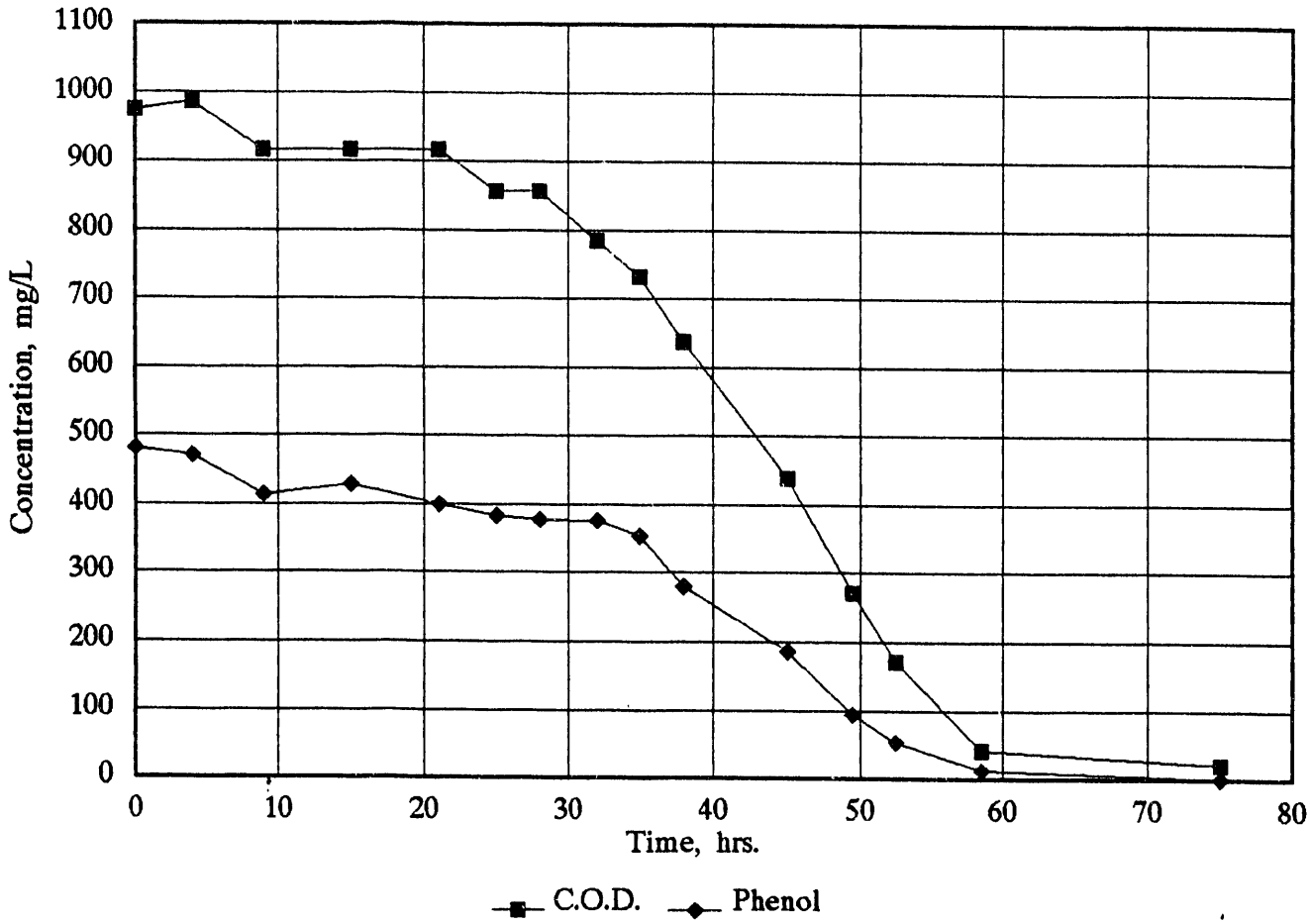

Figure 6-5. COD AND PHENOL VERSUS TIME FOR BATCH EXPERIMENT
(Initial Phenol Concentrations of 450 mg/L)

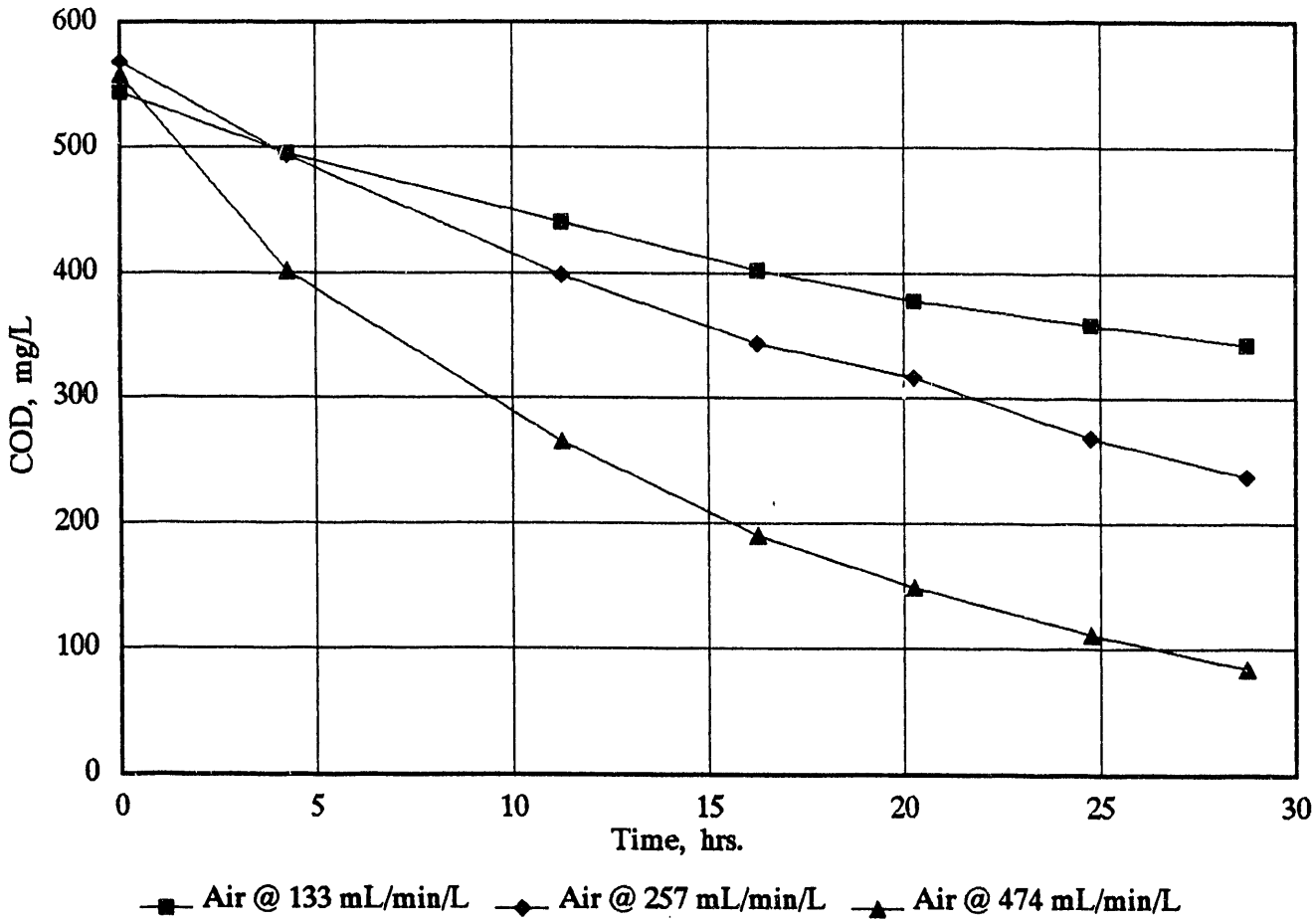

Figure 6-6. CHANGE IN COD WITH TIME DUE TO AIR STRIPPING OF MEK (Initial MEK Concentration of 250 mg/L)

The MEK treatability experiments were conducted and the data corrected for air stripping. The results are shown in Figures 6-7 through 6-10. Figure 6-7 shows the change in COD with time at the different concentrations of MEK, and Figures 6-8 through 6-10 compare the change in COD and MEK with time. The reactor with an initial MEK concentration of about 50 mg/L (COD of 95 mg/L) had a drop in COD to 5 mg/L in 41 hours and a drop in MEK from 43 mg/L to less than 1 mg/L.

The reactor with an MEK concentration of about 100 mg/L initially (Figure 6-9) had a concentration measured by GC of 115 mg/L of MEK and a COD of 180 mg/L. This reactor experienced a biological degradation of MEK to below 1 mg/L in 35 hours, and a reduction in COD to 5 mg/L in 46.5 hours.

Figure 6-10 indicates that the reactor with an MEK concentration initially of about 250 mg/L had a concentration measured by GC of 222 mg/L and a COD of 425 mg/L. The MEK was biodegraded to a concentration less than 1 mg/L and a COD of 7 mg/L in 41.5 hours.

The possibility that aniline was being removed from the reactors by air stripping was also investigated. Upon checking aniline for air stripping at the conditions used during the treatability experiments, it was determined that this effect was not significant (Figure 6-11). The aniline treatability data are presented in Figures 6-12 through 6-15. Figure 6-12 shows the change in COD with time at the different initial aniline concentrations, and Figures 6-13 through 6-15 give the comparative change in COD and aniline with time. In this experiment, unlike the others, the highest concentration of 600 mg/L was biodegraded to a minimum value at a faster rate than the intermediate concentration of 300 mg/L. This unexpected result occurred in both replicates of the experiment and may have been caused by incomplete acclimation of the seed microorganisms to aniline.

At the initial concentration of about 150 mg/L of aniline, the aniline concentration was determined by GC to be 165 mg/L and the COD 371 mg/L. Figure 6-13 shows that the aniline was metabolized by the microorganisms to a concentration less than 1 mg/L in 32 hours and the COD to 6 mg/L in 44 hours.

Figure 6-14 shows that the reactor with an initial aniline concentration of about 300 mg/L had a measured COD concentration of 739 mg/L initially. The concentration of aniline was reduced to less than 1 mg/L in 63 hours at which time the COD was 40 mg/L.

The reactor containing an aniline concentration of about 600 mg/L had an initial COD of 1505 mg/L (Figure 6-15). The aniline concentration was reduced to less than 1 mg/L in 44 hours. The COD after 44 hours was 54 mg/L, a 96.5 percent decrease from the initial COD concentration.

Once the experiments with the individual compounds were completed, TTU initiated three tests with combinations of the compounds. The combinations tested included 1) all four compounds, 2) phenol and aniline, and 3) phenol and MEK. During these tests, the COD was used as the analytical method to track the progress of biodegradation. The results are given in Figure 6-16. A correction was made for the stripping effect of MEK where applicable.

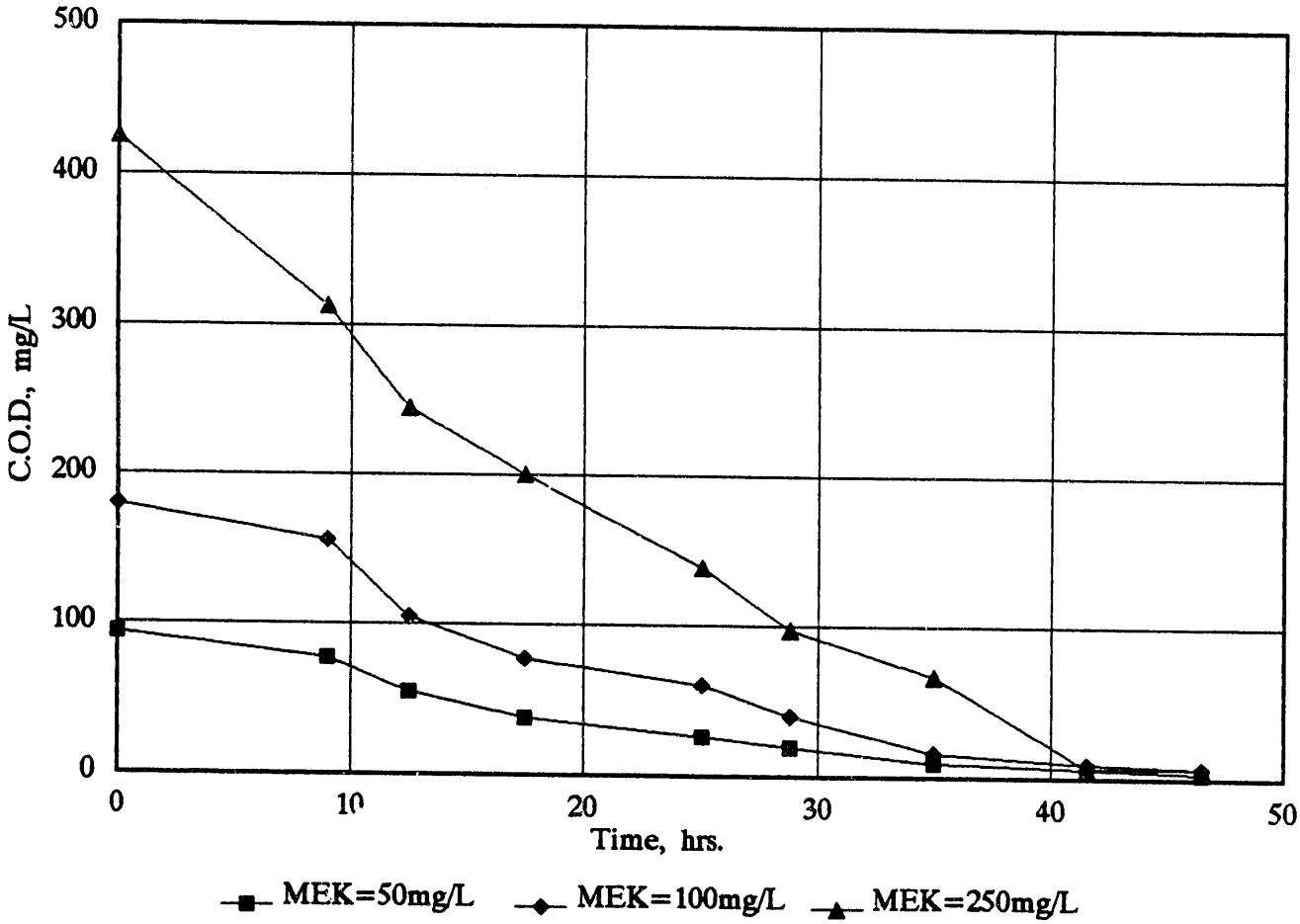

Figure 6-7. CHANGE IN COD WITH TIME FOR MEK BATCH EXPERIMENTS
(Initial MEK Concentrations of 50, 100, and 250 mg/L)

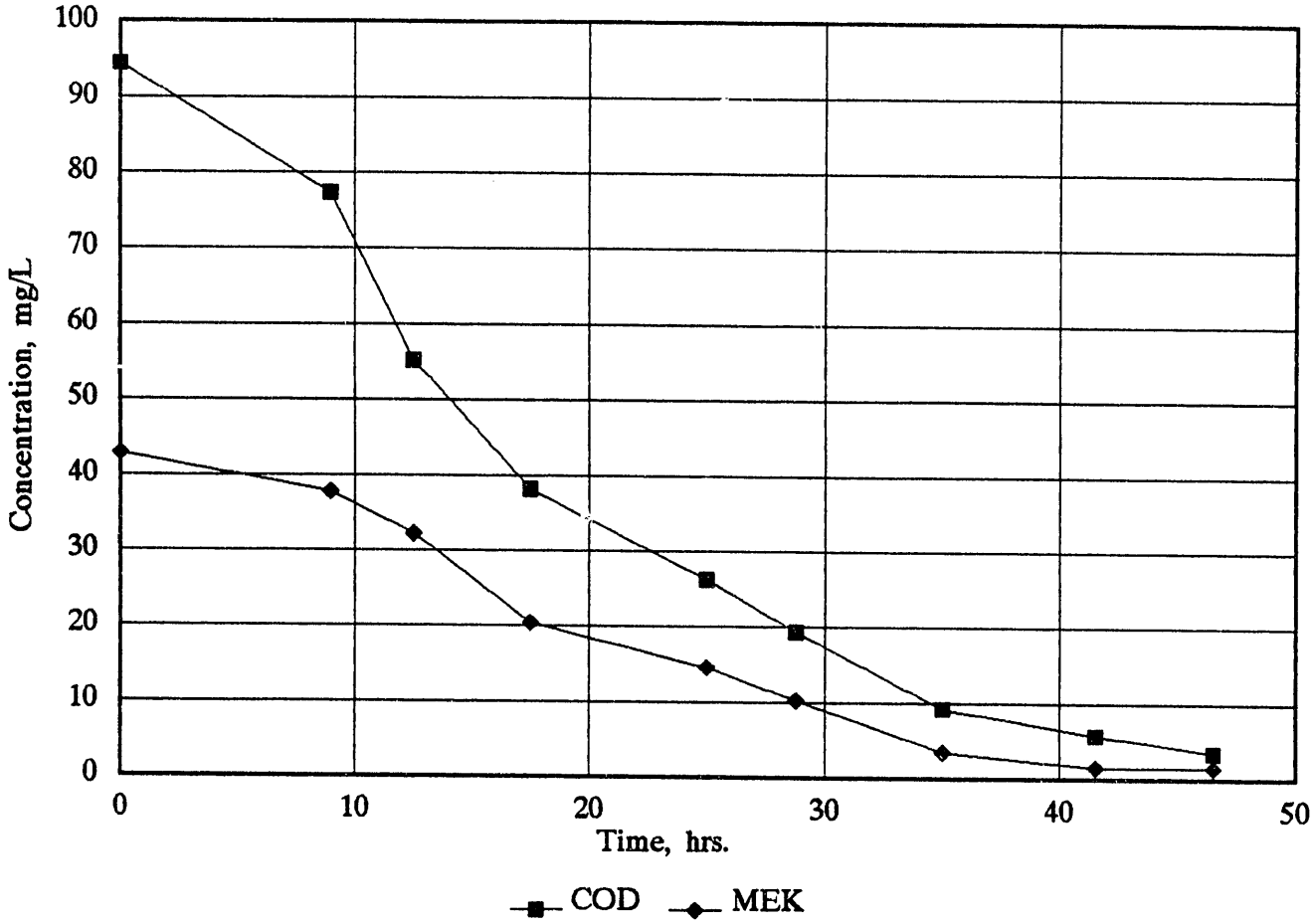

Figure 6-8. CHANGE IN COD AND MEK WITH TIME FOR BATCH EXPERIMENT
(Initial MEK Concentration of 50 mg/L)

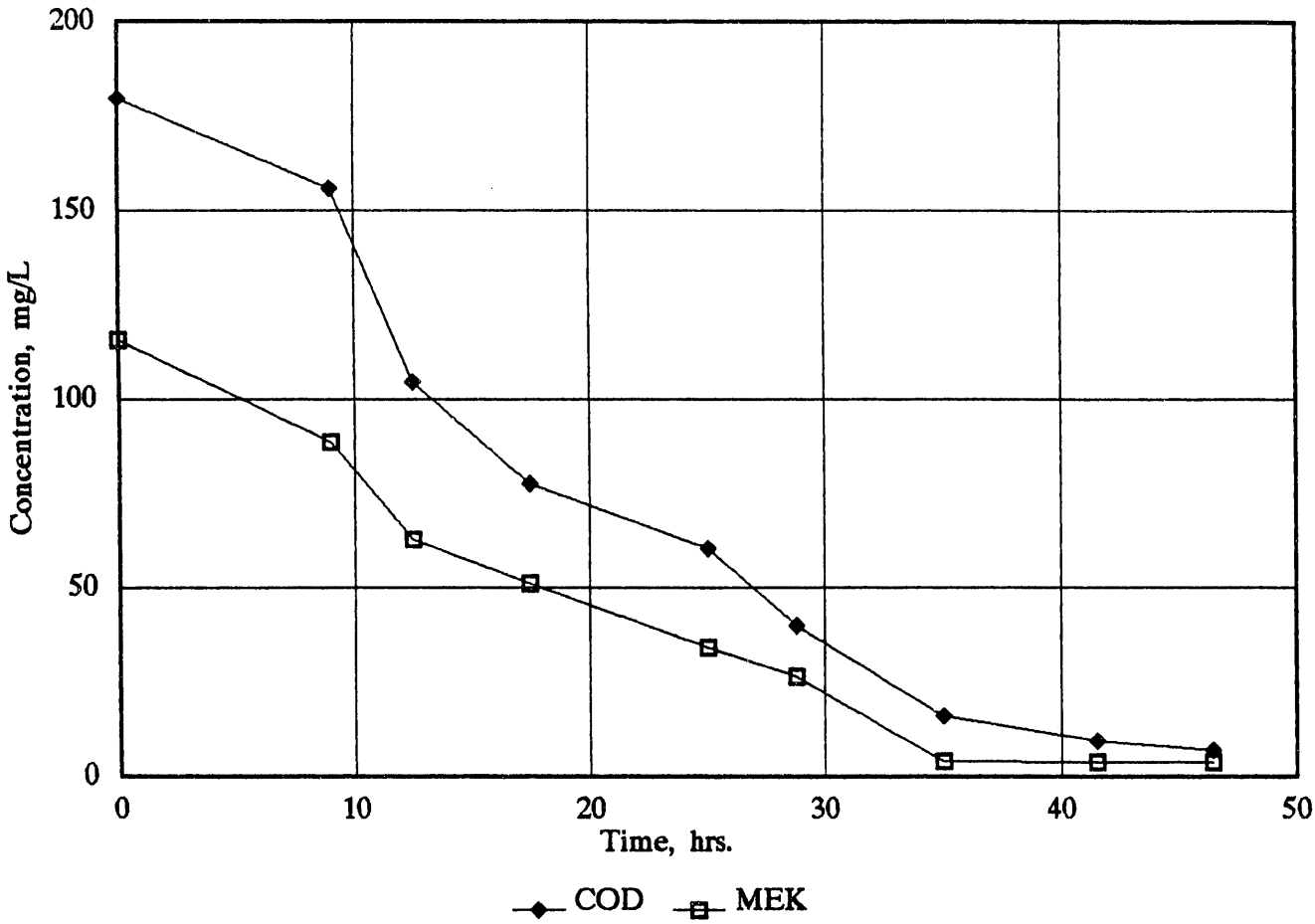

Figure 6-9. CHANGE IN COD AND MEK WITH TIME FOR BATCH EXPERIMENT (Initial MEK Concentration of 100 mg/L)

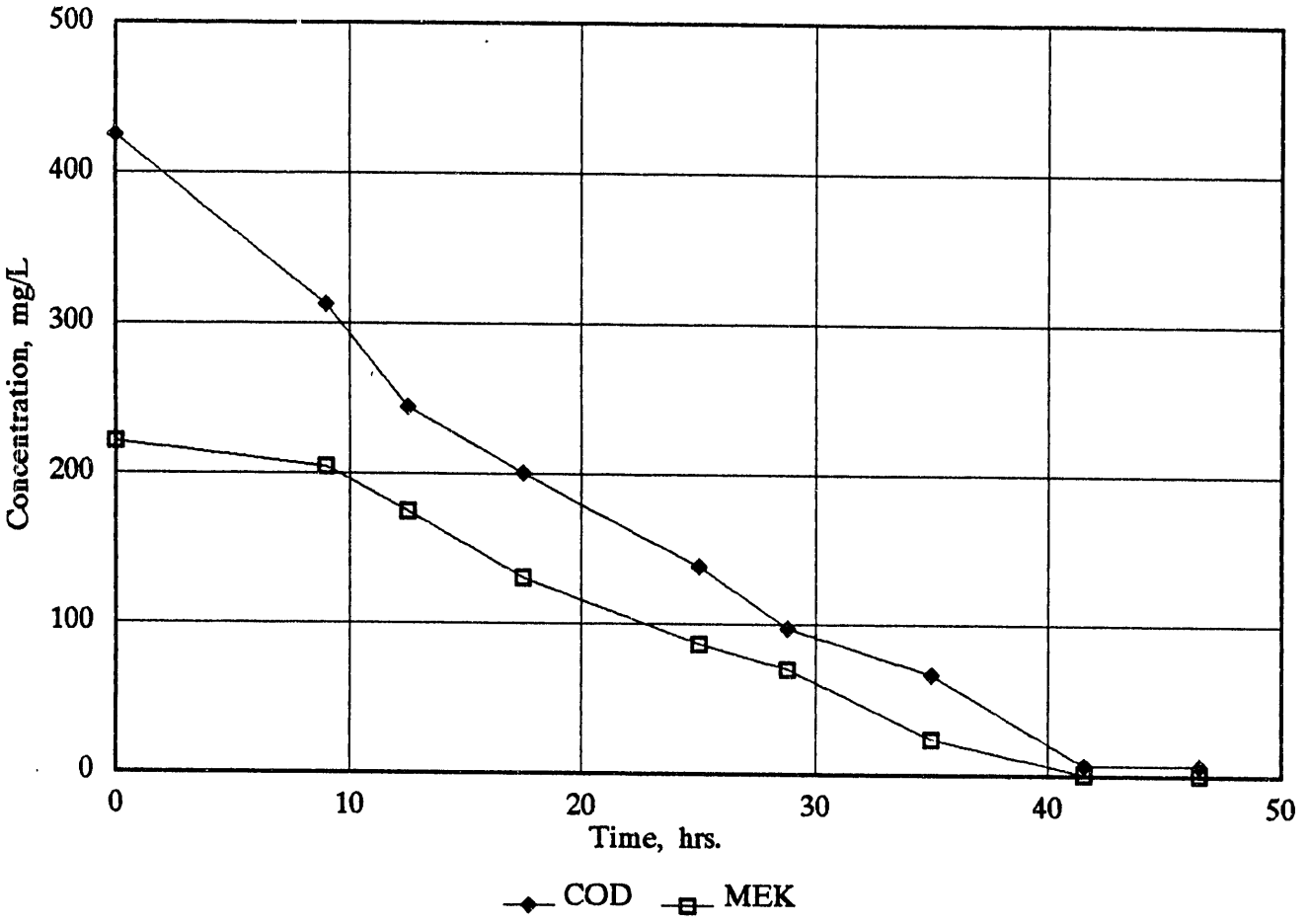

Figure 6-10. CHANGE IN COD AND MEK WITH TIME FOR BATCH EXPERIMENT (Initial MEK Concentration of 250 mg/L)

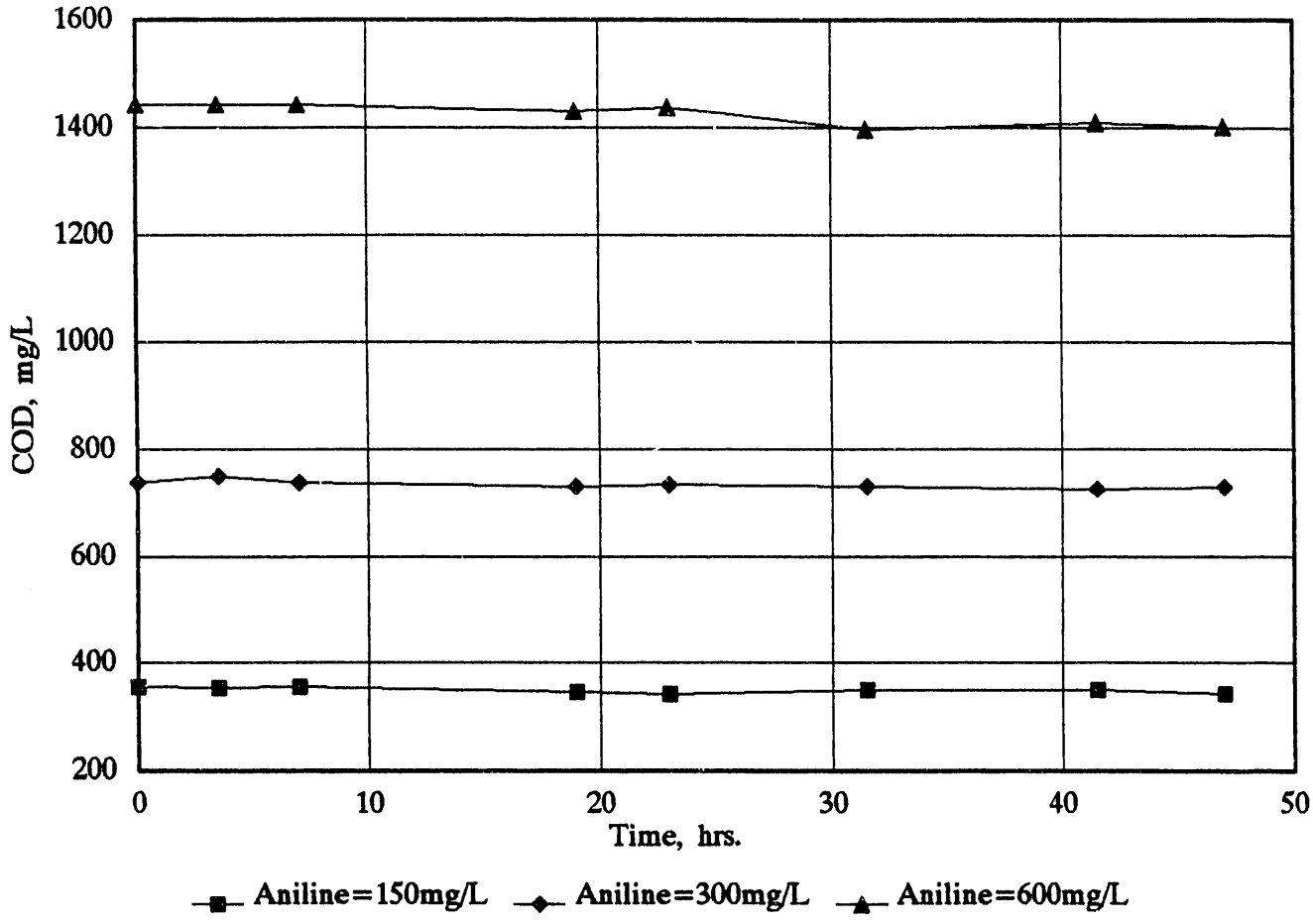

Figure 6-11. CHANGE IN COD WITH TIME FOR ANILINE AIR STRIPPING TESTS
(Initial Aniline Concentrations of 150, 300, and 600 mg/L)

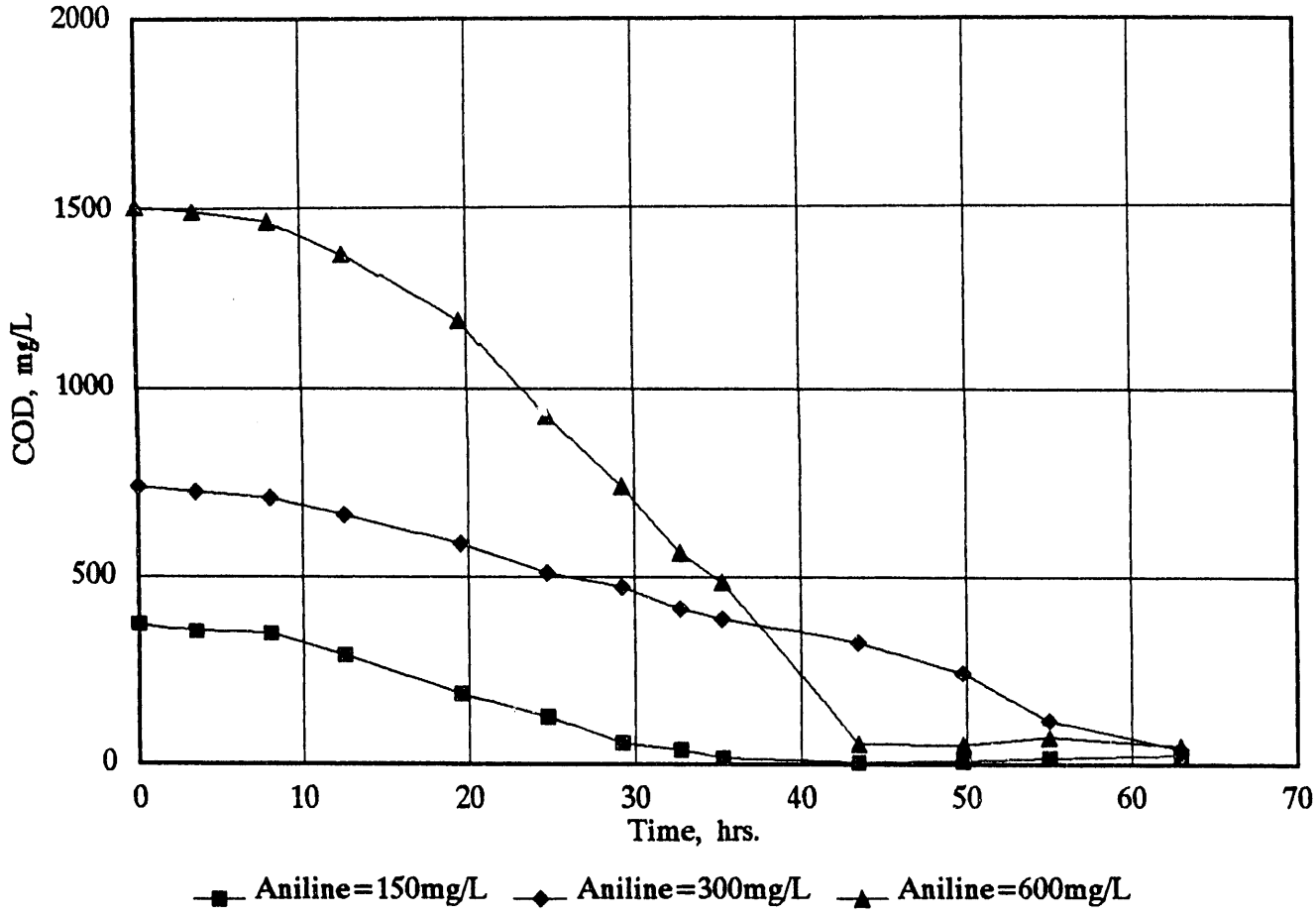

Figure 6-12. CHANGE IN COD WITH TIME FOR ANILINE BATCH EXPERIMENTS
(Initial Aniline Concentrations of 150, 300, and 600 mg/L)

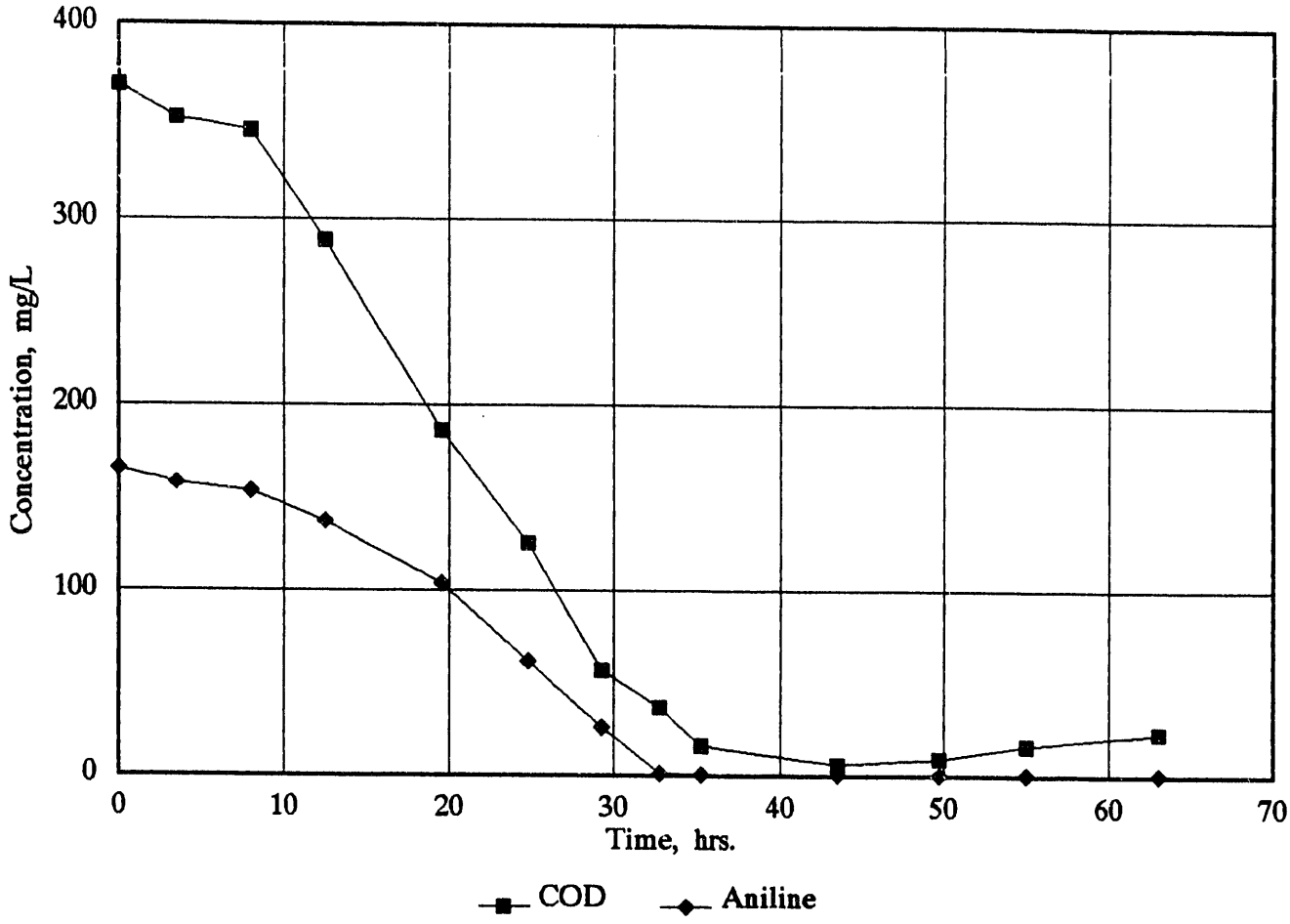

Figure 6-13. CHANGE IN COD AND ANILINE WITH TIME FOR BATCH EXPERIMENT (Initial Aniline Concentration of 150 mg/L)

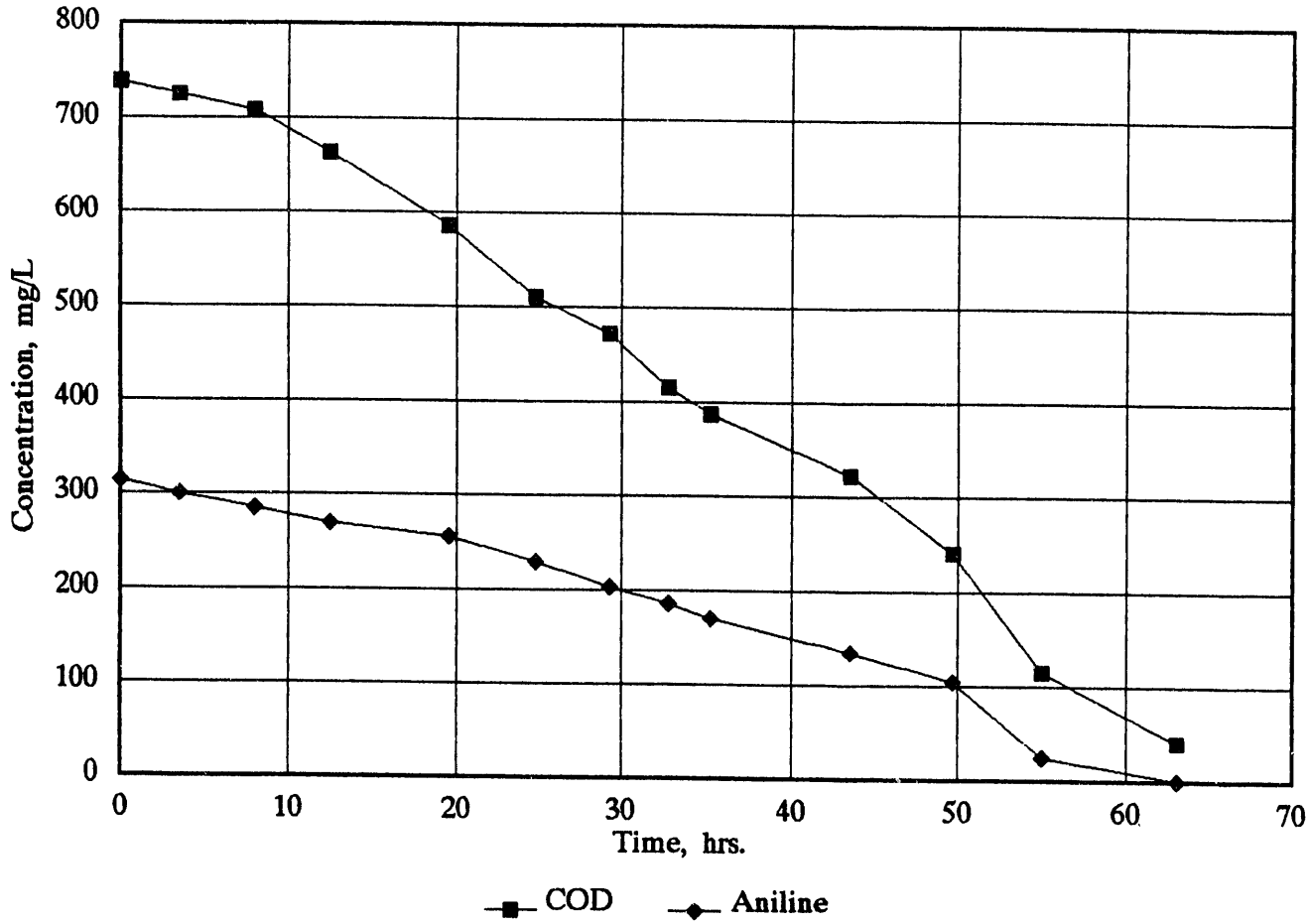

Figure 6-14. CHANGE IN COD AND ANILINE WITH TIME FOR BATCH EXPERIMENT (Initial Aniline Concentration of 300 mg/L)

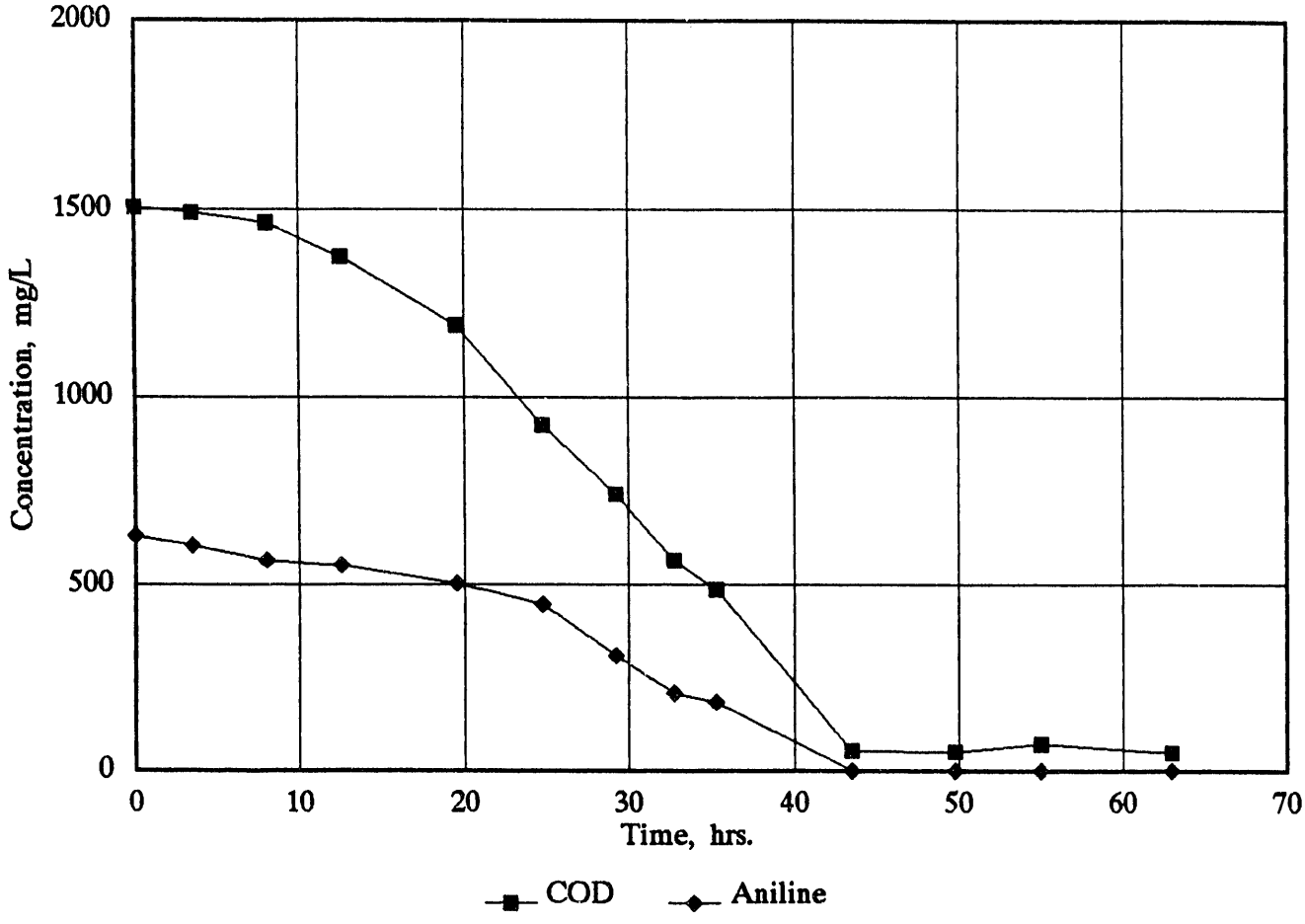

Figure 6-15. CHANGE IN COD AND ANILINE WITH TIME FOR BATCH EXPERIMENT (Initial Aniline Concentration of 600 mg/L)

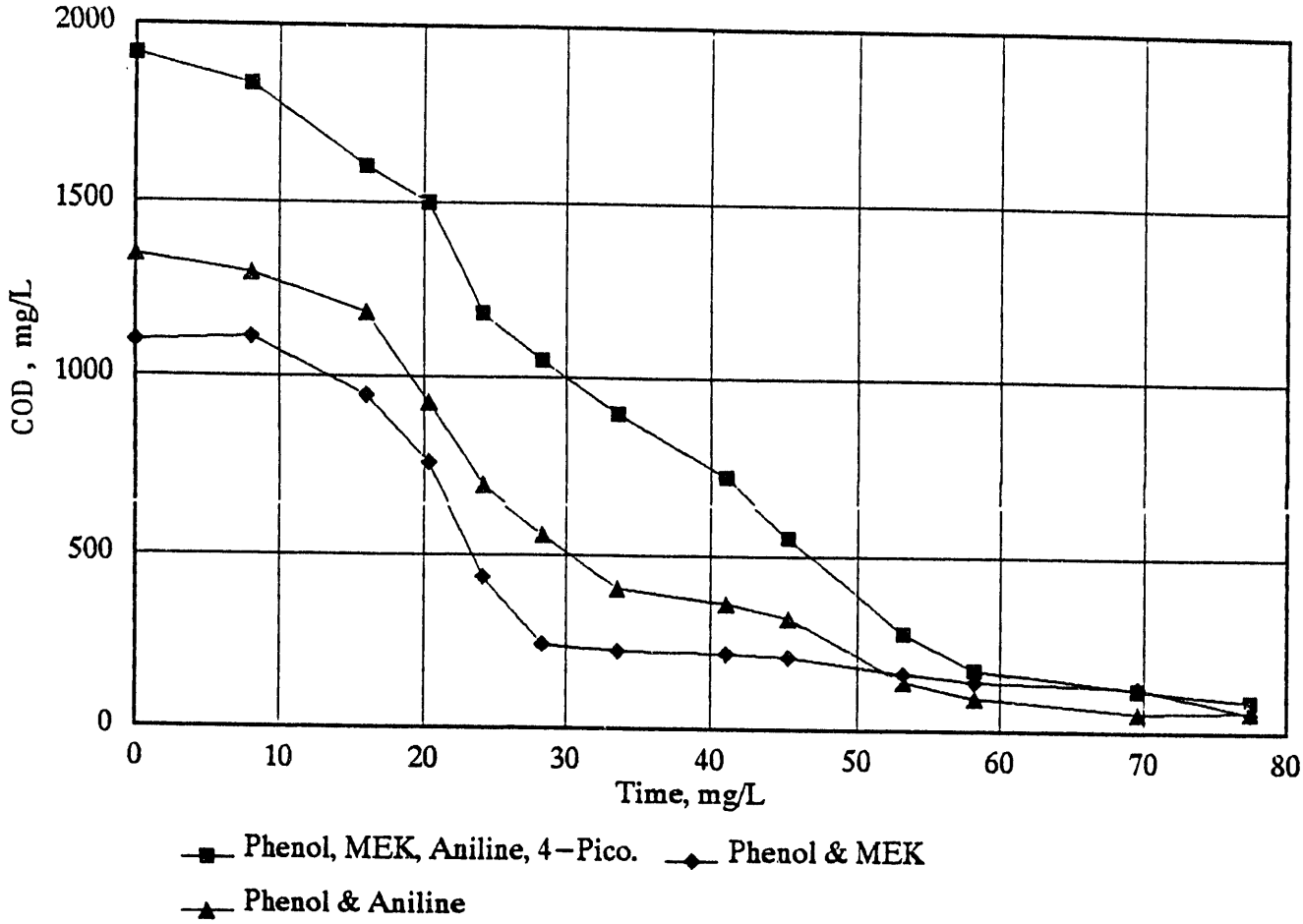

Figure 6-16. CHANGE IN COD VERSUS TIME FOR COMBINATION BATCH EXPERIMENTS (Initial Aniline Concentration of 300 mg/L; Others at 250 mg/L)

In the experiment with all four compounds present, the concentrations of phenol, MEK and 4-methyl pyridine were 250 mg/L; that of aniline was 300 mg/L. The total COD was reduced biologically from an initial value of 1902 to 94 mg/L (95%) after 77 hours. Even though the COD was significantly reduced, this does not mean that 4-methyl pyridine was biodegraded. Previously, TTU had determined that this compound is oxidized to about 18 percent of its theoretical value during the standard COD test. Therefore, the concentration of each individual compound in solution must be determined by GC to confirm its biological removal.

The experiment with phenol and aniline had phenol and aniline concentrations of 250 and 300 mg/L, respectively, which resulted in an initial COD of 1347 mg/L. The COD decreased from this initial value to 53 mg/L in 70 hours. The reactor with phenol and MEK had initial concentrations of each compound of 250 mg/L, which resulted in a COD of 1101 mg/L. The COD was reduced to 40 mg/L after 77 hours.

Conclusions

Based of the results of the experiments described above, the following conclusions can be drawn.

1. Phenol, aniline, and MEK were found to be biodegradable in a batch reactor by microorganisms that had been previously acclimated to the compounds.

2. Microorganisms did not acclimate to 4-methyl pyridine under the experimental conditions of this research.

3. Phenol was readily biodegraded but complete acclimation took prolonged exposure of the microorganisms to the compound.

4. At a concentration of 250 mg/L, MEK will be air stripped to some degree in a batch reactor with air flow rates from 133 to 474 mL/min/L.

5. Aniline at a concentration up to 600 mg/L was not air stripped in a batch reactor with an air flow rate of about 180 mL/min/L.

6. A synthetic waste consisting of a combination of phenol, aniline, MEK, and 4-methyl pyridine is biodegradable in a batch reactor by microorganisms acclimated to the combination of the compounds as indicated by a reduction in the COD.

Pre- and Posttreatment Alternatives

The liquid waste produced during shale hydroretorting contains numerous organic and inorganic components that range in concentration from a trace to several thousand milligrams per liter. In theory, the concentration of each component could, if so desired, be significantly reduced.

The objective of liquid waste treatment is to produce water that has qualities acceptable for reuse or to meet criteria for discharge. Although a single technology would be desirable, the complexity of the chemical composition dictates that more than one operation or process may be needed. The major technology being investigated in this task is that of biological treatment. The objective of this effort on pre- and posttreatment alternatives is to search the literature for alternatives that may be used in conjunction with biological treatment, if needed, to produce an acceptable effluent.

Pretreatment Alternatives. Pretreatment is considered when such treatment either 1) produces a water that is more amenable to biological treatment, or 2) permits the removal of a component(s) under more desirable conditions than exist during or after the primary treatment. In this case, biological treatment is considered to be the primary treatment. Some of the more promising pretreatment techniques are briefly described below.

Steam or air stripping for the removal of H_2S and NH_3 eliminates two major contaminants that could cause problems if not removed prior to biological treatment.[22,23,24] Ammonia in concentrations greater than 500 mg/L are reported to be toxic to microorganisms. Steam stripping has been shown to consistently reduce the concentration of NH_3 to less than 100 mg/L except where high concentrations of strong fixing agents exist. Stripping is accomplished more rapidly at elevated pH and temperature. The addition of a base to adjust the pH to near 10 may also precipitate some metals as hydroxides or salts.

As the pH decreases with NH_3 stripping, H_2S may also be stripped. Alkalinity, pH, temperature, and time are the principal parameters that determine the extent to which NH_3 and H_2S are removed.[25] Removals greater than 99 percent have been reported.

A reduction in the total organic carbon (TOC) may also be observed during stripping. Wastes containing a significant proportion of compounds having low molecular weights and high volatilities have shown greater than 50 percent reduction in TOC as a result of steam stripping.[25] Once separated from the NH_3 and H_2S, the water containing the low molecular weight compounds must be treated, disposed of, or perhaps used for its energy content.

Suspended solids removal by some combination of filtration, flocculation, or sedimentation is frequently included in pretreatment. The addition of alkalinity, nutrients such as phosphorus, and pH adjustment may also be needed.

Posttreatment. The chemical and physical characteristics of the effluent from the biological treatment unit as well as the intended use of the water will dictate the posttreatment methods to be used. At a minimum, it is assumed that biological treatment is followed by sedimentation. Most uses will require filtration for suspended solids removal followed by chemical treatment for bacterial control as minimum treatments. Additional treatment may be required for the removal of refractory organics, dissolved solids, and water stabilization.[26] Some of the available technologies are briefly described below.

Granular activated carbon has been demonstrated to be an effective post or polishing treatment. Although many carbons are available, selection may depend upon adsorption characteristics as well as ease of regeneration. Some compounds are irreversibly adsorbed and contribute to a reduction in the adsorption capacity or fouling of the carbon.[27] Activated carbon also aids in dechlorination.[28]

The concentration of both organics and inorganics may be reduced by reverse osmosis. The rejection of inorganics by this process is well documented. Recently, membranes have been developed that effectively reject some organics at relatively low pressures.[29] Researchers at the University of Kentucky have obtained rejection rates as high as 85 percent with pressures as low as 1.4 MPa[26] (200 psig). Pretreatment with ozone increases the rejection of some compounds. Rejection was shown to increase with increases in ozonation time and pH.

Ionic components may also be removed by electrodialysis. A high-purity product with respect to ionic components is reported to be produced. Few operational problems are expected when the pH is reduced to prevent scale formation.[26]

Inorganic dissolved solids may be removed by ion exchange. This treatment method is usually used to soften hard water and remove other undesirable ions. Some metals and organics have been found to be irreversibly exchanged and, thus, foul the exchanger and reduce adsorption capacity.[30]

Natural processes found in wetlands have proven to be quite effective for the removal of a variety of undesirable inorganic and organic agents.[31] Although these processes represent relatively new technologies, they have been successfully used to remove metals from mine drainage water. Wetlands followed by lagoons with retention times of up to one year also offer the possibility of degrading low concentrations of refractory organic compounds.[26]

Some metals may be removed by activated carbon, activated alumina, and a host of waste products such as hair, sawdust and peanut hulls. For the removal of cadmium and chromium, fly ash has been shown to be an economical alternative to other more expensive agents.[32] It is speculated that the mechanism of removal is chemisorption. Removal has been shown to be pH dependent.

A number of proven and emerging technologies directed toward the cleanup of Superfund sites may also have possible applications as polishing techniques in waste treatment.[31]

Liquid wastes treated for reuse or recycle may be unstable and/or corrosive. Use of appropriate technologies will most likely be necessary to prevent scale formation or corrosion in systems in contact with the treated water.[33]

Subtask 6.4. PFH Systems Analyses

The objective of this subtask was to define the effluent streams, quantities, and compositions for a PFH plant and conduct a thermoeconomic evaluation of the PFH plant. This subtask was comprised of three subtasks: 6.4.1. PFH Process Analyses, 6.4.3. Plant Energy Optimization, and 6.4.4. Economics

Subtask 6.4.1. PFH Process Analyses

The objective of this subtask was to analyze the data obtained in Subtask 5.2 and to refine correlations previously developed for raw shale to describe the performance of beneficiated shale in the PFH process. The refined correlations were incorporated into an existing computer program that simulates the PFH process. The program was used to estimate the compositions and quantities of effluent streams for a commercial-scale PFH plant.

In Subtasks 3.8 and 5.2.1, PFH tests were conducted with beneficiated Alabama shale in a laboratory-scale batch fluidized-bed reactor. Data were generated that relate hydroretorting conditions to the conversion of organic carbon to oil, gas, and residue. The relationships between PFH test conditions and carbon conversions for beneficiated Alabama shale were similar to those observed previously for raw Alabama shale. Carbon conversions depend on temperature, hydrogen pressure, and residence time over the ranges tested of 482° to 593°C (900° to 1100°F), 0 to 7.0 MPa H_2, and 0 to 30 minutes, respectively. Gas yield increases with increasing temperature but is independent of changes in hydrogen pressure. Oil yield increases with increasing hydrogen pressure but decreases with increasing temperature.

The mechanism used to describe carbon conversion includes the simultaneous conversion of carbon to gas, oil, and an active carbon species that can form oil or remain as residue carbon. The correlation constants for six raw Eastern shales were developed in previous work.[1] The correlation constants that apply to the carbon conversion of beneficiated Alabama shale were derived using batch PFH data from Subtasks 3.8 and 5.2.1. Yields are predicted over the ranges of temperature, hydrogen pressure, and residence time that were used in PFH processing.

The products of oil shale retorting include oil, hydrocarbon gases (C_1 to C_5), carbon oxides, H_2S, water, NH_3, water soluble and insoluble gases in low concentrations, and residue shale. The conversion of organic carbon in the kerogen can be simplified to include only oil, hydrocarbon gases, and residue carbon as products. A mechanism describing organic carbon conversion must, however, accurately predict conversions based on the process operating conditions.

Mechanisms for carbon conversion usually describe parallel reactions to produce oil, gas, and char. Sequential reactions account for oil loss by coking and oil cracking. Eastern oil shales have low hydrogen to carbon ratios and retorting these shales in the presence of hydrogen increases the oil yield above thermal retorting yields as a direct function of the hydrogen pressure.

A global mechanism developed previously to describe the carbon conversion achieved during PFH hydroretorting of raw Eastern shales has been shown to also apply to beneficiated Alabama shale. Two oil production pathways are included. Oil can form directly from the kerogen as is the case in several Western shale mechanisms, but significantly more oil can form depending upon the hydrogen pressure.

Experimental

A bulk sample of beneficiated Alabama shale was prepared for laboratory and bennch-scale tests as described in Task 7. The chemical analysis and Fischer Assay (FA) oil yield of a representative sample are presented in Table 6-13. A description of the laboratory-scale PFH unit and its operating procedure were presented in Task 5. In a typical test, a 175- to 200-gram sample of sized shale is charged to a fluidized bed of sand maintained at the desired temperature and hydrogen pressure fcr a selected residence time. The chemical analyses of the product liquids, gases, and residue shale samples are used to determine material balances and oil yields.

Table 6-13. FEED SHALE ELEMENTAL ANALYSIS AND FISCHER ASSAY OIL YIELDS

Shale Member	Alabama Chattanooga
Moisture, wt %	1.87
Ultimate, wt % Dry	
Ash	54.80
Organic Carbon	32.15
Mineral Carbon	0.00
Hydrogen	3.11
Sulfur	9.15
Nitrogen	0.85
Fischer Assay, GPT (L/t)	22.5 (94)

Results and Discussion

The weight loss of shale at PFH conditions is well described as the sum of two simultaneous, first-order reaction paths. The weight losses by the "fast" and "slow" reaction paths are approximately proportional to the carbon conversion to oil and gas, respectively.

$$W = W_{fo} \exp(-k_f t) + W_s \exp(-k_s t) \qquad (6\text{-}1)$$

where

$$k_f = A_f \exp(-E_f/RT) \qquad (6\text{-}2)$$

and

$$k_s = A_s \exp(-E_s/RT) \qquad (6\text{-}3)$$

A determination of the values for the pre-exponential factors and activation energies describing the rates of beneficiated Alabama shale carbon conversion to oil and gas was not in the work scope of this task.

Batch PFH tests were conducted with Alabama shale sized to -20+50 mesh to eliminate mass transfer effects on conversions. Residence times of 20 minutes were used to ensure that all reactions were complete. Organic carbon conversions to oil and gas were obtained in a number of batch tests. These have been used to develop correlations describing organic carbon conversions in relation to temperature and hydrogen pressure.

Relationships exist between the product yields obtained by hydroretorting and both the hydrogen pressure and the temperature. Over the hydrogen pressure range studied (1.4 to 7.0 MPa), there is no effect of pressure on gas formation. Oil yield, however, increases with increasing hydrogen pressure. This result suggests that oil and gas come from different types of carbon in the shale. When temperature is increased in the range of 900° to 1100°F (477° to 593°C), gas yield increases. Conversely, the oil yield obtained from beneficiated Alabama shale decreases with increasing temperature in the range of 900° to 1100°F.

A mechanism is proposed to describe the conversion of beneficiated Alabama shale to products. This mechanism is composed of a set of carbon conversion correlations that describe product yields. The PFH products that containing carbon include hydrocarbon gas (C_{Gas}), oil from two paths (C_{Oil1} and C_{Oil2}), and residue from two paths (C_{Res1} and C_{Res2}). Two intermediate active carbon species (C^* and C^{**}), which can form oil and residue are also included. Constants have been determined empirically.

Several conclusions from the batch PFH tests have been used to develop the proposed carbon conversion mechanism shown in Figure 6-17. Shale organic carbon can form product gas, the first oil product (C_{Oil1}), or an active carbon species (C^*). Product gas appears to be unaffected by oil yield. Oil and gas are proposed to form from different fractions of the shale carbon with the fraction forming gas increasing with temperature. The first oil product, C_{Oil1}, is equivalent to the oil formed with no hydrogen present and has been set equal to the Fischer Assay oil yield.

When no hydrogen is present the active carbon species C^* remains with the shale as residue carbon (C_{Res1}). The presence of hydrogen, however, enables a portion of the C^* carbon to form a second active carbon species C^{**} that can form additional oil. The increase in the oil precursor species C^{**} with increasing hydrogen pressure is reasonable since Eastern shales are hydrogen deficient and need added hydrogen to produce higher oil yields.

The oil precursor C^{**} can form either the second oil product, C_{Oil2}, or additional residue carbon, C_{Res2}. The paths leading to C_{Oil2} and C_{Res2} are parallel and temperature dependent.

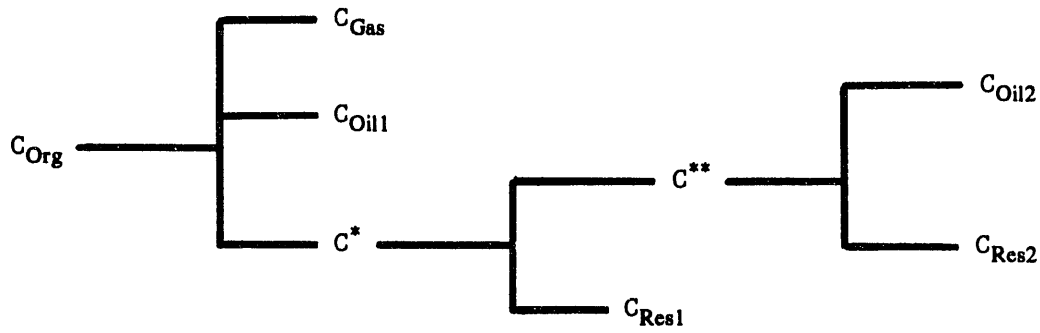

Figure 6-17. PROPOSED MECHANISM FOR PFH ORGANIC CARBON CONVERSION

The set of equations that describe organic carbon conversion by the proposed mechanism is listed below. The rate expressions for gas production, C_{Gas}, and oil production, C^{**}, are described by the proposed slow and fast reaction paths. Batch PFH residence time tests have shown the production of oil is faster than hydrocarbon gas production.

$$-\frac{dC_{Gas}}{dt} = k_{Gas} \cdot C_{Gas} \tag{6-4}$$

$$-\frac{dC^{**}}{dt} = k_{Oil} \cdot C^{**} \tag{6-5}$$

Integrating these equations and performing material balances provides all of the needed carbon conversion correlations for the proposed hydroretorting mechanism.

$$C_{Gas} = C^{o}_{Gas} \cdot (1 - \exp(-k_{Gas}t)) \tag{6-6}$$

$$C^{o} = 1 - C_{Gas} - C_{Oil1} \tag{6-7}$$

$$C^{**} = k_p\, C^{o} \cdot (1 - \exp(-k_{Oil}t)) \tag{6-8}$$

$$C_{Oil} = C_{Oil1} + C_{Oil2} = C^{o}_{Oil1} + C^{o}_{Oil2} \cdot C^{**} \tag{6-9}$$

$$C_{Res} = C_{Res1} + C_{Res2} = C^{o} - C_{Oil2} \tag{6-10}$$

Parameters used in the carbon conversion correlations are defined as follows with temperature in degrees K, hydrogen pressure in MPa, and time in seconds.

$$k_{Gas} = A_{G1} \exp(-E_{G1}/RT) \tag{6-11}$$

$$C^{o}_{Gas} = A_{G2} \exp(-E_{G2}/RT) \tag{6-12}$$

$$k_{p} = 1 - \exp(-a \cdot P_{H_2}{}^{b}) \tag{6-13}$$

$$k_{oil} = A_{01} \exp(-E_{01}/RT) \tag{6-14}$$

$$C^{o}_{oil2} = k_{oil2}/(1 + k_{oil2}) \tag{6-15}$$

$$k_{oil2} = A_{02} \exp(-E_{02}/RT) \tag{6-16}$$

Constants for the carbon conversion correlation for beneficiated Alabama shale are listed in Table 6-14 along with those developed previously for raw Alabama shale. Determination of A_{G1}, E_{G1}, A_{O1}, and E_{O1} were not in the scope of work for this task. Values of the reported correlation constants, including k_p, are based on the results of batch PFH tests.

Carbon conversions for the beneficiated Alabama shale have been calculated over the temperature range from 482° to 593°C (900° to 1100°F) and hydrogen pressures in the range of 0 to 7 MPa for which the correlations are defined. Comparisons of the experimental and calculated organic carbon conversions to oil and gas are presented in Figures 6-18 and 6-19, respectively. Carbon conversions are shown as functions of both temperature and hydrogen pressure.

The fit of the calculated carbon conversions to oil to the best non-linear regression line through the experimental data is within 2 percent of the feed carbon. For the gas, all calculated conversions are within 1 percent of the feed carbon compared to the best fit of the experimental conversions. Scatter among the actual data produces somewhat greater standard deviations between the calculated carbon conversions and the experimental points.

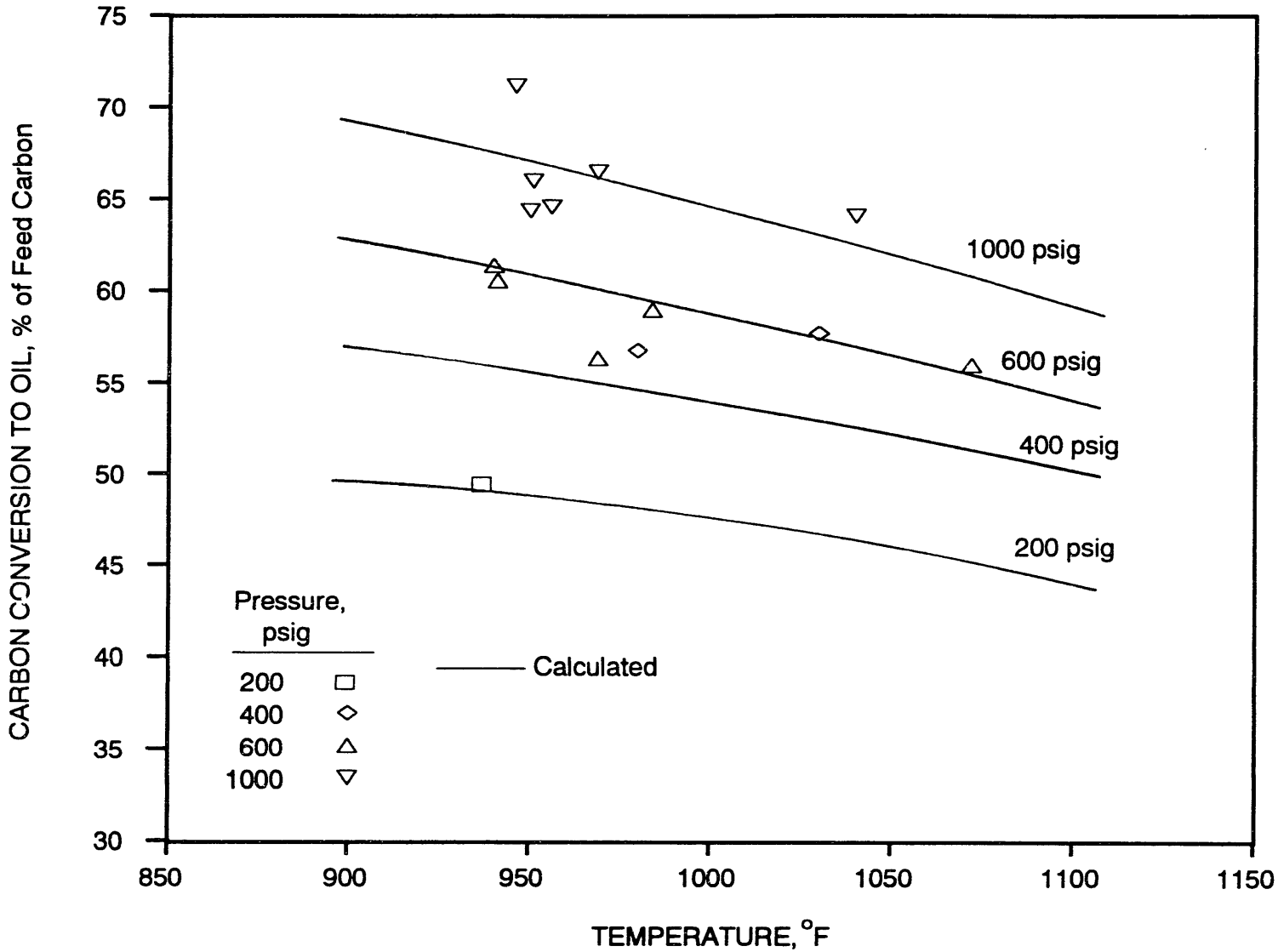

Figure 6-18. COMPARISON OF EXPERIMENTAL AND CALCULATED ALABAMA SHALE CARBON CONVERSIONS TO OIL

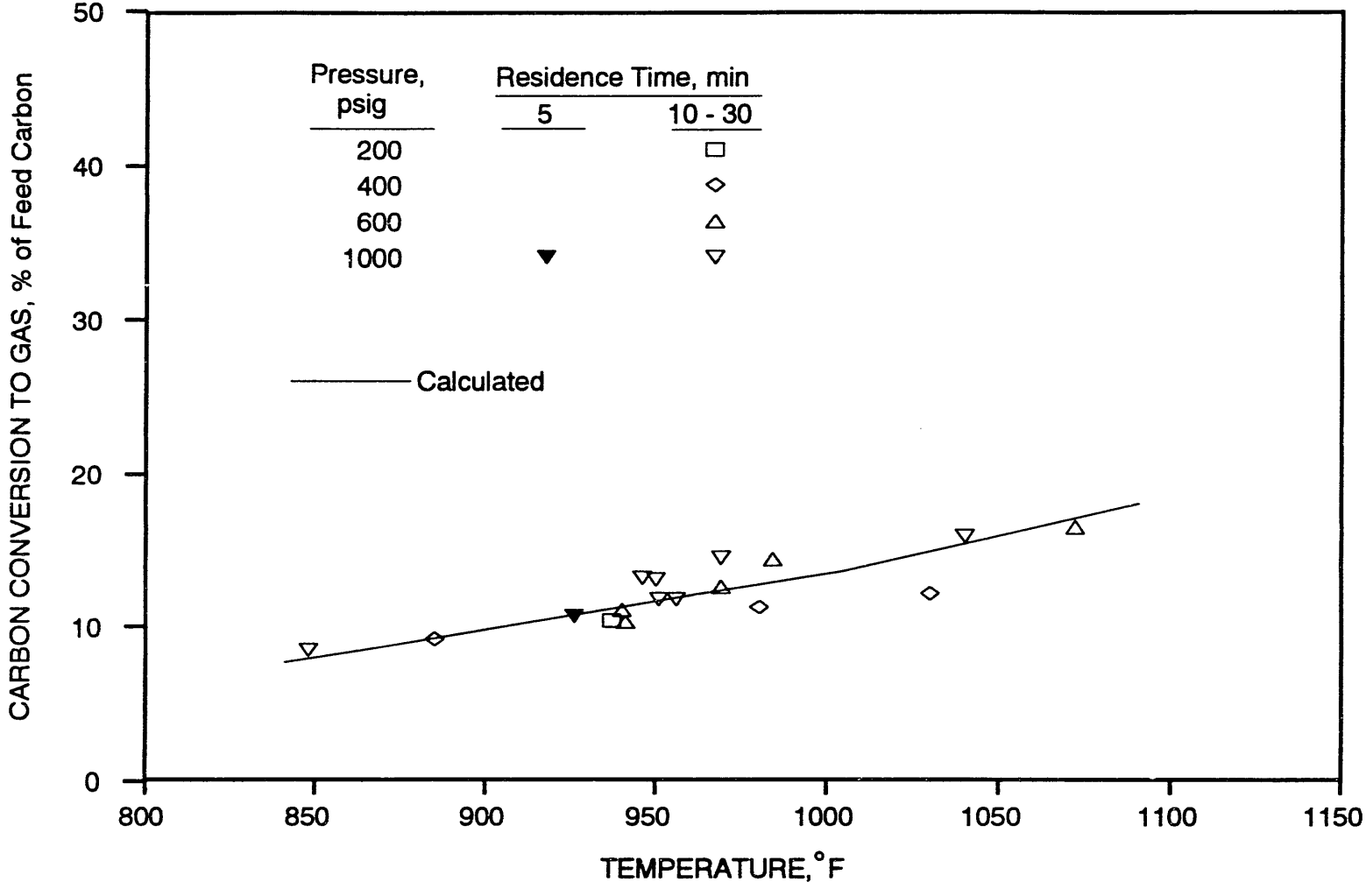

Figure 6-19. COMPARISON OF EXPERIMENTAL AND CALCULATED ALABAMA SHALE CARBON CONVERSIONS TO GAS

Table 6-14. ORGANIC CARBON CORRELATION CONSTANTS

Shale Member	Alabama Chattanooga	
Beneficiated	No	Yes
A_{G2}	12.25	10.73
E_{G2}, cal/g-mole	694	7035
A_{G1}, s^{-1}	ND	ND
E_{G1}, cal/g-mole	ND	ND
$C°_{Oil}$	0.285	0.27
a, P_{H2}^{-1}	0.287	0.37
b	0.73	0.61
A_{02}	3.5×10^{-4}	3.5×10^{-4}
E_{02}, cal/g-mole	-16,450	-16,450
A_{01}, s^{-1}	ND	ND
E_{01}, cal/g mole	ND	ND

ND = Not Determined

Summary

The weight loss and organic carbon conversion achieved by PFH processing of shale have been described by two reaction paths. The fast carbon conversion path produces oil and is complete in 5 to 10 minutes at hydroretorting temperatures of 900° to 1100°F (482° to 593°C). The slow reaction path produces hydrocarbon gases and requires more than 20 minutes to complete at PFH conditions.

Carbon conversion products consist of gas, oil, and residue. The product gas yield increases with increasing temperature and is unaffected by changes in hydrogen pressure. Product oil is the sum of the oil generated with no hydrogen present and the oil generated in a hydrogen atmosphere. The oil generated without hydrogen is equivalent to the Fischer Assay oil yield. With hydrogen present, the fraction of active carbon capable of forming oil increases with increasing hydrogen pressure. This active carbon species can either form oil or remain as residue carbon.

The proposed mechanism describing the PFH organic carbon conversions for beneficiated Alabama shale is based on laboratory-scale data. The predictions of yields in relation to temperature, hydrogen pressure, and residence time can be used to guide the selection of operating conditions for larger bench-scale PFH tests.

The selection of PFH operating conditions affects both the quality and quantity of oil produced. The quality of raw shale oil produced from batch PFH tests was evaluated by determining its specific gravity and carbon to hydrogen (C/H) weight ratio. The data plotted in Figure 6-20 shows that these two measurements are directly related. The relationship is linear for higher C/H ratios and becomes non-linear at lower C/H ratios.

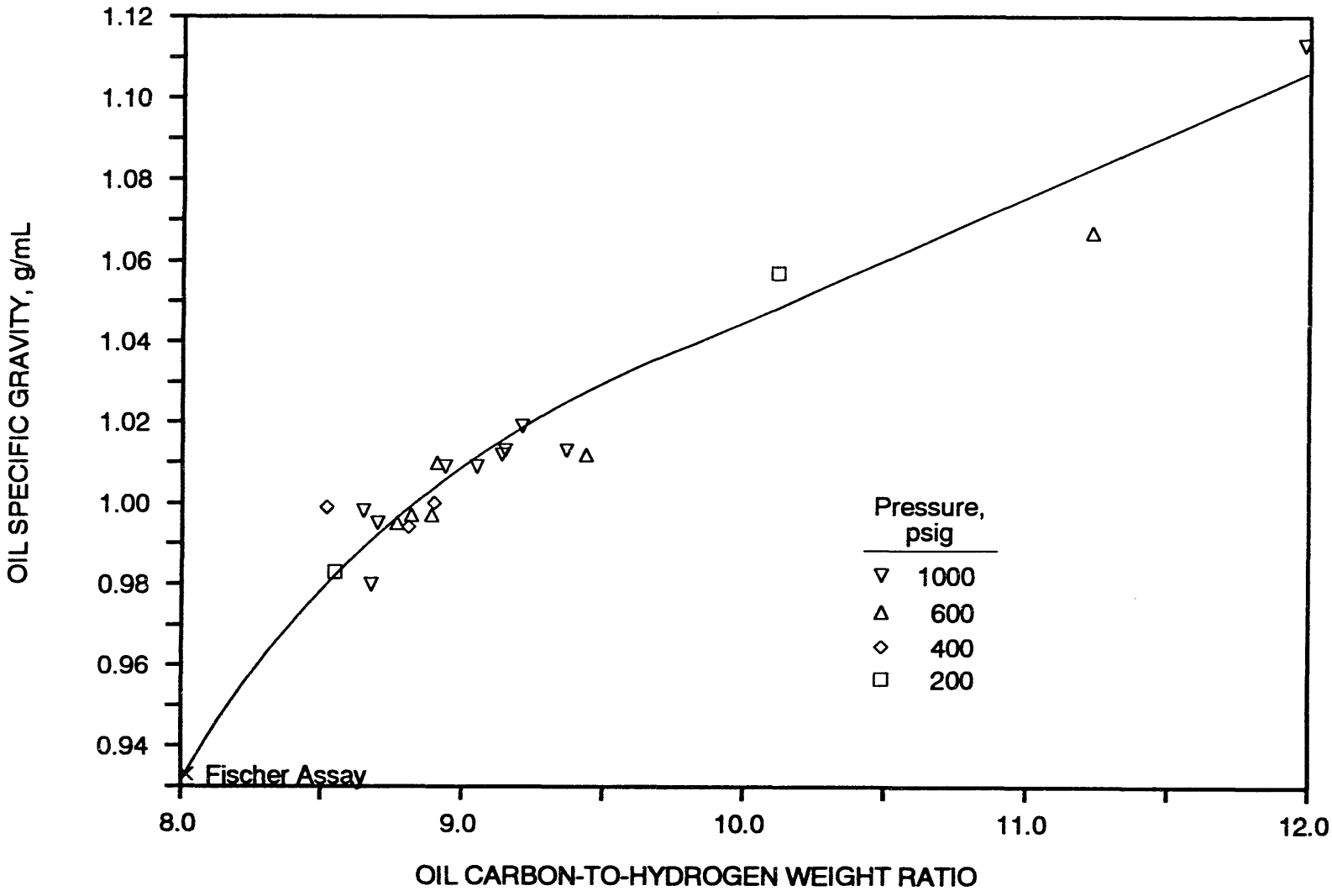

Figure 6-20. COMPARISON OF THE SPECIFIC GRAVITY OF BENEFICIATED ALABAMA SHALE OIL WITH ITS CARBON-TO-HYDROGEN RATIO

A comparison of PFH oil yield and oil quality represented by specific gravity is presented in Figure 6-21 (the oil yield has been normalized as GPT/wt % organic carbon). Oil from the batch PFH tests in this project and Fischer Assay oil from the same shale are included. The quality of the oil from PFH processing is closely related to operating conditions. The quantity of oil generated at 930° to 1060°F (500° to 570°C) increases with increasing hydrogen pressure while the oil specific gravity also increases. The lightest oil is generated under conditions of Fischer Assay with no hydrogen pressure. Increasing hydrogen pressure produces a linear increase in oil specific gravity as well as a significant increase in normalized oil yield. PFH tests conducted at temperatures above 1200°F (650°C) had lower oil yields than those conducted at 930° to 1060°F (500° to 570°C) and the oil was of poorer quality.

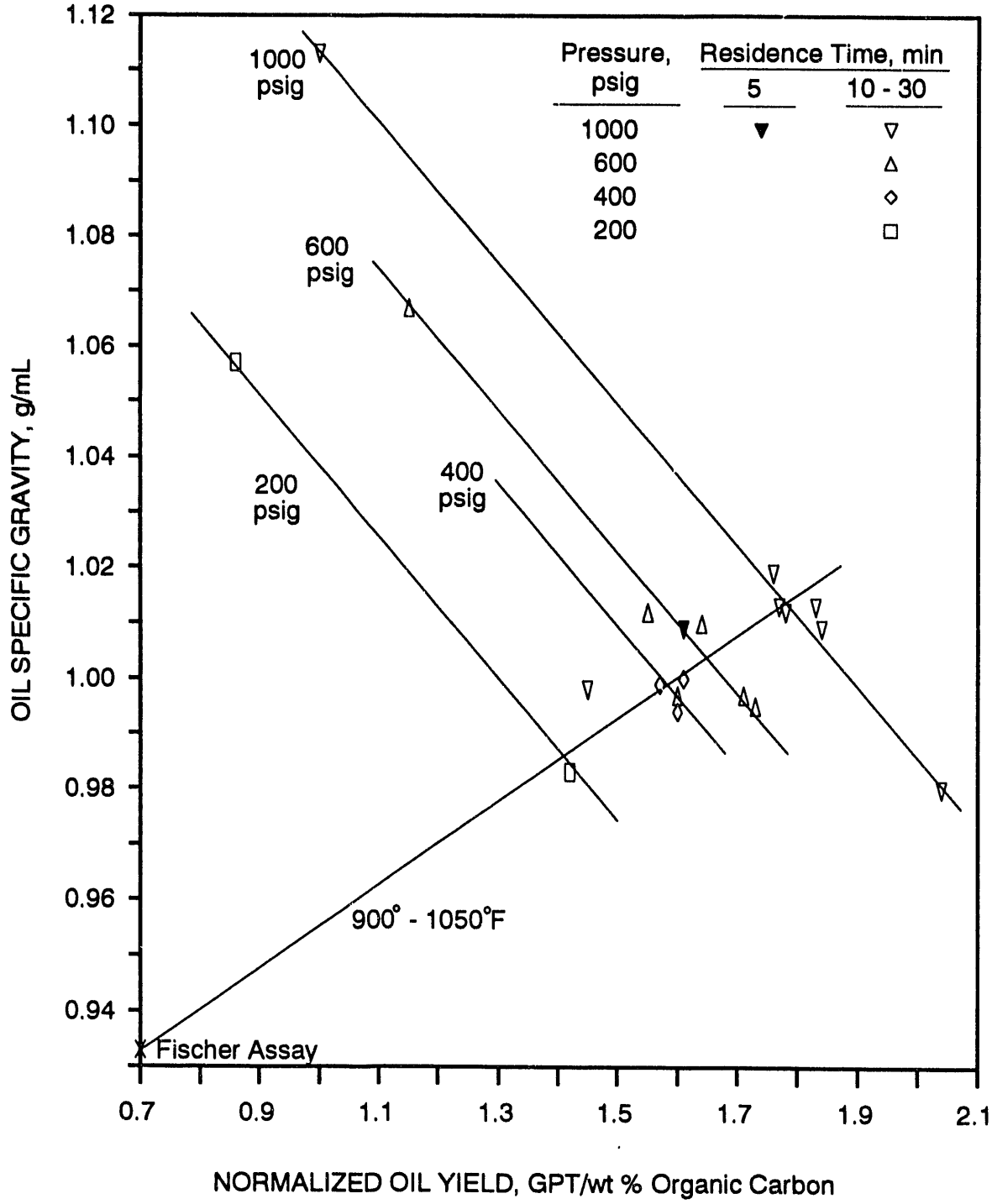

Figure 6-21. COMPARISON OF SHALE OIL SPECIFIC GRAVITY WITH NORMALIZED OIL YIELD

Subtask 6.4.3 Plant Energy Optimization

The objective of this subtask was to provide an initial evaluation of the PFH plant design[1] from thermodynamic and economic viewpoints. The goals were to identify thermodynamic losses, to assist in developing cost-effective solutions to reduce those losses, to improve the understanding of the cost-benefit tradeoffs in the design, to develop recommendations for improving the efficiency and cost effectiveness of the PFH plant, and to facilitate future optimization studies. The evaluation was based on the process flow diagram of the PFH plant shown in Figures 6-22 and 6-23. This subtask was conducted by the Tennessee Technological University (TTU).

To accomplish these objectives

a. the THESIS computer software[2,3] and data supplied by IGT[1] were used to simulate the performance and conduct the detailed thermoeconomic evaluation of the PFH plant and of a steam power plant that uses the spent shale as its main fuel,

b. the exergy method was used to evaluate the performance of each component of the total plant from a thermodynamic viewpoint,

c. the "pinch analysis" method[4] was used to improve the design of the heat exchanger network for the total plant,

d. conventional economic analysis techniques were used to calculate the investment costs for the total plant and various levelized costs, and

e. unique thermoeconomic evaluation techniques[5-8] were applied to calculate the cost of each stream and each product in the PFH plant, to compare different technical options, and to identify the cost sources in each plant component, and the plant areas where design changes are expected to result in the largest reduction in the cost of oil and electricity generated by the total plant.

Background

This section contains a brief introduction to exergy analysis and thermoeconomic evaluation and optimization of energy systems. More details on the methodology are given in References 3 and 5 through 8.

Exergy Analysis. The second law of thermodynamics complements and enhances an energy balance by enabling calculation of both the thermodynamic value of an energy carrier, and the real inefficiencies and losses from processes or systems. The concept of exergy (thermodynamic availability or available energy) is extremely useful for this purpose since an energy analysis generally fails to identify energy waste or the effective use of fuels and energy resources.

Exergy (E) is the maximum useful work attainable from an energy carrier under the conditions imposed by a given environment. Exergy is a thermodynamic property that depends on both the state of the carrier being

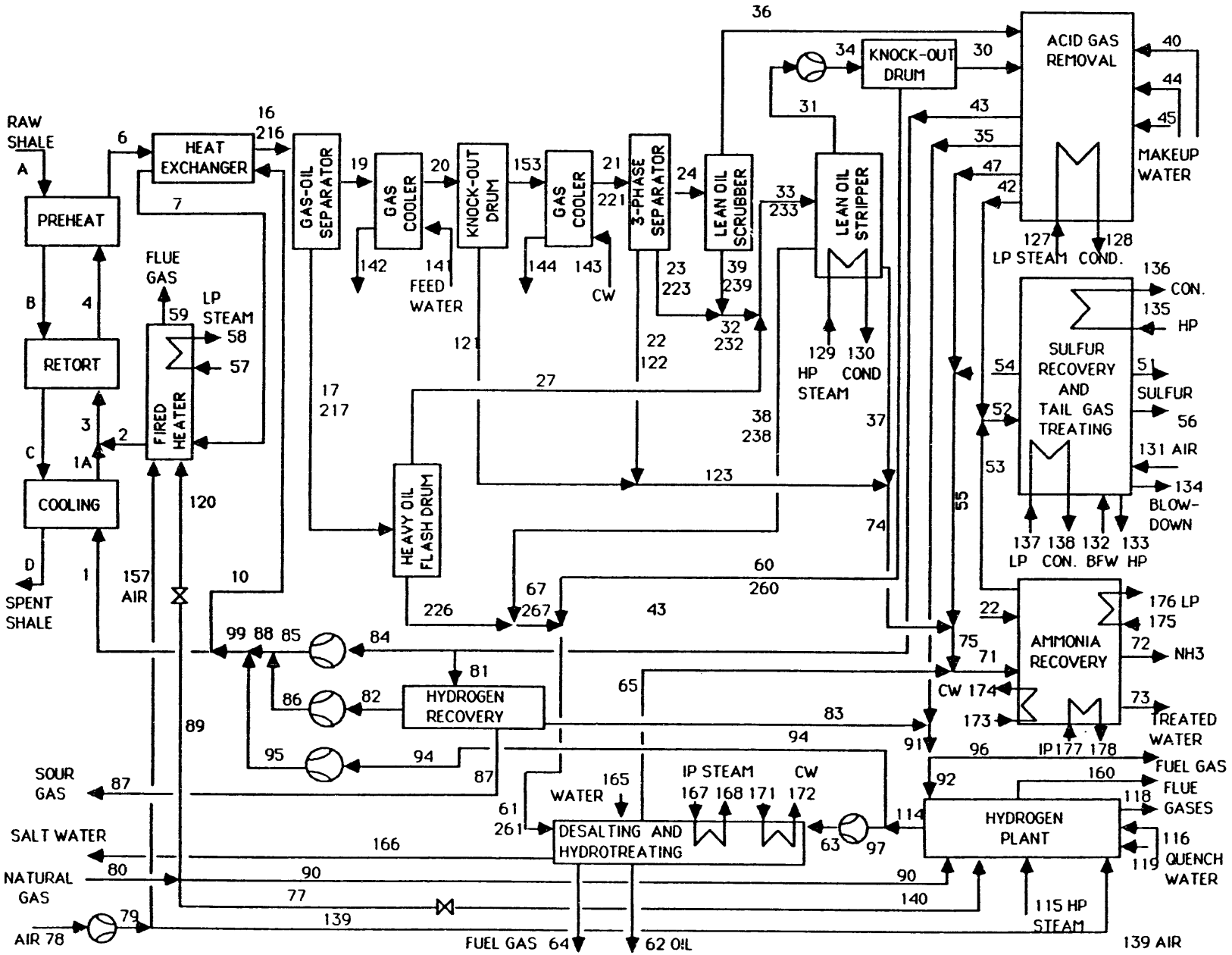

Figure 6-22. FLOW DIAGRAM OF THE PFH PLANT ORIGINAL DESIGN

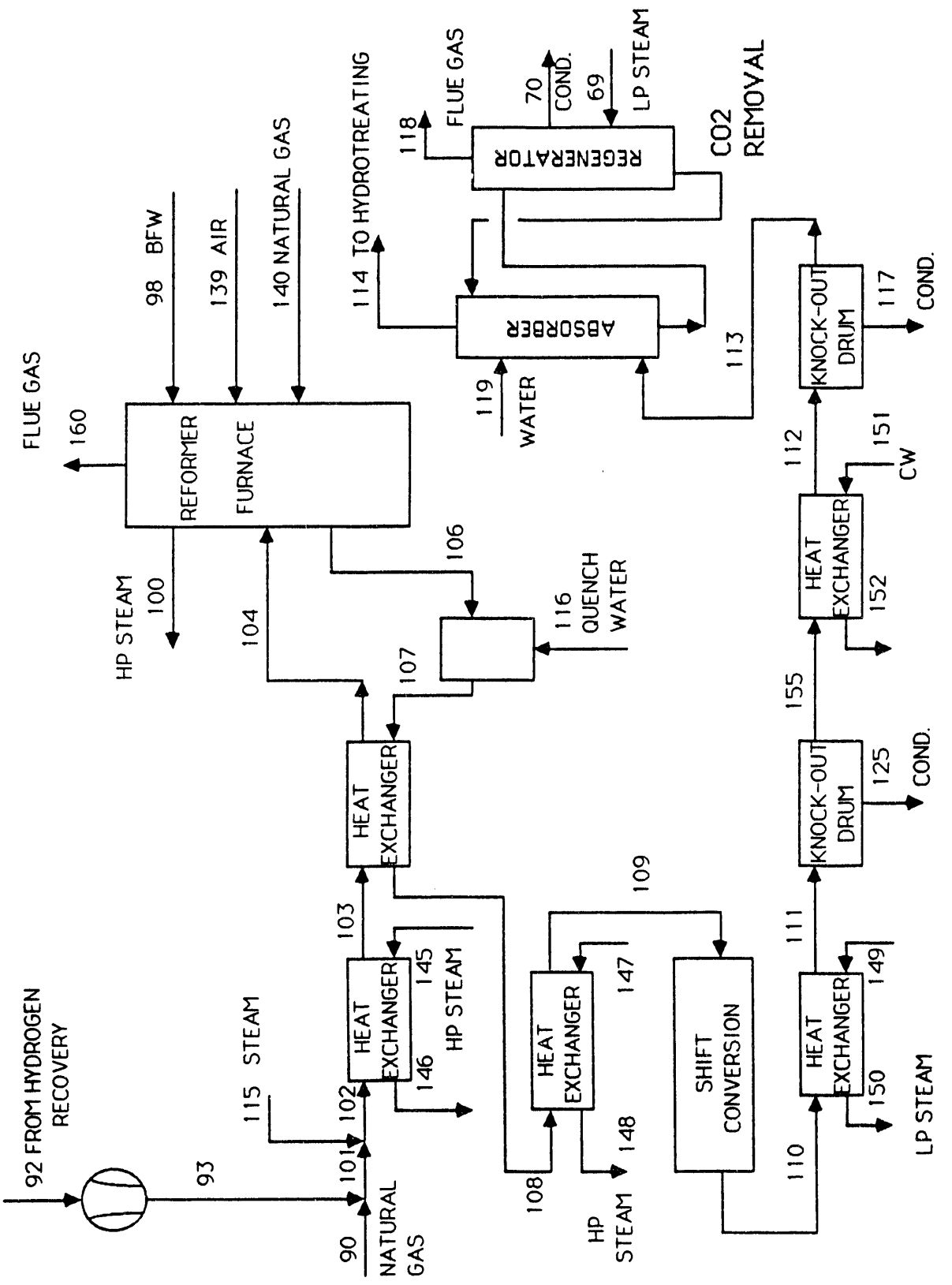

Figure 6-23. FLOW DIAGRAM OF THE HYDROGEN PLANT ORIGINAL DESIGN

considered and the state of the environment. It expresses the maximum capability of the energy carrier to cause changes. In most cases exergy can be considered the useful part of energy, i.e., the part of energy that can theoretically be transformed into any other form of energy.

Unlike total energy, a part of the total exergy supplied to a system is irreversibly destroyed in all processes. The exergy destruction (E_D) usually represents the largest part of what the layman calls "energy waste." The other part of "energy waste" is the exergy loss (E_L), i.e., the exergy transfer out of a system associated with a stream rejected to the environment. The term "destruction" is used to identify the unrecoverable loss of exergy within the system, as distinct from the loss of exergy in an output stream. Both exergy destruction and exergy loss are identified through an exergy analysis.

In addition, an exergy analysis calculates the exergetic efficiency (second-law efficiency) of each plant component. The exergetic efficiency evaluates the true component performance from the thermodynamic viewpoint and is useful in overall plant design evaluations. The definition of exergetic efficiency must be consistent with the purpose of using the system or component being considered.

To understand the term exergetic efficiency, it is helpful to think of each component as having a "product," which represents the desired result from the component, and a "fuel," which represents the driving force for the process, or the resources used to obtain the "product." The exergetic efficiency (ϵ_k) of the component is defined as the ratio of the exergy in the product ($\dot{E}_{P,k}$) to the exergy in the fuel ($\dot{E}_{F,k}$)

$$\epsilon_k = \frac{\dot{E}_{P,k}}{\dot{E}_{F,k}} \tag{3-1}$$

The exergy balance shows that the difference between exergy in the fuel and exergy in the product is the sum of exergy destruction and exergy loss in the component being considered:

$$\dot{E}_{F,k} - \dot{E}_{P,k} = \dot{E}_{D,k} + \dot{E}_{L,k} \tag{3-2}$$

The greater the percentage of the fuel exergy retained in the product, and, thus, the lower the extent of exergy destruction and exergy loss, the higher the exergetic efficiency of the component.

The objectives of an exergy analysis are:

- To identify the thermodynamic losses (exergy destruction and exergy losses) in an energy system and to understand the mechanisms causing the losses (chemical reactions, heat transfer, mixing, friction, etc.).

- To facilitate feasibility and optimization studies during the preliminary design phase of a project, as well as process improvement studies for an existing system.

- To assist in decision-making related to plant operation and maintenance and allocation of research funds.

In an exergy analysis, the exergy flow rate of each stream ($\dot{E}_i$), the flow rate of exergy destruction ($\dot{E}_{D,k}$), and the exergetic efficiency (ϵ_k) of each plant component are calculated, among others. The thermodynamic evaluation of each plant component is also based on the ratios of exergy destruction in a plant component to (a) the total plant exergy destruction ($\sum_k \dot{E}_{D,k}$), Equation 3-3, and (b) the total exergy input to the plant ($\dot{E}_{tot,in}$), Equation 3-4a, as well as the ratio of exergy loss in a component to the total exergy input to the total plant, Equation 3-4b:

$$y_k^* = \frac{\dot{E}_{D,k}}{\sum_k \dot{E}_{D,k}} \tag{3-3}$$

$$y_{D,k} = \frac{\dot{E}_{D,k}}{\dot{E}_{tot,in}} \tag{3-4a}$$

$$y_{L,k} = \frac{\dot{E}_{L,k}}{\dot{E}_{tot,in}} \tag{3-4b}$$

These exergy-destruction and exergy-loss ratios can be used for comparisons among various components of the same plant and among similar components of different plants that use the same fuels as energy input to the total plant.

Thermoeconomic Evaluation. Exergy is not only a measure of the true thermodynamic value of an energy carrier but is also closely related to the economic value of the carrier since users pay only for the useful part of energy. A thermoeconomic analysis combines an exergy analysis with an economic analysis at the component level. The objectives of a detailed thermoeconomic analysis include all the previously mentioned objectives of an exergy analysis in addition to the following:

- To shed light on the cost formation process, and, thus, facilitate studies to effectively reduce the product costs in an energy system.

- To estimate economically optimal operating conditions for a given design configuration.
- To understand the interactions between the thermodynamic performance of each plant component and the cost of the final plant product(s).
- To calculate the production costs of various products generated in the same process.
- To enable cost minimization studies in very complex energy systems.

In addition to mass, energy, and exergy balances, cost balances are formulated for each system component by assigning a cost value to the exergy (not the energy) of each stream entering or exiting the component. This procedure, exergy costing, is based on the finding that exergy is the only rational basis for assigning costs to streams as well as to "energy waste" (exergy destruction and exergy losses) in an energy-conversion process. With the aid of cost balances and some auxiliary assumptions, the cost per unit of exergy for each stream is calculated. Subsequently, we determine the average cost of a) providing a unit of fuel exergy to the k^{th} plant component ($c_{F,k}$), b) generating a unit of product exergy in the k^{th} plant component ($c_{P,k}$), and c) the exergy destruction rate in the k^{th} plant component ($\dot{D}_k$). Using this terminology, the cost balance is written as follows:

$$c_{F,k}\dot{E}_{F,k} + \dot{Z}_k = c_{P,k}\dot{E}_{P,k} + c_{F,k}\dot{E}_{L,k} \qquad (3\text{-}5)$$

Here, $\dot{Z}_k$ expresses the contribution of the investment costs and the operating (excluding fuel) and maintenance (O&M) costs associated with the k^{th} component to the product cost $c_{P,k}$. In the discussion below, these costs are called "capital costs" in order to distinguish them from the exergy costs ("fuel costs") for a plant component.

In the following discussion of the thermoeconomic evaluation we assume that the variables $c_{F,k}$ and $\dot{E}_{P,k}$ remain constant. In addition to the variables given by Equations 3-1, 3-3 and 3-4, the following parameters are used for evaluating the performance of the k^{th} component or group of components from the thermoeconomic viewpoint.

1. The cost rate of exergy destruction in the k^{th} component is calculated in this study from the following relationship:

$$\dot{D}_{D,k} = c_{F,k}\dot{E}_{D,k} \qquad (3\text{-}6)$$

This is the cost of the fuel used to cover the exergy destruction in the component.

2. The relative cost difference (r_k) between average cost per exergy unit of product and average cost per exergy unit of fuel is given by

$$r_k \equiv \frac{c_{P,k} - c_{F,k}}{c_{F,k}} = \frac{\dot{D}_{D,k} + \dot{Z}_k}{c_{F,k}\dot{E}_{P,k}} = \frac{1 - \epsilon_k}{\epsilon_k} + \frac{\dot{Z}_k}{c_{F,k}\dot{E}_{P,k}} \tag{3-7}$$

This equation reveals the real cost sources in the k^{th} system, which are the capital costs ($\dot{Z}_k$) , and the exergy destruction in the system, as expressed by $\dot{D}_{D,k}$. In general, the higher the relative cost difference r_k, the more attention should be paid to the k^{th} system, particularly when the values of $\dot{D}_{D,k}$ and $\dot{Z}_k$ are also high.

3. The thermoeconomic factor f_k

$$f_k = \frac{\dot{Z}_k}{\dot{Z}_k + \dot{D}_{D,k}} \tag{3-8}$$

expresses the contribution of the capital costs to the relative cost difference r_k.

4. For the thermoeconomic evaluation of heat exchangers we use, in addition to those discussed above, the variable z_k defined by:

$$z_k = \frac{\dot{Z}_k}{\dot{E}_{P,k}} \tag{3-9}$$

This variable states the capital costs required to transfer a unit of exergy to the cold stream of the heat exchanger.

These variables are all used in the thermoeconomic evaluation to determine what changes in the plant structure or in a variable (temperature, pressure, etc.) could lead to a decrease in the cost of the final product(s).

In defining the exergetic efficiency of components and in the process of exergy costing, it is appropriate to split the total exergy (superscript TOT) into physical and chemical exergy (superscripts PH and CH, respectively). The chemical exergy can be further split into reaction and environmental exergy[9] (superscripts R and E, respectively). The reaction exergy represents the part of chemical exergy that can be used in technical processes, and, thus, the only cost relevant component of chemical exergy. Therefore, a zero cost is always assigned to the environmental exergy. The splitting of total exergy into its components improves the exergy costing process and makes the efficiency and cost values independent of the reference state used in the exergy calculations.[9]

Thermoeconomic Optimization. A thermoeconomic optimization was not part of the objectives of the current phase of this subtask. This subject is discussed here, however, to demonstrate the potential of this method and what could be done in a later phase of this project.

Cost optimization for a complex energy-conversion system such as the PFH plant is usually expensive and requires knowledge of engineering, science, and business. The goal of optimization is to find the design configuration and the values of the system variables (the temperature, pressure, and chemical composition of flow streams, equipment size, materials, etc.) that minimize the cost of the total plant product(s). This usually involves a trade-off between capital and fuel costs for the entire system. Typical problems in the design and operation of energy systems have many workable solutions - sometimes an infinite number. Selecting the best solution requires engineering judgment, intuition, and critical analysis.

In many cases, a rigorous cost optimization for a complex energy system is not possible because some of the cost functions that are needed to express the capital cost of a component as a function of thermodynamic variables (temperatures, pressures, etc.) are either unavailable or inaccurate. But even in cases in which all the information is available and acceptably accurate, it is expensive and time-consuming to formulate and solve an optimization problem with an extremely large number of equations, constraints, and highly interdependent variables.

Traditionally, design optimization includes the following steps. First, a detailed system configuration is developed; material and energy balances are conducted for this configuration. Then, product costs are estimated through an economic analysis. The third step includes development of a modified/new configuration that accounts for the corresponding material and energy balances. Subsequently the product costs for the new configuration are calculated. Since this is a trial and error process, the last two steps are repeated several times until a solution is achieved.

Development of new process configurations is based, among other factors, on the experience and intuition of design engineers. Several decisions must be made with respect to thermodynamic variables. The final selection criterion, however, is economic. It is apparent that judiciously combining the thermodynamic and economic analyses, as in the thermoeconomic analysis, is advantageous to the optimization process.

Assuming well-designed total system configurations, the contribution of the capital costs to the final product costs decreases with decreasing thermodynamic efficiency (increasing exergy destruction), whereas the fuel cost increases with decreasing efficiency (see Figure 6-24).

Conventional optimization techniques seek the best trade-off between capital costs and fuel costs for the entire system. In thermoeconomics, a fuel is defined for each plant component. Thus the search for an optimum is simplified since these trade-offs can be made at the component level. If the relationship between investment costs and thermodynamic efficiency of the k^{th}

component is known (e.g., Equation 3-10), then the optimal thermodynamic efficiency from the cost viewpoint can be calculated,[8] Equation 3-11.

$$I_k = B_k \left(\frac{\epsilon_k}{1 - \epsilon_k} \right)^{n_k} \dot{E}_{P,k}^{m_k} \tag{3-10}$$

$$\epsilon_k^{OPT} = \frac{1}{1 + F_k} \tag{3-11}$$

with

$$F_k = \sqrt[n_k + 1]{\frac{(\beta_k + \gamma_k) B_k n_k}{\tau c_{F,k} \dot{E}_{P,k}^{(1 - m_k)}}} \tag{3-12}$$

In these equations, β_k is the capital recovery factor, γ_k represents a coefficient which indicates what part of the fixed O&M costs depends on the investment cost I_k, τ is the annual time of plant operation at the nominal capacity and B_k, n_k, and m_k are constants which depend on the component being considered. The variable $F_k^{(n_k+1)}$ is called the thermoeconomic similarity number of the k^{th} component.

The cost optimal values of the relative cost difference, exergy destruction, capital costs, cost of exergy destruction and thermoeconomic factor f can be calculated using Equations 3-13 and 3-17

$$r_k^{OPT} = \frac{n_k + 1}{n_k} F_k = \frac{n_k + 1}{n_k} \left(\frac{1 - \epsilon_k^{OPT}}{\epsilon_k^{OPT}} \right) , \tag{3-13}$$

$$\dot{E}_{D,k}^{OPT} = \dot{E}_{P,k} F_k = \dot{E}_{P,k} \left(\frac{1 - \epsilon_k^{OPT}}{\epsilon_k^{OPT}} \right) , \tag{3-14}$$

$$\dot{Z}_k^{OPT} = \frac{c_F \dot{E}_{P,k} F_k}{n_k} = \frac{c_F \dot{E}_{P,k}}{n_k} \left(\frac{1 - \epsilon_k^{OPT}}{\epsilon_k^{OPT}} \right) , \tag{3-15}$$

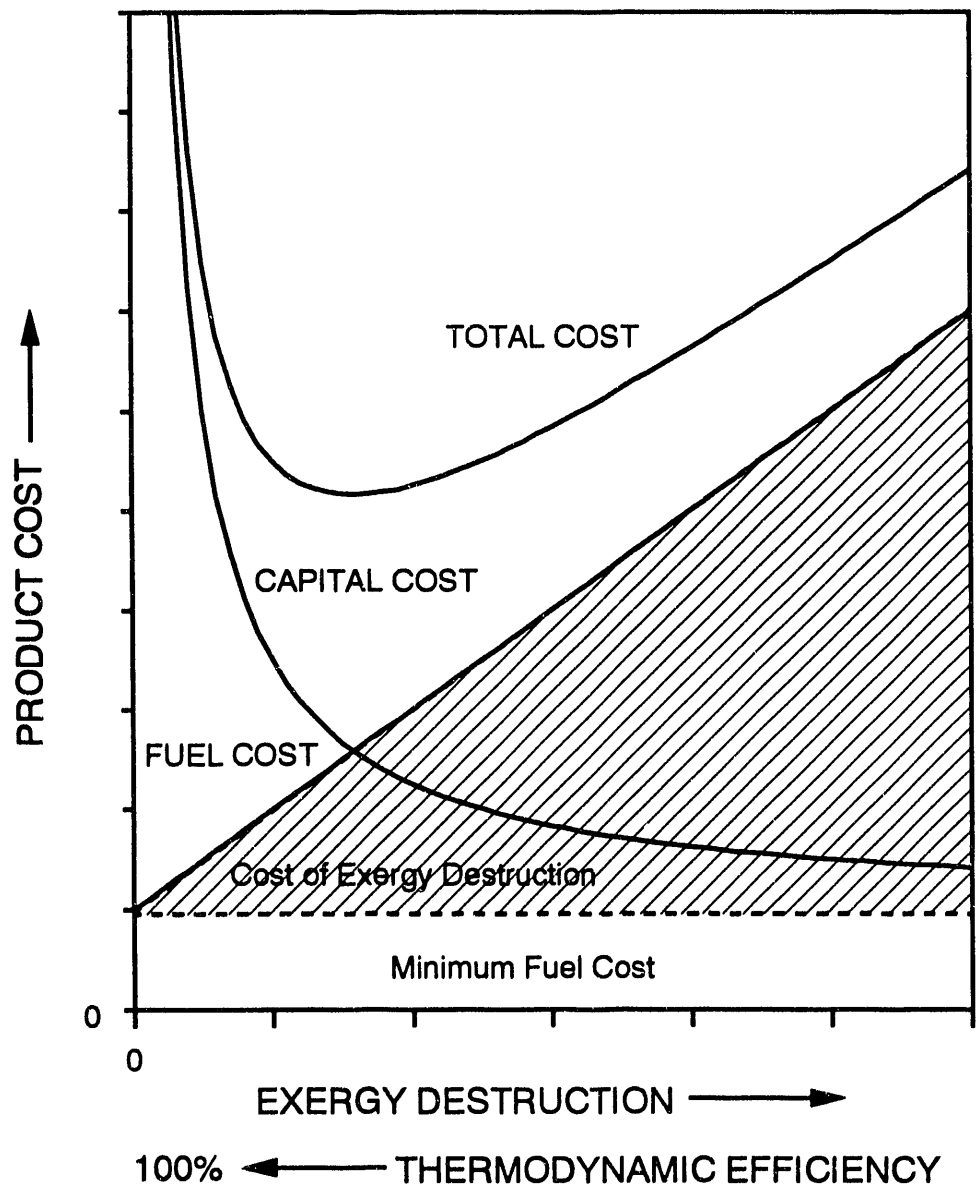

Figure 6-24. CONTRIBUTION OF FUEL AND CAPITAL COSTS TO THE PRODUCT COST AS A FUNCTION OF THE THERMODYNAMIC (Exergetic) EFFICIENCY.

$$\dot{D}_{D,k}^{OPT} = c_{F,k}\dot{E}_{P,k}F_k = c_{F,k}\dot{E}_{P,k}\left(\frac{1 - \epsilon_k^{OPT}}{\epsilon_k^{OPT}}\right) , \qquad (3\text{-}16)$$

and

$$f_k^{OPT} = \frac{1}{1 + n_k} . \qquad (3\text{-}17)$$

All of the above optimization results have been obtained by assuming $\dot{E}_{P,k}$= and $c_{F,k}$ = constant. These assumptions are fulfilled when a single plant component is optimized. It is apparent, however, that these assumptions are not valid when the total plant is optimized and several design changes (including changes in the design structure) are considered simultaneously. In this case, an iterative procedure is required to optimize the total plant. The thermoeconomic variables discussed in the previous section are used in the iteration to achieve a fast convergence.

Benefits of Thermoeconomics. The discussion in this section is more general than the scope of the present project warrants. This is done because thermoeconomics is a significantly younger discipline than exergy analysis and the benefits are not obvious to many energy engineers.

Today, the field of thermoeconomics has matured to the point where it is a valuable analytical tool for the design, operation, and maintenance of energy systems; it is not yet, however, a fully developed discipline. Thus, studies involving further development of the basic aspects of thermoeconomics are currently being carried out in parallel with applications of this field to practical problems.

The effectiveness of reducing costs in the design or operation of an energy system increases when the real causes and sources of costs are understood. A thermoeconomic analysis identifies these sources and indicates the changes required to reduce product costs. This information, complemented by the engineer's intuition and judgment, assists in the effective reduction of the product costs in energy systems on a relatively short time scale compared with traditional approaches. Decisions about the design, operation, and repair or replacement of equipment are facilitated.

In addition, thermoeconomics provides an objective cost allocation to more than one product of the same process. For instance, a thermoeconomic analysis of a cogeneration plant (which produces electricity and process steam) will provide the cost of steam and the cost of electricity separately. The cost ratio of steam to electricity calculated by the analysis does not necessarily have to be reflected in their selling prices, but the plant operators should know the real cost of generating each form of energy. In the current project, thermoeconomics calculates the cost at which the oil and gas

products are generated in the PFH plant and the cost at which the oil and electricity are generated in the combined plant.

The thermoeconomic analysis also shows how much raw fuel is required to produce each stream in the system. Finally, thermoeconomics helps managers decide how to allocate research and development funds to improve plant components that contribute most significantly to the product costs.

It is true that many conclusions obtained by a thermoeconomic optimization could also be obtained through a large number of conventional energy and economic analyses. The advantage of thermoeconomics however is that it replaces an expensive and subjective search for cost reduction with an objective, well-informed, systematic, and, therefore, shorter search in which all of the cost sources are properly identified and evaluated. The savings in both engineering and computer time are significant. Application of thermoeconomic analysis to new energy system concepts and complex installations such as the PFH plant and the combined plant results in significant savings.

Results and Discussion

Simulation. Based on the flow diagrams and the additional information provided by IGT,[1] the thermodynamic performance of the PFH plant was simulated using the THESIS program.[2,3] The computer software calculates the mass flow rate, enthalpy, entropy, exergy, temperature and pressure of each stream. Subroutines for standard components in energy-conversion plants, such as heat exchangers, pumps and some chemical reactors were available with the THESIS set of computer programs. For the remaining components of the PFH plant new subroutines were developed. Since no detailed flow diagrams for the plant areas of sulfur recovery, ammonia recovery and desalting and hydrotreating were available, these areas were treated as a "black box" without a detailed performance simulation. The simulation of these areas should be improved in future studies.

The amount of oil that condenses in some of the plant components is calculated using empirical factors and is not based on a thermodynamic vapor-liquid equilibrium calculation. If a stream contains gases and liquid oil, it is split into a gas and a liquid oil stream. The number assigned to a liquid oil stream is the corresponding gas stream number plus 200. A more flexible calculation of the thermodynamic properties would increase the capabilities of the simulation software.

Based on the simulation results, the following minor changes were made in the flow diagram:

a) Knock out drums were added after Cooler I and the heat exchanger following the shift conversion unit in the hydrogen plant; calculations showed that streams 20 and 111 should contain water condensate.

b) Part of the waste heat from the fired heater was assumed to be used for generating low-pressure steam (50 psig).

Exergy Analysis of the PFH Plant

Tables B1 through B3 in Appendix B present the detailed results obtained from the exergy analysis of the PFH plant. Table B1 shows the mass flow rates, temperatures, pressures and the flow rates of enthalpy and exergy of the material streams in the plant. Table B2 contains the detailed exergy flow rates. For each plant component, Table B3 shows the heat transfer rate, power supplied, exergy destruction flow rate, exergy destruction ratios y^* and y (exergy destruction in the component being considered divided by the sum of exergy destruction in the total plant, and exergy destruction in the component divided by the exergy of raw shale supplied to the PFH plant), and the component exergetic efficiency.

Several observations can be gleaned from Table B3. The exergy destruction in the retorting process (81 MW) is, absolutely taken, high, but, when all reactions taking place in the retorting process are considered, it seems to be relatively low. From a thermodynamic viewpoint, the operation of the retorting unit is very efficient.

The relatively high exergy destruction in the reformer furnace (149 MW) is mainly caused by irreversibilities in a) the combustion of methane, b) the heat transfer from the combustion gases to the steam and gas to be reformed, and c) the chemical reactions during the reforming process. Part of the sensible heat of the flue gas leaving the reformer furnace (stream 160) could be used to produce low-pressure steam and to preheat feedwater.

The addition of steam (stream 115) to stream 101 in the hydrogen plant should occur after stream 101 has been preheated in the first heat exchanger. This change would reduce the surface area of this heat exchanger and, thus, the total investment costs. The total exergy destruction will not be affected by this change.

In the hydrogen plant, the two heat exchangers where stream 102/103 is preheated and stream 108/109 is cooled could be combined into one heat exchanger. This change will reduce the total investment costs.

The exergy destruction in the water quenching of stream 106 at the outlet of the reformer furnace is significant (20.3 MW). The thermoeconomic analysis should determine if using an advanced heat exchanger to cool stream 106/107 and steam addition to stream 108 in lieu of the water quenching would improve the overall economics of the PFH plant.

The estimated overall power consumption in the plant is about 97 MW. The design and operation of the gas compressors should be optimized from the thermoeconomic viewpoint. In addition, the overall plant economics could be improved through a combination of the PFH plant with a steam power plant (or with an intercooled steam-injected gas turbine), which would use the net steam generated in the plant and would provide the required electric power.

The overall exergetic efficiency of 86.73 percent shown in Table B3 for the PFH plant indicates that the overall plant design is thermodynamically

efficient. Some potential, however, still exists for improving the overall efficiency and reducing the costs of the final products.

Thermoeconomic Evaluation of the PFH Plant

The results of the exergy analysis are used as input data for the thermoeconomic analysis. The thermoeconomic evaluation software calculates the

- cost per unit of total, chemical, and physical exergy for each plant stream (Table B4),
- monetary flow rate associated with each exergy form in each plant stream (Table B4),
- cost of fuel, product and exergy destruction for each plant component (Table 6-16), and
- various component related thermoeconomic variables, which assist in the evaluation of the components cost effectiveness (Tables 6-16 and B6).

An estimate of investment costs was provided by IGT to TTU for groups of components as shown in Figure 6-25. No attempt was made to split these costs among the single plant components. The important cost assumptions are summarized in Table 6-15. The results of the thermoeconomic analysis are summarized in Tables 6-16, 6-17, B5 and B6.

Table 6-15. COST ASSUMPTIONS MADE IN THE THERMOECONOMIC ANALYSIS (All values are in 1990 Dollars)

Cost of Beneficiated Oil Shale	$32.34/ton
Cost of Natural Gas	$4.0/MMBtu
Cost of Purchased Electricity	6 ¢/kWh
Electricity Credit	4 ¢/kWh
Market Price of Ammonia	$150.0/ton
Market Price of Sulfur	$70.0/long ton
Plant Economic Life	25 years
Average Inflation Rate	5 %/year
Average Plant Capacity Factor	90.4%

The data in Table 6-16 show that shale retorting is a relatively efficient operation. However, the rates of exergy destruction and cost of exergy destruction in shale retorting are the highest in the plant. Any change in the shale retorting process, which would reduce the exergy destruction in this group, would improve its cost effectiveness. Cost effective changes relate to design changes that would reduce the cost of oil generated by the PFH plant.

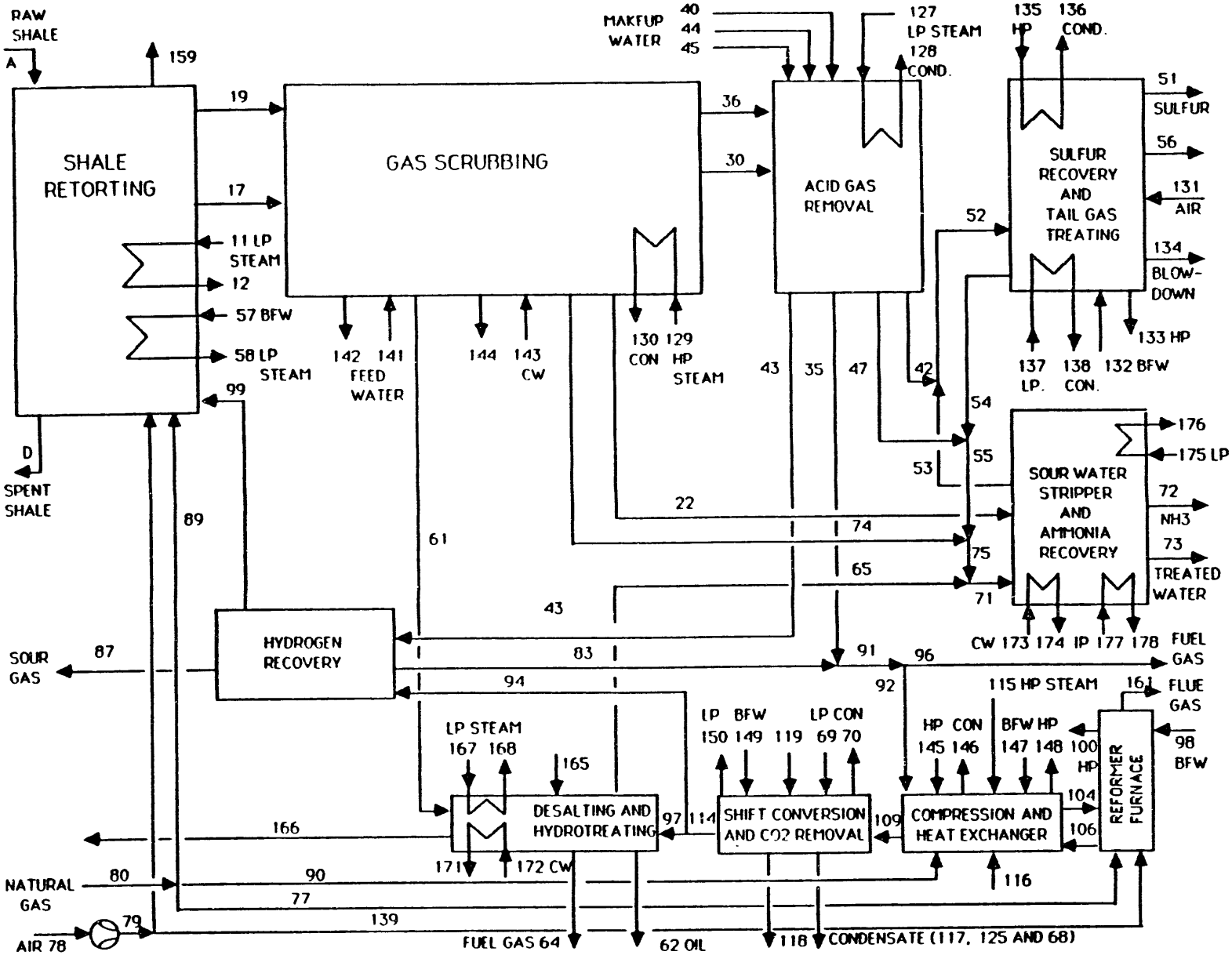

Figure 6-25. BLOCK FLOW DIAGRAM OF THE PFH PLANT USED FOR THE THERMOECONOMIC EVALUATION

Table 6-16. EXERGY DESTRUCTION FLOW RATE ($\dot{E}_D$), EXERGETIC EFFICIENCY (ϵ), COST OF EXERGY DESTRUCTION ($\dot{D}_D$) AND THERMOECONOMIC VARIABLES r AND f FOR SELECTED GROUPS OF PFH PLANT COMPONENTS (Figures 6-22 and 6-25)

Component Group	$\dot{E}_D$ [MW]	ϵ [%]	$\dot{D}_D$ [$/h]	r [%]	f [%]
Shale Retorting	217.8	97.8	2004	4.31	48.4
Gas Scrubbing	21.8	99.8	210	0.98	77.1
Acid Gas Removal	11.4	99.8	110	0.88	78.4
Hydrogen Recovery	30.6	99.5	336	2.78	83.2
Compressor Heat Exchangers	45.7	96.7	733	8.30	58.6
Steam Reformer	152.0	55.8	2275	235.65	66.4
Shift Conversion & CO_2 Removal	73.6	94.3	1313	12.36	51.3
Desalting & Hydrotreating	40.4	99.0	464	6.52	85.2

Table 6-17. PRODUCT COST SUMMARY FOR THE ORIGINAL PFH PLANT (Figures 6-22 and 6-23, Constant 1990 Dollars)

	$/Bbl
Cost of Produced Oil[a]	31.90
Costs of Utilities and Offsites[b]	4.10
Operating Costs	5.65
Sulfur Credit	-0.39
Ammonia Credit	-0.40
Credit for Streams 64 and 96	-2.66
Net Oil Cost	$38.21

a This number is calculated based on the cost flow rate associated with stream 62 after the costs of exergy losses from the PFH plant have been charged to the main product (oil in stream 62). The total capital costs are $1,742 million (1990 $).

b Excluding electric power and natural gas.

The cost effectiveness of gas scrubbing, acid gas removal and hydrogen recovery can be increased mainly through savings in the investment costs as the relatively high values of the factor f indicate. Since the exergy destruction in these component groups is relatively small and to a large extent independent of the investment costs, the general objective for these groups should be to minimize the overall investment costs. The only exception to that is associated with the recycle gas compressors, the cost effectiveness of which would increase by increasing their efficiency, and, consequently, their investment costs.

The cost rate of exergy destruction in compression and heat exchange is relatively large. This group could become more cost efficient by increasing the efficiency of the hydrogen compression process and by adding the high-pressure steam (stream 115) to the hydrogen plant after stream 101 has been preheated in the first heat exchanger.

The value of the thermoeconomic variable r in the reformer furnace is the highest among all plant components. The factor f indicates that this high r value is mainly caused by the high investment costs of this component. Since the cost rates associated with both the exergy destruction and the investment costs are high, particular attention should be paid to this component. A more detailed study is required to optimize this component from the thermoeconomic viewpoint. The same recommendation applies to shift conversion and CO_2 removal group, which shows the second highest r value in the plant.

The calculation of the net oil cost is summarized in Table 6-17. For this calculation, all costs associated with the PFH plant (except the cost of streams 51, 64, 72 and 96 in Figures 6-22 and 6-25) are charged to the oil generated in this plant. Here, in order to make these results comparable with the results of the improved PFH plant design, we did not assume that streams 64 and 96 (fuel gas) are used to reduce the natural gas consumption in the PFH plant; instead a credit is given for streams 64 and 96.

Description of the Combined Plant

The spent shale (stream D) still contains 17.08 percent of organic carbon and has a higher heating value of 3380 Btu/lbm.[1] The thermoeconomic analysis shows, that it would be a waste of $6715/h or 20 percent (Table B4) of the total shale cost, if this stream would not be further used in the plant. An appropriate use for the spent shale is to fuel a conventional steam power plant.

Figure 6-26 shows the flow diagram of a conventional subcritical power plant which could be combined with the PFH plant. The power plant burns the spent shale and the fuel gases (streams 96 and 64) produced in the PFH plant. It provides all the steam and power required in the PFH plant. Waste heat and excess steam from the PFH plant can be used to preheat feedwater. The combined plant has two main products, oil and electricity, and two byproducts, sulfur and ammonia. The connections between the PFH plant and the steam power plant are shown in Figure 6-27.

Exergy Analysis of the Combined Plant

A thermodynamic simulation program was used to predict the performance of the combined plant. The results from the simulation and exergy analysis are given in Tables B7, B8 and B9 (Appendix B). Table B7 shows the mass flow rates, temperatures, pressures and the flow rates of enthalpy and exergy of the material streams in the conventional steam power plant. The corresponding information for the PFH plant is presented in Table B1. Table B9 shows for each plant component, the heat transfer rate, the power supplied (generated), the exergy destruction flow rate, the exergy destruction ratio (the i^{th}

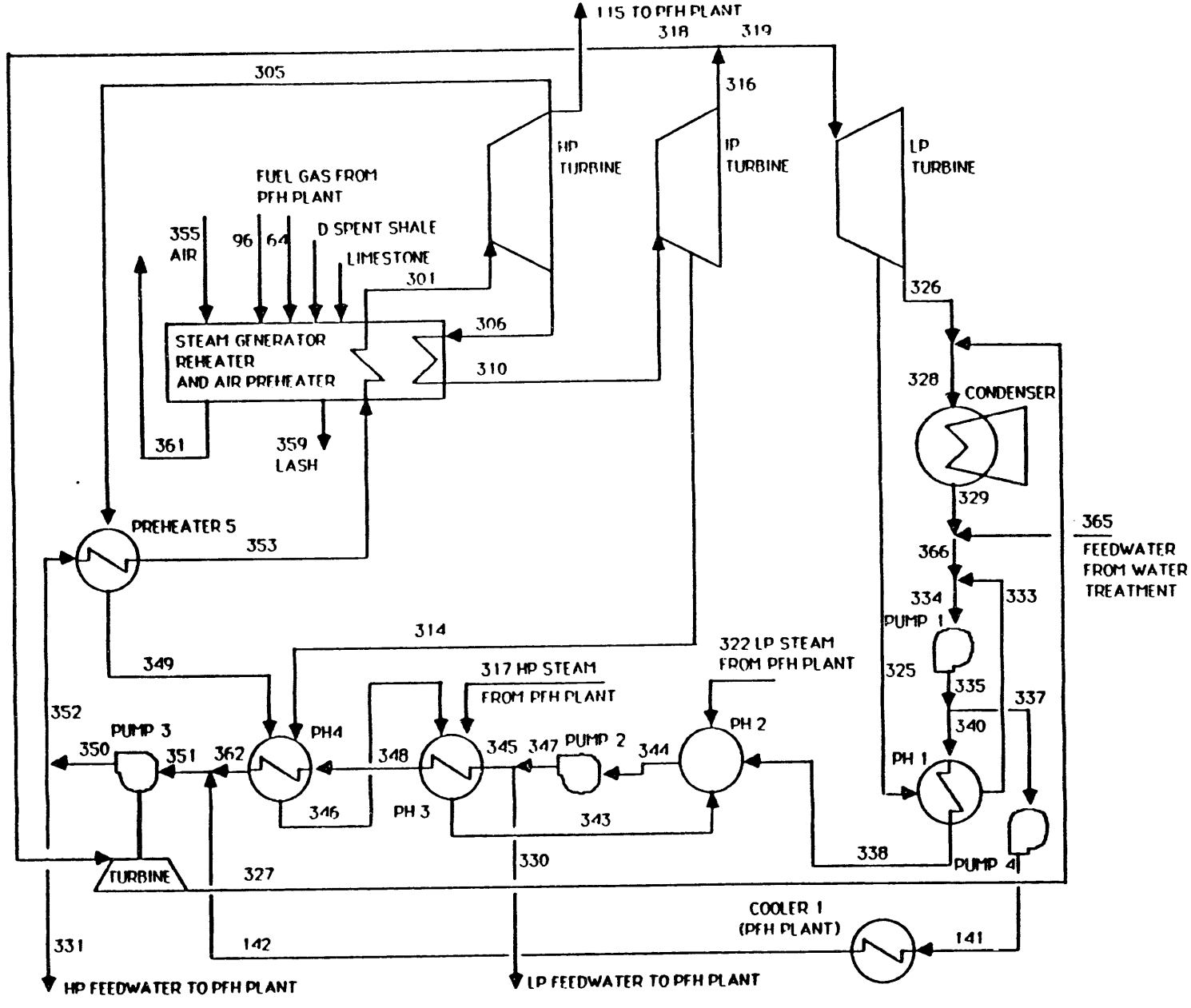

Figure 6-26. FLOW DIAGRAM OF THE ORIGINAL STEAM POWER PLANT

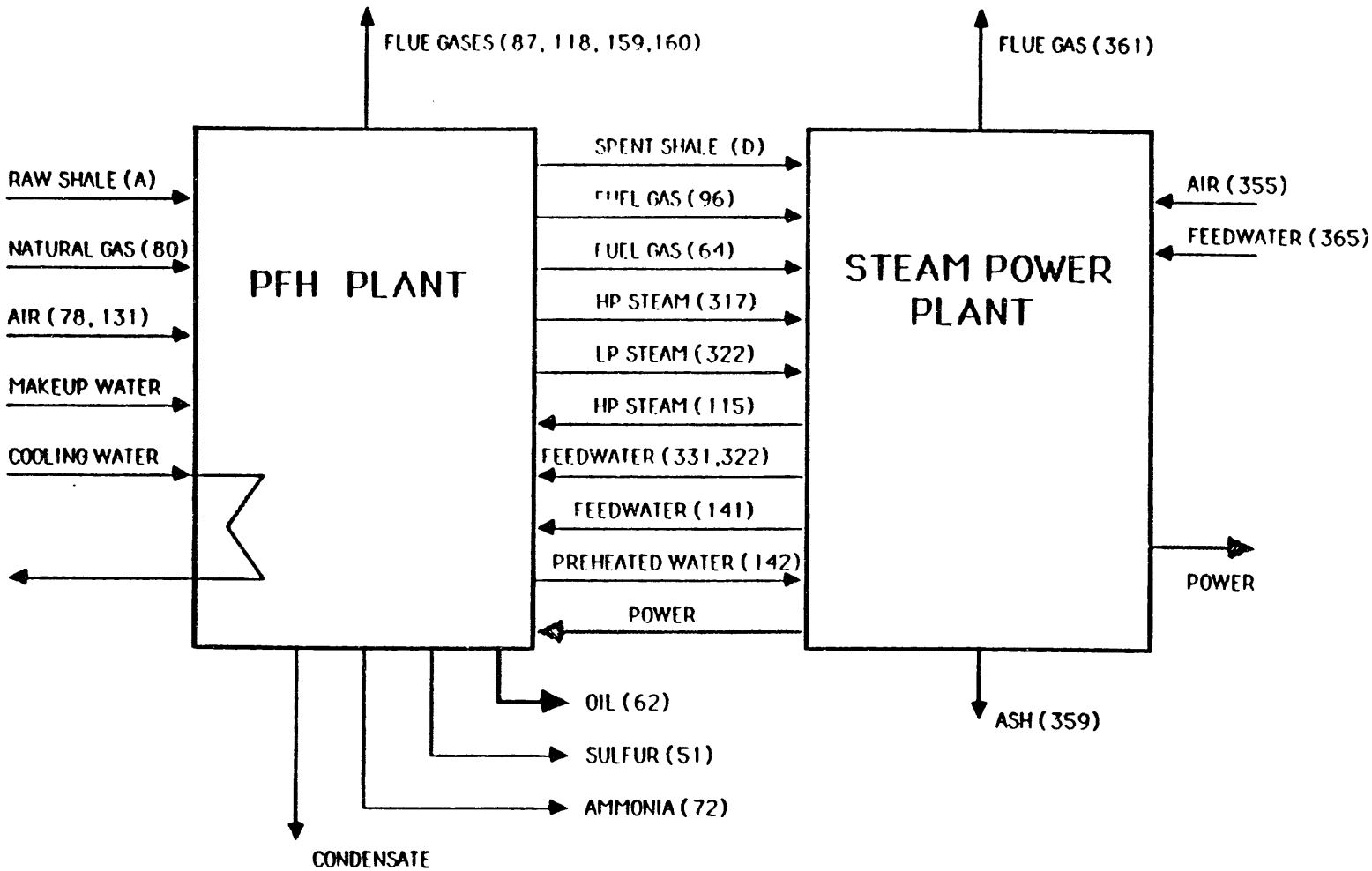

Figure 6-27. INTEGRATION OF PFH PLANT AND STEAM POWER PLANT

component exergy destruction divided by the total plant exergy destruction), the ratio between the component exergy destruction and the exergy of raw shale supplied to the total plant, and the component exergetic efficiency.

The exergy destruction in the steam generator is significant and represents about 50 percent of the total exergy destruction in the combined plant. The exergetic efficiency of the steam generator (51.06 percent, Table B9) is the lowest among all combined plant components. The exergy destruction in the steam turbines is mainly due to friction. State-of-the-art steam turbines were assumed in the design of the power plant. The total exergy destruction in the five feedwater preheaters could be reduced by improving integration between the PFH plant and power plant.

Table B9 shows that the PFH plant with a total exergy destruction of about 697 MW and an exergetic efficiency of 86.73 percent is considerably more efficient than the steam power plant (exergy destruction = 1056 MW; exergetic efficiency = 37.25 percent). This clearly shows that the PFH plant design is energy efficient. It should be noted, however, that there is some potential for cost-effective improvements in the PFH plant design, and a power producing plant has, in general, a lower efficiency than a fuel-conversion plant.

Pinch Analysis of the Combined Plant

Simultaneous with the exergy analysis of the combined power plant, a "pinch analysis"[4] for the total heat exchanger network was conducted. The pinch analysis identifies heat exchangers with a mismatch between the hot and cold side streams. This mismatch leads to an increase in the fuel costs and, sometimes, also in the investment costs for the entire plant. This analysis, combined with the exergy analysis, indicates that the performance of the following heat transfer devices can be improved: 1) Retort product heat exchanger after the preheating unit; 2) LP-steam generator in the fired heater; 3) Heat exchangers using high-pressure and intermediate-pressure steam in the acid gas removal, sulfur recovery, ammonia recovery and desalting and hydrotreating units; 4) Low-pressure steam generator in the hydrogen plant; 5) Cooler in the hydrogen plant; 6) Air preheater in the steam generator; and 7) Cooling of the spent shale.

In addition, elimination of the mixing processes in the hydrogen plant, where high-pressure steam (stream 115) and quench water (steam 116) are used, should have a positive effect on the cost of oil. The potential for optimization, particularly in the hydrogen plant, is significant.

Thermoeconomic Analysis of the Combined Plant

The investment cost data for the power-plant components were based on information reported in another study.[3] Cost indices were used to convert the investment costs associated with the power plant to 1990 dollars, i.e., the same cost basis as the PFH plant investment costs. The detailed results from the thermoeconomic analysis of the combined plant are shown in Tables B10, B11 and B12 and include the following variables:

- Cost flow rates associated with each stream.

- Cost per unit of total, chemical, and physical exergy for each stream.
- Cost of fuel, product, and exergy destruction for each plant component.
- Various thermoeconomic variables to be used in the evaluation of the component cost effectiveness.

Table 6-18 summarizes the most important variables for the thermoeconomic evaluation of the power plant components. The results of the thermoeconomic analysis of the steam power plant show that the steam generator has the lowest exergetic efficiency and the highest exergy destruction rate and cost of exergy destruction rate among all component groups of the combined plant. The relatively low f value indicates that the cost effectiveness of the steam generator might be improved by increasing its efficiency and, consequently, the investment costs of the steam generator. This can be achieved by using a supercritical steam cycle.

The relatively high values of r and f for the low-pressure pump 1 suggest that the least expensive (but equally reliable) pump should be used here. In addition, the number of pumps used in series could be reduced from three to two. The very low f values combined with the relatively high values of the cost of exergy destruction for the preheaters 1, 3, and 4 indicate that the overall cost effectiveness of the combined plant will increase when the temperature differences in these preheaters decrease. This can be achieved through a modification in the heat-exchanger network.

Table 6-19 summarizes the costs of the products generated in the combined plant. The electricity is generated internally at a cost slightly higher than the 4¢/kWh (mid-1990 dollars) credit, which was assumed in the economic analysis. It should be mentioned, however, that the 97 MW of electricity consumed by the PFH plant are now supplied at the same low cost of 4.09 ¢/kWh instead of 6.0 ¢/kWh, which is the cost to purchase electricity. The net cost of oil generated in the combined plant is about $34 per barrel. Thus, the addition of the steam power plant to the PFH plant has an overall positive effect on the cost of oil.

Combined Plant Design Improvements

Based on the results of the combined plant analyses, the following three design modifications were considered in this study:

1. Mod I refers to the design of the heat exchangers used to preheat the hydrogen-rich gas (stream 99 to 3).
2. Mod II refers to the heat exchanger network in the hydrogen plant.
3. Mod III refers to a reduction in the size of the steam power plant by using fuel gas produced in the PFH plant to substitute for part of the natural gas used in the fired heater and the reformer furnace.

Table 6-18. EXERGY DESTRUCTION FLOW RATE ($\dot{E}_D$), EXERGETIC EFFICIENCY (ϵ) COST RATE OF EXERGY DESTRUCTION ($\dot{D}_D$) AND THERMOECONOMIC VARIABLES r AND f FOR COMPONENTS OF THE ORIGINAL STEAM POWER PLANT (Figure 6-26)

Component	$\dot{E}_D$ [MW]	ϵ [%]	$\dot{D}_D$ [$/h]	r [%]	f [%]
Steam Generator	726.3	51.8	5781	123.52	24.5
HP Turbine	11.6	93.8	229	11.86	44.7
IP Turbine	13.0	93.3	255	12.53	42.6
LP Turbine	35.9	86.5	835	20.07	22.4
Pump 1	0.1	72.7	3	211.04	82.2
Preheater 1	1.4	66.4	166	51.70	2.2
Pump 4	0.2	77.2	10	64.82	54.5
Deaerator	1.0	96.3	21	4.99	22.5
Pump 2	0.4	77.2	18	57.67	48.9
Preheater 3	6.9	76.1	180	31.62	0.5
Preheater 4	2.5	89.0	49	13.15	6.1
Pump 3 and Turbine	4.7	70.8	135	60.52	32.0
Preheater 5	3.5	91.9	35	15.37	42.6

Table 6-19. PRODUCT COST SUMMARY FOR THE ORIGINAL COMBINED PLANT (Figures 6-22, 6-23, 6-25 and 6-26, Constant 1990 Dollars)

	$/Bbl
Cost of Produced Oil[a]	33.67
Costs of Utilities and Offsites[b]	4.10
Operating Costs	5.65
Electricity Credit[c]	-8.79
Sulfur Credit	-0.39
Ammonia Credit	-0.40
Net Oil Cost	$33.84

a. Assumes that all fuel and investment costs are charged to the oil. Total capital costs for this case are $2455 million (1990 $).
b. Excluding natural gas.
c. Electricity is produced internally at a cost of 4.09¢/kWh. The cost of electricity generation is included in the cost of $33.67/Bbl given for the oil. The net electricity generated is credited at 4.00 ¢/kWh.

The effects of each modification were initially studied separately and then all three changes were combined. In the following sections, the effects of each design modification on the performance of the original design of the combined plant are discussed. Subsequently, a detailed thermoeconomic analysis of the improved design of the combined plant is presented.

Design Modification I

The heating of the hydrogen rich gas from the thermodynamic state of stream 99 to the state of stream 3 is done in components with relatively low exergetic efficiencies. Particularly, the cooling process in the retorting unit has the lowest efficiency among the heat transfer processes in the combined plant. This is caused by the extremely high temperature differences at the inlet and outlet ($T_C - T_{1A} = 300°F$; $T_D - T_1 = 470°F$). Therefore, an alternative heat exchanger arrangement is suggested in Figure 6-28.

The operating conditions for the reheat and preheat unit and the properties of flow streams 16 and 99 are the same in both designs. A comparison of the thermodynamic properties for the flow streams is given in Table 6-20, which lists only the mass flow rate and temperatures of the streams since all pressure values are the same in both cases.

A comparison of the exergy destruction and the exergetic efficiencies is given in Table 6-21. The preheating (using low-pressure steam) and the splitting of steam 99 after heat exchanger 6/16, along with the significant increase in the mass flow rate of stream 1, lead to a better adjustment of the temperature differences for this group of heat exchangers. Therefore, the exergetic efficiency of all components in Table 6-21 increases or remains constant. The exergy destruction decreases by 9.1 percent from a total of 213.25 MW for this group of components to 190.85 MW. The fuel consumption in the fired heater (stream 120) decreases from 38,188 to 32,382 lb/h (or by 15.2 percent). The fuel savings of $497 per hour, assuming combustion of natural gas, should justify the addition of the heat exchanger surface area required to achieve the changes shown in Figure 6-28 and Table 6-20.

Design Modification II

The exergy and pinch analyses indicate that the heat exchanger arrangement in the hydrogen plant can be improved. To demonstrate the potential for improvement, the design of the hydrogen plant was modified (see Figure 6-29).

In this design, heat exchange between flow streams with high temperature differences and mixing of cold and hot streams is avoided. The conditions at the inlet and outlet of the steam reformer and the shift conversion were kept constant. Most of the waste heat from the hydrogen plant is now used to preheat feedwater in the steam cycle.

The overall effects of these changes in the hydrogen plant can be summarized as follows:

- The exergy destruction in the hydrogen plant is decreased by about 27 percent from 239 to 173 MW.
- The fuel consumption in the reformer furnace is decreased by 14.8 percent from 55,491 to 47,171 lbm/h.
- The total heat exchanger load is decreased by 5.5 percent from 602 to 569 MW.

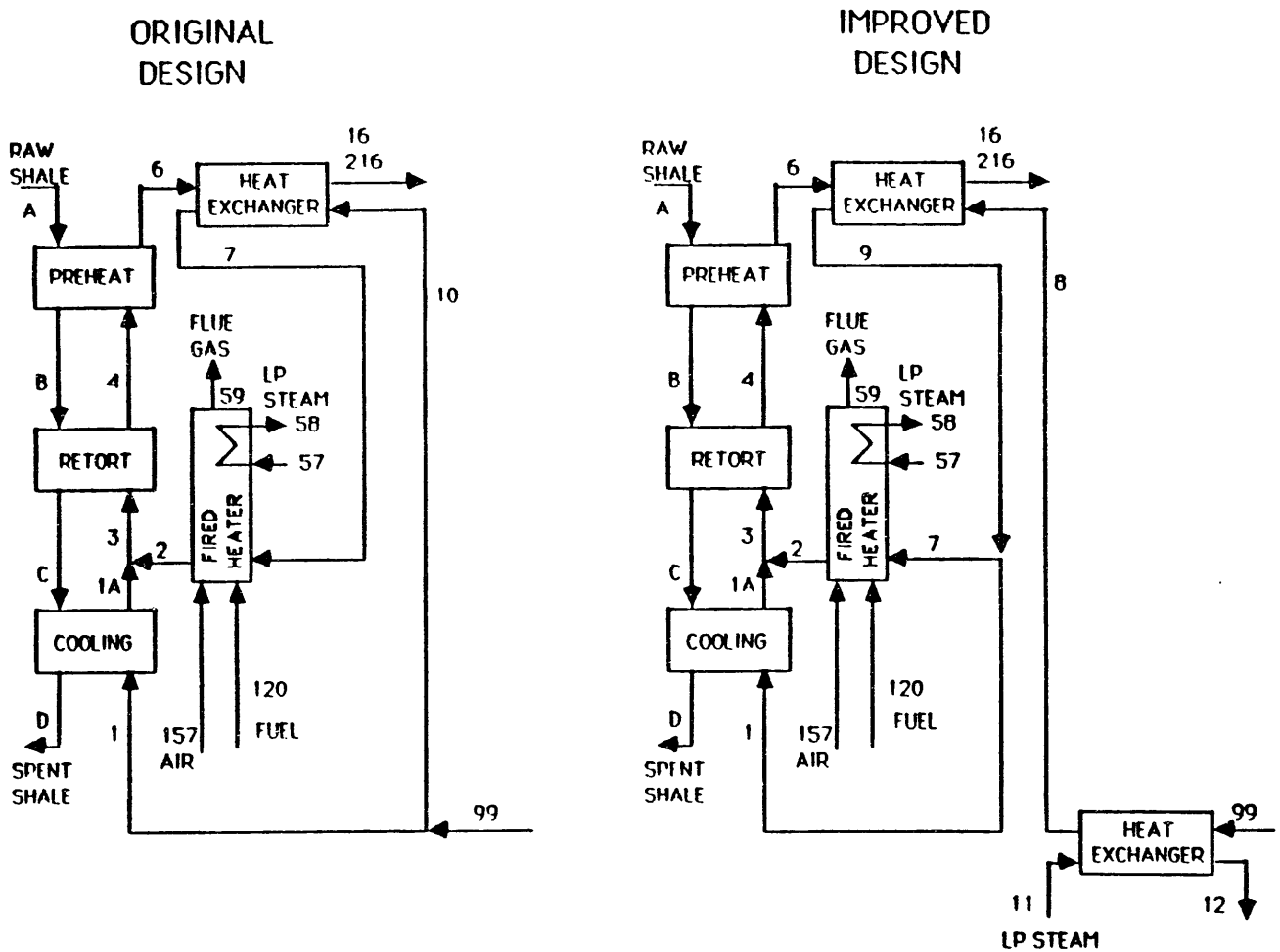

Figure 6-28. COMPARISON OF THE ORIGINAL AND IMPROVED (Modification I) DESIGN OF PART OF THE PFH PLANT

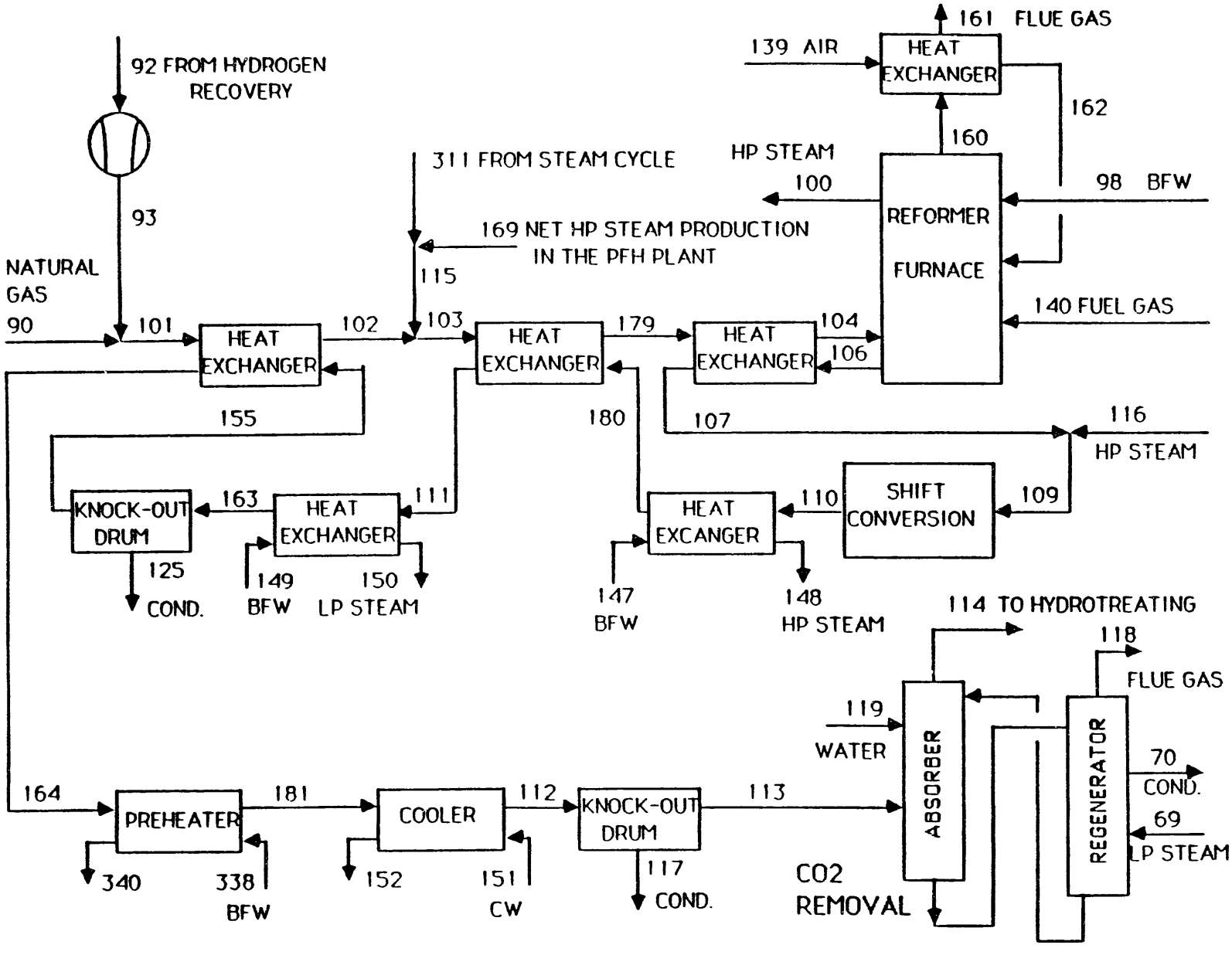

Figure 6-29. FLOW DIAGRAM OF THE IMPROVED HYDROGEN PLANT

- The feedwater preheating in the hydrogen plant allows more steam to be expanded in the low-pressure turbine so that more power is produced. The required cooling is reduced by more than 90 percent from almost 150 to 12 MW.

- The overall efficiency of the combined plant is increased from 70.52 to 71.75 percent (Table 6-22).

Table 6-20. COMPARISON OF THERMODYNAMIC PROPERTIES WHEN MODIFICATION I IS CONDUCTED (Figure 6-28)

	Original Design		Design After Modification I	
Stream No.	Mass Flow Rate, lbm/h	Temperature °F	Mass Flow Rate, lbm/h	Temperature °F
A	2,051,416	60	2,051,416	60
W	37,951	60	37,951	60
B	2,014,142	600	2,014,142	600
C	1,080,818	900	1,080,818	900
D	1,080,818	650	1,080,818	608
1A	160,446	600	287,206	810
1	160,446	180	287,206	517
2	563,750	1400	436,985	1495
3	724,191	1233	724,191	1233
4	1733,417	900	1,733,417	900
6	1,808,642	600	1,808,642	600
7	563,750	511	436,985	517
8	--	--	724,191	262
9	--	--	724,191	517
10	563,749	180	--	--
11	--	--	79,708	298
12	--	--	79,708	298
16	1,439,753	460	1,439,753	460
216	368,890	460	368,890	460
57	55,375	298	45,904	298
58	55,375	298	45,904	298
59	724,928	352	630,755	352
99	724,191	180	724,191	180
120	38,188	85	32,382	85
157	686,745	90	597,928	90

The number of heat exchangers in the hydrogen plant is increased by three and the heat exchanger before the reformer operates at a high temperature level (T_{106} = 1535°F). These changes will increase the investment costs. The fuel savings, however, are significant and the preheating of feedwater in the hydrogen plant reduces the number of preheaters in the steam cycle by two. Therefore, these design changes are expected to be cost effective.

Table 6-21. THE EFFECT OF MODIFICATION I ON THE EXERGY DESTRUCTION ($\dot{E}_D$) AND EXERGETIC EFFICIENCY (ϵ) OF SINGLE COMPONENTS

	Original Design		Design After Modification I	
Component	$\dot{E}_D$, MW	ϵ, %	$\dot{E}_D$, MW	ϵ, %
Preheat	24.15	45.48	24.15	45.48
Retort	81.0	98.2	81.0	98.2
Cooling	6.8	58.4	0.8	95.6
Mixing 1A+2	3.8	99.9	3.4	99.9
Heat Exch. 6/16	3.4	87.5	0.9	96.6
Fired Heater	94.3	60.6	79.7	61.3
Heat Exch. 99/8	--	--	1.7	74.5
Sum	213.25	--	190.85	--

Table 6-22. COMPARISON OF EXERGETIC EFFICIENCY (ϵ) AND NET ELECTRIC POWER GENERATION ($\dot{W}_{net}$) WHEN DESIGN MODIFICATIONS I, II AND III ARE CONDUCTED

Design Modification	ϵ, %	$\dot{W}_{net}$, MW
Original Design	70.52	440
Design Modification I	70.89	438
Design Modification II	71.75	477
Design Modification III	73.92	261
Design Modifications I, II and III	74.98	264

Design Modification III

The thermoeconomic analysis shows that the fuel gas (streams 64 and 96) is produced at a lower cost per exergy unit than the natural gas supplied in the PFH plant from outside (compare the cost of total exergy unit for streams 64, 96 and 80 in Table B4). Thus, the cost effectiveness of the PFH plant must increase if the fuel gas is burned in the fired heater and in the reformer furnace instead of the steam generator of the power plant. The amount of produced fuel gas is not sufficient to completely eliminate the use of natural gas in these components. In addition, to ensure stable combustion of the spent shale in the steam generator, the co-combustion of a small amount of gaseous fuel is required.[11] Therefore, some natural gas is still used in the combined plant for combustion purposes.

Since, based on its exergy value, the fuel gas represents about one third of the power plant fuel, implementation of modification III reduces the power production by about one-third as well. This change results in an increase in the overall efficiency of the combined plant since (a) the oil production is thermodynamically more efficient than the electricity

generation, and (b) the relative weight of electricity generation in the overall efficiency decreases when modification III is implemented.

Combination of Design Modifications I, II and III

The final plant design when modifications I, II and III are considered simultaneously is shown in Figures 6-29, 6-30, and 6-31. The design modifications considered here are almost independent from each other. As Table 6-22 indicates, the sum of the increases in the total efficiency for each one of the modifications I, II and III is almost equal to the increase in total efficiency when modifications I, II and III are considered simultaneously. The detailed results of the thermodynamic simulation for the improved combined plant are given in Tables B13 through B15. The design of the steam cycle is now simpler than the original design. The number of pumps is decreased from four to two. The use of waste heat from the PFH plant to preheat feedwater increases the efficiency of the feedwater preheating.

Thermoeconomic Analysis of the Improved Plant Design

A new thermoeconomic analysis was conducted for the improved design of the combined plant. The detailed results are given in Tables B16 through B18. The most important results are summarized in Table 6-23. Table 6-24 compares the exergy destruction and costs of exergy destruction for some selected plant component groups between original and improved design. The effect of design modifications I, II and III on the cost of oil is shown in Table 6-25. The improvements made in this project decrease the cost of oil from $38.21 per barrel in the original PFH design (or $33.84/Bbl in the original combined plant) to $31.81 per barrel in the improved design.

Figures 6-32 and 6-33 show the sensitivity of net oil cost to changes in the cost of shale, the electricity credit, and the capital recovery factor.

For combustion of spent shale in the combined plant a fluidized bed combustor with limestone desulfurization was assumed. If an alternative desulfurization process (WSA-SNOX[10]), which generates sulfuric acid as a by-product, is used and if the sulfuric acid credit is $70/ton, the net oil cost is reduced by $1 per barrel, as a comparison of Tables 6-25 and 6-26 shows.

Conclusions and Recommendations

In this subtask, the performance of the PFH plant and of a steam power plant combined with the PFH plant were simulated. Detailed exergy and thermoeconomic evaluations were conducted for each plant. These evaluations indicate that

a) shale hydroretorting is a relatively efficient operation from a thermodynamic viewpoint,

b) the cost effectiveness of gas scrubbing, acid gas removal and hydrogen recovery can be increased mainly through savings in the investment costs,

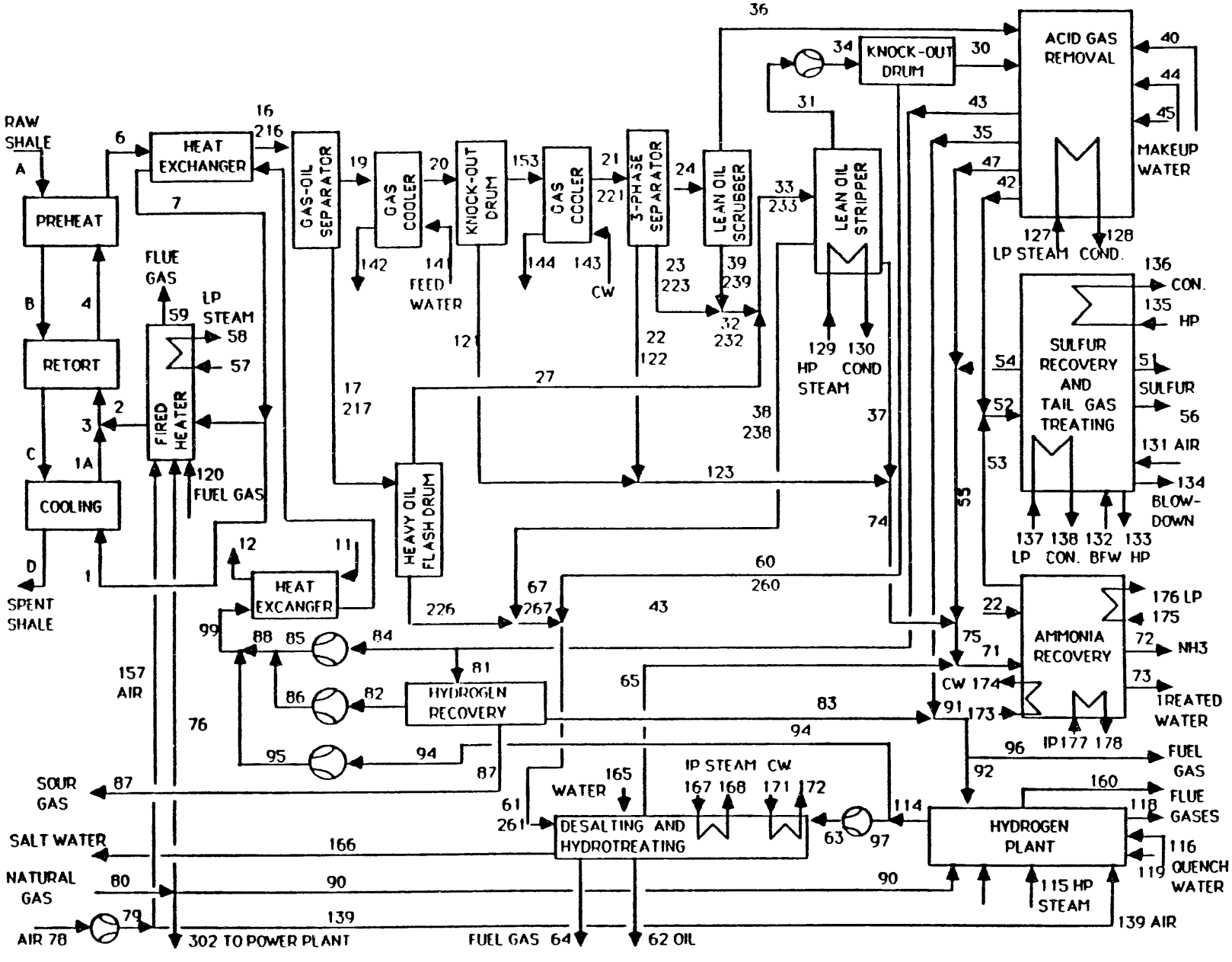

Figure 6-30. FLOW DIAGRAM OF THE IMPROVED PFH PLANT

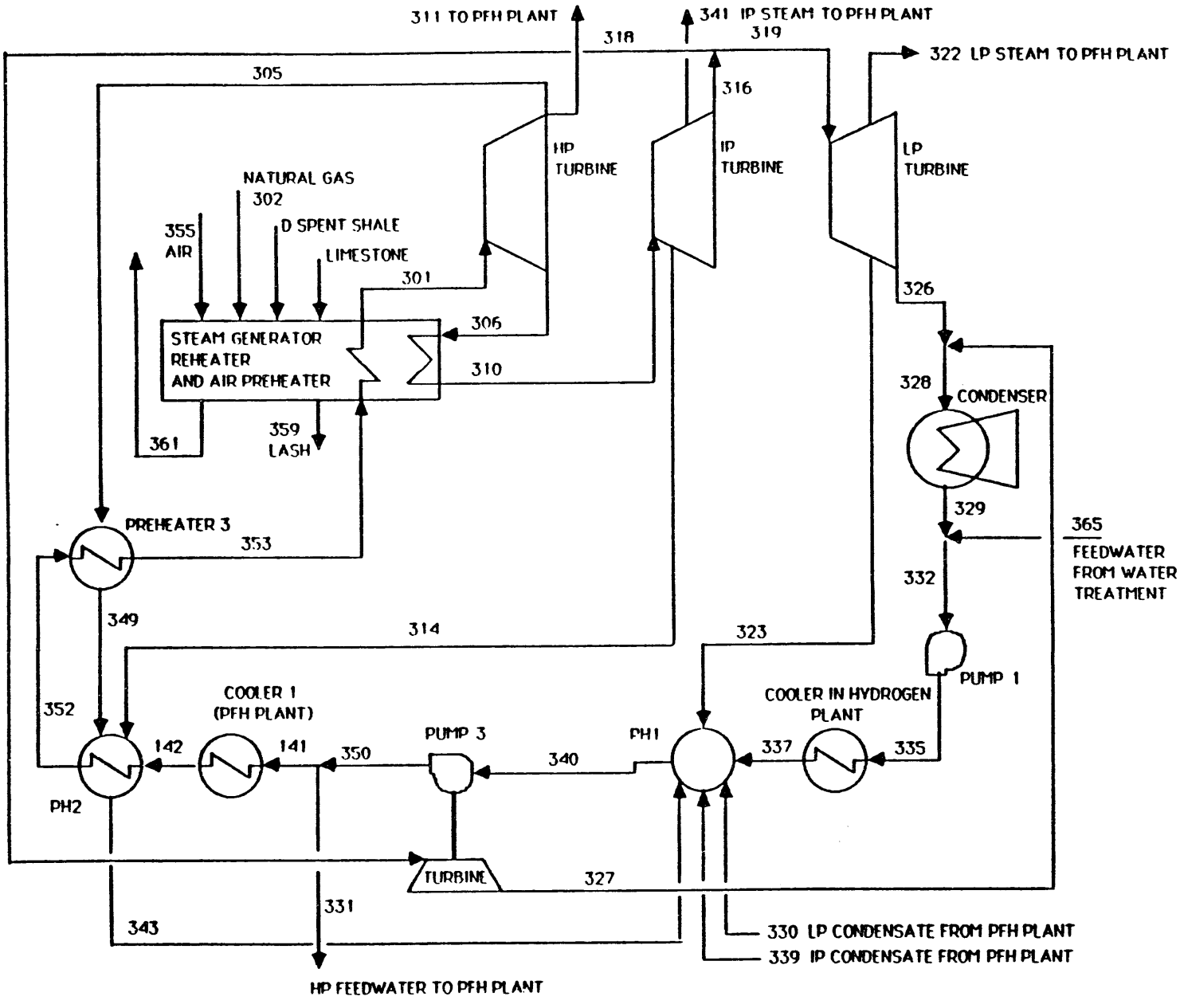

Figure 6-31. FLOW DIAGRAM OF THE POWER PLANT USED IN THE IMPROVED COMBINED PLANT

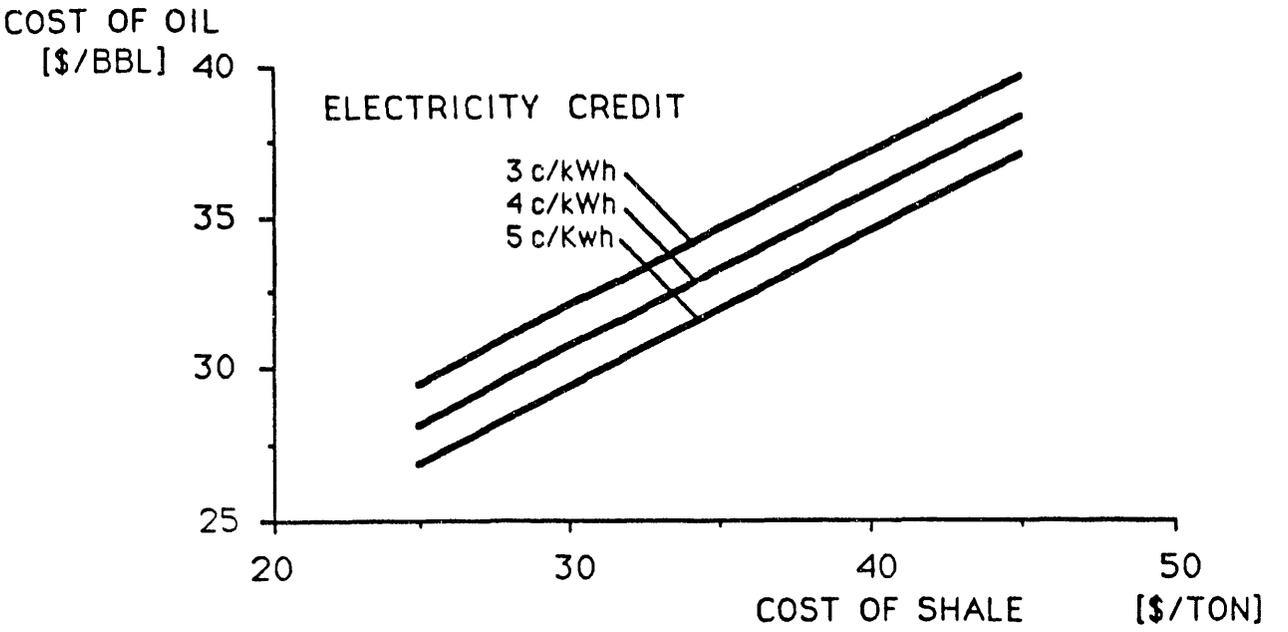

Figure 6-32. SENSITIVITY OF THE NET OIL COST TO CHANGES IN THE COST OF SHALE AND THE ELECTRICITY CREDIT FOR THE COMBINED PLANT IMPROVED DESIGN

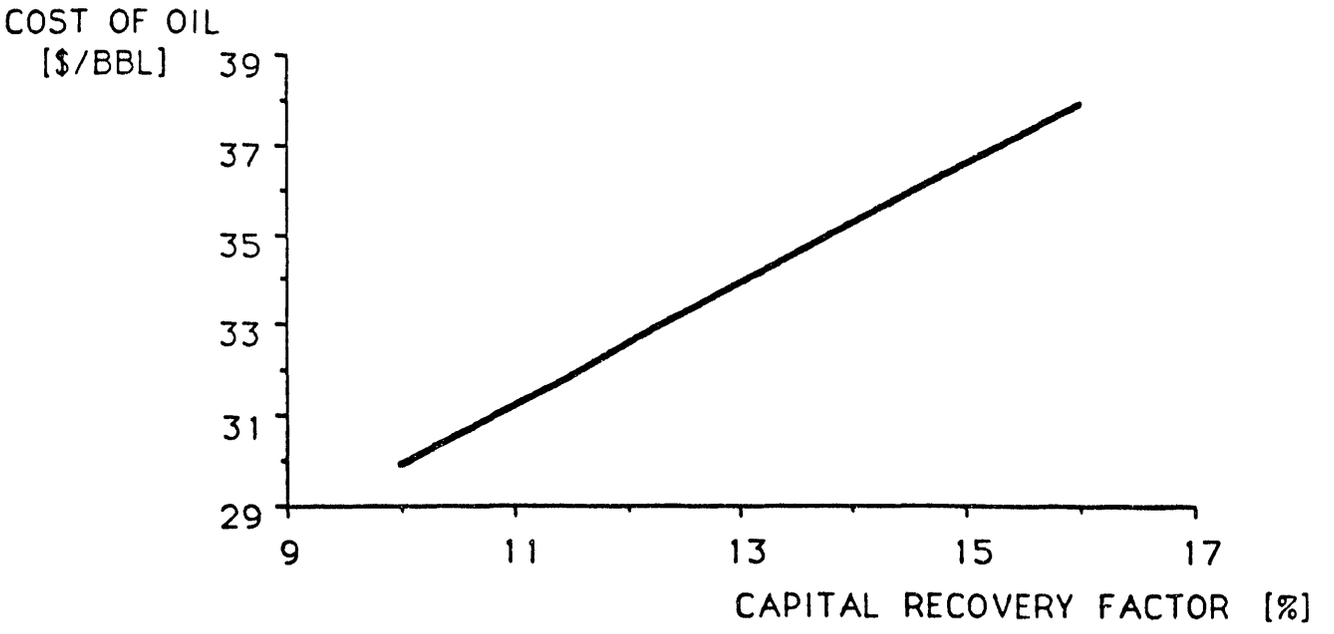

Figure 6-33. SENSITIVITY OF THE NET OIL COST TO CHANGES IN THE CAPITAL RECOVERY FACTOR FOR THE COMBINED PLANT IMPROVED DESIGN

c) the cost effectiveness of the recycle gas compressors would increase by increasing their efficiency,

d) changes in the heat exchanger network that aim at better matching the hot and cold streams and at avoiding cost ineffective exergy destruction result in a simpler and more cost effective overall design, and

e) the net oil cost is considerably reduced when the PFH plant is combined with a conventional steam power plant that uses the spent shale as its primary fuel.

Table 6-23. EXERGY DESTRUCTION FLOW RATE ($\dot{E}_D$), EXERGETIC EFFICIENCY (ϵ), COST RATE OF EXERGY DESTRUCTION ($\dot{D}_D$), AND THERMOECONOMIC VARIABLES r AND f FOR SELECTED GROUPS OF COMPONENTS OF THE COMBINED PLANT IMPROVED DESIGN (Figures 6-25, 6-29, 6-30 and 6-31)

Component Group	$\dot{E}_D$ MW	ϵ %	$\dot{D}_D$ $/h	r %	f %
Shale Retorting	180.1	98.2	1544	4.07	54.9
Gas Scrubbing	19.5	99.8	176	1.01	80.1
Acid Gas Removal	11.4	99.8	102	0.93	79.6
Sulfur Plant	17.8	0.0	0.0	0.00	100.0
Sour Water Stripper & NH_3 Recovery	27.1	0.0	0.0	00.0	100.0
Hydrogen Recovery	34.6	99.5	348	3.05	82.7
Compressor and Heat Exchangers	32.9	99.4	493	1.98	67.8
Steam Reformer	124.4	55.2	1325	356.15	77.2
Shift Conversion & CO_2 Removal	45.6	96.4	720	10.87	65.7
Desalting & Hydrotreating	72.1	98.3	759	7.80	77.9
Steam Generator	510.7	51.4	3408	131.77	28.3
HP Turbine	9.4	92.8	158	14.08	44.8
IP Turbine	9.7	92.9	163	13.99	45.3
LP Turbine	22.4	86.6	440	20.81	25.9
Condenser	47.9	---	---	---	---
Pump 1	0.0	75.9	1	204.70	84.5
Preheater in H_2 Plant	12.1	63.8	126	58.88	3.4
Deaerator	0.8	98.0	12	2.82	29.1
Pump 3 & Turbine	4.0	69.3	81	71.57	38.2
Preheater in PFH Plant	2.7	84.0	20	18.99	0.0
Preheater 2	2.8	88.7	46	13.85	8.1
Preheater 3	2.3	92.5	45	11.95	32.3

Table 6-24. COMPARISON OF EXERGY DESTRUCTION RATE ($\dot{E}_D$) AND COST RATE OF EXERGY DESTRUCTION ($\dot{D}_D$) BETWEEN ORIGINAL (Figures 6-22 and 6-23) AND IMPROVED (Figures 6-29 and 6-30) DESIGN FOR SELECTED PLANT COMPONENTS

	Original Design		Improved Design	
Component Group	$\dot{E}_D$, MW	$\dot{D}_D$, $/h	$\dot{E}_D$, MW	$\dot{D}_D$, $/h
Shale Retorting	217.8	2,004	180.1	1,544
Shift Conversion & CO_2 Removal	73.6	1,313	45.6	720
Compressor & Heat Exchangers	45.7	733	32.9	493
Steam Reformer	152.0	2,275	124.4	1,325

Table 6-25. PRODUCT COST SUMMARY FOR THE COMBINED PLANT IMPROVED DESIGN (Figures 13, 14 and 15, Constant 1990 Dollars)

	$/Bbl
Cost of Produced Oil	28.11
Costs of Utilities and Offsites	4.10
Operating Costs	5.65
Electricity Credit[a]	-5.27
Sulfur Credit	-0.39
Ammonia Credit	-0.40
Net Oil Cost	$31.81

a The electricity is generated at a cost of 3.71 ¢/kWh. Capital costs for this case are $2,222 million (1990 $).

Table 6-26. PRODUCT COST SUMMARY FOR THE COMBINED PLANT IMPROVED DESIGN (Figures 6-29, 6-30, and 6-31) INCLUDING THE WSA-SNOX[10] DESULFURIZATION PROCESS IN THE POWER PLANT (Constant 1990 Dollars)

	$/Bbl
Cost of Produced Oil	29.26
Costs of Utilities and Offsites	4.10
Operating Costs	5.65
Electricity Credit[a]	-5.27
Sulfur Credit	-0.39
Ammonia Credit	-0.40
Sulfuric Acid Credit	-2.16
Net Oil Cost	$30.80

a The electricity is generated at a cost of 4.35 ¢/kWh. Capital costs for this case are $2,377 million (1990 $).

The design improvements discussed here and the reduction in the net oil cost demonstrate the capabilities of the advanced thermoeconomic evaluation techniques applied in this subtask. The potential for further efficiency improvements and reduction in the net oil cost is still significant and should be investigated in future studies. Future work should focus, among others, on the following areas:

Hydrogen Plant

- A rigorous cost optimization of the design of the steam reformer and the shift conversion and CO_2 removal is expected to significantly increase the cost effectiveness of the overall process.

- The option of using pure natural gas in the stream 102 to be reformed, and using stream 92 (from hydrogen to recovery) directly for combustion purposes should be studied. This change should improve the conversion rate in the steam reforming reactor, and, thus, could reduce the investment costs associated with this reactor at constant hydrogen yield.

Acid Gas Removal

- The mass flow rate of stream 36 is less than 2 percent of the mass flow rate of stream 31. If streams 31 and 36 are mixed before the compressor the second acid gas stripper in the acid gas removal becomes redundant.

Heat Exchanger Network of the Combined Plant

- A thermoeconomic optimization of the total heat exchanger network would result in additional savings. The steam use in the lean oil stripper, acid gas removal, sulfur recovery, ammonia recovery and desalting and hydrotreating should be improved. TTU's calculations show that steam at a lower pressure than in the current design should be used in these components.

Electricity Generation

- The economics of electricity generation significantly affect the net oil cost. The optimal capacity of the power plant depends on the cost of generating electricity internally in the combined plant and on the electricity credit. Various options for generating electric power should be compared to determine the most cost-effective option.

PFH Plant Simulation

- A more flexible simulation of the performance of the PFH plant, which will use a more flexible calculation of the thermodynamic properties of the chemical substances involved in this plant and more detailed simulation subroutines for some plant components will facilitate identification of additional opportunities for reducing the net oil cost.

The thermoeconomic evaluation and optimization techniques discussed above are very powerful tools in identifying opportunities for cost savings and in suggesting the necessary design modifications to maximize the savings.

Nomenclature for Subtask 6.4.3

Symbol	Meaning
B	constant in cost equations, $\$/MW^m$
c	cost per exergy unit, \$/GJ
$\dot{D}$	cost flow rate, \$/h
$\dot{E}$	exergy flow rate, MMBtu/h
f	exergoeconomic factor denoting the contribution of the capital costs, Z, to the relative cost difference, r, between fuel and product in a plant component, %
F	variable expressing the criterion of exergoeconomic similarity, dimensionless
$\dot{H}$	enthalpy flow rate, MMBtu/h
I	investment cost, \$
m	capacity exponent in cost equations
$\dot{m}$	mass flow rate, lbm/h
n	efficiency exponent in cost equations
P	pressure, psia
$\dot{Q}$	heat transfer rate, MMBtu/h
r	relative cost difference between average cost per exergy unit of product and average cost per exergy unit of fuel, %
T	temperature, °F
$\dot{W}$	power, MW
y	ratio of exergy destruction (or exergy loss) to total exergy supplied to the plant, %
y^*	ratio of exergy destruction in a component to exergy destruction in the total plant, %
z	ratio of capital costs to product exergy in a heat exchanger, \$/MMBtu
Z	annual capital costs associated with a plant component, \$

Greek letters

β	capital-recovery factor, %
γ	coefficient expressing the part of the annual fixed operating and maintenance costs that depends on the net investment cost for a plant component, %
ϵ	exergetic efficiency, %
τ	annual number of hours of plant operation at the nominal capacity, h

Subscripts

D	exergy destruction
fuel	fuel to the total plant
F	fuel for a component or group of components (according to the definition of exergetic efficiency)
i	stream
in	streams entering a component or system
k	plant component
l	heat loss
L	exergy losses
OM	operation and maintenance
out	streams leaving a component or system
P	product of a component or group of components (according to the definition of exergetic efficiency)
tot	total plant

Superscripts

CH	chemical exergy
E	environmental exergy
OPT	optimum
PH	physical exergy
R	reaction exergy
TOT	total exergy
•	time rate of the corresponding variable

Subtask 6.4.4. Economics

The overall objectives of this task were to prepare a preliminary commercial-scale PFH process design, prepare an economic analysis based on this design, and perform sensitivity studies to evaluate the impact of changes in plant capacity, PFH operating conditions, by-product values and feedstock cost. This task was conducted by IGT.

Overall PFH Process Description

The preliminary commercial-scale PFH oil shale plant design was developed as a grassroots facility, capable of processing densified, beneficiated shale into a synthetic crude oil with a nitrogen content of 500 ppm and an API gravity of 32°. This design is based on the n^{th} plant design rather than a first-of-a-kind facility. The plant is sited in the Eastern U.S. adjacent to an oil shale surface mining facility and a shale beneficiation plant. Beneficiated shale, water, natural gas, and electric power were assumed to be available at the plant battery limits in sufficient quantity to supply process operating requirements. This plant design is a PFH-I configuration, which implies that hydrogen is produced by the conventional process of steam reforming of methane. Hydrogen can also be produced by cracking of methane as discussed in Task 3. This process is termed PFH-II and is expected to have a cost advantage over PFH-I in the production of synthetic crude oil.

Data for hydrogen production via methane cracking were not available when the commercial design was established for this task.

Costs for the beneficiated shale and the beneficiation processing were obtained as factored estimates from a previous study conducted by the engineering firm of Roberts and Schaefer (R & S).[1] The cost for the beneficiation process was adjusted to incorporate column flotation (found to be equivalent to 5 stages of conventional cell flotation) to replace the conventional flotation cells used in the R & S study and to reduce the number of regrind stirred ball mills. The beneficiation cost was also adjusted to delete the lignosulfonate binder (about 15 percent of the annual operating expense of the beneficiation plant) from the briquetting costs based on results of work conducted in Subtask 5.2 in which briquetted shale was prepared without binder and successfully tested in the BSU.

A FORTRAN computer program that simulates the operation of a PFH plant was used to estimate process plant capital and operating costs. The process data generated from this computer program forms the basis for defining the effluent streams and the process economics. The schematic diagram of a conceptual commercial PFH plant is shown in Figure 6-34.

Beneficiated shale (nominally sized to -1/8 inch) is pneumatically conveyed to gas lockhoppers and fed to the fluidized-bed retort. The retort is comprised of three fluidized beds: a preheat section, a retort section, and a cooling section. The shale is hydroretorted at 900°F and 600 psig (482°C and 4.2 MPa). The hydroretorted spent shale from the retort is conveyed to a combustor (fluidized-bed) to generate steam and power. Flue gas from the combustor is processed to remove sulfur dioxide via the WSA-SNOX[2] Process. This

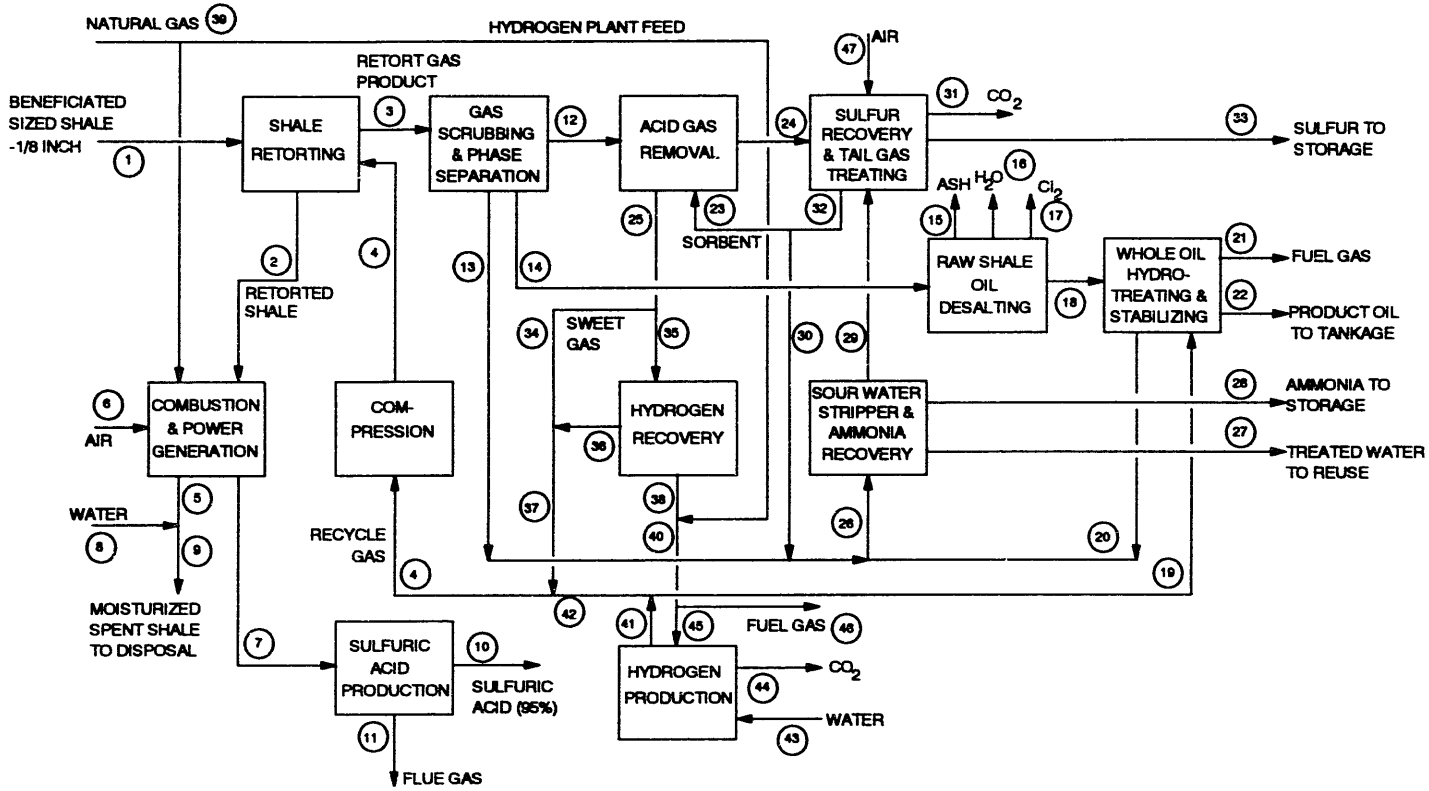

INLET STREAM FLOWS, ton/day

1	24,144	Beneficiated Shale
6	38,723	Air
8	894	Water
39	0	Natural Gas
43	3450	Water
47	1542	Air

OUTLET STREAM FLOWS, ton/day

9	9932	Ash (wet spent shale)
10	2161	Sulfuric Acid + Water
11	39,846	Flue Gas
15	0	Ash
16	0	H_2O
17	0	Cl_2
21	191	Fuel Gas (CH_4)
22	8115	Product Oil
27	1741	Water
28	281	Ammonia
31	1804	CO_2
33	299	Sulfur (S_2)
44	4214	CO_2
46	589	Fuel Gas (CH_4, C_2H_6)

INTERNAL STREAM FLOWS, ton/day

2	12,123	Retorted Shale
3	15,054	Retorted Gas Product
4	3033	H_2
5	9039	Combusted Shale
7	41,807	Combustion Product Gas
12	4856	Scrubber Product Gas
13	1712	Sour Water
14	8486	Raw Oil
18	8486	Clean Raw Oil
19	257	H_2
20	437	H_2S, NH_3, H_2O
23	S(1)	Sorbent
24	234 + S(1)	CO_2 + H_2S + Sorbent
25	4622	Sweet Gas
26	2149 + S(2)	H_2O + CH_4 + H_2S + NH_3 + S_2
29	127 + S(2)	H_2S + CH_4 + S_2
30	S(2)	S(2)
32	S(2) + S(1)	S(2) + Sorbent
34	1636	Sweet Gas
35	3988	Sweet Gas
36	948	H_2
37	2582	Recycle Gas
38	2040	CH_4
40	2040	CH_4
41	708	H_2
42	451	H_2
45	1471	CH_4

Figure 6-34. BLOCK FLOW DIAGRAM OF A COMMERCIAL-SCALE PFH PROCESS

process uses catalytic oxidation of sulfur dioxide to produce sulfuric acid, which is recovered as a by-product.

The retort gases are cooled and scrubbed with lean oil to remove product oil and water from the gas stream. The oil goes to a desalting unit to remove fine solids, and is subsequently hydrotreated, stabilized and sent to tankage. Sour water from both retorting and upgrading is stripped and reused. Ammonia is recovered by selective stripping. Scrubbed retort gases first go to acid gas removal, where H_2S and CO_2 are removed. These acid gases, together with sour gases from the ammonia recovery plant, are sent to sulfur recovery and tail gas treatment.

Sweetened retort gases are split; part is sent to a pressure-swing-adsorption (PSA) hydrogen recovery unit that recovers 97 percent of the hydrogen in the feed stream and the resulting product stream contains 98 percent hydrogen. The rest of the sweetened retort gas is compressed and recycled back to the retorts. The feed to the hydrogen recovery unit is set to maintain a 90 percent hydrogen purity in the recycle gas stream to the retorts. The tail gas from the hydrogen recovery plant is fed to the hydrogen production units, which produce sufficient hydrogen to satisfy the consumption requirements in the retorts and hydrotreaters. No purchased natural gas is required. Hydrogen is produced by conventional steam reforming of methane.

Process Design Data

The data used for the conceptual commercial-scale plant process design are based on results from mini-bench unit (MBU) tests. The MBU test results consist of retort processing conditions, and feed and product information, such as oil quality and yields. The raw MBU test data were reconciled to 100 percent overall and elemental (carbon, oxygen, sulfur, nitrogen and hydrogen) material balances. Basically, the raw gas yield is adjusted first to contain hydrocarbons only up to butane. The gas, oil and sour water yields, and hydrogen consumption are further adjusted to obtain the overall material and elemental closures. Combusted hydroretorted shale data and analyses are also based on MBU test data. The analyses of raw beneficiated, hydroretorted, and combusted Kentucky New Albany shale used for this conceptual commercial design are shown in Table 6-27. The analyses of raw and upgraded shale oil are shown in Table 6-28.

Simulation of PFH Process

The conceptual commercial-scale PFH retort is designed based on 500 tons per hour (454 metric t/h) capacity beneficiated feed, shop fabricated with 10 feet 4 inch (3.15 meter) ID refractory, operating at a shale mass flux of 12,500 lb/h-ft^2 (16.95 kg/s-m^2). The hydrotreater simulation is based on limited pilot plant test results for an oil with similar composition. Chemical hydrogen consumption (1930 SCF/bbl) for the hydrotreating operation is from data based on reducing the nitrogen content in the raw shale oil to 500 ppm in the hydrotreated product oil. The mechanical loss of hydrogen is assumed to be 5 percent of the chemical hydrogen consumption.

Table 6-27. BENEFICIATED KENTUCKY NEW ALBANY SHALE COMPOSITIONS

Component	Feed	Hydroretorted	Combusted
		wt %	
Ash	38.67	73.52	98.73
Organic Carbon	45.72	17.08	0.23
Organic Hydrogen	4.08	0.73	0
Sulfur	4.55	6.41	0.77
Nitrogen	1.28	0.75	0.11
Oxygen (high temp. water)	5.06	1.34	0.14
Hydrogen (high temp. water)	0.64	0.17	0.02
Total	100.00	100.00	100.00
Gross Calorific Value, Btu/lb	9104	3380	~10
Weight, lb	100.00	52.60	39.18

Conversions (Ash Balance), wt %	Hydroretorting	Combustion
Organic Carbon	80.4	99
Organic Hydrogen	90.5	100
Sulfur	25.9	91
Nitrogen	69.2	90
Oxygen (HTW)	86.1	92
Hydrogen (HTW)	86.1	92
Overall Conversion	47.4	25.5

Assume ash is inert in both reactors:
Hydroretorting - 950°F, 600 psig H_2, 5-minute residence time
Fischer Assay - 50.2 GPT, PFH Yield - 88.6 GPT
Combustion - 1600°F, 50 psig, 20% excess air, 5-minute residence time

All other unit operations, such as gas scrubbing and phase separation, acid gas removal, hydrogen recovery, hydrogen production, sulfur recovery, and ammonia recovery plants, are based on conventional process technologies. For example, 99.9 percent of sulfur to the sulfur recovery and tail gas cleaning units is assumed to be recovered using the Claus and SCOT combined process. For the sour water stripping and ammonia recovery operations, the treated water is assumed to contain 50 ppm NH_3 and 10 ppm of H_2S based on the use of the Chevron WWT process.

Economics of the PFH Process

IGT modified the economics subroutines developed previously by Bechtel Group, Inc. and integrated them into the PFH process simulation computer program. Based on the heat and material balances from the process simulations, the economics subroutines are used to estimate the capital and operating costs for a PFH plant with a nominal capacity of 50,000 BPD of raw shale oil, and to calculate the product oil cost in terms of dollars per barrel of hydrotreated oil.

Table 6-28. CHEMICAL ANALYSIS OF THE RAW AND HYDROTREATED OIL FROM THE PFH PROCESS

	Raw Oil	Hydrotreated Oil*
Ultimate Analysis, wt % (dry and solids-free basis)		
Carbon	84.13	86.23
Hydrogen	10.01	12.32
Sulfur	0.93	20 ppm
Nitrogen	1.99	70 ppm
Ash	0.00	0.00
Oxygen (by difference)	2.94	<0.1
C/H Weight Ratio	8.40	7.00
Viscosity, SSU at 100°F	101.4	--
Specific Gravity (60/60°F), g/mL	0.969	0.890
API Gravity, °API	14.5	32
Gross Calorific Value, Btu/lb	17,744	--
Pour Point, °F	-5	--

* Carbon and hydrogen values are calculated, whereas analyses were performed to determine sulfur, nitrogen, and oxygen.

The product oil cost is calculated from four principle components: capital cost, operating cost, utility cost and shale cost. By-product credits are assigned to the sulfur and ammonia recovered from the sour gas streams exiting the retorts. Credits are also generated from the production of surplus power and sulfuric acid from the flue gas from the power plant. The process plants portion of the capital cost is derived from the areas of the conceptual PFH plant as follows:

Area 1. Feed Preparation
Area 2. Shale Retorting
Area 3. Gas Scrubbing and Phase Separation
Area 4. Acid Gas Removal
Area 5. Hydrogen Recovery and Compression
Area 6. Hydrogen Production
Area 7. Claus Sulfur Recovery and SCOT Tail Gas Clean-up
Area 8. Sour Water Treatment and Ammonia Recovery
Area 9. Raw Oil Desalters
Area 10. Hydrotreaters

The capital costs for Area 2 (Retorting) and Area 3 (Gas Scrubbing and Phase Separation) are based on estimates of specific pieces of equipment by using the Questimate™ System from ICARUS, a software system designed to produce estimates for plant renovation and design. This approach was taken to better estimate the costs involved in the relatively unconventional portions of a proposed PFH facility. All vessel and system designs are considered obtainable with present technology. All other plant areas are considered to be of conventional technology and their capital costs are factored based on

capacity using Bechtel economic data from a previous cost estimate done for a hydroretorting plant for HYCRUDE Corporation. Costs for the fluidized-bed combustor and power generation as well as the sulfuric acid plant were estimated based on a report by Foster Wheeler entitled "Topical Report - Fluidized Bed Retorting of Eastern Oil Shale."

The utilities and offsites portion of the capital cost is factored from the total process plant cost and the utility requirements. This portion of the capital cost also contains some fixed amounts for items such as tankage, loading facility, site preparation, etc., which are based on a 50,000 BPD facility. A typical summary of capital costs and the basis for making estimates is shown in Table 6-29.

The operating costs are estimated on a percentage of total fixed capital cost plus other miscellaneous costs derived from previously reported data. The utility cost is based on the amount of raw water and natural gas imported to the plant. A typical summary of annual total operating cost, including the utility costs, is shown in Table 6-30. In terms of mid 1990 dollars, the cost of run-of-mine (ROM) shale is assigned at $4.00/ton; the by-product credits for sulfur and ammonia are assigned at $70/long ton and $150/short ton, respectively. Credit for sulfuric acid is $70/short ton. Surplus power is sold for $0.0435/kWh.

Sensitivity analyses for by-product credits, shale cost, capital recovery, and beneficiation are shown in Table 6-31. A $20/ton change in the price of sulfuric acid changes the oil cost about $1 per barrel. The price of sulfur and anhydrous ammonia has much less an effect on the oil cost. Doubling the price of sulfur from $70 to $140/ton only changes the oil cost (credit) by $0.36 per barrel. Doubling the selling price for anhydrous ammonia from $150 to $300/ton increases the credit for ammonia by $0.81 per barrel. A change of 1 percent in the capital recovery charge changes the cost of oil by about $1 per barrel. The cost of oil is very sensitive to the cost of the ROM shale in the analysis. A $1 change in the ROM shale cost causes a $1.80/bbl change in the cost of oil. This is because it takes about 3-2/3 tons of ROM shale to produce 1 ton of beneficiated shale and each ton of beneficiated shale produces about 2 barrels of oil.

The price of oil is also sensitive to the price at which the surplus power generated from the shale combustion in the form of electricity is sold. A 1¢/kWh change in the price of surplus power sold causes about $1.25 change in the price of oil.

Since the plant is modular, there is only a modest increase in oil cost when the plant size is reduced from 50,000 to 25,000 bbl/day.

Figure 6-35 shows the effects of temperature and pressure on oil yield for hydroretorting Kentucky New Albany shale. The base case used 176 percent of Fischer Assay at 600 psig. The oil yield is sensitive to hydrogen pressure, but not as sensitive to temperature over the range shown in the figure.

Table 6-29. CAPITAL COSTS AND ESTIMATE BASIS FOR A CONCEPTUAL COMMERCIAL-SCALE PFH PLANT

Feedstock: Beneficiated Kentucky New Albany Shale	Capacity, BPSD*	Basis for Cost Estimate
CAPITAL COSTS, MILLIONS (mid 1990 dollars)	52,080	
PROCESS PLANTS		
Shale Crushing and Screening	0	Beneficiated Feed
Retorting	122.0	2 retort modules, at 520 ton/hour/module
Gas Scrubbing and Phase Separation	50.4	2 trains with each train at 50% capacity
Acid Gas Removal	44.0	2 trains with each train at 50% capacity
Hydrogen Recovery and Compression	104.1	3 PSA units with each unit at 33% capacity
Hydrogen Production	310.0	3 reformers and 4 PSA units
Sulfur Recovery and Tail Gas Plants	53.0	2 Claus plants and 1 SCOT plant
Sour Water Stripper and Ammonia Recovery	34.5	1 train at 100% capacity
Raw Shale Oil Desalting	15.1	1 train at 100% capacity
Hydrotreating	100.0	1 train at 100% capacity
Subtotal - Process Plants	833.1	
OFFSITE AND UTILITY PLANTS		
Initial Catalysts and Chemicals	26.3	allowance
Relief and Blowdown	6.6	0.79 of total process plants capital cost
Tankage	21.0	allowance
Interconnecting Piping	131.2	15.75% of total process plants capital cost
Loading Facilities	21.0	allowance
Solid Waste Handling	10.5	allowance
Electrical Distribution	61.8	proportional to total kW distributed
Steam and Power Generation	30.4	proportional to total steam distributed
Water Systems	33.2	linearly proportional to CW circulation
Fire Protection	3.2	0.39% of total process plants capital cost
Sewers and Effluent Treatment	8.2	0.98% of total process plants capital cost
Access Road and Railroad	31.5	allowance
Site Preparation and Improvements	99.8	allowance
Buildings	31.5	allowance
Mobile Equipment	5.3	allowance
Water Supply	42.0	allowance
Subtotal - Offsite and Utility Plants	563.5	
Total Capital Cost	1396.6	

* Based on upgraded shale oil.

Table 6-30. PFH OIL SHALE COST ANALYSIS

Operation:	330 day/year
Plant Life:	25 years
Production Rate:	52,080 barrel/day

Capital Costs	$ million	$/bbl
Process Plant	833.1	6.22
Power Plant	375.0	2.80
Sulfuric Acid Plant	155.0	1.16
Utilities and Offsites	563.1	4.20
Total	1926.2	14.38
Annual Costs and Credits		
Operating Costs	110.8	6.72
Utility Costs	86.5	5.24
Shale Costs	277.4	16.81
Byproduct Credits	-163.8	- 9.53
	310.9	19.24
Summary, $/barrel		33.62

Background Information

Sulfuric Acid	$70/ton
Elemental Sulfur	$70/Long ton
Anhydrous Ammonia	$150/ton
Electricity	$0.0435/kWh
Capital Recovery Charge	11.5%

By-Product Credits	Annual Production Cost, $	$/bbl
Sulfuric Acid (95% 2161 t/d)	54,207,000	3.15
Elemental Sulfur (267 Lt/d)	6,165,000	0.36
Anhydrous Ammonia (253 t/d)	12,518,000	0.73
Exported Power (264 MW)	90,950,000	5.29
		9.53

Shale Costs

ROM Shale	$4/ton
Beneficiated Shale	$14.63/ton
Beneficiation Cost	$19.13/ton

Table 6-31. SENSITIVITY ANALYSES

Sulfuric Acid:	$/ton	$/bbl
	90	32.65
	70*	33.62
	50	34.59
	25	35.80
Electricity:	¢/kWh	
	6	31.50
	5	32.79
	4.35*	33.62
	4	34.07
	3	35.36
	2	36.64
Capital Recovery Charge:	%	
	25	48.01
	20	42.69
	16	38.46
	15	37.35
	14	36.28
	13	35.19
	12	34.14
	11.5*	33.62
	11	33.10
	10	32.07
ROM Shale Cost:	$/ton	
	3	31.77
	4*	33.62
	5	35.47
	6	37.31
	7	39.17
Beneficiated Shale Cost:	$/ton	
	17	32.54
	18	33.05
	19.13*	33.62
	20	34.07
	21	34.57
	22	35.07
	23	35.58
	24	36.09
Plant Size:	bbl/d	
	50,000*	33.62
	25,000	38.25

* Base Case

A capital recovery factor of 0.115 is used. A plant life of 25 years is assumed with an on-stream factor of 90 percent.

The commercial PFH plant, including electric power generation via combustion of hydroretorted shale, is an attractive option to reduce the cost of syncrude production. Since there is a considerable amount of electric power generated as well as chemicals produced, the integrated plant resembles a combination of petroleum refinery, chemical plant, and a power generating station. Such a facility needs to be sited by a suitable shale deposit and beneficiation plant, and where a large base load of electric power, as well as sulfur, sulfuric acid, and ammonia by-products, can be marketed.

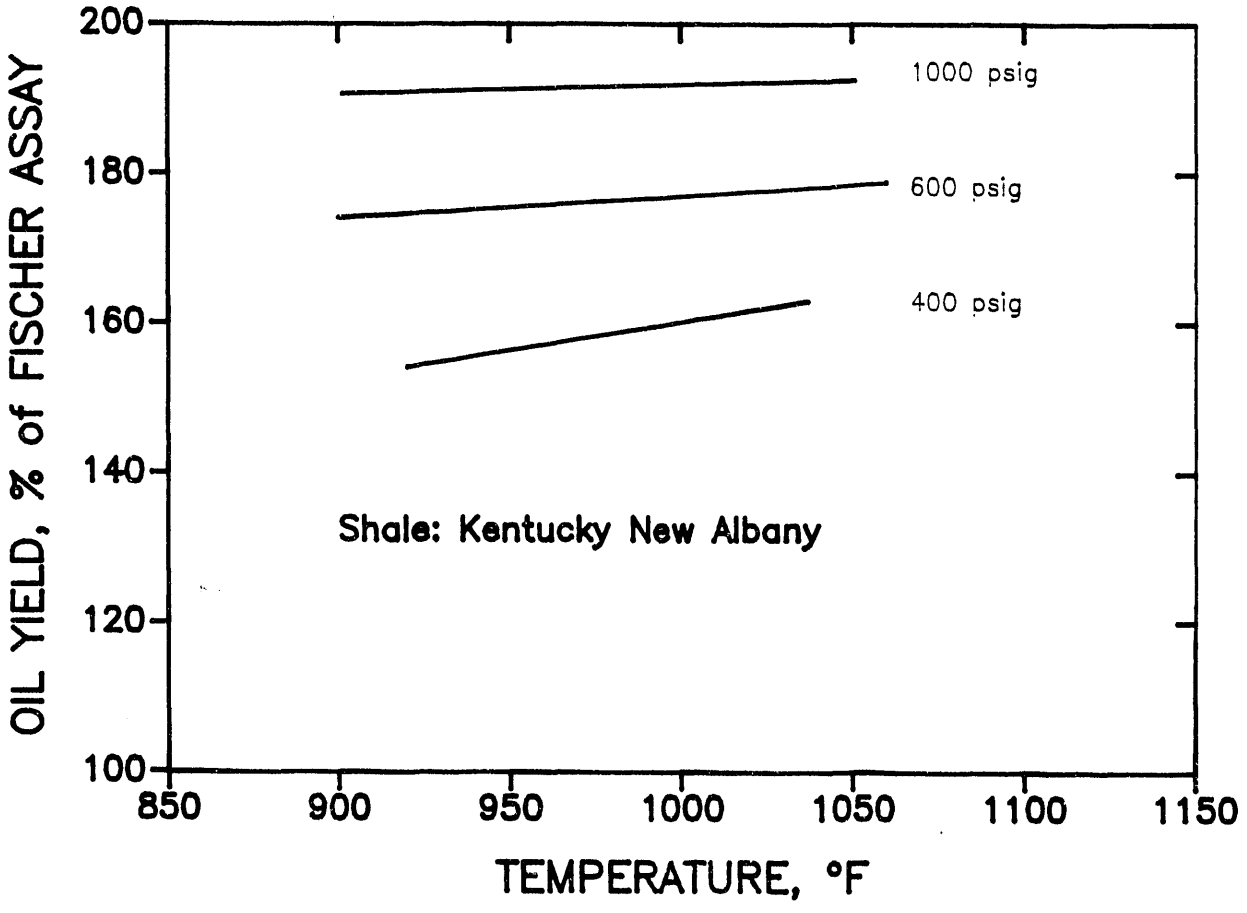

Figure 6-35. EFFECTS OF TEMPERATURE AND PRESSURE ON PFH OIL YIELDS

Task 7. Sample Procurement, Preparation, and Characterization

The objectives of this task were to procure, prepare, and characterize raw and beneficiated Eastern oil shale samples for all of the experimental tasks of the program extension. This task was conducted by the Mineral Resources Institute (MRI) at the University of Alabama.

About 9 tons of Alabama shale were excavated for MRI in June 1991 by the Ashburn & Gray Division of APAC-Alabama (Huntsville) from a specific site in Madison County, Alabama. This site had been previously sampled for MRI shale beneficiation studies. Six tons of shale were shipped to Michigan Technological University (MTU, Houghton) for crushing, grinding and column cell flotation studies. Three tons of shale were shipped to MRI for sample preparation and characterization as well as studies to be conducted by the University of Kentucky Center for Applied Energy Research (UK-CAER).

The 6-ton sample sent to MTU was crushed to pass 5/8 inches and a representative sample was sent to MRI for flotation testing to develop correlations between the oil and carbon contents and density to facilitate column cell flotation operating results at MTU. Analysis of this sample showed that it was lower in Fischer Assay (FA) oil yield than other samples from the same area. Visual inspection revealed contamination by rock components not previously seen in samples from this area. Some contamination may be due to the sample extraction technique used (a large backhoe). Previous samples had been essentially hand loaded after blasting and breaking.

The 3-ton sample shipped to MRI was subsequently hand picked and screened on 4 mesh to remove rock and mud. About 600 pounds of the -4 mesh shale was shipped to UK-CAER to be used in column cell flotation studies.

Chemical analyses of the shale samples sent to MTU, MRI, and UK-CAER are compared in Table 7-1. The results show differences in either the samples or the analytical techniques utilized.

Three bench-scale mechanical cell flotation tests were conducted at MRI using grinding times of 30, 60, and 120 minutes to develop oil and carbon content and density correlations. The feedstock for the rod mill was -10 mesh shale. The mechanical cell flotation tests were conducted to yield a series of products of differing oil and carbon contents and density values without regard to kerogen recovery. Selected results of the flotation tests are shown in Table 7-2. The data show that the sample sent to MTU, while somewhat lower in oil content, would respond to flotation in the same manner as all previous samples taken from the same area. The data also show the previously determined relationship of reduction in oil content with size of grind as well as an increase in density with size of grind.

Figures 7-1 and 7-2 present the density and carbon, and carbon and oil correlations based on linear relationships, respectively, which were developed in the bench scale mechanical cell flotation studies of the MTU sample.

Table 7-1. ANALYSES OF THE ALABAMA OIL SHALE SAMPLES SENT TO MTU, MRI, AND THE UK-CAER

Sample	MTU	MRI	UK-CAER
Proximate Analysis, wt %			
Moisture Content	NA*	1.18	1.36
Fixed Carbon	NA	NA	9.2
Volatile Matter	NA	15.80	14.87
Component, wt %			
Carbon	13.27	15.11	16.46**
Hydrogen	1.59	1.78	NA
Nitrogen	0.47	0.41	NA
Sulfur	7.19	8.15	8.20
Ash	77.28	74.57	72.8
Fischer Assay, GPT	10.5	12.0	14.6

* Not analyzed.
** Organic carbon content.

The objectives of the beneficiation studies of the 6-ton sample sent to MTU were to 1) conduct continuous grinding and column cell flotation studies of the sample, 2) compare the results of treating the ground oil shale in two distinctly different types of column flotation cells, and 3) produce about one ton of flotation concentrate for subsequent PFH studies at IGT. Figure 7-3 shows the flowsheet used at MTU to conduct continuous grinding and column cell flotation studies. Size analysis of selected products from the flowsheet are given in Table 7-3.

Table 7-3. SIZE ANALYSIS OF SELECTED PRODUCTS FROM MTU CONTINUOUS FLOTATION STUDIES

Size Analysis	Rod Mill Feed	Drais Mill Feed	Drais Mill Discharge
	wt %		
-5/8+1/4 inch	54.8	--	--
-1/4+Pan	45.2	--	--
+200 mesh	--	21.7	--
-200+400	--	14.8	--
-400+Pan	--	63.5	--
d_{90}, μm	--	--	12
d_{50}, μm	--	--	4

Table 7-2. FLOTATION TEST RESULTS USED TO DETERMINE OIL:CARBON:DENSITY CORRELATIONS ON MTU SAMPLE

Grinding time, min	Size, μm d_{90}	Size, μm d_{50}	Flotation Product	wt %	FA GPT	Analysis, % C	Analysis, % H	Analysis, % N	Analysis, % S	Density g/mL	Distribution, % Oil	Distribution, % C	Distribution, % H	Distribution, % N	Distribution, % S
			C3 Conc.	40.6	21.3	23.78	2.50	0.67	13.10	2.17	81.3	75.9	67.1	64.8	72.0
30	37.1	12.1	M1-3	33.1	5.2	7.19	1.04	0.29	4.41	2.56	16.3	18.7	22.6	23.3	19.7
			Tailings	26.3	1.0	2.59	0.59	0.19	2.32	2.78	2.4	5.4	10.3	11.9	8.3
			Composite	100.0	10.6	12.72	1.51	0.42	7.39	2.47	100.0	100.0	100.0	100.0	100.0
			C4 Conc.	28.2	26.5	30.13	3.07	0.91	15.11	2.06	69.6	65.2	56.6	58.3	57.4
60	23.7	8.1	M1-4	42.6	6.9	8.96	1.19	0.32	5.67	2.58	27.4	29.3	33.1	30.4	32.5
			Tailings	29.2	1.1	2.44	0.54	0.17	2.56	2.79	3.0	5.5	10.3	11.3	10.1
			Composite	100.0	10.8	13.03	1.53	0.44	7.42	2.49	100.0	100.0	100.0	100.0	100.0
			C4 Conc.	18.3	32.4	37.80	3.79	1.08	15.53	1.87	65.5	55.3	46.1	48.7	39.2
120	16.7	6.1	M1-4	45.3	6.4	10.45	1.35	0.40	7.00	2.53	32.1	37.8	40.6	45.0	43.7
			Tailings	36.4	0.6	2.37	0.55	0.07	3.40	2.83	2.4	6.9	13.3	6.3	17.1
			Composite	100.0	9.0	12.52	1.50	0.41	7.25	2.53	100.0	100.0	100.0	100.0	100.0

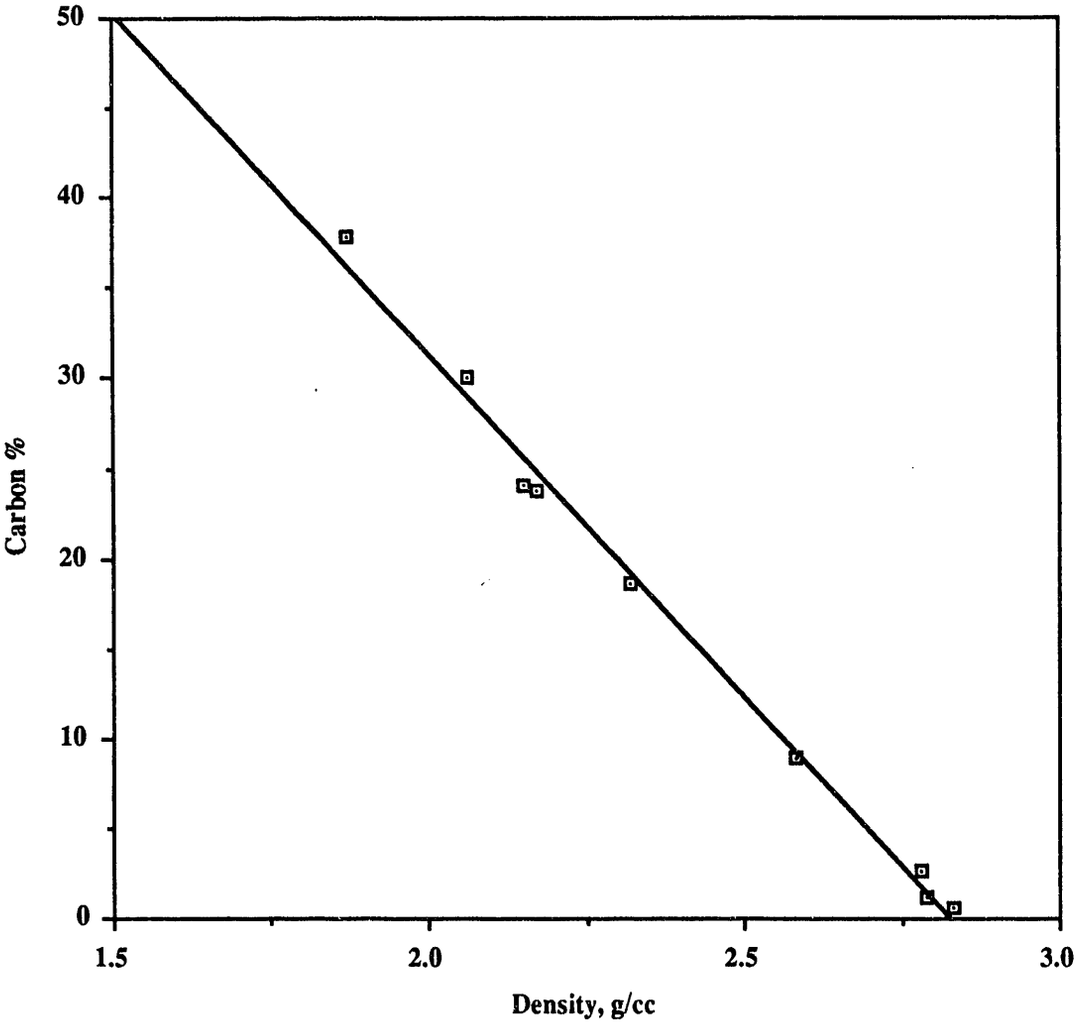

Figure 7-1. MRI CARBON CONTENT:DENSITY CORRELATION
(Mechanical Cell Flotation, MTU Sample)

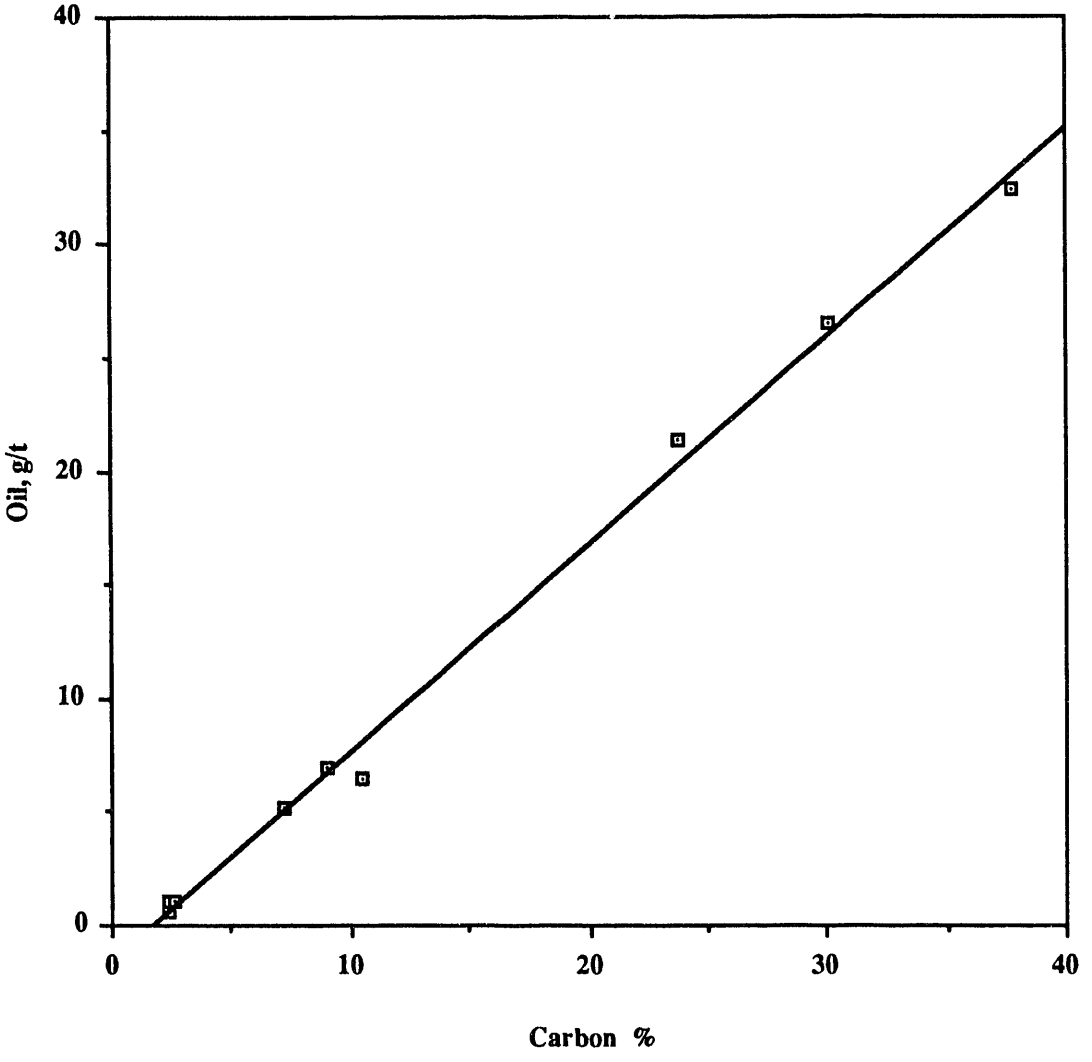

Figure 7-2. MRI FISCHER ASSAY OIL YIELD:CARBON CORRELATION
(Mechanical Cell Flotation, MTU Sample)

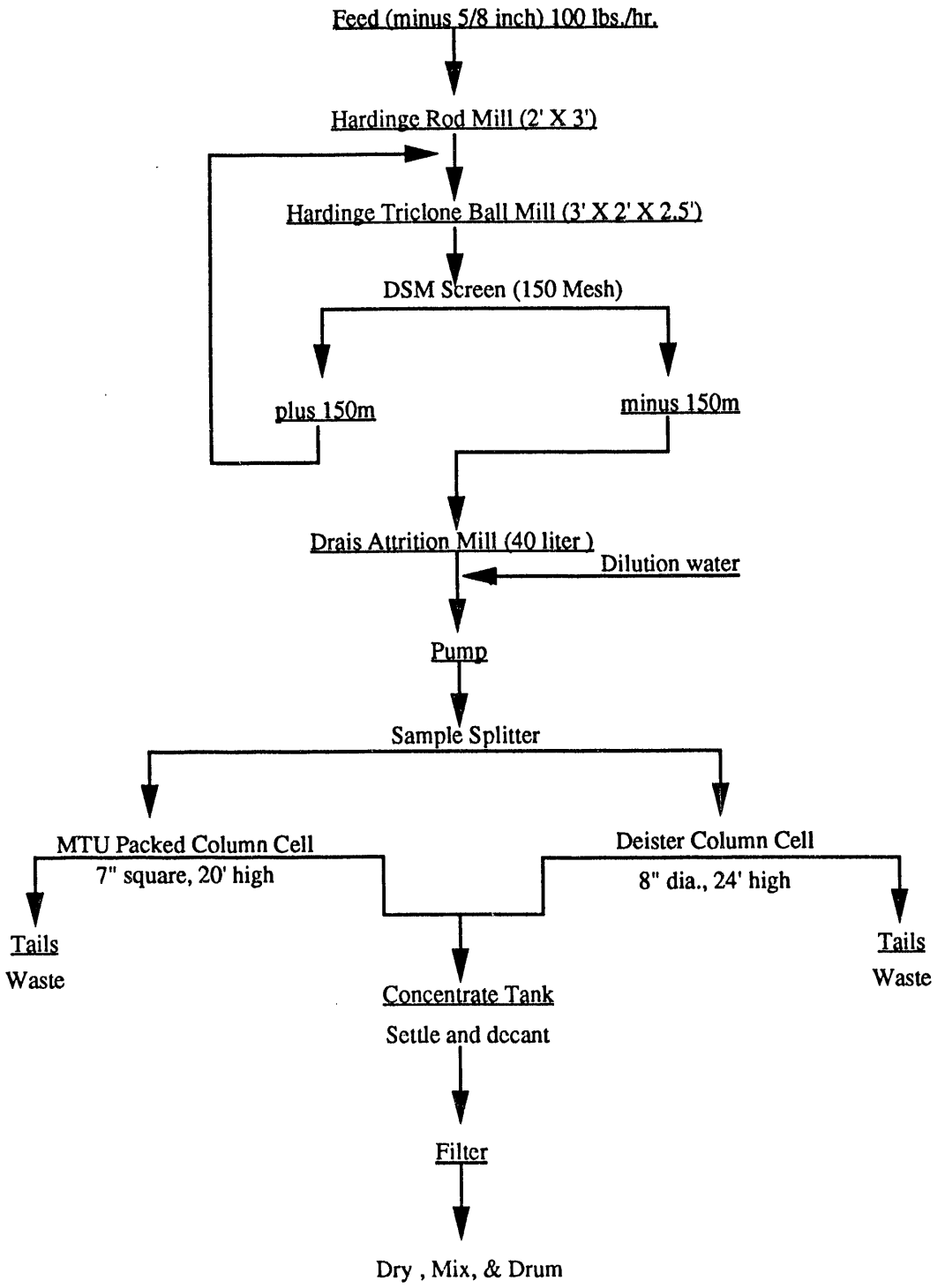

Figure 7-3. FLOWSHEET FOR CONTINUOUS PROCESSING OF ALABAMA OIL SHALE AT MTU

Other average operating conditions for the flowsheet shown in Figure 7-3 are given in Table 7-4.

Table 7-4. AVERAGE OPERATING CONDITIONS FOR MTU GRINDING AND FLOTATION TESTS

Mill Discharges, wt % solids	
Rod	57
Ball	58
Drais	36
Column Cell Feed	5
Dowfroth 250, lb/ton	2.5

MTU personnel monitored the daily production from the two distinctly different column flotation cells by utilizing density measurements of the products. All samples taken during the pilot plant campaign were returned to MRI for analysis. Selected MTU samples, based on high, medium, and low density values, were analyzed for total carbon, hydrogen, nitrogen, and sulfur content.

A comparison of the carbon-density correlations developed from the MRI mechanical cell data and the MTU continuous pilot plant campaign is shown in Figure 7-4. These data indicate some slight differences in the two samples; however, these differences may be the result of the significant differences in the grinding size. The MRI plots were generated from material ground to a d_{90} in the range of 36 to 17 μm; whereas, the MTU column cell feed had an average d_{90} of 12 μm.

The significant differences in the sulfur content of the concentrates (13 to 15 percent sulfur) generated in the MRI mechanical cell studies of the MTU sample and those obtained in column cell concentrates (<9.8 percent sulfur) at MTU can also be attributed to the initial grind size. Studies at MRI have shown that mechanical cell flotation feeds ground to a d_{90} of 11 μm typically yield concentrates containing 7 to 8 percent sulfur, an indication of pyrite liberation with fineness of grind.

Table 7-5 gives a summary of the MTU column cell flotation results based on density analyses of samples taken on a daily operating basis, as well as the calculated concentrate yield from the individual column cell.

Table 7-6 shows the average materials balance results of the MTU packed column cell and the Deister column cell based on oil-carbon-density correlations generated in the MRI mechanical flotation cell studies.

Total concentrate production from the MTU pilot plant campaign amounted to 1500 pounds. After drying and sampling, this bulk concentrate had the analysis given in Table 7-7.

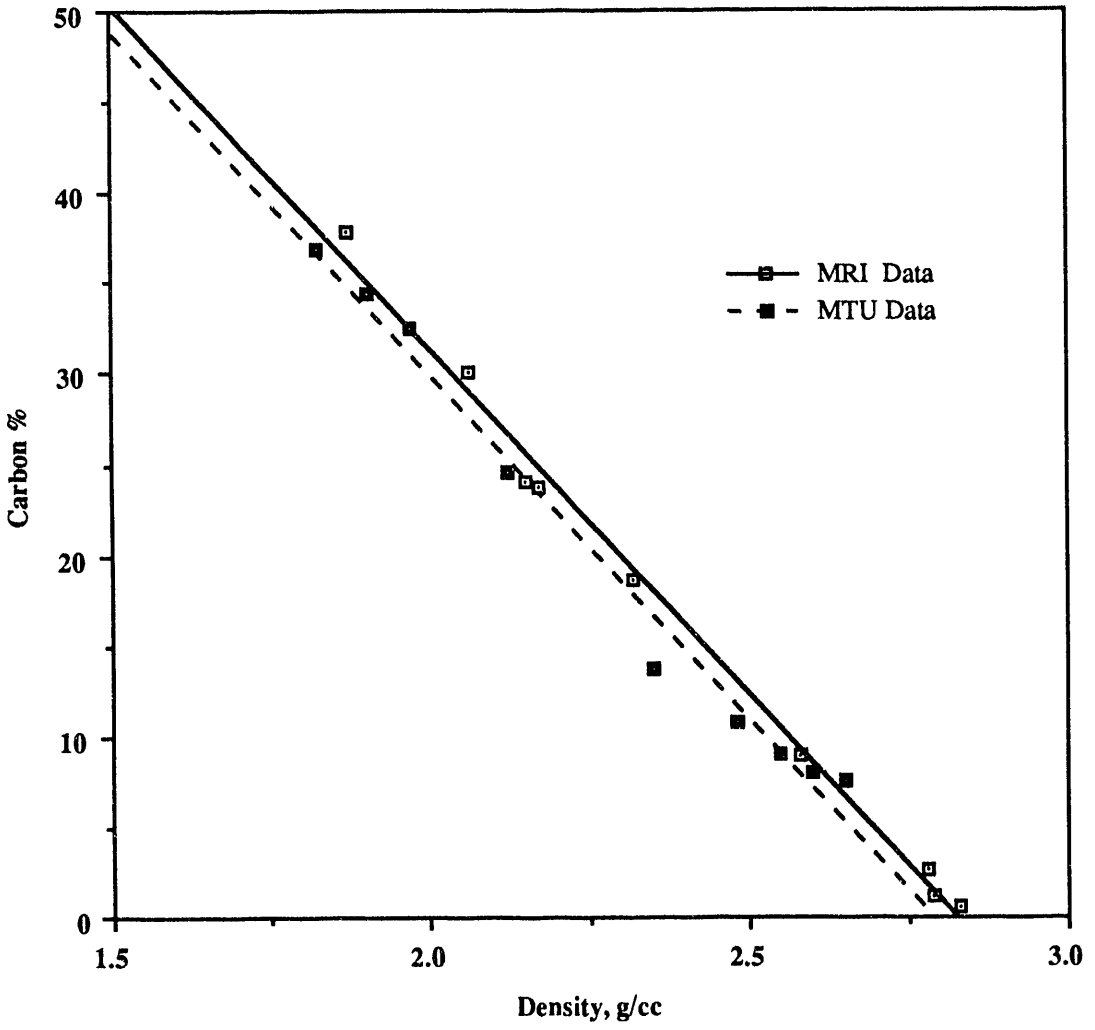

Figure 7-4. COMPARISON OF MRI AND MTU CARBON CONTENT:DENSITY CORRELATIONS

Table 7-5. SUMMARY OF MTU FLOTATION RESULTS BASED ON SAMPLE DENSITY ANALYSES

Product	Number of samples	Density, g/cm^3			Concentrate, wt %		
		Avg.	High	Low	Avg.	High	Low
Column Cell Feed	11	2.41	2.46	2.35	--	--	--
Mtu Cell							
Concentrate	12	1.79	1.92	1.62	20.5	26.0	15.1
Tails	12	2.57	2.65	2.48	--	--	--
Deister Cell							
Concentrate	13	2.00	2.12	1.97	22.6	34.6	13.5
Tails	13	2.53	2.64	2.49	--	--	--
Final Concentrate	10	1.90	1.97	1.82	--	--	--

Table 7-6. AVERAGE MATERIAL BALANCES FOR THE MTU PACKED COLUMN CELL AND THE DEISTER COLUMN CELL

Cell	MTU Packed Column			Deister Column		
Sample	Feed	Conc.	Tails	Feed	Conc.	Tails
Distribution, wt %	100	20.5	79.5	100	22.6	77.4
Oil	100	55	45	100	50	50
Carbon	100	52	52	100	47	53
Fischer Assay, GPT	12.4	33.5	7.0	11.7	26.0	7.0
Carbon Content, wt %	14.6	38.0	9.0	14.9	30.5	10.0

Table 7-7. ANALYSIS OF HEAD SAMPLE OF TOTAL CONCENTRATE PRODUCED AT MTU

Analysis, wt %	MTU Conc.
Carbon	30.65
Hydrogen	3.33
Nitrogen	1.03
Sulfur	8.46
Density, g/cm^3	1.99
Fischer Assay, GPT	25.4

ACKNOWLEDGMENTS

IGT acknowledges the significant work being conducted on this project by the individual subcontractors, their principal investigators, and colleagues -

MRI:	Dr. C. W. Schultz
UK-CAER:	Dr. B. K. Parekh
UN:	Professor M. Misra
TTU:	Professor W. P. Bonner

REFERENCES

Please Note: The references are arranged by numerical order in each report section or subtask as indicated below.

Executive Summary

1. "Pressurized Fluidized-Bed Hydroretorting of Eastern Oil Shales," Final Report for the Period September 1987 throught May 1991 in four volumes, DOE Contract No. DE-AC21-87MC11089, Report No. 11089-47 through -50, March 1992.

Subtask 3.8

1. Plancher H., Miyake G., Venable R. C. and J. C. Petersen J. C., Proceedings of the Can. Tech. Asphalt Assn., 25, pp. 246-262, 1980.

2. Plancher H., Miyake G. and J. C. Petersen, Proceedings of the 13th Oil Shale Symposium, 13, pp. 261-268, Golden, CO, 1980.

Subtask 4.1.4

1. "Pressurized Fluidized-Bed Hydroretorting of Eastern Oil Shales," Final Report for the Period September 1987 throught May 1991, Volume III (Task 4), DOE Contract No. DE-AC21-87MC11089, Report No. 11089-49, March 1992.

Subtask 4.6.2

1. Guirard, B. M., and E. E. Snell, "Biochemical Factors in Growth," Manual of Methods for General Bacteriology, Editor in Chief P. Gerhardt, American Society for Microbiology, pp. 79-111, 1981.

2. Smith, R. W., M. Misra and S. Chen, "Hydrophobic Bacteria as Flocculating Agents for Mineral Suspensions," Engineering Foundation Conference on Dispersion and Aggregation; Fundamentals and Applications, Palm Coast, FL, March 15-20, 1992.

3. Van Loosdrecht, M.C.M., et al., "The Role of Bacterial Cell Wall Hydrophobicity in Adhesion," Appl. Environs., 53, pp. 1893-1897, 1987.

4. Dubel, J., R. W. Smith, M. Misra and S. Chen, "Microorganisms as Chemical Reagents: The Hematite System," Minerals Engineering, Vol. 5, No. 3-5, 1992, pp. 574-556.

5. Misra, M., R. W. Smith, J. Dubel and S. Chen, " Selective Flocculation of Fine Coal with Hydrophobic Mycobacterium Phlei," 1992 The Minerals, Metals and Material Society Annual Meeting, March 1992.

6. Misra, M., S. Chen and R. W. Smith, "Kerogen Aggregation with Mycobacterium phlei," Mineral Bioprocessing, R. W. Smith and M. Misra editors, The Minerals, Metals and Material Society, 1991.

7. Misra, M., S. Chen and R. W. Smith, "Bioflocculation of Finely Divided Solids," Mineral Bioprocessing, R. W. Smith and M. Misra editors, The Minerals, Metals, and Material Society, 1991(a).

8. Smith, R. W., and M. Misra, "Bacterial Flocculation of Phosphate Wastes Using a Hydrophobic Bacterium," 1992 TMS/EPD Proceedings.

9. Smith, R. W., M. Misra and J. Dubel, "Mineral Bioprocessing and the Future," Minerals Engineering, Vol. 4, No. 7-11, 1991, pp. 1127-1141.

10. Buchanan, R. E., and N. E. Gibbons, "Bergley's Manual of Determinative Bacteriology," 8th Edition, The Williams and Wilkins Company, Baltimore, pp. 693-697, 1974.

11. Laskin, A. I., and H. A. Lechevalier, Handbook of Microbiology and Molecular Biology, 2nd Edition, John Wiley and Sons, p. 576, 1987.

12. Pratt, D., "Nutrition of Mycobacterium phlei; Requirement for Rapid Growth Manual of Methods for General Bacteriology," J. of Bacteriol., 1952, 16, pp. 651-657.

Task 5

1. "Pressurized Fluidized-Bed Hydroretorting of Eastern Oil Shales," Final Report for the Period September 1987 throught May 1991, Volume IV (Task 5), DOE Contract No. DE-AC21-87MC11089, Report No. 11089-50, March 1992.

Subtask 6.1

1. Federal Register, Thursday March 29, 1990, Part II Environmental Protection Agency, 40 CFR Part 261 et al., pp. 11845-11846.

2. "Pressurized Fluidized-Bed Hydroretorting of Eastern Oil Shales," Final Report for the Period September 1987 throught May 1991, Volume IV (Task 6), DOE Contract No. DE-AC21-87MC11089, Report No. 11089-50, March 1992.

Subtask 6.2

1. Mensinger, M. C., M. J. Roberts, D. M. Rue and F. S. Lau, "Environmental Data From Moving-Bed Hydroretorting of Three Eastern Oil Shales." Proceedings of the 1988 Eastern Oil Shale Symposium, Lexington, Ky., November 1988.

2. Wentz, C. A., Hazardous Waste Management, New York, Mcgraw-Hill Inc., 1989.

3. Dudley, S. K., "Aerobic Biodegradation Characteristics of Selected Compounds of an Oil Shale Processing Wastewater Using Batch and Continuous Flow Hydraulic Regimes." Ph.D. Dissertation, Tennessee Technological University, May 1991.

4. Noyes Data Corporation, Hazardous Chemicals Data Book 2nd ed., Ed. G. Weiss, Park Ridge, 1986.

5. CRC Press, Inc. CRC Handbook of Chemistry and Physics, 64th ed., Boca Raton, Florida, 1983-1984.

6. Zobell, C. W., "Assimilation of Hydrocarbons by Micro-organisms." Advanced Enzymology, Vol. 10, pp. 443-486, 1950.

7. Ludzalk, F. J., and M. B. Ettinger, "Chemicals Structures Resistant to Aerobic Biochemical Stabilization," Presented at The 14th Industrial Waste Conference, pp. 1173-1200, Purdue University, 1959.

8. Tabak, H. H., C. W. Chambers, and P. W. Kabler, "Microbial Metabolism of Aromatic Compounds," Journal of Bacteriology, Vol. 87, No. 4., pp. 910-919, April 1964.

9. Bayly, R. C. and G. J. Wigmore, "Metabolism of Phenol and Cresols by Mutants of Pseudomonas putida," Journal of Bacteriology, March 1973, pp. 1112-1120.

10. Lallai, A. and G. Mura, "pH Variation During Phenol Biodegradation in Mixed Cultures of Microorganisms," Water Research, Vol. 23, No. 11, 1989, pp. 1335-1338.

11. Lyons, C. D., S. Katz, and R. Bartha, "Mechanisms and Pathways of Aniline Elimination from Aquatic Environments," Applied and Environmental Microbiology, Sept. 1984, pp. 491-496.

12. Wyndham, R. C., "Evolved Aniline Catabolism in Acinetobacter Calcoaceticus during Continuous Culture of River Water," Applied and Environmental Microbiology, April 1986, pp. 781-789.

13. Paris, D. F., and N. L. Wolfe, "Relationships Between Properties of a Series of Anilines and Their Transformation by Bacteria," Applied and Environmental Microbiology, May 1987, pp. 911-916.

14. N. J. Sax, Dangerous Properties of Industrial Materials, 6th ed. (1984).

15. Merck Index, 10th ed., 1983, p. 1067.

16. Ettinger, E. B., R. J. Lishka, and R. C. Kroner, "Persistence of Pyridine Bases in Polluted Water," Industrial and Engineering Chemistry, April 1954, p. 791.

17. Stafford, D. A. and A. G. Callely, "Properties of a Pyridine-Degrading Organism," Journal of General Microbiology, Vol. 63, Sept.-Nov. 197C, XIV.

18. Watson, K. G. and R. B. Cain, "Microbial Metabolism of the Pyridine Ring," Biochemical Journal, Vol. 146, 1975, pp. 157-172.

19. Kuhn, E. K. and J. M. Suflita, "Microbial Degradation of Nitrogen, Oxygen and Sulfur Heterocyclic Compounds Under Anaerobic Conditions: Studies with Aquatic Samples," Environmental Toxicology and Chemistry, Vol. 8, 1989, pp. 1149-1158.

20. Van Nostrand Reinhold Company, Handbook of Environmental Data on Organic Chemicals. New York, 1977. 1977.

21. Standard Methods for the Examination of Water and Wastewater, APHA, AWWA, and WPCF, Washington, D.C., 1989.

22. Ganczarczyk, J. and D. Elion, "Extended Aeration of Coke-Plant Effluents," Proceedings, 33rd Purdue Industrial Waste Conference, pp. 895-902, Lafayette, Indiana, May 1978.

23. Tsai, K.-C., M. A. Kamer and J. H. Gray, "Steam Stripping of Coal Liquifaction Waste for Ammonia and Sulfide Removal," Proceedings, 37th Purdue Industrial Waste Conference, pp. 465-473, Lafayette, Indiana, May 1982.

24. Tsai, K.-C., S. E. Shelby, Jr., M. Ziegler and A. S. Slesinger, "Air and Steam Stripping of High-Strength Ammonia Wastes," Proceedings, 36th Purdue Industrial Waste Conference, pp. 924-933, Lafayette, Indiana, May 1981.

25. Lewis, R. C., and G. D. Rawlings, "Laboratory Treatability Testing of Selected Oil Shale Process Wastewaters," Proceedings, 36th Purdue Industrial Waste Conference, pp. 341-349, Lafayette, Indiana, May 1981.

26. Hicks, R. E., R. F. Probstein, I. Wei, D. S. Farrier, J. Lotwala, and T. E. Phillips, Proceedings, 13th Oil Shale Symposium, pp. 321-344, Colorado, School of Mines, Golden Colorado, 1980.

27. Grant, Terry M. and C. Judson King, "Irreversible Adsorption of Phenolic Compounds by Activated Carbons," Ph.D. Thesis, Lawrence Berkley Laboratory, Berkley, California, December 1988.

28. Osantowski, R. and R. V. Hendricks, "Physical/Chemical and Biological Treatment of Coke-Plant Wastewater," Proceedings, 36th Purdue Industrial Waste Conference, pp. 168-176, Lafayette, Indiana, May 1981.

29. Bhattacharyya, D. and M. E. Williams, "Separation of Hazardous Organics by Low Pressure Reverse Osmosis Membranes - Phase II," EPA/600/52-91/045, January 1992.

30. Wastewater Engineering, Treatment, Disposal, and Reuse, Third Edition, Metcalf and Eddy, Inc., Revised by G. Tchobanglous and F. L. Burton, McGraw-Hill, Inc., 1991.

31. The Superfund Innovative Technology Evaluation Program: Technology Profiles, Fourth Edition, EPA/540/5-91/008, p. 54-55, November 1991. U.S. EPA Office of Solid Waste and Emergency Response, Washington, D.C.

32. Viraraghavan, T. and G.A.K. Rao, "Removal of Cadmium and Chromium from Wastewater Using Fly Ash," Proceedings, 45th Purdue Industrial Waste Conference, pp. 517-527, Lafayette, Indiana, May 1991.

33. Process Chemistry for Water and Wastewater Treatment, L. Benefield, J. Judkins, Jr., and B. Weand, Prentice-Hall, Inc., Englewood Cliffs, New Jersey, 1982.

Subtask 6.4.1

1. Burnham, A. K., "Reaction Kinetics and Diagnostics for Oil Shale Retorting", Symp. Syn. Fuels From Oil Shale II, 175-202, Nashville, TN, 1981.

2. Allred, V. D., "Kinetics of Oil Shale Pyrolysis", Chem. Eng. Progr., 62(8), 35, 1966.

3. Burnham, A. K. and Braun, R., "General Model of Oil Shale Pyrolysis", In-Situ, 9(1), 1, 1985.

4. Wall, G. C. and Smith, S. J., "Kinetics of Production of Individual Products From the Isothermal Pyrolysis of Seven Australian Oil Shales", Fuel, 66(3), 345, 1987.

5. Lau, F. S., Rue, D. M., Purwani, D. V. and Rex, R. C., "Gasification Characteristics of Eastern Oil Shale", Proc. 1986 East. Oil Shale Symp., 53-60, Lexington, KY, 1987.

6. Roberts, M. J., Rue, D. M. and Lau, F. S., "Pressurized Fluidized Bed Hydroretorting of Six Eastern Shales in Batch and Continuous Laboratory-Scale Reactors", Proc. 1990 East. Oil Shale Symp., 323-341, Lexington, KY, 1991.

Subtask 6.4.3

1. Institute of Gas Technology, "PFH Plant Design - Performance and Cost Data," series of private communications, June 1991 through April 1992.

2. Eisermann, W., Hasberg, W. and Tsatsaronis, G., "THESIS -A Computer Program for the Simulation and Design of Energy-Conversion Plants," Brenstoff-Wärme-Kraft, Vol. 36, 1984, No. 1-2, pp. 45-51.

3. Tsatsaronis, G. and Winhold, M., "Thermoeconomic Analysis of Power Plants," EPRI AP-3651, RP 2029-8, Final Report, Electric Power Research Institute, Palo Alto, CA, August 1984.

4. Linnhoff, B., et al., A User Guide on Process Integration for the Efficient Use of Energy, The Institution of Chemical Engineers, England, 1983.

5. Tsatsaronis, G., Winhold, M. and Stojanoff, C. G., "Thermoeconomic Analysis of Gasification-Combined-Cycle Power Plants," EPRI AP-4734, RP 2029-8, Final Report, Electric Power Research Institute, Palo Alto, CA, August 1986.

6. Tsatsaronis, G., "Thermoeconomic Analysis and Optimization of Energy Systems." Progress in Energy and Combustion Science, to be published, 1992.

7. Tsatsaronis, G. and Valero, A., "Thermodynamics Meets Economics," Mechanical Engineering, August 1989, pp. 84-86.

8. Tsatsaronis, G. and Pisa, J., "Exergoeconomic Evaluation and Optimization of Energy Systems - Application to the CGAM Problem," to be presented at the International Symposium on Efficiency, Costs, Optimization and Simulation of Energy Systems (ECOS '92), June 15-18, 1992, Zaragoza, Spain, and to be published in Thermoeconomic Analysis of Energy Systems, ASME, New York, 1992.

9. Tsatsaronis, G., Pisa, J. J. and Gallego, L. M., "Chemical Exergy in Exergoeconomics," Thermodynamic Analysis and Improvement of Energy Systems, Proceedings of the International Symposium, Beijing, China, June 5-8, 1989, Pergamon Press, pp. 195-200.

10. Gaire, R. J., Mozzella, G. and Hand, T. J., "Fluidized-Bed Retorting of Eastern Oil Shale," 1989 Eastern Oil Shale Symposium, November 15-17, 1989.

11. Wallman, P. H., "Coproduction of Oil and Electric Power from Colorado Oil Shale," Lawrence Livermore National Laboratory L-365, Livermore, CA, Energy Vol. 17, No. 4, pp. 313-319, 1992.

Subtask 6.4.4

1. Johnson, L. R., and R. H. RIley, "The Beneficiation of Eastern Oil Shales to Produce Oil Shale Concentrate for Retorting: An Engineering Study," Work performed for MRI under Grant No. DE-FG-21-85LC11066, Roberts and Schaeffer Company, December 1988.

2. Gaire, R. J., Mozzella, G. and Hand, T. J., "Fluidized-Bed Retorting of Eastern Oil Shale," 1989 Eastern Oil Shale Symposium, November 15-17, 1989.

Appendix A. University of Nevada (Reno) Data Analysis Procedure

The data can be rearranged making use of the following expressions (16).

$$t/V=\text{slope X } V+\text{intercept} \quad . \quad . \quad . \quad . \quad . \quad . \quad . \quad . \quad . \quad . \quad (1)$$

or

$$t/V=(\mu\kappa\gamma_c/2A^2\Delta p)V+\text{intercept} \quad . \quad . \quad . \quad . \quad . \quad . \quad . \quad . \quad . \quad . \quad (2)$$

where: t is time after application of vacuum, V is filtrate volume, μ is viscosity of water, γ_c is filter cake resistance, A is filter area, Δp is pressure drop across the filter and

$$\kappa=m_s\rho_F/m_F/((1-\varepsilon)\rho_s-\varepsilon\rho_F m_s/m_F). \quad . \quad . \quad . \quad . \quad . \quad . \quad . \quad . \quad . \quad (3)$$

where : ε is the porosity of the cake, ρ_F is the density of water, ρ_s is the density of the solids, m_s is the mass of the solids and m_F is the mass of the filtrate.

These expressions indicate that if t/V is plotted as a function of V the slope of the straight line curve generated should yield the expression from which filter cake resistance (γ_c) can be calculated:

$$\text{slope}=\mu\kappa\gamma_c/2A^2\Delta p \quad . \quad . \quad . \quad . \quad . \quad . \quad . \quad . \quad . \quad . \quad . \quad . \quad . \quad . \quad . \quad . \quad (4)$$

APPENDIX B. Results of the Exergetic and Thermoeconomic Evaluation of the PFH Process Design Conducted by Tennessee Technological University

TABLE B1

MASS FLOW RATE, TEMPERATURE, PRESSURE, AND FLOW RATES OF ENTHALPY AND EXERGY FOR EACH STREAM OF THE PFH PLANT ORIGINAL DESIGN (FIGURES 22 AND 23)

Stream	$\dot{m}$ [lb/hr]	T [°F]	P [psia]	$\dot{H}$ [MMBtu/hr]	$\dot{E}$ [MMBtu/hr]
A	2051416	60.0	620.0	-5052.69	19079.93
W	37951	60.0	620.0	-260.15	0.04
B	2014142	600.0	620.0	-4504.64	19148.73
C	1080822	900.0	620.0	-4104.43	3969.82
D	1080822	650.0	620.0	-4207.43	3914.08
1A	160446	600.0	43.3	-57.18	4060.69
1	160446	180.0	620.0	-143.60	4028.12
2	563750	1400.0	620.0	452.05	14681.83
3	724195	1232.0	620.0	394.87	18729.66
4	1733417	900.0	615.0	-588.43	33660.39
6	1808642	600.0	610.0	-1403.68	33509.22
7	563749	510.8	651.9	-268.62	14202.83
10	563749	180.0	661.9	-504.59	14122.59
16	1439753	460.4	600.0	-1612.39	26856.14
17	1853	460.4	590.0	-4.37	23.92
19	1437899	460.4	595.0	-1608.03	26831.20
20	1437899	130.0	590.0	-2148.65	26677.89
21	1050352	100.0	575.0	-995.71	22849.09
22	3845	100.0	570.0	-10.15	14.26
23	1194	100.0	570.0	-0.72	25.63
24	1040956	100.0	570.0	-955.15	22808.92
25	1853	460.4	590.0	-4.37	23.92
26	364020	100.0	30.0	-90.66	6456.97
27	6723	470.2	30.0	-4.13	110.09
30	15840	100.0	100.0	-11.19	315.14
31	115894	100.0	20.0	-20.51	2095.49
32	126097	100.0	19.5	-22.16	2272.69
33	132820	107.7	19.5	-27.01	2382.31
34	115894	158.5	100.0	-18.42	2098.92
35	14629	100.0	90.0	-10.47	304.57
36	900004	100.0	560.0	-932.33	20274.14
37	918	100.0	20.0	-6.26	0.00
38	1083	100.0	20.0	-0.22	22.22
39	124903	100.0	19.5	-21.44	2247.35
40	91	90.0	100.0	-0.62	0.00
41	1302	100.0	90.0	-1.25	10.65
42	27153	100.0	18.0	-38.80	189.27
43	875234	100.0	550.0	-901.04	20095.45
44	726	90.0	90.0	-4.96	0.00
45	355	90.0	560.0	-2.42	0.00

TABLE B1 (Continued)

Stream	$\dot{m}$ [lb/hr]	T [°F]	P [psia]	$\dot{H}$ [MMBtu/hr]	$\dot{E}$ [MMBtu/hr]
46	25124	100.0	550.0	-33.80	180.95
47	0	100.0	18.0	0.00	0.00
48	26426	36.9	90.0	-35.05	190.44
51	25258	99.7	14.7	0.10	202.64
52	37822	99.7	14.7	-50.47	272.09
53	10670	100.0	14.7	-11.67	82.99
54	14676	99.7	14.7	-100.02	0.04
55	14676	99.7	14.7	-100.02	0.04
56	10492	99.7	14.7	-40.86	1.45
57	55375	297.7	64.7	-366.33	2.41
58	55375	297.7	64.7	-315.85	18.26
59	724925	351.7	17.4	-845.42	34.09
60	2706	100.0	100.0	-0.96	55.40
61	3789	100.0	20.0	-1.18	77.53
62	690516	100.0	14.7	-205.89	13481.27
63	60591	193.4	2119.9	-51.84	1914.69
64	50289	100.0	100.0	-90.60	817.00
65	30750	100.0	14.7	-102.30	160.66
67	1083	100.0	20.0	-0.22	22.22
68	478	100.0	259.6	-3.26	0.00
69	78513	297.7	64.7	-447.82	25.89
70	80849	297.7	64.7	-535.22	3.42
71	222828	120.8	14.7	-1405.87	161.62
72	10812	100.0	214.7	-12.45	93.66
73	205191	130.0	25.0	-1392.16	1.16
74	177402	130.5	20.0	-1203.55	0.97
75	192078	128.2	14.7	-1303.57	1.00
77	55491	100.0	320.0	-111.10	1239.24
78	1684636	60.0	14.7	-6.83	1.52
79	1684636	90.5	17.4	5.60	12.05
80	96678	100.0	320.0	-193.57	2159.05
81	348343	100.0	550.0	-358.61	7997.99
82	123892	100.0	214.7	-100.74	3693.29
83	223015	100.0	16.7	-249.70	4254.18
84	526891	100.0	550.0	-542.42	12097.46
85	526891	137.5	661.9	-523.40	12111.85
86	123892	246.5	680.0	-66.46	3739.41
87	1436	250.0	20.0	-7.99	0.42
88	650784	171.7	661.9	-589.86	15845.00
89	38188	100.0	320.0	-76.46	852.83
90	2999	100.0	320.0	-6.01	66.98
91	237644	100.0	16.7	-260.17	4557.53
92	192370	100.0	16.7	-210.60	3689.27
93	192370	242.4	320.0	-197.68	3715.21

TABLE B1 (Continued)

Stream	$\dot{m}$ [lb/hr]	T [°F]	P [psia]	$\dot{H}$ [MMBtu/hr]	$\dot{E}$ [MMBtu/hr]
94	73412	100.0	259.6	-75.15	2277.35
95	73412	226.8	706.2	-58.34	2299.50
96	45273	100.0	16.7	-49.56	868.25
97	60591	100.0	259.6	-62.02	1879.63
98	129369	488.8	614.7	-829.01	16.24
99	724195	180.0	661.9	-648.19	18141.95
100	129369	488.8	614.7	-734.74	58.86
101	195369	239.8	320.0	-203.68	3782.03
102	747971	502.3	320.0	-3279.18	4021.67
103	747971	502.3	320.0	-3279.18	4021.67
104	747971	800.0	310.0	-3151.09	4087.88
105	747971	1535.0	310.0	-2804.38	4321.13
106	748129	1535.0	310.0	-2181.08	4699.61
107	894848	1099.2	310.0	-3174.97	4631.30
108	894848	867.0	300.0	-3303.06	4547.28
109	894848	760.0	290.0	-3360.80	4510.90
110	895010	900.0	290.0	-3362.98	4510.03
111	895010	333.7	279.6	-3670.21	4352.13
112	895010	100.0	269.6	-4165.46	4219.74
113	523420	100.0	264.6	-1633.39	4218.08
114	134003	100.0	259.6	-137.17	4156.97
115	552602	648.9	653.5	-3075.50	284.05
116	146719	140.0	310.0	-993.89	1.10
117	371590	100.0	264.6	-2532.07	1.22
118	388939	100.0	259.6	-1495.67	82.85
119	2336	90.0	260.0	-15.82	0.02
120	38188	85.2	17.4	-76.46	845.77
121	172126	130.0	580.0	-1167.60	1.22
122	4358	100.0	575.0	-29.69	0.02
123	176484	129.3	575.0	-1197.29	1.23
124	177402	130.5	20.0	-1203.55	0.97
127	127156	297.7	64.7	-725.27	41.92
128	127156	297.7	64.7	-841.20	5.54
129	64105	488.8	614.7	-364.08	29.17
130	64105	488.8	614.7	-410.79	8.05
131	54110	60.0	14.7	-0.22	0.05
132	104175	488.8	614.7	-667.56	13.08
133	93757	488.8	614.7	-532.48	42.66
134	10417	488.8	614.7	-66.76	1.31
135	38587	488.8	614.7	-219.15	17.56
136	38587	488.8	614.7	-247.27	4.84
137	21592	297.7	64.7	-123.16	7.12
138	21592	297.7	64.7	-142.84	0.94
139	997893	90.0	17.4	3.19	7.13

TABLE B1 (Continued)

Stream	$\dot{m}$ [lb/hr]	T [°F]	P [psia]	$\dot{H}$ [MMBtu/hr]	$\dot{E}$ [MMBtu/hr]
140	55491	85.2	17.4	-111.10	1228.97
141	1772437	97.3	580.2	-12080.84	7.13
142	1772437	397.4	522.1	-11538.95	145.37
143	2012317	60.0	14.7	-13793.88	2.16
144	2012317	94.0	14.7	-13725.57	4.30
147	79234	488.8	614.7	-507.74	9.95
148	79234	488.8	614.7	-450.00	36.05
149	336978	297.7	64.7	-2229.28	14.69
150	336978	297.7	64.7	-1922.04	111.10
151	6199940	60.0	14.7	-42498.89	6.66
152	6199940	140.0	14.7	-42003.64	41.27
153	1265773	130.0	580.0	-981.05	26675.68
154	1045994	100.0	575.0	-965.92	22849.25
155	895010	333.7	279.6	-3670.21	4352.13
157	686742	90.0	17.4	2.19	4.91
160	1053376	542.8	17.4	-1172.19	73.46
165	36483	60.0	22.0	-250.08	0.04
166	36483	224.3	22.0	-244.08	0.83
167	198881	677.0	164.7	-1097.51	92.27
168	198881	364.8	164.7	-1301.77	13.48
171	3789075	60.0	14.7	-25973.07	4.07
172	3789075	114.0	14.7	-25768.80	14.00
173	1084245	60.0	14.7	-7432.20	1.16
174	1084245	114.0	14.7	-7373.75	4.01
175	30148	297.7	64.7	-199.44	1.31
176	30148	297.7	64.7	-171.95	9.94
177	30148	364.8	164.7	-197.33	2.04
178	30148	677.0	164.7	-166.37	13.99
216	368890	460.4	600.0	-27.25	6561.34
217	368890	460.4	590.0	-27.25	6561.34
221	215422	100.0	575.0	-53.65	3821.13
223	215422	100.0	570.0	-53.65	3821.13
225	368890	460.4	590.0	-27.25	6561.34
226	364020	100.0	30.0	-90.66	6456.97
232	231470	100.0	19.5	-57.65	4105.80
233	231470	107.7	19.5	-56.93	4105.86
238	246395	100.0	20.0	-61.37	4370.53
239	16049	100.0	19.5	-4.00	284.67
254	215422	100.0	575.0	-53.65	3821.13
260	97348	100.0	100.0	-24.24	1726.75
261	707763	100.0	20.0	-176.27	12554.24
262	690516	100.0	14.7	-205.89	13481.27
267	610415	100.0	20.0	-152.03	10827.50

TABLE B2

FLOW RATES OF PHYSICAL, REACTION, ENVIRONMENTAL, CHEMICAL, AND TOTAL TOTAL EXERGY OF EACH STREAM IN THE ORIGINAL PFH PLANT (FIGURES 22 AND 23)

Stream	$\dot{E}^{PH}$ [lb/hr]	$\dot{E}^{R}$ [MMBtu/hr]	$\dot{E}^{E}$ [MMBtu/hr]	$\dot{E}^{CH}$ [MMBtu/hr]	$\dot{E}^{TOT}$ [MMBtu/hr]
A	0.000	18384.374	696.643	19078.932	19079.932
W	0.000	0.000	0.041	0.041	0.041
B	97.934	18390.731	661.155	19051.886	19148.730
C	119.404	3523.011	327.634	3850.645	3969.825
D	63.657	3523.011	327.634	3850.645	3914.079
1A	135.423	3700.493	24.500	3924.993	4060.685
1	103.344	3900.271	24.500	3924.771	4028.115
2	891.576	13704.171	86.084	13790.255	14681.831
3	1014.642	17604.439	110.583	17715.021	18729.664
4	944.073	32158.941	557.383	32716.322	33660.395
6	720.044	32195.799	593.377	32789.176	33509.219
7	447.705	13669.083	86.043	13755.126	14202.831
10	367.466	13669.083	86.043	13755.126	14122.592
16	595.822	25861.584	398.737	26260.320	26856.145
17	0.575	22.965	0.383	23.348	23.923
19	594.203	25838.615	398.383	26237.000	26831.203
20	440.891	25838.615	398.383	26237.000	26677.891
21	421.228	22139.611	288.253	22427.863	22849.092
22	0.348	8.564	5.346	13.910	14.258
23	0.205	24.889	0.533	25.422	25.628
24	419.180	22106.158	283.580	22389.738	22808.918
25	0.575	22.965	0.383	23.348	23.923
26	0.210	6250.601	206.154	6456.755	6456.965
27	0.476	106.577	3.036	109.613	110.089
30	1.032	306.792	7.314	314.106	315.138
31	0.676	2032.748	62.067	2094.814	2095.490
32	0.660	2204.322	67.711	2272.033	2272.693
33	0.744	2310.899	70.663	2381.562	2382.305
34	4.107	2032.748	62.067	2094.814	2098.921
35	0.917	300.160	3.490	303.650	304.567
36	408.872	19651.154	214.116	19865.270	20274.143
37	0.001	0.000	0.001	0.001	0.002
38	0.008	21.883	0.331	22.215	22.223
39	0.643	2179.433	67.276	2246.709	2247.353
40	0.000	0.000	0.000	0.000	0.000
41	0.067	6.632	3.953	10.585	10.652
42	0.187	118.282	70.806	189.087	189.275
43	404.352	19539.504	151.588	19691.094	20095.445
44	0.001	0.000	0.001	0.001	0.002
45	0.001	0.000	0.000	0.000	0.001

TABLE B2 (Continued)

Stream	$\dot{E}^{PH}$ [lb/hr]	$\dot{E}^{R}$ [MMBtu/hr]	$\dot{E}^{E}$ [MMBtu/hr]	$\dot{E}^{CH}$ [MMBtu/hr]	$\dot{E}^{TOT}$ [MMBtu/hr]
46	2.427	111.650	66.874	178.524	180.951
47	0.000	0.000	0.000	0.000	0.000
48	1.336	118.282	70.827	189.108	190.444
51	0.006	0.000	202.637	202.637	202.643
52	0.025	170.251	101.814	272.064	272.090
53	0.004	51.969	31.013	82.982	82.985
54	0.021	0.000	0.016	0.016	0.037
55	0.021	0.000	0.016	0.016	0.037
56	0.013	0.017	1.416	1.433	1.446
57	2.354	0.000	0.059	0.059	2.414
58	18.197	0.000	0.059	0.059	18.257
59	23.886	0.000	10.204	10.204	34.090
60	0.106	54.394	0.895	55.289	55.395
61	0.028	76.277	1.221	77.498	77.527
62	0.398	13125.380	355.497	13480.876	13481.274
63	81.208	1826.223	7.257	1833.479	1914.688
64	4.587	801.838	10.579	812.417	817.005
65	0.064	135.099	25.493	160.593	160.657
67	0.008	21.883	0.331	22.215	22.223
68	0.001	0.000	0.001	0.001	0.002
69	25.801	0.000	0.084	0.084	25.885
70	3.338	0.000	0.084	0.084	3.422
71	0.824	135.099	25.700	160.799	161.623
72	1.765	91.667	0.227	91.894	93.659
73	0.893	0.027	0.236	0.263	1.156
74	0.781	0.000	0.191	0.191	0.971
75	0.789	0.000	0.206	0.206	0.996
77	10.891	1212.039	16.309	1228.349	1239.240
78	0.000	0.000	1.519	1.519	1.519
79	10.529	0.000	1.519	1.519	12.049
80	18.976	2111.665	28.414	2140.079	2159.055
81	160.932	7776.723	60.333	7837.056	7997.988
82	93.629	3583.945	15.721	3599.666	3693.294
83	1.386	4192.732	60.063	4252.794	4254.181
84	243.420	11762.781	91.257	11854.039	12097.459
85	257.813	11762.781	91.257	11854.039	12111.851
86	139.748	3583.945	15.721	3599.666	3739.414
87	0.337	0.046	0.041	0.088	0.425
88	395.446	15346.726	102.830	15449.556	15845.003
89	7.495	834.115	11.224	845.339	852.835
90	0.589	65.510	0.881	66.392	66.980
91	1.471	4492.893	63.164	4556.057	4557.527
92	1.190	3636.951	51.131	3688.082	3689.272
93	27.132	3636.951	51.131	3688.082	3715.214

TABLE B2 (Continued)

Stream	$\dot{E}^{PH}$ [lb/hr]	$\dot{E}^{R}$ [MMBtu/hr]	$\dot{E}^{E}$ [MMBtu/hr]	$\dot{E}^{CH}$ [MMBtu/hr]	$\dot{E}^{TOT}$ [MMBtu/hr]
94	55.911	2212.642	8.792	2221.435	2277.346
95	78.070	2212.642	8.792	2221.435	2299.505
96	0.280	855.941	12.033	867.974	868.254
97	46.147	1826.223	7.257	1833.479	1879.626
98	16.102	0.000	0.139	0.139	16.241
99	472.048	17559.369	110.533	17669.900	18141.947
100	58.725	0.000	0.139	0.139	58.864
101	27.704	3702.461	51.869	3754.330	3782.034
102	266.957	3702.461	52.248	3754.709	4021.666
103	266.957	3702.461	52.248	3754.709	4021.666
104	333.171	3702.461	52.248	3754.709	4087.880
105	566.425	3702.461	52.248	3754.709	4321.134
106	578.545	4085.046	36.017	4121.063	4699.607
107	510.077	4085.046	36.175	4121.220	4631.297
108	426.055	4085.046	36.175	4121.220	4547.276
109	389.675	4085.046	36.175	4121.220	4510.896
110	421.444	4041.178	47.409	4088.587	4510.031
111	263.539	4041.178	47.409	4088.587	4352.126
112	131.153	4041.178	47.409	4088.587	4219.740
113	129.126	4041.178	47.776	4088.953	4218.080
114	102.058	4038.865	16.048	4054.914	4156.971
115	283.459	0.000	0.593	0.593	284.052
116	0.947	0.000	0.158	0.158	1.104
117	0.818	0.000	0.399	0.399	1.217
118	25.447	2.313	55.095	57.408	82.855
119	0.015	0.000	0.002	0.002	0.017
120	0.426	834.115	11.224	845.339	845.766
121	1.031	0.000	0.185	0.185	1.216
122	0.014	0.000	0.005	0.005	0.018
123	1.039	0.000	0.190	0.190	1.229
124	0.781	0.000	0.191	0.191	0.971
127	41.786	0.000	0.137	0.137	41.923
128	5.406	0.000	0.137	0.137	5.542
129	29.099	0.000	0.069	0.069	29.168
130	7.979	0.000	0.069	0.069	8.048
131	0.000	0.000	0.049	0.049	0.049
132	12.966	0.000	0.112	0.112	13.078
133	42.559	0.000	0.101	0.101	42.660
134	1.297	0.000	0.011	0.011	1.308
135	17.516	0.000	0.041	0.041	17.557
136	4.803	0.000	0.041	0.041	4.844
137	7.096	0.000	0.023	0.023	7.119
138	0.918	0.000	0.023	0.023	0.941
139	6.230	0.000	0.900	0.900	7.130

TABLE B2 (Continued)

Stream	$\dot{E}^{PH}$ [lb/hr]	$\dot{E}^{R}$ [MMBtu/hr]	$\dot{E}^{E}$ [MMBtu/hr]	$\dot{E}^{CH}$ [MMBtu/hr]	$\dot{E}^{TOT}$ [MMBtu/hr]
140	0.619	1212.039	16.309	1228.349	1228.968
141	5.227	0.000	1.903	1.903	7.130
142	143.463	0.000	1.903	1.903	145.366
143	0.000	0.000	2.161	2.161	2.161
144	2.142	0.000	2.161	2.161	4.303
147	9.862	0.000	0.085	0.085	9.947
148	35.967	0.000	0.085	0.085	36.052
149	14.325	0.000	0.362	0.362	14.687
150	110.738	0.000	0.362	0.362	111.100
151	0.000	0.000	6.658	6.658	6.658
152	34.615	0.000	6.658	6.658	41.273
153	436.904	25838.617	400.154	26238.771	26675.676
154	420.757	22139.611	288.878	22428.488	22849.246
155	263.539	4041.178	47.409	4088.587	4352.126
157	4.287	0.000	0.619	0.619	4.907
160	58.632	0.000	14.828	14.828	73.459
165	0.001	0.000	0.039	0.039	0.040
166	0.789	0.000	0.039	0.039	0.828
167	92.052	0.000	0.214	0.214	92.265
168	13.270	0.000	0.214	0.214	13.484
171	0.000	0.000	4.069	4.069	4.069
172	9.928	0.000	4.069	4.069	13.997
173	0.000	0.000	1.164	1.164	1.164
174	2.841	0.000	1.164	1.164	4.006
175	1.282	0.000	0.032	0.032	1.314
176	9.907	0.000	0.032	0.032	9.939
177	2.012	0.000	0.032	0.032	2.044
178	13.954	0.000	0.032	0.032	13.986
216	18.212	6334.214	208.910	6543.124	6561.336
217	18.212	6334.214	208.910	6543.124	6561.336
221	0.124	3699.007	121.999	3821.006	3821.130
223	0.124	3699.007	121.999	3821.006	3821.130
225	18.212	6334.214	208.910	6543.124	6561.336
226	0.210	6250.601	206.154	6456.755	6456.965
232	0.133	3974.580	131.087	4105.667	4105.801
233	0.189	3974.580	131.087	4105.667	4105.856
238	0.142	4230.848	139.539	4370.386	4370.528
239	0.009	275.573	9.089	284.662	284.671
254	0.124	3699.007	121.999	3821.006	3821.130
260	0.056	1671.562	55.130	1726.693	1726.749
261	0.408	12153.013	400.823	12553.836	12554.244
262	0.398	13125.380	355.497	13480.876	13481.274
267	0.352	10481.450	345.692	10827.144	10827.495

TABLE B3

HEAT TRANSFER RATE ($\dot{Q}$), POWER ($\dot{W}$), EXERGY DESTRUCTION FLOW RATE ($\dot{E}_D$), EXERGY DESTRUCTION RATIO y^*, RATIO OF EXERGY DESTRUCTION TO THE EXERGY OF SHALE (y), AND EXERGETIC EFFICIENCY (ϵ) FOR EACH COMPONENT IN THE ORIGINAL PFH PLANT (FIGURES 22 AND 23)

Component	$\dot{Q}$ [MW]	$\dot{W}$ [MW]	$\dot{E}_D$ [MW]	y^* [%]	y [%]	ϵ [%]
PREHEAT	2.07	0.00	24.15	1.70	0.39	45.48
RETORT	26.65	8.24	81.00	5.71	1.30	98.18
COOLING	4.86	0.00	6.79	0.48	0.11	58.43
MIXING (1A+2=3)	0.00	0.00	3.77	0.27	0.06	99.93
HEAT EXCHANGER	0.00	0.00	3.37	0.24	0.05	87.46
GAS-OIL SEPARATOR	0.00	0.00	0.30	0.02	0.00	100.00
GAS COOLER I	0.00	0.00	4.42	0.31	0.07	90.17
KNOCK-OUT DRUM I	0.00	0.00	0.29	0.02	0.00	100.00
GAS COOLER II	0.00	0.00	0.97	0.07	0.02	39.27
3-PHASE SEPARATOR	0.00	0.00	0.08	0.01	0.00	100.00
LEAN OIL SCRUBBER	0.77	0.00	0.81	0.06	0.01	99.99
LEAN OIL STRIPPER	16.94	1.96	8.13	0.57	0.13	99.57
ACID GAS REMOVAL	34.37	0.75	11.41	0.80	0.18	99.81
GAS COMPRESSOR 31/34	1.22	1.93	0.92	0.07	0.01	52.11
KNOCK-OUT DRUM III	5.27	0.00	0.48	0.03	0.01	99.92
CLAUS & SCOT UNITS	21.70	1.31	17.73	1.25	0.28	79.53
HEAVY OIL FLASH DRUM	18.51	0.00	5.34	0.38	0.09	99.72
HYDROGEN RECOVERY	0.05	0.00	14.68	1.03	0.24	99.37
RECYCLE GAS COMPR. 82/86	10.05	21.16	7.64	0.54	0.12	63.89
RECYCLE GAS COMPR. 84/85	0.00	5.87	1.65	0.12	0.03	71.87
RECYCLE GAS COMPR. 94/95	5.07	10.53	4.03	0.28	0.06	61.69
COMPR. TO H_2 PLANT 92/93	7.63	12.02	4.42	0.31	0.07	63.26
MIXING WITH NATURAL GAS	0.00	0.00	0.05	0.00	0.00	100.00
STEAM ADDITION 115	0.00	0.00	13.02	0.92	0.21	98.91
HEAT EXCHANGER 102/103	0.00	0.00	0.00	0.00	0.00	0.00
FEED PROD. HEAT EXCHANGER	0.00	0.00	5.22	0.37	0.08	78.81
REFORMER FURNACE	0.00	0.00	148.97	10.50	2.39	56.28
QUENCH WATER	0.00	0.00	20.34	1.43	0.33	98.52
HEAT EXCHANGER 108/109	0.00	0.00	3.01	0.21	0.05	71.76
SHIFT CONVERSION	0.64	0.00	0.25	0.02	0.00	99.98
HEAT EXCHANGER 110/111	0.00	0.00	18.02	1.27	0.29	61.06
KNOCK-OUT DRUM IV	0.00	0.00	0.00	0.00	0.00	100.00
HEAT EXCHANGER 111/112	0.00	0.00	28.65	2.02	0.46	26.15
KNOCK-OUT DRUM V	0.00	0.00	0.13	0.01	0.00	99.99
ABSORBER/REGENERATOR	22.78	1.01	1.22	0.09	0.02	99.90
COMPR. TO DES. & HYDR.	15.78	19.75	9.47	0.67	0.15	52.03
DESALTING & HYDROTREATING	54.76	5.09	30.74	2.17	0.49	99.27
SW TRTM. & NH_3 RECOVERY	3.57	3.50	2.94	0.21	0.05	94.66
NATURAL GAS THROTTLING	0.00	0.00	5.08	0.36	0.08	99.17
FIRED HEATER	0.00	0.00	94.29	6.64	1.51	60.60
AIR FAN 78/79	0.00	3.83	0.75	0.05	0.01	80.49
PFH PLANT	**252.29**	**96.95**	**697.22**	-----	**13.27**	**86.73**

TABLE B4

COSTS ASSOCIATED WITH PHYSICAL, CHEMICAL, AND TOTAL EXERGY OF EACH STREAM IN THE ORIGINAL PFH PLANT (FIGURE 25)

Stream	Physical Exergy Cost Flow [$/hr]	Cost of Physical Exergy Unit [$/GJ]	Chemical Exergy Cost Flow [$/hr]	Cost of Chemical Exergy Unit [$/GJ]	Total Exergy Cost Flow [$/hr]	Cost of Total Exergy Unit [$/GJ]
A	0.00	0.00	33275.74	1.65	33275.74	1.65
D	111.01	1.65	6715.20	1.65	6826.21	1.65
17	52.85	2.67	18472.76	2.67	18525.61	2.67
19	1671.61	2.67	73809.77	2.67	75481.38	2.67
22	0.98	2.67	0.00	0.00	0.98	0.07
30	2.90	2.67	883.64	2.67	886.54	2.67
35	2.77	2.86	917.17	2.86	919.94	2.86
36	1150.24	2.67	55884.86	2.67	57035.10	2.67
40	0.00	0.00	0.00	0.00	0.00	0.00
42	0.00	0.00	0.00	0.00	0.00	0.00
43	1158.99	2.72	56440.57	2.72	57599.57	2.72
44	0.00	0.00	0.00	0.00	0.00	0.00
45	0.00	0.00	0.00	0.00	0.00	0.00
47	0.00	0.00	0.00	0.00	0.00	0.00
51	0.00	0.00	788.69	3.69	788.69	3.69
52	0.01	0.38	0.00	0.00	0.01	0.00
53	0.01	2.53	0.00	0.00	0.01	0.00
54	0.00	0.00	0.00	0.00	0.00	0.00
55	0.00	0.00	0.00	0.00	0.00	0.00
56	0.00	0.00	0.00	0.00	0.00	0.00
57	13.28	5.35	0.00	0.00	13.28	5.22
58	78.60	4.09	0.00	0.00	78.60	4.08
61	1.23	2.67	36735.85	2.76	36737.08	2.76
62	1.12	2.67	48381.50	3.40	48382.62	3.40
64	20.91	4.32	2915.68	3.40	2936.60	3.41
65	0.00	0.00	0.00	0.00	0.00	0.00
68	0.00	0.00	0.00	0.00	0.00	0.00
69	119.86	4.40	0.00	0.00	119.86	4.39
70	15.51	4.40	0.00	0.00	15.51	4.29
71	2.20	2.53	0.00	0.00	2.20	0.01
72	0.00	0.00	669.63	6.91	669.63	6.78
73	0.00	0.00	0.00	0.00	0.00	0.00
74	2.20	2.67	0.00	0.00	2.20	2.14
75	2.20	2.64	0.00	0.00	2.20	2.09
77	0.00	0.00	5305.75	4.09	5305.75	4.06
78	0.00	0.00	0.00	0.00	0.00	0.00
79	157.91	14.21	0.00	0.00	157.91	12.42
80	0.00	0.00	9243.89	4.09	9243.89	4.06
83	3.97	2.72	12189.78	2.72	12193.76	2.72
87	0.00	0.00	0.00	0.00	0.00	0.00
89	0.00	0.00	3651.37	4.09	3651.37	4.06

TABLE B4 (Continued)

Stream	Physical Exergy Cost Flow [$/hr]	Cost of Physical Exergy Unit [$/GJ]	Chemical Exergy Cost Flow [$/hr]	Cost of Chemical Exergy Unit [$/GJ]	Total Exergy Cost Flow [$/hr]	Cost of Total Exergy Unit [$/GJ]
90	0.00	0.00	286.77	4.09	286.77	4.06
91	6.74	4.35	13106.95	2.73	13113.69	2.73
92	5.46	4.35	10609.94	2.73	10615.40	2.73
94	254.88	4.32	12924.98	5.51	13179.86	5.49
96	1.29	4.35	2497.01	2.73	2498.29	2.73
97	210.37	4.32	10667.74	5.51	10878.11	5.49
98	117.11	6.89	0.00	0.00	117.11	6.83
99	1607.80	3.23	60183.88	3.23	61791.68	3.23
100	744.77	12.02	0.00	0.00	744.77	11.99
104	1518.80	4.32	10896.72	2.75	12415.52	2.88
106	2637.37	4.32	18786.40	4.32	21423.78	4.32
109	1776.39	4.32	21193.77	4.87	22970.16	4.83
114	465.24	4.32	23592.72	5.51	24057.96	5.49
115	1649.52	5.52	0.00	0.00	1649.52	5.50
116	0.00	0.00	0.00	0.00	0.00	0.00
117	0.00	0.00	0.00	0.00	0.00	0.00
118	0.00	0.00	0.00	0.00	0.00	0.00
119	0.00	0.00	0.00	0.00	0.00	0.00
127	194.11	4.40	0.00	0.00	194.11	4.39
128	25.11	4.40	0.00	0.00	25.11	4.29
129	238.03	7.75	0.00	0.00	238.03	7.73
130	65.27	7.75	0.00	0.00	65.27	7.69
131	0.00	0.00	0.00	0.00	0.00	0.00
132	94.30	6.89	0.00	0.00	94.30	6.83
133	187.19	4.17	0.00	0.00	187.19	4.16
134	0.00	0.00	0.00	0.00	0.00	0.00
135	143.28	7.75	0.00	0.00	143.28	7.73
136	39.28	7.75	0.00	0.00	39.28	7.69
137	32.96	4.40	0.00	0.00	32.96	4.39
138	4.26	4.40	0.00	0.00	4.26	4.29
139	93.43	14.21	0.00	0.00	93.43	12.42
141	71.91	13.04	0.00	0.00	71.91	9.56
142	460.80	3.04	0.00	0.00	460.80	3.00
143	0.00	0.00	0.00	0.00	0.00	0.00
144	0.00	0.00	0.00	0.00	0.00	0.00
147	71.72	6.89	0.00	0.00	71.72	6.83
148	190.73	5.03	0.00	0.00	190.73	5.01
149	80.83	5.35	0.00	0.00	80.83	5.22
150	520.34	4.45	0.00	0.00	520.34	4.44
151	0.00	0.00	0.00	0.00	0.00	0.00
152	0.00	0.00	0.00	0.00	0.00	0.00
157	64.48	14.26	0.00	0.00	64.48	12.46
159	103.17	4.09	0.00	0.00	103.17	2.87
160	253.25	4.09	0.00	0.00	253.25	3.27

TABLE B5

POWER ($\dot{W}$), EXERGY DESTRUCTION ($\dot{E}_D$), EXERGY DESTRUCTION RATIO (y^*), RATIO OF EXERGY DESTRUCTION TO THE EXERGY OF SHALE (y), AND EXERGETIC EFFICIENCY (ϵ) FOR COMPONENT GROUPS IN THE ORIGINAL PFH PLANT (FIGURE 25)

Group	$\dot{W}$ [MW]	$\dot{E}_D$ [MW]	y^* [%]	y [%]	ϵ [%]
Shale Retorting	8.24	217.80	14.37	3.89	97.8
Gas Scrubbing	3.98	21.83	1.44	0.39	99.8
Acid Gas Removal	0.75	11.41	0.75	0.20	99.8
Sulfur Recovery	1.31	17.79	1.17	0.32	---
Sour Water Stripper & NH_3 Recovery	3.50	27.27	1.80	0.49	---
Hydrogen Recovery	37.60	30.64	2.02	0.55	99.5
Compressor and Heat Exchangers	12.02	45.73	3.02	0.82	96.7
Steam Reformer	0.00	151.98	10.02	2.72	55.8
Shift Conversion & CO_2 Removal	1.01	73.58	4.85	1.32	94.3
Desalting & Hydrotreating	25.02	40.40	2.66	0.72	99.0

TABLE B6

VARIOUS THERMOECONOMIC VARIABLES FOR COMPONENT GROUPS IN THE ORIGINAL PFH PLANT (FIGURE 25)

Group	r [%]	ϵ [%]	$\frac{\dot{Z}}{\dot{E}_{P,k}c_{F,k}}$ [%]	$\frac{1-\epsilon}{\epsilon}$ [%]	f [%]
Shale Retorting	1878.46	4.31	2.22	2.00	47.33
Gas Scrubbing	707.75	0.98	0.22	0.75	76.94
Acid Gas Removal	398.01	0.88	0.19	0.68	78.24
Hydrogen Recovery	1663.64	2.78	0.47	2.25	82.81
Compressor & Heat Exchangers	1036.15	8.30	3.44	4.49	56.61
Steam Reformer	4489.99	235.65	79.25	46.60	37.03
Shift Conversion & CO_2 Removal	1381.54	12.36	6.02	5.64	48.36
Desalting & Hydrotreating	2677.81	6.52	0.96	5.22	84.41

TABLE B7

MASS FLOW RATE, TEMPERATURE, PRESSURE, AND FLOW RATES OF ENTHALPY AND EXERGY FOR EACH STREAM OF THE ORIGINAL STEAM POWER PLANT (FIGURE 26)

Stream	$\dot{m}$ [lb/hr]	T [°F]	P [psia]	$\dot{H}$ [MMBtu/hr]	$\dot{E}$ [MMBtu/hr]
301	4225479	1000.4	2422.1	-22912.31	2814.63
302	95562	83.8	16.7	-140.16	1680.35
305	348522	648.8	653.5	-1939.71	179.14
306	3324356	648.8	653.5	-18501.84	1708.72
310	3324356	1000.4	588.7	-17834.84	2084.33
314	140613	831.9	313.7	-765.70	76.18
316	2954714	589.6	110.5	-16425.79	1241.31
317	199668	488.8	614.7	-1133.99	90.85
318	174724	589.6	110.5	-971.32	73.40
319	2779989	589.6	110.5	-15454.47	1167.90
321	2779989	589.3	108.3	-15454.47	1164.79
322	165091	297.7	64.7	-941.64	54.43
325	88598	161.7	4.9	-512.17	14.97
326	2691391	112.3	1.4	-15738.41	244.52
327	174724	118.2	1.6	-1015.90	18.00
328	2866116	112.3	1.4	-16754.30	260.92
329	2866116	103.6	1.4	-19521.67	7.93
330	165091	258.3	590.3	-1098.62	5.48
331	210085	411.8	2860.1	-1363.88	19.77
333	88598	105.8	4.2	-603.27	0.26
334	3517733	96.7	1.4	-23984.27	7.99
335	3517733	96.8	65.3	-23983.43	8.67
337	1772437	96.8	65.3	-12084.24	4.37
338	1745296	149.1	61.4	-11808.09	14.07
339	229029	365.9	164.7	-1498.84	15.63
340	1745296	96.8	65.3	-11899.19	4.30
341	229029	677.0	164.7	-1263.88	106.25
342	2599190	247.6	57.7	-17327.82	74.70
343	688803	267.3	162.4	-4578.08	23.79
344	2828218	257.3	57.7	-18826.66	88.85
345	2663127	258.3	590.3	-17722.10	88.45
346	489135	351.7	273.0	-3208.29	30.84
347	2828218	258.3	590.3	-18820.71	93.94
348	2663127	344.6	554.9	-17486.30	162.92
349	348522	427.1	568.7	-2257.69	33.17
350	4435564	411.8	2860.1	-28795.79	417.35
351	4435564	405.0	521.6	-28840.36	378.10

TABLE B7 (Continued)

Stream	$\dot{m}$ [lb/hr]	T [°F]	P [psia]	$\dot{H}$ [MMBtu/hr]	$\dot{E}$ [MMBtu/hr]
352	4225479	411.8	2860.1	-27431.91	397.58
353	4225479	481.0	2688.6	-27113.93	531.71
354	174724	588.5	102.4	-971.32	72.65
355	4678288	60.0	14.7	-18.96	4.22
356	4678288	121.0	20.3	50.09	62.04
357	4678288	482.0	18.4	468.29	173.28
359	793283	800.3	14.5	-4100.64	48.45
361	5061552	320.0	14.7	-5062.54	418.43
362	2663127	410.0	521.6	-17301.40	232.80
363	1772437	97.3	580.2	-12080.84	7.13
364	552602	648.8	653.5	-3075.53	284.04
365	563019	60.0	14.7	-3859.34	0.60
366	3429135	96.5	1.4	-23381.01	7.74
369	688803	408.8	273.0	-4342.29	113.12
370	489135	421.5	313.7	-3023.39	105.84

TABLE C8

FLOW RATES OF PHYSICAL, REACTION, ENVIRONMENTAL, CHEMICAL AND TOTAL EXERGY OF EACH STREAM IN THE ORIGINAL STEAM POWER PLANT (FIGURE 26)

Stream	$\dot{E}^{PH}$ [MMBtu/hr]	$\dot{E}^{R}$ [MMBtu/hr]	$\dot{E}^{E}$ [MMBtu/hr]	$\dot{E}^{CH}$ [MMBtu/hr]	$\dot{E}^{TOT}$ [MMBtu/hr]
301	2810.090	0.000	4.538	4.538	2814.628
302	0.576	1657.779	21.997	1679.776	1680.352
305	178.766	0.000	0.374	0.374	179.140
306	1705.151	0.000	3.570	3.570	1708.721
310	2080.760	0.000	3.570	3.570	2084.330
314	76.028	0.000	0.151	0.151	76.179
316	1238.135	0.000	3.173	3.173	1241.308
317	90.636	0.000	0.214	0.214	90.850
318	73.216	0.000	0.188	0.188	73.404
319	1164.919	0.000	2.985	2.985	1167.904
321	1161.808	0.000	2.985	2.985	1164.793
322	54.252	0.000	0.177	0.177	54.430

TABLE B8 (Continued)

Stream	$\dot{E}^{PH}$ [MMBtu/hr]	$\dot{E}^{R}$ [MMBtu/hr]	$\dot{E}^{E}$ [MMBtu/hr]	$\dot{E}^{CH}$ [MMBtu/hr]	$\dot{E}^{TOT}$ [MMBtu/hr]
325	14.871	0.000	0.095	0.095	14.967
326	241.628	0.000	2.890	2.890	244.518
327	17.809	0.000	0.188	0.188	17.997
328	257.847	0.000	3.078	3.078	260.925
329	4.853	0.000	3.078	3.078	7.931
330	5.306	0.000	0.177	0.177	5.483
331	19.542	0.000	0.226	0.226	19.767
333	0.166	0.000	0.095	0.095	0.261
334	4.212	0.000	3.778	3.778	7.990
335	4.893	0.000	3.778	3.778	8.670
337	2.465	0.000	1.903	1.903	4.368
338	12.195	0.000	1.874	1.874	14.070
339	15.381	0.000	0.246	0.246	15.627
340	2.428	0.000	1.874	1.874	4.302
341	106.005	0.000	0.246	0.246	106.251
342	71.912	0.000	2.791	2.791	74.703
343	23.051	0.000	0.740	0.740	23.791
344	85.817	0.000	3.037	3.037	88.854
345	85.594	0.000	2.860	2.860	88.454
346	30.318	0.000	0.525	0.525	30.843
347	90.899	0.000	3.037	3.037	93.937
348	160.063	0.000	2.860	2.860	162.923
349	32.791	0.000	0.374	0.374	33.166
350	412.589	0.000	4.763	4.763	417.352
351	373.335	0.000	4.763	4.763	378.099
352	393.046	0.000	4.538	4.538	397.584
353	527.177	0.000	4.538	4.538	531.715
354	72.465	0.000	0.188	0.188	72.653
355	0.000	0.000	4.219	4.219	4.219
356	57.821	0.000	4.219	4.219	62.040
357	169.064	0.000	4.219	4.219	173.282
359	48.448	0.000	0.000	0.000	48.448
361	77.680	0.000	340.746	340.746	418.426
362	229.940	0.000	2.860	2.860	232.800
363	5.227	0.000	1.903	1.903	7.130
364	283.444	0.000	0.593	0.593	284.038
365	0.000	0.000	0.605	0.605	0.605
366	4.054	0.000	3.683	3.683	7.737
369	112.381	0.000	0.740	0.740	113.121
370	105.318	0.000	0.525	0.525	105.843

TABLE B9

HEAT RATE ($\dot{Q}$), POWER ($\dot{W}$), EXERGY DESTRUCTION FLOW RATE ($\dot{E}_D$), EXERGY DESTRUCTION RATIO (y^*), RATIO OF EXERGY DESTRUCTION TO THE EXERGY OF SHALE (y), AND EXERGETIC EFFICIENCY (ϵ) FOR EACH POWER PLANT COMPONENT

	Component	$\dot{Q}$ [MW]	$\dot{W}$ [MW]	$\dot{E}_D$ [MW]	y^* [%]	y [%]	ϵ [%]
46	Steam Generator	0.00	20.56	746.84	52.64	12.00	51.06
47	HP Turbine	0.00	-173.69	14.67	1.03	0.24	92.21
48	IP Turbine	0.00	-178.22	15.38	1.08	0.25	92.06
49	LP Turbine	0.00	-228.65	36.67	2.58	0.59	86.18
50	Pump 1	0.00	0.26	0.06	0.00	0.00	77.07
51	Pump 4	0.00	1.05	0.24	0.02	0.00	77.24
52	Preheater 1	0.00	0.00	1.45	0.10	0.02	66.42
53	Preheater 2	0.00	0.00	1.01	0.07	0.02	96.28
54	Pump 2	0.00	1.83	0.34	0.02	0.01	81.24
55	Preheater 3	0.00	0.00	6.87	0.48	0.11	76.06
56	Preheater 4	0.00	0.00	2.53	0.18	0.04	89.01
57	Pump 3	0.00	13.06	1.56	0.11	0.03	88.06
58	Turbine 5	0.00	-13.06	3.18	0.22	0.05	80.44
59	Preheater 5	0.00	0.00	3.47	0.24	0.06	91.89
60	Condenser	810.50	0.00	74.15	5.23	1.19	---
	Steam Power Plant	810.50	-536.44	908.42	56.57	13.40	37.25
	PFH Plant	252.29	96.95	697.22	43.43	9.39	86.73
	Total Plant	1062.73	-439.50	1605.64	---	---	70.52

TABLE B10

COSTS ASSOCIATED WITH PHYSICAL, CHEMICAL, AND TOTAL EXERGY OF EACH STREAM IN THE COMBINED PLANT ORIGINAL DESIGN (FIGURES 25, 26 AND 27)

Stream	Physical Exergy Cost Flow [$/hr]	Cost of Physical Exergy Unit [$/GJ]	Chemical Exergy Cost Flow [$/hr]	Cost of Chemical Exergy Unit [$/GJ]	Total Exergy Cost Flow [$/hr]	Cost of Total Exergy Unit [$/GJ]
A	0.00	0.00	33275.74	1.65	33275.74	1.65
D	111.01	1.65	6715.20	1.65	6826.21	1.65
17	52.85	2.67	18472.76	2.67	18525.61	2.67
19	1671.61	2.67	73809.77	2.67	75481.38	2.67
22	0.98	2.67	0.00	0.00	0.98	0.07
30	2.90	2.67	883.64	2.67	886.54	2.67
35	2.77	2.86	917.17	2.86	919.94	2.86
36	1150.24	2.67	55884.86	2.67	57035.10	2.67
40	0.00	0.00	0.00	0.00	0.00	0.00
42	0.00	0.00	0.00	0.00	0.00	0.00
43	1158.99	2.72	56440.57	2.72	57599.57	2.72
44	0.00	0.00	0.00	0.00	0.00	0.00
45	0.00	0.00	0.00	0.00	0.00	0.00
47	0.00	0.00	0.00	0.00	0.00	0.00
51	0.00	0.00	788.69	3.69	788.69	3.69
52	0.01	0.38	0.00	0.00	0.01	0.00
53	0.01	2.53	0.00	0.00	0.01	0.00
54	0.00	0.00	0.00	0.00	0.00	0.00
55	0.00	0.00	0.00	0.00	0.00	0.00
56	0.00	0.00	0.00	0.00	0.00	0.00
57	13.28	5.35	0.00	0.00	13.28	5.22
58	78.60	4.09	0.00	0.00	78.60	4.08
59	103.17	4.09	0.00	0.00	103.17	2.87
61	1.23	2.67	36735.85	2.76	36737.08	2.76
62	1.12	2.67	48381.50	3.40	48382.62	3.40
64	20.91	4.32	2915.68	3.40	2936.60	3.41
65	0.00	0.00	0.00	0.00	0.00	0.00
68	0.00	0.00	0.00	0.00	0.00	0.00
69	119.86	4.40	0.00	0.00	119.86	4.39
70	15.51	4.40	0.00	0.00	15.51	4.29
71	2.20	2.53	0.00	0.00	2.20	0.01
72	0.00	0.00	669.63	6.91	669.63	6.78
73	0.00	0.00	0.00	0.00	0.00	0.00
74	2.20	2.67	0.00	0.00	2.20	2.14
75	2.20	2.64	0.00	0.00	2.20	2.09
77	0.00	0.00	5305.75	4.09	5305.75	4.06
78	0.00	0.00	0.00	0.00	0.00	0.00
79	157.91	14.21	0.00	0.00	157.91	12.42
80	0.00	0.00	9243.89	4.09	9243.89	4.06
83	3.97	2.72	12189.78	2.72	12193.76	2.72
87	0.00	0.00	0.00	0.00	0.00	0.00

TABLE B10 (Continued)

Stream	Physical Exergy Cost Flow [$/hr]	Cost of Physical Exergy Unit [$/GJ]	Chemical Exergy Cost Flow [$/hr]	Cost of Chemical Exergy Unit [$/GJ]	Total Exergy Cost Flow [$/hr]	Cost of Total Exergy Unit [$/GJ]
89	0.00	0.00	3651.37	4.09	3651.37	4.06
90	0.00	0.00	286.77	4.09	286.77	4.06
91	6.74	4.35	13106.95	2.73	13113.69	2.73
92	5.46	4.35	10609.94	2.73	10615.40	2.73
94	254.88	4.32	12924.98	5.51	13179.86	5.49
96	1.29	4.35	2497.01	2.73	2498.29	2.73
97	210.37	4.32	10667.74	5.51	10878.11	5.49
98	117.11	6.89	0.00	0.00	117.11	6.83
99	1607.80	3.23	60183.88	3.23	61791.68	3.23
100	744.77	12.02	0.00	0.00	744.77	11.99
104	1518.80	4.32	10896.72	2.75	12415.52	2.88
106	2637.37	4.32	18786.40	4.32	21423.78	4.32
109	1776.39	4.32	21193.77	4.87	22970.16	4.83
114	465.24	4.32	23592.72	5.51	24057.96	5.49
115	1649.52	5.52	0.00	0.00	1649.52	5.50
116	0.00	0.00	0.00	0.00	0.00	0.00
117	0.00	0.00	0.00	0.00	0.00	0.00
118	0.00	0.00	0.00	0.00	0.00	0.00
119	0.00	0.00	0.00	0.00	0.00	0.00
127	194.11	4.40	0.00	0.00	194.11	4.39
128	25.11	4.40	0.00	0.00	25.11	4.29
129	238.03	7.75	0.00	0.00	238.03	7.73
130	65.27	7.75	0.00	0.00	65.27	7.69
131	0.00	0.00	0.00	0.00	0.00	0.00
132	94.30	6.89	0.00	0.00	94.30	6.83
133	187.19	4.17	0.00	0.00	187.19	4.16
134	0.00	0.00	0.00	0.00	0.00	0.00
135	143.28	7.75	0.00	0.00	143.28	7.73
136	39.28	7.75	0.00	0.00	39.28	7.69
137	32.96	4.40	0.00	0.00	32.96	4.39
138	4.26	4.40	0.00	0.00	4.26	4.29
139	93.43	14.21	0.00	0.00	93.43	12.42
141	71.91	13.04	0.00	0.00	71.91	9.56
142	460.80	3.04	0.00	0.00	460.80	3.00
143	0.00	0.00	0.00	0.00	0.00	0.00
144	0.00	0.00	0.00	0.00	0.00	0.00
147	71.72	6.89	0.00	0.00	71.72	6.83
148	190.73	5.03	0.00	0.00	190.73	5.01
149	80.83	5.35	0.00	0.00	80.83	5.22
150	520.34	4.45	0.00	0.00	520.34	4.44
151	0.00	0.00	0.00	0.00	0.00	0.00
152	0.00	0.00	0.00	0.00	0.00	0.00
157	64.48	14.26	0.00	0.00	64.48	12.46
160	253.25	4.09	0.00	0.00	253.25	3.27

TABLE B10 (Continued)

Stream	Physical Exergy Cost Flow [$/hr]	Cost of Physical Exergy Unit [$/GJ]	Chemical Exergy Cost Flow [$/hr]	Cost of Chemical Exergy Unit [$/GJ]	Total Exergy Cost Flow [$/hr]	Cost of Total Exergy Unit [$/GJ]
301	16352.61	5.52	0.00	0.00	16352.61	5.51
305	1040.28	5.52	0.00	0.00	1040.28	5.50
306	9922.69	5.52	0.00	0.00	9922.69	5.50
310	12015.16	5.47	0.00	0.00	12015.16	5.46
314	439.01	5.47	0.00	0.00	439.01	5.46
316	7149.50	5.47	0.00	0.00	7149.50	5.46
317	741.38	7.75	0.00	0.00	741.38	7.73
318	422.78	5.47	0.00	0.00	422.78	5.46
319	6726.72	5.47	0.00	0.00	6726.72	5.46
322	252.02	4.40	0.00	0.00	252.02	4.39
325	85.87	5.47	0.00	0.00	85.87	5.44
326	421.40	1.65	0.00	0.00	421.40	1.63
327	31.06	1.65	0.00	0.00	31.06	1.64
328	452.46	1.66	0.00	0.00	452.46	1.64
329	8.46	1.65	0.00	0.00	8.46	1.01
330	39.56	7.07	0.00	0.00	39.56	6.84
331	130.52	6.33	0.00	0.00	130.52	6.26
333	0.29	1.65	0.00	0.00	0.29	1.05
334	8.75	1.97	0.00	0.00	8.75	1.04
335	34.18	6.62	0.00	0.00	34.18	3.74
338	106.30	8.26	0.00	0.00	106.30	7.16
337	17.22	6.62	0.00	0.00	17.22	3.74
339	88.82	5.47	0.00	0.00	88.82	5.39
340	16.96	6.62	0.00	0.00	16.96	3.74
341	612.12	5.47	0.00	0.00	612.12	5.46
342	492.63	6.49	0.00	0.00	492.63	6.25
343	40.20	1.65	0.00	0.00	40.20	1.60
344	581.45	6.42	0.00	0.00	581.45	6.20
345	638.18	7.07	0.00	0.00	638.18	6.84
346	52.87	1.65	0.00	0.00	52.87	1.62
347	677.74	7.07	0.00	0.00	677.74	6.84
348	1393.10	8.25	0.00	0.00	1393.10	8.10
349	57.19	1.65	0.00	0.00	57.19	1.63
350	2755.70	6.33	0.00	0.00	2755.70	6.26
351	2300.41	5.84	0.00	0.00	2300.41	5.77
352	2625.19	6.33	0.00	0.00	2625.19	6.26
353	3634.58	6.53	0.00	0.00	3634.58	6.48
355	0.00	0.00	0.00	0.00	0.00	0.00
359	84.49	1.65	0.00	0.00	84.49	1.65
361	135.47	1.65	0.00	0.00	135.47	0.31
362	1839.61	7.58	0.00	0.00	1839.61	7.49
365	0.00	0.00	0.00	0.00	0.00	0.00
366	8.46	1.98	0.00	0.00	8.46	1.04

TABLE B11

POWER ($\dot{W}$), EXERGY DESTRUCTION ($\dot{E}_D$), EXERGY DESTRUCTION RATIO (y^*), RATIO OF EXERGY DESTRUCTION TO THE EXERGY OF SHALE (y), AND EXERGETIC EFFICIENCY (ϵ) FOR COMPONENTS OF THE COMBINED PLANT ORIGINAL DESIGN (FIGURES 25, 26 AND 27)

Component	$\dot{W}$ [MW]	$\dot{E}_D$ [MW]	y^* [%]	y [%]	ϵ [%]
Shale Retorting	8.24	217.80	14.37	3.89	97.8
Gas Scrubbing	3.98	21.83	1.44	0.39	99.8
Acid Gas Removal	0.75	11.41	0.75	0.20	99.8
Sulfur Recovery	1.31	17.79	1.17	0.32	---
Sour Water Stripper & NH_3 Recovery	3.50	27.27	1.80	0.49	---
Hydrogen Recovery	37.60	30.64	2.02	0.55	99.5
Compressor and Heat Exchangers	12.02	45.73	3.02	0.82	96.7
Steam Reformer	0.00	151.98	10.02	2.72	55.8
Shift Conversion & CO_2 Removal	1.01	73.58	4.85	1.32	94.3
Desalting & Hydrotreating	25.02	40.40	2.66	0.72	99.0
Steam Generator	0.00	726.28	47.91	12.99	51.8
HP Turbine	180.37	11.60	0.77	0.21	93.8
IP Turbine	184.30	12.98	0.86	0.23	93.3
LP Turbine	235.07	35.86	2.37	0.64	86.5
Pump 1	0.26	0.08	0.00	0.00	72.7
Preheater 1	0.00	1.45	0.10	0.03	66.4
Pump 4	1.05	0.24	0.02	0.00	77.2
Deaerator	0.00	1.01	0.07	0.02	96.3
Pump 2	1.83	0.44	0.03	0.01	77.2
Preheater 3	0.00	6.87	0.45	0.12	76.1
Preheater 4	0.00	2.53	0.17	0.05	89.0
Pump 3 & Turbine	0.00	4.73	0.31	0.08	70.8
Preheater 5	0.00	3.47	0.23	0.06	91.9

TABLE B12

VARIOUS THERMOECONOMIC VARIABLES FOR COMPONENTS OF THE COMBINED PLANT ORIGINAL DESIGN (FIGURES 25, 26 AND 27)

Component	$\dot{Z}$ [$/hr]	r [%]	$\frac{1-\epsilon}{\epsilon}$ [%]	$\frac{\dot{Z}}{\dot{E}_{P,k}c_{F,k}}$ [%]	f [%]
Shale Retorting	1878.46	4.31	2.22	2.00	47.33
Gas Scrubbing	707.75	0.98	0.22	0.75	76.94
Acid Gas Removal	398.01	0.88	0.19	0.68	78.24
Hydrogen Recovery	1663.64	2.78	0.47	2.25	82.81
Compressor & Heat Exchangers	1036.15	1.98	0.64	1.32	67.32
Steam Reformer	4489.99	235.65	79.25	46.60	37.03
Shift Conversion & CO_2 Removal	1381.54	12.36	6.02	5.64	48.36
Desalting & Hydrotreating	2677.81	6.52	0.96	5.22	84.41
Steam Generator	1879.16	123.37	93.22	13.50	12.65
HP Turbine	185.17	11.84	6.56	4.72	41.82
IP Turbine	189.21	12.51	7.19	4.73	39.66
LP Turbine	241.32	20.05	15.57	3.74	19.35
Pump 1	14.16	210.61	37.64	55.69	59.67
Preheater 1	3.76	51.70	50.56	0.75	1.47
Pump 4	11.70	64.73	29.48	21.40	42.06
Deaerator	6.21	4.99	3.87	1.07	21.65
Pump 2	17.19	57.60	29.46	17.86	37.74
Preheater 3	0.87	31.62	31.47	0.11	0.36
Preheater 4	3.18	13.15	12.34	0.71	5.45
Pump 3 & Turbine	63.58	60.44	41.15	12.02	22.61
Preheater 5	26.30	15.35	8.83	5.65	39.03

TABLE B13

MASS FLOW RATE, TEMPERATURE, PRESSURE, AND FLOW RATES OF ENTHALPY AND EXERGY FOR EACH STREAM OF THE COMBINED PLANT IMPROVED DESIGN (FIGURES 29, 30 AND 31)

Stream	$\dot{m}$ [lb/hr]	T [°F]	P [psia]	$\dot{H}$ [MMBtu/hr]	$\dot{E}$ [MMBtu/hr]
A	2051416	60.0	620.0	-5052.69	19079.93
W	37951	60.0	620.0	-260.15	0.04
B	2014142	600.0	620.0	-4504.64	19148.73
C	1080818	900.0	620.0	-4104.32	3969.81
D	1080818	606.7	620.0	-4223.79	3905.95
1A	287206	810.1	43.3	-19.68	7314.38
1	287206	516.7	620.0	-134.17	7253.33
2	436985	1493.8	620.0	414.25	11426.63
3	724191	1231.8	620.0	394.58	18729.35
4	1733417	900.0	615.0	-588.43	33660.39
6	1808642	600.0	610.0	-1403.68	33509.22
7	436985	516.5	562.1	-204.88	10996.44
8	724191	261.7	572.1	-575.49	18135.48
9	724191	516.5	562.1	-339.53	18223.80
11	79748	297.7	64.7	-454.86	26.29
12	79748	297.7	64.7	-527.57	3.48
16	1439753	460.4	600.0	-1612.39	26856.14
17	1853	460.4	590.0	-4.37	23.92
19	1437899	460.4	595.0	-1608.03	26831.20
20	1437899	332.3	590.0	-1756.62	26772.67
21	1222478	100.0	575.0	-2168.46	22848.83
22	3845	100.0	570.0	-10.15	14.26
23	1194	100.0	570.0	-0.72	25.63
24	1040956	100.0	570.0	-955.15	22808.92
25	1853	460.4	590.0	-4.37	23.92
26	364020	100.0	30.0	-90.66	6456.97
27	6723	470.2	30.0	-4.13	110.09
30	15840	100.0	100.0	-11.19	315.14
31	115894	100.0	20.0	-20.51	2095.49
32	126097	100.0	19.5	-22.16	2272.69
33	132820	107.7	19.5	-27.01	2382.31
34	115894	158.5	100.0	-18.42	2098.92
35	14629	100.0	90.0	-10.47	304.57
36	900004	100.0	560.0	-932.33	20274.14
37	918	100.0	20.0	-6.26	0.00
38	1083	100.0	20.0	-0.22	22.22
39	124903	100.0	19.5	-21.44	2247.35
40	91	90.0	100.0	-0.62	0.00
41	1302	100.0	90.0	-1.25	10.65
42	27153	100.0	18.0	-38.80	189.27
43	875234	100.0	550.0	-901.04	20095.45

TABLE B13 (Continued)

Stream	$\dot{m}$ [lb/hr]	T [°F]	P [psia]	$\dot{H}$ [MMBtu/hr]	$\dot{E}$ [MMBtu/hr]
44	726	90.0	90.0	-4.96	0.00
45	355	90.0	560.0	-2.42	0.00
46	25124	100.0	550.0	-33.80	180.95
48	26426	36.9	90.0	-35.05	190.44
51	25258	99.7	14.7	0.10	202.64
52	37822	99.7	14.7	-50.47	272.09
53	10670	100.0	14.7	-11.67	82.99
54	14676	99.7	14.7	-100.02	0.04
55	14676	99.7	14.7	-100.02	0.04
56	10492	99.7	14.7	-40.86	1.45
57	44235	297.7	64.7	-292.64	1.93
58	44235	297.7	64.7	-252.31	14.58
59	616868	351.7	17.6	-716.90	29.14
60	2706	100.0	100.0	-0.96	55.40
61	3789	100.0	20.0	-1.18	77.53
62	690516	100.0	14.7	-205.89	13481.27
63	61233	192.2	1717.5	-52.55	1927.00
64	50295	100.0	100.0	-91.69	799.24
65	30752	100.0	14.7	-102.30	160.68
67	1083	100.0	20.0	-0.22	22.22
68	567	100.0	210.3	-3.87	0.00
69	79244	297.7	64.7	-451.99	26.13
70	81580	297.7	64.7	-537.59	3.46
71	222831	101.0	14.7	-1411.02	161.18
72	10815	100.0	214.7	-12.45	93.68
73	205191	130.0	25.0	-1392.16	1.16
74	177402	101.5	20.0	-1208.70	0.47
75	192078	101.3	14.7	-1308.72	0.51
76	222	110.4	18.4	-0.44	4.91
78	1348744	60.0	14.7	-5.47	1.22
79	1348744	92.4	17.6	5.08	10.33
80	7594	80.3	320.0	-15.29	169.58
81	348343	100.0	550.0	-358.61	7997.99
82	123892	100.0	214.7	-100.74	3693.29
83	223015	100.0	16.7	-249.70	4254.18
84	526891	100.0	550.0	-542.42	12097.46
85	526891	137.5	661.9	-523.40	12111.85
86	123892	246.5	680.0	-66.46	3739.41
87	1436	250.0	20.0	-7.99	0.42
88	650784	171.7	661.9	-589.86	15845.00
90	2999	100.0	320.0	-6.01	66.98
91	237644	100.0	16.7	-260.17	4557.53
92	192370	100.0	16.7	-210.60	3689.27
93	192370	242.4	320.0	-197.68	3715.21
94	73407	100.0	210.3	-75.27	2267.32

TABLE B13 (Continued)

Stream	$\dot{m}$ [lb/hr]	T [°F]	P [psia]	$\dot{H}$ [MMBtu/hr]	$\dot{E}$ [MMBtu/hr]
95	73407	226.8	572.1	-58.35	2289.66
96	45273	100.0	16.7	-49.56	868.25
97	61233	100.0	210.3	-62.78	1891.30
98	330906	488.8	614.7	-2120.47	41.54
99	724191	180.0	572.1	-648.20	18118.47
100	330906	488.8	614.7	-1879.34	150.56
101	195369	239.8	320.0	-203.68	3782.03
102	195369	297.7	310.0	-197.72	3783.49
103	747971	445.0	310.0	-3304.69	4009.17
104	747971	1463.1	290.0	-2840.70	4292.01
105	747971	1535.0	290.0	-2804.26	4318.57
106	748129	1535.0	290.0	-2167.28	4705.80
107	748129	822.7	280.0	-2514.78	4467.93
109	894640	758.8	280.0	-3346.87	4517.79
110	894802	900.0	280.0	-3349.89	4516.27
111	894802	551.7	260.3	-3539.85	4405.32
112	894802	100.0	220.3	-4148.12	4220.43
113	528290	100.0	215.3	-1650.61	4218.62
114	134641	100.0	210.3	-138.05	4158.62
115	552602	558.8	614.7	-3106.97	266.25
116	146510	488.8	614.7	-832.09	66.66
117	366512	100.0	215.3	-2497.51	1.15
118	393082	100.0	210.3	-1511.04	81.94
119	2336	90.0	260.0	-13.35	0.01
120	40873	110.4	18.4	-59.59	719.94
122	176484	100.0	575.0	-1202.44	0.74
123	176484	100.0	575.0	-1202.44	0.74
124	177402	101.5	20.0	-1208.70	0.47
127	127156	297.7	64.7	-725.27	41.92
128	127156	297.7	64.7	-841.20	5.54
129	64105	488.8	614.7	-364.08	29.17
130	64105	488.8	614.7	-410.79	8.05
131	54110	60.0	14.7	-0.22	0.05
132	104175	488.8	614.7	-667.56	13.08
133	93757	488.8	614.7	-532.48	42.66
134	10417	488.8	614.7	-66.76	1.31
135	38587	488.8	614.7	-219.15	17.56
136	38587	488.8	614.7	-247.27	4.84
137	21592	297.7	64.7	-123.16	7.12
138	21592	297.7	64.7	-142.84	0.94
139	772674	91.8	17.6	2.82	5.91
140	54911	110.4	18.4	-79.90	965.83
141	2916007	293.7	2860.1	-19287.21	146.21
142	2916007	343.7	2802.9	-19138.63	195.21
143	400357	60.0	14.7	-2744.34	0.43

TABLE B13 (Continued)

Stream	$\dot{m}$ [lb/hr]	T [°F]	P [psia]	$\dot{H}$ [MMBtu/hr]	$\dot{E}$ [MMBtu/hr]
144	400357	296.3	14.7	-2278.82	100.21
147	100821	488.8	614.7	-646.07	12.66
148	100821	488.8	614.7	-572.60	45.87
149	117602	297.7	64.7	-778.00	5.13
150	117602	297.7	64.7	-670.77	38.77
151	1122554	60.0	14.7	-7694.80	1.21
152	1122554	140.0	14.7	-7605.13	7.47
153	1437899	332.3	580.0	-1756.59	26770.50
154	1045994	100.0	575.0	-965.92	22849.25
155	894802	351.7	250.3	-3647.07	4356.91
157	576070	92.2	17.6	2.15	4.41
160	827484	542.8	17.6	-918.18	57.60
161	827484	217.7	14.7	-991.63	24.60
162	772674	476.3	17.6	76.26	26.94
163	894802	351.7	250.3	-3647.07	4356.91
164	894802	340.2	240.3	-3653.03	4352.13
165	36483	60.0	22.0	-250.08	0.04
166	36483	224.3	22.0	-244.08	0.83
167	198881	677.0	164.7	-1097.51	92.27
168	198881	364.8	164.7	-1301.77	13.48
169	276282	488.8	614.7	-1569.11	125.71
171	3789075	60.0	14.7	-25973.07	4.07
172	3789075	114.0	14.7	-25768.80	14.00
173	1084256	60.0	14.7	-7432.28	1.16
174	1084256	114.0	14.7	-7373.83	4.01
175	30148	297.7	64.7	-171.96	9.94
176	30148	297.7	64.7	-199.44	1.31
177	30148	677.0	164.7	-166.37	13.99
178	30148	364.8	164.7	-197.33	2.04
179	747971	712.9	300.0	-3188.20	4065.49
180	894802	766.9	270.0	-3423.36	4469.95
216	368890	460.4	600.0	-27.25	6561.34
217	368890	460.4	590.0	-27.25	6561.34
221	215422	100.0	575.0	-53.65	3821.13
223	215422	100.0	570.0	-53.65	3821.13
225	368890	460.4	590.0	-27.25	6561.34
226	364020	100.0	30.0	-90.66	6456.97
232	231470	100.0	19.5	-57.65	4105.80
233	231470	107.7	19.5	-56.93	4105.86
238	246395	100.0	20.0	-61.37	4370.53
239	16049	100.0	19.5	-4.00	284.67
254	215422	100.0	575.0	-53.65	3821.13
260	97348	100.0	100.0	-24.24	1726.75
261	707763	100.0	20.0	-176.27	12554.24

TABLE B13 (Continued)

Stream	$\dot{m}$ [lb/hr]	T [°F]	P [psia]	$\dot{H}$ [MMBtu/hr]	$\dot{E}$ [MMBtu/hr]
262	690516	100.0	14.7	-205.89	13481.27
267	610415	100.0	20.0	-152.03	10827.50
301	2916007	1000.4	2422.1	-15811.81	1942.38
302	4373	80.3	320.0	-8.80	97.65
305	251254	648.8	653.5	-1398.37	129.14
306	2388433	648.8	653.5	-13292.92	1227.66
310	2388433	1000.4	588.7	-12813.71	1497.52
311	276320	648.9	653.5	-1537.86	142.04
314	152853	831.9	313.7	-832.35	82.81
316	2006551	589.6	110.5	-11154.78	842.97
318	140583	589.6	110.5	-781.52	59.06
319	1865968	589.6	110.5	-10373.26	783.91
321	1865968	589.3	108.3	-10373.26	781.82
322	129652	488.4	64.7	-726.80	47.66
323	26966	488.4	64.7	-151.16	9.91
326	1709351	112.3	1.4	-9995.21	155.35
327	140583	118.2	1.6	-817.39	14.48
328	1849934	112.3	1.4	-10812.59	168.55
329	1849934	103.6	1.4	-12600.25	5.12
330	129652	297.7	64.7	-857.71	5.65
331	286699	293.7	2860.1	-1896.30	14.37
332	2412953	93.5	1.4	-16459.60	4.98
335	2412953	93.5	58.0	-16459.08	5.40
337	2412953	260.9	55.1	-16053.66	78.20
339	229029	365.9	164.7	-1498.84	15.63
340	3202707	287.2	55.1	-21219.37	129.68
341	229029	677.0	164.7	-1263.88	106.25
343	404108	334.1	273.0	-2657.99	22.87
349	251254	427.1	568.7	-1627.61	23.91
350	3202707	293.7	2860.1	-21183.51	160.58
352	2916007	408.8	2718.9	-18940.59	269.59
353	2916007	481.0	2688.6	-18711.35	366.94
354	140583	588.5	102.4	-781.52	58.46
355	3373489	60.0	14.7	-13.67	3.04
356	3373489	121.0	20.3	36.12	44.74
357	3373489	482.0	18.4	337.68	124.95
358	1080818	606.7	14.7	-4223.79	3905.95
359	793283	800.3	14.5	-4100.64	48.45
361	3665734	320.0	14.7	-3476.15	370.40
365	563019	60.0	14.7	-3859.34	0.60
370	404108	421.5	313.7	-2459.95	102.98

TABLE B14

FLOW RATES OF PHYSICAL, REACTION, ENVIRONMENTAL, CHEMICAL, AND TOTAL EXERGY OF EACH STREAM IN THE COMBINED PLANT IMPROVED DESIGN (FIGURES 29, 30 AND 31)

Stream	$\dot{E}^{PH}$ [MMBtu/hr]	$\dot{E}^{R}$ [MMBtu/hr]	$\dot{E}^{E}$ [MMBtu/hr]	$\dot{E}^{CH}$ [MMBtu/hr]	$\dot{E}^{TOT}$ [MMBtu/hr]
A	0.000	18384.370	686.406	19079.932	19079.932
W	0.000	0.000	0.041	0.041	0.041
B	97.934	18390.730	661.155	19051.886	19148.730
C	119.404	3523.008	327.631	3850.640	3969.814
D	55.539	3523.008	327.631	3850.640	3905.952
1A	288.850	6982.086	43.855	7025.944	7314.375
1	227.789	6981.689	43.854	7025.543	7253.332
2	737.257	10622.645	66.725	10689.369	11426.627
3	1014.435	17604.334	110.583	17714.916	18729.352
4	944.073	32158.941	557.383	32716.322	33660.395
6	720.044	32195.799	593.377	32789.176	33509.219
7	338.103	10591.723	66.616	10658.339	10996.441
8	471.992	17553.086	110.399	17663.482	18135.477
9	560.320	17553.086	110.399	17663.482	18223.805
11	26.207	0.000	0.086	0.086	26.292
12	3.390	0.000	0.086	0.086	3.476
16	595.822	25861.584	398.737	26260.320	26856.145
17	0.575	22.965	0.383	23.348	23.923
19	594.203	25838.615	398.383	26237.000	26831.203
20	535.672	25838.615	398.383	26237.000	26772.672
21	422.662	22139.609	286.559	22426.168	22848.832
22	0.348	8.564	5.346	13.910	14.258
23	0.205	24.889	0.533	25.422	25.628
24	419.180	22106.156	283.581	22389.738	22808.918
25	0.575	22.965	0.383	23.348	23.923
26	0.210	6250.601	206.154	6456.755	6456.965
27	0.476	106.577	3.036	109.613	110.089
30	1.032	306.792	7.314	314.106	315.138
31	0.676	2032.748	62.067	2094.814	2095.490
32	0.660	2204.322	67.711	2272.033	2272.693
33	0.744	2310.899	70.663	2381.562	2382.305
34	4.107	2032.748	62.067	2094.814	2098.921
35	0.917	300.160	3.490	303.650	304.567
36	408.872	19651.154	214.116	19865.270	20274.143
37	0.001	0.000	0.001	0.001	0.002
38	0.008	21.883	0.331	22.215	22.223
39	0.643	2179.433	67.276	2246.709	2247.353

TABLE B14 (Continued)

Stream	$\dot{E}^{PH}$ [MMBtu/hr]	$\dot{E}^{R}$ [MMBtu/hr]	$\dot{E}^{E}$ [MMBtu/hr]	$\dot{E}^{CH}$ [MMBtu/hr]	$\dot{E}^{TOT}$ [MMBtu/hr]
40	0.000	0.000	0.000	0.000	0.000
41	0.067	6.632	3.953	10.585	10.652
42	0.187	118.282	70.806	189.087	189.275
43	404.352	19539.502	151.590	19691.094	20095.445
44	0.001	0.000	0.001	0.001	0.002
45	0.001	0.000	0.000	0.000	0.001
46	2.427	111.650	66.874	178.524	180.951
48	1.336	118.282	70.827	189.108	190.444
51	0.006	0.000	202.637	202.637	202.643
52	0.025	170.251	101.814	272.064	272.090
53	0.004	51.969	31.013	82.982	82.985
54	0.021	0.000	0.016	0.016	0.037
55	0.021	0.000	0.016	0.016	0.037
56	0.013	0.017	1.416	1.433	1.446
57	1.881	0.000	0.048	0.048	1.928
58	14.536	0.000	0.048	0.048	14.584
59	18.903	0.000	10.234	10.234	29.137
60	0.106	54.394	0.895	55.289	55.395
61	0.028	76.277	1.221	77.498	77.527
62	0.398	13125.380	355.497	13480.876	13481.274
63	79.292	1840.449	7.261	1847.711	1927.003
64	4.521	784.316	10.405	794.721	799.241
65	0.064	135.119	25.493	160.613	160.677
67	0.008	21.883	0.331	22.215	22.223
68	0.001	0.000	0.001	0.001	0.002
69	26.041	0.000	0.085	0.085	26.126
70	3.369	0.000	0.085	0.085	3.454
71	0.364	135.119	25.700	160.819	161.183
72	1.765	91.687	0.227	91.914	93.679
73	0.893	0.027	0.236	0.263	1.156
74	0.281	0.000	0.191	0.191	0.471
75	0.299	0.000	0.206	0.206	0.506
76	0.003	4.841	0.065	4.906	4.910
78	0.000	0.000	1.216	1.216	1.216
79	9.115	0.000	1.216	1.216	10.331
80	1.486	165.859	2.232	168.091	169.577
81	160.932	7776.723	60.332	7837.055	7997.987
82	93.629	3583.945	15.721	3599.666	3693.294
83	1.386	4192.732	60.063	4252.794	4254.181
84	243.420	11762.781	91.257	11854.039	12097.459
85	257.813	11762.781	91.257	11854.039	12111.852
86	139.748	3583.945	15.721	3599.666	3739.414

TABLE B14 (Continued)

Stream	$\dot{E}^{PH}$ [MMBtu/hr]	$\dot{E}^{R}$ [MMBtu/hr]	$\dot{E}^{E}$ [MMBtu/hr]	$\dot{E}^{CH}$ [MMBtu/hr]	$\dot{E}^{TOT}$ [MMBtu/hr]
87	0.337	0.046	0.041	0.088	0.425
88	395.446	15346.724	102.832	15449.556	15845.003
90	0.589	65.510	0.881	66.392	66.980
91	1.471	4492.892	63.164	4556.056	4557.527
92	1.190	3636.951	51.131	3688.082	3689.272
93	27.132	3636.951	51.131	3688.082	3715.214
94	52.255	2206.359	8.704	2215.063	2267.318
95	74.593	2206.359	8.704	2215.063	2289.656
96	0.280	855.941	12.033	867.974	868.254
97	43.589	1840.449	7.261	1847.711	1891.300
98	41.186	0.000	0.355	0.355	41.541
99	454.985	17553.086	110.399	17663.482	18118.469
100	150.209	0.000	0.355	0.355	150.564
101	27.704	3702.461	51.869	3754.330	3782.034
102	29.157	3702.461	51.869	3754.330	3783.487
103	254.456	3702.461	52.248	3754.709	4009.165
104	537.301	3702.461	52.248	3754.709	4292.010
105	563.862	3702.461	52.248	3754.709	4318.571
106	575.635	4094.001	36.160	4130.161	4705.796
107	337.768	4094.001	36.160	4130.160	4467.928
109	387.469	4094.001	36.317	4130.317	4517.786
110	419.461	4049.121	47.689	4096.810	4516.271
111	308.506	4049.121	47.688	4096.810	4405.315
112	123.620	4049.121	47.689	4096.810	4220.429
113	121.503	4049.121	47.993	4097.114	4218.618
114	95.845	4046.808	15.966	4062.774	4158.619
115	265.658	0.000	0.593	0.593	266.252
116	66.506	0.000	0.157	0.157	66.663
117	0.753	0.000	0.394	0.394	1.147
118	23.960	2.313	55.668	57.982	81.942
119	0.015	0.000	0.003	0.003	0.018
120	0.468	710.054	9.415	719.469	719.937
122	0.550	0.000	0.190	0.190	0.740
123	0.550	0.000	0.190	0.190	0.740
124	0.281	0.000	0.191	0.191	0.471
127	41.786	0.000	0.137	0.137	41.923
128	5.406	0.000	0.137	0.137	5.542
129	29.099	0.000	0.069	0.069	29.168
130	7.979	0.000	0.069	0.069	8.048
131	0.000	0.000	0.049	0.049	0.049
132	12.966	0.000	0.112	0.112	13.078
133	42.559	0.000	0.101	0.101	42.660

TABLE B14 (Continued)

Stream	$\dot{E}^{PH}$ [MMBtu/hr]	$\dot{E}^{R}$ [MMBtu/hr]	$\dot{E}^{E}$ [MMBtu/hr]	$\dot{E}^{CH}$ [MMBtu/hr]	$\dot{E}^{TOT}$ [MMBtu/hr]
134	1.297	0.000	0.011	0.011	1.308
135	17.516	0.000	0.041	0.041	17.557
136	4.803	0.000	0.041	0.041	4.844
137	7.096	0.000	0.023	0.023	7.119
138	0.918	0.000	0.023	0.023	0.941
139	5.216	0.000	0.697	0.697	5.913
140	0.628	952.567	12.639	965.206	965.834
141	143.076	0.000	3.132	3.132	146.208
142	192.076	0.000	3.132	3.132	195.208
143	0.000	0.000	0.430	0.430	0.430
144	99.778	0.000	0.430	0.430	100.208
147	12.549	0.000	0.108	0.108	12.657
148	45.766	0.000	0.108	0.108	45.874
149	4.999	0.000	0.126	0.126	5.126
150	38.646	0.000	0.126	0.126	38.773
151	0.000	0.000	1.206	1.206	1.206
152	6.267	0.000	1.206	1.206	7.473
153	533.505	25838.615	398.383	26237.000	26770.504
154	420.757	22139.609	288.880	22428.488	22849.246
155	260.102	4049.121	47.688	4096.810	4356.912
157	3.892	0.000	0.520	0.520	4.411
160	43.855	0.000	13.744	13.744	57.598
161	10.857	0.000	13.744	13.744	24.600
162	26.243	0.000	0.697	0.697	26.939
163	260.102	4049.121	47.688	4096.810	4356.912
164	255.326	4049.121	47.689	4096.810	4352.135
165	0.001	0.000	0.039	0.039	0.040
166	0.789	0.000	0.039	0.039	0.828
167	92.052	0.000	0.214	0.214	92.265
168	13.270	0.000	0.214	0.214	13.484
169	125.413	0.000	0.297	0.297	125.710
171	0.000	0.000	4.069	4.069	4.069
172	9.928	0.000	4.069	4.069	13.997
173	0.000	0.000	1.164	1.164	1.164
174	2.842	0.000	1.164	1.164	4.006
175	9.907	0.000	0.032	0.032	9.940
176	1.282	0.000	0.032	0.032	1.314
177	13.954	0.000	0.032	0.032	13.986
178	2.012	0.000	0.032	0.032	2.044
179	310.780	3702.461	52.248	3754.709	4065.489
180	373.143	4049.121	47.688	4096.810	4469.952

TABLE B14 (Continued)

Stream	$\dot{E}^{PH}$ [MMBtu/hr]	$\dot{E}^{R}$ [MMBtu/hr]	$\dot{E}^{E}$ [MMBtu/hr]	$\dot{E}^{CH}$ [MMBtu/hr]	$\dot{E}^{TOT}$ [MMBtu/hr]
216	18.212	6334.214	208.910	6543.124	6561.336
217	18.212	6334.214	208.910	6543.124	6561.336
221	0.124	3699.007	121.999	3821.006	3821.130
223	0.124	3699.007	121.999	3821.006	3821.130
225	18.212	6334.214	208.910	6543.124	6561.336
226	0.210	6250.601	206.154	6456.755	6456.965
232	0.133	3974.580	131.087	4105.667	4105.801
233	0.189	3974.580	131.087	4105.667	4105.856
238	0.142	4230.848	139.539	4370.386	4370.528
239	0.009	275.573	9.089	284.662	284.671
254	0.124	3699.007	121.999	3821.006	3821.130
260	0.056	1671.562	55.130	1726.693	1726.749
261	0.408	12153.013	400.823	12553.836	12554.244
262	0.398	13125.380	355.497	13480.876	13481.274
267	0.352	10481.450	345.692	10827.144	10827.495
301	1939.246	0.000	3.132	3.132	1942.378
302	0.856	95.508	1.285	96.793	97.649
303	1.963	95.508	1.285	96.793	98.756
304	2217.978	0.000	319.778	319.778	2537.756
305	128.875	0.000	0.270	0.270	129.145
306	1225.092	0.000	2.565	2.565	1227.657
307	71.087	0.000	0.666	0.666	71.752
308	2288.220	0.000	319.847	319.847	2608.067
309	543.590	0.000	0.000	0.000	543.590
310	1494.954	0.000	2.565	2.565	1497.519
311	141.739	0.000	0.297	0.297	142.036
314	82.646	0.000	0.164	0.164	82.810
316	840.818	0.000	2.155	2.155	842.973
318	58.909	0.000	0.151	0.151	59.060
319	781.909	0.000	2.004	2.004	783.913
321	779.821	0.000	2.004	2.004	781.825
322	47.519	0.000	0.139	0.139	47.659
323	9.883	0.000	0.029	0.029	9.912
326	153.511	0.000	1.836	1.836	155.347
327	14.329	0.000	0.151	0.151	14.480
328	166.562	0.000	1.987	1.987	168.548
329	3.133	0.000	1.987	1.987	5.120
330	5.512	0.000	0.139	0.139	5.651
331	14.067	0.000	0.308	0.308	14.375
332	2.393	0.000	2.591	2.591	4.985
335	2.808	0.000	2.591	2.591	5.399

TABLE B14 (Continued)

Stream	$\dot{E}^{PH}$ [MMBtu/hr]	$\dot{E}^{R}$ [MMBtu/hr]	$\dot{E}^{E}$ [MMBtu/hr]	$\dot{E}^{CH}$ [MMBtu/hr]	$\dot{E}^{TOT}$ [MMBtu/hr]
337	75.610	0.000	2.591	2.591	78.201
339	15.381	0.000	0.246	0.246	15.627
340	126.238	0.000	3.439	3.439	129.677
341	106.005	0.000	0.246	0.246	106.251
343	22.439	0.000	0.434	0.434	22.873
349	23.640	0.000	0.270	0.270	23.909
350	157.142	0.000	3.439	3.439	160.581
352	266.454	0.000	3.132	3.132	269.585
353	363.806	0.000	3.132	3.132	366.938
354	58.305	0.000	0.151	0.151	58.456
355	0.000	0.000	3.042	3.042	3.042
356	41.695	0.000	3.042	3.042	44.737
357	121.911	0.000	3.042	3.042	124.953
359	48.448	0.000	0.000	0.000	48.448
361	50.549	0.000	319.847	319.847	370.396
365	0.000	0.000	0.605	0.605	0.605
370	102.549	0.000	0.434	0.434	102.983

TABLE B15

HEAT TRANSFER RATE ($\dot{Q}$), POWER ($\dot{W}$), EXERGY DESTRUCTION FLOW RATE ($\dot{E}_D$), EXERGY DESTRUCTION RATIO (y^*), RATIO OF EXERGY DESTRUCTION TO THE EXERGY OF SHALE (y), AND EXERGETIC EFFICIENCY (ϵ) FOR EACH COMPONENT OF THE COMBINED PLANT IMPROVED DESIGN (FIGURES 29, 30 AND 31)

Component	$\dot{Q}$ [MW]	$\dot{W}$ [MW]	$\dot{E}_D$ [MW]	y^* [%]	y [%]	ϵ [%]
Preheat	2.07	0.00	24.15	2.12	0.43	45.48
Retort	26.53	8.24	80.91	7.10	1.43	98.18
Cooling	1.46	0.00	0.83	0.07	0.01	95.59
Mixing 1A+2=3	0.00	0.00	3.42	0.30	0.06	99.94
Heat Exchanger	0.00	0.00	1.00	0.09	0.02	96.28
Gas-Oil Separator	0.00	0.00	0.30	0.03	0.01	100.00
Gs Cooler I	0.00	0.00	0.00	0.00	0.00	0.00
Knock-Out Drum I	0.00	0.00	0.64	0.06	0.01	99.99
Gas Cooler II	0.00	0.00	0.22	0.02	0.00	99.24
3-Phase Separator	0.00	0.00	0.21	0.02	0.00	100.00
Lean Oil Scrubber	0.77	0.00	0.81	0.07	0.01	99.99
Lean Oil Stripper	16.94	1.96	8.13	0.71	0.14	99.57
Acid Gas Removal	34.37	0.75	11.41	1.00	0.20	99.81
Gas Compressor 31/34	1.22	1.93	0.92	0.08	0.02	52.11
Knock-Out Drum III	5.27	0.00	0.48	0.04	0.01	99.92
Claus & Scot Units	21.70	1.31	17.73	1.56	0.31	79.53
Heavy Oil Flash Drum	18.51	0.00	5.34	0.47	0.09	99.72
Hydrogen Recovery	0.00	0.00	14.68	1.29	0.26	99.37
Recycle Gas Compr. 82/86	10.05	21.16	7.64	0.67	0.14	63.89
Recycle Gas Compr. 84/85	0.00	5.87	1.65	0.14	0.03	71.88
Recycle Gas Compr. 94/95	5.14	10.63	4.09	0.36	0.07	61.56
Compr. to H_2 Plant 92/93	7.63	12.02	4.42	0.39	0.08	63.26
Mixing with Natural Gas	0.00	0.00	0.05	0.00	0.00	100.00
Preheat 101/102	0.00	0.00	0.97	0.09	0.02	30.43
Mixing with Steam 115	0.00	0.00	11.89	1.04	0.21	99.00
Preheat 179/104	0.00	0.00	2.44	0.21	0.04	87.14
Preheat 179/104	0.00	0.00	3.33	0.29	0.06	95.23
Reformer Furnace	0.00	0.00	124.36	10.92	2.20	55.20
Heat Recovery Boiler HP	0.00	0.00	3.84	0.34	0.07	71.72
Heat Recovery Boiler LP	0.00	0.00	4.32	0.38	0.08	69.51
Knock-Out Drum IV	0.00	0.00	0.00	0.00	0.00	100.00
Cooling by Water	0.00	0.00	2.53	0.22	0.04	42.10
Knock-Out Drum V	0.00	0.00	0.19	0.02	0.00	99.98

TABLE B15 (Continued)

Component	$\dot{Q}$ [MW]	$\dot{W}$ [MW]	$\dot{E}_D$ [MW]	y^* [%]	y [%]	ϵ [%]
CO_2 Removal	22.88	1.02	1.23	0.11	0.02	99.90
Compression before D&H	16.15	20.16	9.70	0.85	0.17	51.90
Desalting Hydrotreating	54.92	5.13	59.54	5.23	1.06	98.60
NH_3 Recovery	2.07	3.50	8.00	0.70	0.14	86.70
Fired Heater	0.00	0.00	75.40	6.62	1.34	63.98
Air Fan	0.00	3.26	0.58	0.05	0.01	82.07
Steam Generator	0.00	14.09	524.77	46.06	9.30	50.75
HP Turbine	0.00	-119.87	10.12	0.89	0.18	92.21
IP Turbine	0.00	-125.60	10.82	0.95	0.19	92.07
LP Turbine	0.00	-143.58	23.15	2.03	0.41	86.12
Condenser	523.91	0.00	47.90	4.20	0.85	0.00
Pump 1	0.00	0.16	0.04	0.00	0.00	77.17
Preheater in H2Plant	0.00	0.00	12.90	1.13	0.23	62.32
Deaerator	0.00	0.00	0.76	0.07	0.01	98.04
Pump 2	0.00	10.51	1.45	0.13	0.03	86.18
Turbine	0.00	-10.51	2.55	0.22	0.05	80.45
Preheater in PFH Plant	0.00	0.00	2.79	0.25	0.05	83.72
Preheater 1	0.00	0.00	2.78	0.24	0.05	88.71
Preheater 2	0.00	0.00	2.31	0.20	0.04	92.51
Sum	771.36	-277.86	1139.25	100.00	20.19	98.32
PFH Plant	362.54	96.94	663.83	43.62	8.81	85.62
Steam Power Plant	523.87	-361.10	774.89	56.38	11.39	36.74
Total Plant	771.36	-264.16	1406.72	100.00	25.02	74.98

TABLE B16

COSTS ASSOCIATED WITH PHYSICAL, CHEMICAL, AND TOTAL EXERGY OF EACH STREAM IN THE COMBINED PLANT IMPROVED DESIGN (FIGURES 25, 29, 30 AND 31)

Stream	Physical Exergy Cost Flow [$/hr]	Cost of Physical Exergy Unit [$/GJ]	Chemical Exergy Cost Flow [$/hr]	Cost of Chemical Exergy Unit [$/GJ]	Total Exergy Cost Flow [$/hr]	Cost of Total Exergy Unit [$/GJ]
A	0.00	0.00	33074.44	1.64	33074.44	1.64
D	96.27	1.64	6674.56	1.64	6770.83	1.64
11	127.75	4.62	0.00	0.00	127.75	4.61
12	16.53	4.62	0.00	0.00	16.53	4.51
17	49.15	2.48	17180.20	2.48	17229.35	2.48
19	1554.64	2.48	68645.21	2.48	70199.85	2.48
22	0.91	2.48	0.00	0.00	0.91	0.06
30	2.70	2.48	821.81	2.48	824.51	2.48
35	2.58	2.67	855.62	2.67	858.21	2.67
36	1069.75	2.48	51974.53	2.48	53044.28	2.48
40	0.00	0.00	0.00	0.00	0.00	0.00
42	0.00	0.00	0.00	0.00	0.00	0.00
43	1078.80	2.53	52535.07	2.53	53613.87	2.53
44	0.00	0.00	0.00	0.00	0.00	0.00
45	0.00	0.00	0.00	0.00	0.00	0.00
47	0.00	0.00	0.00	0.00	0.00	0.00
51	0.00	0.00	788.69	3.69	788.69	3.69
52	0.00	0.00	0.00	0.00	0.00	0.00
53	0.00	0.00	0.00	0.00	0.00	0.00
54	0.00	0.00	0.00	0.00	0.00	0.00
55	0.00	0.00	0.00	0.00	0.00	0.00
56	0.00	0.00	0.00	0.00	0.00	0.00
57	19.84	10.00	0.00	0.00	19.84	9.75
58	43.81	2.86	0.00	0.00	43.81	2.85
61	1.14	2.48	34343.56	2.58	34344.70	2.58
62	1.04	2.48	45172.28	3.18	45173.32	3.18
64	21.58	4.53	2662.98	3.18	2684.57	3.18
65	0.00	0.00	0.00	0.00	0.00	0.00
68	0.00	0.00	0.00	0.00	0.00	0.00
69	274.75	10.00	0.00	0.00	274.75	9.97
70	35.54	10.00	0.00	0.00	35.54	9.75
71	0.73	1.91	0.00	0.00	0.73	0.00
72	0.00	0.00	755.23	7.79	755.23	7.64
73	0.00	0.00	0.00	0.00	0.00	0.00
74	0.73	2.48	0.00	0.00	0.73	1.48
75	0.73	2.33	0.00	0.00	0.73	1.38
76	0.00	0.00	21.19	4.09	21.19	4.09
78	0.00	0.00	0.00	0.00	0.00	0.00

TABLE B16 (Continued)

Stream	Physical Exergy Cost Flow [$/hr]	Cost of Physical Exergy Unit [$/GJ]	Chemical Exergy Cost Flow [$/hr]	Cost of Chemical Exergy Unit [$/GJ]	Total Exergy Cost Flow [$/hr]	Cost of Total Exergy Unit [$/GJ]
79	142.91	14.86	0.00	0.00	142.91	13.11
80	0.00	0.00	726.05	4.09	726.05	4.06
83	3.70	2.53	11346.29	2.53	11349.99	2.53
87	0.00	0.00	0.00	0.00	0.00	0.00
90	0.00	0.00	286.77	4.09	286.77	4.06
91	6.28	4.05	12201.91	2.54	12208.20	2.54
92	5.09	4.05	9877.33	2.54	9882.41	2.54
94	249.49	4.53	11162.46	4.78	11411.95	4.77
96	1.20	4.05	2324.59	2.54	2325.78	2.54
97	208.11	4.53	9311.24	4.78	9519.36	4.77
98	299.24	6.89	0.00	0.00	299.24	6.83
99	1424.71	2.97	55310.49	2.97	56735.20	2.97
100	1852.41	11.69	0.00	0.00	1852.41	11.66
104	2074.65	3.66	14497.85	3.66	16572.50	3.66
106	2748.32	4.53	19719.08	4.53	22467.40	4.53
107	1612.64	4.53	19719.10	4.53	21331.74	4.53
111	1472.93	4.53	19559.87	4.53	21032.80	4.53
114	457.60	4.53	20473.70	4.78	20931.30	4.77
115	1805.18	6.44	0.00	0.00	1805.18	6.43
116	588.29	8.38	0.00	0.00	588.29	8.36
117	0.00	0.00	0.00	0.00	0.00	0.00
118	0.00	0.00	0.00	0.00	0.00	0.00
119	0.00	0.00	0.00	0.00	0.00	0.00
120	0.00	0.00	2168.39	2.86	2168.39	2.85
127	203.70	4.62	0.00	0.00	203.70	4.61
128	26.35	4.62	0.00	0.00	26.35	4.51
129	257.40	8.38	0.00	0.00	257.40	8.36
130	70.58	8.38	0.00	0.00	70.58	8.31
131	0.00	0.00	0.00	0.00	0.00	0.00
132	0.00	0.00	0.00	0.00	0.00	0.00
133	0.00	0.00	0.00	0.00	0.00	0.00
134	0.00	0.00	0.00	0.00	0.00	0.00
135	154.94	8.38	0.00	0.00	154.94	8.36
136	42.48	8.38	0.00	0.00	42.48	8.31
137	34.59	4.62	0.00	0.00	34.59	4.61
138	4.47	4.62	0.00	0.00	4.47	4.51
139	81.78	14.86	0.00	0.00	81.78	13.11
140	0.00	0.00	2909.01	2.86	2909.01	2.85
141	830.52	5.50	0.00	0.00	830.52	5.38
142	958.72	4.73	0.00	0.00	958.72	4.65
143	0.00	0.00	0.00	0.00	0.00	0.00
144	0.00	0.00	0.00	0.00	0.00	0.00

TABLE B16 (Continued)

Stream	Physical Exergy Cost Flow [$/hr]	Cost of Physical Exergy Unit [$/GJ]	Chemical Exergy Cost Flow [$/hr]	Cost of Chemical Exergy Unit [$/GJ]	Total Exergy Cost Flow [$/hr]	Cost of Total Exergy Unit [$/GJ]
147	91.17	6.89	0.00	0.00	91.17	6.83
148	249.77	5.17	0.00	0.00	249.77	5.16
149	52.75	10.00	0.00	0.00	52.75	9.75
150	213.39	5.23	0.00	0.00	213.39	5.22
151	0.00	0.00	0.00	0.00	0.00	0.00
152	0.00	0.00	0.00	0.00	0.00	0.00
155	1241.84	4.53	19559.87	4.53	20801.70	4.53
157	61.13	14.89	0.00	0.00	61.13	13.13
59	81.65	4.09	0.00	0.00	81.65	2.66
161	32.72	2.86	0.00	0.00	32.72	1.26
164	0.00	0.00	19559.87	4.53	19559.87	4.26
165	0.00	0.00	0.00	0.00	0.00	0.00
166	0.00	0.00	0.00	0.00	0.00	0.00
167	452.55	4.66	0.00	0.00	452.55	4.65
168	65.24	4.66	0.00	0.00	65.24	4.59
169	1105.26	8.35	0.00	0.00	1105.26	8.33
171	0.00	0.00	0.00	0.00	0.00	0.00
172	0.00	0.00	0.00	0.00	0.00	0.00
173	0.00	0.00	0.00	0.00	0.00	0.00
174	0.00	0.00	0.00	0.00	0.00	0.00
175	48.30	4.62	0.00	0.00	48.30	4.61
176	6.25	4.62	0.00	0.00	6.25	4.51
177	68.60	4.66	0.00	0.00	68.60	4.65
178	9.89	4.66	0.00	0.00	9.89	4.59
180	1781.54	4.53	19559.87	4.53	21341.41	4.53
301	9576.18	4.68	0.00	0.00	9576.18	4.67
302	0.00	0.00	418.09	4.09	418.09	4.06
305	636.40	4.68	0.00	0.00	636.40	4.67
306	6049.62	4.68	0.00	0.00	6049.62	4.67
310	7349.43	4.66	0.00	0.00	7349.43	4.65
311	699.92	4.68	0.00	0.00	699.92	4.67
314	406.30	4.66	0.00	0.00	406.30	4.65
316	4133.59	4.66	0.00	0.00	4133.59	4.65
318	289.61	4.66	0.00	0.00	289.61	4.65
319	3843.99	4.66	0.00	0.00	3843.99	4.65
322	233.61	4.66	0.00	0.00	233.61	4.65
323	48.59	4.66	0.00	0.00	48.59	4.65
326	266.11	1.64	0.00	0.00	266.11	1.62
327	24.84	1.64	0.00	0.00	24.84	1.63
328	290.95	1.66	0.00	0.00	290.95	1.64
329	5.43	1.64	0.00	0.00	5.43	1.01

TABLE B16 (Continued)

Stream	Physical Exergy Cost Flow [$/hr]	Cost of Physical Exergy Unit [$/GJ]	Chemical Exergy Cost Flow [$/hr]	Cost of Chemical Exergy Unit [$/GJ]	Total Exergy Cost Flow [$/hr]	Cost of Total Exergy Unit [$/GJ]
330	58.15	10.00	0.00	0.00	58.15	9.75
331	81.65	5.50	0.00	0.00	81.65	5.38
332	5.43	2.15	0.00	0.00	5.43	1.03
335	19.17	6.47	0.00	0.00	19.17	3.37
337	371.24	4.65	0.00	0.00	371.24	4.50
339	75.62	4.66	0.00	0.00	75.62	4.59
340	597.26	4.48	0.00	0.00	597.26	4.37
341	521.14	4.66	0.00	0.00	521.14	4.65
343	38.90	1.64	0.00	0.00	38.90	1.61
349	40.98	1.64	0.00	0.00	40.98	1.62
350	912.17	5.50	0.00	0.00	912.17	5.38
352	1371.14	4.88	0.00	0.00	1371.14	4.82
353	1987.80	5.18	0.00	0.00	1987.80	5.13
355	0.00	0.00	0.00	0.00	0.00	0.00
359	83.98	1.64	0.00	0.00	83.98	1.64
361	87.63	1.64	0.00	0.00	87.63	0.22
365	0.00	1.64	0.00	0.00	0.00	0.00

TABLE B17

POWER ($\dot{W}$), EXERGY DESTRUCTION ($\dot{E}_D$), EXERGY DESTRUCTION RATIO (y^*), RATIO OF EXERGY DESTRUCTION TO THE EXERGY OF SHALE (y), AND EXERGETIC EFFICIENCY (ϵ) FOR GROUPS OF THE COMBINED PLANT IMPROVED DESIGN (FIGURES 25, 29, 30 AND 31)

Group	$\dot{W}$ [MW]	$\dot{E}_D$ [MW]	y^* [%]	y [%]	ϵ [%]
Shale Retorting	8.24	180.08	15.10	3.22	98.2
Gas Scrubbing	3.98	19.52	1.64	0.35	99.8
Acid Gas Removal	0.75	11.41	0.96	0.20	99.8
Sulfur Recovery	1.31	17.79	1.49	0.32	0.0
Sour Water Stripper & NH_3 Recovery	3.50	27.12	2.27	0.49	0.0
Hydrogen Recovery	37.60	34.58	2.90	0.62	99.5
Compressor & Heat Exchangers	12.02	32.89	2.76	0.59	99.4
Steam Reformer	0.00	124.36	10.43	2.22	55.2
Shift Conversion & CO_2 Removal	1.01	45.62	3.82	0.82	96.4
Desalting & Hydrotreating	25.02	72.11	6.04	1.29	98.3
Steam Generator	14.09	510.68	42.81	9.13	51.4
HP Turbine	123.07	9.38	0.79	0.17	92.8
IP Turbine	129.30	9.71	0.81	0.17	92.9
LP Turbine	147.95	22.35	1.87	0.40	86.6
Condenser	0.00	47.90	4.02	0.86	0.0
Pump 1	0.16	0.04	0.00	0.00	75.9
Preheater in Hydrogen Plant	0.00	12.13	1.02	0.22	63.8
Deaerator	0.00	0.76	0.06	0.01	98.0
Pump 3 & Turbine	0.00	4.01	0.34	0.07	69.3
Preheater in PFH Plant	0.00	2.73	0.23	0.05	84.0
Preheater 2	0.00	2.78	0.23	0.05	88.7
Preheater 3	0.00	2.31	0.19	0.04	92.5

TABLE B18

VARIOUS THERMOECONOMIC VARIABLES FOR GROUPS OF THE COMBINED IMPROVED DESIGN (FIGURES 25, 29, 30 AND 31)

Group	$\dot{Z}$ [$/hr]	r [%]	$\frac{1-\epsilon}{\epsilon}$ [%]	$\frac{\dot{Z}}{\dot{E}_{P,k}c_{F,k}}$ [%]	f [%]
Shale Retorting	1878.46	4.07	1.84	2.15	53.89
Gas Scrubbing	707.75	1.01	0.20	0.80	79.94
Acid Gas Removal	398.01	0.93	0.19	0.73	79.44
Sulfur Recovery	797.68	0.00	0.00	0.00	100.00
Sour Water Stripper & NH_3 Recovery	522.91	0.00	0.00	0.00	100.00
Hydrogen Recovery	1663.64	3.05	0.53	2.44	82.25
Compressor & Heat Exchangers	1036.15	1.98	0.64	1.32	67.32
Steam Reformer	4489.99	356.15	81.17	60.28	42.62
Shift Conversion & CO_2 Removal	1381.54	10.87	3.72	6.44	63.37
Desalting & Hydrotreating	2677.81	7.80	1.72	5.644	76.60
Steam Generator	1347.70	131.77	94.43	16.11	14.57
HP Turbine	128.16	14.08	7.78	5.53	41.55
IP Turbine	134.64	13.99	7.66	5.56	42.04
LP Turbine	154.07	20.81	15.42	4.47	22.46
Condenser	94.79	0.00	0.00	0.00	100.00
Pump 1	7.80	204.70	31.69	56.78	64.18
Preheater in Hydrogen Plant	4.48	58.88	56.86	1.27	2.19
Deaerator	4.77	2.82	2.00	0.80	28.58
Pump 3 & Turbine	50.14	71.57	44.25	15.92	26.46
Preheater in PFH Plant	0.00	18.99	18.99	0.00	0.00
Preheater 2	4.05	13.85	12.73	0.98	7.15
Preheater 3	21.24	11.95	8.10	3.44	29.84

END

DATE
FILMED
7/16/93